PERFORMANCE OF FULL-SCALE ULTRA-HIGH PERFORMANCE FIBER-

REINFORCED CONCRETE COLUMN SUBJECTED TO EXTREME EARTHQUAKE-

TYPE LOADING AND EFFECT OF SURFACE PREPARATION ON THE COHESION

AND FRICTION FACTORS OF THE AASHTO INTERFACE SHEAR EQUATION

by

GUILLERMO PALACIOS

Presented to the Faculty of the Graduate School of

The University of Texas at Arlington in Partial Fulfillment

of the Requirements

for the Degree of

MASTER OF SCIENCE IN CIVIL ENGINEERING

THE UNIVERSITY OF TEXAS AT ARLINGTON

May 2015

Acknowledgements

Abstract

PERFORMANCE OF FULL-SCALE ULTRA-HIGH PERFORMANCE FIBER-

REINFORCED CONCRETE COLUMN SUBJECTED TO EXTREME EARTHQUAKE-

TYPE LOADING AND EFFECT OF SURFACE PREPARATION ON THE COHESION

AND FRICTION FACTORS OF THE AASHTO INTERFACE SHEAR EQUATION

Guillermo Palacios, M.S.

The University of Texas at Arlington, 2015

Supervising Professor: Shih-Ho Chao

Buildings in areas of high seismicity may be subjected to large axial stresses as well as severe earthquake loading. In order to protect the integrity of these buildings, concrete columns must possess high compressive strength and adequate ductility. While the use of high strength concrete (HSC) may appear as an attractive alternative and can reduce the section size of first story columns, its increase in strength leads to an increase in brittleness compared to that of normal strength concrete. For that reason, HSC requires a large amount of transverse reinforcement to maintain adequate ductility, which leads to severe congestion in placement of the reinforcing bars and adds to the cost and effort. A solution may be found in ultra-high-performance fiber-reinforced concrete (UHP-FRC). UHP-FRC is an innovative material which provides high compressive strength (25-30 ksi) and shear strength as well as improved compressive ductility and excellent confinement characteristics. The addition of high strength steel microfibers into the high strength concrete mix can reduce the need for excessive transverse reinforcement. The UHP-FRC mixture used in this research was created to maximize the dense particle packing concept, and it is essentially self-consolidating. Even though UHP-FRC provides

iv

superior material properties, there is limited test data available on its full-scale structural application. The performance of full-scale modern high-rise moment frame columns, with both normal strength concrete and UHP-FRC, tested under very large cyclic displacement reversals up to collapse is presented and discussed in the first part of this thesis. The use of UHP-FRC completely changes the typical failure mode of concrete columns as it improves confinement and prevents concrete crushing. Experimental results showed that the UHP-FRC column exhibited higher peak strength and greater drift capacity before succumbing to significant strength degradation compared to a conventional normal strength reinforced concrete column.

The achievement of composite action of concrete bridge deck systems relies heavily on the bond between the precast beams and the cast in-place concrete slabs. Two important components responsible for resisting horizontal shear are the cohesion and/or aggregate interlock, and the friction between the crack faces. The second part of this thesis investigates the influence of surface preparation on the cohesion and friction factors of the nominal interface shear resistance equation of the AASHTO LRFD Bridge Design Specifications (2014). A systematic surface preparation method was developed to recreate the different International Concrete Repair Institute (ICRI) Concrete Surface Profiles (CSPs) from which a series of push-off tests were performed to assess the contribution of the cohesion factor and the friction factor used in the AASHTO interface shear equation. An experimental program was developed made up of component push-off tests and full-scale composite box and slab beam tests. The experimental results suggest that the cohesion factor used by AASHTO may be considered un-conservative as both the cohesion factor and friction factor are not only dependent on the surface roughness, but also can be limited by the strength of the concrete matrix. The effect of a

smoother surface finish typically formed with the use of SCC was also investigated in the

full-scale specimens.

Table of Contents

viii

List of Illustrations

xvi

xvii

xviii

xxi

List of Tables

Chapter 1

Introduction

<u>1.1 Part I: Overall Experimental Program</u>

This thesis will describe a part of the first phase of the two-phase NEES (Network for Earthquake Engineering Simulation) research program entitled "Full-Scale RC and HPFRC Frame Sub-assemblages Subjected to Collapse-Consistent Loading Protocols for Enhanced Collapse Simulation and Internal Damage Characterization." This project is a collaborative effort between University of Texas at Arlington, University of Minnesota, California State University at Chico, and the University of Illinois at Urbana-Champaign. The first phase of this project sets out to perform full-scale tests on a series of modern high-rise moment frame columns with both normal strength concrete and UHP-FRC under very large cyclic displacement reversals up to collapse (Nojavan et al., 2014). The second phase of this multi institutional project focuses on the full-scale sub-assemblage testing of beam column connections (Choi and Chao, 2015).

The overall objective of this project is to investigate the behavior of full-scale reinforced concrete (RC) and high-performance fiber reinforced concrete (HPFRC) frame components when subjected to collapse-level loading, and then to use the experimental results (mechanical response and internal imaging) to develop improved component models that will enable the accurate modeling of structural collapse for the implementation in the next generation of performance-based seismic design procedures.

The experiments in the first phase of the project comprise of two different types of modern high-rise moment frame column specimens, perimeter frame columns of cross-sectional dimensions of 36x28 in. and space frame columns with cross-sectional dimensions of 28x28 in., both of which were be tested at the NEES Multi-Axial Sub-assemblage Testing (MAST) Laboratory at the University of Minnesota. This thesis will

primarily focus on the characteristics and behavior of the two space frame column specimens, more specifically on the UHP-FRC column specimen SP8.

High strength concrete (HSC) is often utilized as a cost-effective design solution in the lower stories of high-rise buildings. There are many advantages to the use of HSC in high-rise buildings, particularly in the column members. HSC has the potential of reducing section sizes hence reducing some construction costs due to labor and formwork, while maximizing the rentable floor space (Mwafy et al., 2015). However, the brittleness of HSC makes it a less attractive material for structures in high seismic areas. This is due to the fact that extensive transverse reinforcement is needed in the column cages in order to provide adequate confinement to maintain strength and ductility. The addition of excessive transverse reinforcement can lead to severe congestion in the plastic hinge regions of the columns, thus creating great difficulties during construction and concrete placement. The use of HSC can also have an effect on the seismic performance of such columns, as HSC are susceptible to early cover spalling, which leads to a decrease in strength (ACI-441R, 1996). Researchers have improved the confinement and seismic performance of concrete columns through the use of fiber-reinforced concrete (normal strength 5-8 ksi. with moderate compressive ductility). Additional dowel reinforcement, combined with debonding techniques to prevent damage concentration (Aviram et al., 2010), have also been used. However, these techniques could complicate the design, and they have been known to fail in the prevention of concrete deterioration, crushing, and bar buckling. In recent years, the development of ultra-high-performance fiber-reinforced concrete (UHP-FRC) has provided an innovative material that shares the advantages of HSC and can resolve it's brittleness issue while maintaining constructability. The superior mechanical properties of UHP-FRC offer a new alternative to design earthquake-resistant moment frame members.

While the capabilities of UHP-FRC suggest it to be a valuable alternative in earthquake resistant structures, it has yet to be tested in large scale structural applications. The first part of this thesis primarily focuses on the characteristics and behavior of two full-scale space frame column specimens consisting of a normal strength concrete specimen (SP5) and a specimen with its plastic hinge region cast with UHP-FRC (SP8), both tested under large cyclic reversals.

1.2 Part II: Overall Experimental Program

The shear resistance at the interface between the precast element and the cast in-place (CIP) element is of paramount importance in order to ensure the successful transfer of stresses in composite concrete bridges. Sufficient shear resistance prevents the relative slip between the two elements thus fostering composite action. A good connection between the two components of the composite system can be achieved by artificially roughening the interface, providing a bonding agent, and/or using shear connectors or ties, mostly in the form of extended stirrups or hooks. When a crack between the surfaces occurs, the horizontal shear reinforcement elongates across the crack providing a clamping force at the interface which controls the crack width. In order for the horizontal shear reinforcement to develop its yield strength before pullout or debonding, the bars must be sufficiently anchored on both sides of the interface. It is believed that the clamping action of the reinforcement only comes into play after the crack between the surfaces slightly opens. The horizontal shear stress due to bending is equal in magnitude to the vertical shear stress and can be derived either based on the classical strength of materials approach or an alternative considering the shear force at the strength limit state as given by AASHTO Section C5.8.4.2 (AASHTO, 2014).

The horizontal shear at the interface is resisted by a combination of:

(1) Resistance of the protrusions on the crack faces to shearing (i.e. cohesion and/or aggregate interlock) also referred to as "cohesion factor" by AASHTO,

(2) Friction between the crack faces, and

(3) Dowel action of the reinforcement.

The AASHTO nominal shear resistance of the interface plane is given by:

$$V_{ni} = cA_{cv} + \mu\left(A_{vf}f_y + P_c\right)$$

(1-1)

The nominal shear resistance should however not be greater than the lesser of:

$$V_{ni} \leq K_1 f_c' A_{cv}, \text{ or}$$

(1-2)

$$V_{ni} \leq K_2 A_{cv}$$

(1-3)

For a cast in-place concrete slab on clean concrete girder surfaces, free of laitance with a surface roughened to an amplitude of 0.25 in.:

c = cohesion factor = 0.28 ksi;

μ = friction factor = 1.0;

A_{cv} = interface area (in^2);

K_1 = fraction of concrete strength available to resist interface shear = 0.3;

K_2 = limiting interface shear resistance = 1.8 ksi for normal weight concrete

Equation (1-2) is a limit preventing shearing or crushing of aggregates whereas equation (1-3) is due to lack of sufficient experimental data beyond the limit K_2.

The shear friction concept is used in today's design specifications for horizontal shear transfer, to describe the behavior of a cracked material or an interface between two elements. Before cracking, interface shear is believed to be transferred mainly through concrete and through both concrete and reinforcing bars after cracking. Loss of contact at the interface will result in failure to transmit shearing forces. The loss of contact can

occur due to crushing of the interlocking aggregates and cement paste. This occurs when either of these components reaches their compressive capacity which is directly related to concrete strength. When the two sides of a cracked specimen try to shear past each other, friction resists their motion. Friction is assisted by the clamping force provided by the dead load of the CIP slab as well as that provided by the reinforcement bridging the interface.

Horizontal cracks between the precast beams and the CIP decks have been noticed in several older TxDOT bridges. Figure 1 below shows horizontal cracks on an older bridge located at the Riverside Drive Underpass at I-35 in Austin, Texas. These cracks could result from shrinkage or excessive shear forces. Shrinkage of the deck can induce significant stresses along the interface between the precast beam and the CIP deck leading to cracking or slip if shear resistance at the interface is insufficient. More details regarding the cracks are discussed in Section 7.5.2.

Figure 1. Interface cracks on Riverside Dr. Underpass at I-35

As shown in the AASHTO equation (Eq. 1-1), the three major contributions to the horizontal shear resistance are (1) cohesion and/or aggregate interlock, (2) friction

between the crack faces, and (3) dowel action of the reinforcement. The objective of this research is therefore two-fold:

1. Determine the influence of horizontal shear reinforcement on interface shear despite limited development:

TxDOT specifies a 5 in. thick composite concrete deck to be used on prestressed slab beams and box beams. AASHTO LRFD Bridge Design Specifications (2014) section 5.8.4.1 requires that all reinforcement crossing the interface should be fully developed on both sides of the interface by embedment, hooks, or other methods to develop the design yield stress. AASHTO Section 5.11.2.4 provides guidelines for determining the development length needed for standard hooks in tension. The equation provided results in an embedded length of 6.7 in. not possible in a 5 in. CIP slab. However, horizontal shear reinforcement does not qualify to be considered as "standard hooks" according to the AASHTO definition and there is no equation suitable for typically horizontal shear reinforcement. Since the shear friction action of the interface shear reinforcement relies on yielding of the bars (Item 3 of Eq. 1-1), a short embedded length inside the composite slab can fail by premature pullout due to localized concrete fracture prior to yielding, thus providing insufficient clamping force. The embedded length of interface shear reinforcement is only 2 in. in current TxDOT prestressed slab beams and box beams (Figure 2).
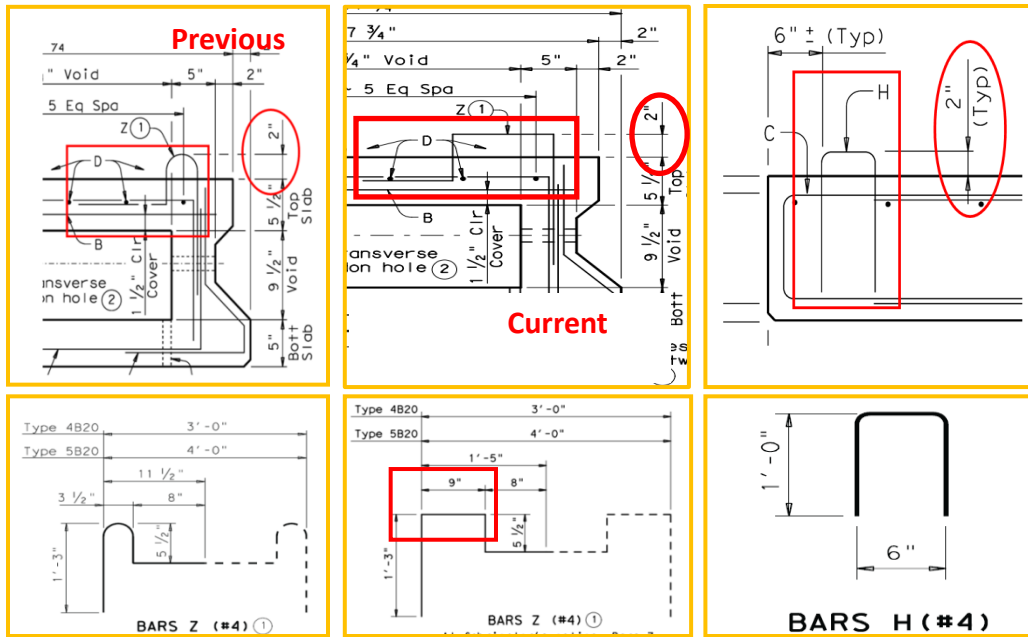
Figure 2. Standard TxDOT box and slab beam details

2. Determine the influence of different surface profiles on interface shear strength:

AASHTO Section 5.8.4.3 (AASHTO, 2014) specifies c = 0.28 ksi and μ = 1.0 for a surface roughened to an amplitude of 0.25 in. This indicates that both the cohesion factor c and friction factor μ are affected by the surface roughness. Current TxDOT standards state that "Finished, unformed surfaces must not have distortions greater than 0.25 in." (TxDOT, 2004). A number of the precast plants in Texas typically give a wood float finish on box and slab beams. This is done by sliding a wooden float across the top of the wet concrete resulting in a coarse finish. This is why it is very important to investigate the effects of a wood float surface finish on the shear transfer across an interface. An effective means to improve the horizontal shear resistance is to specify a rougher finish (i.e. amplitude of roughness greater than 0.25 in.) on top of the beam to improve horizontal shear capacity. An experimental study carried out by Saemann and

7

Washa (1964) has shown that the horizontal shear strength is increased by increasing the surface roughness.

Also, TxDOT is moving towards using the ICRI (International Concrete Repair Institute) guidelines for concrete surface preparation as a measure of surface roughness. The ICRI guidelines offer nine distinct surface configurations graded from smooth to very rough. These configurations are identified as concrete surface profiles (CSPs) ranging from CSP 1 which is nearly flat to CSP 9 which is very rough (Figure 3). The Precast Panel-Fabrication Standard recommends that the top of the panel should be finished to a roughness between a CSP 6 and a CSP 9. Therefore, by investigating these different surface configurations, we can recommend the roughness that will lead to an improvement to the horizontal shear resistance of composite TxDOT beams.
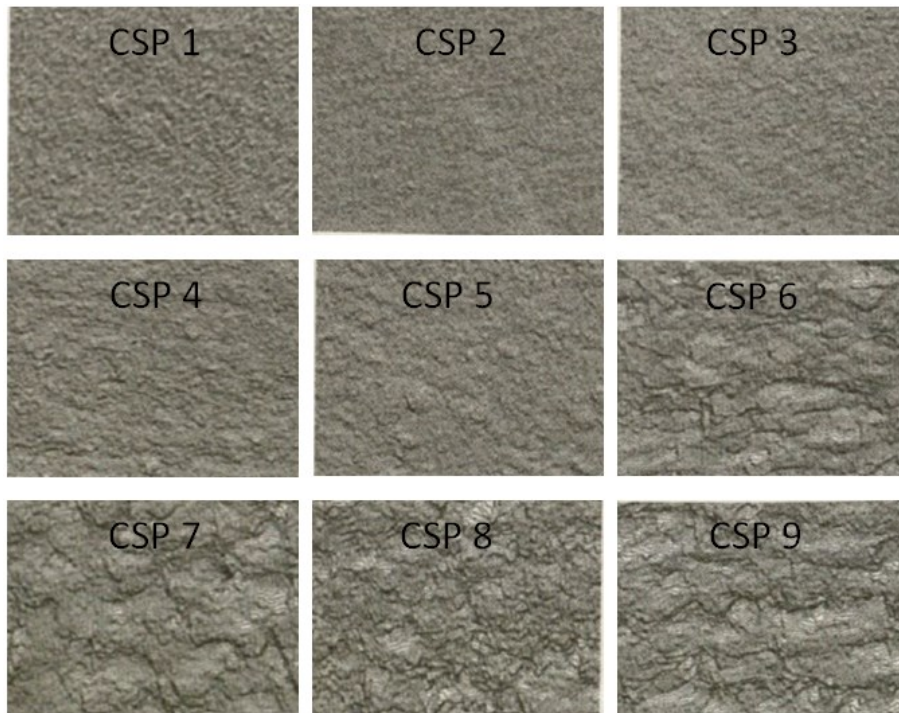
Figure 3. ICRI concrete surface profiles (CSPs)

A complete experimental investigation was carried out as part of TxDOT project No. 0-6718 comprising of 7 Tasks as shown in the flowchart on Figure 4 to investigate if adequate horizontal shear capacity is provided by the 5 in. concrete deck on slab and box beams, despite lack of reinforcement development. The first three tasks correspond to small-scale push-off tests to investigate the three major components of horizontal shear resistance: (1) cohesion and/or aggregate interlock, (2) friction between the crack faces, and (3) dowel action of the reinforcement. A simple bar pullout test was also used to evaluate the influence of the bend curvature on the bond and slip characteristics of the horizontal shear reinforcement. Alternative details for surface roughness and bar geometries were also investigated. The second phase of this research consists of testing several full-scale composite box and slab beams with current TxDOT detailing and alternative details to investigate the overall composite behaviors that may be overlooked in the small-scale component tests.

```
┌─────────────────────────┐
│   TxDOT Project 0-6718   │
└─────────────────────────┘
            │
            ▼
┌─────────────────────────────────┐
│            Task 1               │
│  Literature Review and Field    │
│  Trips to Bridge Sites and      │
│      Precast Plants             │
└─────────────────────────────────┘
```

```
┌─────────────────────┐              ┌─────────────────────┐
│    Push-off Test     │              │      Task 5          │
│                      │              │   Bar Pullout Test   │
└─────────────────────┘              └─────────────────────┘
          │                                    │
          ▼                                    ▼
┌──────────────────────────────┐   ┌──────────────────────────────┐
│           Task 2             │   │           Task 6             │
│ Evaluate Horizontal Shear    │   │ Full-Scale Composite Beam    │
│ Component: cA_cv             │   │     Test: current practice   │
│ (cohesion and/or aggregate   │   └──────────────────────────────┘
│ interlock)                   │
└──────────────────────────────┘
          │
          ▼
┌──────────────────────────────┐
│           Task 3             │
│ Evaluate Horizontal Shear    │
│ Component: μP_c              │
│ (friction between the crack  │
│ faces)                       │
└──────────────────────────────┘
          │
          ▼
┌──────────────────────────────┐
│           Task 4             │
│ Evaluate Horizontal Shear    │
│ Component: μA_{vf}f_y        │
│ (dowel action of the         │
│ reinforcement)               │
└──────────────────────────────┘
```

Task 2: Evaluate Horizontal Shear Component: cA_{cv} (cohesion and/or aggregate interlock)

Task 3: Evaluate Horizontal Shear Component: μP_c (friction between the crack faces)

Task 4: Evaluate Horizontal Shear Component: $\mu A_{vf}f_y$ (dowel action of the reinforcement)

```
┌──────────────────────────────┐
│           Task 7             │
│ Full-Scale Composite Beam    │
│ Test (Further Investigation) │
└──────────────────────────────┘
            │
            ▼
┌──────────────────────────────┐
│           Task 8             │
│ Final Report (Research       │
│ Findings and Design          │
│ Recommendations)             │
└──────────────────────────────┘
```

Figure 4. TxDOT project No. 0-6718 experimental investigation

This thesis aims to examine the effects of different surface preparations through an experimental study and focuses on the shear transfer through concrete or "concrete action", which consists of the cohesion or interlock of aggregate protrusions, and the

friction resulting from the normal compressive stress. AAHSTO (2014) simplifies the "concrete action" into two terms, the cohesion factor (*c*), and the friction factor (*μ*).This thesis will report a literature review and survey of each of the 50 state's Departments of Transportations (DOTs) regarding their current practice (Task 1). The results of the push-off tests relating to the concrete components of cohesion and aggregate interlock (Task 2) and the friction between the crack faces (Task 3) will also be reported. This study will also relate the component test results to a full-scale beam investigation, more specifically the effect of surface preparation on the horizontal shear strength of full-scale box and slab beams with no horizontal shear reinforcement (Task 6) and the effect of the smooth finish typically created by SCC on the horizontal shear strength of full-scale composite box and slab beams with a reduced area (Task 7). All other tasks in relation to the development of the horizontal shear reinforcement, and relative to the embedment length and bar curvature not reported in this thesis may be found elsewhere (Waweru, 2015).

1.3 Organization of Thesis

This thesis is comprised of two different research projects and thus organized into two major parts. Chapter 1 will introduce the two individual research projects and their respective overall testing programs as well as discuss the organization of the report.

Part I will be covered in Chapter 2 through Chapter 6, and will discuss the performance of a full-scale ultra-high performance fiber-reinforced concrete column subjected to extreme earthquake type loading. Chapter 2 will present a literature review on the advantages and applications of HSC, followed by the current ACI 318 seismic design confinement provisions for concrete columns. Previous tests on concrete columns subjected to earthquake type loading and a brief introduction to UHP-FRC will also be presented. Chapter 3 will discuss the experimental program including a preliminary small-

scale column study and the full-scale column design, construction, instrumentation, test setup, and loading protocol. Chapter 4 will address the full-scale column experimental testing covering test observations and the response of the two full-scale column specimens. Chapter 5 will report the test results including the elastic behavior of the UHP-FRC specimen, a seismic comparison between two specimens, a brief investigation on the effectiveness of transverse reinforcement of columns extending into the footing, followed by a discussion of UHP-FRC and the ACI 318-14 seismic design provisions. Finally, the summary, conclusion, and recommendations of this UHP-FRC research project will be summarized in Chapter 6.

Part II will be covered in Chapter 7 through Chapter 11, describing the effect of surface preparation on the concrete contributions of the horizontal shear strength of composite box and slab beams, more specifically the cohesion and friction factors of the AASHTO equation. A literature review on horizontal shear will be presented in Chapter 7. Chapter 8 will explain the experimental program including design, construction, and test setup of both the push-off style component tests and the full-scale beam testing. Chapter 9 will discuss the test results and observations. Finally, the summary, conclusion, and recommendations for this project will be summarized in Chapter 10.

Chapter 2

Part I: Literature Review

This section describes important characteristics and applications of HSC, including the typical behavior of HSC columns. The ACI 318-14 seismic design provisions are also presented more specifically in relation to the confinement of high strength moment frame concrete columns. This is followed by a review of prior research on reinforced concrete columns subjected to earthquake-type loading, including HSC columns and columns which incorporated seismic performance enhancing techniques. A brief introduction to UHP-FRC will also be presented.

2.1 Introduction

In ancient times many great civilizations from the early Egyptians to the Romans have constructed monuments using a mixture of sand, water, aggregate and a paste-like material we would now refer to as cement. Historically, concrete is considered one of the world's oldest building materials, and with these great monuments withstanding the test of time we continue to use concrete in a number of structures today. However, through the development of various admixtures the characteristics of concrete have greatly improved. More specifically an advanced material that is in essence an enhanced from conventional concrete, High strength concrete (HSC). HSC offers a wider range of applications and improved properties that result in stronger, stiffer, and more durable and economical solutions to a number of engineering projects. These characteristics have helped HSC become a more popular alternative in modern day structural designs and construction.

2.2 Applications of HSC in RC structures

As the term "high strength" has varied in the past, it is difficult to categorize or compare older HSC structures from those built today. However, one of the earliest and

most popular buildings that has adopted HSC is the 311 South Wacker building located in Chicago, Il which was once the highest reinforced concrete building in the world when it was completed in 1990 (Figure 5). The building has 71 stories and is 969 feet tall utilizing concrete with compressive strengths up to 12,000 psi (Portland Cement Association, 1994).

Figure 5. 311 South Wacker Drive, Chicago USA (Portland Cement Association, 1994)

Beyond that, HSC has been applied to major part of high rise buildings including the skyscrapers shown in Figure 6 (Portland Cement Association, 1994). HSC is often utilized as a cost-effective design solution in the lower stories of high-rise buildings. There are many advantages to the use of HSC in high-rise buildings, particularly in the column members. Additionally, Thomsen and Wallace (1994) described the benefits of using HSC in regions of moderate to severe seismic risk. The benefits include: Increasing the strength and stiffness of a column, allowing the use of smaller columns, increasing the safety of a design by satisfying the strong column-weak girder concept, allowing for more rapid construction by attaining higher strengths at an early age, and reducing the anchorage lengths requirements. Mwafy et al. (2015) also concluded that HSC also has

the potential of reducing section sizes hence reducing some construction costs due to labor and formwork, while maximizing the rentable floor space.

* Reinforced concrete frame
† Composite concrete/steel frame
** Also includes one experimental column of 17,000 psi
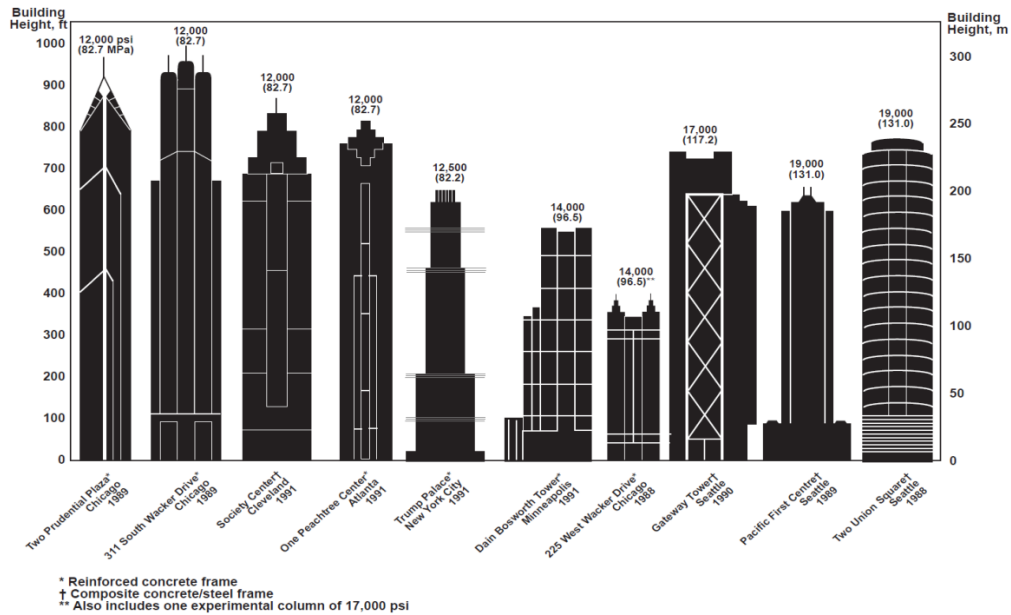
Figure 6. HSC buildings in the United States (Portland Cement Association, 1994)

<u>2.3 Advantages of High Strength Concrete</u>

The properties of HSC are attained through modifications in the mix design and curing of normal strength concrete. The following are the most common modifications that are used to obtain high strength concrete (Caldarone, 2009):

1. Reducing w/cm ratio and introducing water reducing admixtures (WRA) or high-range water-reducers (HRWR): This is the most important improvement as it creates many benefits not only to the fresh concrete mixture, but also to the hydrated product. The loss of slump due to the lower w/cm ratio can be corrected by using HRWR so that the workability can be maintained. Also, without adding the excess amount of water required for workability purposes, reduces the possibility of bleeding, segregation, air pocket after hydration, and a weaker transition zone. Therefore, a denser and more uniform matrix is created resulting in a stronger concrete.

2. Using mineral admixtures: mineral admixtures with pozzolanic and cementitous properties such as fly ash, or ground furnace slag, are introduced into the concrete mix with three main purposes:

   a) Provide a supplement source of silica and reduce the heat of hydration,

   b) provides a finer particle to densify the packing of concrete,

   c) as a cementitous material replacement.

3. Stronger aggregate: while fine aggregates, mostly sand, do not have a significant effect on the strength and modulus of elasticity, the properties of the coarse aggregates highly affect the mechanical properties of the concrete. This can be explained due to two factors,

   1) coarse aggregates occupy the largest volume of any constituent in the concrete,

   2) the weaker zone in concrete microstructure also known as "transition zone" (the surround area of coarse aggregates). The strength of the transition zone controls the bond strength between the paste phase and aggregates phase, it also depends on the physical properties of the aggregates e.g. shapes, roughness, etc. Therefore, in HSCs, the aggregates have to be designed carefully so that the difference in strength between the aggregate and the paste will not cause a lower strength transition zone.

   Figure 7 summarizes the important characteristics of HSC along with the structural advantage resulting from such characteristics. Typically, HSC has a low w/cm ratio with the addition of HRWR and mineral admixtures (fly ash, silica-fume). Therefore, HSC has lower air voids and defects compared to NSC which results in less micro

cracking, stronger and more consistent transition zone strength, higher bond strength, and lower permeability. HSC concrete has many other notable performance characteristics relative to the long-term performance of the concrete structure, such as abrasion resistance, freeze-thaw resistance, fire protection, and reduced creep (ACI-363R, 2010).
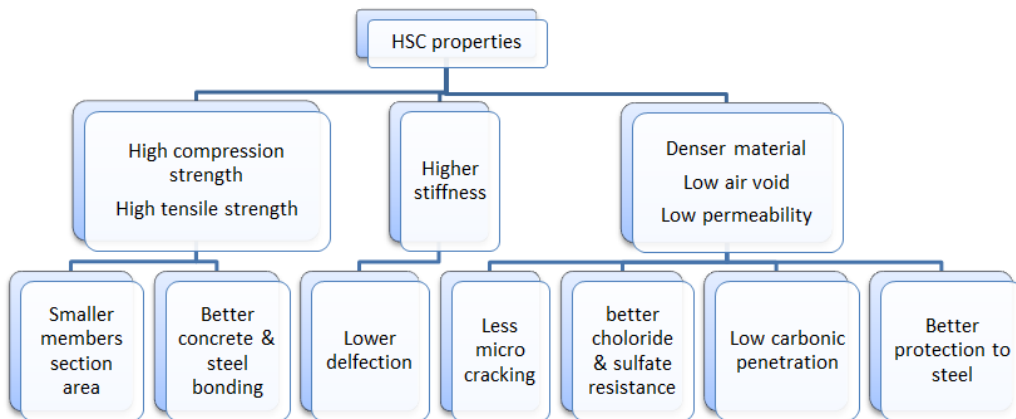
Figure 7. Advantages of HSC properties

2.3.1 Strength

HSC as per ACI 363R-10 (2010) is defined as concrete that has a specified compressive strength of 8,000 psi. or greater. Figure 8 shows the stress-strain curves for concrete with various high compressive strengths. It can be observed form Figure 8 that as the compressive strength increases so does the slope of the initial linear portion of the stress-strain curve; demonstrating that there is a direct relation between the modulus of elasticity and the compressive strength of HSC. It is important to note that while there are many advantages to HSC its increase in strength also comes with an increase in brittleness as denoted by the post-peak behavior of the stress-strain curves shown in Figure 8. As mentioned previously, the higher modulus of elasticity can be attributed to

the higher volume and increased elastic modulus of the aggregate used within the mix as well as the lower w/c ratio.
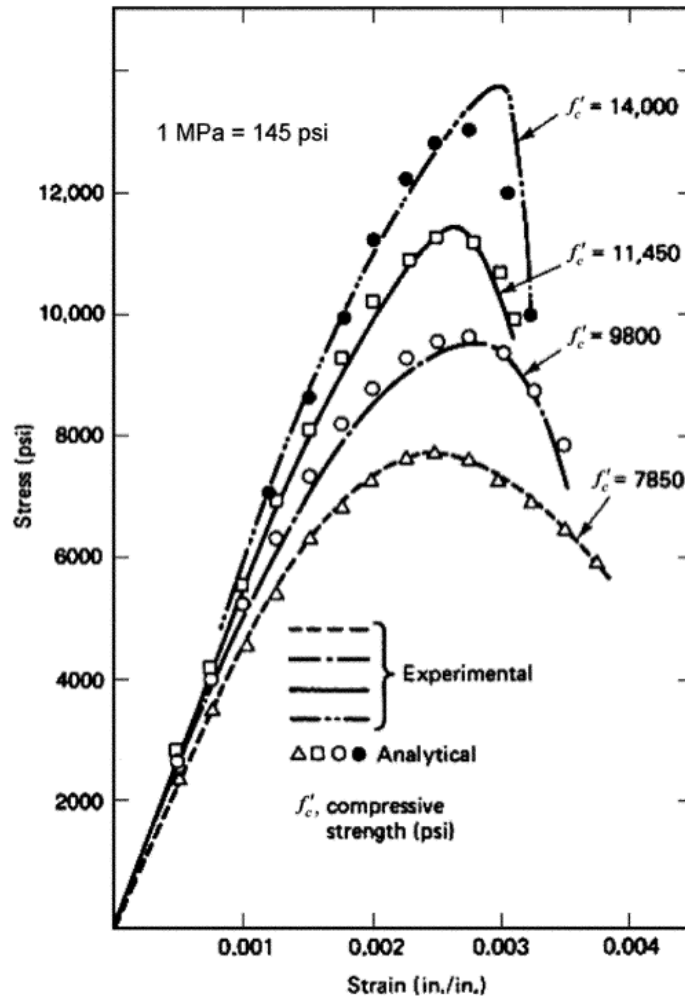
Figure 8. Stress-strain curves for concrete in compression (ACI-363R-11, 2011)

2.3.2 Stiffness

The stiffness of concrete is typically represented by the modulus of elasticity. The modulus of elasticity is defined as the ratio of normal stress to the corresponding strain for compressive stresses below the proportional limit of a material. As shown in Figure 8, the slope of the linear portion of the curves for HSCs are generally steeper than that of

NSCs and also from Figure 9, we can see that the modulus of elasticity is increased when the compressive strength increases.

Table 1 shows different suggestions for the prediction of modulus of elasticity of HSCs. However, this property varies and is highly dependent on the testing methods and definitions (ACI 363R-10, 2010).

Table 1. Suggested equations for predicting modulus of elasticity of HSC (ACI 363R-10, 2010)

Author	Year	Recommend E_c , (psi)
Martinez et al	1982	$E_c = 40,000(f_c')^{0.5} + 106$ for 3000 psi $< f_c' < 12,000$
Cook	1989	$E_c = w_c{*}2.55(f_c')^{0.315}$
Ahmad and Shah	1985	$E_c = w_c{*}2.5(f_c')^{0.325}$ (psi) for $f_c' < 12,000$ psi
Berke et al	1992	$E_c = 2,778(CF) + 6189(SF) + 452,545(LN(age)) + 1,796,695$
Tomosawa and Noguchi	1993	$E_c = 4.86 \times 106 k_1 \cdot k_2(w_c /150)^2 \times (f_c' /8700)^{1/3}$
Radain et al	1993	$E_c = 2,101,775 + 26,200(f_c')^{0.5}$
ACI 318-14	2014	$E_c = 57,000(f_c')^{0.5}$

The expressions above do not predict the modulus of elasticity with very high accuracy as shown by the wide variety of test data collected by ACI in Figure 9. The E_c value is highly dependent on many other factors such as aggregate type, mix design proportioning, and curing conditions.
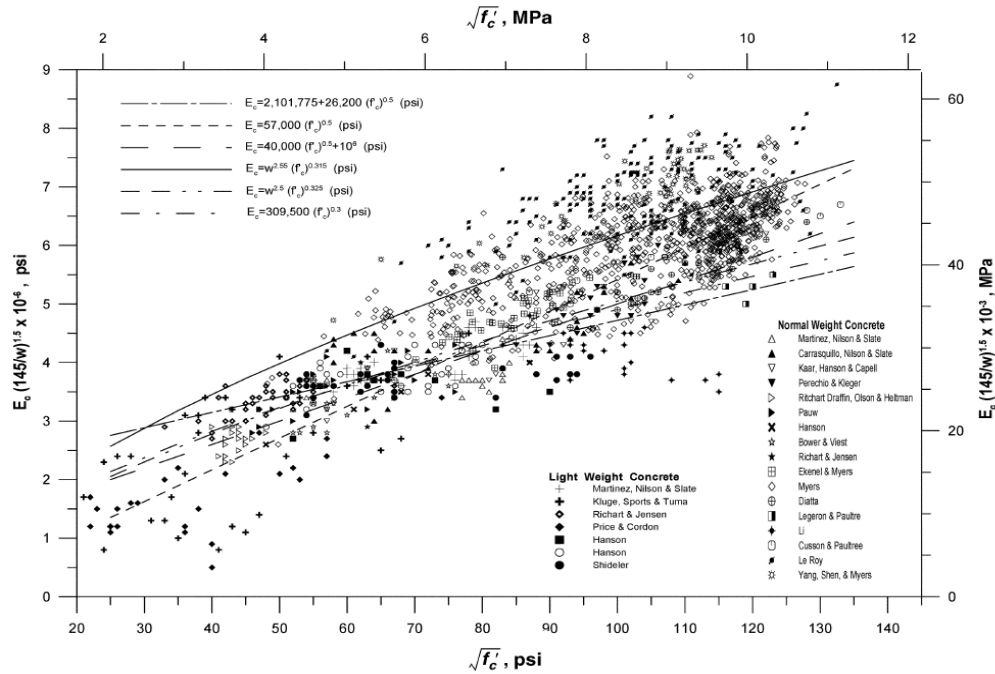
Figure 9. Elastic modulus and square root of concrete strength relationship (ACI 363R-10, 2010)

2.3.3 Ductility

Concrete is generally a brittle material with low tensile capacities. Additionally, the higher the compressive strength, the less ductile the concrete behaves. Therefore, under a plain concrete comparison, HSC will perform more brittle than NSC. However, in reinforced concrete columns, if the lateral reinforcement is adequately designed, HSC is capable of performing with higher strength and ductility than NSC. Also in flexural members, HSC will reduce the depth of the neutral axis; consequently the tensile steel

strain will be higher for the same bending condition compared to NSC, and more ductile behavior can be achieved. Figure 10 shows a stress-strain curve comparison between HSC and low-strength concrete. Figure 8 shows that the post-peak behavior of the low-strength concrete has a less steep slope compared to that of the higher strength concrete, representing a relatively higher ductility than that observed in HSC.
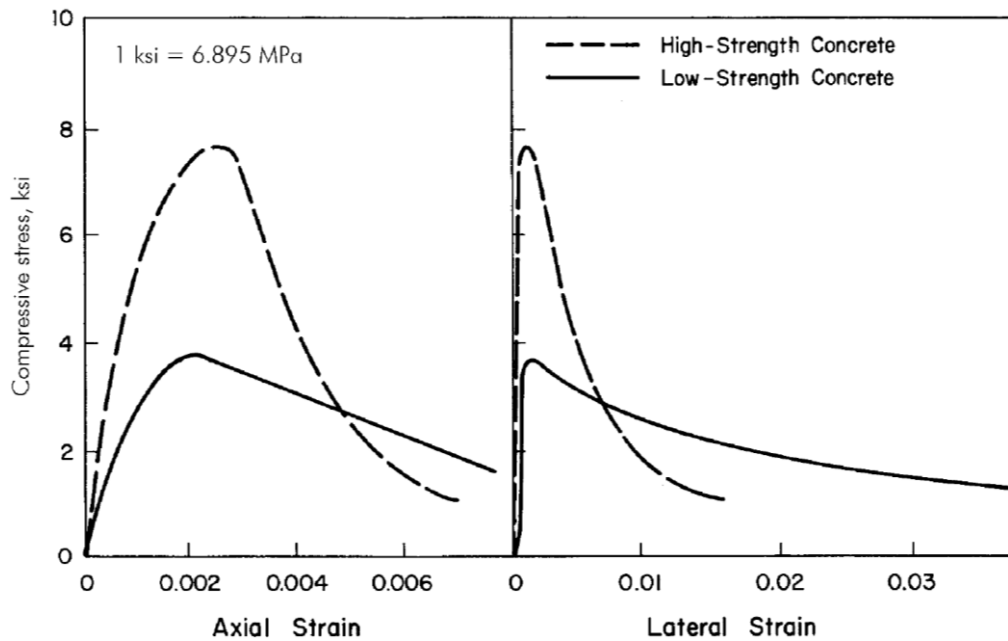
Figure 10. Axial and lateral stress-strain curve (ACI 363R-10, 2010)

2.4 Typical behavior of HSC columns

Despite numerous advantageous characteristics of HSC over NSC, the full benefit of HSC in RC columns cannot be achieved unless the columns are designed with proper consideration to their material limitations. As discussed in the previous sections, most concrete mechanical properties are empirically correlated to the uniaxial compressive strength. Furthermore, as the design concrete strength is specified by the engineer depending on the structural situation, an improved structural performance can generally be obtained through an increase in concrete strength.

2.4.1 HSC column subjected to concentric axial loading

From the stress-strain information shown in Figure 10, let's compare two RC columns subjected to concentric loading, one made from NSC and the other made from HSC, both designed with the same reinforcement ratio. As the applied load increases, the concrete will crush and eventually fail the column. The comparison between the two cases can be observed in Figure 11 and Figure 12.

ε=0.001
- Concrete reaches significant nonlinearity, stiffness decreases.
- Steel still linearly elastic, starts to pick up larger portion of total load.

ε=0.002
- Concrete achieves peak stress, exhibits plastic behavior and will not be able to take any extra load.
- Steel starts yielding but may take all applied load.

ε=0.003
- Concrete literally fails by crushing.
- Steel completely yields and may fail by buckling.

Figure 11. NSC column under axial compression

ε=0.001	ε=0.002	ε=0.003	ε=0.0035
• Concrete behaves linear elastic • Steel still linearly elastic. • Both material taking load as normal.	• Concrete stiffness decreases • Steel starts yielding and eventually takes a higher portion of the load	• Concrete reaches its peak strength but does not fail • Steel yields and reaches peak strength • Column section still works under compatible condition	• Concrete literally fails by crushing. • Steel completely yields and may fail by buckling.

Figure 12. HSC column under axial compression

From the comparison charts, it can be observed that in the case of HSC, the complete steel area has yielded when the concrete reaches its maximum strength. Thus, there is improved compatibility between the concrete and the reinforcing steel in the HSC case, than in the NSC case.

ACI 318-14 suggests an equation for the nominal capacity of a member subject to axial compression based on the superposition of concrete strength and reinforced steel strength:

$$P_n \; = \; 0.85 f_c' \left(A_g - A_{st} \right) + f_y A_{st} \qquad (2\text{-}1)$$

For comparison, let's assume a concrete column cast with 6 ksi concrete and reinforced with 60 ksi steel with a 1% reinforcing ratio. Substituting the steel strength with 10f'$_c$ and substituting A$_{st}$ with 0.01A$_g$, the equation above can be rewritten as:

$$P_n \; = \; 0.85 f_c' \left(A_g - 0.01 A_g \right) + 10 f_c' \times 0.01 A_g \qquad (2\text{-}2)$$

$$P_n = 0.9415 f_c' A_g \qquad \text{(2-3)}$$

$$A_g = \frac{P_n}{0.9415 f_c'} \qquad \text{(2-4)}$$

If the concrete strength is replaced with 12,000 psi, thus the P_n will be approximately doubled in value or the A_g will be reduced by approximately half. However, in practice a column is very rarely subjected to a purely concentric load, thus further discussion on the advantages of HSC under combined loading must be considered.

2.4.2 HSC column subjected to eccentric loading

For a typical column design, assuming the column is non-slender and the P-Δ effects may be ignored, the capacity of a column subjected to eccentric loading can then be represented by the interaction diagram shown in Figure 13. For a simple comparison, the balanced failure condition will be considered, where concrete crushes and steel yields at the same time.
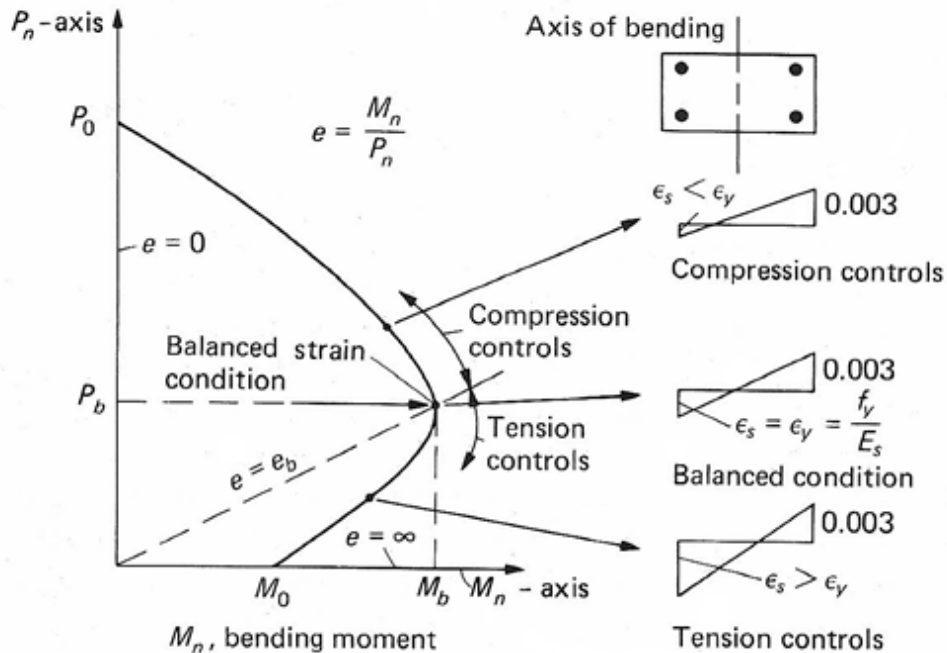
Figure 13. Column interaction diagram (ASDIP, 2015)

Assuming that both NSC and HSC crush at a strain of 0.003 and the reinforcing steel yields at strain of 0.002, the stress diagram can be visualized for both cases as shown in Figure 14.

(a) Stress distribution NSC

(b) Stress distribution HSC

(c) Equivalent rectangular stress block (two parameters)
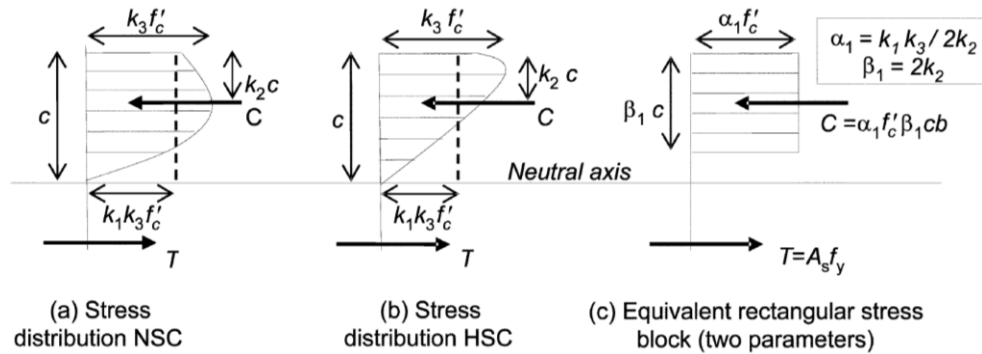
Figure 14. Compressive stress distribution (ACI 363R-10, 2010)

From Figure 14, considering the case of HSC with a compressive strength of 12 ksi, and NSC with a compressive strength of 6 ksi, the peak compressive stress for HSC would be twice as high compared to the case of NSC, thus the slope of stress distribution curve will be much steeper. This suggests that there is an uneven stress distribution in HSC resulting in a shorter depth of the compressive stress block for HSC compared to NSC. From Figure 14, the value of c and k_2 for the HSC case must smaller than in the NSC case. Through the use of similar triangles, if c is smaller, thus the tensile strain will be larger and so the members will be more ductile. k_1 and k_3 are factors that equalize of distribution of the compressive stress into an equivalent stress block. Hence, the steeper the stress distribution, the smaller the k_1 and k_3 factors are. Therefore, the compressive stress block will be smaller for HSC.

2.4.3 Concrete cover

Some researchers have observed that concrete cover in HSC columns spalled prior to them reaching their nominal capacity (ACI 441R-96, 1996; Razvi and Saatcioglu, 1994; Foster, 2001).

This phenomenon is not typically observed in NSC columns. Collins et al. (1993) attributed the cover spalling to differential shrinkage between the cover shell and the HSC around the reinforcement. The steel bars also restrain this shrinkage and therefore cause micro-cracking along the bar-concrete interface. Cusson and Paultre (1994) attributed the early cover spalling to the close spacing of the transverse reinforcement. The mechanism of the separation between the concrete cover and the core concrete due to shrinkage can be seen in Figure 15.

a) Shrinkage in Shell Concrete   b) Presence of Bars Restraining Shrinkage   c) Resulting Propagation of Cracks and Cover Spalling
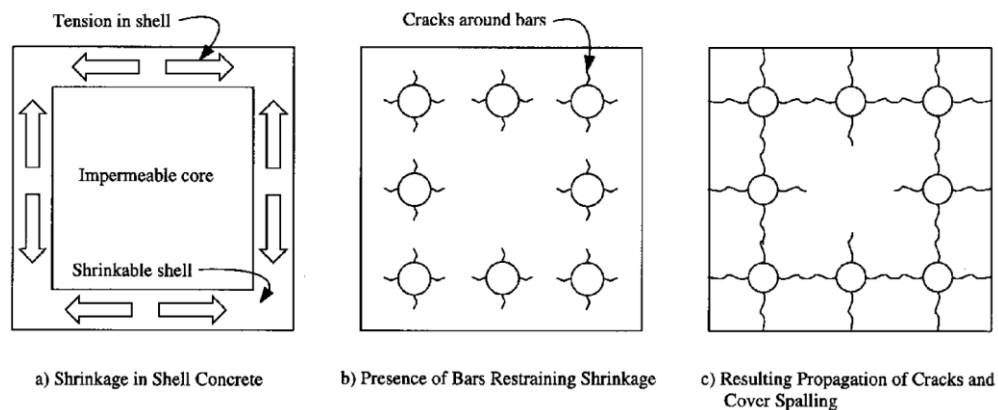
Figure 15. Cracking pattern in HSC columns due to drying shrinkage (ACI 441R-96, 1996)

Foster (2001) developed a spalling mechanism by observing the cover-core interface cracking. He indicate that cracking must first happen between the cover and the core concrete, and the spalling is the result of a triaxial stress state of the concrete cover area, he suggested that the triaxial compression stress state is occurring in the concrete core while a compression-tension state is occurring for the cover concrete resulting in spalling (Figure 17).

The significance of cover spalling in HSC columns can be seen in Figure 16. Point A represents when the cracking of the concrete cover initiates. This is followed by a decrease in strength due to the reduction in concrete area until point B. After this point

the behavior of the column becomes highly dependent on its confinement detailing. If the column is not adequately confined there will be sharp decrease in the column strength. If the column is confined normally it will regain its strength back to its original peak strength and then the strength will decrease in a ductile manner. However, if the column is highly confined the column can actually regain its strength well past its original peak strength and maintain its increased strength with good ductility. Therefore, the proper confinement of concrete columns is of great importance.
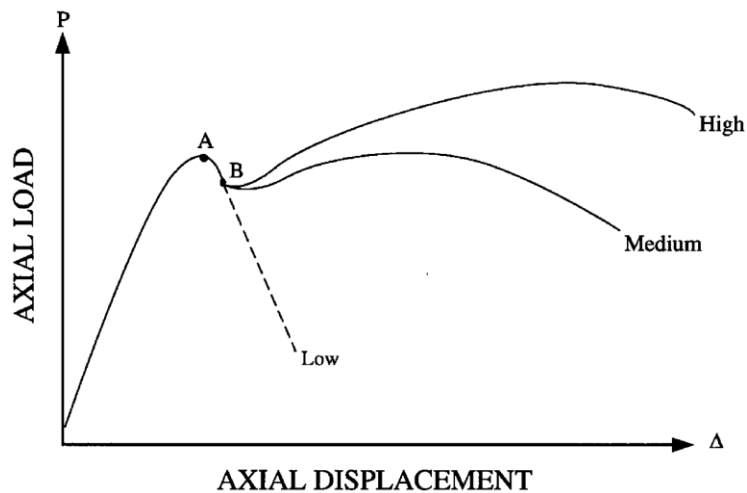
Figure 16. Behavior of HSC under concentric load (ACI 441R-96, 1996)

Additionally, ACI 363R-10 reported that the relative lateral strain in HSC is less than that of NSC because of less micro-cracking being present in HSC under the same axial strain. This affects the interaction between concrete and lateral reinforcement, meaning that the triaxial stress distribution in HSC is different to NSC and the effectiveness of lateral reinforcement in HSC is lower than that in NSC.

The phenomenon of early cover spalling and less effective transverse reinforcement are the disadvantages of using HSC in columns; however, these issues can be corrected by adequate confinement detailing or the introduction of steel fibers.

2.4.4 Confinement Effect
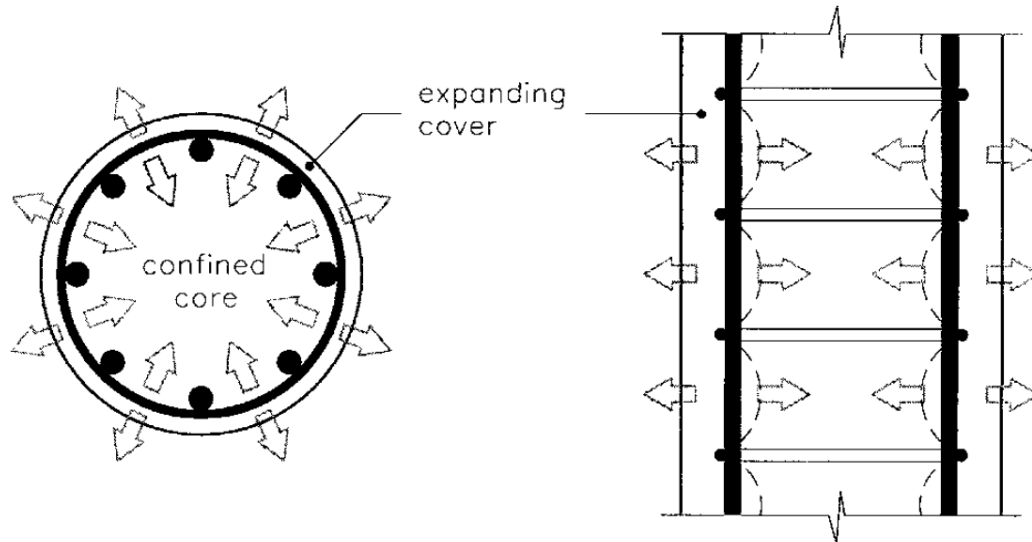
Figure 17. Mechanics of cover spalling (Foster, 2001)

Figure 17 explains how the strength of a concrete column can still be regained even after the initiation of cover spalling due to the confinement effect. Confinement stress is considered as uniform stress in the case of circular hoops or spiral transverse reinforcement (Figure 18). While the contribution of the longitudinal reinforcement is typically ignored in circular steel arrangements, it is accounted for in the strength model for confined concrete of rectangular sections, where its contribution can be more significant (Mander et al., 1988).
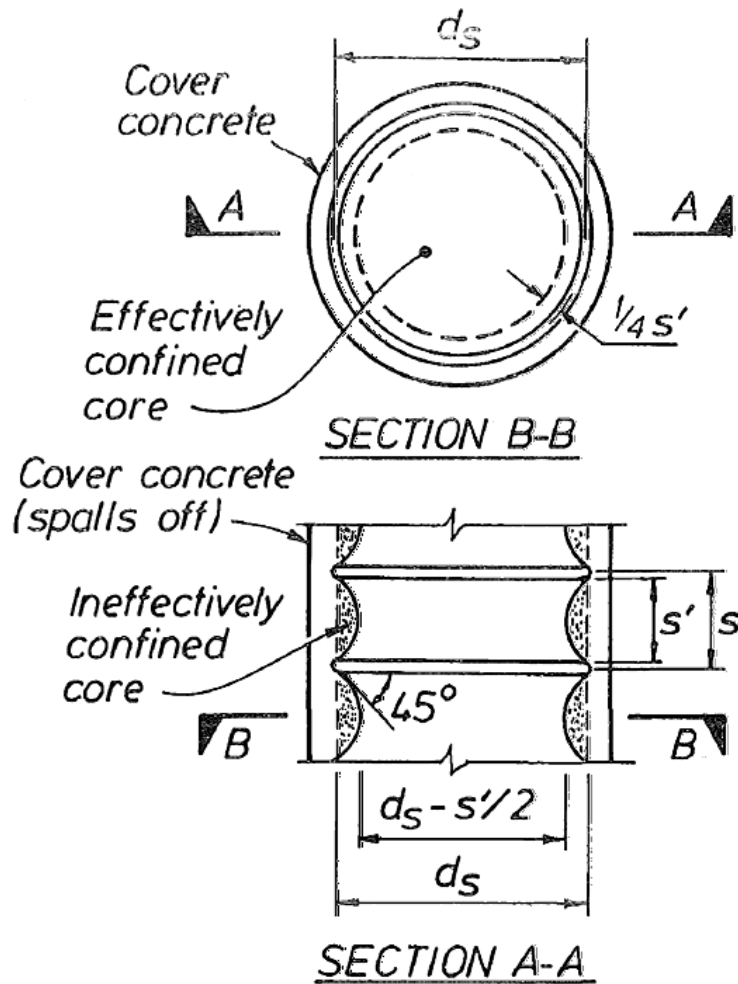
Figure 18. Effective area of circular or spiral confined concrete (Mander et al., 1988)

The effective area of the circular confined concrete shown in Figure 18 can be calculated as

$$A_e = \frac{\pi}{4}\left(d_s - \frac{s\prime}{2}\right)^2 = \frac{\pi}{4}d_s\left(1 - \frac{s\prime}{2d_s}\right)^2 \qquad (2\text{-}5)$$

where s' is the clear distance between spirals or hoops and d_s is the diameter of spiral or hoop from bar center to center. From this equation, the effective area does not depend on the longitudinal reinforcement arrangement, though the area of the longitudinal bars is accounted for in the calculated core area:

29

$$A_{cc} = \frac{\pi}{4} d_s^2 (1 - \rho_{cc}) \qquad (2\text{-}6)$$

where, ρ_{cc} is the ratio of longitudinal reinforcement to area of core concrete. The effectiveness of steel confinement is present by the factor

$$k_e = \frac{A_e}{A_{cc}} \qquad (2\text{-}7)$$

A visual schematic of the effective area for rectangular columns is shown in Figure 19.
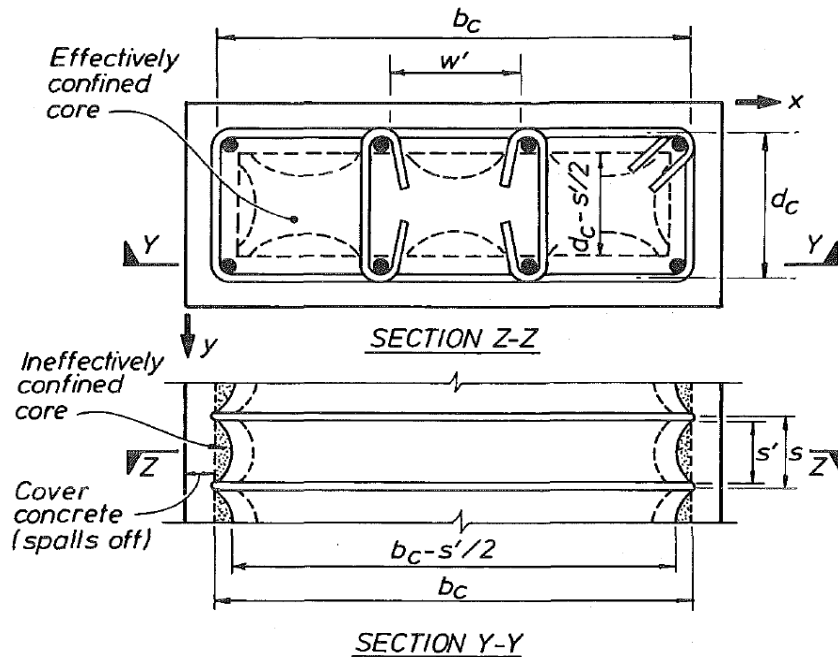
Figure 19. Effective area of rectangular hoop confined concrete section (Mander et al., 1988)

In the case of a rectangular section, the contribution of the longitudinal reinforcement is accounted for in the effective area of the confined concrete section. The effective area is defined as

$$A_e = \left(b_c d_c - \sum_{i=1}^{n} \frac{(w'_i)^2}{6} \right) \left(1 - \frac{s'}{2b_c} \right) \left(1 - \frac{s'}{2d_c} \right) \qquad (2\text{-}8)$$

30

where, d_c and b_c are the center to center dimension of the hoops. The term in the summation operation is achieved from Figure 20, where the clear distance between 2 longitudinal bars is defined as w, the "arch effect" is expected to occur at an angle of 45°, the ineffective area caused by the "arch effect" is then defined as $\frac{w^2}{6}$.
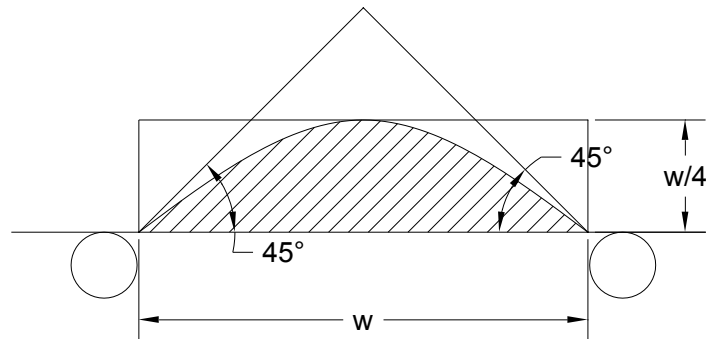
Figure 20. Ineffective concrete area caused by "arch effect"

2.4.5 Transverse reinforcement

Transverse reinforcement plays an important role in the columns strength and ductility regardless if HSC or NSC is used. Transverse reinforcement in concrete columns have four main functions: to confine the core concrete from crushing, provide shear resistance, support the longitudinal reinforcement from buckling after the loss of concrete cover, and to facilitate the construction of the reinforcing cages. All of these roles are of great importance, but the most significant contribution of transverse reinforcement is in providing confinement which improves the strength of the core concrete. Figure 16 point B shows how the strength can be regained, indicating the point that the transverse reinforcement engages the concrete core and creates the confinement effect. The additional strength is significantly affected by the amount of transverse reinforcement. As discussed in section 2.4.4, the use of transverse reinforcement in different configurations, such as circular spirals, or hoops, affects the calculation of effective area and thus the

total strength of the column section. ACI 441R-96 reported the effects of transverse reinforcement in HSC columns (Figure 21).
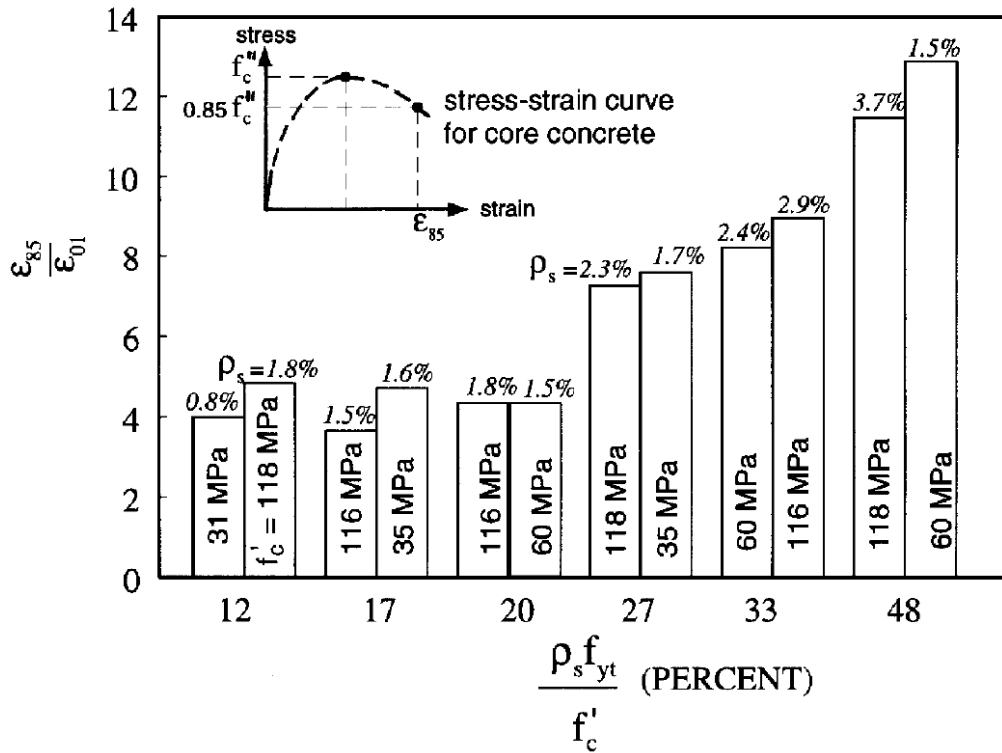
Figure 21. Ductility ratio of columns with different concrete strengths (ACI 441R-96, 1996)

An important quality of a well-designed concrete column is the capability to maintain its strength after the ultimate stress has been reached. The main parameter of this case is the axial ductility ratio, which is defined as the ratio of the strain at a stress equal to $0.85f'_c$ after the maximum stress is reached, to the strain at maximum peak stress. The lager this ratio, the longer the column can maintain strength before collapse. Figure 21 shows that columns with different concrete strengths and different volumetric ratios of transverse reinforcement can have a similar ductility ratio depending on their level of reinforcement ratio and yield strength to concrete compressive strength (Razvi and Saatcioglu, 1994). They also suggested based on previous research on HSC

columns that members with low volumetric ratio may exhibit a lower experimental strength than the calculated nominal values as shown in Figure 22.
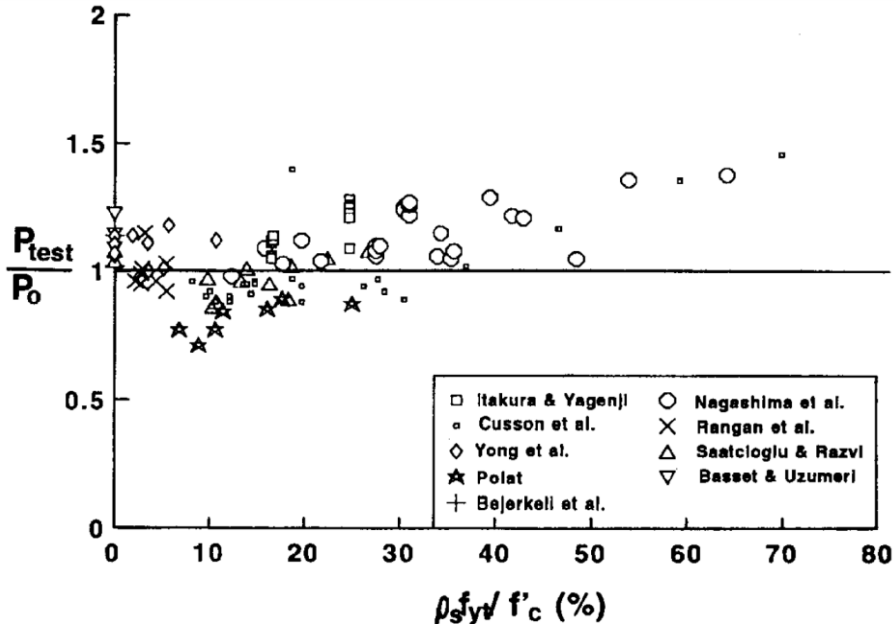
Figure 22. Comparison of experimental and calculated concentric strength of columns

(Razvi and Saatcioglu, 1994)

Cusson and Paultre (1994) suggested that when high strength steel is used in combination with a well confined HSC column, the tensile strength of the transverse reinforcement is utilized more effectively. According to the authors, the yield strength of the confinement steel determines the upper limit of the confining pressure. The higher the pressure applied to the concrete core, the higher the strength and ductility of the concrete column.

Figure 23, shows four different column reinforcement arrangements that were tested with two different hoop yield strengths. It can be observed that the higher yield strength does not come into effect in columns that are not well confined (configuration A), and show similar strength and ductility as columns with lower transverse reinforcement

yield strength. In addition, If a hoop configuration is chosen that provides adequate confinement to the concrete core, the contribution of the higher transverse reinforcement yield strength becomes more evident as there is a notable increase in the strength and ductility of the concrete column in comparison to the column with a lower transverse reinforcement yield strength.
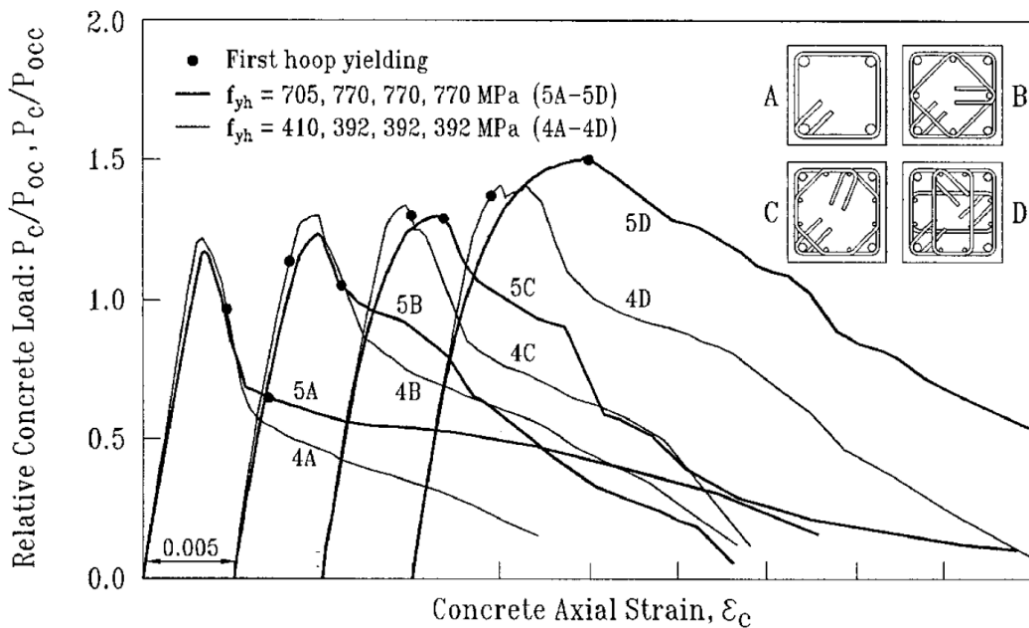
Figure 23. Effect of transverse reinforcement yield strength and configuration on column performance (Cusson and Paultre, 1994)

2.5 ACI 318-14 Seismic Design Provisions

Due to the brittle nature of concrete, in order for columns in areas of high seismicity to behave with adequate strength and ductility, enough confinement reinforcement must be provided. Confinement is typically provided by transverse reinforcement in the form of overlapping spirals, circular hoops, or rectilinear hoops with or without cross-ties. Chapter 18 of ACI 318-14 contains provisions considered to be the minimum requirements for earthquake-resistant structures. More specifically, section

34

18.7.5 describes the requirements of the transverse reinforcement in relation to confining the concrete section and providing lateral support to the longitudinal reinforcement.

Transverse reinforcement is required by ACI over a minimum length where flexural yielding normally occurs (ACI 318-14 18.7.5.1), typically referred to as the plastic hinge region. This region is defined as the largest of:

a) The depth of the member at the joint face or section where flexural yielding is likely to occur;

b) One-sixth of the clear span of the member; and

c) 18 in.

For locations where axial load and flexural demands are high such as the base of a building, this length is increased by 50% (ACI 318-14 R18.7.5.1).

Section 18.7.5.2 provides requirements for the configuration of the transverse reinforcement. Figure 24 shows an example of the requirements for the transverse reinforcement configuration in columns.

Consecutive crossties engaging the same longitudinal bar have their 90-degree hooks on opposite sides of column

$6d_b$ extension

$6d_b \geq 3$ in.

A_{sh2}

A_{sh1}

x_i x_i x_i

b_{c1}

b_{c2}

The dimension x_i from centerline to centerline of laterally supported longitudinal bars is not to exceed 14 inches. The term h_x used in Eq. (18.7.5.3) is taken as the largest value of x_i.

Transverse reinforcement	Conditions		Applicable expressions	
A_{sh}/sb_c for rectilinear hoop	$P_u \leq 0.3A_g f'_c$ and $f'_c \leq 10{,}000$ psi	Greater of (a) and (b)	$0.3\left(\dfrac{A_g}{A_{ch}}-1\right)\dfrac{f'_c}{f_{yt}}$	(a)
			$0.09\dfrac{f'_c}{f_{yt}}$	(b)
	$P_u > 0.3A_g f'_c$ or $f'_c > 10{,}000$ psi	Greatest of (a), (b), and (c)	$0.2k_f k_n \dfrac{P_u}{f_{yt}A_{ch}}$	(c)
ρ_s for spiral or circular hoop	$P_u \leq 0.3A_g f'_c$ and $f'_c \leq 10{,}000$ psi	Greater of (d) and (e)	$0.45\left(\dfrac{A_g}{A_{ch}}-1\right)\dfrac{f'_c}{f_{yt}}$	(d)
			$0.12\dfrac{f'_c}{f_{yt}}$	(e)
	$P_u > 0.3A_g f'_c$ or $f'_c > 10{,}000$ psi	Greatest of (d), (e), and (f)	$0.35k_f\dfrac{P_u}{f_{yt}A_{ch}}$	(f)

Figure 24. Example of transverse reinforcement requirements (ACI 318-14, 2014)

Section 18.7.5.3 refers to the spacing requirements of the transverse reinforcement within the plastic hinge region defined in section 18.7.5.3. This requirement is intended to restrain the longitudinal reinforcement from buckling after concrete spalling. The transverse reinforcement spacing shall not exceed the smallest of the following:

a) One-quarter of the minimum member dimension;

b) Six times the diameter of the smallest longitudinal bar; and

c) s_o as defined by

$$s_o = 4 + \frac{14 - h_x}{3}$$

The amount of confinement reinforcement in this region is then defined by ACI 318-14 18.7.5.4. as shown in Figure 24. ACI 318-14 has introduced a concrete strength factor (k_f) and a confinement effectiveness factor (k_n) which are defined as

$$k_f = \frac{f'_c}{25{,}000} + 0.6 \geq 1.0$$

$$k_n = \frac{n_l}{n_l - 2}$$

The confinement effectiveness factor takes into consideration the spacing of the longitudinal reinforcement and decreases the required confinement for columns with closely spaced laterally supported longitudinal reinforcement. Additionally, the concrete strength factor increases the required confinement for columns with compressive strengths greater than 10,000 psi because such columns can experience brittle failure if not well confined (ACI 318-14, R18.7.5.4).

The requirements stated in ACI section 18.7.5 are to account for the brittleness of concrete and thus prevent the loss of the axial load capacity of the columns after the loss of the shell concrete due to cover spalling. After cover spalling the longitudinal reinforcement is more susceptible to buckling, hence the transverse reinforcement is appropriately detailed to also prevent such mechanisms. The transverse reinforcement required in 18.7.5.4 is a function of concrete strength, this means that as the specified concrete strength increases so does the amount of required reinforcement in the plastic hinge region. For example, due to the additional concrete strength factor, if the concrete strength of a column designed with 5 ksi concrete was increased to 30 ksi the required transverse reinforcement amount would be increased by 180% making construction and concrete placement nearly impossible.

2.6 Prior column testing and seismic performance enhancing techniques

The previous section described the typical characteristics of NSC and HSC columns. The typical failure mechanism of a concrete column subjected to seismic loading has been described by many researchers as initiating with flexural cracking, followed by crushing of the concrete, loss of concrete cover resulting in a loss in flexural capacity. Some flexural capacity is retained due to the confinement provided by the transverse and longitudinal reinforcement. As the cyclic reversals continue the

37

buckling/fracture of the longitudinal reinforcement is observed along with possible bulging and opening of the transverse reinforcement.

Bae and Bayrak (2008) tested a series of five full-scale column specimens with dimensions as shown in Figure 25. Each column specimen was tested under cyclic lateral load reversals subjected to a constant axial load in order to investigate the effect of the L/h ratio and axial load on the behavior of RC columns. The columns were design in accordance to Chapter 21 of the ACI 318-05 code with 6,000 psi normal weight concrete. The researchers reported the typical failure mechanism of concrete columns previously described where the column specimens eventually failed by buckling of the longitudinal bars due to the extensive crushing of the core concrete and cover concrete. One of the column specimens at the end of testing can be seen in Figure 26. The researchers observed the opening of transverse reinforcement despite the use of 135-degree hooked anchorages and recommended extending the specified length of the anchorages from 6db to 15db, a length where the hoops did not open. The researchers also suggested from test observations that at low axial load levels (P/Po = 0.2), it may be possible to relax the confining reinforcement requirements of ACI 318-05.
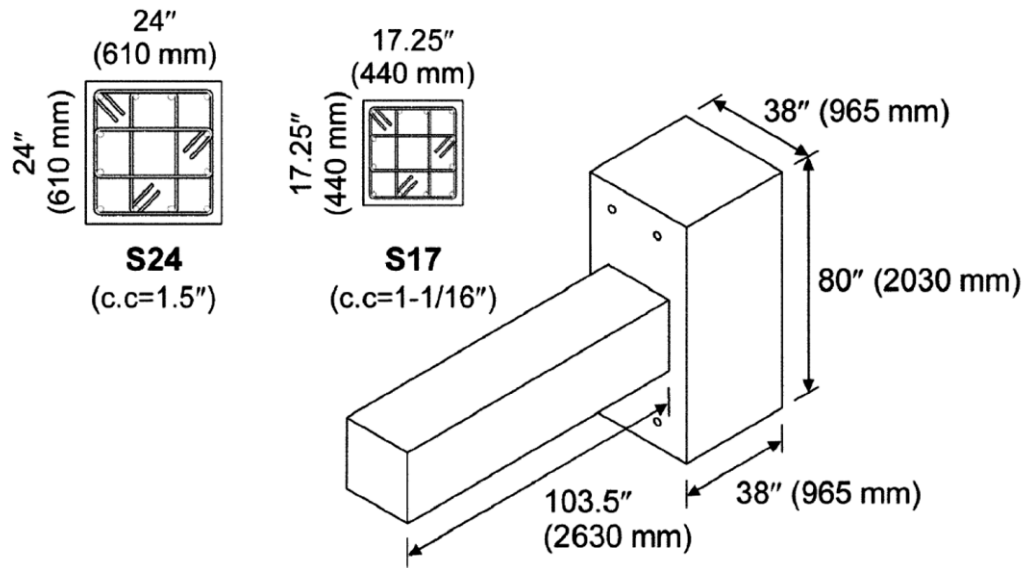
Figure 25. Dimensions and layout of specimens tested by Bae and Bayrak (2008)

Figure 26. Specimen S24-4UT after failure (Bae, 2005)

Legeron and Paultre (2000) studied the behavior of HSC columns under cyclic flexure and constant axial load. The researchers tested six large scale specimens with a target concrete strength of 100 MPa (14.5 ksi) in order to investigate the influence of the volumetric ratio of the confining reinforcement and the axial load level. The specimen dimensions and testing setup can be seen in Figure 27. To study the effect of the confining reinforcement, the tie configuration was kept constant and the spacing of ties was varied from 60 mm (2.36 in.) to 130 mm (5.12 in.). The researchers observed the main failure mechanism to be the buckling and rupture of the longitudinal reinforcement with significant concrete damage visible as shown in Figure 28. From the figure, the relationship between axial load level and plastic hinge length can also be seen. As the axial load level increases, so does the length of the plastic hinge region. It was also noticed that the region just above the base stub remained undamaged due to a confinement effect provided by the base stub. The researchers concluded that for axial load levels less than or equal to 15% of the gross axial load capacity, approximately 50% of the confinement reinforcement is necessary, similarly observed by Bae and Bayrak (2008) for NSC columns. Legeron and Paultre (2000) stated that HSC can be used in seismic zones provided that it is adequately confined, and that high-yield strength steel may be a solution for columns subjected to a high-axial load-level where excessive high reinforcement ratios may be necessary, typically difficult to use in practice.
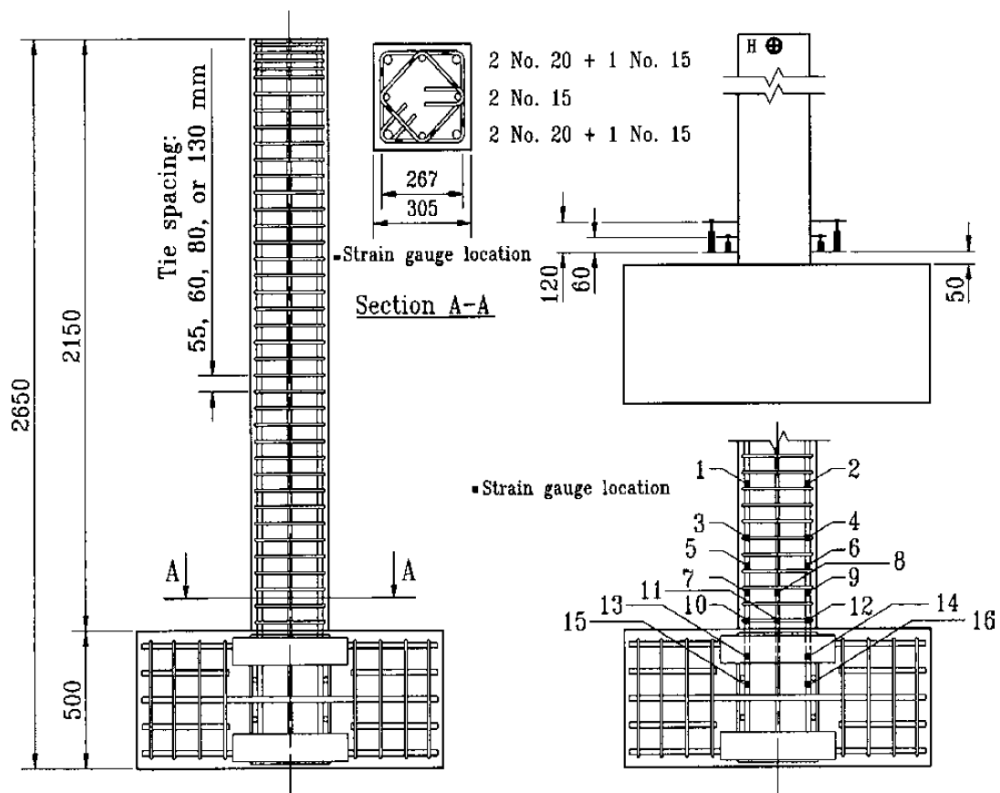
Figure 27. Specimen configuration (Legeron and Paultre, 2000)
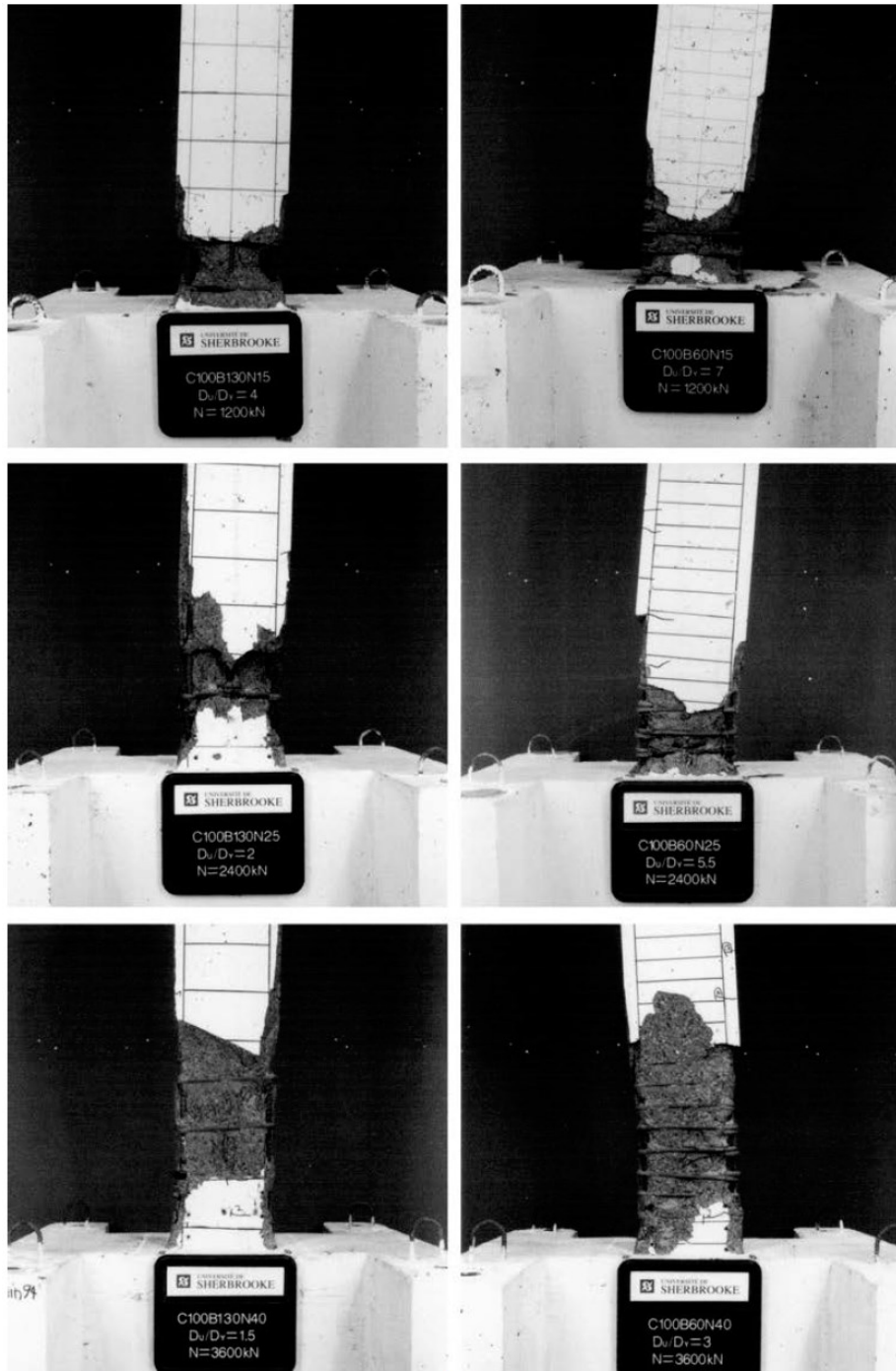
Figure 28. Testing specimen damage and plastic hinge region after testing (Legeron and Paultre, 2000)

Sugano (1996) tested five ultra-high strength concrete column specimens laterally reinforced with ultra-high-strength steel bars under reversed cyclic loading and constant axial compression to investigate the influence of axial stress level and capacity of lateral reinforcement. The column specimens were constructed with a specified compressive strength of 120 MPa (17.4 ksi) and lateral reinforcement with yield strength of 1,380 MPa (200 ksi). The column specimen configuration can be seen in Figure 29. Sugano (1996) noticed that the effect of the capacity of the transverse reinforcement was more notable for specimens with high axial load ratios compared to low axial load ratios. For this reason, as shown in Figure 30 the two column specimens subjected to high axial load with lower lateral reinforcement capacity failed in a brittle compressive manner (UC10H and UC15H) while the specimen with high axial load and high lateral reinforcement capacity (UC20H) failed in flexure along with the lower axial load specimens (UC15L and UC20L). Sugano (1996) concluded that in order for the brittle ultra-high strength concrete to have sufficient ductility, relatively more capacity of lateral reinforcement is required compared to that of lower strength concrete. This confinement can be found in the form of high or ultra-high strength lateral reinforcement.
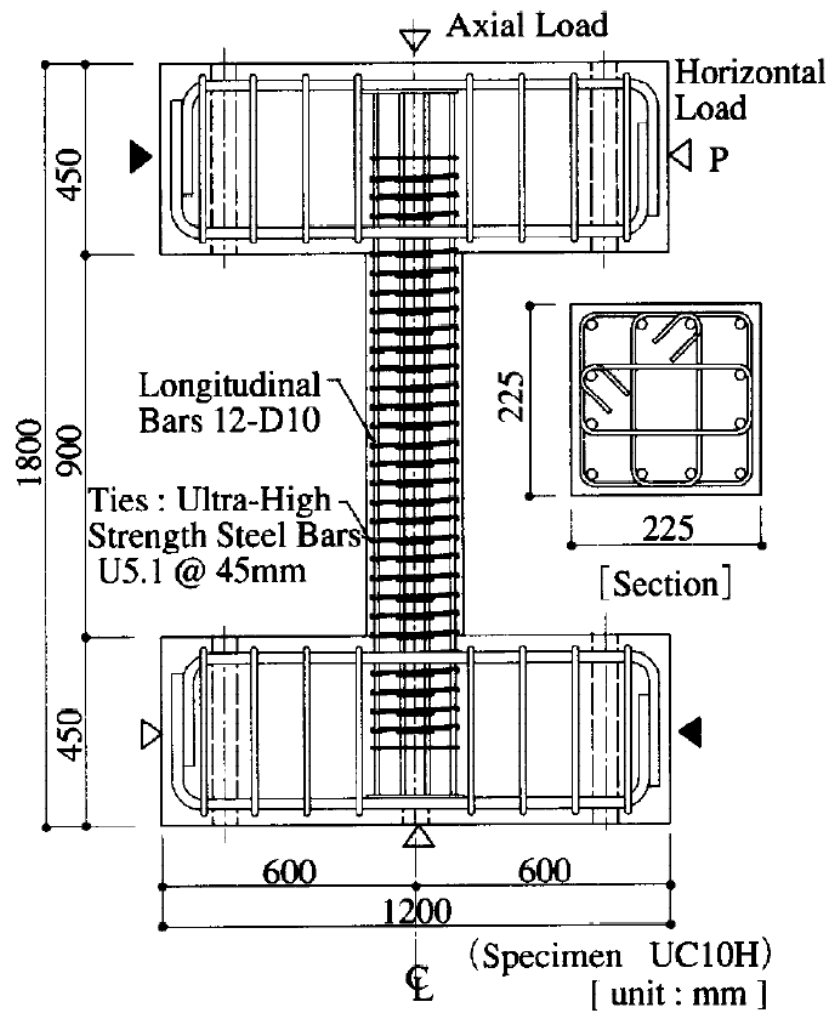
Figure 29. Column specimen configuration (Sugano, 1996)

UC10H
$\sigma_0/f_c'=0.62$
$P_w \cdot f_{yh}=11.0$MPa
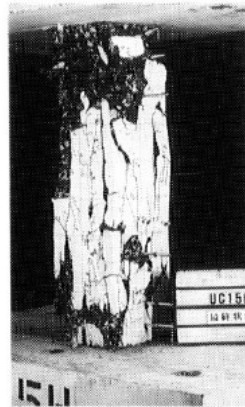
UC15H
$\sigma_0/f_c'=0.62$
$P_w \cdot f_{yh}=16.9$MPa
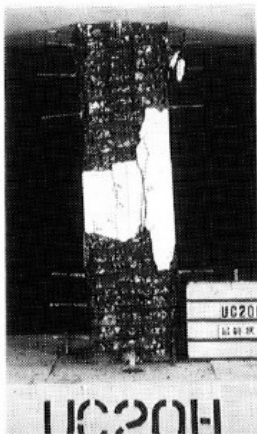
UC20H
$\sigma_0/f_c'=0.62$
$P_w \cdot f_{yh}=21.7$MPa
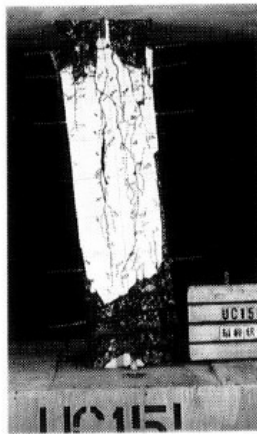
UC15L
$\sigma_0/f_c'=0.36$
$P_w \cdot f_{yh}=16.9$MPa
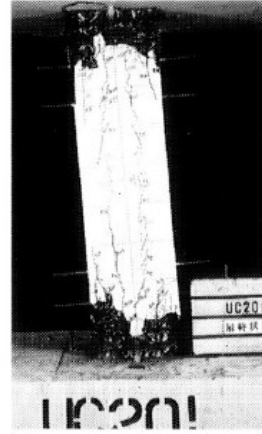
UC20L
$\sigma_0/f_c'=0.36$
$P_w \cdot f_{yh}=21.7$MPa

Figure 30. Column specimens after failure (Sugano, 1996)

Foster (2001) investigated the behavior of HSC columns, more specifically the mechanism of early cover spalling and its effect on lower than anticipated failure loads.

Foster suggested that the addition of steel fibers to the concrete mix would be an effective way to improve the ductility of HSC columns and prevent early cover spalling.

Additional methods to improve the confinement and seismic performance of concrete columns through the use of more modern design techniques have been investigated. For example, Aviram et al. (2010) tested two quarter scale circular bridge column specimens with high performance fiber-reinforced concrete (HPFRC) under bidirectional cyclic loading. The column specimens were detailed with additional dowel reinforcement and debonding techniques so as to force the inelastic deformations to occur slightly above the column base. In specimen S1 long dowels were used and the upper portions of the dowels were debonded with the use of plastic tubes. Specimen S2 used shorter dowels terminating in the plastic hinge region, and the main longitudinal bars were debonded. Both columns were compared to a reference column of the same geometry cast with regular reinforced concrete. The enhanced techniques showed an improved maximum ductility of 10.7% and 5.4% drift ratios for the S1 and S2 columns respectively compared to the reference column which had a maximum ductility of 3.9% drift ratio. However, while such techniques may improve the seismic performance and ductility of the concrete columns they could complicate the design and construction; in addition they fail in the prevention of concrete deterioration, crushing, and bar buckling and result in the same failure mechanism as that of regular RC as shown in Figure 31.

Figure 31. Specimen S1 after 10.7% drift ratio (Aviram et al., 2010).

2.7 Brief introduction to UHP-FRC

Ultra-high performance concrete (UHPC) and ultra-high performance fiber-reinforced concrete (UHP-FRC) were introduced in the mid-1990s (Willie et al., 2011). As Willie et al. (2011) explains, this relatively new material initially required special treatments to obtain high compressive strengths such as special curing techniques through heat, pressure, or excessive vibration. Rossi (2000), defines UHPC as a concrete or cement composite that uses a relatively high binder ratio, a water to cementitous ratio (or water to binder ratio) less than 0.2, and show a compressive strength in excess of about 22 ksi. Naaman and Willie (2010) later add that UHP-FRC composite materials exhibit, after first cracking, a strain-hardening behavior in tension with the development of multiple cracking, thus, in effect, developing a new stand-alone structural material with outstanding compressive strength and useful tensile properties.

This new material is based on the optimization of the particle packing concept. In essence, the high packing density of the particles reduces the presence of defects or air voids, thus increasing the strength of the material. More current UHP-FRC research aims at developing UHP-FRC with no special treatments while using materials that are commercially available (Wille et al., 2011).

UHP-FRC is an innovative material which provides high compressive strength (25-30 ksi.) and shear strength as well as improved compressive ductility and excellent confinement characteristics. UHP-FRC shares the advantages of HSC mentioned in the previous sections with a uniaxial compressive strength of approximately in excess of 23 ksi. However, UHP-FRC does not share the brittleness observed in HSC with the integration of high strength straight steel microfibers which contribute to higher shear and tensile capacities, thus reducing the need for excessive transverse reinforcement typically necessary in HSC columns. UHP-FRC exhibits a tensile strain-hardening response up to large strains (0.5 to 1.0 percent), accompanied by a multiple cracking process. Thus, large deformations are needed to cause visible damage in UHP-FRC members. Even though UHP-FRC provides superior material properties most of the prior research has involved small-scale material testing, with limited test data available on its full-scale structural application.

Chapter 3

Part I: Experimental Program

3.1 Introduction

The experimental program briefly describes the development of the UHP-FRC mix for large scale casting and its mechanical properties. This is followed by a small-scale column study that was done to observe the influence of fiber volume and volumetric ratio on the confinement effect of concrete columns used to conceptualize the full-scale column design. The design, construction, and instrumentation of the full-scale column specimens are also discussed. In addition, the test setup and loading protocol used for both specimens is presented.

3.2 Material characteristics of UHP-FRC

The development of a suitable UHP-FRC mix for large-scale column casting with characteristics such as high compressive strength and ductility, tensile ductility, and good flowability, which are all critical properties for concrete columns subjected to seismic loading, is discussed elsewhere (Aghdasi, 2013).

The optimized mix had a flow diameter of 8 in. which allows for a very flowable pour through the reinforcing cage and removes the need for external vibration, as the mix was observed to be essentially self-consolidating. The compressive characteristics of the UHP-FRC mix obtained through the compressive testing of 2.78 in. cubes are shown in Figure 32 and Table 2. The compressive strength of the UHP-FRC mix at testing day was found to be 22.9 ksi and continued to increase to a 28-day compressive strength of 25.0 ksi.
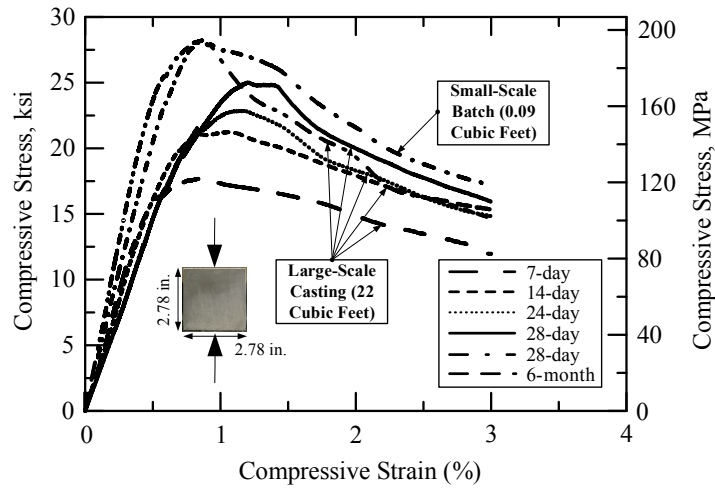
- 1 in. = 25.4 mm
- 1 Cubic Feet = 0.0283 Cubic Meter
- Each curve is based on average of two 2.78-in.-cubes
- 24-day was when the full-scale column was tested

Figure 32. Compressive stress-strain curve of 2.78 in. UHP-FRC cubes (Aghdasi, 2013)

Table 2. Results of compressive testing of 2.78 in. UHP-FRC cubes (Aghdasi, 2013)

	σ_{pc}*, ksi (MPa)	ε_{pc}† (%)	% of σ_{pc} at ε_c
7-day	17.7 (122.0)	0.86	67.6
14-day	21.2 (146.2)	1.08	69.1
24-day	22.9 (157.9)	1.17	64.8
28-day	25.0 (172.4)	1.22	63.7
6-month	28.3(195.1)	0.87	54.3

* Peak tensile strength; † Strain at peak tensile strength

Furthermore, the tensile characteristics of the developed UHP-FRC mix are shown in Figure 33 and Table 3. Based on the tensile tests, an average peak tensile strength of 1.11 ksi was obtained corresponding to a tensile strain of 0.15%.
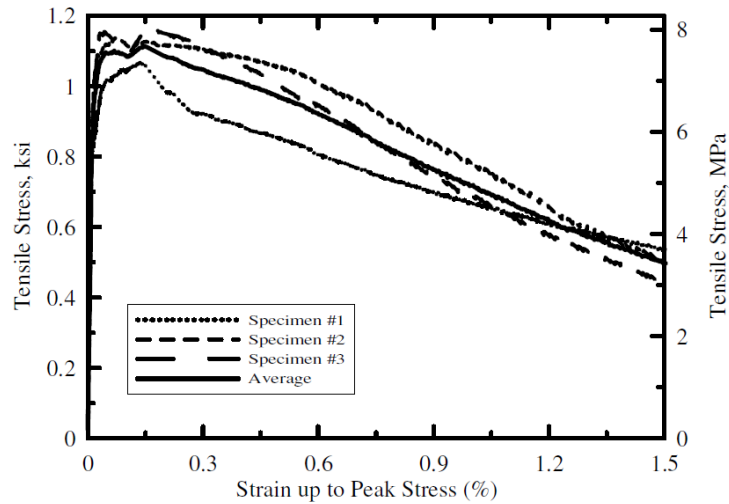
Figure 33. Tensile stress-strain curves of UHP-FRC mix produced in large scale casting

(Aghdasi, 2013)

Table 3. Tensile properties of the developed UHP-FRC mix (Aghdasi, 2013)

Specimen #	σ_{pt}, ksi (MPa)	ε_{pt} (%)
1	1.07 (7.4)	0.14
2	1.14 (7.9)	0.08
3	1.16 (8.0)	0.17
Average	1.11 (7.7)	0.15

3.3 Small-scale column confinement study

As the material characteristics of UHP-FRC suggest possible advantages for its use in structural applications, a small-scale parametric study was conducted to determine the influence of various parameters on the confinement effect of concrete columns. The parameters for this investigation include the transverse reinforcement ratio, concrete strength, and fiber volume fraction. Each of these parameters is well known to have a significant influence on the confinement effect and ultimate strength of concrete columns under axial compression. The addition of steel fibers can improve many properties

51

normal reinforced concrete such as strength and ductility (Aoude et al., 2009). On the other hand, adequate design of transverse reinforcement can also provide a similar improvement to RC members. Hence there is a need to investigate the relationship between confinement provided due to fiber volume, and confinement provided due to transverse reinforcement.

3.3.1 Specimen Design

Due limitations of the testing facility, the specimens were designed so that the nominal strength of each specimen was lower than 400 kips. From compressive testing of UHP-FRC cubes, the compressive strength is approximately between 25 ksi to 30 ksi. The required specimen dimension for a square column will then be:

$$\text{b} = \sqrt[2]{\frac{400 \text{ kip}}{27 \text{ ksi}}} = 3.85 \text{ in}$$

Therefore, based on the limitations a 3.5x3.5 in. square column section was chosen. The height of the columns was designed to prevent slenderness but large enough to accommodate the larger tie spacing. Based on these criteria, a 9 in. column height was chosen to satisfy all the conditions. To prevent any additional confinement, all the specimens are also designed without concrete cover. The nominal axial strength of the columns is then calculated as follows:

$$\text{P}_\text{n} = 27 \times (3.5^2 - 4 * 0.1) + 60 \times 4 \times 0.1 = 343 \text{ ksi}$$

Longitudinal reinforcement ratio:

$$\rho_\text{l} = \frac{\text{n} \times \text{A}_\text{sl}}{\text{b} \times \text{h}} = \frac{4 \times 0.1}{3.5^2} = 3.26\%$$

Transverse reinforcement ratio A,B,C-2:

$$\rho_\text{s} = \frac{\text{n} \times \text{A}_\text{st}}{\text{b} \times \text{s}} = \frac{2 \times 0.1}{3.5 \times 2.25} = 2.54\%$$

Transverse reinforcement ratio A,B,C-4:

$$\rho_s = \frac{n \times A_{st}}{b \times s} = \frac{2 \times 0.1}{3.5 \times 4.5} = 1.26\%$$

The column specimen is 3.5x3.5x9.75 in. high and is reinforced with 4 No. 3 longitudinal reinforcement and No. 3 bars welded together as transverse reinforcement. The ties are made from 4 No. 3 bars, welded together at the 4 corners. A steel template was used to ensure the consistency of the stirrups and steel cages and also a steel cap was used to keep column ends in a parallel plane. Figure 34 shows the typical specimen reinforcement design for a tie spacing of 2.25 in.
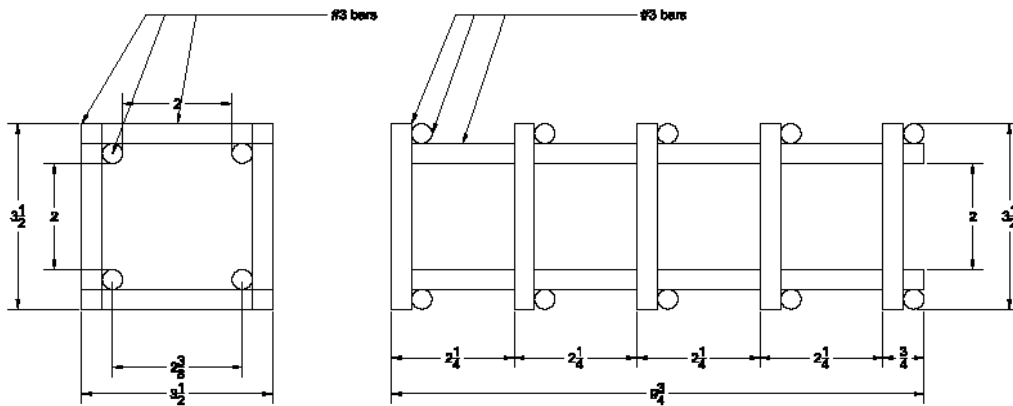
Figure 34. Steel cage design with 2.25 in. tie spacing

3.3.2 Specimen Fabrication

The following pictures show the specimen reinforcement, formwork, and casting procedure. Figure 35 shows the finished reinforcing cage for the specimen with 2.25 in tie spacing.
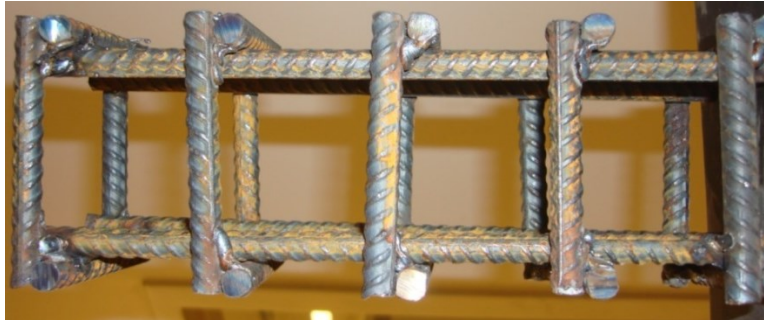
Figure 35. The steel cage with 2.25 in stirrup spacing

The assembly of formwork is shown in Figure 36. It is comprised of timber formwork clamped with a steel cap to ensure dimension precision and prevent any bulging during casting.
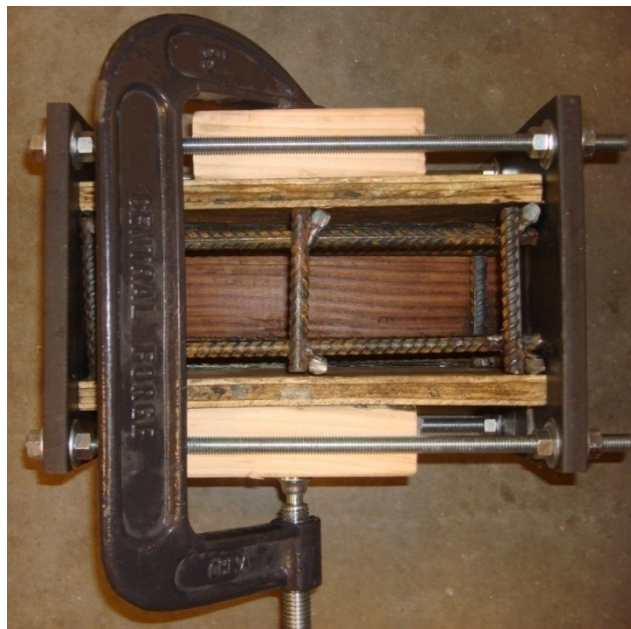
Figure 36. Formwork and steel case ready for casting

The clamp is also utilized to keep the formwork tightly pressed with the cage to eliminate any concrete cover. Prior to casting, all the dimensions of the columns are measured and the bolts are then tightened so that the differences in lengths between all specimens are less than 1/8 in (Figure 37).

Figure 37. Tolerance checking to make sure the different is less than 1/8 in.
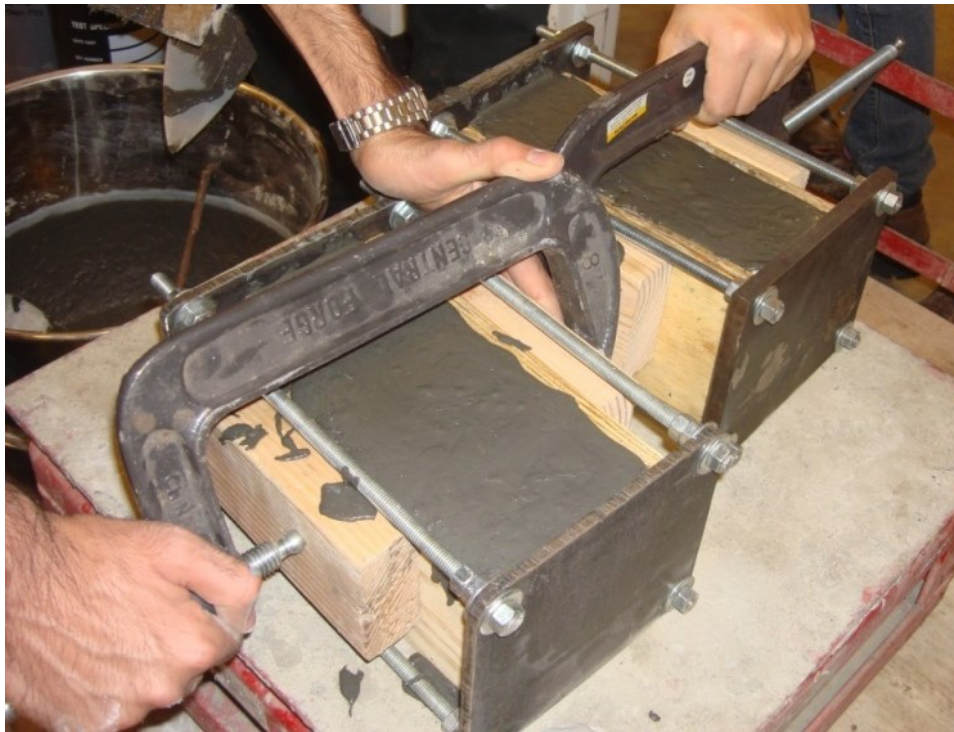
Figure 38. Small-scale specimen casting

After formwork removal, the specimens were grinded on all sides and smoothened to ensure proper contact during testing; they were then marked and placed in the curing room (Figure 39).

Figure 39. Specimens B2 and B4 after formwork removal and grinding

3.3.3 Small-scale column testing

To observe the deformation of the specimens in both the longitudinal and lateral directions, five linear varying differential transformers (LVDTs) were utilized as the diagram indicates shown in Figure 40. The LVDT 04 and 05 are placed in the same location and measure in opposite directions relative to external reference points to observe the movements of the testing machine during the experiments. A picture of the actual test setup used is shown in Figure 41.
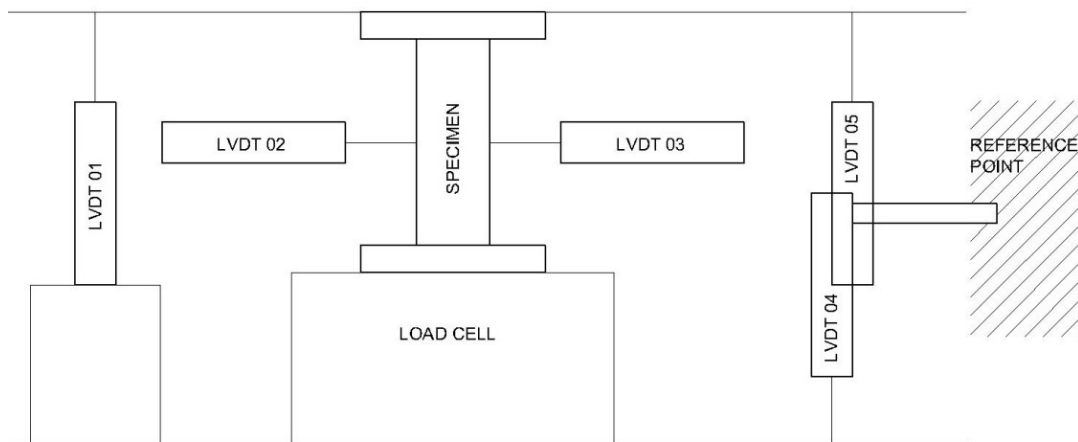
Figure 40. Small-scale column test setup

The specimens were loaded until the peak capacity was reached after which the end of testing was determined due to failure based on the following criterion:

- At least one of the ties has ruptured,

- longitudinal bar has ruptured,

- The specimens has a wide crack opening indicating tie failure

Figure 41. Test setup with LVDTs and load cell

3.3.4 Test Results and Observations

A summary of the test results is shown in Table 4. Note that the highlighted rows in gray correspond to a normal strength concrete (NSC) of 5 ksi with no added fibers.

Table 4. Summary of small-scale column test results

ID	ρ_s	V_f (%)	Concrete Type	Column Strength (ksi)
A3		0	NSC	7.26
A4	1.26	0	UHPC	15.72
B4		3	UHP-FRC	18.79
C4		5	UHP-FRC	22.91
A1		0	NSC	8.78
A2	2.54	0	UHPC	19.5
B2		3	UHP-FRC	22.27
C2		5	UHP-FRC	23.04

As shown in Table 4, by doubling the transverse reinforcement ratio from 1.26 to 2.54 a 21% increase in strength was seen by the NSC columns. The failure of the NSC column occurred very quickly and began by the brittle crushing and spalling of the cover concrete. Once the crushing initiated the core concrete's cross sectional area was reduced which lowered the column strength. With the reduction in compressive stresses being sustained by the concrete a portion of the stresses were then transferred to the longitudinal reinforcement which soon after began to buckle. The transverse reinforcement is meant to confine the concrete in the core of the column as well as prevent the longitudinal reinforcement from buckling. As the load increases the transverse reinforcement can no longer withstand the tensile stresses and eventually ruptures leading to the failure of the column. Therefore, there is a direct relationship between the confinement provided by the transverse reinforcement and the ultimate strength of the concrete column. The NSC specimens A3 and A1 are shown in Figure 42 and Figure 43 respectively. The additional transverse reinforcement in specimen A1 clearly confined the crushing to a specific section of the column around the mid height rupturing two hoops but maintaining a greater area of core concrete than that of specimen A3. Specimen A3 shows more crushing and spalling throughout the height of the column as well as a ruptured hoop at mid height which is a consequence of its lack of confinement and attributes to its lower ultimate strength.
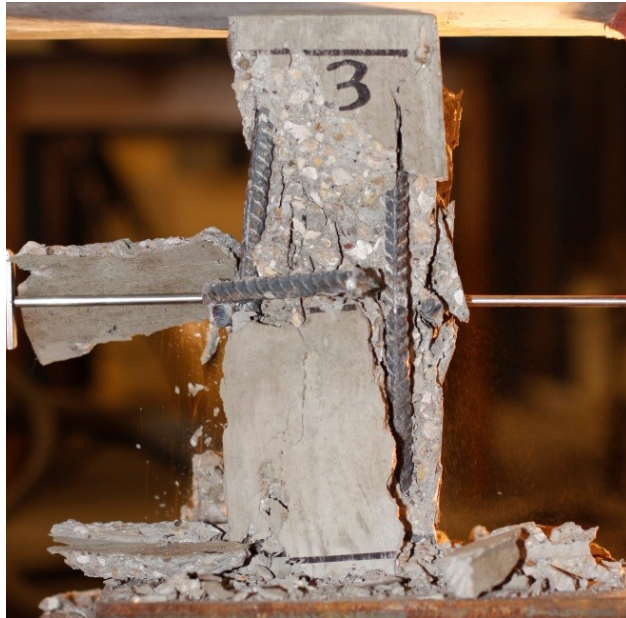
Figure 42. Crushing of specimen A3
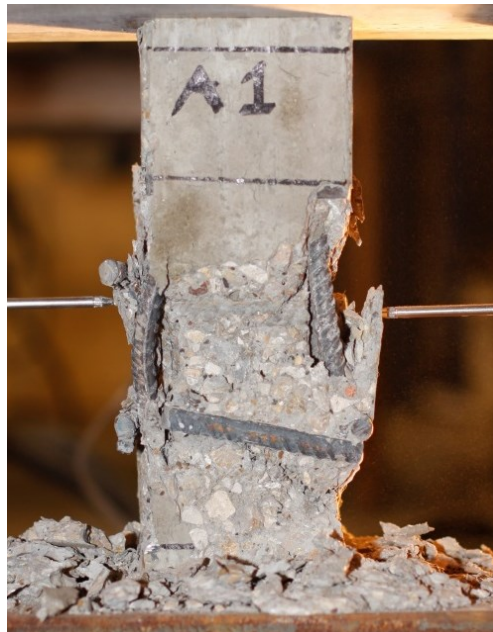
Figure 43. Crushing of specimen A1

A similar observation can be made for the ultra-high performance concrete (UHPC) 28 ksi concrete columns, in which by doubling the transverse reinforcement ratio

the column showed a strength increase of 24% from specimen A2 to specimen A4. The failure mode of the UHPC columns was also controlled by the failure of the transverse reinforcement and occurred the same way as that of NSC however a few differences were observed. Because of the reduced number of defects and higher strength of UHPC, the reduction of the crushing and failure of the columns occurred slightly slower than that of the NSC columns however the failure was more explosive due to the higher stress levels. The most important difference observed was that more of the core concrete remained intact after crushing compared to that of the NSC which attributes to the increased strength of the UHPC columns. Most of the crushing occurred at the concrete cover and outer regions near the reinforcement. Specimens A4 and A2 can be seen in Figure 44 and Figure 45 respectively.

Figure 44. Crushing of specimen A4
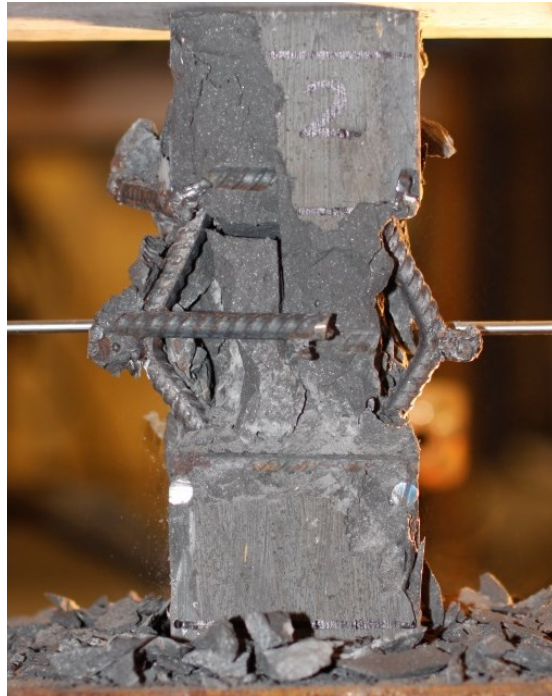
Figure 45. Crushing of specimen A2

The addition of fibers to the concrete mix greatly altered the behavior and confinement effect in the column specimens. Figure 46 shows a plot of the effect of transverse reinforcement ratio and fiber volume fraction on UHPC columns. It can be observed that as the fiber volume fraction increases so does the concrete strength regardless of the transverse reinforcement ratio. However, it is important to note that at a fiber volume fraction of 5% the ultimate strength for the columns with a transverse reinforcement ratio of 1.26 and 2.54 is equal. This suggests that the confinement interaction between the fibers and transverse reinforcement ratio at high fiber volume fractions is mainly controlled by the behavior of the fibers and not the transverse reinforcement.
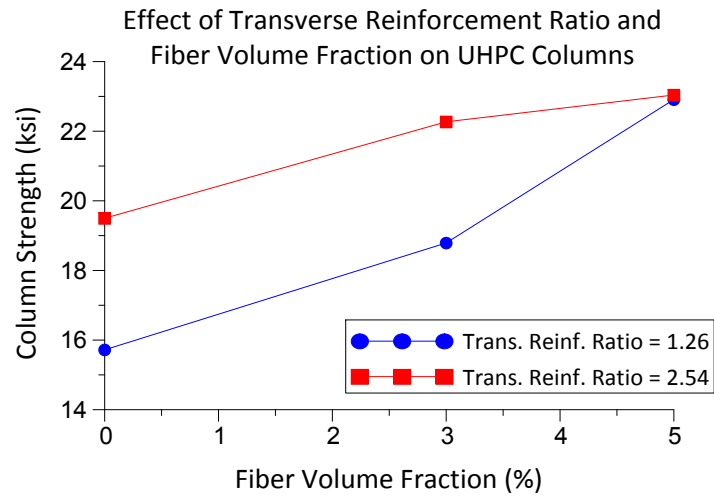
Figure 46. The effect of transverse reinforcement ratio and fiber volume fraction on

UHPC columns

Specimens B2 and B4 were made with UHP-FRC with a fiber volume fraction of 3%. In this case doubling the transverse reinforcement ratio only increased the strength of the UHP-FRC column by 18.5% because the confinement is no longer dependent on solely the transverse reinforcement but a combination of both the transverse reinforcement ratio and the fiber volume fraction. The failure mode for the UHP-FRC columns was very different compared to that of NSC and UHPC columns without fibers. As the column was loaded a number of micro cracks began to develop with only a few visible on the exterior surface but many occurring within the interior of the column as it begins to expand laterally. Without fibers the column would exhibit brittle behavior and continue to spall and crush as observed with the previous specimens. However, with the addition of fibers the cracks were restrained from opening and the tensile stresses were then transferred through the concrete by the fibers causing a bulging effect. The fibers were engaged in confining the core concrete as the compressive stresses continued to increase. A sudden explosive bulging then occurred, however, only a small amount of

spalling is observed. This explosive bulging represents the fibers pulling out and rupturing as they can no longer withstand the tensile stresses and prevent the cracks from opening. Once the fibers have begun to fail more spalling of the concrete cover is seen around the reinforcing bars. Since the fibers can no longer transfer the stresses through the concrete the longitudinal bars are forced to sustain some of the compressive stresses which lead to buckling of the longitudinal reinforcement and eventually rupturing the transverse reinforcement. This failure mode sequence is a much more ductile process compared to that of the previous specimens without fibers. However, it is important to note how the failure regions were still similar to those of the other specimens for each respective transverse reinforcement ratio. Specimen B4 experienced spalling along the height of the column parallel to the direction of loading with the rupture of the hoop at mid height. Specimen B2 had a more localized failure region in which two hoops failed due to the buckling of the longitudinal reinforcement. It can also be observed that the buckling of the longitudinal reinforcement has more curvature compared to that of the previous specimens due to the higher compressive stresses. Specimens B4 and B2 can be seen in Figure 47 and Figure 48 respectively. Also visible in the figures is the interface between the inner core concrete and the exterior spalling cover concrete in which the fibers pull out or break.

Figure 47. Crushing of specimen B4

Figure 48. Crushing of specimen B2

As shown in Table 4 and Figure 46 very interesting behavior was observed with specimens C2 and C4. The results showed that in the case of UHP-FRC with a volumetric fiber fraction of 5%, doubling the transverse reinforcement ratio had no effect on the ultimate strength of the column. This means that the confinement effect and ultimate strength was predominantly controlled by the volumetric fiber fraction and not the transverse reinforcement ratio. The failure mode was also different than that of specimens B2 and B4 with a volumetric fiber fraction of 3%. The failure of C4 began with micro cracking followed by a very explosive burst as the concrete cracked but was held together by the high percentage of fibers which resulted in significant bulging. Once the fibers could no longer restrain the bulging spalling began and spread along the height of the column as previously seen with specimens with a transverse reinforcement ratio of 1.26. The buckling of the longitudinal reinforcement followed as well as the rupture of the hoop. However, the interior core remained almost completely intact with only slight spalling visible. Even though specimens C4 and C2 had the same strength, the behavior of C2 was much more impressive. The failure mode also began with micro cracking and a sudden explosive burst that lead to bulging. As the load increased, the bulging continued and the fibers were able to restrain the cracking and lateral expansion with the help of the transverse reinforcement. Two hoops where then exposed appearing to be ruptured however the specimen remained completely intact due to the high volume of fibers providing confinement to the core concrete. The core concrete was not clearly visible since there was no significant spalling of the cover concrete. Specimens C4 and C2 can be seen in Figure 49 and Figure 50 respectively.

Figure 49. Crushing of specimen C4
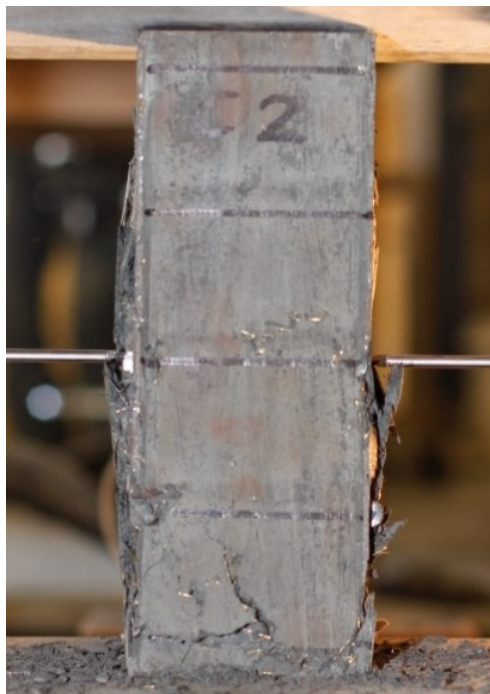
Figure 50. Crushing of specimen C2

The compressive tests performed suggest that parameters such as concrete strength, transverse reinforcement ratio, and most importantly fiber volume fraction have a significant influence on the confinement effect and ultimate strength of columns under axial compression. It was observed for columns without fibers that the ultimate strength of the column is dependent on the concrete strength and the confinement provided by the transverse reinforcement in which the failure of the column is predominantly controlled by the failure of the hoop. By doubling the transverse reinforcement ratio of the NSC columns a 21% increase in strength of was observed. Similarly for UHPC, doubling the transverse reinforcement ratio resulted in a 24% increase in strength. The failure of the UHPC was more concentrated to the region in which the transverse reinforcement failed and the longitudinal reinforcement buckled. More core concrete remained intact compared to that of the NSC columns, with the crushing and spalling occurring only at the cover concrete.

The addition of fibers to the UHPC mix greatly altered the behavior and confinement effect of the columns. By doubling the transverse reinforcement ratio of UHP-FRC columns with a fiber volume fraction of 3% an increase in strength of 18.5% was observed. The increase in strength was lower compared to that of the previous specimens tested without fibers. This is because the confinement effect is shared by both the transverse reinforcement and the steel fibers. As the loading is increased the concrete expands laterally and cracks. The cracks are then restrained from opening by the fibers resulting in a confining pressure to the core concrete and bulging of the column. Therefore under a higher fiber volume fraction a higher percentage of fibers will be able to bridge the cracks applying a greater confinement pressure which results in less concrete spalling and a lower reduction in the cross section of the core concrete. It can be observed that as the fiber volume fraction increases so does the concrete

strength regardless of the transverse reinforcement ratio. However, it is important to note that at a fiber volume fraction of 5% the ultimate strength for the columns with a transverse reinforcement ratio of 1.26 and 2.54 is equal. This suggests that the influence of the interaction between the fibers and transverse reinforcement ratio on the confinement effect at high fiber volume fractions is mainly controlled by the fibers and not the transverse reinforcement. This proposes that with the addition of a high volume fraction, such as 5%, the transverse reinforcement ratio may be reduced by up to 50%.

<div align="center">3.4 Full-scale specimen geometry and design</div>

Each full-scale column specimen was comprised of a 75x75x23 in. loading block, a column section placed at a 45 degree angle, and a 84x84x30 in. footing block. The footing block and loading block where reinforced with two layers of No. 8 bars placed in each direction. The space frame column is a 106 in. tall square column representing a part of a column bent in double-curvature at the ground floor of a prototype 20-story building. The column has cross-sectional dimensions of 28x28 in. and is reinforced with 12 No. 8 bars (ASTM A706 Grade 60) distributed evenly around the perimeter of the cross-section.

Although using HSC for high-rise building members such as columns is beneficial, the increasing brittleness of concrete with high compressive strength has become a major concern, especially for seismic applications. For this reason, proper confinement (that is, transverse reinforcement) of concrete is essential for the safe use of HSC. Figure 51 shows the typical reinforcement for a seismic resistant reinforced concrete moment frame column with normal strength concrete (5 ksi.). The congestion of steel reinforcement is mainly due to transverse reinforcement requirements (ACI 318-14, 2014). The amount of transverse reinforcement largely depends on compressive strength. ACI ITG-4.3R (2007) indicates that when the concrete compressive strength is

increased from normal strength to ultra-high strength, significant amounts of transverse reinforcement are needed to confine the concrete in order to prevent premature brittle failure even though this is practically impossible due to the already congested reinforcing cage for normal strength concrete (Figure 51). However, the necessary amount of transverse reinforcement is considerably less when UHP-FRC is used due to the much enhanced confinement caused by the addition of microfibers as demonstrated by the previous small scale column study. This allows the transverse reinforcement amount used in UHP-FRC to be the same as that used in the plastic hinge region of a normal strength RC column, significantly less than the typical reinforcement amount required for concretes with such high strengths. The transverse reinforcement consists of groups of three overlapping ties bent from No. 5 bars (ASTM A615 Grade 60) spaced at 5 in. for the first 42 in. near the plastic hinge region, and 6 in. for the remainder of the height of the specimen above the plastic hinge region (Figure 52).

Figure 51. Typical confinement reinforcement used in normal strength columns for RC moment frames (photo curtesy of Dr. Shih-Ho Chao)
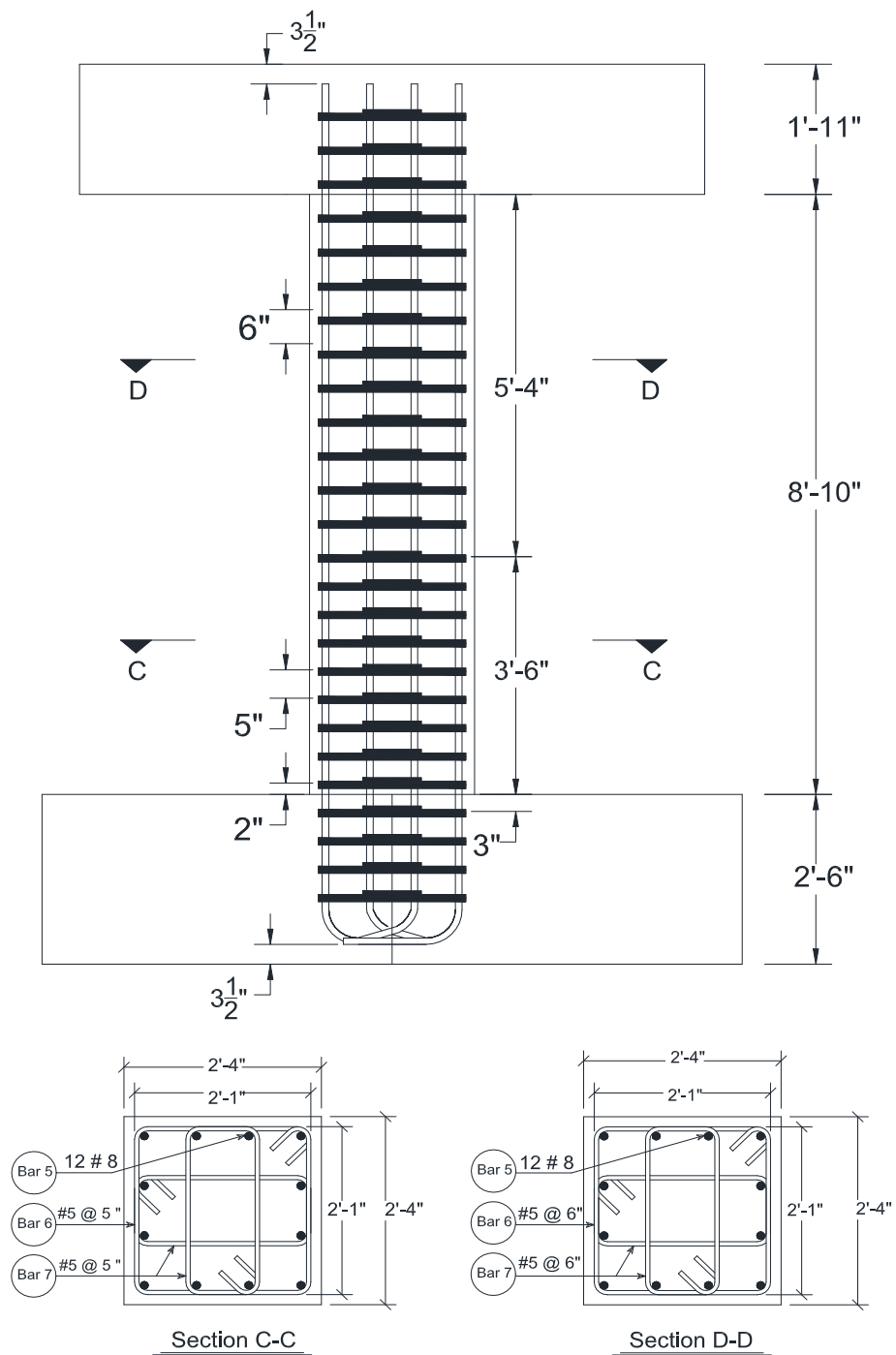
Figure 52. Full-scale space frame column specimen design

3.5 Specimen Construction

All of the column specimens were constructed at the UTA Civil Engineering Laboratory Building (CELB). Each specimen was built in three major parts and cast vertically to simulate real world construction as accurately as possible. Prior to the start of construction all steel strain gauges were placed on the reinforcing bars. The reinforcing cage for the footing block and column cage were constructed separately but simultaneously. Once the footing block cage was completed, it was placed inside the formwork and the truss support frame was erected as shown in Figure 53. After the column cage was completed and instrumented with concrete strain gauges as shown (Figure 54), it was placed inside the footing cage (Figure 55), centered, and secured with high-strength straps to the truss frame to prevent it from moving during casting (Figure 56).

Figure 53. Footing block reinforcement and formwork

Figure 54. Completed column reinforcement cage

Figure 55. Placing of the column cage into the footing block
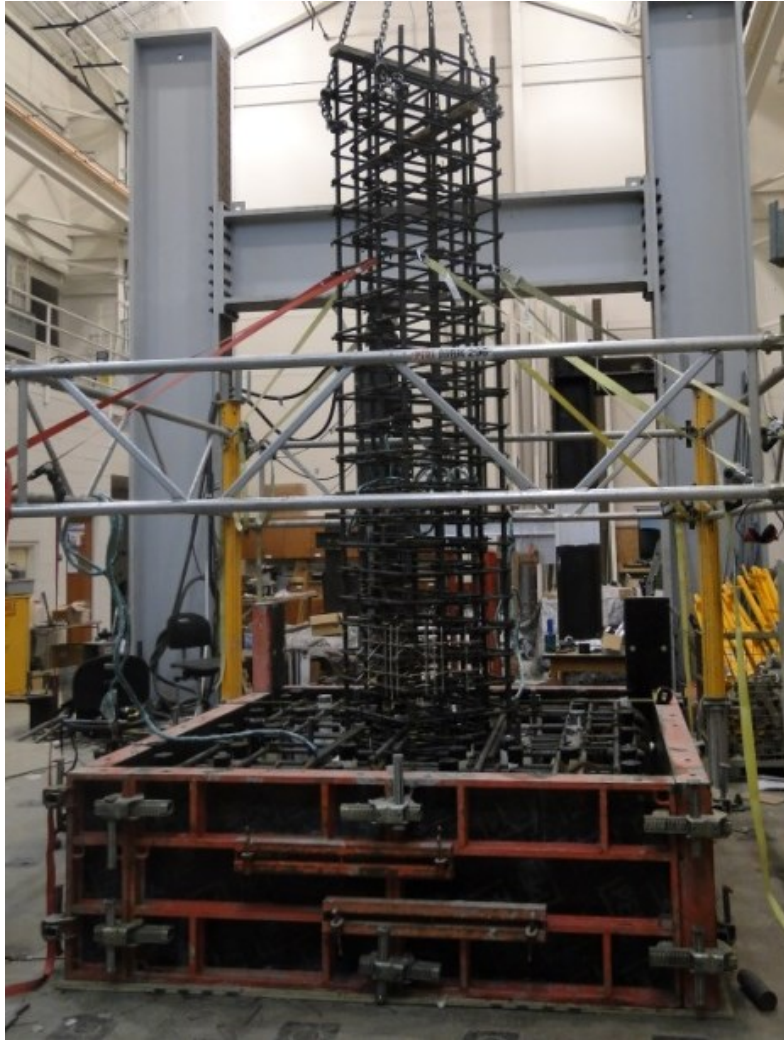
Figure 56. Centered and secured column cage

The bottom block was cast using 5 ksi concrete provided by a ready mix truck as shown in Figure 57.Twelve concrete cylinders were made to be tested under uniaxial compression and track the concrete strength progression. After the bottom block concrete had gained sufficient strength, the formwork for the column and the platform were placed (Figure 58). The loading block reinforcing cage was constructed (Figure 59) and placed on the platform together with the loading block formwork. The remainder of specimen SP5 was cast using 5 ksi concrete provided by a ready mix truck. The concrete

was poured into a large bucket which was then lifted with a crane to pour the concrete into the column section as shown in Figure 60.

Figure 57. Footing block casting

Figure 58. Loading block cage and formwork

Figure 59. Column formwork and loading block platform

Figure 60. Final column and loading block casting

After two days of curing the formwork was removed and the column specimen prepared for shipping. Four post-tensioning rods were used to protect the specimen from cracking during lifting and transportation. The finished SP5 column specimen can be seen in Figure 61. The column was removed from the CELB by the use of heavy duty forklifts (Figure 62) and placed on a flatbed truck to be transported to the University of Minnesota (Figure 63).

Figure 61. SP5 column specimen

Figure 62. Removing specimen from CELB

Figure 63. Shipping of column specimen to Minnesota

Both column specimens SP5 and SP8 were built with the same construction sequence. However, there are two key differences between the two space frame columns. The differences featured in specimen SP8 include:

1. The first 40 in. above the footing was cast with UHP-FRC

While the capabilities of UHP-FRC may suggest it to be a valuable alternative in earthquake resistant structures it has still yet to be tested in large scale structural applications. To further explore its capabilities, the first 40 in. of the column section of specimen SP8 was cast with UHP-FRC. Since no tests had been conducted with UHP-FRC on full scale structural elements, it presented an interesting construction challenge. In order to correctly mix the UHP-FRC in large quantities a special concrete mixer had to be designed. The mixer was designed and fabricated with the help of a local manufacturing company and can be seen in Figure 64. The column formwork was set up prior to casting to a height of 40 in. above the footing surface (Figure 64). All of the dry materials for the casting were premeasured and placed inside of a large bucket (Figure 65). The dry material is then added to the mixture slowly followed by water and super plasticizer. The microfibers are added last as shown in (Figure 66). In order to pour the 40 in. section the mixer must be elevated to a height well above the section to allow the UHP-FRC concrete to flow downwards into the column formwork. The mixer was raised with the crane and placed on an elevated platform as shown in Figure 66. An extension is placed to guide the UHP-FRC mix towards the column section. The UHP-FRC concrete is then poured into the formwork until it is completely filled (Figure 68). The UHP-FRC mix proved to be essentially self-consolidating and required no vibration.

Figure 64. Mixer and formwork for 40 in. UHP-FRC section

Figure 65. Premeasured dry materials

Figure 66. Pouring dry material and addition of micro-fibers

Figure 67. Elevated mixer ready for pouring

Figure 68. Pouring of UHP-FRC 40 in. section

Figure 69. UHP-FRC section after casting

After the casting of the UHP-FRC section the remainder of the column SP8 was cast identically to that of column SP5. The completed specimen SP8 can be seen in Figure 70.

Figure 70. Space frame column specimen SP8

2. The bottom two layers of transverse reinforcement below the footing were removed

As section 5.3 will discuss, currently ACI Section 18.10.6.4g specifies that for a special boundary element terminating at a footing, mat, or pile cap, the special boundary element transverse reinforcement shall extend at least 12 in. into the footing, mat, or pile cap. In the case where columns or boundary element have an edge located within one-half the footing depth from an edge of the footing, ACI Section 18.13.2.3 states that the transverse reinforcement must extend into the footing, mat, or pile cap and be developed for f_y in tension. The exact distance that the transverse reinforcement shall extend is not clearly defined.

In order to investigate these provisions and the necessity of the continuation of the transverse reinforcement within the footing section, specimen SP5 was constructed with the recommended ACI provisions and the transverse reinforcement was extended completely to the bottom of the footing. On the other hand, in column SP8 the lowest two layers of the transverse reinforcement were removed and both areas were extensively instrumented to study their behavior during testing (Figure 71).
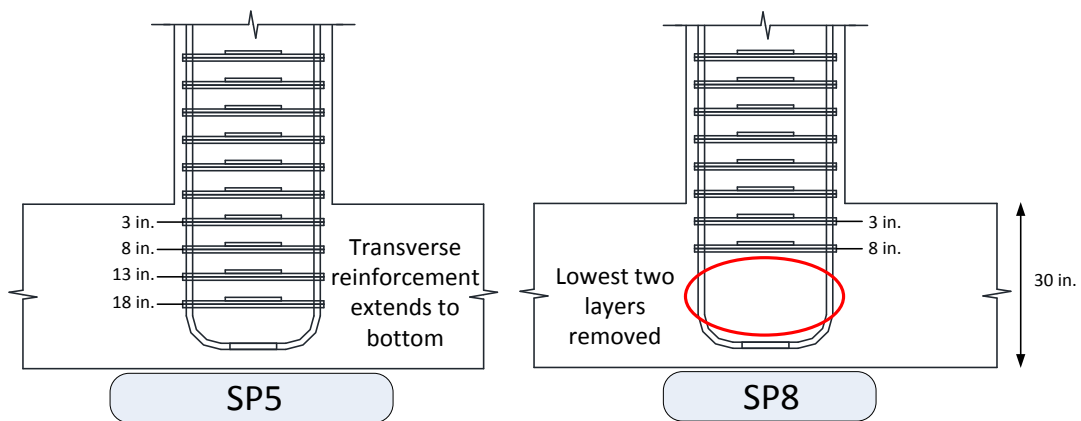
Figure 71. Column SP5 and SP8 transverse reinforcement into footing details

<u>3.6 Specimen instrumentation</u>

In order to compare and evaluate the major differences in strain deformation between the RC column and the UHP-FRC column, both specimens were extensively instrumented with steel strain gauges placed on the longitudinal and transverse reinforcing bars up to a height of 48 in. above the footing. To measure the internal strains of the concrete during testing, each specimen was instrumented with embedded concrete strain gauges. The concrete strain gauges for the RC specimen and the UHP-FRC specimen were located in the same locations to provide a direct comparison of the concrete performance during testing.

3.6.1 Steel Strain Gauges

The determination of the strain development within both the longitudinal and transverse reinforcement used in the specimens of this study is essential to analyzing the behavior of reinforced concrete columns. This information can be gathered by installing strain gauges directly to the surface of the steel reinforcement prior to constructing the reinforcing cage and pouring the concrete. In order to obtain accurate data from these sensors, a special procedure was used that creates a smooth, flat surface to which the strain gauge is attached, and ensures protection of the device from damage due to the conditions of casting and pouring. This procedure involves different forms of grinding to obtain a smooth and more efficient contact surface prior to the installation of the strain gauge (Figure 72). Once the strain gauge is applied following the manufacturers recommendations (Figure 73), various forms of sealants and waterproofing layers are applied to protect the strain gauges during construction and casting (Figure 74). Finally, the strain gauge is covered with moisture sealing rubber tape and liquid tape to further protect the stain gauge. A zip tie is also placed on the wire near the gauge to prevent and accidental wire pull-outs during construction (Figure 75). A more extensive explanation of

the standard procedure followed for the instillation of the steel strain gauges can be found in Appendix B.

Figure 72. Grinding of the reinforcing bars
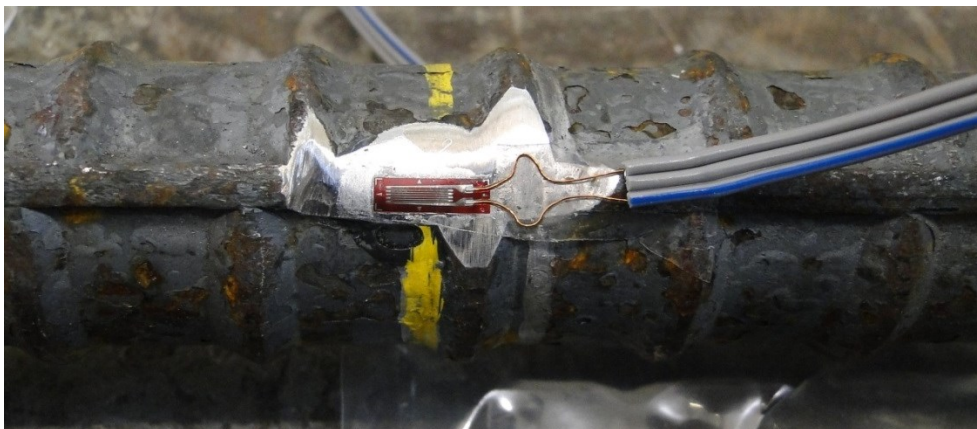
Figure 73. Applied strain gauge

Figure 74. Application of coat A

Figure 75. Completed strain gauge instillation

The locations of each of the strain gauges used in both specimens are shown in Figure 76 through Figure 78. Figure 76 shows the location of the strain gauges installed on the longitudinal reinforcement that are in the direction of the applied cyclic loading. The strain gauges shown in Figure 77 correspond to the previously observed plastic hinge locations, thus these strain gauges were added to obtain a comparison between the two specimens near the plastic hinge region. Figure 78 displays the locations of the strain gauges placed on the transverse reinforcement.

The notation of the steel strain gauge alphanumerical labels is described as follows. The first letters designate the type of strain gauge. For example, "SL" describes a strain gauge located on the longitudinal reinforcement; "STR" describes a strain gauge located on the transverse reinforcement. In the case of the longitudinal reinforcement, the first numerical terms describe the designated longitudinal bar number as shown in the strain gauge location drawings. In the case of the transverse reinforcement, the first numerical terms correspond to the location of the strain gauge on the transverse reinforcement as shown in the strain gauge location drawings. The final numerical terms, in both cases, correspond to the elevation of the strain gauge location with respect to the footing surface or ground "G". Note, a positive number describes a location above the footing, while a negative number describes a location within the footing.
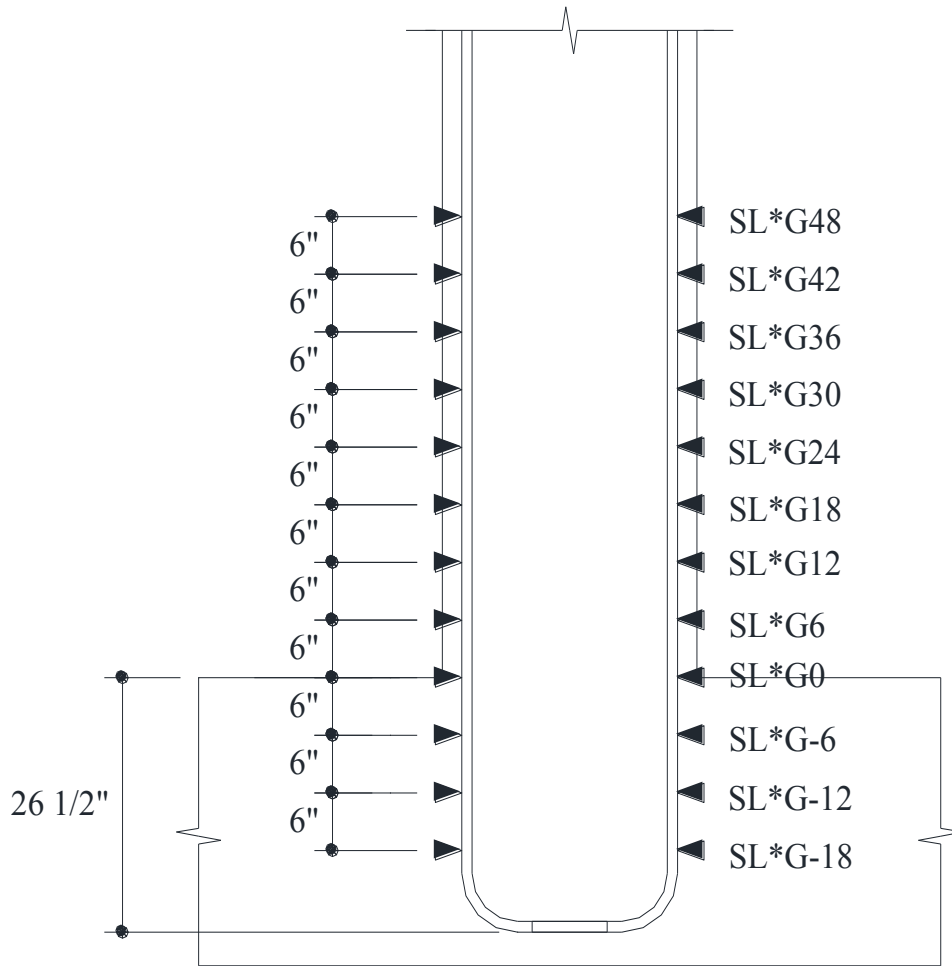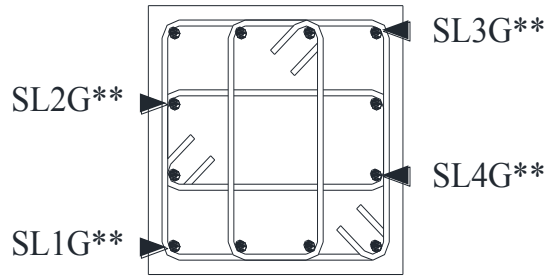
Figure 76. Strain gauges on longitudinal bars

SL6G**   SL3G**

SL2G**   SL7G**

SL5G**   SL4G**

SL1G**   SL8G**

SL*G14.5

5"   SL*G9.5

9 1/2"
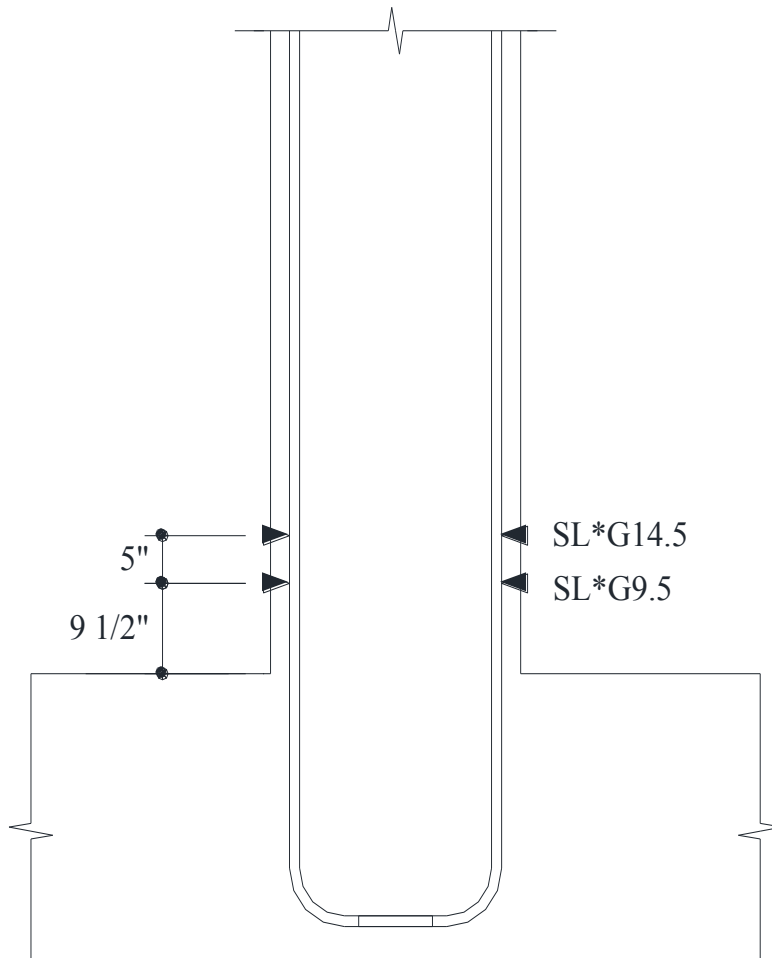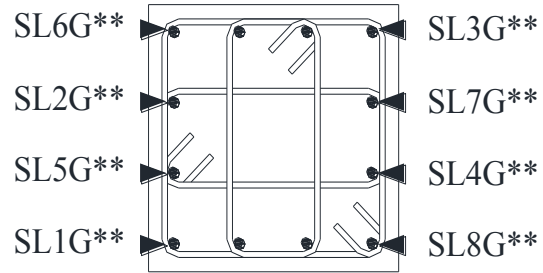
Figure 77. Strain gauge locations near plastic hinge
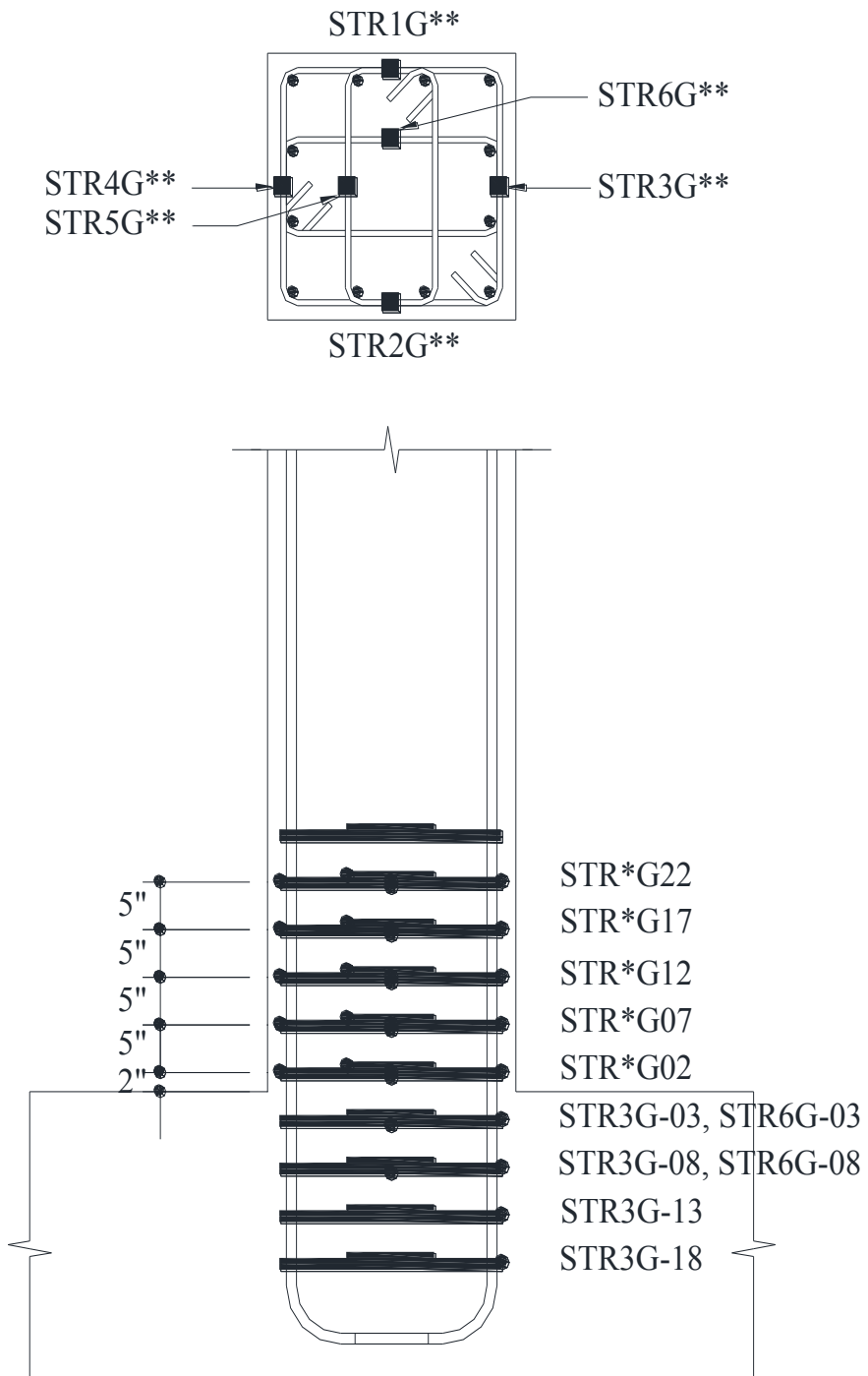
Figure 78. Strain gauge locations on transverse reinforcement

3.6.2 Concrete Strain Gauges

Concrete strain gauges are used to measure the strain in the concrete during testing of the RC columns. This information is very useful in measuring the confinement provided by each of the column specimens. Based on this information, observations may be made with respect to column size, concrete strength, and hoop spacing to optimize the design of the reinforcement.

To measure strains in the concrete during testing each specimen was instrumented with concrete strain gauges. The concrete strain gauges are embedded within the concrete. A length of steel wire is tensioned within the concrete strain gauge. As the concrete deforms, the steel wire is pulled or loosened and strains are measured between the two flanges of the concrete gauge. An example of the concrete strain gauge can be seen in Figure 79.

Figure 79. Concrete strain gauges

The location of the concrete gauges was determined initially by the possible locations of the plastic hinge. The concrete gauge locations for SP5 are shown in Figure 80, Figure 81 and Figure 82. Note that the direction of the gauge in Figure 80

corresponds to the longitudinal direction; while Figure 81 and Figure 82 correspond to the transverse direction with reference to the height and width of the cross-section respectfully.

The notation used to label each concrete strain gauge describes the location of that particular concrete strain gauge in space. For example, on the cross sectional view shown on the top of Figure 80 the label CL1G**, the C represents that the gauge is a concrete strain gauge. The L signifies that the gauge is oriented in the longitudinal direction. The transverse direction along the height of the cross section is represented by H, and the transverse direction along the width of the cross section is represented by B. The 1 defines the gauge number. The G** refers to the elevation of the strain gauges from the top face of the footing block or "Ground". For example, in the drawing shown on the bottom of Figure 80, CL*G15, the G15 signifies that the gauge is located 15 inches from the surface of the footing block or "Ground".

Specimen SP8 was instrumented according to the drawings shown in Figure 81 through Figure 87. The differences in the instrumentation of the concrete strain gauges are due to the differences between specimen SP5 and SP8. Additional concrete strain gauges were placed below the footing to evaluate the behavior of the concrete during testing with the removal of the transverse reinforcement.
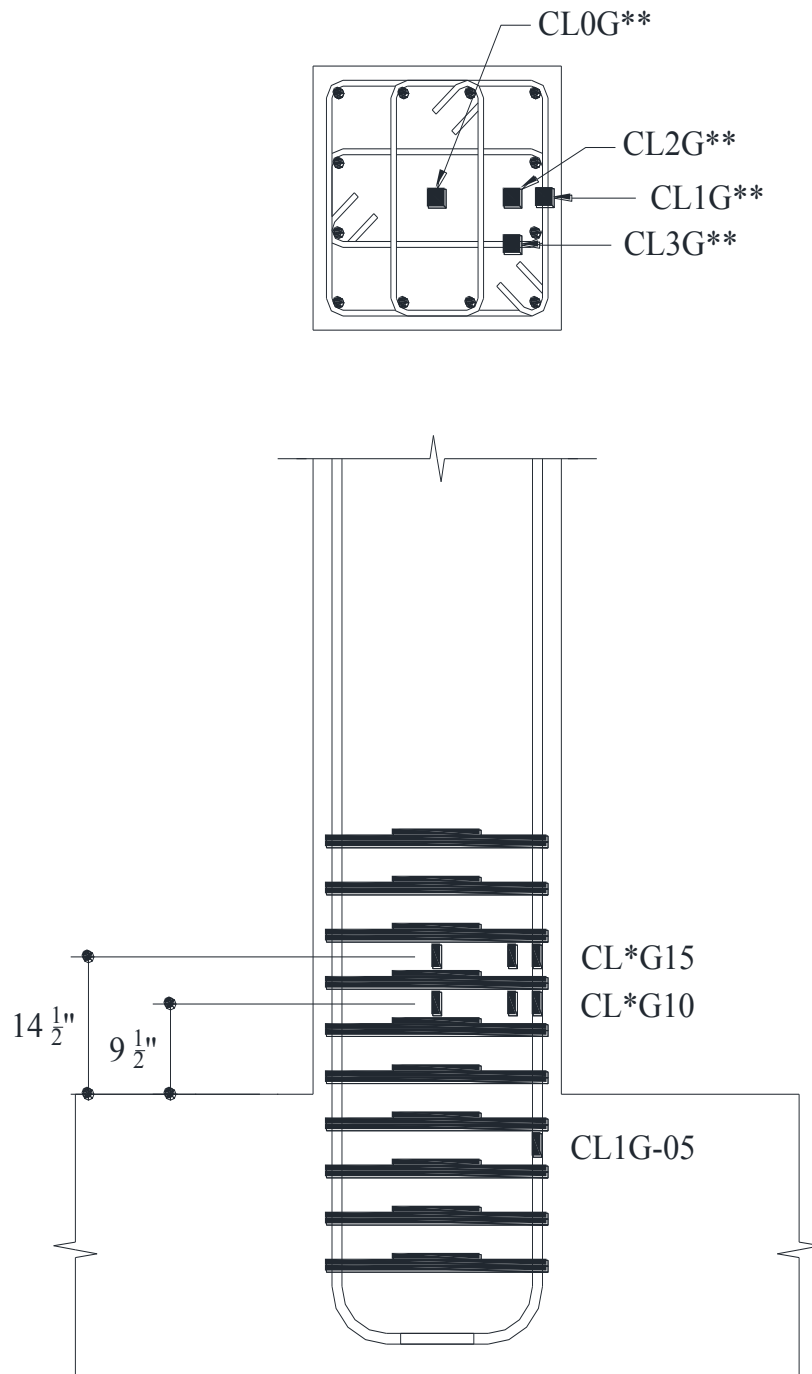
Figure 80. SP5 concrete strain gauge CL series location

CTRH1G**
CTRH2G**
CTRH3G**

CTRH4G**

CTRH*G15
CTRH*G12
CTRH*G10
CTRH*G07

$14\frac{1}{2}"$

$9\frac{1}{2}"$

CTRH2G-05

CTRH4G-05
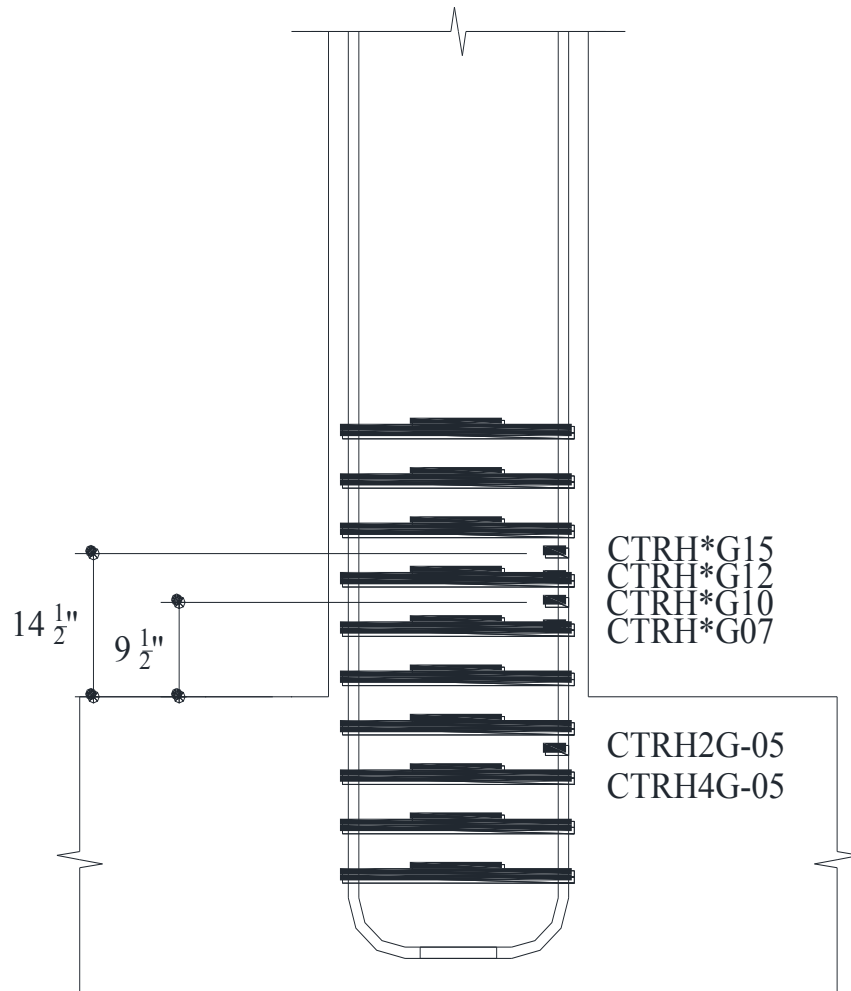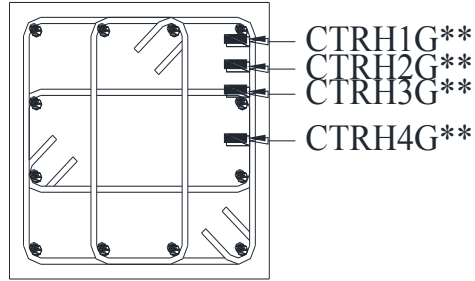
Figure 81. SP5 concrete strain gauge CTRH series location

CTRB1G**
CTRB2G**
CTRB3G**
CTRB4G**

CTRB*G15
CTRB*G12
CTRB*G10
CTRB*G07

$14\frac{1}{2}$"

$9\frac{1}{2}$"
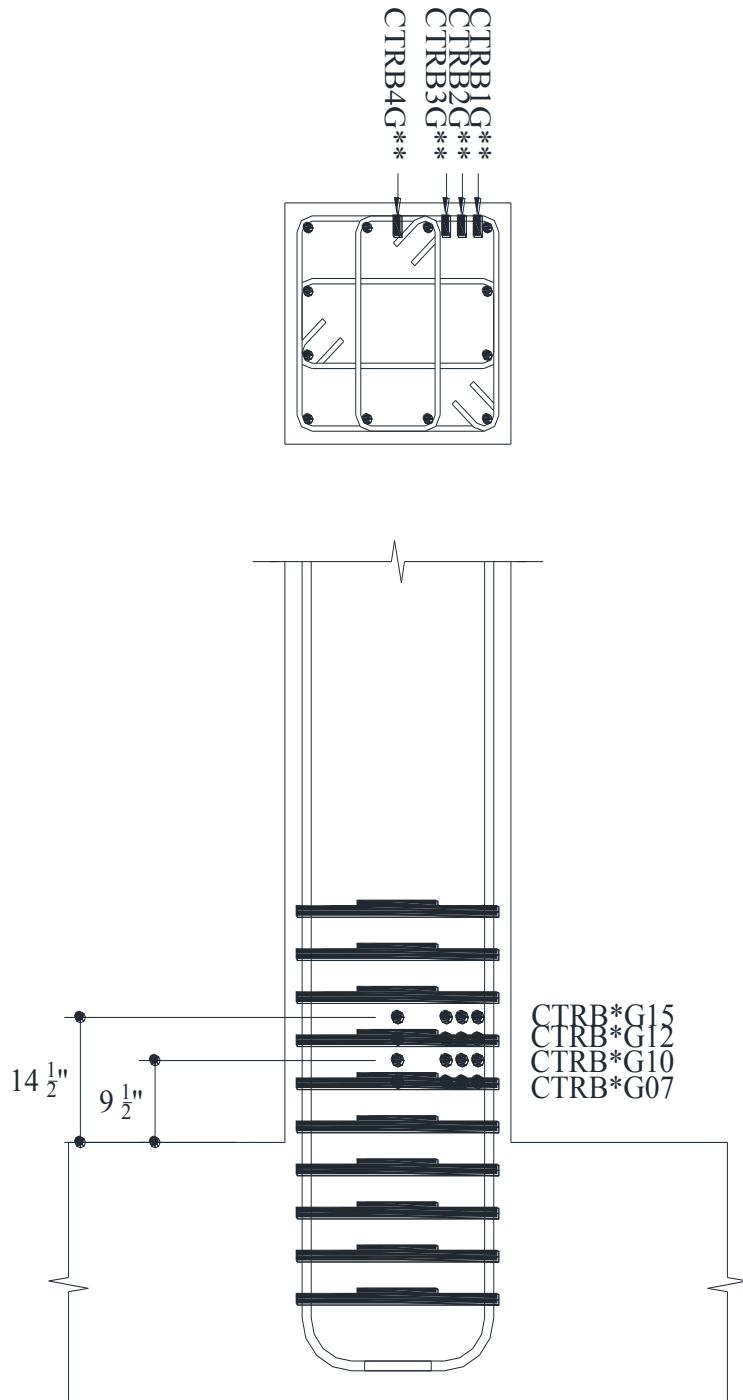
Figure 82. SP5 concrete strain gauges CTRB series locations

96
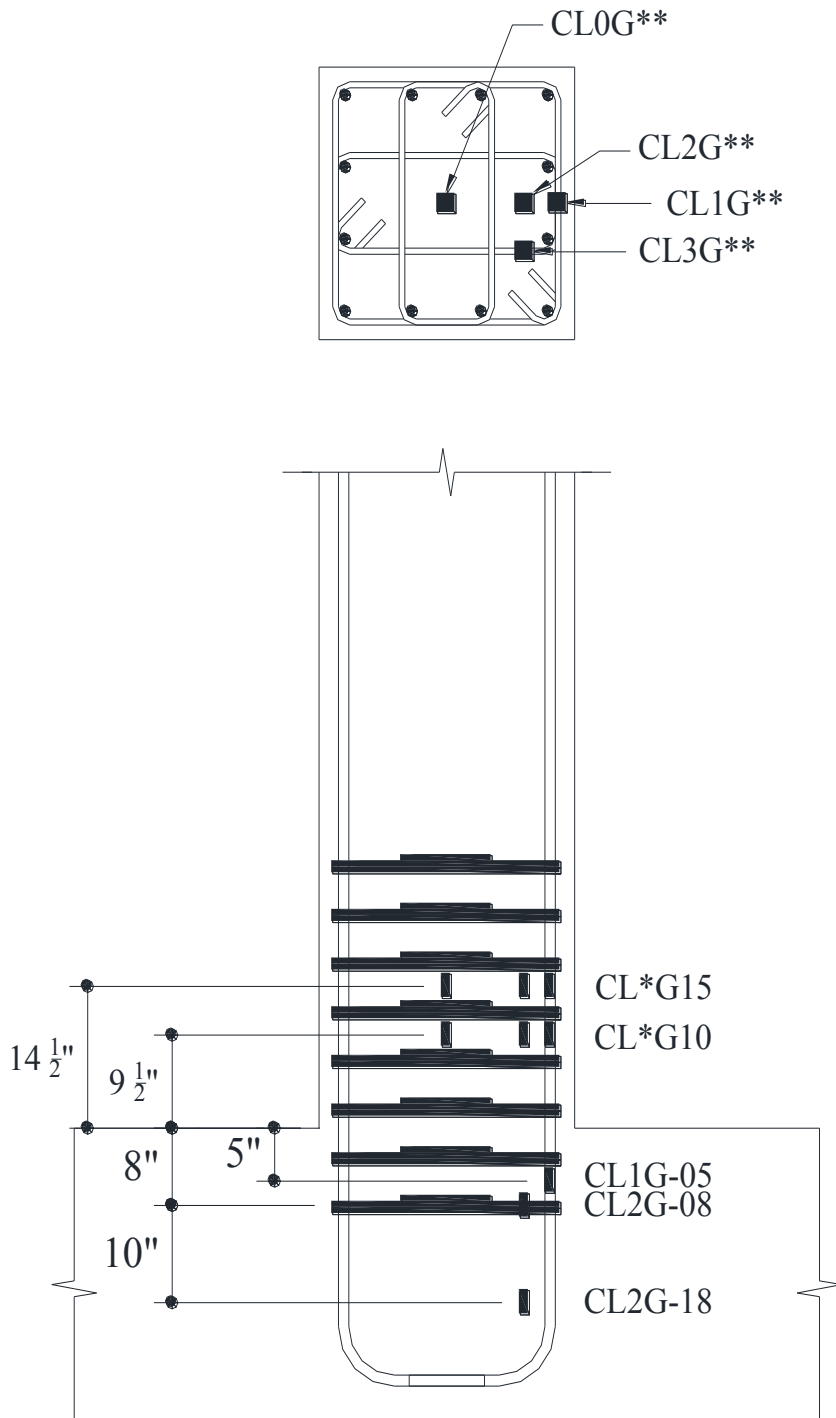
Figure 83. SP8 concrete strain gauge CL series locations

CTRH1G**
CTRH2G**
CTRH3G**

CTRH4G**

CTRH*G15
CTRH*G12
CTRH*G10
CTRH*G07

$14 \frac{1}{2}$"

$9 \frac{1}{2}$"

5"

CTRH2G-05
CTRH4G-05
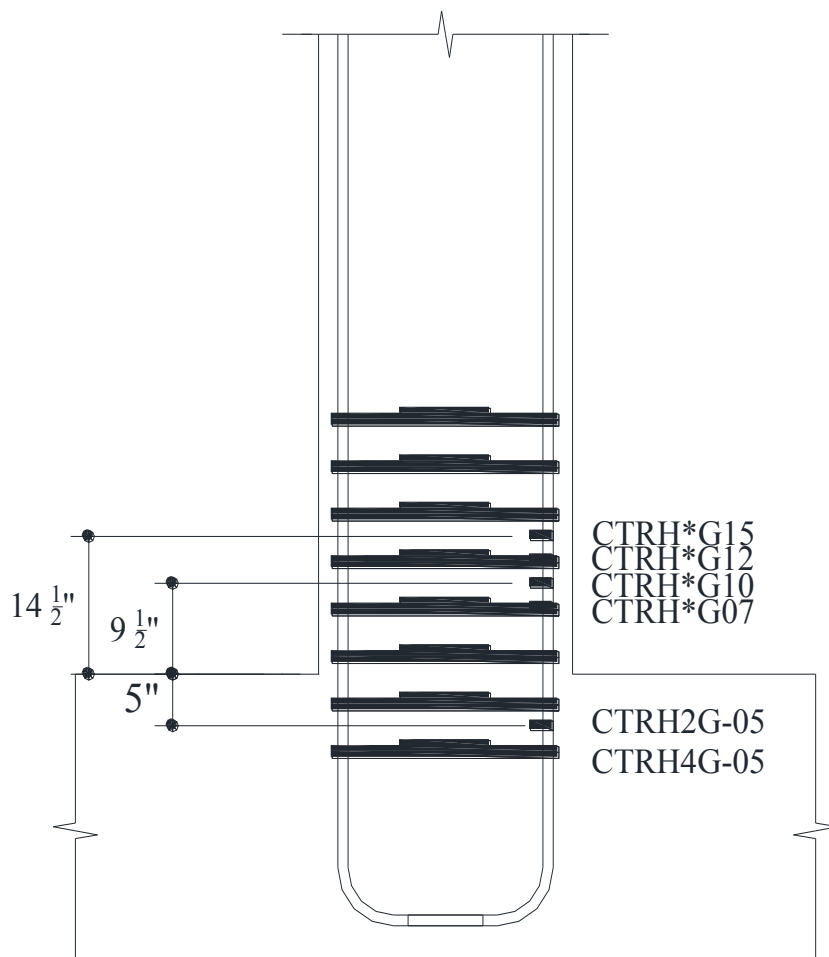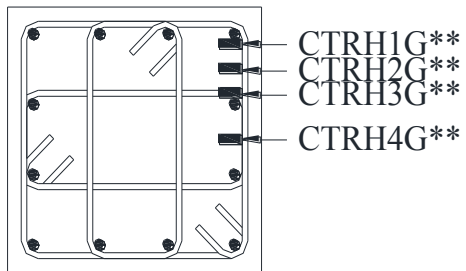
Figure 84.SP8 concrete strain gauge CTRH series locations

CTRH5G**

8"

10"

CTRH5G-08

CTRH5G-18
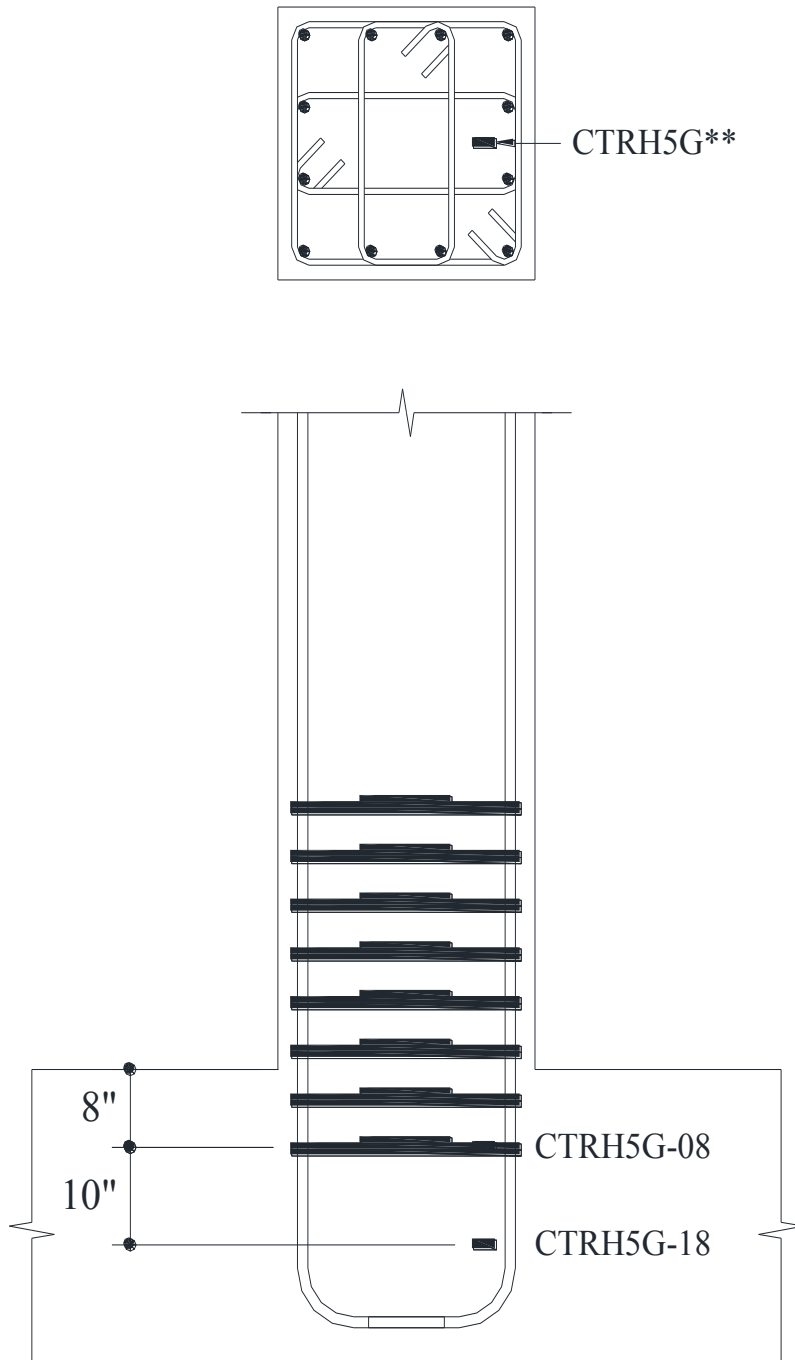
Figure 85. Additional SP8 concrete strain gauge CTRH series locations

CTRB1G**
CTRB2G**
CTRB3G**
CTRB4G**

CTRB*G15
CTRB*G12
CTRB*G10
CTRB*G07

$14\frac{1}{2}$"

$9\frac{1}{2}$"
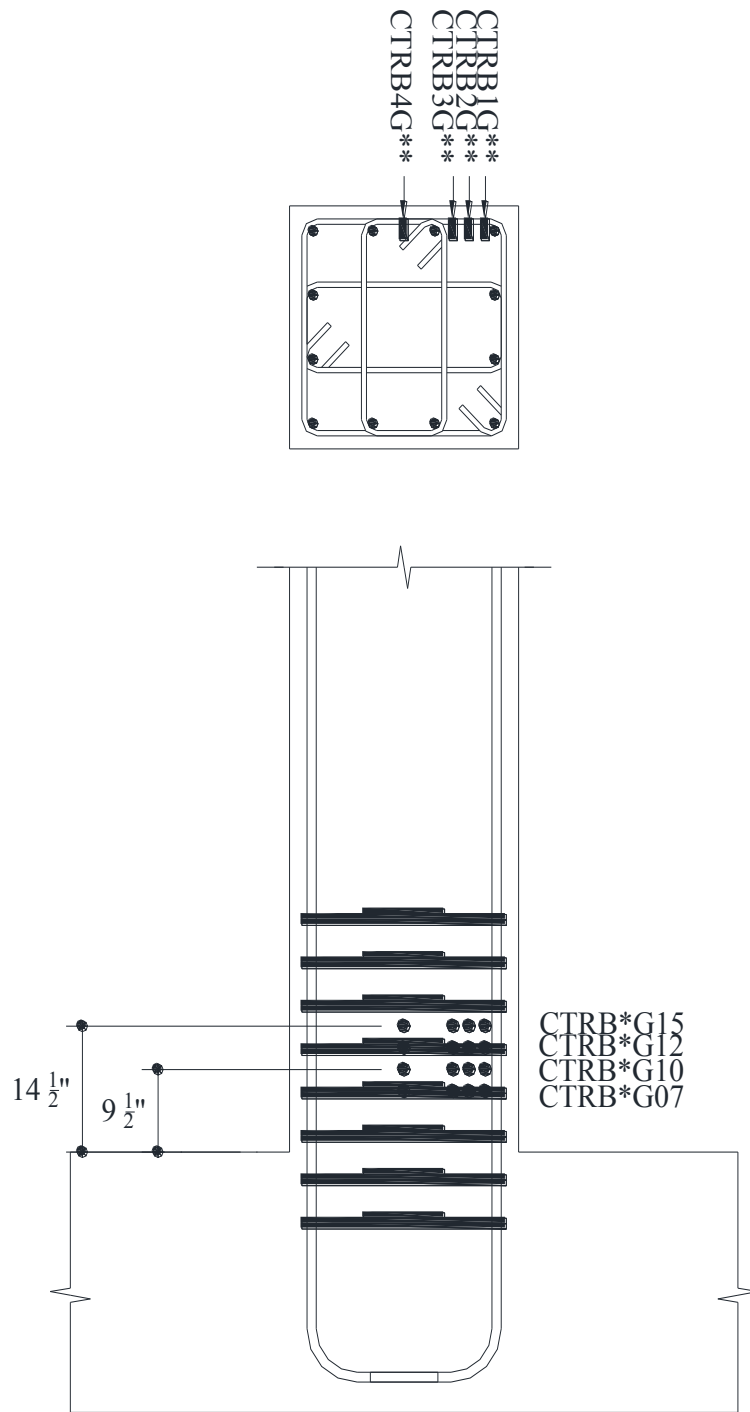
Figure 86. SP8 concrete strain gauge CTRB series locations
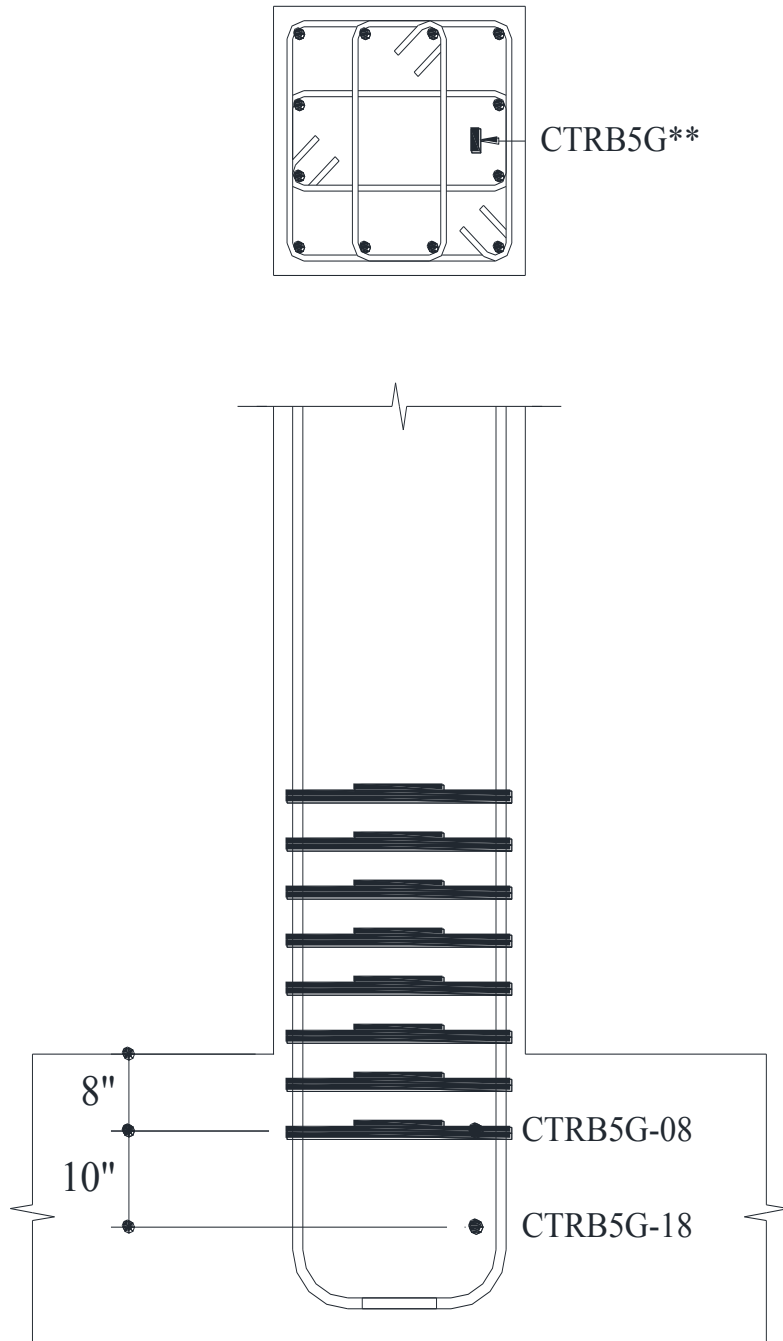
Figure 87. Additional SP8 concrete strain gauge CTRB series locations

CTRB5G**

8"

CTRB5G-08

10"

CTRB5G-18

The Multi-Axial Subassemblage Testing (MAST) Laboratory located at the University of Minnesota is one of the largest laboratories of its kind in the world (Figure 88). The laboratory is used to test a variety of structural elements up to 29 ft. tall under various extreme loading conditions. The sophisticated six degrees-of-freedom (DOF) control system allows for multi-directional loading schemes while being able to maintain a constant axial load that may more accurately simulate the loading effects of an earthquake. Additionally, the combination of actuators (4 vertical and 4 horizontal) are capable of exerting a total vertical force of 1,320 kips and a horizontal force of 880 kips (French et al., 2004).
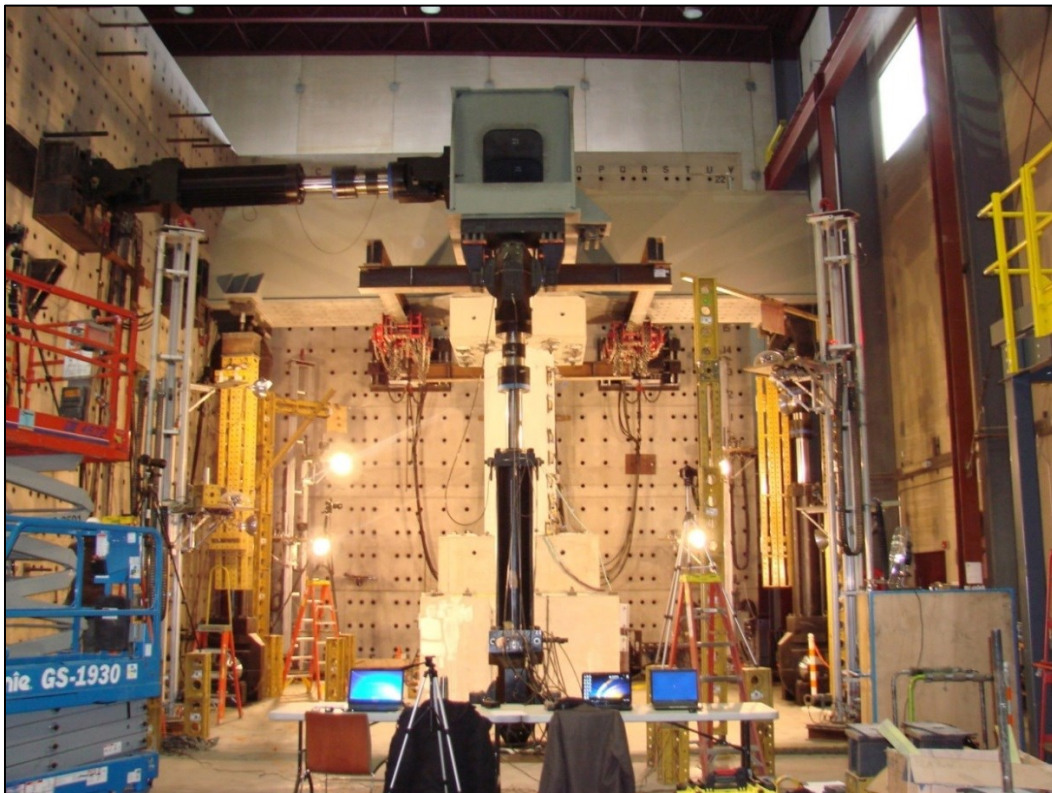
Figure 88. MAST testing facilities

The footing block of the column specimen was post-tensioned to a base block which was fixed to the strong floor of the laboratory. The loading block of the column specimen was post-tensioned to the crosshead which will apply the loading during testing (Figure 89). Each specimen was instrumented with LVDTs along the height of the column on both the NW and SE sides (Figure 90 and Figure 91) as well as string potentiometers to measure displacements during testing (Figure 92). Furthermore, cameras were positioned in the North-west, South-east, and South-west faces of the column in addition to the remote control telepresence system of the MAST facilities (Figure 88).

Figure 89. Overall test setup
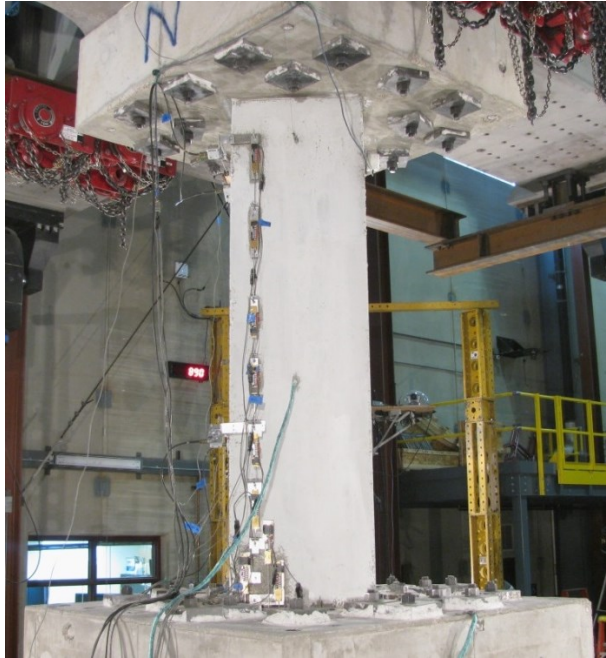
Figure 90. NW LVDTs
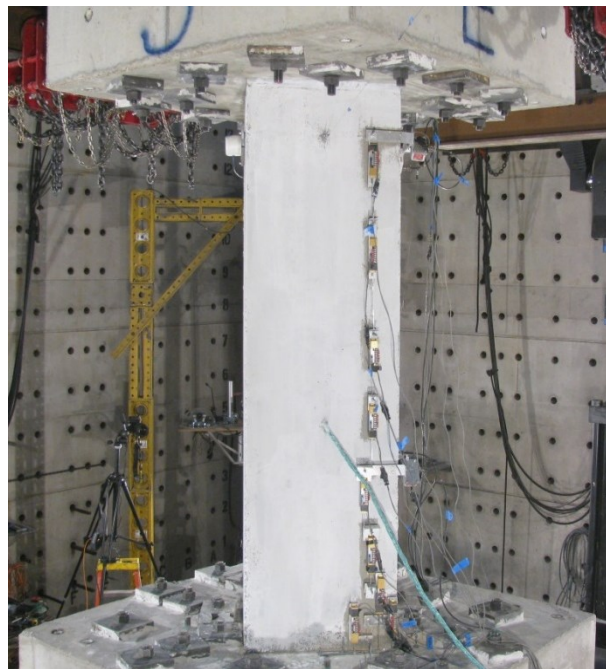
Figure 91. SE LVDTs
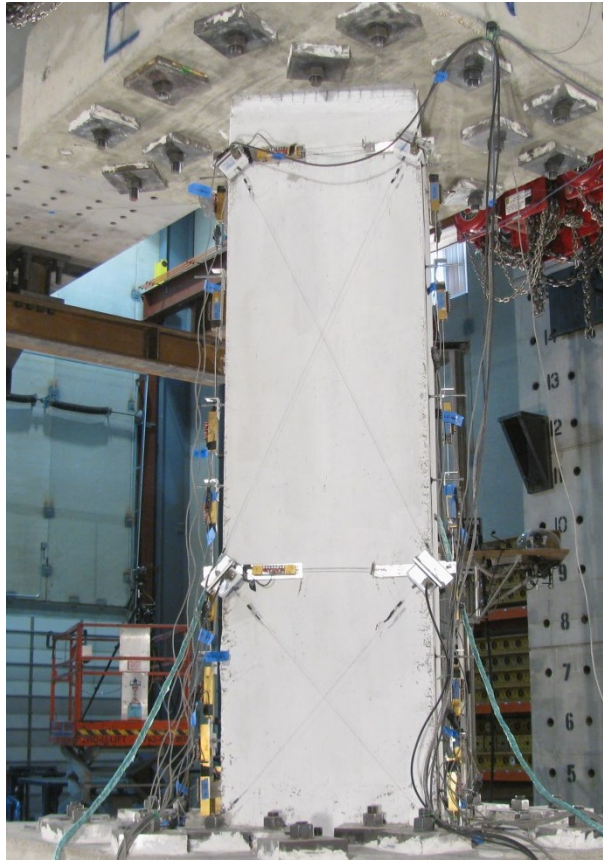
Figure 92. String potentiometers

3.8 Loading Protocol

The same cyclic loading protocol was used for both specimens; the loading protocol used in this study was in accordance with ACI 374-05 (2005). An axial load of 1,176 kip was applied at the beginning of each test and kept vertical and constant throughout the entirety of the test. After the application of the axial load, the specimens were subjected to the reverse cyclic loading protocol. Figure 93 shows the applied loading protocol where three fully reversed cycles were applied at each drift level gradually increasing in magnitude. In between each increasing drift level, intermediate cycles were applied at a magnitude of 1/3 of the preceding drift level. The criteria for stopping the test was based on the displacement limitations of the crosshead actuators or

until the specimen's strength degraded to 20 percent or less of their peak resistance exhibited during the test in both directions.

As shown in Figure 94, the test unit was rotated 45 degrees with respect to the principal directions of the footing and laboratory floor. Thus, the corresponding MAST control coordinate system will be rotated by 45 degrees about the +Z axis to an x'-y'-z' system as shown in Figure 94. The general orientation of the MAST laboratory is kept for identification of the specimen surfaces.
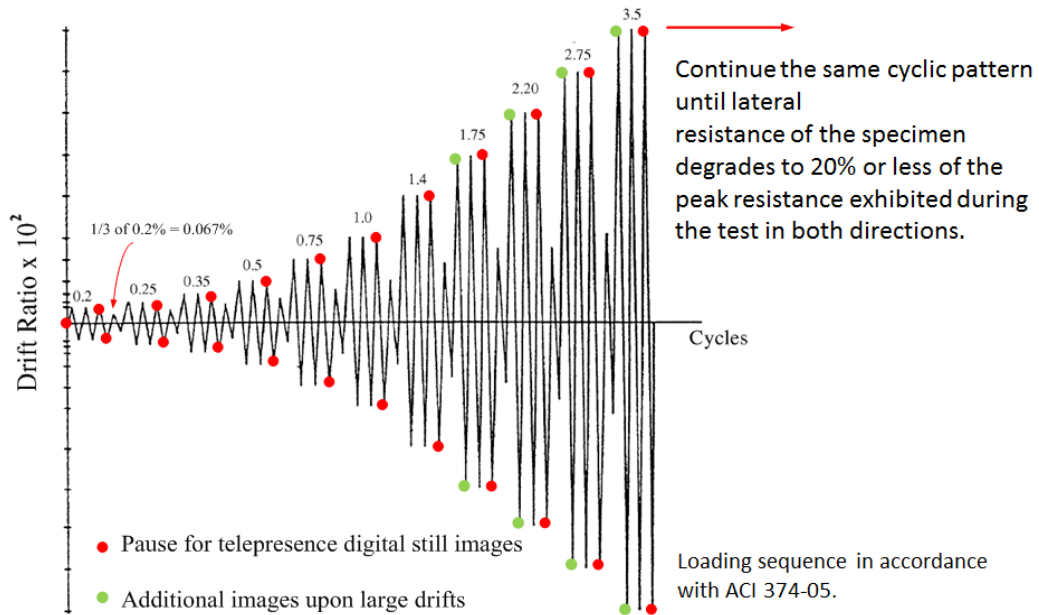
Figure 93. Reversed cyclic loading protocol for column specimens
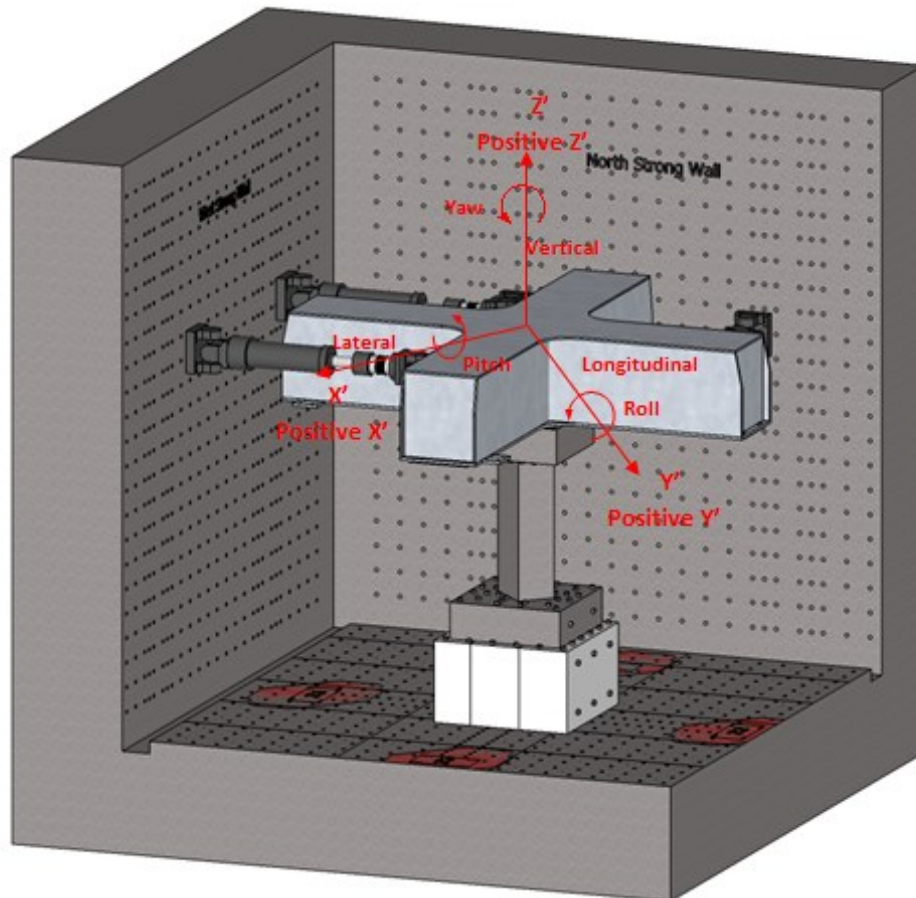
Figure 94. Overview of test setup with the rotated MAST control coordinate system

Chapter 4

Part I: Experimental Testing

The results for the two column specimens subjected to the reverse cyclic loading protocol described previously are described in this chapter. The general response of each specimen is presented. Observations made during the testing of each specimen and a comparison of the strain gauge information is also reported.

<u>4.1 Test Observations</u>

This section describes test observations on both specimens and offers a visual comparison between the seismic performance of an RC column (SP5) and a column with its plastic hinge region cast with UHP-FRC (SP8). Prior to the start of the cyclic loading protocol, an initial axial load of 1,176 kip was first applied at the beginning of each test and kept vertical and constant throughout the entirety of the test.

At approximately 0.5% drift the first flexural crack was observed in SP5 at approximately 14 in., 22 in., and 32 in. above the footing surface as shown in Figure 95. Specimen SP8 is displayed on the right with no visible cracking.
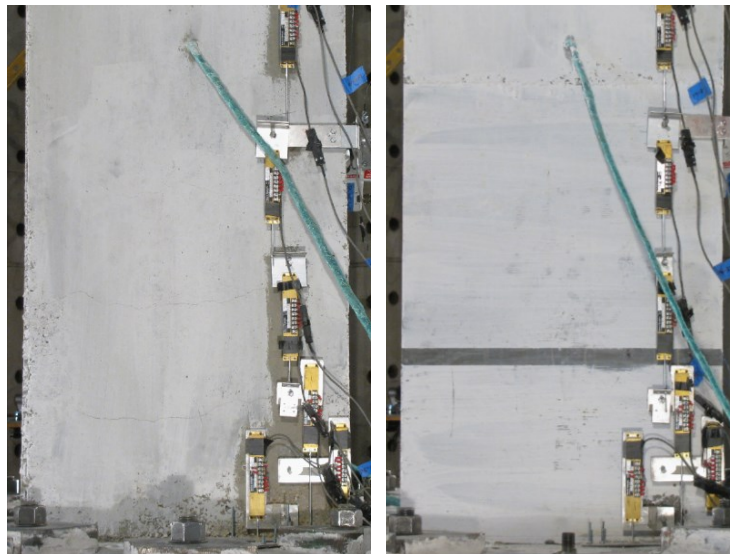
Figure 95. Column specimen SP5 and SP8 at 0.5% drift

The first longitudinal bar yielding was observed at 0.75% for both column specimens at the column base. At 1.0% drift a longitudinal crack was observed along with concrete crushing at the south-west corner of column SP5 and no visible damage observed in SP8 as shown in Figure 96.

Figure 96. Column specimen SP5 and SP8 at 0.75% drift

A strength decrease was observed for column SP5 at 1.4% drift. The concrete crushing observed at the south-west corner increased and also the flexural crack width (Figure 97). No cracking was observed in the UHP-FRC section of column SP8 at this drift level and the column's lateral strength continued to increase.

At 2.75% it was noticed that the lateral strength of column SP5 decreased in both the positive and negative directions. More significant concrete crushing is now visible on the column corners (Figure 98).

Figure 97. Column specimen SP5 and SP8 at 1.4% drift
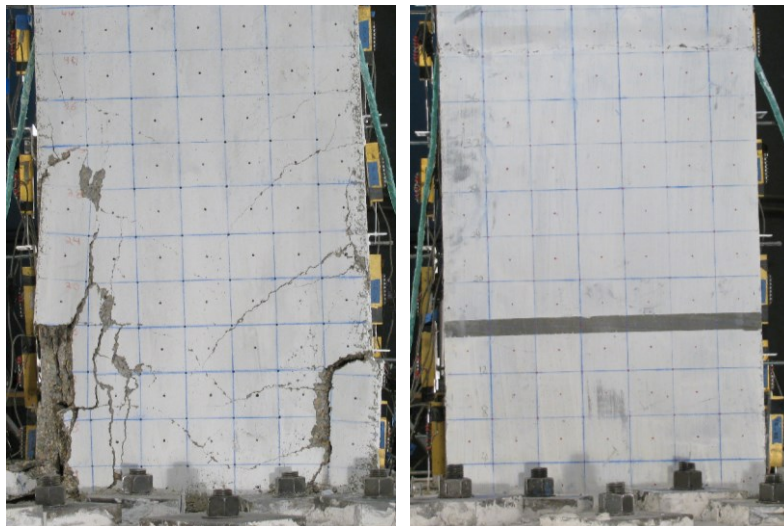
Figure 98. Column specimen SP5 and SP8 at 2.75% drift

At 5.5% drift there is severe damage to the SP5 column. The failure mechanisms typically observed with RC columns subjected to cyclic loading were present during the testing of specimen SP5. These mechanisms are observable in Figure 99, in which there is severe concrete crushing present in the column faces located in the direction of

loading. Longitudinal bar buckling and rupture was also observed in the direction of loading, consistent with the significant strength degradation seen during testing. At this point in the test, there is still no perceivable damage to the UHP-FRC section of column SP8. However, there was noticeable concrete damage to the RC footing block as well as a separation between the column section and the footing section (Figure 100).
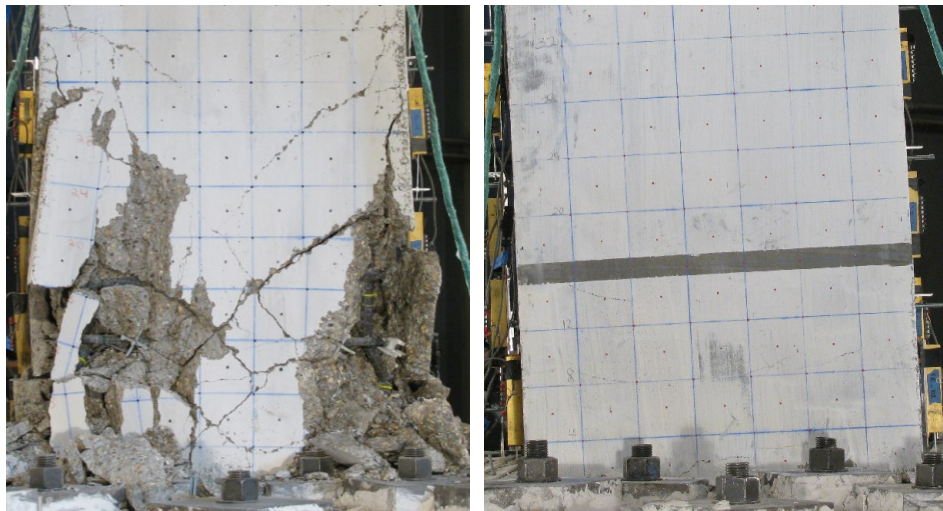
Figure 99. Column specimen SP5 and SP8 at 5.5% drift

Figure 100. Damage and separation at the column-footing interface

Specimen SP8 failed in a very different manner than that of SP5, mainly due to the low-cycle fatigue and rupture of the longitudinal reinforcement at the column-footing interface. The column specimen SP8 dropped to less than 20% of its lateral peak strength at a drift of 8.6%. The UHP-FRC section remained intact with no visible damage, thus SP8 failed solely due to the behavior of the longitudinal reinforcement which ruptured at the interface (Figure 101).

Figure 101. SP8 column specimen after testing

<u>4.2 Response of Test Specimens</u>

The cyclic response of specimen SP5 and specimen SP8 are shown in Figure 102 and Figure 103 respectively. Specimen SP5 reached maximum lateral peak strength of 192 kips at 1.38% drift. Specimen SP8 reached maximum lateral peak strength of 222 kips at 2.17% drift.
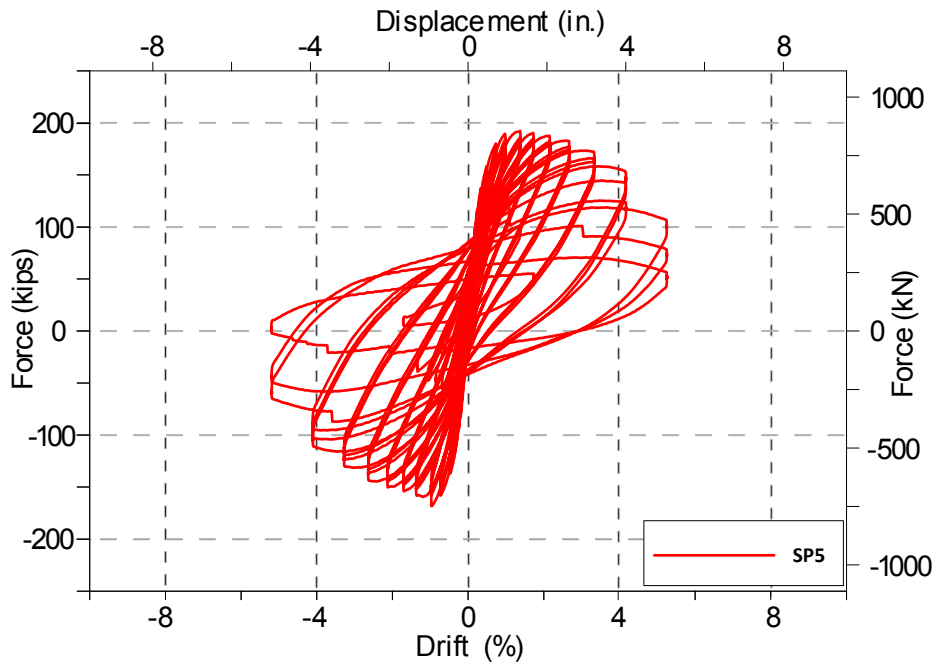
Figure 102. Lateral force vs. drift behavior of SP5
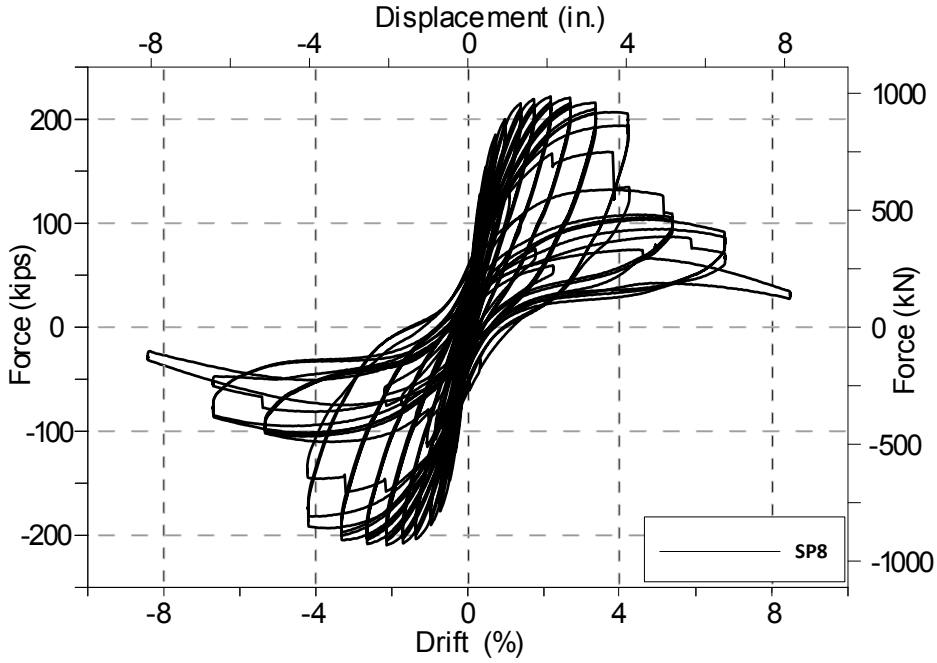
Figure 103. Lateral force vs. drift behavior of SP8

Specimen SP5 failed in a typical manner common to conventional concrete columns. The typical failure modes of normal strength concrete columns subjected to seismic loading includes, concrete crushing, yielding of hoops, and buckling/fracture of the longitudinal reinforcement each contributing to a loss in load carrying capacity. Figure 104 shows a representation of the strain profile for the longitudinal bars of column specimen SP5, more specifically bar SL2G in both the positive and negative directions. It can be observed from Figure 104 that yielding of the longitudinal reinforcement in the column section initiated at a loading of 180 kip or about 0.75% drift. As the test continued, the concrete damage became more significant and the cover eventually spalled off exposing the longitudinal bars to large tensile and compressive strains with only the transverse reinforcement providing support. Figure 105 shows the strain profile for the transverse reinforcement of column SP5, more specifically STR4G, which is the positioned near the longitudinal bar SL2G shown in Figure 104. It can be observed in Figure 105, that the transverse reinforcement experienced the largest strains in the negative direction due to the expansion of the concrete core in that specific direction. However, it is important to point out that at a loading in the negative direction of 168 kips (approximately -1.00% drift), which is the peak strength of the column in the negative direction and just prior to the load degradation, it can be seen that at a height of 12 in. there is a decrease in the strain of the transverse reinforcement. This represents significant concrete damage to this region, which was later observed after the end of testing, and is consistent with the observed longitudinal bar buckling and rupture of bar SL2G.

After reaching its peak strength in the negative direction, the longitudinal bars have essentially yielded in the plastic hinge region and the concrete reaches its maximum compressive stress and crushes, at this point the typical column failure

mechanism is triggered. This can also be verified by observing the concrete strain gauges CTRH3G shown in Figure 106. The concrete strain gauges were only placed on one side of the column, but it can be expected that since the column has a symmetrical cross-section and is also being loaded with symmetric cyclic reversals, that the concrete sections on both sides will exhibit very similar behavior. It can be seen in Figure 106 that there is a sudden rise in concrete strain after the peak loading corresponding to cracking or crushing in the area where the concrete gauge is located. Naturally, the highest observed strain first occurs at 10 in. above the surface, as this is the area with the least confinement since this gauge is located in between two hoops (located at 7 in. and 12 in.). Once concrete crushing is initiated in a localized region, this makes the surrounding concrete more susceptible to crushing, as the stresses are redistributed to the remaining concrete that is still intact, leading to increased concrete cyclic degradation.

Essentially, the damage progression and strength degradation of the column is initiated by the concrete behavior and its strength limitations. Column SP5 after the end of testing is shown in Figure 107, it can be seen that there is a significant reduction in core concrete in the region between 7 in. to about 15 in. above the footing surface, consistent with the recorded strains previously discussed. Longitudinal bar buckling and rupture is also visible as well as a hoop that has opened.
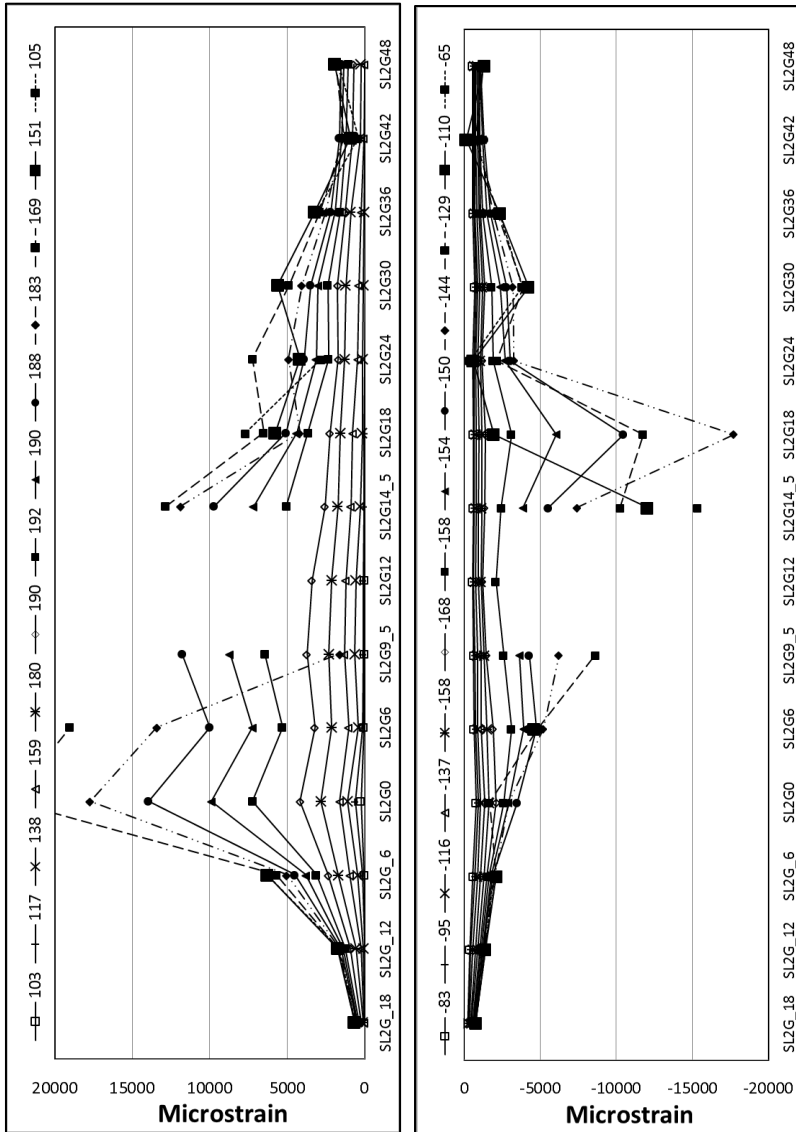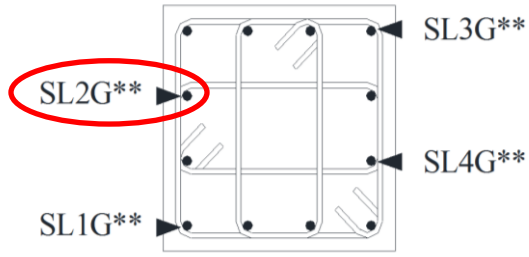
Figure 104. SP5 strain profile of SLG2 in the positive and negative directions

116
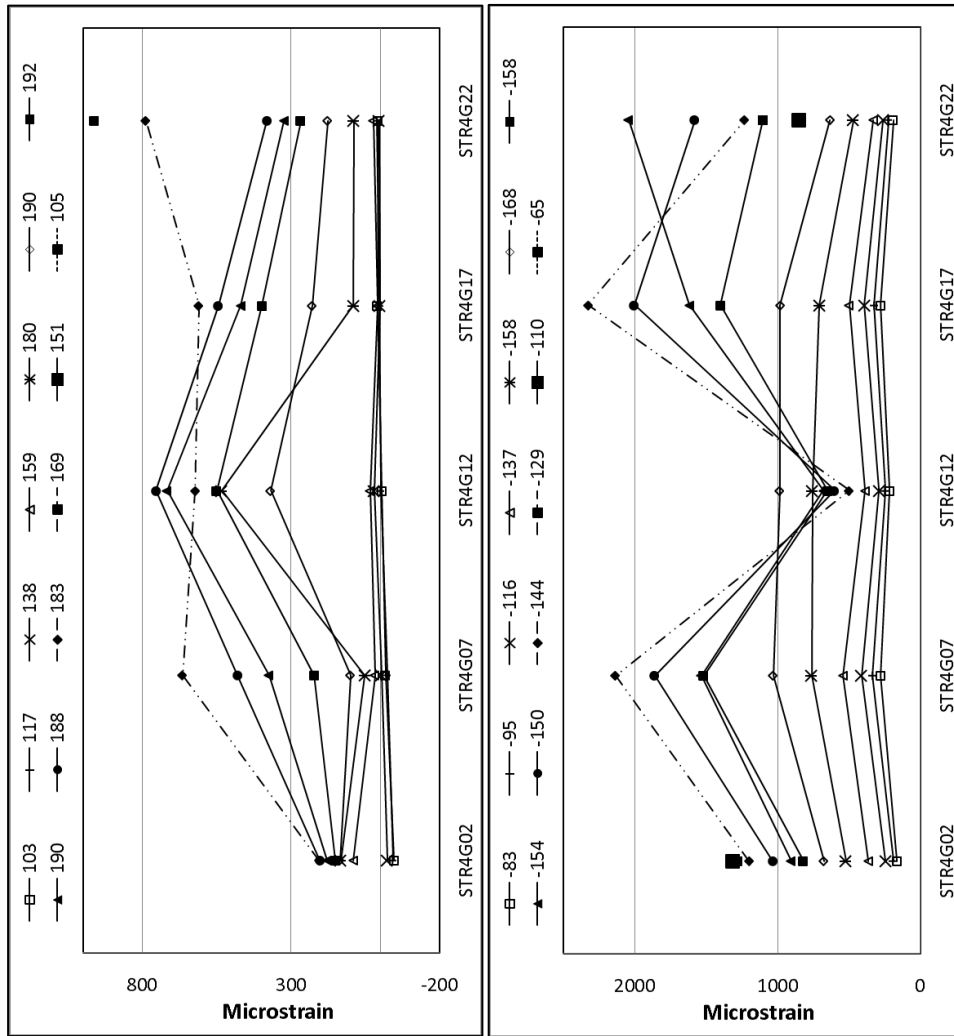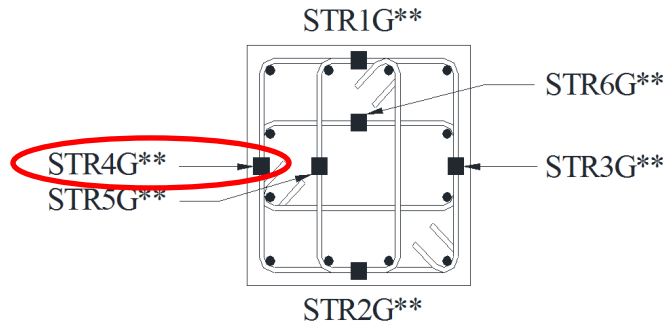
Figure 105. SP5 strain profile of STR4G in the positive and negative directions
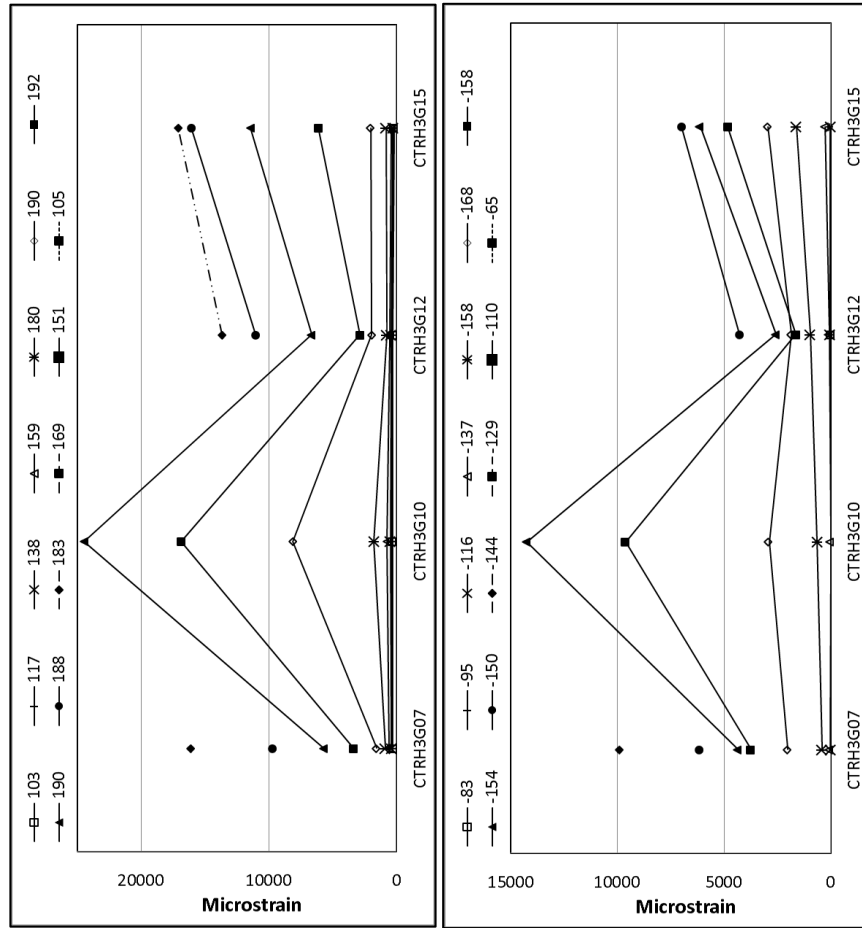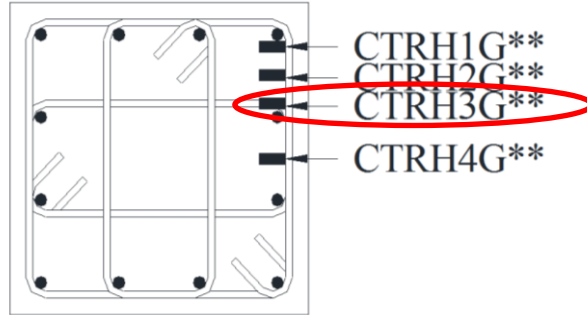
Figure 106. SP5 strain profile of CTRH3G in the positive and negative directions

Figure 107. Column SP5 after testing

Specimen SP8 having its plastic hinge region cast with UHP-FRC failed in a very different way compared to specimen SP5. A distinct failure mechanism was observed with concentrated yielding located at the column footing interface. Figure 108 shows the strain profile for the longitudinal bar SL2G along the height of column SP8. With no visible concrete damage to the UHP-FRC region through the entirety of the test the longitudinal reinforcement remained very well protected during testing. This allowed for the longitudinal reinforcement to fully develop in both tension and compression without the risk of bar buckling or rupture which was observed in specimen SP5. The highest strain concentrations were observed at the column footing interface where the column eventually failed due to the low cycle fatigue of the longitudinal reinforcement. This suggests that because of the high compressive strength and ductility of UHP-FRC a smaller equivalent compressive stress block is expected with higher strains well past 0.003 before crushing, thus the design may be improved so that additional longitudinal reinforcement may be added while still remaining tension-controlled and an even higher strength and ductility may achieved than that observed in SP8.

Higher strains were also observed in the longitudinal reinforcement within the footing compared to the longitudinal reinforcement of specimen SP5; this is attributed to the high bonding strength of UHP-FRC and is responsible for the increased deformation of column SP8. Chao (2005) stated that the unique characteristics of HPFRCCs can significantly enhance the bonding characteristics of reinforcing bars and pre-stressing strands embedded in concrete matrices because of multiple cracking due to fiber bridging as shown in Figure 109. After testing it was also visible how some of the longitudinal bars remained in the column section and pulled out of the footing section (Figure 110).

The transverse reinforcement in SP8 essentially remained elastic with minor strain being recorded well below 50% of yielding (Figure 111). This is due to the high confinement and compressive ductility of UHP-FRC which recorded very minor strains in the direction of loading and almost zero strain (below 120 microstrain) through the entirety of the test (Figure 112) in the opposing direction. There was no visible damage to the surface of the UHP-FRC section and the very low strains recorded by the internal concrete gauges, signifying that no significant cracking or crushing was present within the column section. As previously presented with the small-scale column testing, the strain observations in the full-scale specimen suggest that the transverse reinforcement may be reduced in the region where UHP-FRC is used, this is contrary to the case in which HSC is used.
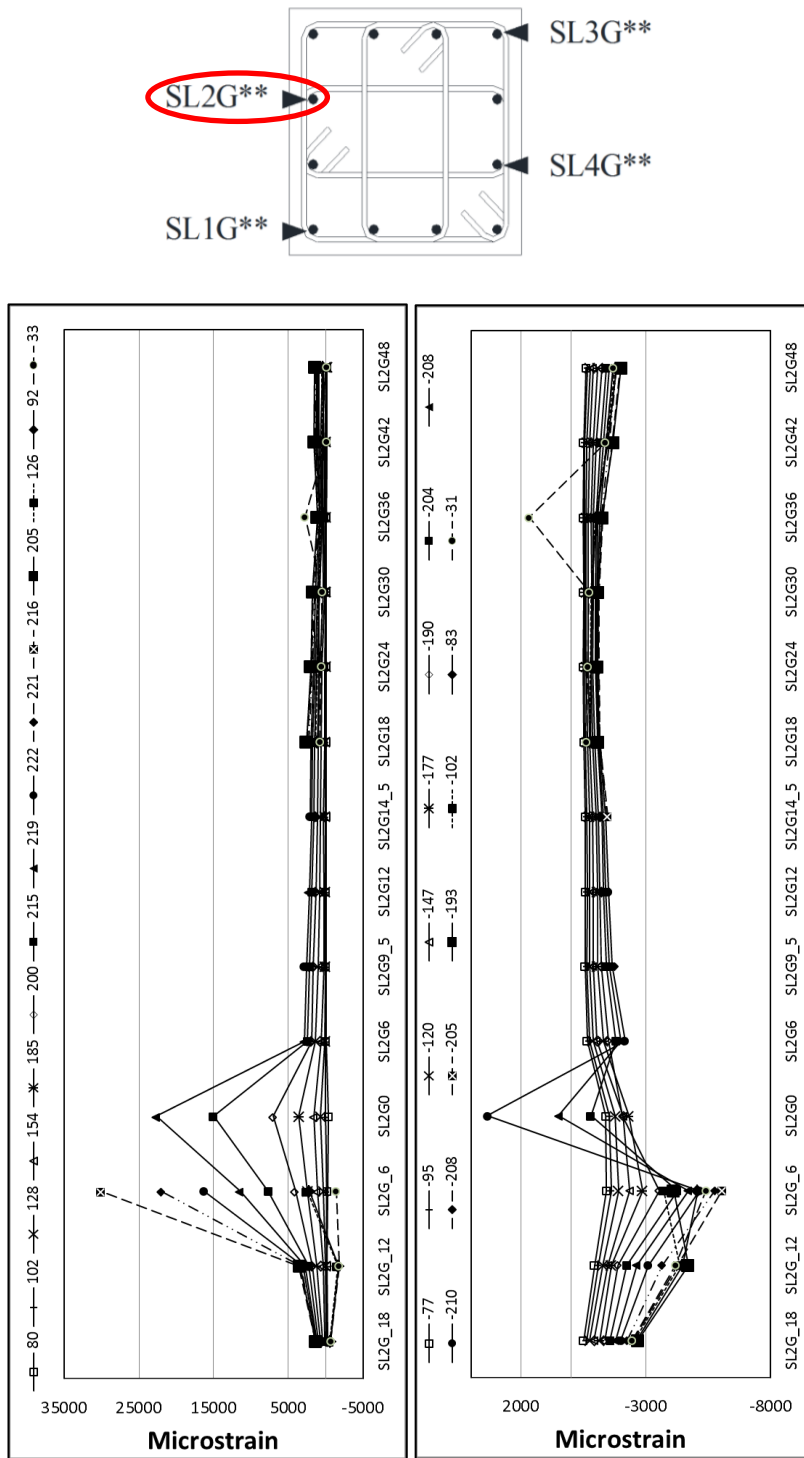
Figure 108. SP8 strain profile of SLG2 in the positive and negative directions
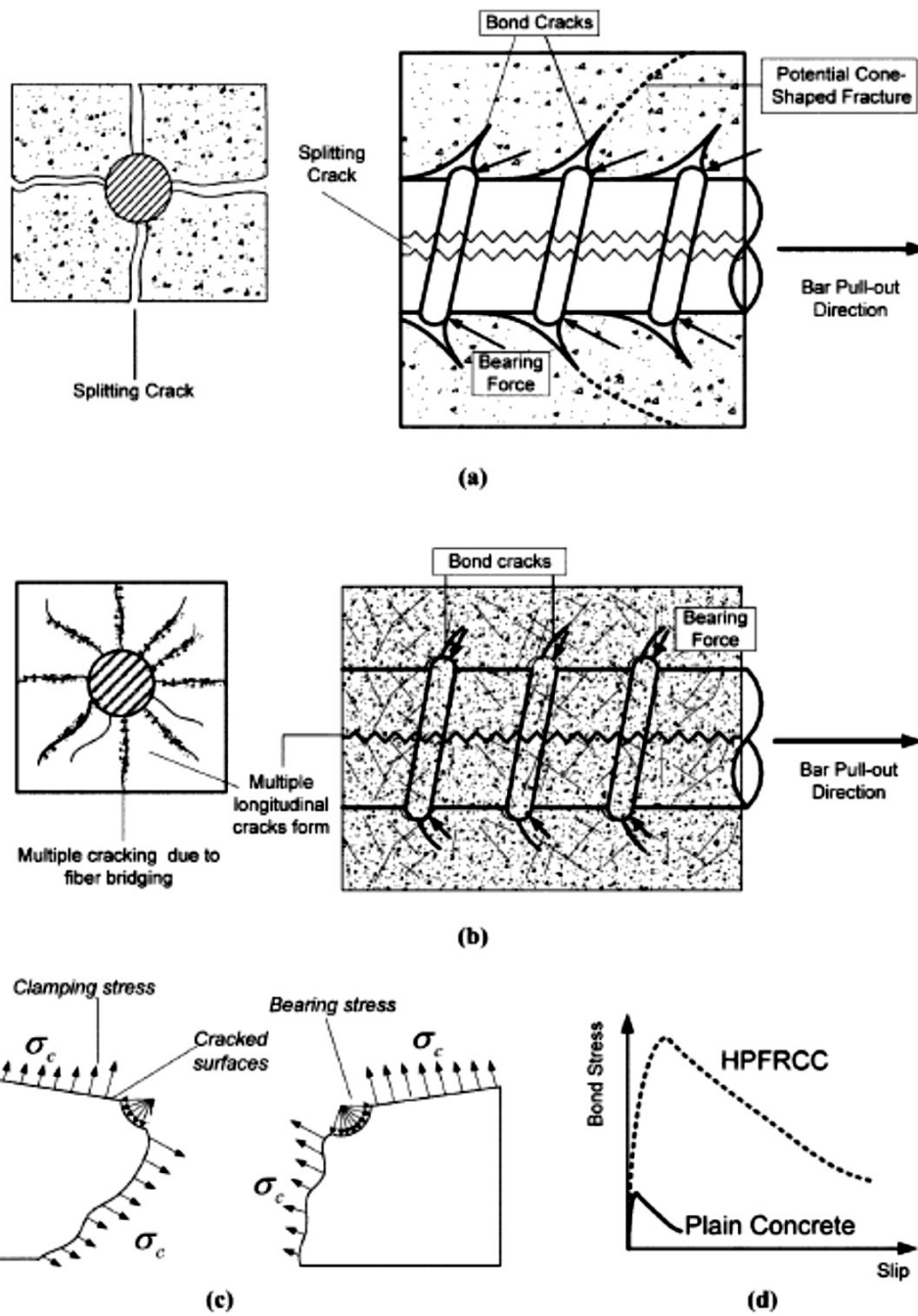
Figure 109.Differences in bond mechanism of reinforcing bars in conventional and HPFRCC concrete (Chao, 2005)

Figure 110. Longitudinal bar pull-out from footing after testing
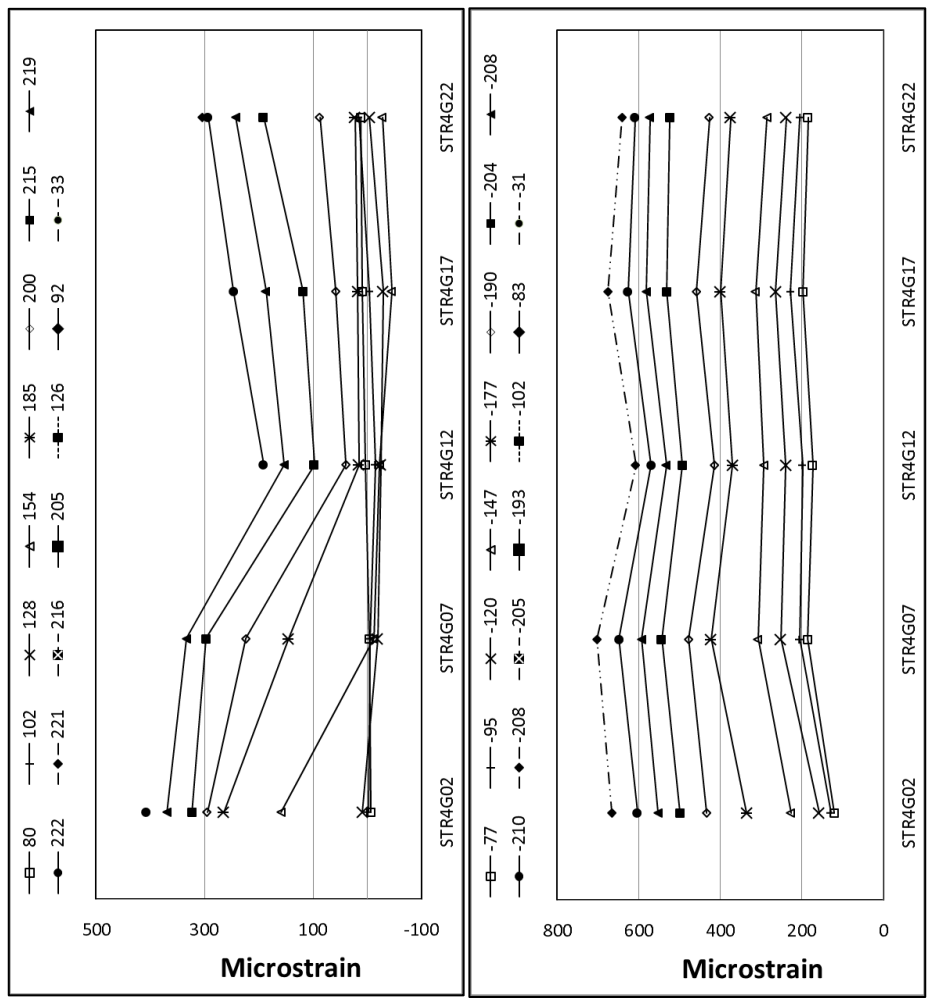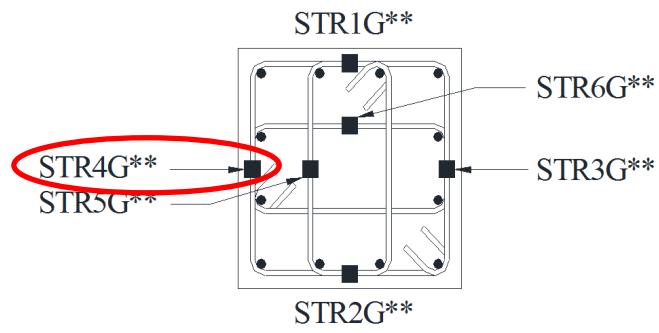
Figure 111. SP8 strain profile of STR4G in the positive and negative directions
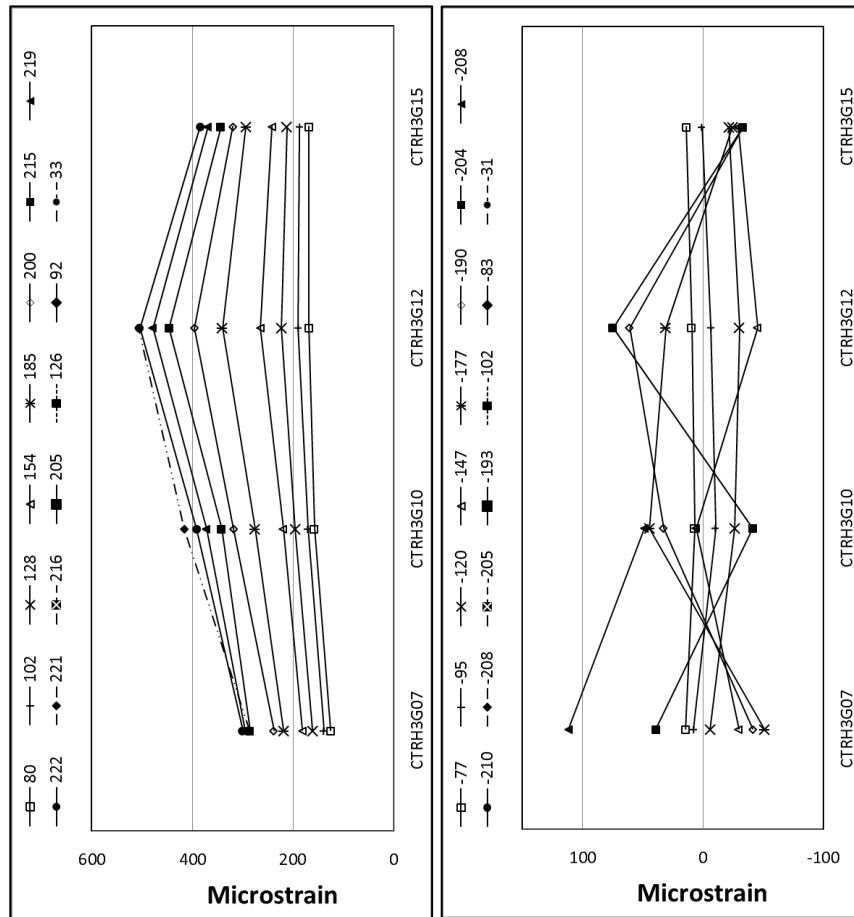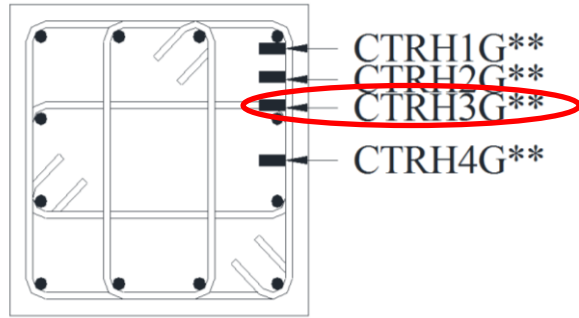
Figure 112. SP8 strain profile of CTRH3G in the positive and negative directions

125

Chapter 5

Part I: Discussion of Test Results

In this chapter a continuation of the analysis of the test data will be presented as a form of discussions into key aspects observed during testing. First the unique characteristics of UHP-FRC will be explored through a comparison of the elastic behavior of both specimens. Next, a closer look at the damage progression and failure mechanisms of each column specimen will be discussed as well as another look at the use of UHP-FRC and how its material characteristics improve the seismic performance of structural members. The discussion of test results will be concluded with a brief investigation into the effectiveness of transverse reinforcement of columns extending into the footing.

5.1 Elastic behavior of column specimens

The determination of an accurate modulus of elasticity of the developed UHP-FRC mix is of great importance when calculating the deflection of structural members. ACI offers a simplified equation to predict the modulus of elasticity for normal weight plain concrete in terms of concrete strength

$$E_c = 57,000\sqrt{f'_c}$$

Previous equations describing the relationship between modulus of elasticity and concrete strength of UHP-FRC have been derived based on compression tests of 3 in. diameter 6 in. long cylinders (Graybeal, 2007). The equation derived by Graybeal (2007) follows the same form as the previously mentioned ACI equation.

$$E_c = 46,200\sqrt{f'_c}$$

It has also been observed that a disparity in concrete strength and compressive strain may be present when comparing different size and different geometry specimens cast with the same high strength concrete mix (del Viso et al., 2008). The specimen

geometry of the high strength concrete cylinder and cube specimens tested by del Viso et al. (2008) and the corresponding compressive stress-strain curves are shown in Figure 113. As differences in UHP-FRC mix designs and casting sizes may vary significantly, this will also introduce additional variables not considered in previous research.
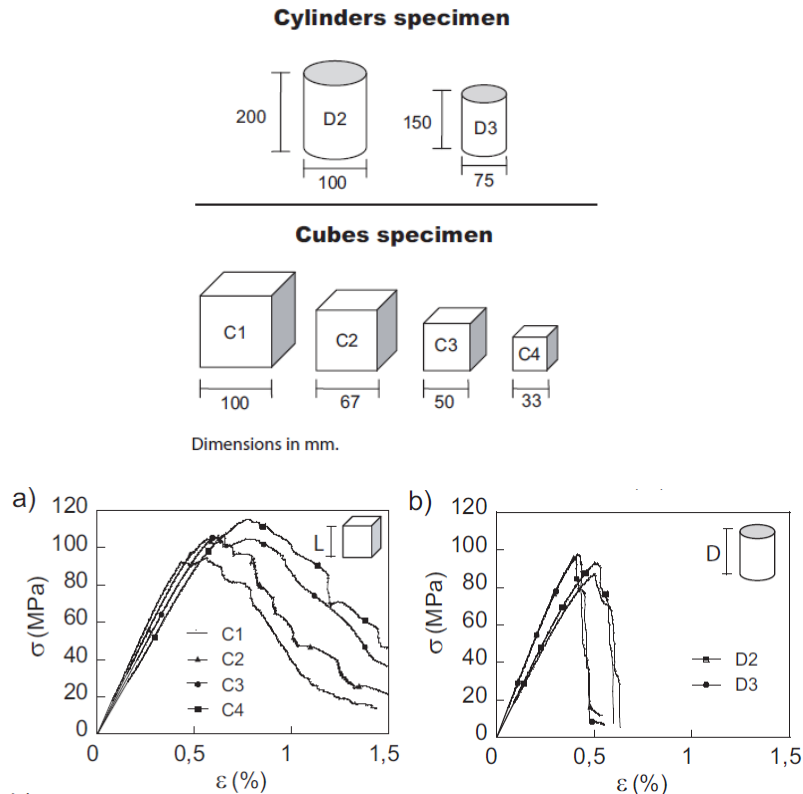
Figure 113. Specimen geometry and compressive stress-strain curves (del Viso et al., 2008)

In order to eliminate such discrepancies the modulus of elasticity was approximated directly from the full-scale column test. Prior to the start of the test, a small displacement cycle was applied in both directions; no concrete cracking was induced at this loading. The modulus of elasticity of the normal strength concrete column specimen was approximated using the test results through a simplified structural analysis approach.

It can be idealized that the modulus of elasticity of the upper portion of column SP8 will have a modulus of elasticity (E), and thus the UHP-FRC section will have a modulus of elasticity (vE), where v is a modification factor used to obtain the modulus of elasticity of only the UHP-FRC section in terms of the modulus of elasticity of the RC section. Through structural analysis and linear regression iteration, a composite modulus of elasticity of 4,000 ksi was obtained for specimen SP5. Considering the volume of the longitudinal reinforcement is less than 1.5% of the total volume, the modulus of elasticity of the concrete alone was found to be 3,700 ksi or 90% of that predicted by the ACI equation for the modulus of elasticity of normal strength concrete. Interestingly, the derived modulus of elasticity of the UHP-FRC section was found to be 95% of that of normal strength concrete (3,500 ksi), or about 50% of the modulus of elasticity predicted by Graybeal's equation. Figure 114 shows a comparison of the SP8 test results with the linear displacement calculated from the approximated elastic modulus and the predicted elastic modulus calculated from Graybeal's equation. It should be noted that the elastic modulus equation derived by Graybeal was obtained from a commercially available UHP-FRC mix, while the UHP-FRC mix used for the SP8 column specimen was specifically developed for large scale casting at The University of Texas at Arlington (Aghdasi, 2013). This suggests that as UHP-FRC is still a new material, the previously developed equations should be used with caution as further research is still required in exploring various types of mix designs and their effect on the modulus of elasticity in relation to large scale castings.

Figure 114. Force vs. displacement of SP8

After the initial application of the axial force (1,176 kips), it was also observed that the UHP-FRC column displaced longitudinally 5% more than the RC column; this is consistent with the 5% difference previously observed in the modulus of elasticity (Figure 115).
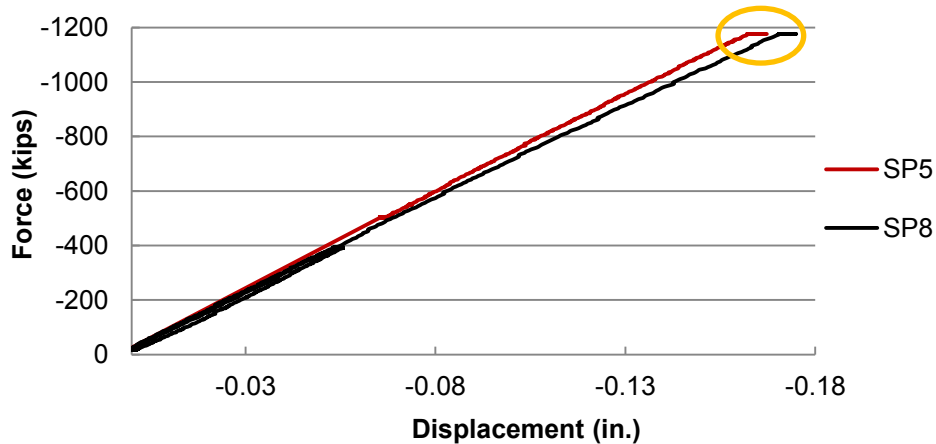
Figure 115. Axial force vs. axial displacement of SP5 and SP8

A unique strain distribution was also observed for the UHP-FRC column under the initial axial loading. The concrete strain gauges embedded within the column cross-section in the longitudinal position at 10 in. above the footing surface showed opposing compressive strain distributions for the RC column and the UHP-FRC column. In the RC column a higher compressive strain was observed in the core of the column while in the UHP-FRC column lower strains were observed in the core with slightly higher strains observed along the perimeter of the cross-section which includes the longitudinal reinforcement and the surrounding concrete (Figure 116).
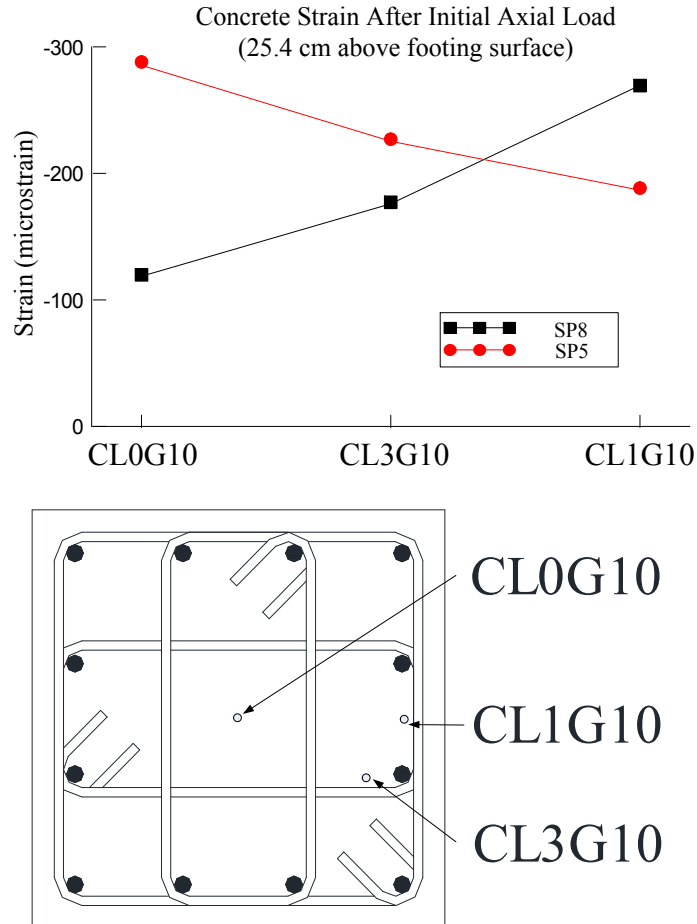
Figure 116. Concrete strain distribution after initial axial load;

A comparison of the average backbone curves for both columns can be seen in Figure 117. The first longitudinal bar yielding was observed near 0.75% drift for both specimens, this indicates that the column behavior at drifts before 0.75% is primarily controlled by the elastic mechanical properties of the concrete. Initially the RC column has a moderately higher lateral stiffness than the UHP-FRC column up to about 0.4% drift. After this point, the concrete cracking sustained by the RC column subjected to cyclic reversals becomes significant and the rate of the lateral load increase drops corresponding to the decrease in the moment of inertia, lowering the stiffness of the RC column. However, while the modulus of elasticity of UHP-FRC may initially be 5% lower than that of normal strength concrete, due to the very high compressive ductility of the UHP-FRC no cracking is observed at 0.4% drift and thus the load can be sustained longer.
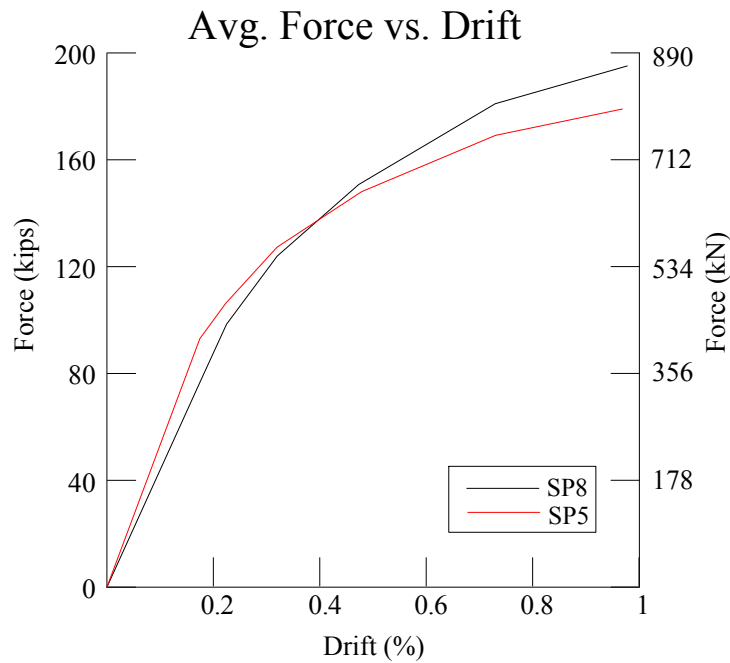
Figure 117. Comparison of full-scale RC and SP8 UHP-FRC column specimens

5.2 Seismic Performance Comparison

The force versus drift response and backbone comparison shown in Figure 118 and Figure 119 indicate that the UHP-FRC column could maintain strength up to nearly 4% drift ratio while the conventional reinforced concrete column deteriorated very fast after 1% drift ratio. While the axial load ratio ($P_u/A_g f'_c$) for the conventional concrete was 0.3, it dropped to 0.06 with the addition of UHP-FRC to the column due to the high compressive strength of the UHP-FRC. This smaller axial load ratio minimized the detrimental influence of the axial load effect at the post-elastic stage.
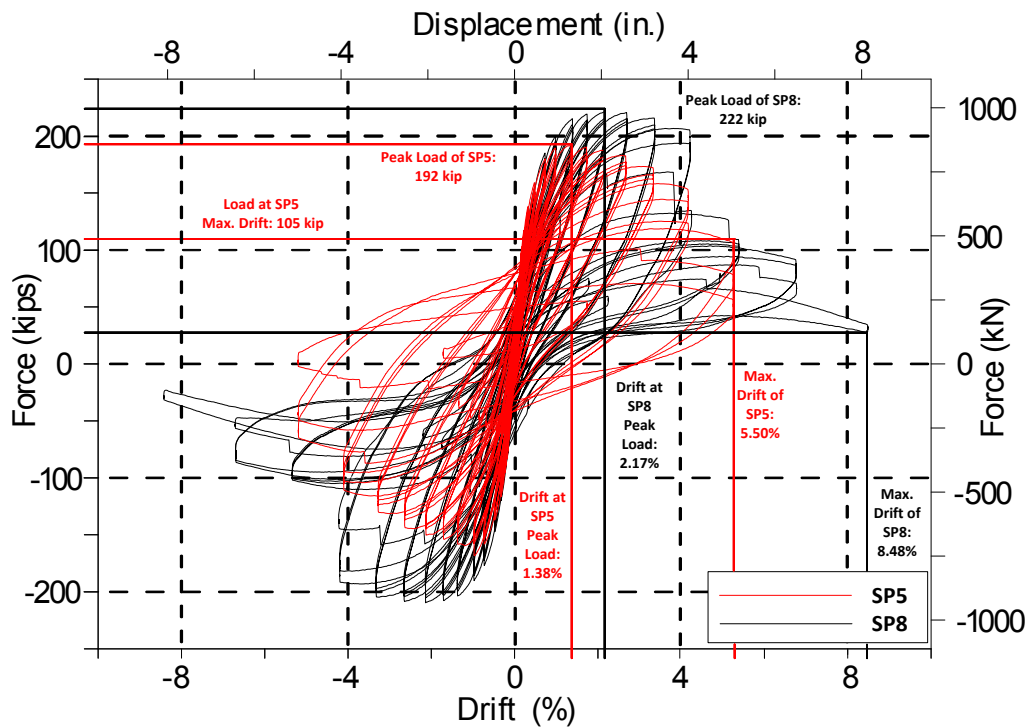
Figure 118.SP5 and SP8 force vs. drift comparison
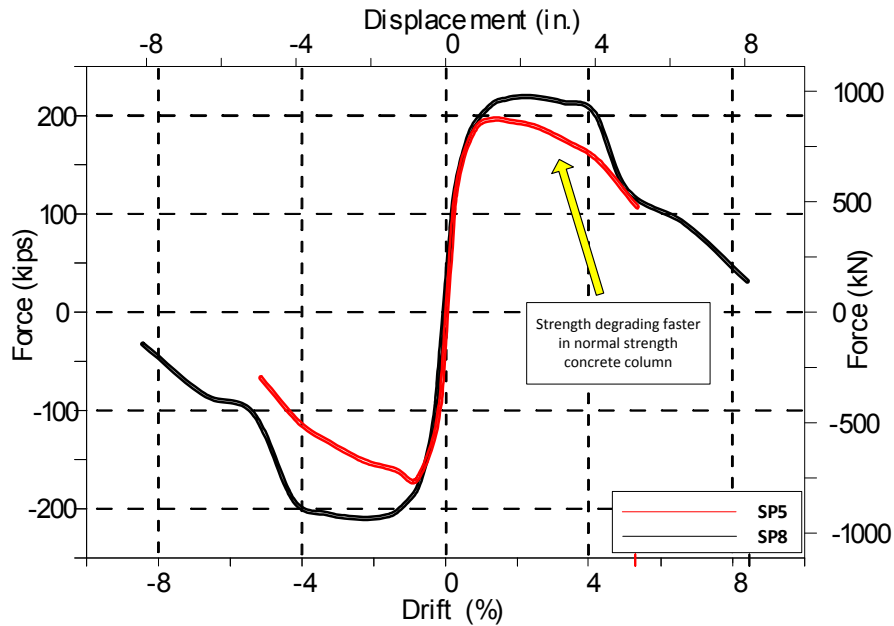
Figure 119. SP5 and SP8 backbone curve comparison

5.2.1 Direct strain gauge comparison

It is important to analyze the strain gauge information at similar loading for both column specimens to further understand the differences in the behavior of the RC column SP5 and the UHP-FRC column SP8. This comparison is done at a loading of 190 kips for column SP5, close to the peak load of 192 kips, and a load of 185 kips for SP8. First, observations will be made on the longitudinal and transverse reinforcement, followed by observations on the differences found in the embedded concrete strain gauges. The label notation and strain gauge location drawings were previously discussed in section 3.6 of this thesis.

Figure 120 shows the strain gauge locations corresponding to the longitudinal reinforcement. Figure 121 shows a strain profile for the longitudinal reinforcement in tension referred to as bars SL1 and SL2. Within the footing region, where conventional

133

concrete is used for both specimens, the strains in the longitudinal bars of both columns at this point are nearly identical. It can be easily seen that the highest strain is observed at the interface between the column and the footing for both columns, SP5 being slightly higher than SP8. It was also observed that in both cases the corner bar (SL1) recorded higher strains than the inner bar (SL2). Interestingly, a drop in strain occurs 6 inches above the footing for both SP5 and SP8. This may be due to a possible stub confinement effect that has been previously mentioned by other researchers (Legeron and Paultre, 2000; Bae and Bayrak, 2008), in which additional confinement is provided by the stub section. After this section, the strain profile for both specimens is noticeably different. In the case of SP5, the strain again rises at 9.5 in. above the footing, similar distance to which bar buckling was observed at the end of testing. At a height above 9.5 in. the strain is seen to gradually decrease as the distance from the footing surface is increased.

Within the plastic hinge region it was observed that specimen SP5 had higher strain values well above yielding up to a height of about 18 in. above the footing surface. However, in specimen SP8 no stub confinement effect was present and the only recorded strain above yielding was observed precisely at the column-footing interface much lower strains were recorded within the plastic hinge region well below yielding and steadily decreasing up to a height of 30 in. Above 30 inches the there is a slight increase in strain up to a height of 42 in. (the region where the UHP-FRC section ends and RC begins) then once again drops to nearly zero strain at 48 inches. At 42 inches the recorded strain is nearly identical for both SP5 and SP8, the major differences are observed within the UHP-FRC section, or the first 40 in.
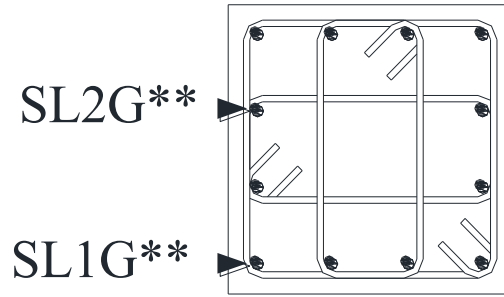
Figure 120. Location of longitudinal bar strain gauges
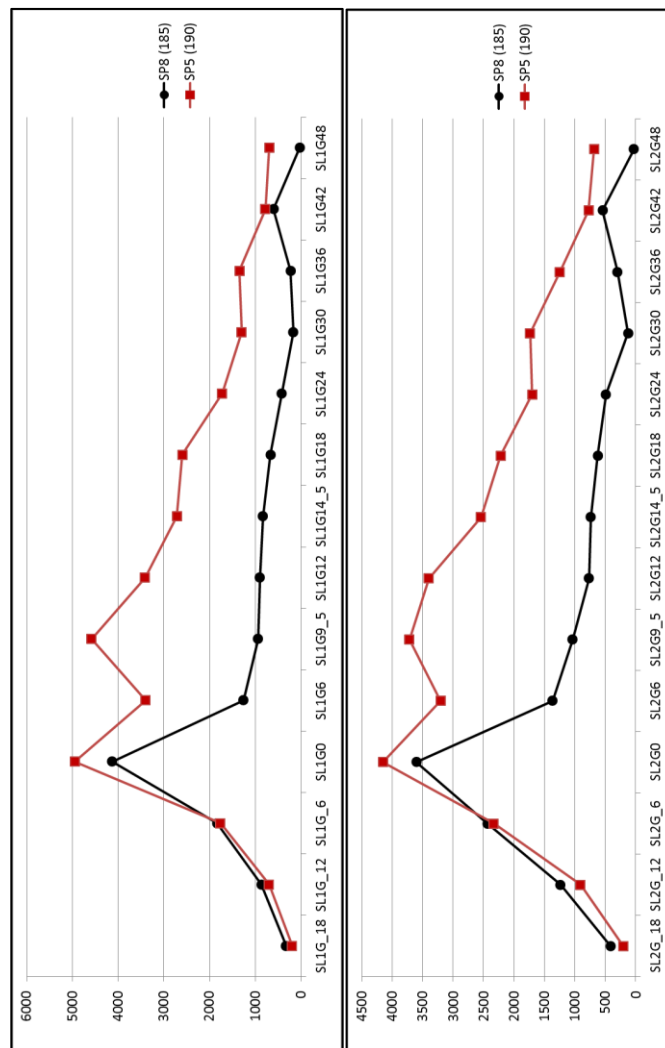
Figure 121. Comparison of bars SL1 and SL2

135

Figure 122 shows a comparison of the two longitudinal bars in compression (SL3 and SL4). It can be observed that for column SP5 the corner bar (SL3) has higher peak compressive strains than the inner bar (SL4), while SP8 the strain distribution in the two bars appear to be nearly identical. SP5 shows higher compressive strains in the longitudinal bars compared to SP8 suggesting that most of the compressive forces in specimen SP8 are being shared by both the reinforcing bars and the UHP-FRC, while in the case of SP5 the increased concrete degradation during the cyclic loading reversals has lowered the concrete contribution and distributed a larger amount of compressive stresses to the longitudinal reinforcement. SP5 has peak compressive stresses at the interface. Within the footing the compressive strains decrease rapidly, while along the height of the column the compressive strains decrease steadily. However, SP8 has a peak compressive strain 6 in. within the RC footing with significant strains also being observed at the interface. In the region within the footing higher strains where observed for column SP8 compared to column SP5, and at 45 in. above the footing surface, outside the UHP-FRC region, both specimens recorded nearly identical strains.
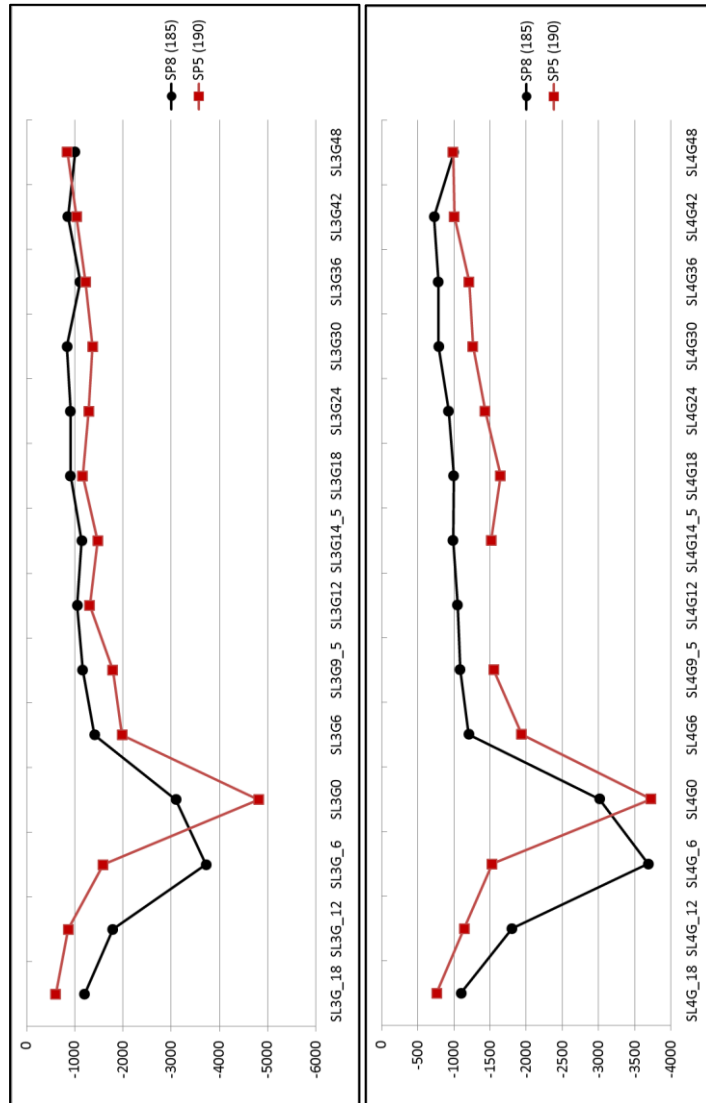
Figure 122. Comparison of bars SL3 and SL4 in compression

In comparing the transverse reinforcement, it should be noted that some concrete crushing was beginning to be observed near this loading, no significant damage had yet occurred, thus the transverse reinforcement had not yet been fully engaged. With this in mind, most of the observed strains at this loading were very minor and thus only some noticeable comparisons will be discussed.

The first notable comparison is made in the core region of the columns, strain gauge location STR6 (Figure 123). Figure 124 shows the strain of the inner hoop at location STR6. From Figure 124 it can be observed that within the inner core of the column, SP8 recorded very minor strains (below 150 microstrain) while STR6 in SP5 showed significant strain close to yielding more specifically at 7 in. above the footing surface. This is also consistent with the bar buckling observed near this height after testing (Figure 136).
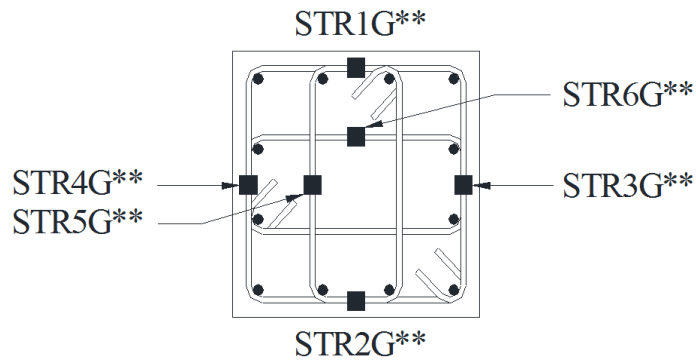
Figure 123. Transverse reinforcement strain gauge locations
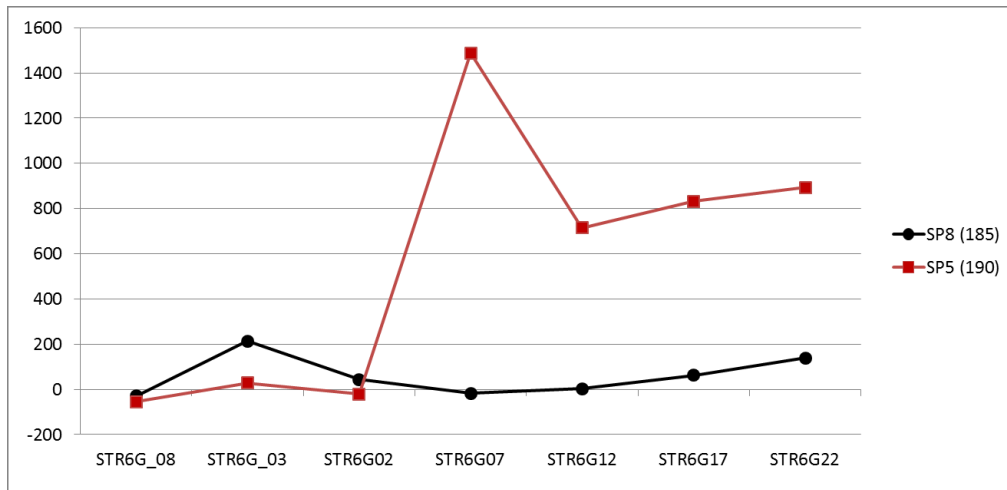
Figure 124. STR6 along column height

Figure 125 and Figure 126 show the transverse reinforcement strain comparison at a cross-section located at 12 in. and 22 in. respectively. Even though significant concrete damage is not visible in the exterior of the two column specimens, it can already be perceived that the strains in the transverse reinforcement of SP5 are greater than that observed in SP8.
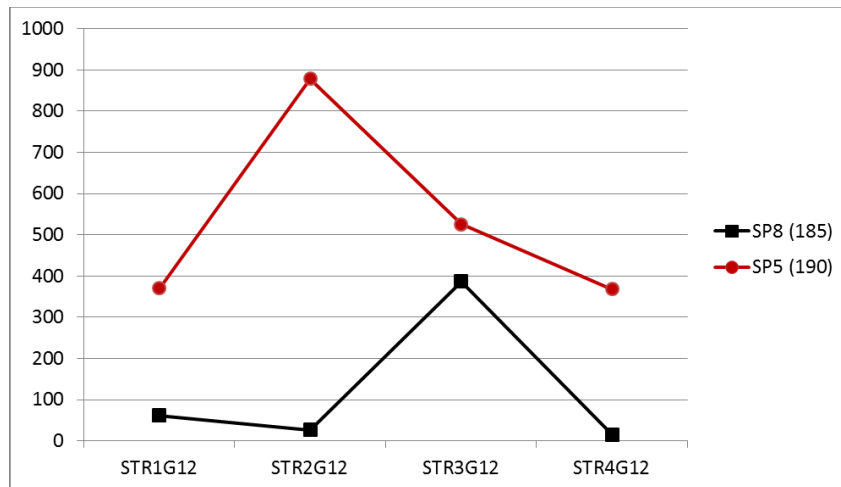
Figure 125. Transverse reinforcement strain at 12 in.
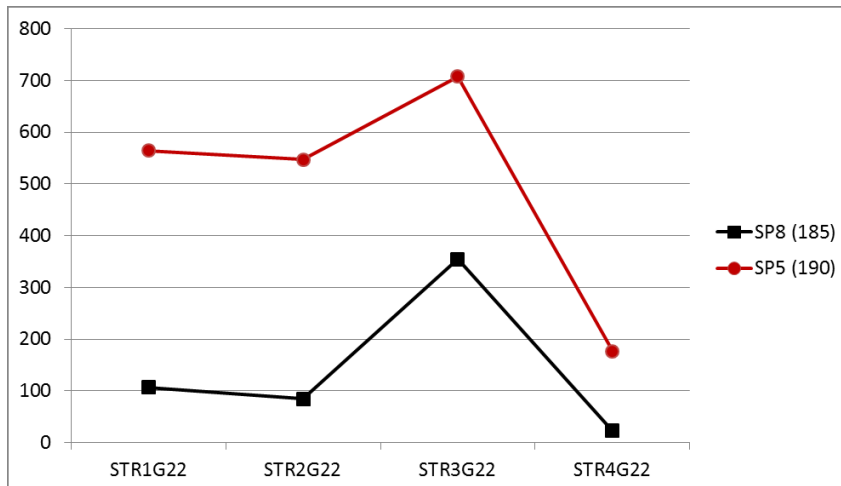
Figure 126. Transverse reinforcement strain at 22 in.

The comparison between the embedded concrete strain gauges is of great importance as it directly evaluates the differences between the conventional concrete used in SP5 and the UHP-FRC mix used in SP8. Figure 127 shows the locations of the CTRH concrete strain gauge series. These gauges are located in the positive direction of loading.
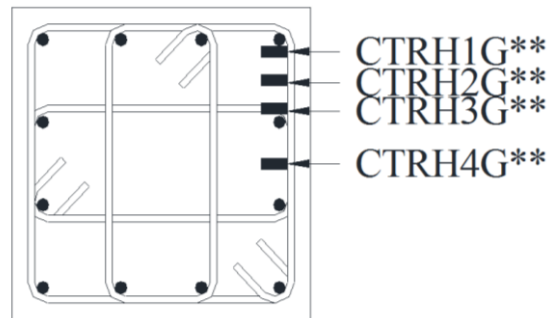
Figure 127. CTRH series locations

Figure 128 through Figure 131 show the comparison of the CTRH concrete strain gauge series along the height of the column. All peak strain values of column SP5 occurred at 10 in. above the footing surface, this location is consistent with the reduction in core concrete and buckling of the longitudinal reinforcement observed after the end of testing. The concrete strain gauges CTRH1, CTRH2, and CTRH3 located near the corner exhibited higher strains than CTRH4 at locations in between hoops. Lower strain values can be seen at 7 and 12 in. due to confinement from the transverse reinforcement. No such hoop confinement effect was observed in SP8 suggesting a possible reduction in transverse reinforcement would not greatly affect the confinement of the UHP-FRC core. All SP8 values were below 1,000 microstrain with the highest strain being 5 in. into the footing.
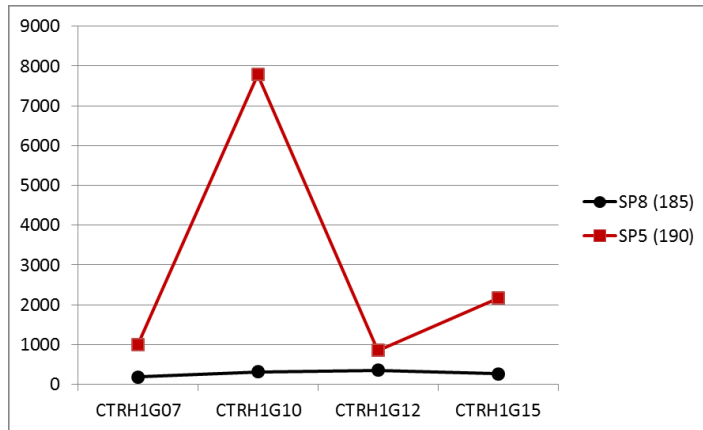
Figure 128. CTRH1 series along height
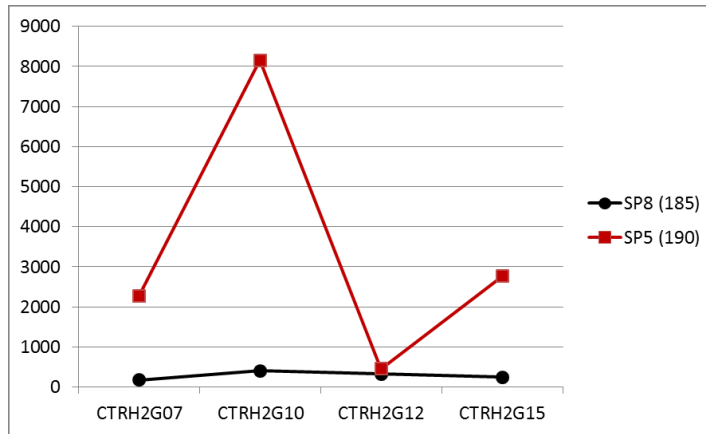
Figure 129. CTRH2 series along height
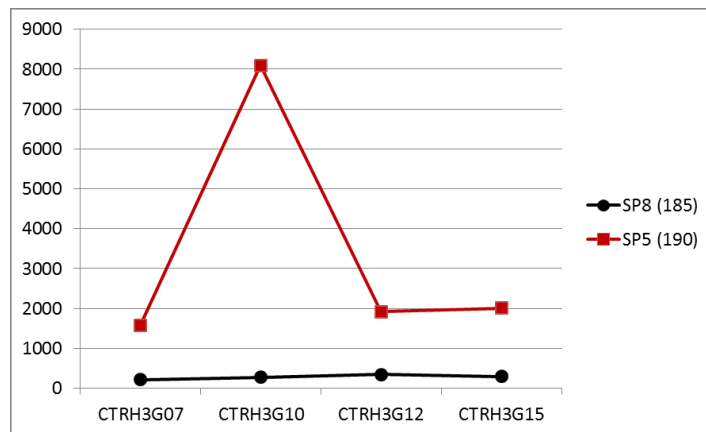
Figure 130. CTRH3 series along height

141
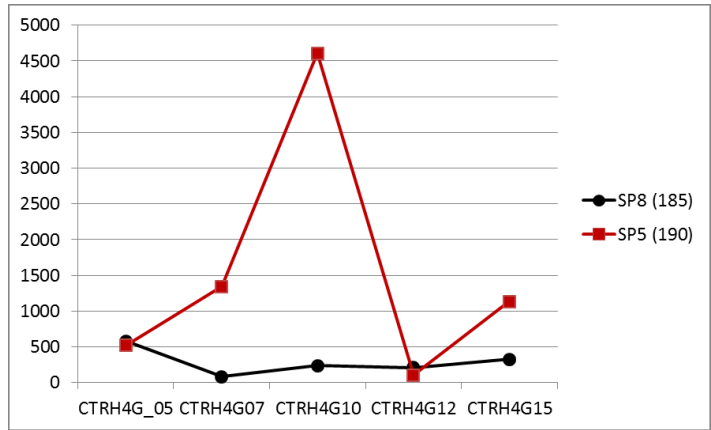
Figure 131. CTRH4 series along height

The locations of the CTRB concrete strain gauge series can be seen in Figure 132. The CTRB series was placed perpendicular to the direction of loading, hence the strain recorded in this direction was generally lower compared to the CTRH series. In this case, both column specimens recorded minor strains but the same trend being observed (Figure 133 and Figure 134). SP5 recorded very minor strains all below 1000 microstrain and SP8 recorded even lower strains all below 312 microstrain.
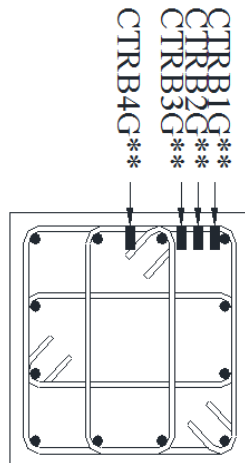
Figure 132. CTRB series locations
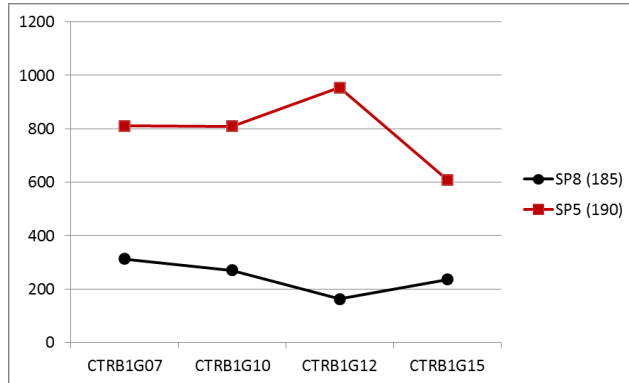
Figure 133. CTRB1 series along height
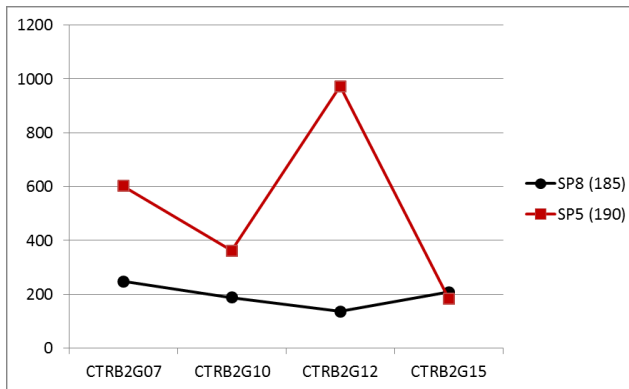
Figure 134. CTRB2 series along height

Figure 135. SP5 at the end of testing

143

Figure 136. SP5 bar buckling and rupture

The strain gauge observations were consistent with the damage observed at the end of the testing of column SP5 with the highest reduction in core concrete was seen to be between 7 in. and 12 in. Bar buckling was also observed in this region. From this direct comparison it is clear to see the differences in the strain distribution of the two specimens due to the properties of UHP-FRC. No hoops yielded up to the peak load of column SP8 suggesting that transverse reinforcement may be reduced with the use of UHP-FRC potentially reducing costs and facilitating construction. The highest hoop strain was observed 3 in. below the footing surface.

5.3 Effectiveness of transverse reinforcement of columns extending into footing

As previously discussed, In order for buildings in areas of high seismicity to perform adequately during an earthquake they must be properly detailed. However, some detailing can be overly conservative and may lead to congestion of the reinforcing bars and increased difficulties during construction and concrete placement. If some of the reinforcement can be reduced, it would facilitate the construction process allowing the building to be finished quickly and more efficiently. One problematic area in which the reinforcement may be reduced is the transverse reinforcement of columns extending into footings. Therefore, additionally to the comparison of columns SP5 and SP8 a brief investigation was done on the effectiveness of the transverse reinforcement of columns extending into the footing for all eight full-scale column specimens.

5.3.1 ACI Provisions

Currently, ACI 318-14 section 18.10.6.4g specifies that for a special boundary element terminating at a footing, mat, or pile cap, the special boundary element transverse reinforcement shall extend at least 12 in. into the footing, mat, or pile cap. In the case where columns or boundary element have an edge located within one-half the footing depth from an edge of the footing, ACI 318 section 18.13.2.3 states that the transverse reinforcement must extend into the footing, mat, or pile cap and be developed for f_y in tension (Figure 137). The exact distance that the transverse reinforcement shall extend is not clearly defined. The detailing specified in ACI 318 section 18.10.6.4g and section 18.13.2.3 aim to prevent failure of the column within the footing such as an edge failure of the footing, pile cap, or mat. However, no full-scale testing has been conducted to verify such provisions.

Recent tests performed on full-scale modern high-rise moment frame columns with both normal strength concrete and UHP-FRC under extreme loading conditions have

shown that damage is primarily concentrated above the footing region. No footing failure was observed with minor strain recorded in the transverse reinforcing bars of the column region located within the footing.
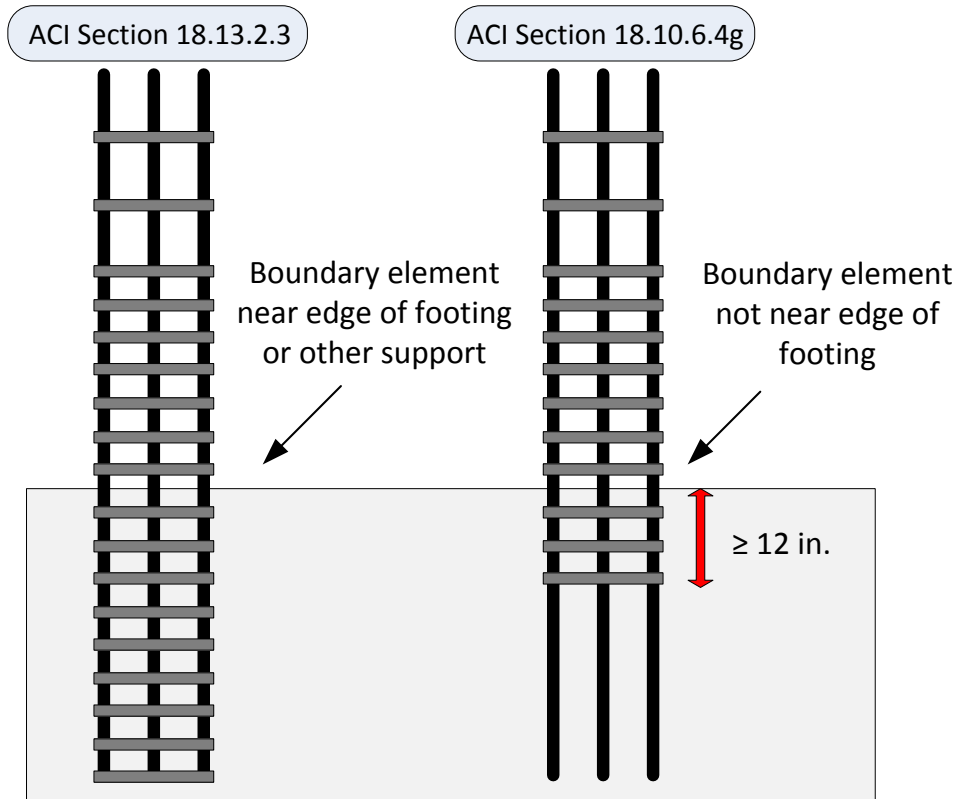
Figure 137. Reinforcing details for footings, mats, and pile caps per ACI sections 18.13.2.3 and 18.10.6.4g

In a number of structural situations concrete is exposed to a combination of stresses which greatly alter its behavior. In a classical study Richart et al. (1928) tested a series of concrete cylinders applying a liquid pressure along laterally while simultaneously loading them under axial compression. The researchers discovered that the general strength and ductility of concrete is greatly increased under the confinement

of triaxial compression. This is the case for the concrete located in the column section below the footing surface where it is confined under triaxial compression by the applied loading and surrounding concrete, thus this area would be significantly stronger than its uniaxial compressive strength. To validate the necessity of transverse reinforcement below the surface of the footing block. The test specimens were designed according to a prototype 20-story high rise building in accordance with Chapter 18 of ACI 318-14. A series of eight full-scale reinforced concrete columns were tested under various loading protocols created to simulate extreme-earthquake type loading with large lateral displacements.

5.3.2 Specimen Description

A total of eight full-scale specimens were investigated to demonstrate the effectiveness of the column transverse reinforcement located within the footing. Two different types of cross-sectional dimensions were examined, six perimeter frame columns with dimensions of 36x28 in., and two space frame columns with dimensions of 28x28 in. one of which was constructed with UHP-FRC in the plastic hinge region (SP8). Each specimen was comprised of a 75x75x23 in. loading block, a 106 in. tall column section placed at a 45 degree angle, and a 84x84x30 in. footing block. The loading block and the footing block were both reinforced with two layers of No. 8 flexural reinforcement placed in both directions (Figure 139). The perimeter frame columns were reinforced with 16 No. 9 longitudinal bars and the space frame columns were reinforced with 12 No. 8 longitudinal bars. No. 5 transverse reinforcement was used for both columns spaced at 5 or 6 in. depending on the distance from the column base. The transverse reinforcement was spaced at 5 in. within the footing and extended along the length of the column below the base for both types of columns with the exception of SP7 and SP8. In specimens SP7 and SP8, the bottommost two layers of transverse reinforcement were removed within

147

the footing as shown in Figure 138. The No. 8 and No. 9 longitudinal bars met the requirements of ASTM A706 Grade 60 while the No. 5 transverse reinforcing bars were ASTM A615 Grade 60.

All specimens were constructed at the University of Texas at Arlington and cast in the upright position as to simulate real world construction (Figure 139). The footing block was cast first with self-consolidation concrete with a specified 28-day compressive strength of 5,000 psi. After the concrete had hardened the column formwork was erected and the column and loading block sections were subsequently cast. After casting, the specimens were then shipped to the University of Minnesota for testing.
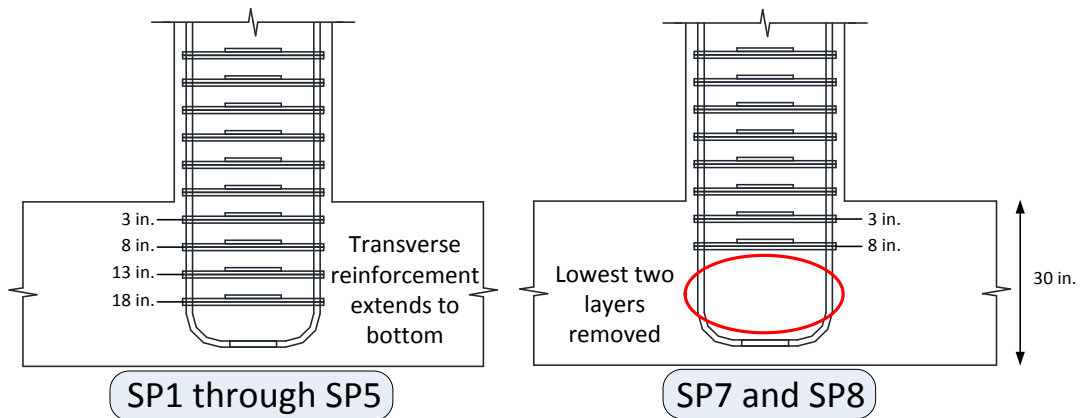
Figure 138. Column specimen transverse reinforcement layout within footing

Figure 139. SP3 column and footing cage prior to casting

5.3.3 Instrumentation within footing

The column transverse reinforcement below the footing was instrumented with rebar strain gauges and concrete strain gauges were also utilized located as shown in Figure 140 and Figure 141 respectively. Concrete strain gauges were utilized to measure the strain in the areas in which the transverse reinforcement was removed. The concrete strain gauges were placed at 5 in, 8 in., and 18 in. below the footing surface on the south-east end parallel to the direction of loading.
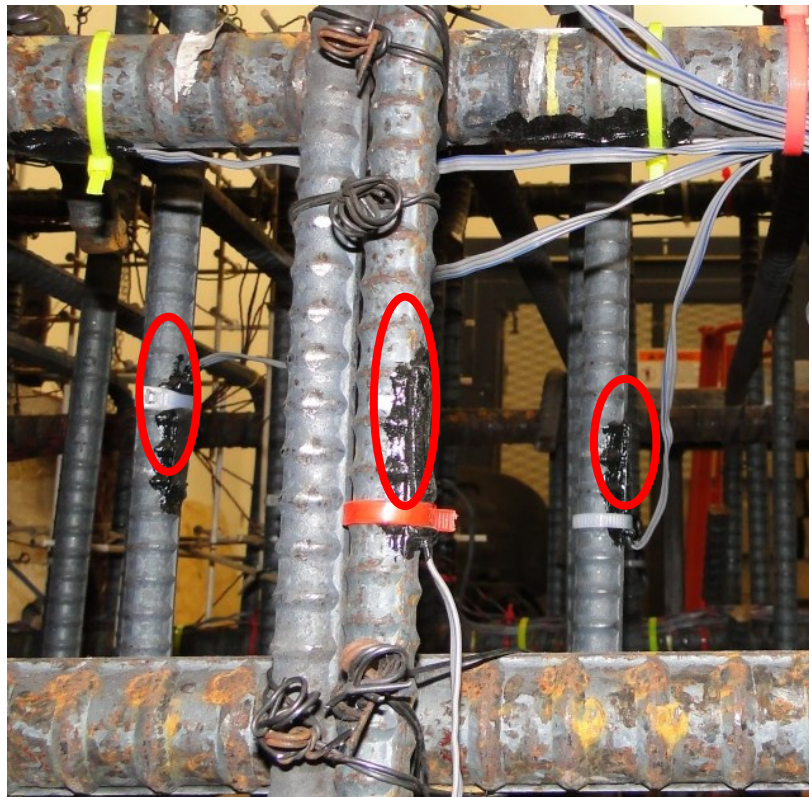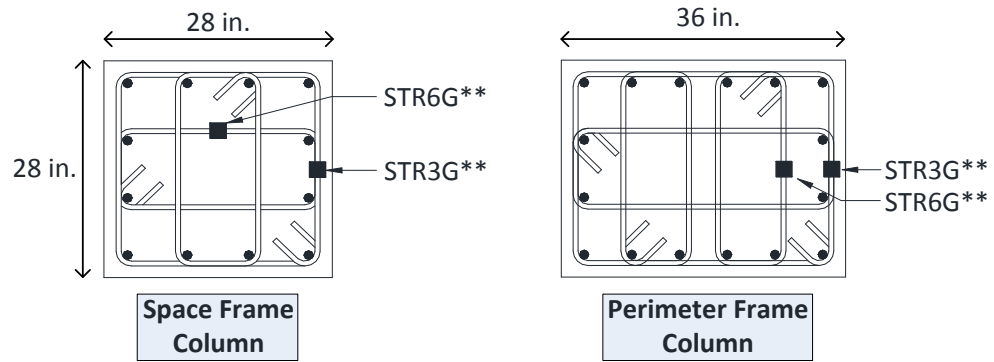
Figure 140. Location of rebar strain gauges for space frame and perimeter frame columns

Space Frame Column

CL2G**
CL1G**

CTRH2G**
CTRH4G**
CTRH5G**
CTRB5G**

Perimeter Frame Column

CL2G**
CL1G**

CTRH2G**
CTRH4G**
CTRH5G**
CTRB5G**
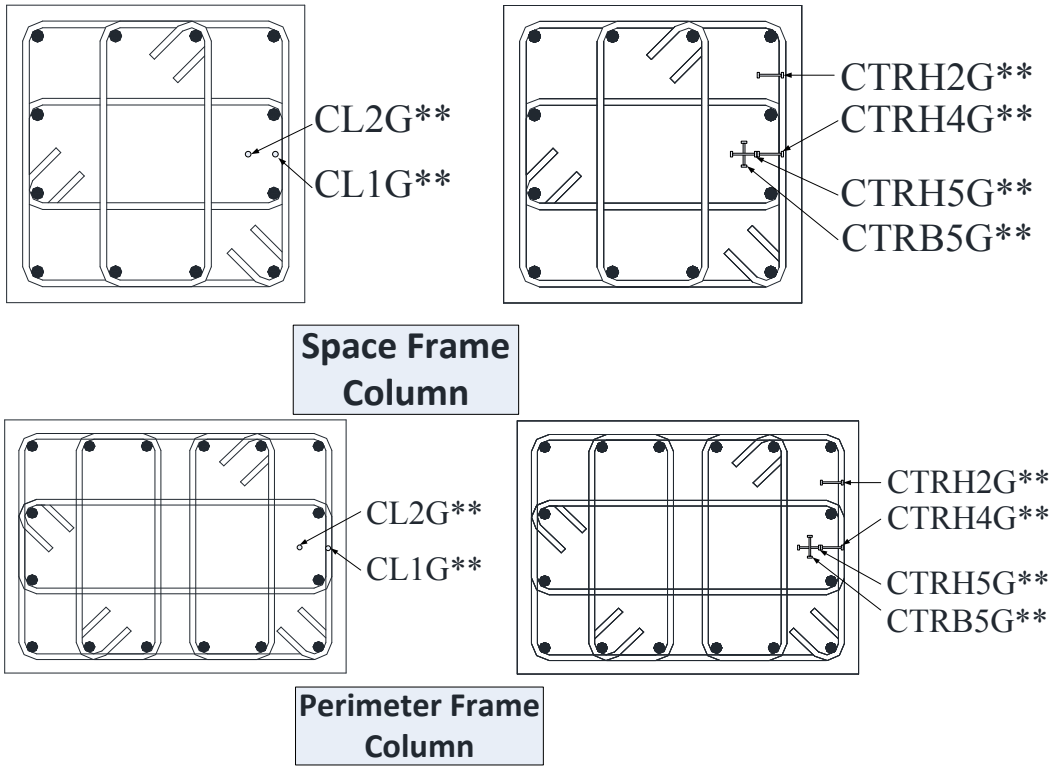
Figure 141. Location of concrete strain gauges for space frame and perimeter frame columns

5.3.4 Loading Protocols

All specimens were tested at the MAST laboratories located at the University of Minnesota. The eight column specimens were tested under six distinct loading protocols. Before the start of the loading protocol, each specimen was first subjected to an axial load of 756 kips, or 1,176 kips corresponding to 0.15f'cAg, or 0.3f'cAg (for 5 ksi concrete) for the perimeter frame columns and space frame columns respectively. The six loading protocols were made up of a monotonic loading protocol (SP1), a near collapse loading protocol (SP6), five cyclic loading protocols based on ACI 374-05 (SP2, SP3, SP4, SP5 and SP8) , and one bi-directional cyclic loading protocol also based on ACI 374-05 (SP7). The six loading protocols can be seen in Figure 142. Two criteria were established for stopping the test. The first criterion is defined by strength degradation, in which the residual strength drops to 20 percent of the peak strength. The second criterion is controlled by the maximum stroke angle of the hydraulic actuators.
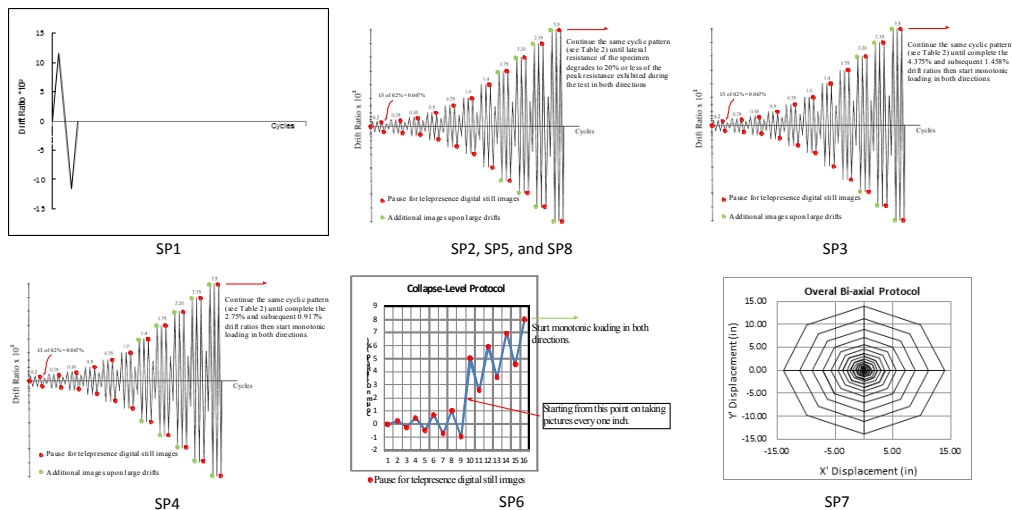
Figure 142. Applied loading protocols

5.3.5 Summary of experimental results

Most damage was concentrated to the plastic hinge region of the column above the footing (Figure 143). No footing failure was observed in any of the eight columns with

very minor damage detected in the column region located within the footing. The strain gauge data recorded minor strain in the footing below yielding. The load deflection envelopes of the eight specimens are shown in Figure 144 and the strain gauge results of the eight specimens are summarized in Table 5 and Table 6. Figure 145 shows the transverse reinforcement strain profile of column specimen SP5 within the footing and the concrete strain gauges located within column SP8. It is important to note that the strain is significantly reduced as the distance from the footing surface is increased, and all hoops remain well below yielding. More importantly, In the region where the transverse reinforcement was removed (SP8), the concrete strain was recorded continued to be minor. Observations are consistent with all 8 full-scale column tests under varying loading protocols.

Figure 143. SP3 column subjected to a symmetric cyclic loading protocol

Backbone Curve Column Comparisson
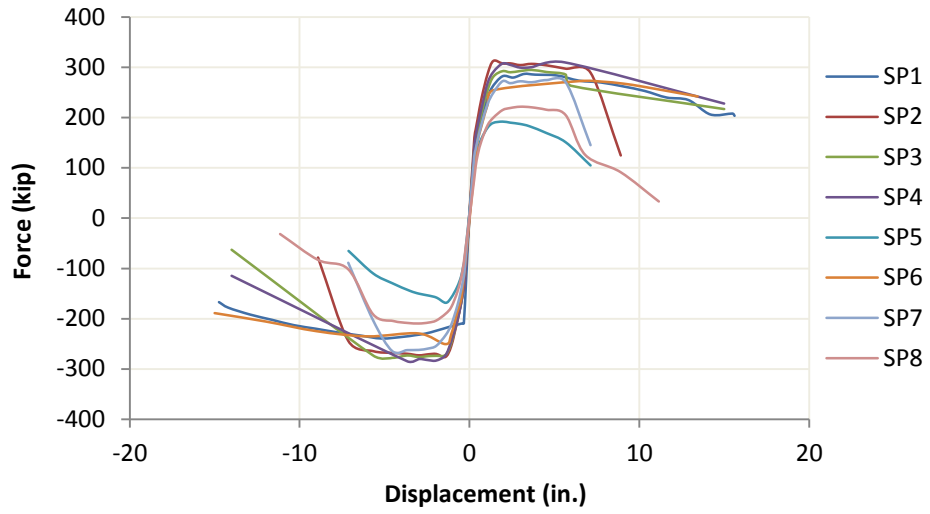
Figure 144. Backbone curve column comparison of all test specimens

Table 5. Summary of column performance and maximum transverse reinforcement strain

within footing

Specimen	Peak Force (Kips)	Disp. At Peak Force (in)	Max Hoop Strain in Footing at Peak Force (microstrain)	Max Hoop Strain in Footing (microstrain)	Disp. At Peak Strain (in)
SP1	290	4	862	1383	15.6
	-240	-5.15	195		
SP2	314	1.39	259	1063	2.13
	-278	-1.4	392		
SP3	296	2.97	626	642	3.66
	-278	-4.52	-84		
SP4	310	6.11	805	960	13.98
	-288	-1.95	-20		
SP5	192	1.95	167	921	-2.21
	-168	-1.4	40		
SP6	280	4.44	1661	2339	13.41
	-257	-1.41	-28		
SP7-Y	279	4.54	1903	1988	7.13
	-268	-4.54	-259		
SP8	222	2.97	1376	1683	4.52
	-209	-2.97	362		

Table 6. Concrete strain gauge summary for locations with no transverse reinforcement

Specimen	Max Strain (microstrain)			
	CTRH5G_08	CTRH5G_18	CTRB5G_08	CTRB5G_18
SP7 Y Pos	2672	174	1057	170
SP7 Y Neg	1525	11	117	117
SP7 X Pos	1811	20	396	318
SP7 X Neg	1479	43	1092	102
SP8 Pos	443	225	329	121
SP8 Neg	142	25	139	64
All	2672	225	1092	318
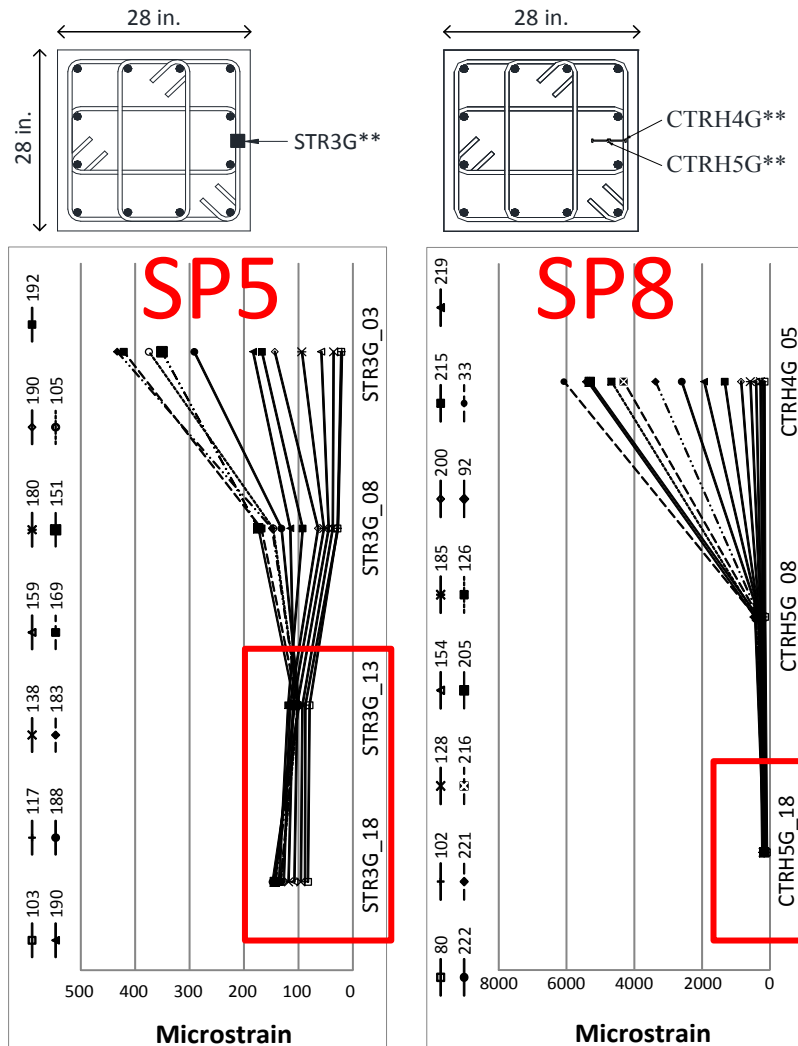
Figure 145. SP5 transverse reinforcement strain profile

The first perimeter frame column specimen (SP1) was tested under monotonic displacement in both directions reaching peak strength of 290 kips at 4 in. displacement. No yielding was observed in any of the transverse reinforcement below the footing. The highest strain observed was STR6G_03 with a strain of 0.001383. The second perimeter frame column specimen (SP2) was tested under a cyclic loading protocol based in part on the guidelines provided by ACI 374-05. SP2 reached a peak strength of 313 kips at

1.39 in. The highest strain observed for SP2 occurred 3 in. below the footing in STR68_08 at only 0.000813 well below yielding. The third perimeter frame column specimen (SP3) was tested under a symmetric cyclic loading protocol with a peak strength of 296 at 2.97 in. The highest strain below the footing was observed on STR3G_03 at .000642 well below yielding. The fourth specimen (SP4) was subjected to a symmetric cyclic loading protocol followed by a monotonic push. SP4 reached a peak strength of 310 kips at 6.11 in. The highest strain observed below the footing was once again on the first transverse reinforcement 3 in. under the surface STR3G_03 at only .000937. The fifth specimen (SP5) is a space frame column. SP5 was also tested under a symmetric cyclic loading protocol and reached a peak strength of 192 kips at 1.95 in. The highest strain observed on the space frame specimen occurred in the negative direction and was 3 inches below the surface at STR3G_03 at only .000639. Specimen SP6 was a perimeter frame column subjected to more realistic near collapse loading protocol with unsymmetrical loading reversals. SP6 had a peak strength of 280 kip at 4.44 in. The transverse reinforcement 3 in. below the footing of SP6 at STR3G_03 had the highest strain of all tests and came the closest to yielding with a strain of .002334. SP7 was a perimeter frame column subjected to a bi-directional symmetric cyclic loading protocol and had the 2 bottommost transverse reinforcement bars removed. SP7 had a peak strength in the y-direction of 279 kip at 4.54 in. The highest strain recorded for SP7 was STR3G_03 with .001988 occurring in the positive y direction. The last specimen was tested was a space frame column subjected to the same symmetric cyclic loading protocol as the previous space frame column SP5. However, the major differences in SP8 were that the two bottommost transverse reinforcing bars had been removed and the first 40 in. of the column above the footing was cast with UHP-FRC. As previously presented, due to the characteristics of UHP-FRC, specimen SP8 failed in a distinct

manner and reached a peak load of 222 kips at 2.97 in. The highest strain below the footing was observed at STR3G_03 with .001683 still below yielding.

5.3.6 Observations of strain within footing

The longitudinal bars below the footing are well confined by concrete from all sides even when the column is located near the edge of the footing. Test results showed that no footing failure was observed in two types of columns subjected to a variety of very demanding loading protocols with large displacement reversals as would be seen in severe earthquakes. It was also observed that the transverse reinforcement below the footing recorded minor strain well below yielding during all eight tests, the highest strain being observed at a distance of 3 in. below the footing. The current ACI provisions that require the transverse reinforcement at the footing ends to extend to 12 in. below the footing surface, or in some cases the total length of the column within the footing, may be relaxed to only the first hoop below the footing surface or 8 in. below the footing surface. The suggestions are based on experimental test results that demonstrate that the transverse reinforcement in the footing region will not yield even during extreme conditions. The experimental results also showed that even with the removal of the last two transverse reinforcement layers to a length of only 8 in. below the footing surface, the performance of the column specimen was not affected and the concrete strains recorded were still considerably low.

<u>5.4 Discussion of UHP-FRC and ACI 318-14 seismic design provisions</u>

As introduced in Chapter 2, concrete is one of the world's oldest building materials and through the development of various admixtures the characteristics of concrete have greatly improved. For example, high strength concrete offers a wider

range of applications and higher quality properties which help it become a more popular alternative in today's structural designs and construction.

UHP-FRC is an emerging new material that takes a giant leap into the future of modern structural design. The mechanical characteristics are far superior to those of any previously developed concrete material; analogous to the improved strength and ductility of steel and the more brittle cast iron. UHP-FRC offers an interesting design alternative to be used in situations where typical reinforced concrete design is not feasible and when structural elements are subjected to extreme loading conditions. One interesting application is in the lower story columns of mid to high-rise moment-frame concrete structures located in seismic regions. The use of UHP-FRC in concrete columns can completely change the failure modes typically observed in conventional and high strength concrete columns subjected to earthquake type loading.

As presented in Chapter 2, the requirements currently stated in ACI 318-14 section 18.7.5 are to account for the brittleness of concrete and thus prevent a decrease in the axial load capacity of the columns after the loss of the shell concrete due to cover spalling. After cover spalling the longitudinal reinforcement is more susceptible to buckling, hence the transverse reinforcement is appropriately detailed to also prevent such mechanisms. The transverse reinforcement required in 18.7.5.4 is a function of concrete strength, this means that as the specified concrete strength increases so does the amount of reinforcement in the plastic hinge region. The excessive amount of transverse reinforcement required in such regions could result in construction difficulties and possible issues during concrete placement.

Typically, an increase in concrete strength will also result in an increase in brittleness, as is the case for HSC. However, UHP-FRC offers both high strength and high ductility due to the inclusion of high strength steel micro fibers, characteristics that

are not accounted for in ACI 318. The experimental test results presented in the previous chapters suggest that many of the current seismic design provisions in ACI 318 can be relaxed if UHP-FRC is used.

Requirements put into place to provide confinement, mainly the requirements of section 18.7.5 may be relaxed as shown in the small-scale column specimens and the full-scale testing. The small-scale column testing showed that by increasing the volumetric fiber fraction the same high column axial strength can be achieved regardless of the transverse reinforcement ratio. This suggests that the fibers are the main contributor to the confinement effect of UHP-FRC columns. The full-scale column testing verified the observations, as no concrete damage was observed and the transverse reinforcement in the UHP-FRC region was essentially elastic recording only very minor strains. Therefore, provisions regarding the amount (18.7.5.4), spacing (18.7.5.3), and arrangement (18.7.5.2) of transverse reinforcement may be significantly reduced if UHP-FRC is used. Additionally, detailing requirements such as the 135° seismic hooks are no longer necessary as the transverse reinforcement is not expected to open during earthquake loading if UHP-FRC is used due to the additional steel microfibers.

Essentially the design of UHP-FRC columns can be greatly simplified by reducing the confinement requirements. Furthermore, longitudinal reinforcement requirements (18.7.4) should be further explored along with the structural-stress strain characteristics. This suggests that because of the high compressive strength and ductility of UHP-FRC a smaller equivalent compressive stress block is expected, with higher strains well past 0.003 before concrete crushing, thus the design may be improved so that additional longitudinal reinforcement may be added while still remaining a tension-controlled section and an even higher strength and ductility may achieved than that observed in SP8. Additional requirements such as mechanical and lap splices in plastic

160

hinge regions may also be relaxed if UHP-FRC is used due to the improved bonding characteristics exhibited by UHP-FRC. The suggested improvements will not only simplify the design of UHP-FRC members, but also greatly simplify the construction of buildings in areas of high seismicity.

Chapter 6

Part I: Summary, Conclusions, and Recommendations

6.1 Summary

Two full-scale column specimens were tested at the NEES MAST facility at the University of Minnesota. The typical failure mode was observed in the RC column for normal strength concrete columns subjected to seismic loading. The first observable flexural cracks were seen at 0.5% drift at 8 in. and 16 in. above the footing. The first longitudinal bar yielded at 0.75% drift. The failure of the RC column initiated with concrete crushing at the corners of the column at 1.0% drift, soon after the crushing a decrease in strength was observed at 1.4% drift. As the cyclic reversals continued, the concrete cover was eventually lost, followed by the bulging and opening of the transverse reinforcement, and then the buckling and fracture of the longitudinal reinforcement. This deterioration resulted in a significant decrease in strength and eventual failure of the RC column.

The use of UHP-FRC completely changes the typical failure mechanism observed in concrete columns due to its high strength and high compressive ductility. There was no visible concrete damage observed in the plastic hinge region of the UHP-FRC column throughout the test. This allowed the longitudinal reinforcement to be utilized to its ultimate tensile capacity without buckling. Furthermore, transverse reinforcement in the UHP-FRC region recorded only minor strains of less than 50% yielding, suggesting that the transverse reinforcement may be significantly reduced in UHP-FRC columns allowing for less congestion and greater ease of construction.

Figure 144 compares both specimens, at similar loadings of 190 kip (SP5) and 185 kip (SP8), close to peak loading, with embedded concrete gauges at a cross-section of 10 in. above the footing and strain gauges on the longitudinal reinforcement along the height of the columns in the positive loading direction. This shows the measured concrete

tensile strains in the UHP-FRC column to be significantly lower than those in the RC column. Additionally, at the same loading, the longitudinal reinforcement of the RC column measured strains above yielding up to a height of 18 in., while the longitudinal reinforcement of the UHP-FRC column showed only a concentrated yielding at the interface between the column and footing surface at 6 in. below the footing surface.

Figure 145 compares both columns at 5.25% drift showing significant concrete crushing and bar buckling in the RC column with no visible damage detected in the UHP-FRC column. The UHP-FRC column failure was due to low cycle fatigue of the longitudinal reinforcement at the interface between the footing and the column section. The RC column reached a maximum lateral peak strength of 192 kips at 1.38% drift while the UHP-FRC specimen reached a lateral peak strength of 222 kips at 2.17% drift.

Overall the deformation of both columns during testing can be attributed to two very different mechanisms. Longitudinal bar yielding was recorded in the RC column from 6 in. below the footing to 36 in. above the footing with observable bar buckling and rupture within that range. However, the longitudinal bar yielding of the UHP-FRC column was concentrated from the column footing interface and penetrated 12 in. into the footing. Higher strains were also observed in the longitudinal reinforcement within the footing of column SP8 compared to the longitudinal reinforcement of specimen SP5; this is attributed to the high bonding strength of UHP-FRC and is responsible for the increased deformation of column SP8.
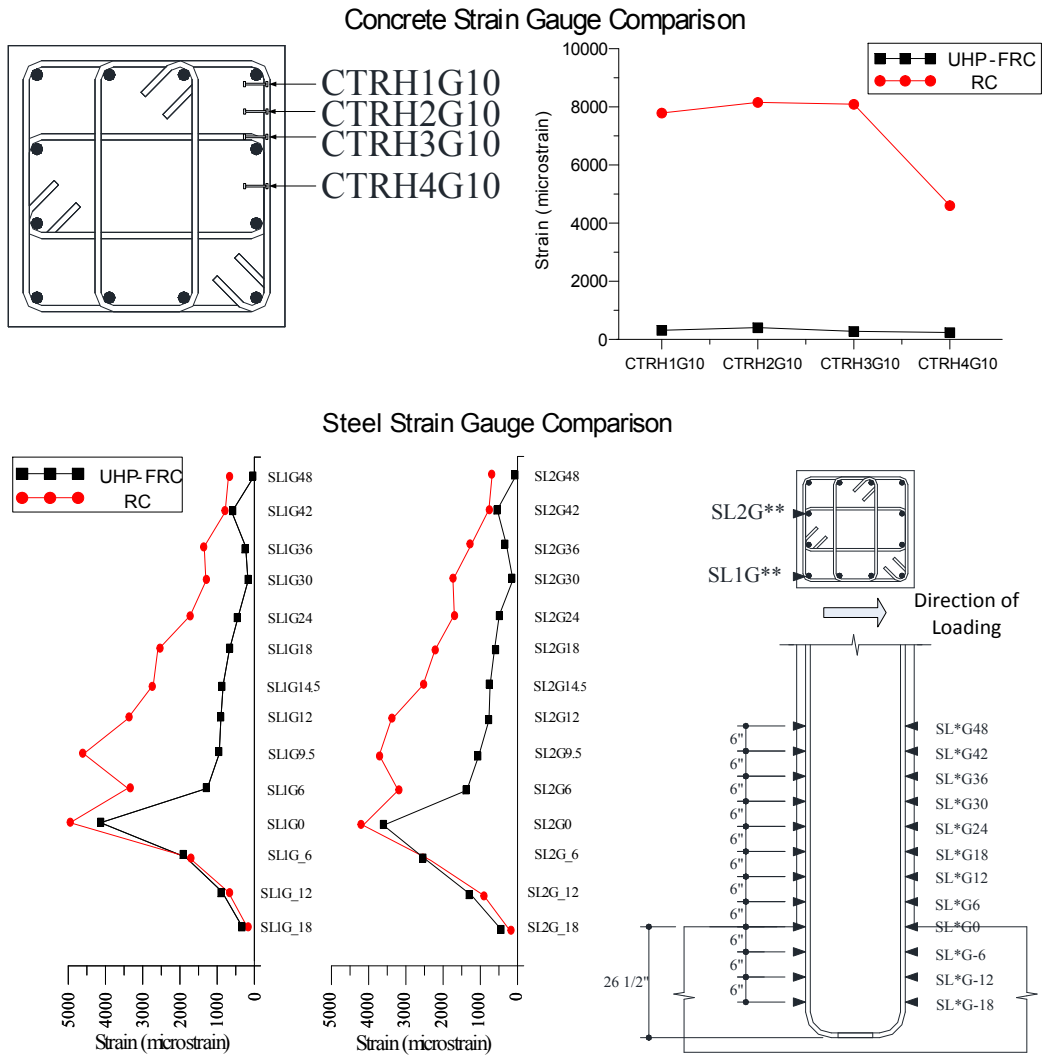
Figure 144. Concrete gauge and strain gauge comparison between RC and UHP-FRC

specimens
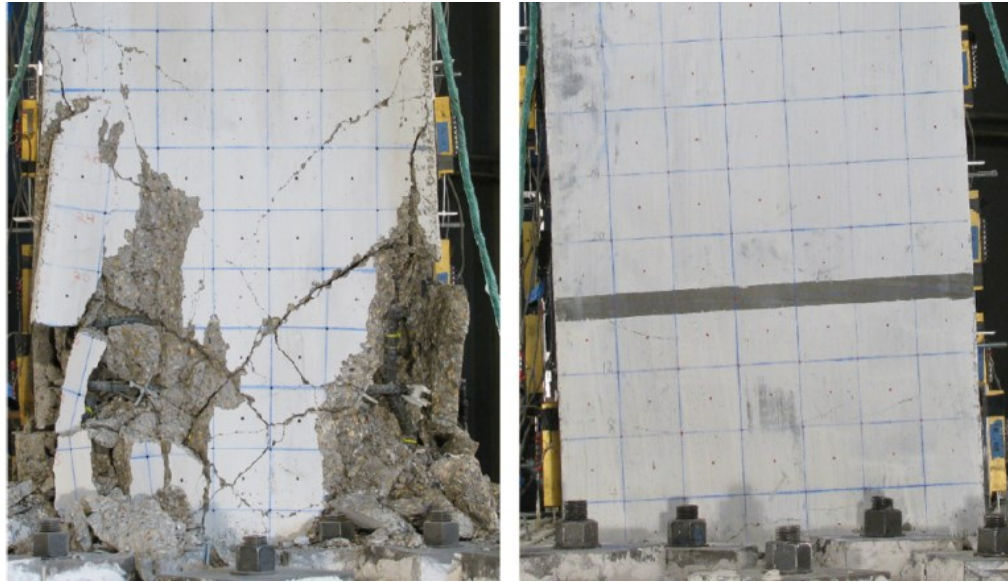
Figure 145. Comparison of RC (left) and UHP-FRC (right) specimens at 5.50% drift

6.2 Conclusions and Recommendations

1. At moderate drifts (1.0~2.0%), damage in UHP-FRC column was very minor compared to the RC column. This can result in cost-savings in post-earthquake repairs in buildings constructed with UHP-FRC columns.

2. The measured concrete strains as well as strains in the transverse reinforcement were essential in the elastic range for the UHP-FRC column; this suggests that the transverse reinforcement in UHP-FRC columns can be considerably reduced.

3. UHP-FRC column exhibited higher strength and greater drift capacity before significant strength degradation compared to the RC column.

4. The seismic performance of the UHP-FRC column such as strength or ductility was solely dependent on the tension/low-cycle fatigue behavior of the longitudinal reinforcing bars. Other factors such as bar buckling, concrete spalling, concrete crushing, and failure of hoops were eliminated in the UHP-FRC column.

5. The experimental test results presented in the previous chapters suggest that many of the current seismic design provisions in ACI 318-14 can be relaxed if UHP-FRC is used. More specifically the confining requirements and amount of transverse reinforcement necessary for columns cast using concrete with a compressive strength higher than 10,000 psi.

6. While further research is still needed on the full-scale applications of UHP-FRC, this study proposes that UHP-FRC columns have advantageous characteristics compared to that of RC and HSC columns and may be a viable design solution for seismic regions in the near future.

7. Additionally, it was also observed that the transverse reinforcement below the footing recorded minor strain well below yielding during all eight full-scale tests of columns subjected to a variety of very demanding loading protocols with large displacement reversals as would be observed in severe earthquakes. The current ACI provisions that require the transverse reinforcement at the footing ends to extend to 12 in. below the footing surface, or in some cases the total length of the column within the footing, may be relaxed to only the first hoop below the footing surface or 8 in. below the footing surface.

Chapter 7

Part II: Literature Review

This section underlines the principles of horizontal shear and corresponding research studies contributing to the understanding of the shear resistance between precast beams and CIP composite concrete slabs. The testing methods used by prior researchers to identify the key components of shear resistance, are also discussed.

7.1 Introduction

7.1.1 Interface (or Horizontal) Shear
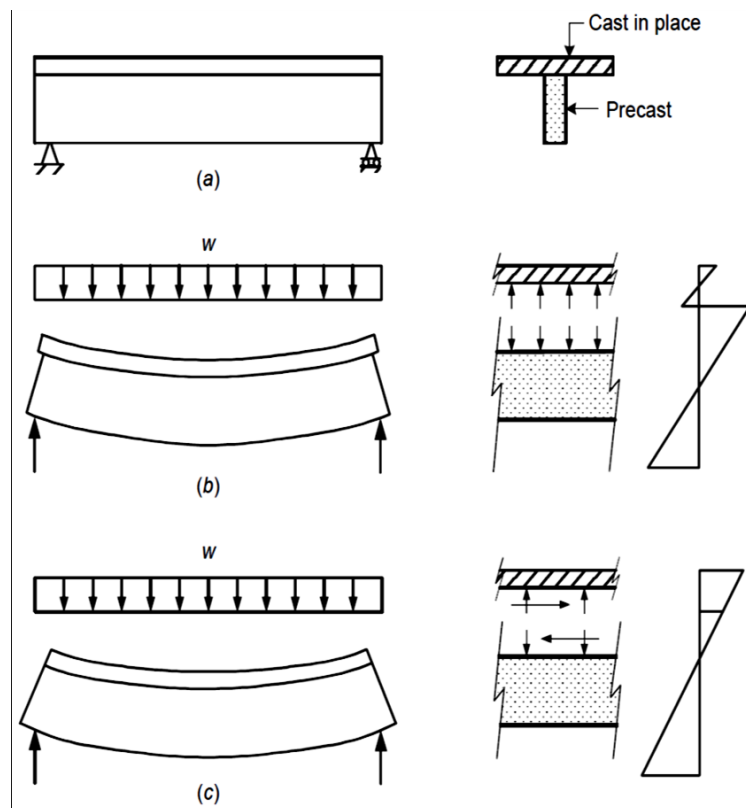
Figure 146. (a) Typical precast beam and CIP slab. (b) Non-composite action. (c) Composite action (Naaman, 2012)

The horizontal shear stress at the interface between the precast beam and the CIP slab is generated by the loads acting on the composite section only. They are the additional dead load and live load, if the precast beam is unshored, to which only the slab weight is added when the precast beam is shored. The horizontal shear stress due to bending is equal in magnitude to the vertical shear stress (Figure 146 and Figure 147) and can be derived either based on the classical strength of materials approach or an alternative considering the shear force at the strength limit state as given by AASHTO Section C5.8.4.2 (AASHTO, 2014).
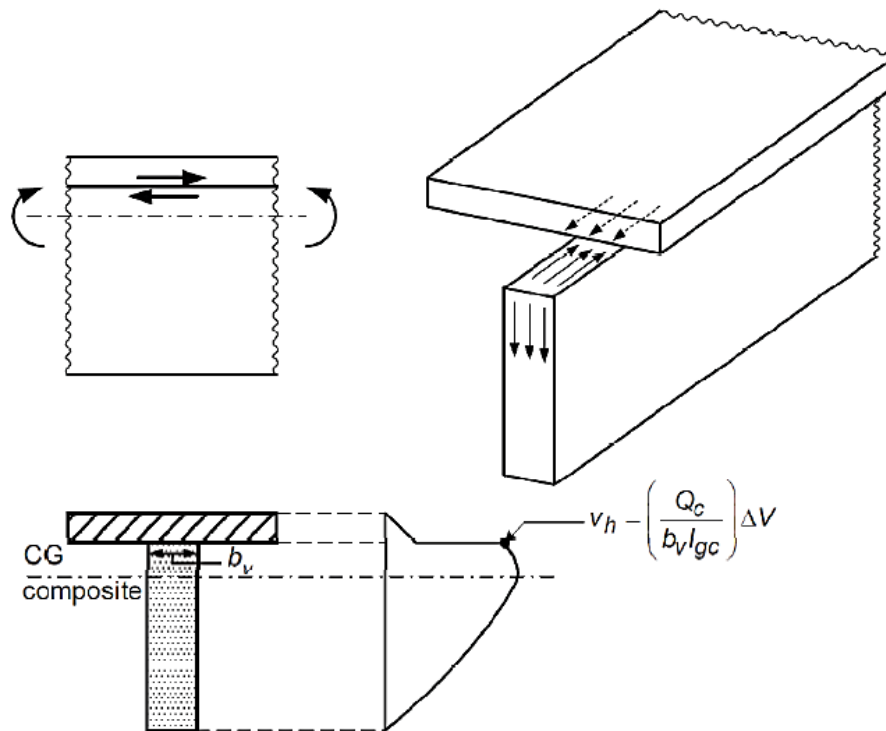
Figure 147. Interface horizontal shear stress (Naaman, 2012)

The horizontal shear is resisted by a combination of:

(1) Resistance of the protrusions on the crack faces to shearing (i.e. cohesion and/or aggregate interlock). For simplicity, AASHTO uses the term "cohesion factor" to capture the effects of this contribution listed,

(2) Friction between the crack faces, and

(3) Dowel action of the reinforcement.

Mast (1968), Hanson (1960), and Kaar et al. (1960) first introduced the shear friction equation (Eq. 1-1). This was the basis of the shear-friction design procedure found in Section 22.9 of ACI 318-14.

$$v_{nh} = \rho_v f_y \mu \qquad\qquad (7\text{-}1)$$

v_{nh} = nominal horizontal shear stress

μ = friction coefficient between the two surfaces

A number of assumptions and limitations were used in formulating the shear friction equation as listed below (Kamel, 1996):

- Interface must be clean and free of laitance,

- Well confined concrete,

- Reinforcement crossing the interface must be well anchored,

- A certain level of relative slip at the interface is permitted,

- Bond and cohesion do not develop shear resistance, only friction does,

- Bar size is limited to ¾ in. and yield strength of 60 ksi for the steel crossing the interface,

- Shear resistance is based on the ultimate load after cracking and is not valid when fatigue or slip is critical,

- The equation is only valid for normal weight concrete,

- The coefficient of friction does not depend on the concrete strength,

- The coefficient of friction is apparent and applicable to low stress levels only,

- Clamping stress is limited to $0.15f'_c$.

Following research by Hanson (1960) and Kaar et al. (1960), the American Concrete Institute (ACI) Code in its 1963 provisions introduced the design guidelines for steel crossing the interface between CIP slabs and precast beams. Push-off tests were found to be a relatively simple and inexpensive way of determining the horizontal shear strength compared to conducting full-scale tests on composite beams. The concept of "shear friction" was modified in the ACI Code (1970) based on push-off tests by Kriz et al. (1965), Birkeland and Birkeland (1966), Mast (1968), and Hofbeck et al. (1969). The Prestressed Concrete Institute (PCI) Design Handbook uses a procedure for calculating the shear strength based on the research conducted by Shaik (1978). Shaik's (1978) and Birkeland's (1966) equations provides a close representation of the test data but does not include the effect of concrete strength.

<u>7.2 Push-off Tests</u>

The push-off test has been used to verify the concept of shear friction in laboratory experiments. Two L-shaped components are used to form the push-off specimen. One L-shaped concrete component represents the precast section with or without steel reinforcing extending from the lower leg. The second L-shaped component is cast on top of the precast specimen and the combined unit is loaded in direct shear along the interface. A typical push-off specimen is shown in Figure 148.
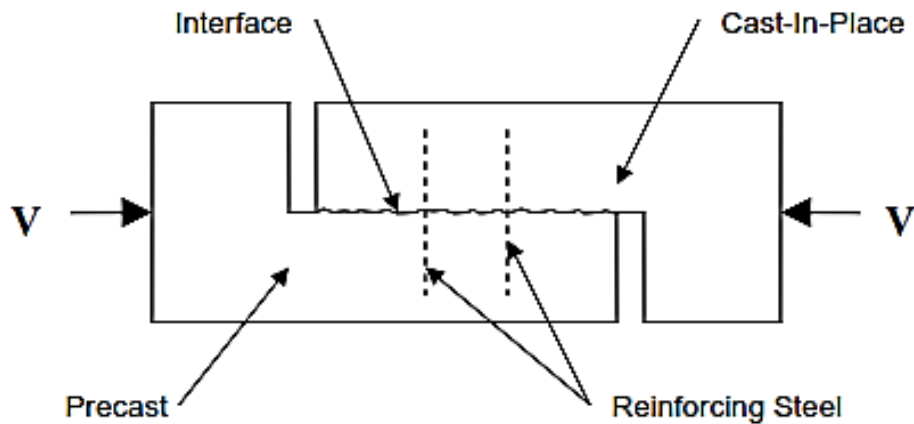
Figure 148. Typical push-off specimen (Scholz, 2004)

The push-off test has been used extensively by Birkeland (1966), Mast (1968), and Mattock (1969, 1972, and 1976) to quantify horizontal shear capacity between a precast and CIP concrete interface. The following is a summary on the different experiments carried out on interface shear using push-off specimens.

Menkulasi and Roberts-Wollmann (2002, 2003) modified the push-off test to represent a precast deck panel system with a haunch space between two precast L-shaped components and included a shear pocket block-out in the deck component. They performed three series of 12 push-off tests with three varying parameters: the haunch height, the mortar type, and shear connectors. For push-off specimens without shear connectors, a maximum shear stress of 125 psi was realized.
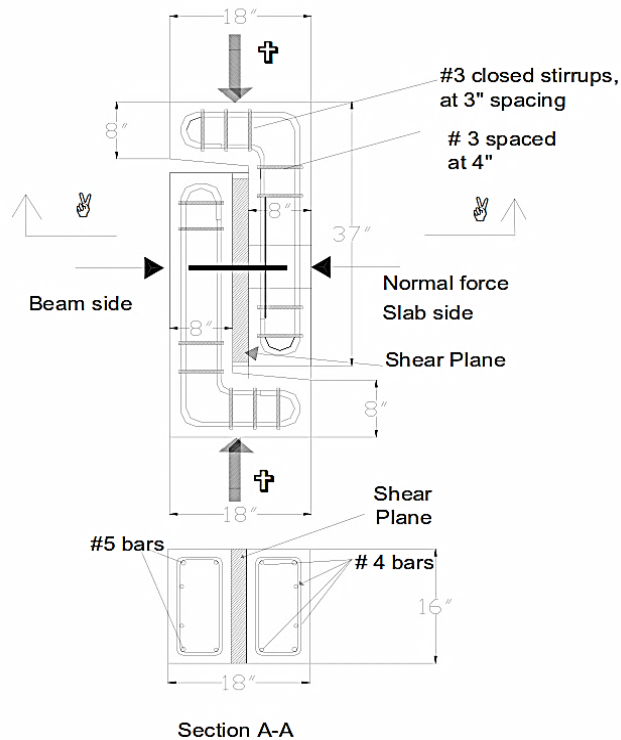
Figure 149. Typical push-off test specimen (Menkulasi and Wollmann, 2003)

They compared their tests results to the ACI 318-11 (2011), AASHTO Specification for Highway Bridges (2012) and AASHTO LRFD Bridge Design Specifications (2012) design equations for horizontal shear strength and found that the AASHTO LRFD method best predicted the precast deck panel system's behavior. The researchers then developed equations for predicting the horizontal shear strength based on their test data.

For un-cracked interfaces the nominal horizontal shear resistance in terms of stress (ksi.) is:

$$v_{nh} = 0.16 + 0.51\left(A_{vh} \times f_y + P_n\right) / \left(b_v s\right) \quad \text{(best-fit equation)} \quad (7\text{-}2)$$

For cracked interfaces the nominal horizontal shear resistance in terms of stress (ksi.) is:

$$v_{nh} = 0.02 + 0.86\left(A_{vh} \times f_y + P_n\right)/\left(b_v s\right) \quad \text{(best-fit equation)} \quad \text{(7-3)}$$

where:

v_{nh} = the nominal horizontal shear resistance in terms of stress (ksi.)

A_{vh} = area of reinforcement that crosses the interface (in.)

f_y = yield stress of the reinforcement (ksi.)

b_v = width of the interface (in.)

s = length of the interface (in.)

Scholz (2004) investigated the mortar or grout system used to connect precast panels to bridge girders by filling the space in the horizontal shear pockets and the haunches. Several important mortar characteristics were identified and investigated in order to create specifications that indicate the required performance criteria for mortars. He conducted push-off tests on 6 specimens with three different mortar types; a rake surface finish was provided to the specimens with an amplitude of ¼ in. Each test consisted of two L-shaped concrete blocks, one representing the girder and one representing the deck panel slab. The shear pocket and haunch were filled with mortar. The specimen was then loaded directly along the center line of the haunch up to failure (Figure 150). A small normal force (2.5 kips) was also provided to simulate the clamping stress resulting from the tributary weight of a deck panel per girder spacing as well as other dead loads.

173
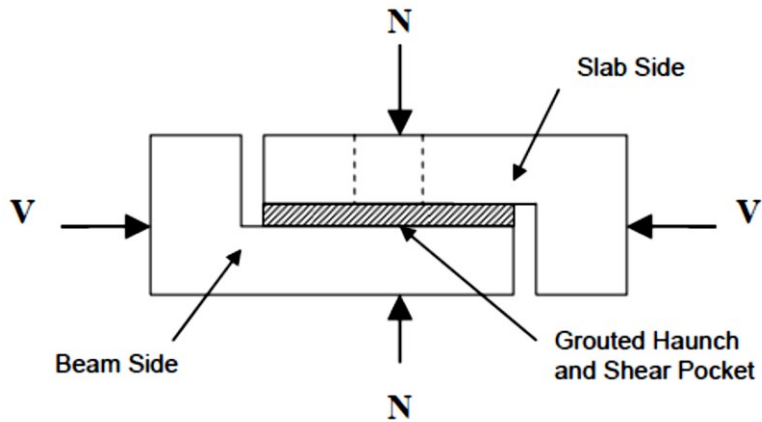
Figure 150. Typical push-off specimen (Scholz, 2004)

He concluded that sandblasting is unnecessary because it did not significantly increase the bonding capabilities of a concrete surface which had already been raked to amplitude of ¼ in. He recommended a ¼ in. amplitude on the top flange of conventional girders.

Trejo and Kim (2010) used the push-off test to assess the performance of different shear connector designs. Figure 151 shows a schematic of the push-off sample tested in the laboratory.
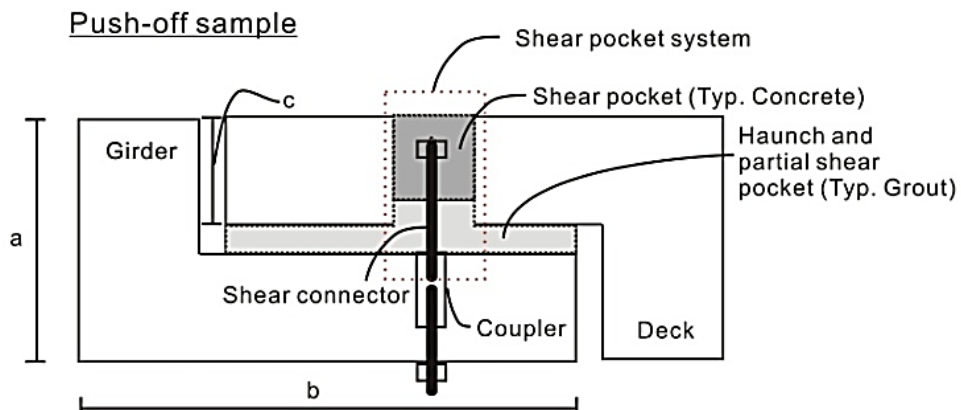
Figure 151. Push-off specimen with shear pocket (Trejo and Kim, 2010)

The 1.25 in and 0.75 in. (32 and 19 mm) diameter all-thread rods were used as shear connectors, as recommended by TxDOT personnel. The researchers identified five stages of shear transfer and failure mechanisms (Figure 152):

• Initial adhesion loss (Stage 1),

• Shear key action (Stage 2),

• Shear key action failure at peak load (Stage 3),

• Dowel action of the shear connectors at sustained load (Stage 4), and

• Final failure of the system (Stage 5).
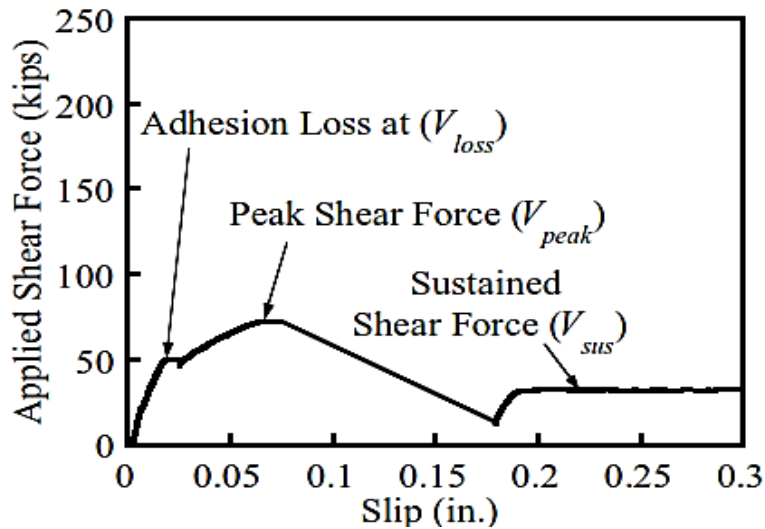
Figure 152. Typical failure mode (Trejo and Kim, 2010)

From the results gathered, the researchers proposed a new design equation to estimate the shear capacity of the girder-haunch-deck systems.

$$\min \begin{cases} V_{peak} = c' \cdot n \cdot A'_{cv} + \mu_p \cdot (\Sigma A_{sc} \cdot f_y) \cdot n \\ V_{sus} = \mu_r (A_s f_y + P_n) \cdot n \end{cases} \tag{7-4}$$

V_{loss} is the shear force at the adhesion loss,

V_{peak} is the peak shear force,

V_{sus} is the sustained or post-peak force,

c is the adhesion stress on the interface between girder and deck,

A_{cv} is the effective interface area of concrete engaged in shear transfer (haunch and deck contact area),

c' is the interlock of the crack surface in the shear pocket system,

A' is the effective interface area of the concrete engaged in shear transfer (referred to as the cracked area in the shear pocket system),

A_{sc} is the cross-sectional area of shear connectors,

f_y is the yield strength of the shear connector,

μ_p is the coefficient of friction at peak shear force for surfaces roughened to an amplitude of approximately 0.20 to 0.25 in. (5 to 6.4 mm),

μ_r is the coefficient of friction at sustained force (herein 80 percent of V_{sus}) for surfaces roughened to an amplitude of approximately 0.20 to 0.25 in. (5 to 6.4 mm), and

P_n is a permanent normal force to the shear plane.

n is the number of pockets per overhang panel.

The results from the test revealed that the roughened surface on the girder provides a stronger adhesion between the haunch material and the adjacent girder surface in the push-off specimens. However, dowel action of the shear connectors was seen as likely the main source of the interface shear capacity after shear key failure.

National Cooperative Highway Research Program (NCHRP) (2008) investigated the shear capacity of headed-studs as shear connectors between concrete panels and

structural steel girders. The researchers conducted push-off tests on the systems with four and eight headed-studs (each 1.25 in. (32 mm) in diameter). Cross ties and steel tube systems were used to confine the grout in the shear pocket that surrounds the shear connectors so as to improve the interface shear capacity. The results from the test indicated that push-off tests are sufficient to reflect the performance of full-size specimens. They also found that the HSS (hollow structural section) steel tubes could effectively confine the grout that surrounds the shear studs in the shear pockets. However, test results showed high peak loads with relatively low ductility. They proposed design recommendations to achieve the peak shear resistance of the system based on this study.

Hanson (1960) studied the composite action between concrete girders with CIP concrete slabs. He tested 62 push-off specimens and 10 composite T-beams to investigate the horizontal shear transfer strength. The push-off specimens contained horizontal shear reinforcement embedded 4 in. into the 7 in CIP slab. The horizontal shear reinforcement was positioned in most cases at the center of the shear length (which varied from 6 in., 12 in. or 24 in.) but in some specimens two or three horizontal shear reinforcements were placed evenly on the shear length.
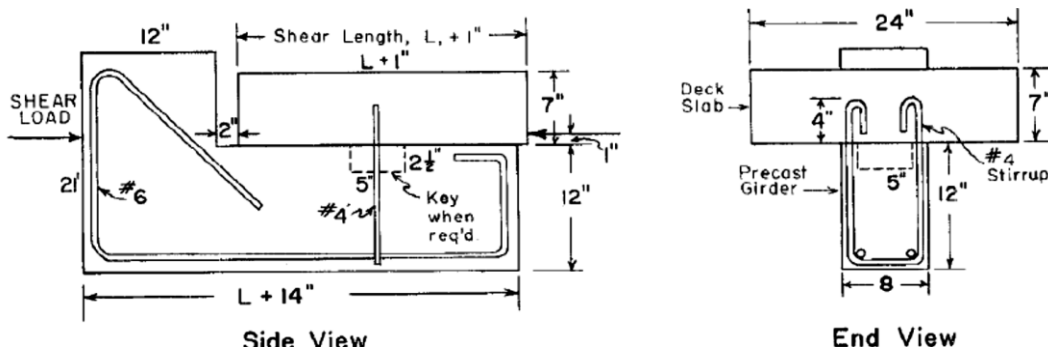
Figure 153. Typical push-off specimen (Hanson, 1960)

Several finishes were applied at the interface;

- Smooth: surface trowelled to a relatively smooth condition.

- Rough: surface roughened by scraping with the edge of a metal sheet (3/8 in. amplitude)

- Bond: concrete cast directly on to a dry girder surface.

- Un-bonded: surface painted with a silicone compound to prevent the new concrete from bonding with the precast concrete.

- Smooth aggregate bare: aggregates protruding on the surface.

- Rough aggregate bare: no paste on projecting aggregates.

- Shear keys: 5 in. square in the direction of the shear force and 2.5 in. deep into the girder concrete.

Test results indicated that the shear keys led to a slight change in the shear-slip curves. The contact area was found to act as a unit and failed without the effects of the key being realized. This indicated that the bond had to be broken before the shear key acts. Although concrete strength was not the main focus in this research, tests revealed that shear stress appeared to be approximately proportional to the concrete strength of the CIP slab.

Birkeland and Birkeland (1966) postulated that a crack that forms in a monolithic concrete block along the failure plane will lead to slippage along the shear plane when an external shear load V is applied. The slippage is resisted by the friction μP resulting from the clamping force P. They also showed that the tension T due to reinforcement across the interface produced the equivalent of the external clamping force P (Figure 154).

178
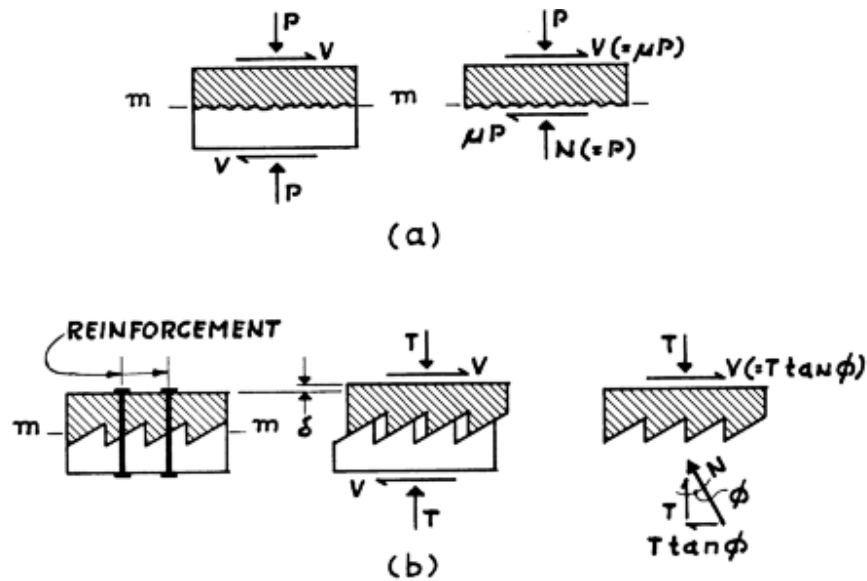
Figure 154. Shear friction hypothesis (Birkeland and Birkeland, 1966)

They then introduced a parabolic function for the horizontal shear strength at the interface as shown below:

$$v_{nh} = 33.5\sqrt{r_v f_y} \text{ (psi)} \tag{7-5}$$

They supported their hypothesis by the use of Hanson's (1960) push-off test to represent rough-bonded and rough-unbounded specimens, Anderson's (1960) push-off specimens to simulate building connections, and Mast's (1968) specimens to prove the design of horizontal shear connection between the precast longitudinal strips of a barrel shell roof. The strength data was then plotted to compare their hypothesis to the test data from these researchers. They then concluded that the shear friction hypothesis is an extremely useful tool which is simple and easy to apply and suggested that a test program be conducted to specifically verify the hypothesis.

Hofbeck et al. (1969) investigated the horizontal shear transfer across a plane for cracked and pre-cracked interfaces. The clamping stress, concrete strength, and reinforcement yield strength were investigated by testing 38 push-off specimens. The

researchers concluded that a pre-existing crack along the shear plane reduced the ultimate shear transfer and increased the horizontal slip. A 250 psi reduction in the shear strength was expected for a 4,000 psi normal weight concrete with clamping stresses between 200 psi and 1,000 psi. The reduction was higher for lower values of clamping stress. For clamping stresses above 1,000 psi, there is a very slow rate of increase in the interface shear strength of initially un-cracked specimens with an increase in clamping stress, while the strength of the initially cracked specimens continued to increase at the same rate as for lower clamping stresses. Consequently, the horizontal shear strength for cracked and un-cracked interface was approximately equal for a clamping stress of 1,340 psi as shown in Figure 155.
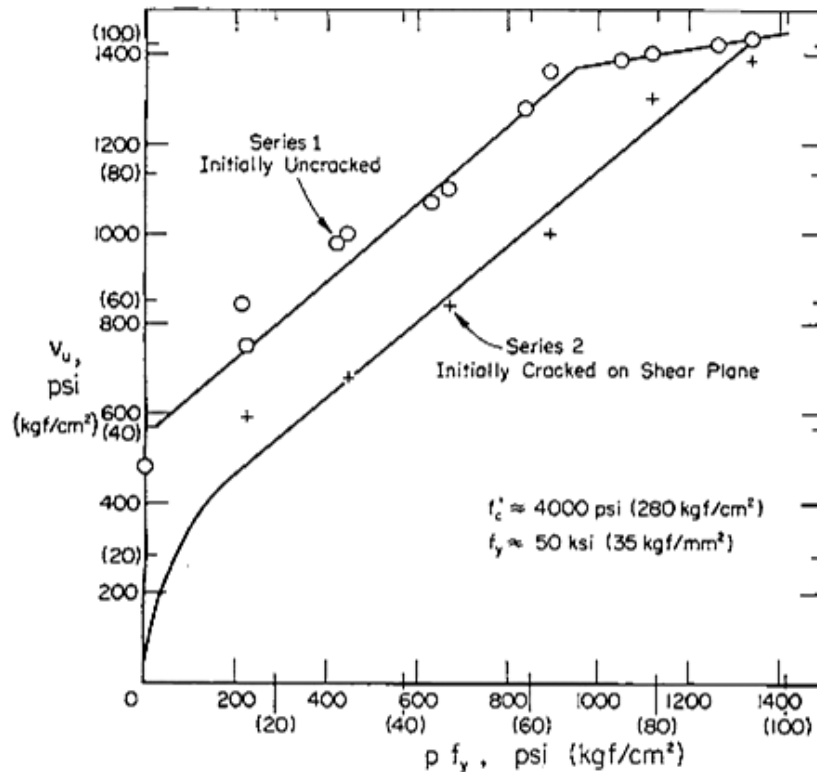
Figure 155. Push-off test results (Hofbeck et al., 1969)

Hofbeck et al. (1969) also noted that the shear strength of initially cracked specimens is not directly proportional to the amount of reinforcement. Specimens with a pre-existing interface crack were found not to be affected by the concrete strength for values of clamping stress of up to 600 psi. Changes in strength, size and spacing of grade 60 reinforcement did not affect the horizontal shear strength for the same clamping stresses.

They also concluded that dowel action does not contribute significantly to the shear transfer strength of initially un-cracked specimens but has a significant effect in initially cracked specimens. Hence the shear friction theory was found adequate in estimating the shear strength for the case of initially cracked specimens with a friction coefficient of $\mu = 1.4$ but conservative in the case of an un-cracked interface.

Kamel (1996) carried out push-off tests to evaluate the performance of several different types of shear connection schemes under ultimate horizontal shear stress and fatigue. A series of tests were carried out on specimens having a double shear interface and a single shear interface. Among the steel shear connectors applied were headed and headless high-strength bars and reinforcement stirrups whereas the type of interface included debonded shear keys, bonded roughened interfaces, unbonded roughened interfaces, smooth interfaces (both debonded and bonded). The roughened interface was applied to the top surface of the precast concrete section using a stiff bristled brush. The brush was moved in a circular motion to produce a ¼ in. amplitude on the surface. Specimens containing a roughened interface were used to evaluate the ability to remove the top concrete deck from the bottom girder using a 60 pound jack hammer.

Results from his fatigue tests showed that the specimens behaved in a similar manner under ultimate strength as an identical specimen that was not subjected to fatigue after the test was completed. He thus concluded that fatigue will have no effect on the service or ultimate capacity of these types of connections. The author concluded that the steel connectors do not necessarily contribute to the shear resistance in bonded systems until the bond is broken. He also suggested that a spacing greater than 24 in. currently specified by AASHTO Standard Specifications (2014) can be applied for design for sections with bonded interfaces. The author observed that the shear stress for debonded smooth interface was generally constant for all levels of clamping stress whereas the shear stress for debonded shear keys was seen to increase with increase in clamping stress. The author observed that all three components of the horizontal resistance contributed to the resistance in his fatigue tests.

Mattock and Hawkins (1972) conducted investigations to show how concrete strength, shear plane characteristics, reinforcement and direct stress (stresses acting

parallel or transverse to the shear plane) affect the interface shear strength of reinforced concrete. Pull-off and modified push-off specimens were used to study the influence of direct stresses acting parallel and transverse to the shear plane respectively.
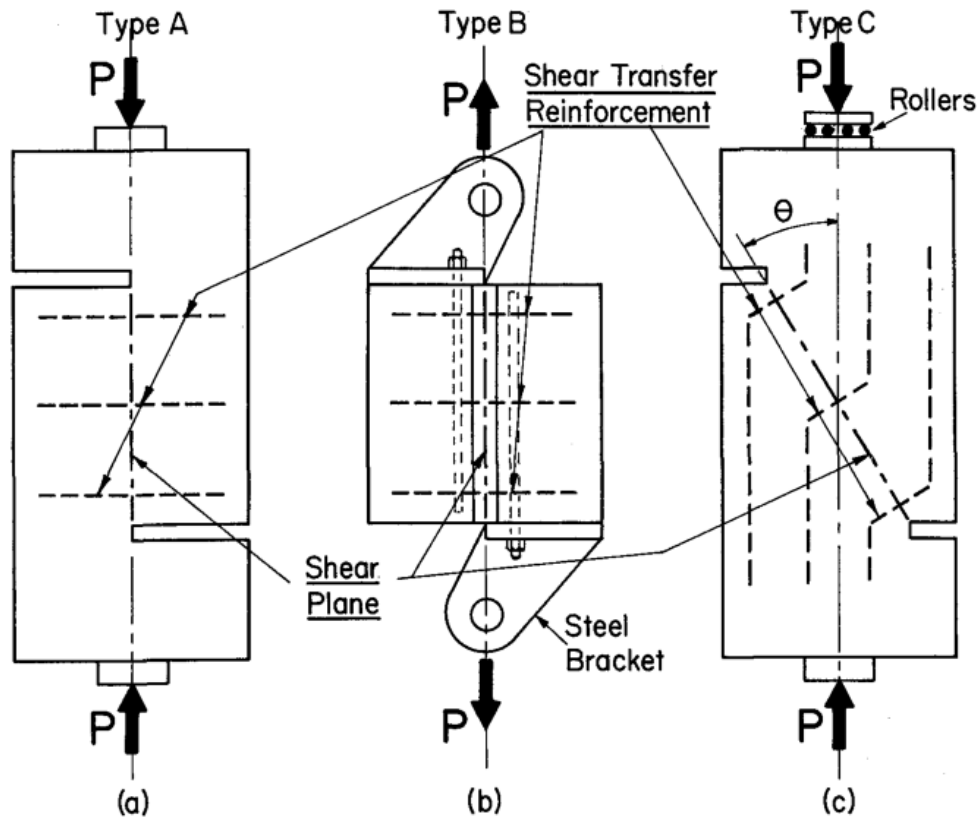
Figure 156. (a) Push-off; (b) Pull-off; and (c) Modified push-off specimens (Mattock, 1969)

The length and width of the shear planes were 10x5 in., 12x4.75 in. and 12x6 in. in the push-off, pull-off and modified push-off specimens, respectively. The specimens were monotonically loaded to failure and slip measured along the shear plane as well as lateral separation at the shear plane.

Mattock also tested pre-cracked shear transfer specimens to account for the possibility of a crack existing along the shear plane. The results showed that the slip in a

pre-cracked specimen was greater in all stages of loading than for an un-cracked specimen. Furthermore, the ultimate shear strength is reduced if the specimen is also under-reinforced. This decrease was seen to happen more in the push-off specimens than in the pull-off specimens. They also found out that for values of ρf_y below 600 psi, the concrete strength does not appear to affect the shear strength. On the other hand, for higher values of ρf_y, the shear strength is lower for the lower strength concrete.

They then conducted an analytical study to determine the influence that direct stress parallel to the shear plane has on the shear strength. They concluded that the shear strength of initially cracked concrete with moderate amount of reinforcement is primarily developed by frictional resistance to sliding between the faces of the crack and by dowel action of the reinforcement crossing the crack.

Mattock et al. (1976) investigated the shear transfer strength of lightweight aggregate concrete. They tested both initially un-cracked specimens and specimens cracked in the shear plane. Ten series of push-off specimens with a shear plane of 50 in^2 were tested. For the initially un-cracked specimens, no slip along the shear plane nor separation across the shear plane occurred until the formation of diagonal tension cracks in the region of the shear plane. Slip occurred along the pre-crack in the shear plane from the commencement of the loading and at a progressively increasing rate. They concluded that the shear strength of lightweight concrete is less than that of sand and gravel concrete (normal weight concrete) having the same compressive strength.

Mattock, Johal, and Chow (1975) conducted tests on six series of specimens, four corbel type push-off specimens and two standard push-off specimens, in order to

view the influence of moment or tension acting on the shear plane has on shear transfer as well as to validate the assumptions made in Section 11.5 of ACI 318-71. The researchers discovered that there is no interaction between moment and shear transfer, meaning that an additional applied moment will not reduce the shear transfer across a crack. Furthermore, the assumptions made in section 11.5 of ACI 318-71 that reinforcement needed to carry both shear and tension across a crack can simply be added were validated by the test results. The results also found that it is more appropriate to add the normal stress parameter to the reinforcement parameter when calculating shear transfer strength. They then concluded that the design equation provided by ACI 318-71 were conservative for small values of ρf_y and unnecessarily limited the ultimate shear transfer stress to 800 psi. They instead suggested the equations proposed by Birkeland (1968) where, $v_u = 33.5\sqrt{\rho_v f_y}$, and Mattock (1974) where, $v_u = 400 + 0.8\rho f_y$ but not less than $0.3 f_c'$, were both equally acceptable and more economical for design use.

Walraven, Frenay and Pruijssers (1987) conducted a statistical analysis to propose new shear friction equations for determining the shear capacity of the cracked interface of reinforced concrete members. They based their research on existing test data collected from 88 push-off test results by Hofbeck (1969), Frenay (1985), Walraven (1981) and Pruijssers (1985). They proposed that the influence of concrete strength is a basic parameter to consider in calculating the horizontal shear strength. From their analysis they concluded that the traditional shear friction equation without cohesion term is conservative especially in the region of low reinforcement ratios or high concrete strengths. Also that great accuracy can be achieved by considering the concrete strength

as a basic parameter. They formulated an equation that is accurate over a wide range of parameters.

Khan and Mitchell (2002) carried out an experimental study on fifty push-off specimens with cracked, pre-cracked, and cold-joint interfaces to determine if the current ACI provisions were applicable for high strength concrete. They designed the specimens to be identical to those used by Hofbeck (1969), Mattock (1976), and Anderson (1960) for comparison purposes. The cold-joint specimens were not floated or intentionally roughened but left as cast. Results showed that the un-cracked and cold-joint specimens developed diagonal cracks between $15^{°}$ and 45° to the shear plane at loads between 50% and 75% of the peak ultimate capacity. On the other hand, in the pre-cracked specimens, slip between the two faces began immediately upon load application. Cracking away from the shear plane was not observed until significant yielding of the reinforcement had occurred. They concluded that the ACI 318-99 shear friction provisions give a conservative estimate for the interface shear strength for high-strength concrete.

Paulay, Park, and Phillips (1974) investigated the contribution of dowel action, surface preparation, and reinforcement content towards the shear strength of construction joints subjected to monotonic and cyclic loading. They tested thirty-six push-off specimens having varying surface preparation and three different amounts of reinforcement across the joints. To eliminate shear transfer in some of the specimens, bond was minimized by spraying varnish on some rough surfaces or applying melted wax on some smooth surfaces. The purpose of these specimens was to determine the load-slip relationship for dowel action. The researchers concluded that for design purposes,

the contribution of the dowel action of the reinforcement should be ignored. Although significant dowel forces can be generated, excessive slips are expected along the joint.

Kent et al. (2012) carried out an in-depth review of previous work on interface shear as well as complementing it with an experimental study. The researchers set out to prove that the interface shear equations in ACI 318-08 are more conservative than those of AASHTO. They also argued that that the inclusion of the cA_{cv} term in AASHTO increases the shear-friction capacity to unwarranted levels and does not help to calibrate the equation with existing experimental data as asserted in the commentary of the AASHTO provisions. They tested eight typical push-off specimens having steel ties across the interface that simulated interface reinforcement. No. 3 and No. 4 bars were tested having two steel grades, ASTM A1035/A1035M high-strength (f_y = 100 ksi) steel and ASTM A615/A615M (f_y = 60 ksi) steel.

(a) test specimen   (b) instrumentation
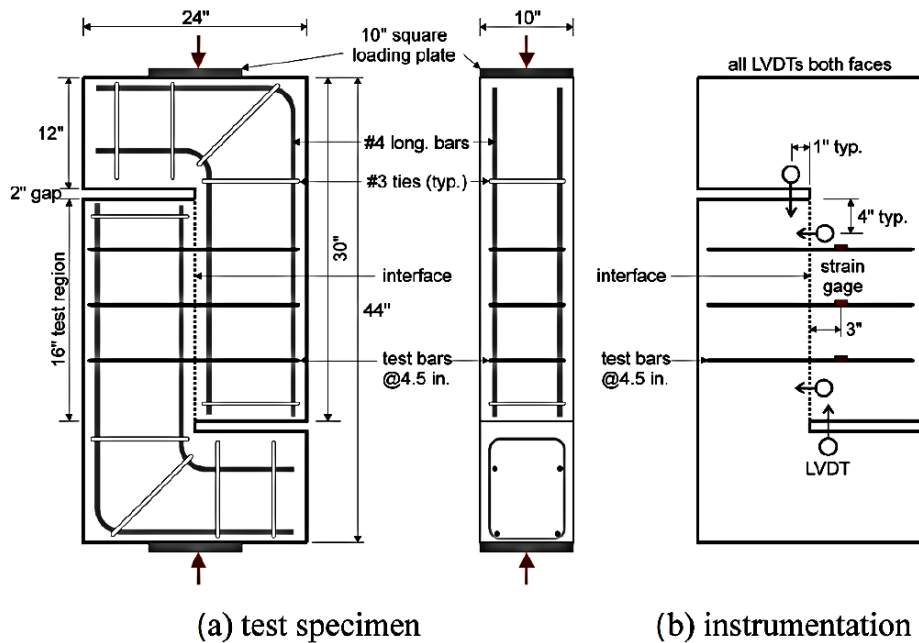
Figure 157. Typical push-off specimen (Kent et al., 2012)

It was observed that the use of ASTM A1035/A1035M high-strength steel instead of ASTM A615/A615M steel at the interface did not increase the shear friction capacity of the specimens significantly. This is because the ultimate shear capacity was controlled by concrete behavior and was reached well before steel yielding occurred. They therefore suggested that the clamping force is a function of the steel modulus rather than the yield strength.

The researchers concluded that while the reinforcing ratio affects the shear-friction capacity, the steel grade does not. He also concluded, similar to Park and Paulay (1974), that due to the complex nature of the shear friction mechanism, it is not possible to explicitly separate all parameters contributing to shear-friction behavior or establish explicit predictive behavior. They concluded that the AASHTO (2007) relationship for shear friction capacity does not capture the mechanism of shear friction and incorrectly implies that the interface reinforcement yields as the ultimate capacity is reached.

7.3 Full-scale Beam Tests

Hanson (1960) studied the composite action between concrete beam girders with CIP concrete slabs. He tested 62 push-off specimens and 10 composite T-beams to investigate the horizontal shear transfer strength. The beams were designed to reach high horizontal shear at the interface at a load well below flexural failure. The beams were tested in two series: in series-I the beams were tested under two point loading, while in series-II the beams were tested under three point loading.
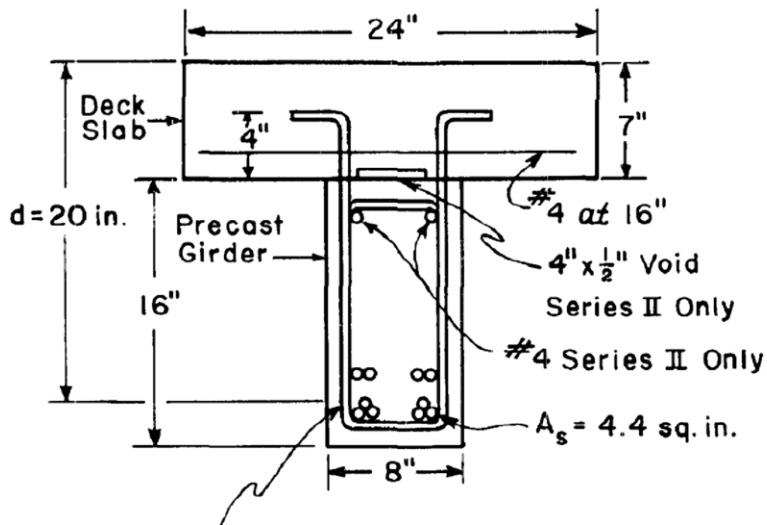
Figure 158. Cross section of beams (Hanson, 1960)
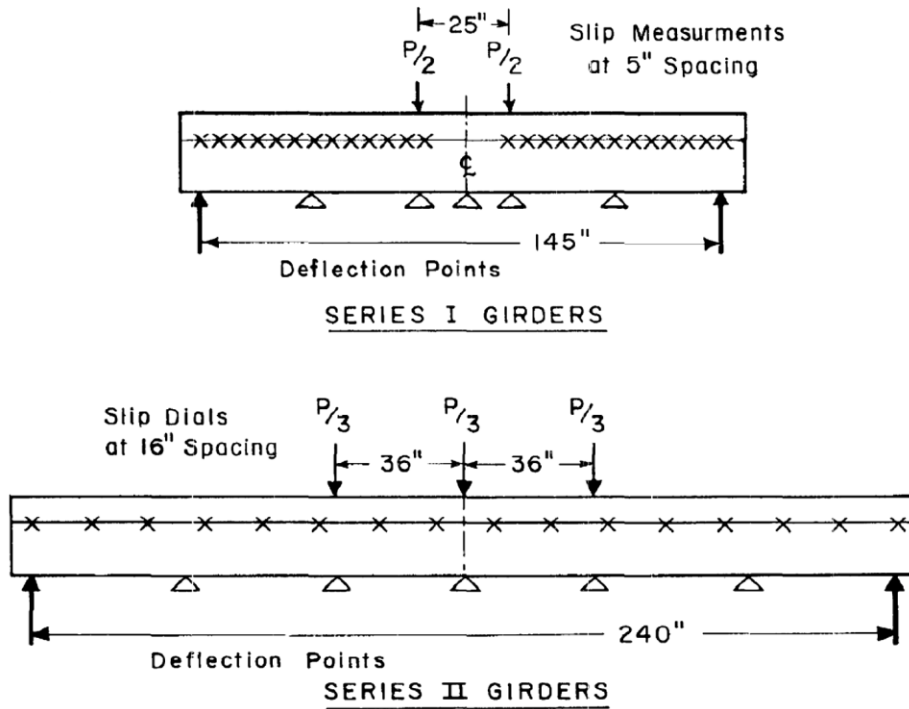
Figure 159. Test set-up for series I and II (Hanson, 1960)

From the results of the beam test, Hanson concluded that composite action was lost at the critical slip value of 0.005 in. He suggested a maximum shearing stress for composite action to be 500 psi for a roughened bonded interface with concrete strengths between 3,000 psi and 5,000 psi. If additional steel reinforcement crossing the interface is to be provided in excess of the required amount, an additional horizontal shear capacity of 175 psi may be added for each percent of stirrup reinforcement.

Loov and Patnaik (1994) conducted an extensive study on the horizontal shear strength of composite concrete beams with roughened interface for a wide range of steel ratios. Sixteen composite beams with different geometries (Figure 160) were tested. The major variables in their study were the clamping stress and the concrete strengths. The clamping stress was varied by adjusting the amount of steel crossing the interface and the width of the precast concrete girder. The interface was left as-cast with some aggregate protruding. The beams were simply supported and loaded with a point load at the center span. The beams were designed to be strong in vertical shear and flexure so that the first mode of failure is horizontal shear. Their test showed that slip was insignificant up to a horizontal shear stress of 220 to 290 psi. It increased with stress up to a slip ranging from 0.01 to 0.03 in. They also observed that there was little difference between the shear stress at a slip of 0.2 in. and the shear stress at peak load.

(a)
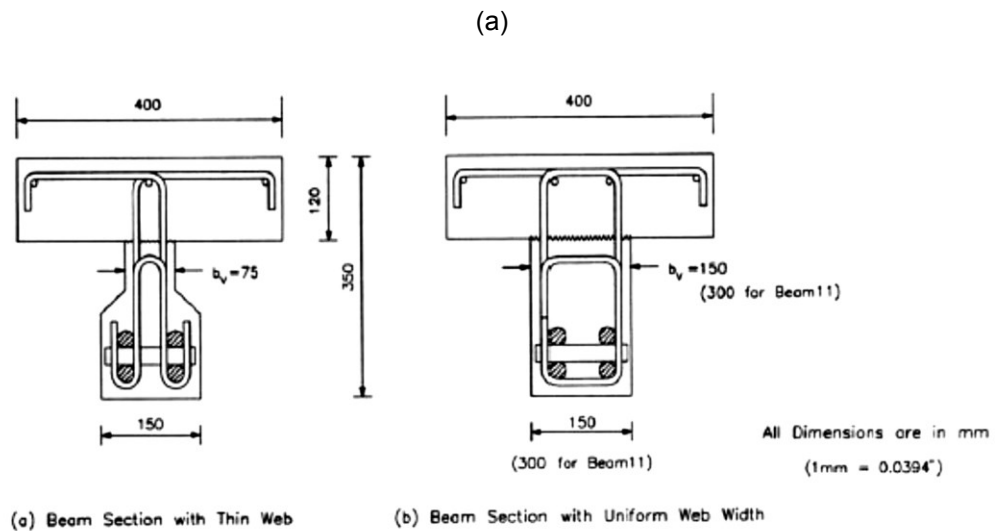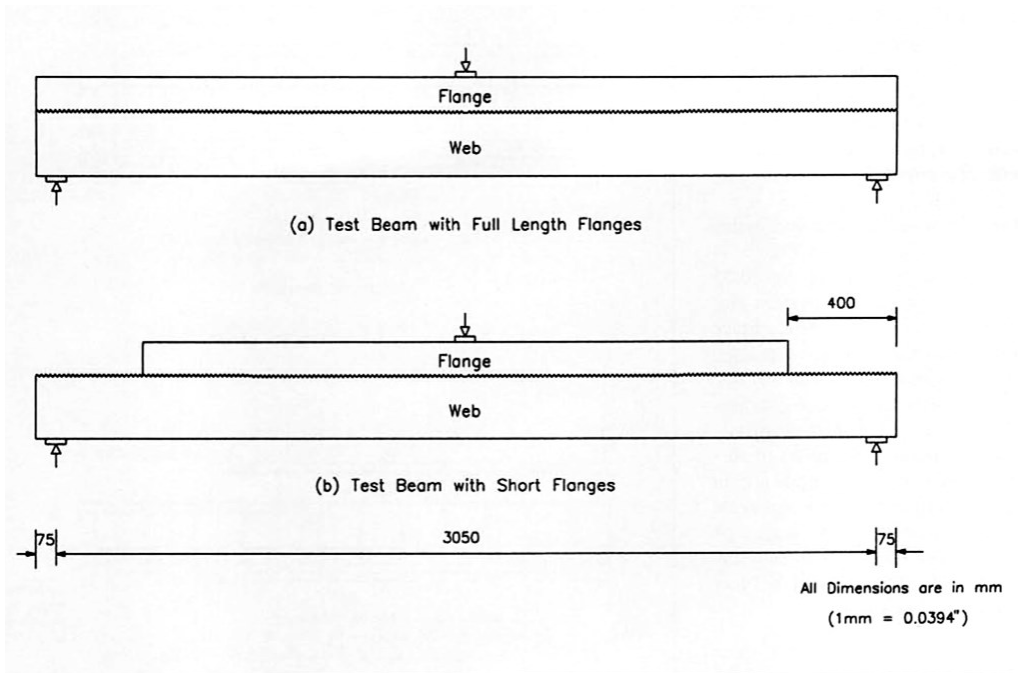
(b)

Figure 160. Typical test beams (Loov and Patnaik, 1994)

Their results showed that stirrups were not stressed until a horizontal shear stress of about 220-290 psi (Figure 161) and did not yield at a slip of 0.005 in. as was

proposed by Hanson (1960) but instead began to yield at a slip of 0.02 in. He concluded that elastic analysis using cracked transformed section properties is a valid assumption and a simple method for estimating the horizontal shear stresses in composite concrete beams at failure.
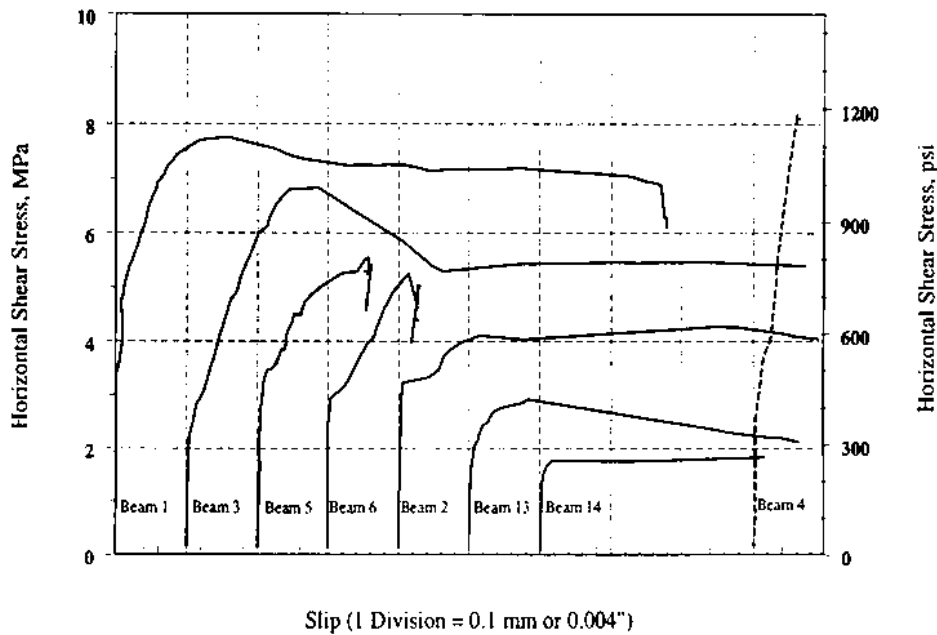
Figure 161. Test results for beams 1 through 6 and beams 13 and 14 (Loov and Patnaik, 1994)

Seible and Latham (1990) conducted preliminary studies on the horizontal shear transfer behavior of overlaid reinforced concrete bridge decks combined with experimental results of the effects of interface preparations and dowels on horizontal load transfer. Shear block tests, full-scale transverse bridge deck slab panel tests and a full-scale prototype bridge deck tests were conducted. They investigated seven different surface preparations. These included:

- Monolithic: specimen cast monolithically.

- Lubricated: a rough construction joint was sprayed with a bond breaking agent to eliminate chemical bond between the old and new concrete.

- Surface rough: wood float finish and light sandblasted interlayer surface

- Scarified: grooves greater than 1/8 in. deep cut into the old concrete with a jack hammer.

- Lubricated and dowels.

- Surface rough and dowels.

- Scarified and dowels.

Results from the shear block and slab panel test showed that the vertical construction joint performance is evidently influenced by the surface preparation. Also that the dowel-reinforced specimens were controlled by dowel yield at a level of ρ_d=0.28% dowel reinforcement. The lubricated specimens exhibited very early delamination of the interlayer and independent flexural cracks developed in the old and new concrete slabs. The surface rough specimens had flexural crack propagation into the overlay with only temporary arrests and slight horizontal deviations. Failure occurred by delamination well above the flexural yield limits. Differences in behavior between surface rough and scarified specimens were only noticed at ultimate failure. They also came to the conclusion that the 0.07% dowel reinforcement did not influence the crack pattern development and was not sufficient to control the ultimate delamination crack. They stated that interface dowels are only beneficial in confining the crack after the fact. The following conclusions were made by the researchers:

1) A delamination of a rough and clean interface is not likely to occur under service and overloads.

2) Reinforcement dowels in horizontal construction joints for full depth structural concrete overlays are not effective as long as a rough and clean interface is provided.

The minimum interface reinforcement of 0.08% by AASHTO (1983) proved inefficient once delamination occurred. The dowel reinforcement ratio of 0.28% provided in the shear blocks was clearly sufficient to control interlayer slip behavior.

Kovach and Naito (2008) investigated the shear friction of girder-deck systems having no shear connectors. Their research aimed to determining if there was a possibility of increasing the allowable horizontal shear capacity between a precast beam and CIP slab without the use of horizontal shear reinforcements. Their findings suggested that the cohesion and adhesion between the girder and deck could provide sufficient shear resistance. In addition, they concluded that the interface roughness had a pronounced effect on the composite shear action and a sufficient level of roughness could help obtain a high level of horizontal shear capacity. The surface condition, cohesion, and adhesion therefore should be considered for the design and practice.

7.4 Review of Design and Code Equations

Mast Equation:

Mast was the first researcher to propose the following linear shear friction equation. It was later modified by Birkeland and Anderson (1960):

$$v_n = \rho_v f_y \mu \tag{7-6}$$

Loov and Patnaik (1994) however concluded from their research that this equation is very conservative for low clamping stresses and unsafe for sections with high clamping stresses.

Saemann and Washa Equation:

Saemann and Washa (1964) came up with Eq. 7-7 for determining the horizontal shear strength of a composite section from tests performed on full-size beams. The effects of surface conditions were not included in the equation since it was discovered that the contributions from surface conditions were diminished as the amount of reinforcement crossing the interfaces increased.

$$Y = \frac{2700}{X+5} + 300P\left(\frac{33-X}{X^2+6X+5}\right)psi \tag{7-7}$$

where Y = ultimate shear strength

P = percent of steel crossing interface

X = effective depth of the section

The first part of the equation represents the shear strength when no reinforcing steel is crossing the interface whereas the second part represents the strength due to clamping force when reinforcing steel is used.

Birkeland Equation:

Birkeland and Birkeland (1966) were the first to propose a parabolic equation for the horizontal shear strength (Equation 2-10):

$$v_n = 33.5\sqrt{\rho_v f_y} \; psi \tag{7-8}$$

This equation only included the clamping stress multiplied by a factor and did not account for the concrete strength or varying surface treatments.

Walraven Equations:

In his numerous tests on push-off specimens, he developed the following equations which consider the concrete compressive strength:

$$v_n = C_3(0.0007\rho_v f_y)^{C_4} \quad psi \tag{7-9}$$

Where,

$$C_3 = 16.8(f_c')^{0.406}$$
$$C_4 = 0.0371(f_c')^{0.303} \tag{7-10}$$

Mattock Equations:

Mattock (1969) proposed an equation for horizontal shear strength as shown below:

$$v_n = 0.8 \times A_{vf} f_y + A_c k_1 \tag{7-11}$$

Mattock further modified and simplified Walraven's equation by eliminating the c factors:

$$v_n = 400 + 0.8\rho_v f_y \ psi$$
$$v_n \leq 0.3 f_c' \ psi \tag{7-12}$$

From his research on lightweight concrete, Mattock et al. (1976) also concluded that the shear strength of lightweight concrete is less than that of normal weight concrete.

Loov Equation:

Loov (1978) was among the first researchers to incorporate the influence of concrete strength directly into the horizontal shear equation (Equation 2-15).

$$v_n = k\sqrt{\rho_v f_y f_c'} \qquad (7\text{-}13)$$

k = 0.5 for initially un-cracked surface

Hsu et al. (1987) proposed a k =0.66 on a similar equation for both cracked and un-cracked interfaces.

Shaikh Equation:

Shaikh (1978) developed Equation 7-14 for horizontal shear strength which was adapted by PCI Design Handbook (1992) as the basis for their design equations.

$$v_n = \phi \rho_v f_y \mu_e \qquad (7\text{-}14)$$

Where,

$$\phi = 0.85 \text{ for shear}$$

$$\mu_e = \frac{1000\lambda^2}{v_n}$$

λ= 1.0 for normal weight concrete

λ= 0.85 for sand-lightweight concrete

λ=0.75 for all lightweight concrete

The PCI Design Handbook (1992) uses a simplified form of the equation as shown below:

$$v_n = \lambda\sqrt{1000\phi\rho_v f_y} \leq 0.25 f_c' \lambda^2 \text{ and } 1000\lambda^2 \text{ psi} \qquad (7\text{-}15)$$

Loov and Patnaik Equation:

As mentioned above, Loov and Patnaik (1994) combined the equation by Loov (1978) with the horizontal strength of composite beam without shear connectors. The equation is applicable for both high and low clamping stresses:

$$v_n = k\lambda\sqrt{(15+\rho_v f_y)f_c'} \leq 0.25 f_c' \text{ psi} \qquad (7\text{-}16)$$

k =0.6

λ = same as used by PCI

In 2001, Patnaik proposed a linear variation on his previous shear equations:

$$v_n = 87 + \rho_v f_y \leq 0.2 f_c' \text{ and } 800 \text{ psi}$$
$$v_n = 0 \quad \text{for } \rho_v f_y \leq 50 \text{ psi} \qquad (7\text{-}17)$$

7.4.1 2014 AASHTO LRFD Bridge Design Specifications for Horizontal Shear

The specifications propose that the interface shear transfer should be considered across a plane at:

- An existing or potential crack,

- An interface between two concretes cast at different times,

- An interface between dissimilar materials, or

- The interface between different elements of the cross-section.

The nominal shear resistance of the interface plane is represented as a linear equation as shown:

$$V_{ni} = cA_{cv} + \mu(A_{vf}f_y + P_c) \tag{7-18}$$

The nominal shear resistance should however not be greater than the lesser of:

$$V_{ni} \leq K_1 f'_c A_{cv}, \text{ or}$$
$$V_{ni} \leq K_2 A_{cv}$$

Where,

c = cohesion factor

μ = friction factor

A_{cv} = interface area (in^2)

A_{vf} = area of shear reinforcement crossing the shear plane within area A_{cv} (in^2)

The AASHTO provisions give the following recommendations for the cohesion and friction factors.

For normal weight concrete placed against a clean concrete surface, free of laitance and intentionally roughened 0.25 inches

c = 0.24 ksi

μ = 1.0

For concrete placed against clean, hardened concrete not intentionally roughened but free of laitance and clean

c = 0.075 ksi

μ = 0.6

For a CIP concrete slab on clean concrete girder surfaces, free of laitance and intentionally roughened 0.25 inches

c = 0.28 ksi

μ = 1.0

ACI 318-14 Section 16.4 recommends the equations for horizontal shear design. ACI outlines that the design of horizontal shear is based on the following equation.

$$V_u \leq \phi V_{nh} \qquad \text{(ACI equation 17-1)} \qquad\qquad (7\text{-}19)$$

Where,

V_u = factored shear strength

V_{nh} = nominal horizontal shear resistance

ϕ = strength reduction factor (0.75)

The horizontal shear resistance is determined as follows:

$$If \ V_u \leq \phi 500 b_v d \ \text{then,}$$

For contact surfaces that are clean, free of laitance and intentionally roughened,

$$V_{nh} \leq 80 b_v d$$

For contact surfaces that are clean, free of laitance, but not intentionally roughened, having minimum tie reinforcement,

$$V_{nh} \leq 80 b_v d$$

For contact surfaces that are clean, free of laitance, having minimum tie reinforcement and intentionally roughened to a full amplitude of approximately ¼ in.,

$$V_{nh} = (260 + 0.6 \rho_v f_y)\lambda b_v d \leq 500 b_v d$$

If $V_u \geq \phi 500 b_v d$ then,

$$V_{nh} = A_{vf} f_y \mu \leq \min \ (0.2 f_c' A_c \ \text{or} \ 800 A_c)$$

Where,

b_v = width of the interface (in.)

d = distance from the extreme compression fiber to centroid of tension reinforcement for the entire composite section (in.)

A_{vf} = area of shear reinforcement crossing the interface (in^2)

f_y = yield stress of the shear reinforcement (psi)

μ = coefficient of friction which depends on surface

= 1.0λ for concrete placed against hardened concrete with intentionally roughened surface.

= 1.4λ for concrete cast monolithically.

= 0.6λ for concrete placed against hardened concrete with surface not intentionally roughened.

= 0.7λ for concrete anchored to as-rolled structural steel by headed studs or by reinforcing bars.

λ = 1.0 for normal weight concrete

λ = 0.85 for sand-lightweight concrete

λ = 0.75 for all lightweight concrete

A_c = area of concrete engaged in shear transfer (in^2)

$$\rho_v = \frac{A_v}{b_v s}$$

7.5 Review of Site Visits and Study of Common Practices in 50 States

7.5.1 Introduction

As a part of the research project, site visits were conducted on bridges in Austin as well as Fort Worth to observe possible horizontal shear cracks. In addition, visits were made to two precast plants in Texas to observe their typical beam fabrication and surface finishing processes. A survey was also conducted to get a comprehensive overview of the horizontal shear reinforcement and surface preparation details for box and slab beams of all 50 DOTs in the United States.

7.5.2 Site Visits

Riverside Bridge (Austin, TX)

A visit was made to the Riverside Bridge (Intersection of I-35 and Riverside Rd.) to observe possible horizontal shear cracks. The location of the bridge and design drawings can be seen in Figure 162. Observation of the bridge revealed extensive horizontal cracks at the end spans and the middle span of the bridge. Crack widths as wide as 10 mm were measured. It is important to note however that this is an older bridge which uses an asphaltic concrete overlay of 2 in. as opposed to a 5 in. CIP concrete slab. There was therefore no horizontal shear reinforcement at the interface. The only composite section on the beam was observed to be between the precast beam and the sidewalk. The interface at this section was also observed to be very smooth (Figure 163).

(a)

Transverse
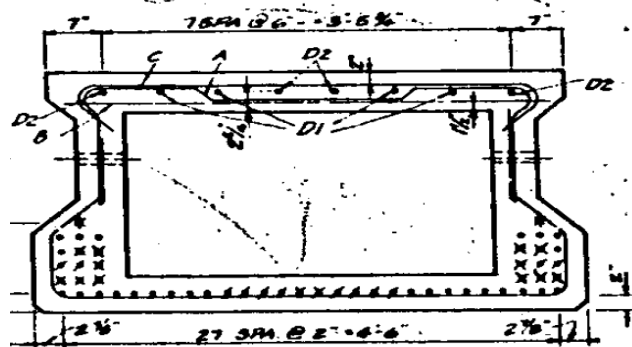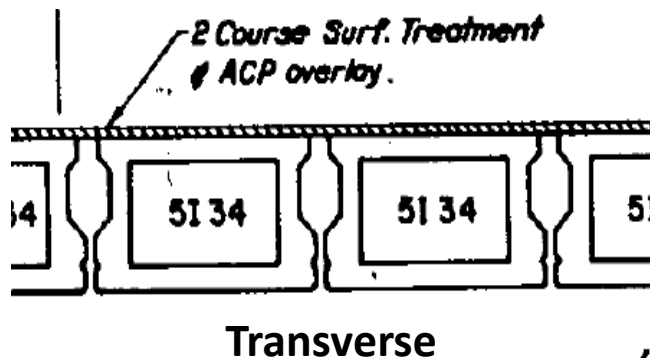
(b)

Figure 162. Riverside bridge location and design drawings
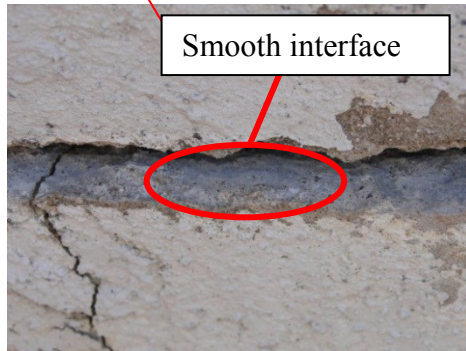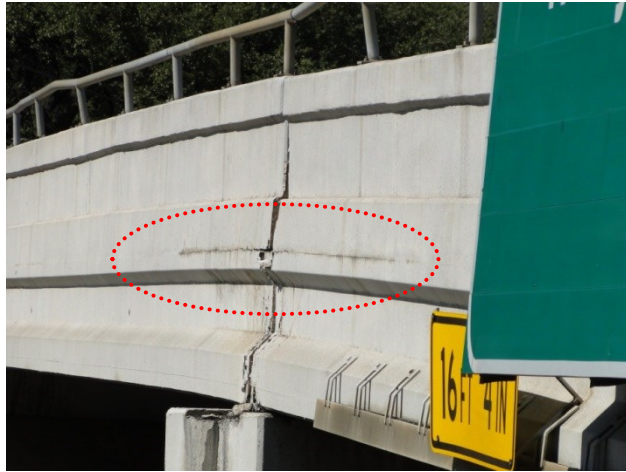
Figure 163. Horizontal shear cracks at the interface of beam and sidewalk

Ft. Worth Bridge Site Visits

Two bridge sites were visited in Ft. Worth, TX to observe the possible occurrence of interface shear cracks. The first bridge was also an older bridge located near the intersection of E Long Avenue and Beach St (Figure 164). This bridge was constructed with concrete box beams and a 2 in. asphalt overlay on the surface. These types of bridges use shear keys to connect the girder and the deck and do not use any type of steel reinforcing along the interface.

Figure 164. Location of Long Ave. Bridge

It was witnessed on arrival that this bridge did not have any interface shear damage; however other forms of damage were observed. A number of shear cracks and crushing was observed at the ends of the girders. Figure 165 shows an example of some of the observed shear cracks. Horizontal shear cracks were present on the girders but did not extend into the deck interface.

Figure 165. Shear cracks observed at the South-West end of the Long Ave. Bridge

The second bridge that was visited was located at Cattlebaron Dr. at Silver Creek (Figure 166). The bridge is a slab beam bridge with a CIP reinforced concrete deck similar to the bridges that we are currently investigating. As this bridge was newly constructed, there was no visible damage to study.
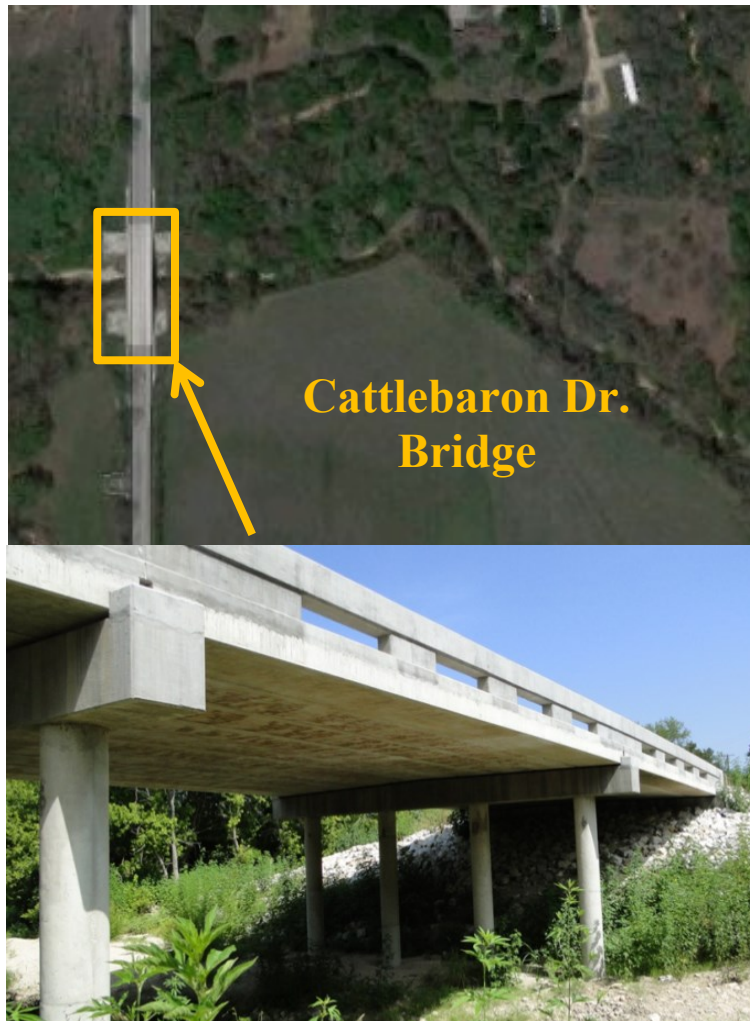
Figure 166. Location of Cattlebaron Dr. Bridge

7.5.3 Plant Visits

Texas Prestressed Concrete

A visit to the Texas Prestressed Concrete Plant in Elm Mott, Tx was done to view the typical process involved in manufacturing a slab beam. River gravel (¾ in.) was used as the coarse aggregates while river sand was used as the fine aggregates. Horizontal

shear reinforcement (Grade 60, No. 4 bar) is spaced at 12 in. and has an embedment length of 2 in. as per TxDOT specifications (Figure 167 and Figure 168).

Figure 167. Spacing of horizontal shear reinforcement

Figure 168. Horizontal shear reinforcement details

The slab beams are typically finished by using a wood float as shown in Figure 169. On comparing the surface finish with the CSP surface profiles, it was observed that

the surface roughness for the conventional concrete slab beam was between a CSP 6 and a CSP7 (Figure 171) while an SCC slab had a surface roughness of CSP 4 (Figure 170).

Figure 169. Application of wood float finish

Figure 170. SCC concrete surface compared to CSP 4

Figure 171. Wood float concrete surface compared to CSP 6 and CSP 7

Texas Prestressed Concrete typically does not fabricate box beams due to their complicated construction and cost. The plant mentioned that they would be willing to

change their process of roughening the surface if a faster method (say broom or rake finish) was specified.

Bexar Concrete Works LTD

Unlike Texas Prestressed Concrete, Bexar uses ¾ in. limestone aggregates for the coarse aggregate and manufactured sand as the fine aggregates. They fabricate both box and slab beams.

Figure 172. Finished box beam

The horizontal shear reinforcement of the box beam is spaced at approximately 12 in. spacing and 8 in. at the ends. The horizontal shear reinforcement is 2 in. high with a width of 3.5 in. The horizontal reinforcements are placed at a distance of 6 in. from the edge of the box beam (Figure 173).

Figure 173. Horizontal shear reinforcement details

A wood float finish is provided for the surfaces of all TxDOT box and slab beams fabricated at the plant. The wood float finish created a surface roughness between CSP 7 and CSP 9 as shown in Figure 174.

Figure 174. Box beam surface roughness compared to CSPs

Bexar provides a broom finish on precast panels (Figure 175), suggesting that other methods of surface preparation may be applied to box and slab beams if necessary.

Figure 175. Surface finish on precast panel

7.5.4 Review of Other Department of Transportation Practices

An investigation was conducted on other DOT practices pertaining to the construction of box and slab beams. The main focus of the study was on the details of the horizontal shear reinforcement and the surface roughness implemented. Some of states do not have either box beams or slab beams and although others do use them; they do not have the plans on their website. The table below summarizes the findings on all the states.

Table 7. Review of DOT Practices

STATE	BOX BEAM	SLAB BEAM
Alabama	No box beam	Has slab beam
Alaska	No box beam	No slab beam
Arizona	Have both box and slab beams. Do not have any standard drawings just follow AASHTO specifications	
Arkansas	No box beam	No slab beam
California	Has box beam (no response on horizontal shear reinforcement details)	Has slab beam
Colorado	Has box beam	Has slab beam
Connecticut	Has box beam	Has slab beam
Delaware	Has box beams	Has slab beams
Florida	No box beam	Has slab beam
Georgia	Has box beam	No slab beam
Hawaii		
Idaho	Has box beam	Has slab beam
Illinois	Has box beams	No slab beams
Indiana	Has box beam (No information on beams on website)	No slab beam
Iowa	Do not typically use box beam or slab beams	
Kansas	No box beam	No slab beam
Kentucky	Has box beam	No slab beam
Louisiana	Box beams rarely used	No slab beam
Maine	Has box beam	Has slab beam
Maryland	No box beam	Has slab beam
Massachusetts	Has box beam	Has deck beam
Michigan	Has box beam	No slab beam

Table 8. Review of DOT Practices – continued.

Minnesota	Has rectangular beam	No slab beam
Mississippi	No slab or box beams	
Missouri	Has box beam	Has slab beam
Montana	No box beam	No slab beam
Nebraska	No box beam	No slab beam
Nevada	No information on beams on website	
New Hampshire	Has box beam	Has slab beam
New Jersey	Has box beam	Has slab beam
New Mexico	Rarely use box beam	No slab beam
New York	Has box beam	Has slab beam
North Carolina	Has box beam	Has slab beam
North Dakota	Has box beam	No slab beam
Ohio	Has box beam	Has slab beam
Oklahoma	No box beam	No slab beam
Oregon	Has box beam	Has slab beam
Pennsylvania	Has box beam	No slab beam
Rhode Island	Has box beam	Has slab beam
South Carolina	No box beam	Has slab beam
Tennessee	Has box beam	No slab beam
South Dakota	No box beam	No slab beam

Table 9. Review of DOT Practices – continued.

Texas	Has slab beam	Has box beam
Utah	No box beam	No slab beam
Vermont	Plans not available on website (no response)	
Virginia	Use them infrequently so no statewide standard available	
Washington	No box beam	Has slab beam
West Virginia	Has box beam	No slab beam
Wisconsin	Has box beam	No slab beam

There are generally five surface finishes that are applied on fresh concrete.

- **As-placed roughness:** No attempt is made to smooth or roughened the surface after concrete is poured and vibrated.

- **Float finish:** After concrete is poured and vibrated, a rough wooden float is run through the surface to smoothen it.

- **¼" rake finish:** A rake is run across the interface transverse to the beam length leaving a very rough textured finish.

- **Rough broom finish:** A stiff broom is run across the surface of the beam in the transverse direction.

- **Sheepsfoot voids:** This represents a mechanical surface finish consisting of 1 in. diameter, ½ in. deep impressions made at a spacing of 3½ in.

The DOT survey suggest that only three kinds of finishes are currently being used; that is the broom, rake, and wood float finish as will be seen below. From the study conducted it has been observed that there are essentially five types of horizontal shear reinforcement as shown below.

217

<u>Type 1</u>

This type has been used by three of the states (West Virgina, North Dakota and Ohio) investigated although the width (w) and the embedded length (h) of the horizontal shear reinforcement varies.
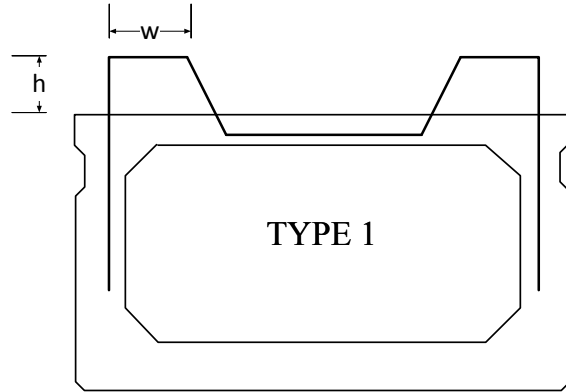
Figure 176. Type 1 horizontal shear reinforcement

<u>Type 2</u>

This is one of the least used horizontal reinforcement. It is used in two of the states (Michigan and Maryland). This kind of reinforcement almost runs the entire width of the beam.
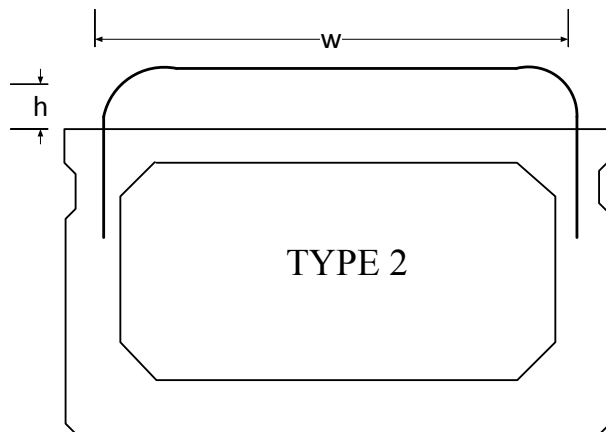
Figure 177. Type 2 horizontal shear reinforcement

The third type of horizontal shear reinforcement is in use in Colorado and Missouri. A 90° curvature is utilized in this kind of reinforcement.
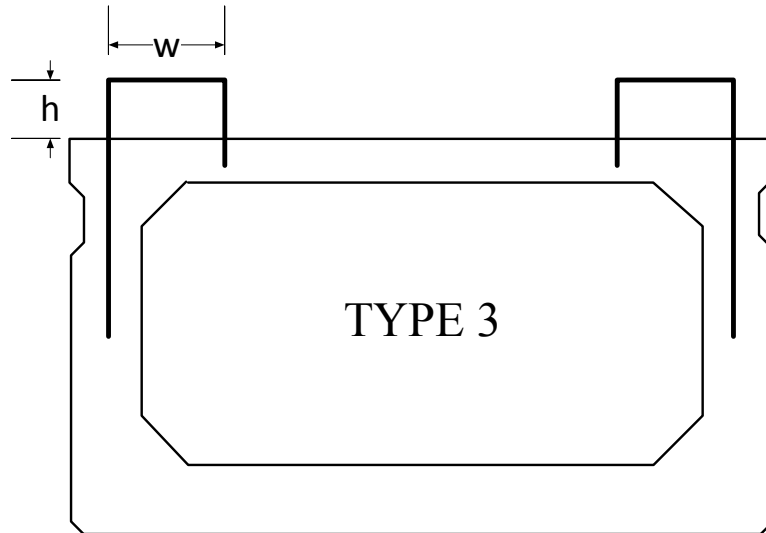
Figure 178. Type 3 horizontal shear reinforcement

Type 4

Three states (Washington, Alabama and Missouri) use this type of reinforcement that utilizes a 90° curvature as seen.
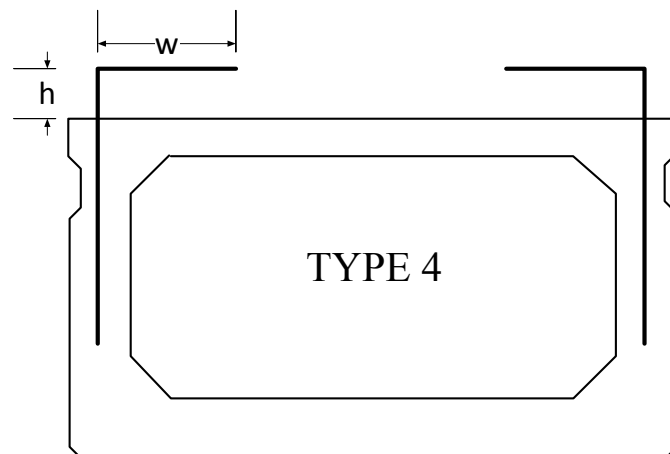
Figure 179. Type 4 horizontal shear reinforcement

<u>Type 5</u>

The fifth type is the most popular horizontal shear reinforcement. Eight of the states investigated use this type of reinforcement. A 180° curvature is utilized in this kind of reinforcement. This type of reinforcement has also been used perpendicular to the cross-section in Maine and Massachusetts. It is designed in accordance to AASHTO.
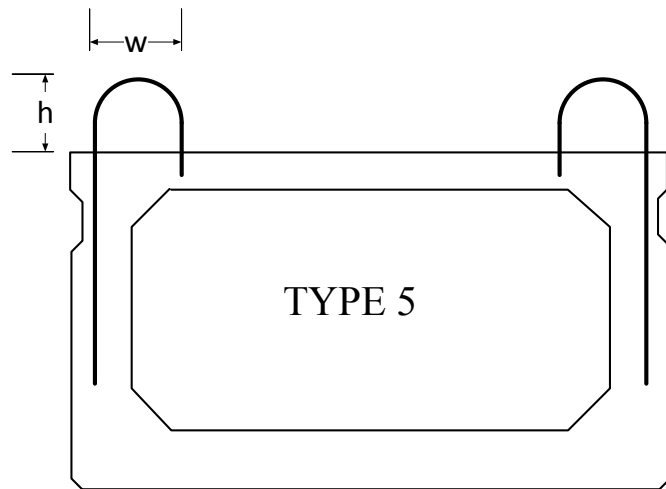
Figure 180. Type 5 horizontal shear reinforcement
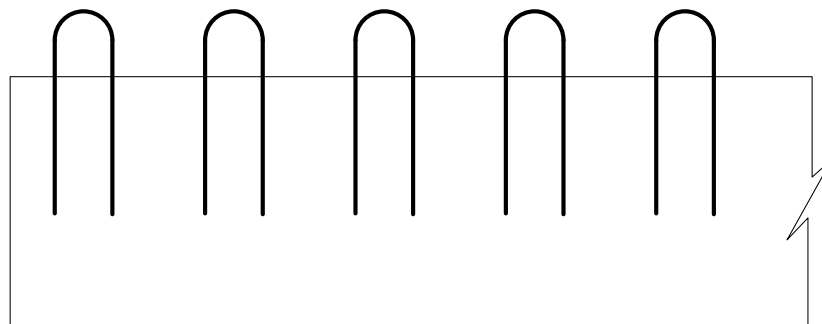
Figure 181. Type 5 horizontal shear reinforcement (perpendicular to cross-section)

A wood float surface finish is also shown to be the most used finishing method on the beam surfaces. The table below gives a summary of the findings.

Table 10. Summary of DOT Surface Finish Survey

State	Type of horizontal shear reinforcement	Width (in.)	Embedded length (in.)	Surface finish
Ohio	Type1	9	2	Wood float
North Dakota	Type 1	6	3	Wood float
West Virginia	Type 1	7	5	Wood float
Maryland	Type 2	-	2.125	-
Michigan	Type 2	31	2.75	Wood float
Colorado	Type 3	-	2.5	Wood float
Missouri	Type 3	9	2	-
Texas	Type 3	6	2	Wood float
Florida	Type 3	12	2.5	-
Missouri	Type 4	6	2.5	-
Alabama	Type 4	4	2.5	Rake finish

Table 11. Summary of DOT Surface Finish Survey – continued.

Washington	Type 4	9	2.5	Wood float
Indiana	Type 5	-	21/8	Scoring
Kentucky	Type 5	-	2.5	Wood float
Maine	Type 6	(perpendicular to cross-section)	3	Wood float
Massachusetts	Type 6	(perpendicular to cross-section)	2	Rake finish
Minnesota	Type 5	3	6	Broom finish
Pennsylvania	Type 5	4	3	Broom finish
Rhode Island	Type 6	-	2	Rake finish
Texas	Type 5	3.5	2	Wood float

It is clear from this study that the width of horizontal shear reinforcement used in other states is generally greater than that used in TxDOT practice. Also of interest is the effectiveness of using the reinforcement perpendicular to the cross-section. Therefore, the testing matrix proposed in Task 5 (Waweru, 2015) is justified as it will determine the effectiveness of different widths and curvatures of the reinforcement. The DOT review also shows that although wood float finish is the most popular finish being used, other types of finishing (e.g. broom finish and rake finish) should be considered for their effectiveness.

Chapter 8

Part II: Experimental Program

8.1 Introduction

The experimental program is divided into two sections; component tests and full-scale tests. Section 8.2 will describe the component tests made up of push-off type testing to evaluate the cohesion and aggregate interlock and friction components of the AASHTO equation including the specimen design, construction and each distinct test setup. Section 8.3 will discuss the full-scale testing of composite box and slab beams including each respective design, construction and the full-scale test setup.

8.2 Component Tests

The push-off type test as commonly used for shear friction studies (Hofbeck et al., 1969; Mattock and Hawkins, 1972; Kahn and Mitchell, 2002) was utilized to evaluate the Task 2 shear resistance component cA_{cv}. To isolate the horizontal shear component of cohesion and aggregate interlock, no interface reinforcement was used, and the specimens were tested in the vertical position as shown below in Figure 220. By placing the specimens vertically the shear resistance from μP_c was eliminated.

The Task 3 shear component μPc was evaluated using another form of push-off test different to that used in Task 2. No interface reinforcement was used to eliminate any contribution from the shear reinforcement. This time the specimens were tested horizontally so that the dead load coming from the slab and other superimposed dead load will be mobilized. Various surface roughness amplitudes were investigated for both Task 2 and Task 3 specimens as shown in the testing matrix in Table 12.

223

Table 12. Task 2 and Task 3 Testing Matrix

Push-off Test Specimens	Shear Resistance Components		Number of Tests
	cA_{cv}	μP_c	
	Task 2	Task 3	
Wood Float Finish	3	3	6
ICRI surface roughness: CSP 6	3	3	6
ICRI surface roughness: CSP 7	3	3	6
ICRI surface roughness: CSP 8	3	3	6
ICRI surface roughness: CSP 9	3	3	6
			Total 30

A dead load was provided on the Task 3 specimens in the form of a compression force of 20 kips. This load does not depict the exact load that is applied on the composite beam but it was chosen so as to give a clearer picture of the difference in the friction coefficient between the different surface profiles. It was found from Task 2 that the largest variations between the test results are approximately 10 kips. In order to ensure that the friction induced by the vertical load is not less than 10 kips, a slightly larger vertical load (20 kips) was used to make sure the contribution from friction can be easily identified.

Since the push-off specimen is representative of a cast in-place slab supported by a precast girder, an additional dead weight corresponding to its tributary area must be added. According to the TxDOT standard drawings and the riverside bridge plans, slab and box beams are typically between 3'-11" and 5' wide and are usually placed side by side or with a maximum spacing of 3 inches for the slabs as shown below.
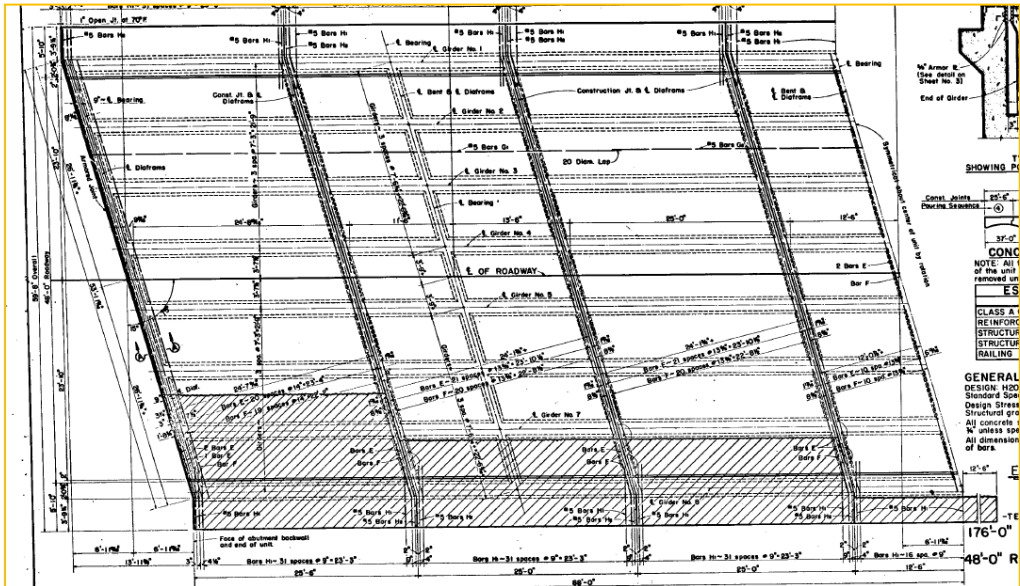
Figure 182. Riverside bridge plans
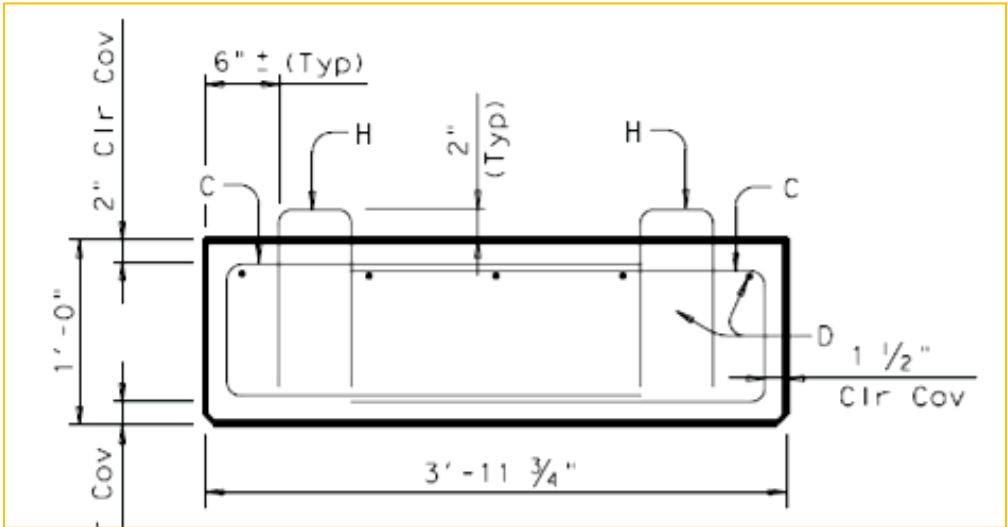
Figure 183. Typical slab beam section
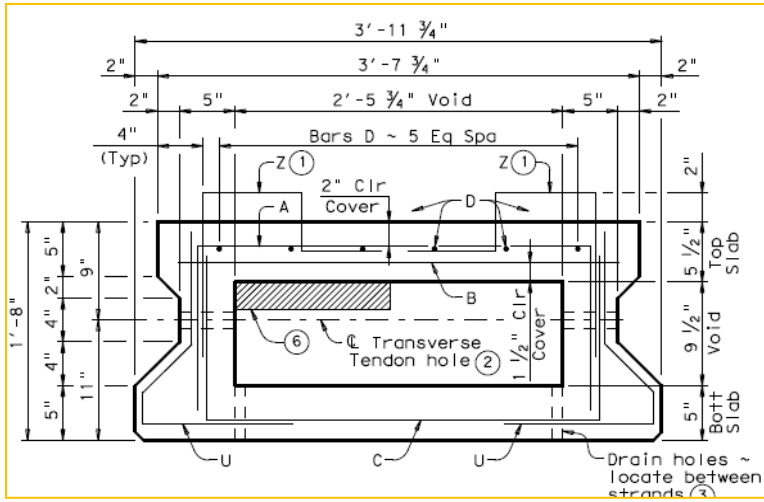
Figure 184. Typical box beam section
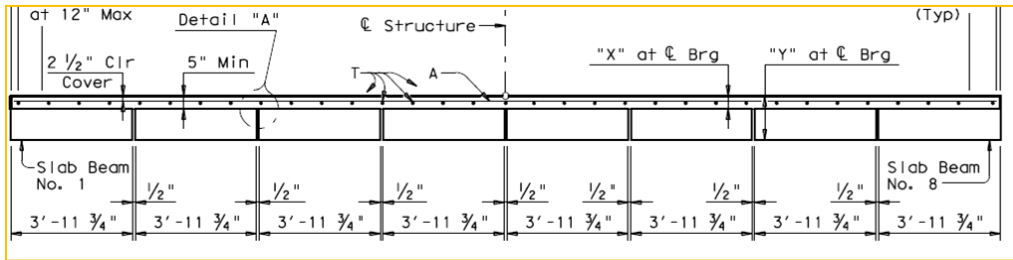
Figure 185. Typical transverse section.

Figure 186. Girder spacing according to TxDOT practice

The test specimens already include the portion of the slab directly above it and so the tributary area needing to be added will be:

Girder Width in inches:

$$3' - 11\frac{3}{4}" = 47.75 \ in.$$

Total Tributary Area per foot:

$$T = (47.75 \ in.) \times 12 in. = 573 \frac{in^2}{ft}$$

Volume per foot assuming a 5 in. thick slab:

$$V = 573 \frac{in^2}{ft} \times 5 in = 2865 \frac{in^3}{ft} = 1.66 \frac{ft^3}{ft}$$

Total weight per foot assuming the density of reinforced concrete is 150 pcf.:

$$W_T = 1.66 \frac{ft^3}{ft} \times 150 \ pcf = 248.70 \frac{lb}{ft} = 0.249 \frac{kip}{ft}$$

Weight per square foot acting on the girder:

$$W_G = \frac{.248 \frac{kip}{ft}}{3.92 \ ft} = 0.06 \frac{kip}{ft^2}$$

The interface of the test specimen has dimensions of 14"x18", or 1.16 feet wide by 1.5 feet long, giving a total interface area of 252 in². According to these dimensions the total dead load being applied at the interface is then

$$DL = 0.06 \frac{kip}{ft^2} \times (1.16 \ ft \times 1.5 \ ft) = 0.10 kips$$

Subtracting the weight of the existing cast in place part of the specimen, the additional dead weight needed to be added is then

$$DW = 0.10\,kips - [\frac{\left(252\,in^2 \times 5in\right)}{\left(12\,in\right)^3} \times 0.150\frac{kip}{ft^3}] = 0 \text{ kips.}$$

This means that the dead load provided by the cast in place part of the specimen is the exact dead load needed to simulate the actual bridge dead loading. As was mentioned earlier this dead load is not enough to clearly demonstrate the effect of the friction has on the interface shear strength hence a higher value of 20 kips was added as a normal force for the Task 3 specimens.

8.2.1 Push-off Specimen Design

Geometry and Reinforcing

Each test specimen measured 30x14x10 in., this size was chosen to provide a shear interface area of 252 in^2 (18x14 in.). The reinforcing cage for the specimen is shown below in Figure 188. Also to prevent flexural failure from occurring, minimum longitudinal and transverse reinforcement was provided. No. 4 longitudinal bars were placed at both the top and bottom of the specimen spaced at 3 in. on center. No. 3 lateral reinforcement was also provided at 5 in. spacing. The reinforcement layout chosen was similar to the one used by Mattock. It should be noted that this reinforcement layout provides a higher reinforcement ratio as compared to that used in actual girder/deck (Figure 187).
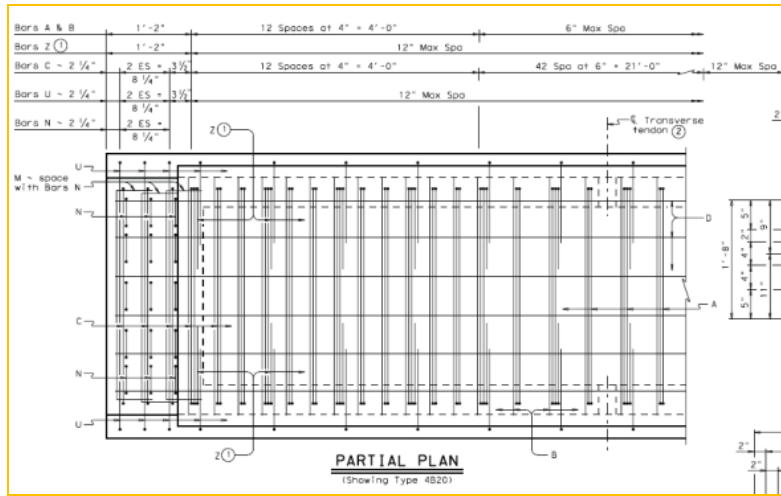
Figure 187. TxDOT box beam reinforcement layout
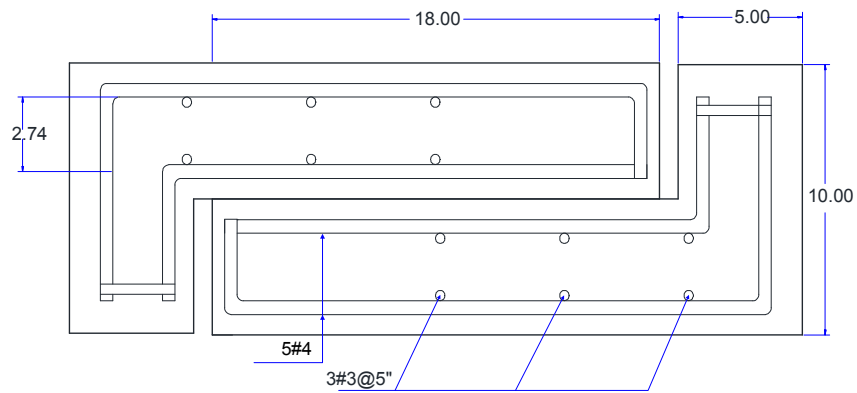
Figure 188. Reinforcement layout
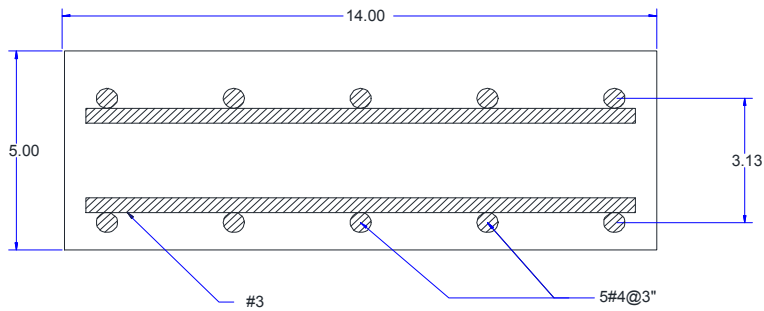
Figure 189. Cross-sectional view of reinforcement layout

229

Figure 190. Caging for precast part of specimen

Concrete Mix Design

The concrete mix used was in accordance to TxDOT specifications. The precast box and slab beams are typically cast with concrete class "H", while the CIP slab is commonly cast with concrete class "S" (Table 13). The concrete for the push-off specimens was ordered from a local ready mix provider. The concrete mix design per the ready mix supplier is displayed on

Table 14. TxDOT concrete class "H" was delivered to the lab on first to simulate the precast portion of the specimen, after that section had hardened concrete class "S" was cast on top to simulate the CIP deck. Cylinders were also prepared for each casting to test the compressive strength of the each mix after 28 days.

Table 13. TxDOT Concrete Class H and Class S Specifications

Class of concrete	Design strength, Min 28-day f'c (psi)	Maximum W/C ratio	Coarse aggregate grades
"H" (Precast)	5,000	0.45	3-6
"S" (CIP)	4,000	0.45	2-5

Table 14. Ready-mix Concrete Mix Design

Properties	Class H	Class S
Type III cement	611 lb	423 lb
Fly ash	-	141 lb
Lime	1840 lb	1840 lb
Coarse aggregates (3/4")	1331 lb	1255 lb
Fine aggregates	Not specified	50%
Retarder	9.02 oz	11.3 oz
Water-cement ratio	0.45	0.45

*Quantities per cubic yard of concrete.

Surface Preparation

After contacting a number of precast plants it was found that TxDOT box and slab beams are typically given a wood float finish. This is done by sliding a wooden float across the top of the wet concrete as shown in Figure 191, resulting in a coarse finish as shown in Figure 192. A similar type of finish was observed on site while visiting the precast plants as shown in Figure 193 and Figure 194. This is why it is of great importance to investigate the effects of a wood float surface finish on the shear transfer across an interface.

Figure 191. Applying a wood float finish (Texas Prestressed, Elm Mott, Texas; I-girder)

Figure 192. Wet concrete surface after wood float finish

Figure 193. Surface finish on Lampassas River Bridge (Waco, TX)

Figure 194. A closer view of the surface finish on Lampassas River Bridge

ICRI concrete surface profiles (CSP's) were utilized to observe the influence interface roughness has on the horizontal shear transfer. Six types of concrete surface profiles were used to establish a spectrum of relations between the friction forces and amplitude of the surface roughness. Two specimens were cast for each surface roughness which includes WF, CSP 6, 7, 8, and 9.

8.2.1.1 Surface Preparation Method

After an unsuccessful initial method in which a stamping approach was used to generate different surface profiles, a modified method of surface preparation was then developed by using a number of concrete tools such as concrete rakes and brooms that will expose aggregate along the interface. The tools used are shown in Figure 195 through Figure 199. The method provides a systematic way to obtain each of the CSP

finishes and is explained in Table 15. Figure 200 through Figure 206 show the method preparation and surface profiles next to the CSP samples.

Figure 195. Wood float
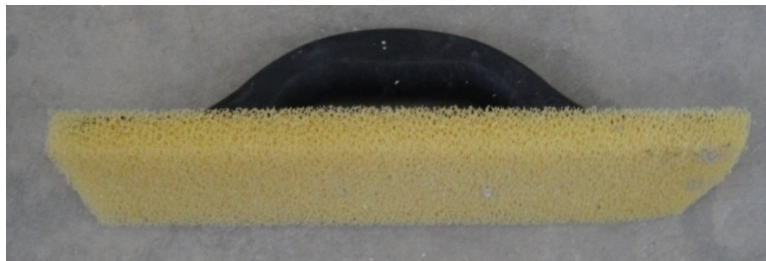
Figure 196. Coarse sponge float

Figure 197. Rubber float

Figure 198. Concrete rake

Figure 199. Concrete broom

Table 15. Modified CSP Surface Preparation Method.

Surface Finish	Tools	Technique
CSP 5	Rubber Float	Slide two times in the same direction.
CSP 6	Concrete Broom	One brush in the same direction.
CSP 7	Sponge Float	Slide three times in the same direction.
CSP 8	Concrete Broom	One brush back and forth.
CSP 9	Concrete Rake, Concrete Broom, Sponge Float	Slide once with rake, once with broom, once with sponge, in that order all in the same direction.

**The method is done after the concrete has been leveled using a concrete trowel or wood float immediately after casting. Thirty minutes later, the sponge float is lightly passed to remove any excess water due to bleeding and then each respective technique is performed.

Figure 200. Surface preparation using a concrete broom

Figure 201. Surface preparation using a sponge float
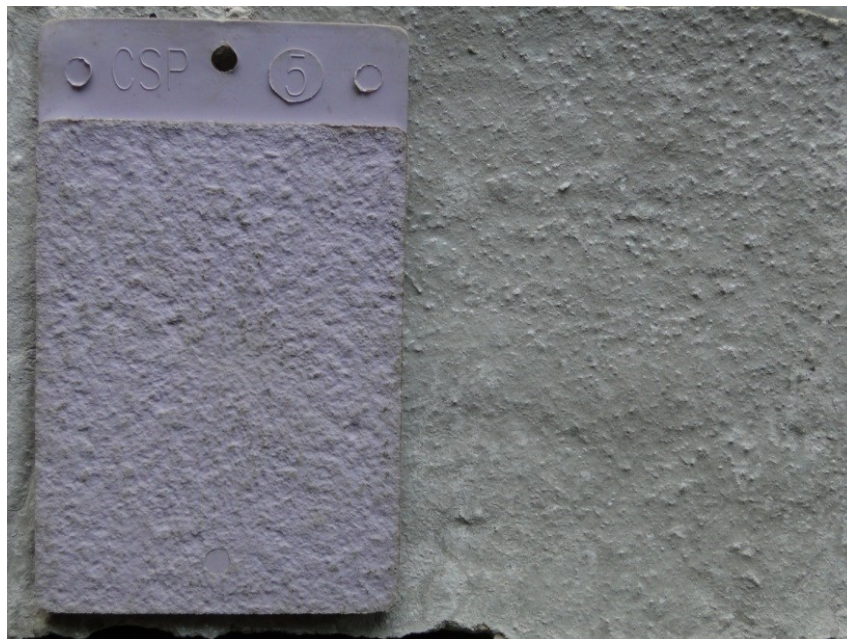
Figure 202. CSP 5 finish using the modified method of preparation
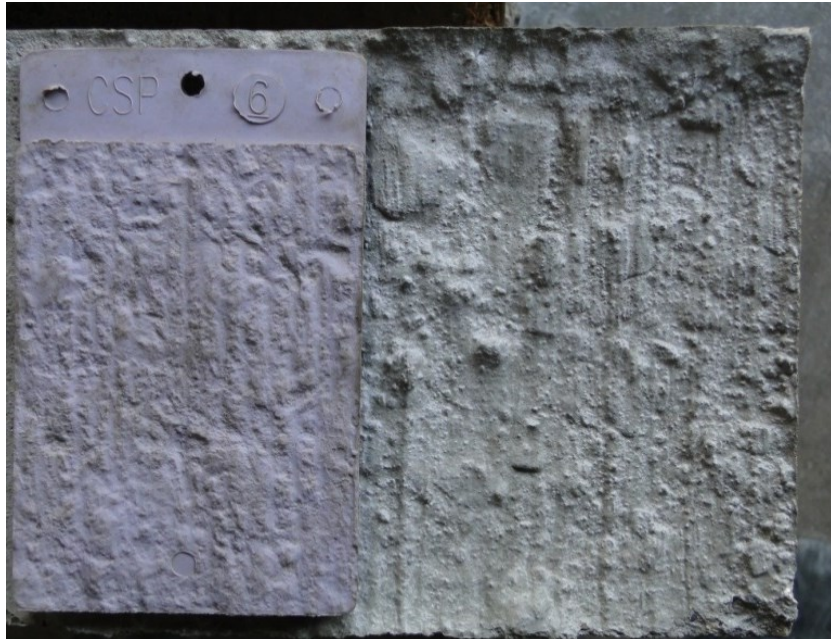
Figure 203. CSP 6 finish using the modified method of preparation

Figure 204. CSP 7 finish using the modified method of preparation

Figure 205. CSP 8 finish using the modified method of preparation
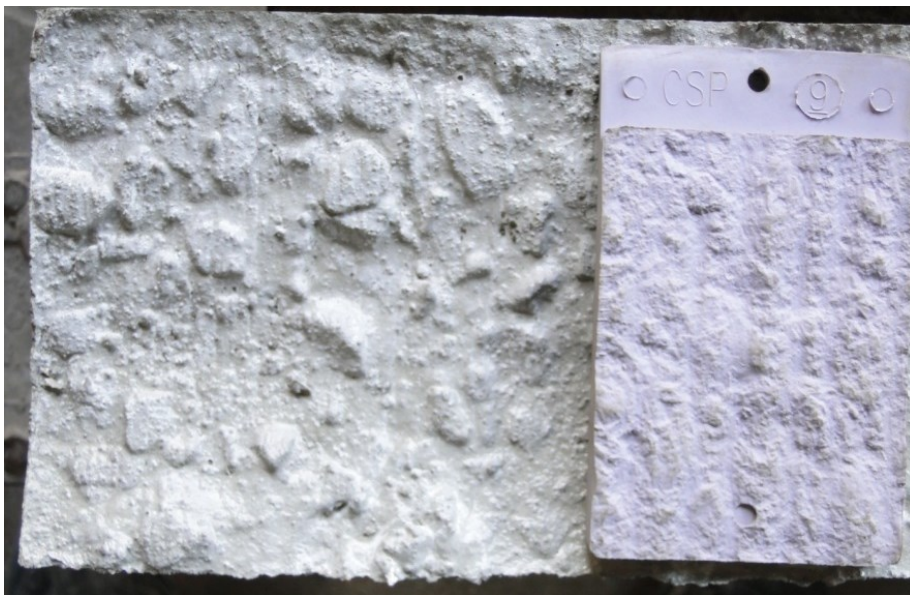
Figure 206. CSP 9 finish using the modified method of preparation

From the photos it can be seen that the CSP finishes can be successfully reproduced by the developed surface method.

8.2.2 Specimen Construction

Concrete was delivered to the UTA CELB for the casting of the precast part of the push-off specimen with concrete class "H". After the concrete was cast on the precast part of the specimen, the surfaces were first finished by a wooden float after which the processes mentioned in Table 15 for making the surface profiles were employed. Figure 202 through Figure 206 show the different surfaces made. As can be seen, the surfaces closely matched those of the CSP molds. The specimens were covered by a plastic sheet after the surface preparation was completed to avoid moisture loss during curing.

Figure 207. Specimen formwork

Figure 208. Wood float finish on all specimens

(a)
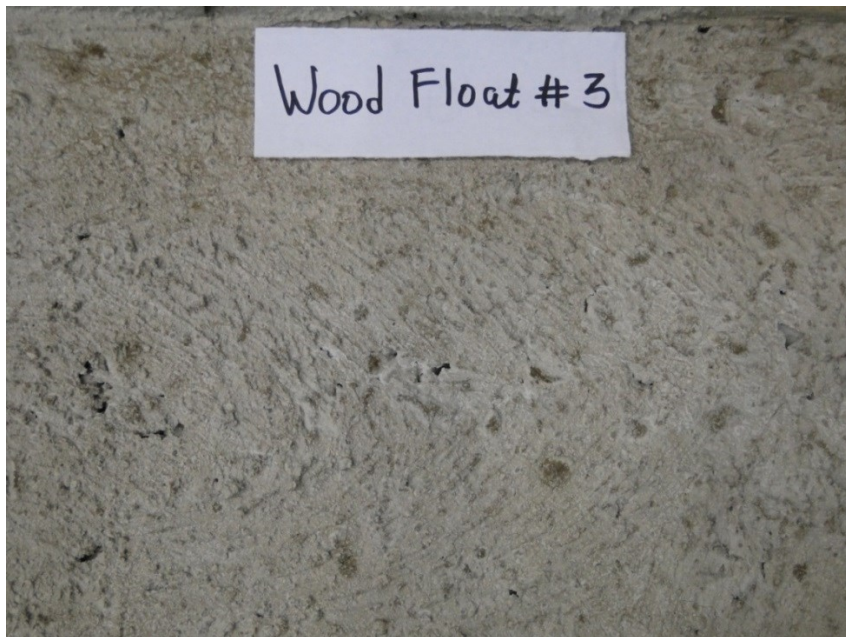
Wood Float #3

(b)

Figure 209. Wood float finished surface

(a) Brush once in same direction

(b) Finished surface.

Figure 210. CSP 6

(a) Slide three times in the same direction.

(b) Finished concrete surface.

Figure 211. CSP 7

(a) Brush once back and forth.

(b) Finished surface

Figure 212. CSP 8

(a) Slide once with rake. and brush once with broom.

(b) Slide once with sponge float.

(c) Finished surface

Figure 213. CSP 9

Figure 214. Finished specimens

The surfaces of the precast section were air blown to remove dust and dirt particles prior to the next concrete casting. The reinforcement cage was then placed and the concrete (Class "S") for the CIP portion of the specimen was cast as shown below.

Figure 215. CIP caging and formwork

Figure 216. Casting of CIP part of specimens

Figure 217. Finished specimens

The specimens were then covered with a plastic sheet and cured for 28 days after which they were demolded and prepared for testing. The concrete strength after 28 days was 4.5 ksi for the precast part and 5.0 ksi for the CIP part.

Figure 218. Demolded specimens

8.2.3 Task 2: Test Setup and Instrumentation

Push-off tests similar to the tests done by Hofbeck et al. (1969), Mattock and Hawkins (1972) (Figure 219), and Kahn and Mitchell (2002) were conducted in the vertical position for evaluating the cohesion component of the AASHTO (2014) nominal interface shear equation. The specimens had no interface shear reinforcement and by

249

testing the specimens in the vertical position the effects of the dead load due to the CIP slab were removed.
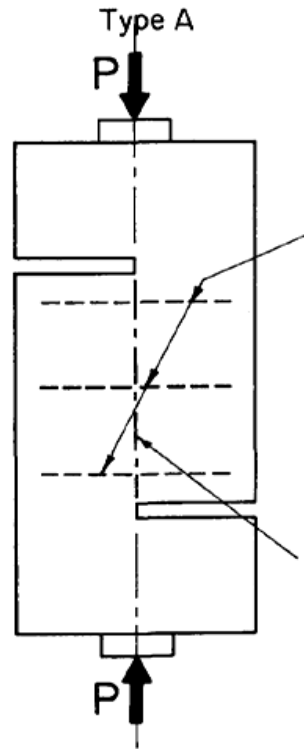
Figure 219. Push-off tests used by Mattock and Hawkins (1972)

The test setup for the vertical push-off test used in Task 2 is shown in Figure 220. It consists of a 400-kip compression machine, a load cell, a W12x79 steel section used as the loading beam, and two loading strips. A wide flange section was chosen as it gives a more direct load distribution since the load can be transferred through the web and onto the loading strip (Figure 220). A 16x1x0.5 in. steel plate was welded underneath the middle of wide flange section and was used as one of the loading strips. The second loading strip (16x1x0.5 in.) was placed underneath the specimen at the midpoint. These two loading strips were used to minimize the eccentricity of the load, which could lead to undesirable flexural stresses in the specimens. Lateral bracing was placed on both sides

to restrain the concrete sections when separation occurs at failure. The load cell was secured to the machine to prevent it from falling after a sudden failure. Each test specimen was instrumented with two linear varying differential transformers (LVDTs) placed on each of the segments to measure the slip between the precast and CIP parts during testing.
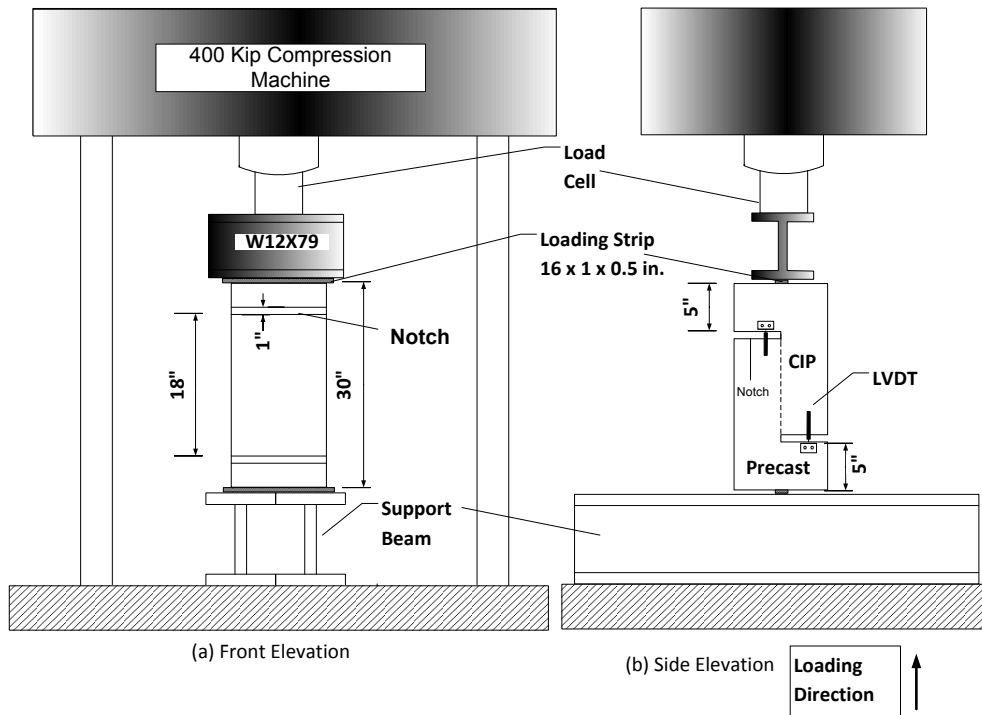
Figure 220. Schematic view of Task 2 test setup

8.2.4 Task 3: Test Setup

The test setup for the horizontal push-off test is shown in Figure 221. The specimen was placed horizontally such that the contribution from the normal force will be mobilized. The specimen will have no interface reinforcement and by subtracting the values obtained from the Task 2 results due to the cohesion and aggregate interlock component, the shear resistance from (μPc) can be calculated. It consists of a 400 kip compression machine applying the compression load, a load cell to record the load being

applied, a hydraulic cylinder that applies the horizontal force on the interface and a W8x24 loading beam. A 14x14x2 in. plate was used to transfer the compression load to the specimen. To ensure that the load is uniformly applied to the specimen through the loading beam, grout was applied uniformly below the loading plate. A plastic sheet was then placed on top of the grout before placing the loading plate. The specimen was instrumented with two linear variable differential transformers LVDTs placed on both the CIP and precast parts to measure the slip during testing. A loading strip of 16x1x0.5 in. was used on both sides to ensure the load was transferred to the interface.
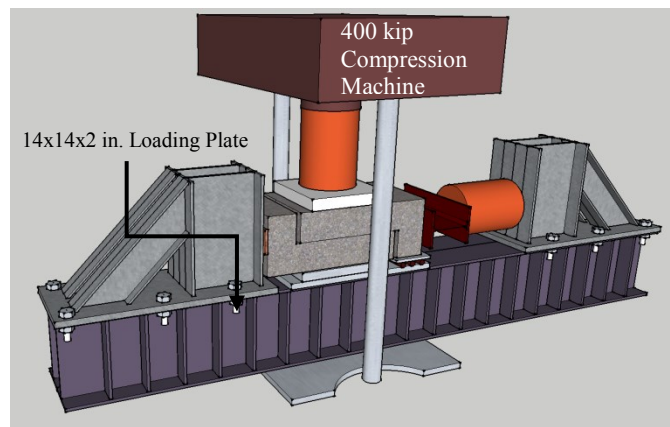
(a)
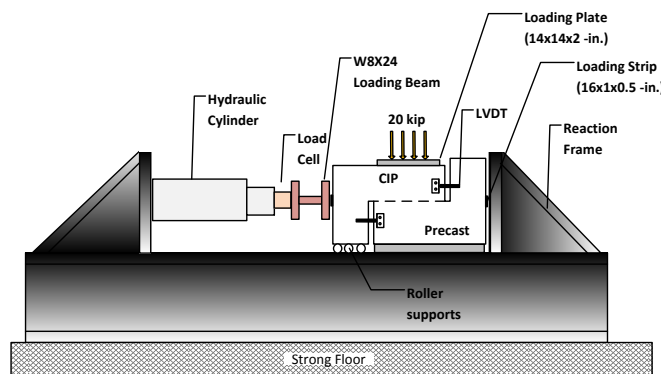
(b)

Figure 221. Schematic of Task 3 test setup (horizontal push-off test)
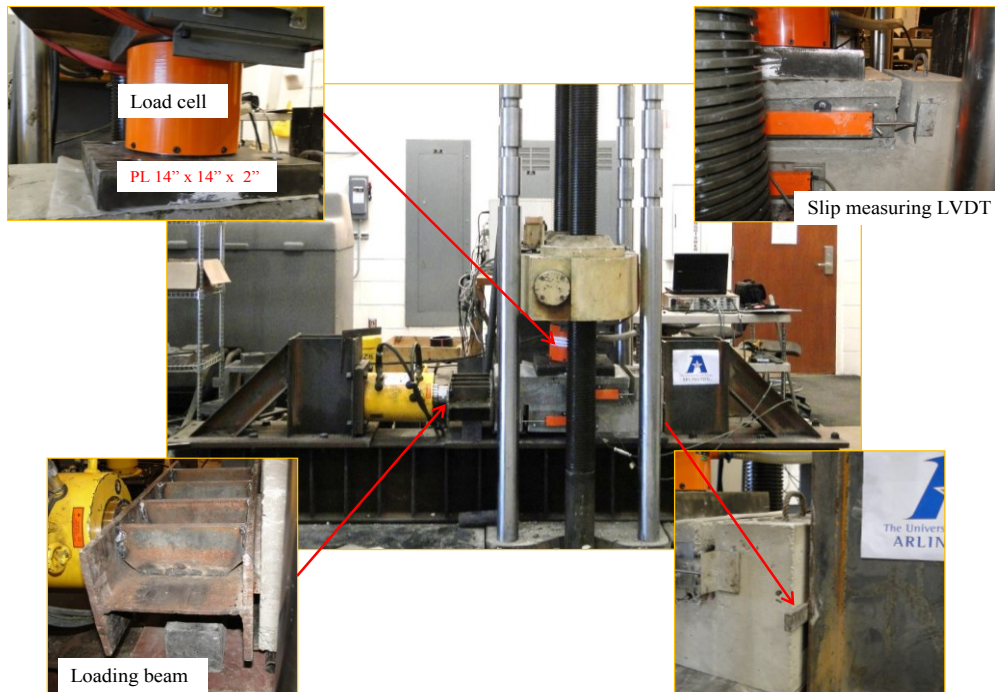
Figure 222. Details of Task 3 test setup

To reduce any load eccentricities, the actual position of the loading beam and load cell were marked on the center of the specimen. The top surface of the specimen was grouted and the 2 in. thick plate was placed in-between the specimen and the load cell. The compressive force was vertically applied first by the 400-kip machine and kept constant at 20 kips after which the horizontal force was applied. The horizontal load was applied at a rate of approximately 100 lb/sec, up to failure.

Since some friction was expected to be generated between the compression loading plate and the plastic sheet on top of the specimen, a test was conducted to find out how much this would contribute to the total shear recorded. The set-up utilized one segment of a failed specimen to analyze the friction contribution as shown in Figure 223. The rollers were used so that there was no shear between the specimen and the plate on top of the roller and then a compression load of 20 kips was applied to the specimen.

This compression load was kept constant while a horizontal load was progressively applied.
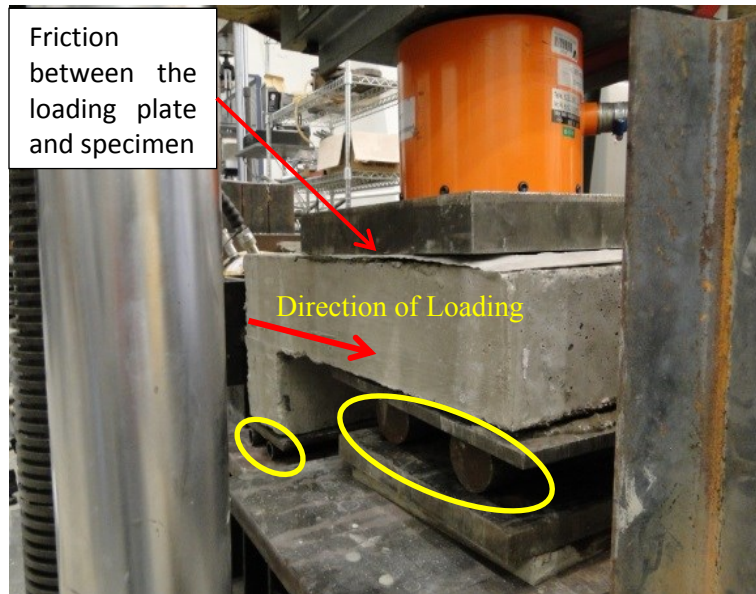
Figure 223. Component test used to analyze the friction contribution of test setup

The specimen moved almost immediately when the force was applied. It was discovered that the contribution from these two factors was only about 0.5 kips. Therefore it does not adversely affect the Test 2 results.

8.3 Full-Scale Composite Beam Tests

8.3.1 Task 6: Current TxDOT Provisions

8.3.1.1 Task 6: Current TxDOT Provisions Specimen Design

A total of two slab and two box full-scale beams were tested for Task 6. One of the box beams was designed using the current reinforcement detailing according to TxDOT so as to represent a typical beam used in practice. Strain gauges were mounted on the horizontal shear reinforcement to measure the strain of the bars during testing. In the second box beam, the flexural reinforcement was increased so as to force a

horizontal shear failure and evaluate the horizontal shear strength of the beam as a whole. The same detailing was used for the two slab beams as shown in Table 16.

Table 16. Testing Matrix for Task 6.

Full-Scale Beam Test	Number of Tests
30-ft Composite Box Beam, 4B20	2
30-ft Composite Slab Beam, 4SB12	2

PGSuper Beam Analysis and Design

PGSuper was used to design the box and the slab beams for Task 6. A 30 ft long composite beam was selected for both the slab and box beams due to the lifting constraints of the crane in the UTA CELB. The beam selected was one that did not exceed the crane capacity of 15 tons. The PGSuper analysis determined that the box beam type 4B20 and slab beam 4SB12, having a length of 30 ft, were the optimum choice of beams to be used for this task. The design of the beams was done according to the current TxDOT standards using the PSBSD and BBSDS standard drawings as guidelines. To increase the shear demand and simulate the most critical condition, more prestressing strands were added to the beam. The analysis determined that a flexural failure will occur before shear or horizontal shear failure occurs.

Moment Capacity

The results from the analysis show that the moment capacity of each beam is more than two times the moment demand. Using the setup shown in Figure 224 the expected failure load was calculated to be 81 kips for typical TxDOT slab beams and 160 kips for box beams. The moment diagram for the test setup can be seen in Figure 224. This was calculated using the maximum moment.
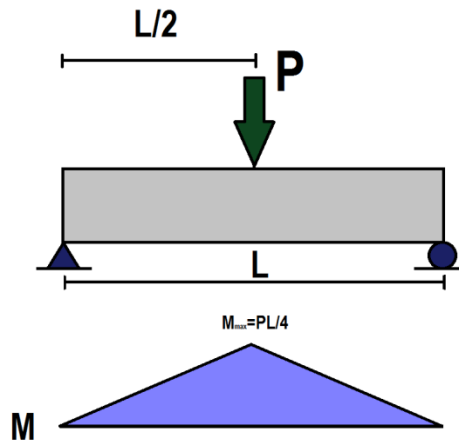
Figure 224. Moment diagram of simply supported beam with point load at midspan

Shear Capacity

In order for the beam to fail in shear, a peak load of 472 kips for the box beam and 597 kips for the slab beam would be expected with regards to the maximum shear (highlighted). Therefore the load needed to fail the beam by shear is much higher than that needed to fail the beam by flexure hence it was expected that the beam will fail in flexure. Figure 225 shows the shear diagram for the case of a simply supported beam with a point load applied at midspan.
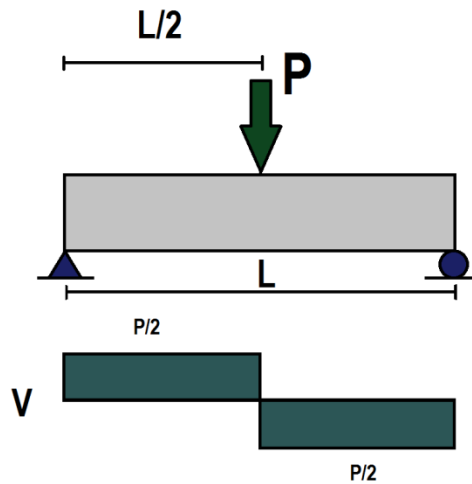
Figure 225. Shear diagram of simply supported beam with point load at midspan

Horizontal Shear Strength

The results from the horizontal shear strength shows that the design horizontal interface shear strength is at least four times that of the interface shear demand. The load needed to fail the beam by horizontal shear is significantly higher than that needed to cause a flexural failure. It is therefore unlikely that a horizontal shear failure will occur before flexural failure. The results observed in Waweru (2015) from the Task 5 tests indicate that the bar pulls out before yielding. Therefore, the yield stress indicted in the AASHTO interface shear equation was replaced with the highest bar stress recorded in Task 5 (f_s = 36 ksi), in which the results are shown in the last column.

Table 17 summarizes the maximum moment, shear, and horizontal shear results from the PGSuper design for the two current TxDOT standard beams. The peak load shows the expected load needed to fail the beam in flexure. This peak load has been calculated based on a point load application as shown on Figure 226.
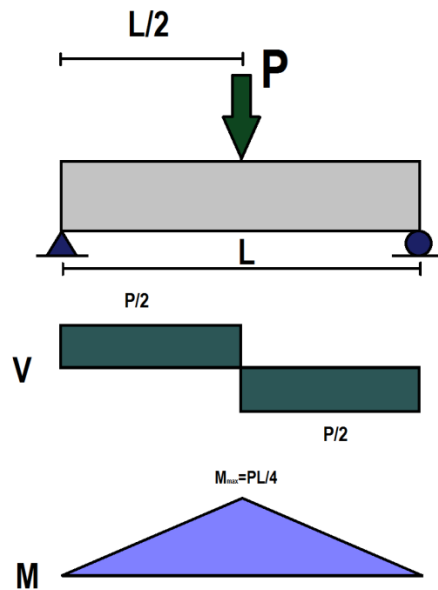
Figure 226. Shear and moment diagrams of simply supported beam with point load at midspan

Table 17. Maximum moment, shear, and horizontal shear from PGSuper Design

Beam Type	No. of Strands	Mu* (kip-ft)	ΦMn (kip-ft)	Vu (kip)	ΦVn (kip)	Vui (kip/ft)	Vni (kip/ft)	Weight (lb)	Peak Load (kips)
4SB12	14	427.63	593.14	57.48	337.59	50.50	173.29	25,380	82
4B20	16	452.83	1161.13	88.05	304.15	40.12	175.58	25,950	161

* Based on HL-93 loading

A comparison was made between the beam with the maximum horizontal shear demand and the beam proposed for this design to determine the difference in the shear demand between the two. From the analysis, it was found that a 65 ft box beam 5B20 and a 50ft slab beam 5SB15 provided the maximum possible horizontal shear demand. This has been tabulated in Table 18.

Table 18. Shear Stress demand comparison.

Beam Type	Span Length (ft)	Shear Stress Demand (kip/ft2)
4B20	30	10.99
5B20	65	15.48
4SB12	30	12.70
5SB15	50	14.66

Specimen Drawings and Dimensions

Due to the design modification to the number of strands, a slight change was made in the standard drawings to take into account these changes.

From the PGSuper results, it was decided that horizontal shear reinforcement be eliminated on one of the slab beams and one of the box beams to evaluate their contribution on horizontal shear resistance. Flexural reinforcement was increased on the beams without shear reinforcement so as to force a horizontal shear failure in order to investigate horizontal shear strength as a whole. Since PGSuper does not consider mild-steel flexural reinforcement in calculating the moment, hand calculations were performed to determine the moment capacity of the beams.

Table 19 summarizes the moment capacity as well as the peak load required to fail the specimen by flexure.

Table 19. Moment capacity and peak load of over-reinforced beams

Beam Type	No. of Strands	No. of bars	Mu* (kip-ft)	ΦMn (kip-ft)	ΦVn (kip)	Vui (kip/ft)	Vni (kip/ft)	Weight (lb)	Peak Load (kips)
4SB12	14	12	427.63	1163.43	337.59	50.50	173.29	26,338	160
4B20	16	15	452.83	2126.15	304.15	40.12	175.58	27,148	310

The bars were placed in the most convenient spacing to avoid obstruction of voids and strands (Figure 227and Figure 228). Since Flexicore of Texas provides a rake finish on all slab and box beams, a rake finish was provided on all the specimens.
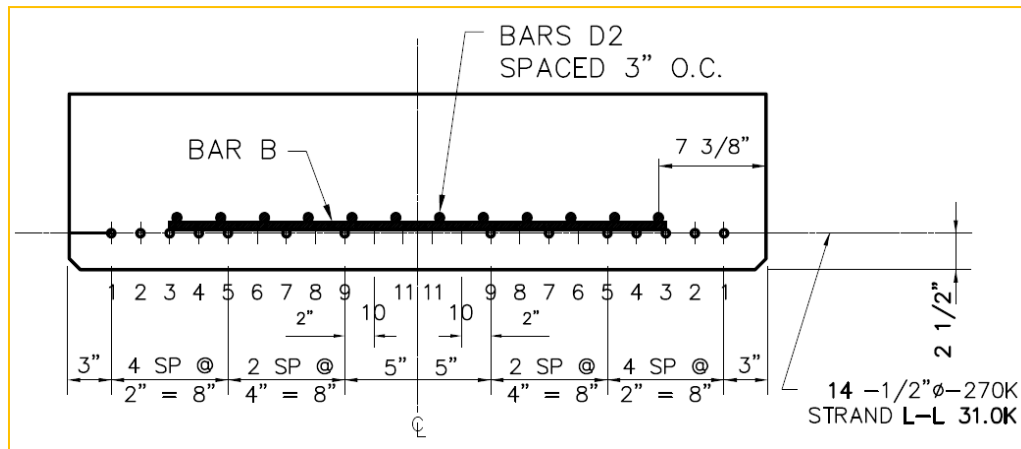
Figure 227. Slab beam without shear reinforcement
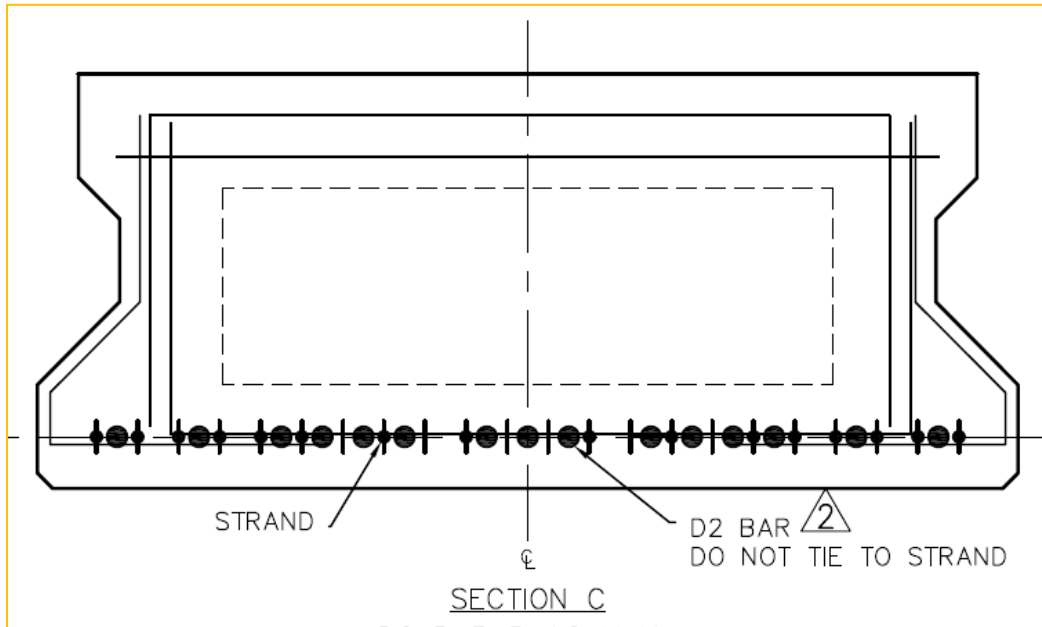
Figure 228. Box beam without shear reinforcement

8.3.1.2 Task 6: Current TxDOT Instrumentation and Casting

Instrumentation

Given the difficulty in placing strain gauges on the prestress strands, it was decided that two #3 bars will be placed along the strand with strain gauges mounted on them. From ACI Sec. 12.2.2 (Equation 8-1), a developmental length of 30 in was determined to be adequate to avoid bar pullout before yielding. Given that the yield strength of the bar may be as high as 100 ksi, the developmental length was doubled to 60 in.

$$l_d = \left(\frac{f_y \Psi_t \Psi_e}{25\lambda\sqrt{f_c'}}\right) d_b \qquad\qquad (8-1)$$

These bars will be placed 30 in both ways from the center of the beam.
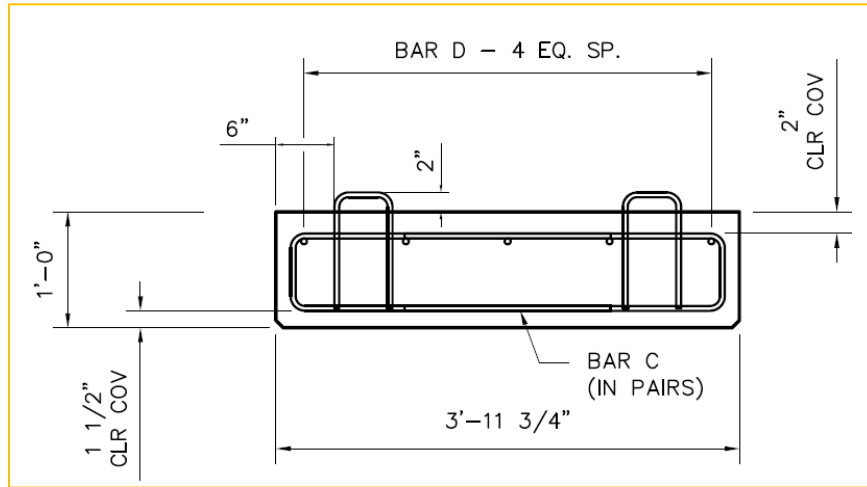
Figure 229. Slab beam section
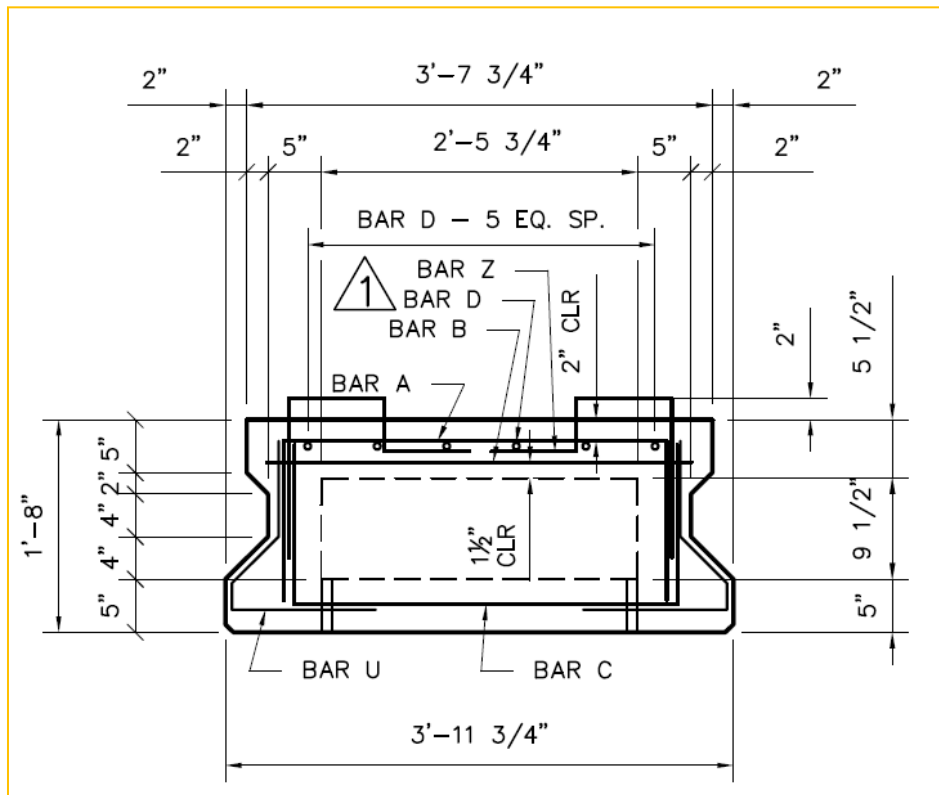
Figure 230. Box beam section

261

Specimen Preparation

- *Box Beam Specimen*

The beams were fabricated at Flexicore of Texas located in Pearland, TX. First, the prestressing bed was cleaned and sprayed with water due to the high temperatures on the day of casting. The prestressing strands were then drawn and stressed at a jacking force of 31 kips per strand. The longitudinal reinforcement was then placed in the bed as well as the end mat reinforcement. The Bars C were then positioned at a spacing of 6 in. whereas Bars U were placed at a spacing of 9 in. Strain gauges were installed on the longitudinal reinforcement and on Bars C so as to monitor the strains on the bars. The reinforcement layout is as shown in Figure 231. The horizontal shear reinforcement at both ends of the beam and the center were strain gauged on both sides of the bar. Cylinders were also made to test the compressive strength of the mix after 28 days.
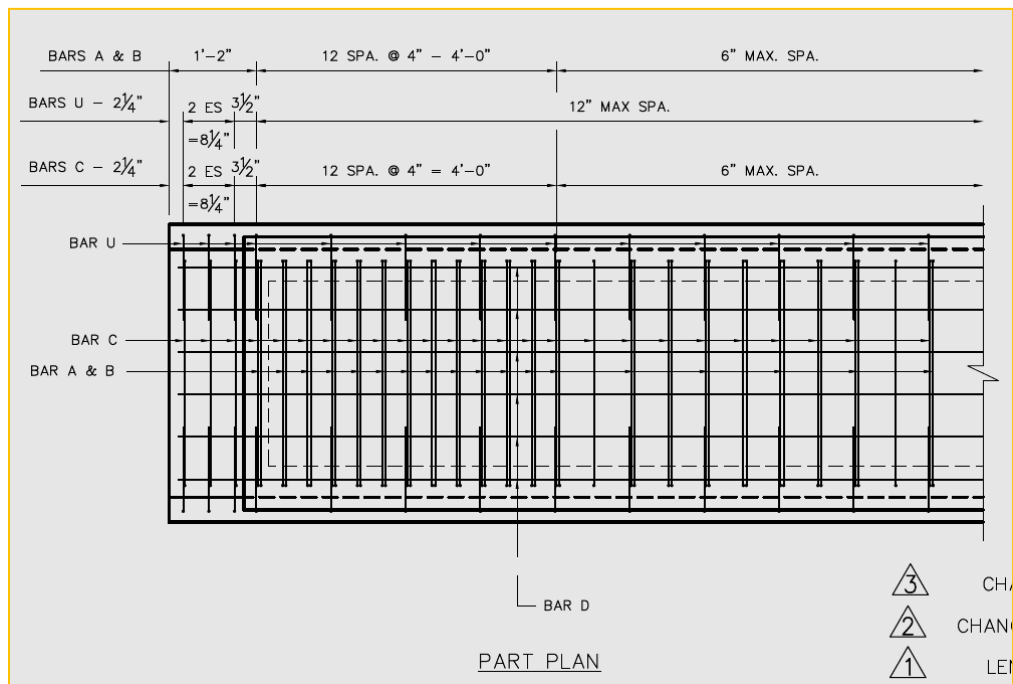
Figure 231. TxDOT box beam reinforcement layout

(a)
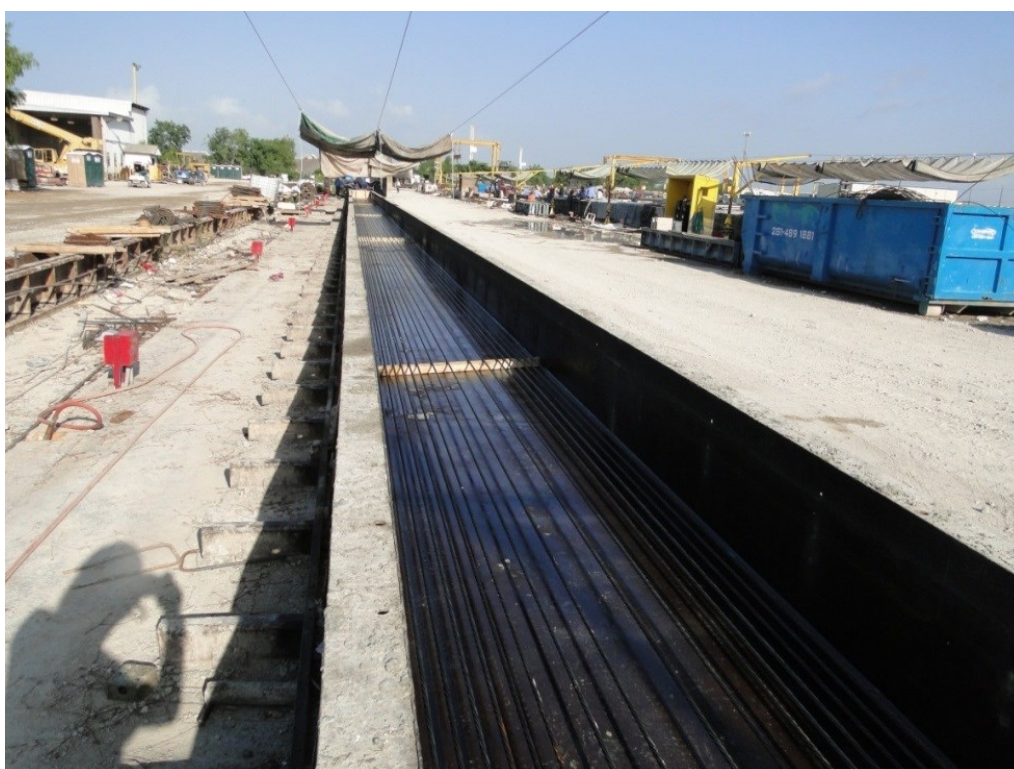
(b)

Figure 232. Prestressing of strands

(a)

(b)

Figure 233. Strain gauge application of Bar U

Figure 234. Strain gauges on longitudinal reinforcement
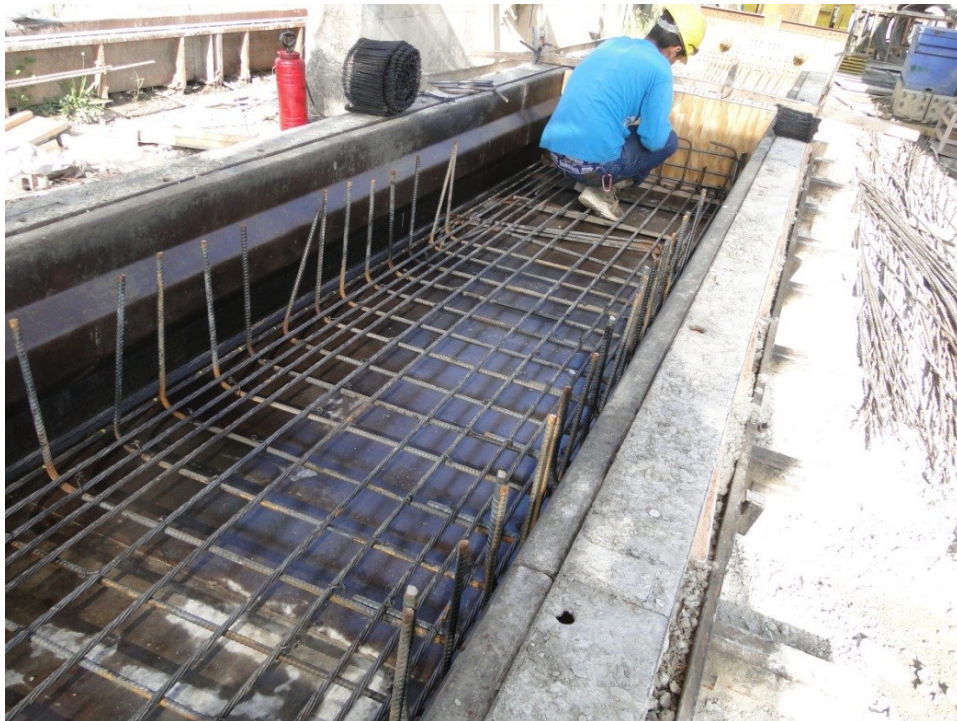
Figure 235. Placement of Bar C

(a)

(b)

Figure 236. Placing of No. 3 longitudinal bars

Figure 237. Placing of Bars U

(a)

(b)

Figure 238. Placing of No. 8 longitudinal bars

Figure 239. End mat reinforcement

The concrete mix used was chosen according to TxDOT specifications. Box and slab beams are typically cast with concrete class "H", while the CIP slab is cast with concrete class "S". The two box beams were cast in two sections. After the bottom reinforcement was placed, the concrete was poured to a height of 5 in. after which Styrofoam was placed to create the hollow section of the box beam (Figure 240 to Figure 242).

Figure 240. Concrete pouring

Figure 241. Concrete poured to 5 inches

Figure 242. Placement of the Styrofoam

The reinforcement cage for the top portion of the box beam was then placed using a crane and concrete poured to the top of the box beams. As the concrete was poured the horizontal shear reinforcement was adjusted to its correct location and the surface was initially finished using a wood float.

(a)

(b)

Figure 243. Top reinforcement for box beam with horizontal shear reinforcement

Figure 244. Top reinforcement for box beam without horizontal shear reinforcement

(a)

(b)

Figure 245. Casting of the top part of the box beam with horizontal shear reinforcement

271

Flexicore of Texas provides a rake finish to all their box and slab beams therefore a rake finish was provided on all of the Task 6 beam specimens to simulate what is typically done in practice. The rake was passed through the wet concrete surface transverse to the beam length as demonstrated in Figure 246.

Figure 246. Rake finish

After placing, the horizontal shear reinforcements were then lightly scrubbed by a steel wool to remove concrete from their surfaces.

Figure 247. Cleaning of horizontal shear reinforcement

Figure 248. Finished box beam

The specimens were then covered to avoid moisture loss during curing. The prestressing strands were cut the next day and the beam specimens demolded for storage. The concrete strength after 28 days was 11 ksi for the precast box beams.

Figure 249. Finished box beam specimens

- *Slab Beam Specimen*

After the prestressing strands were stressed, the longitudinal bars were placed for the slab beams. The bars were supported on top of the strands by #4 bars placed transversely at intervals along the length of the slab beam without shear reinforcement (Figure 252). The stirrups (Bar C) were then placed with the stirrups containing strain gauges at 9 inch spacing from the center of the beams. The longitudinal bars with strain gauges were placed at the furthest bar from right beam edge, at the center and 13 in. from the left edge (Figure 251).
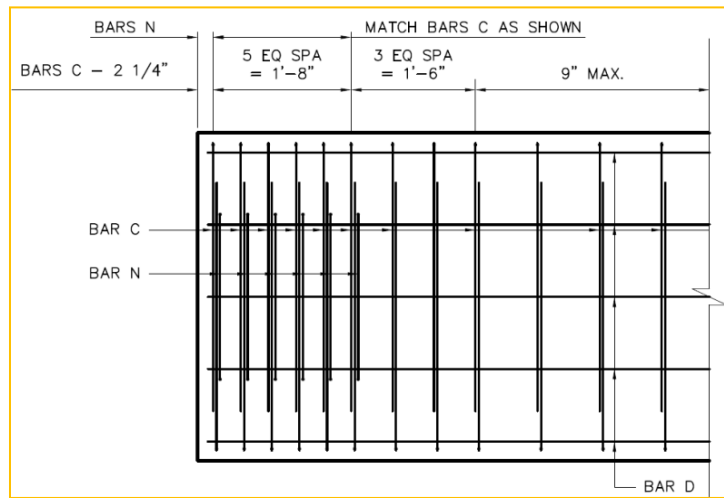
Figure 250. TxDOT slab beam reinforcement layout
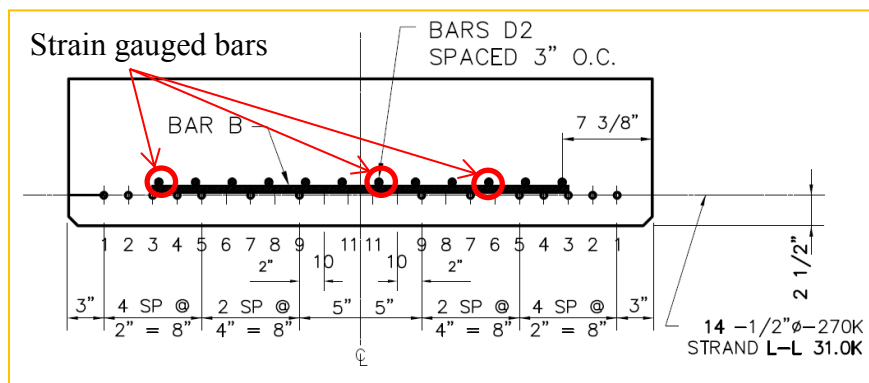
Figure 251. Slab beam section
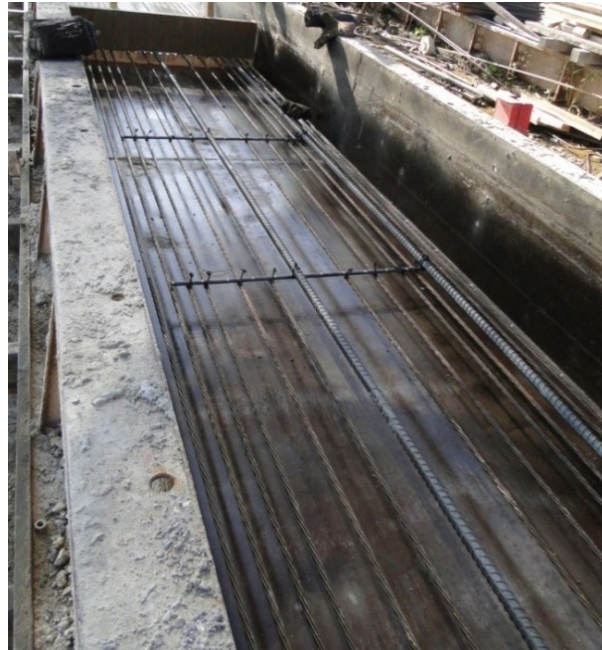
Figure 252. Placement of strands and flexural reinforcement

Figure 253. Placing of strain gauged stirrups

(a)

(b)

Figure 254. Placing of No. 8 longitudinal bars on slab beam without shear reinforcement

(a)

(b)

(c)

Figure 255. Placing of No. 3 longitudinal bars on slab beam with shear reinforcement

Figure 256. Stirrup spacing

(a)

(b)

Figure 257. Completed slab beam reinforcement

The concrete was cast using Class "H" concrete mix according to TxDOT specifications. The slab beams were cast in one single pour. A rake finish was applied on the wet concrete surface in the transverses direction before the beams were covered for curing.

Figure 258. Slab beam casting

(a)

(b)

(c)

Figure 259. Rake finish

A longitudinal line was then made on the wet concrete at 6 in. from the edge to mark the position where the horizontal shear reinforcement would be placed. The horizontal shear reinforcement bars were then pushed into the wet concrete until a height of 2 in. remained above the concrete surface (Figure 260). The concrete strength after 28 days was 10 ksi for the precast slab beams.

(a)

(b)

Figure 260. Placing of horizontal shear reinforcement

Figure 261. Finished slab beam with horizontal shear reinforcement
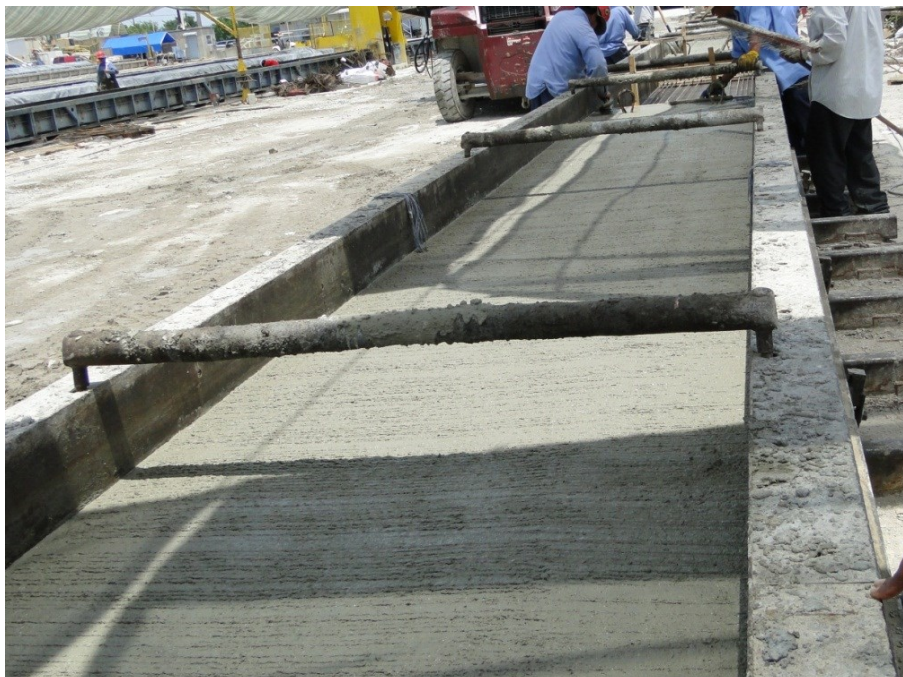
Figure 262. Finished slab beam without horizontal shear reinforcement

Cast in-Place Casting

The horizontal shear reinforcement was instrumented with strain gauges at midspan and near the ends of the beams prior to casting. The reinforcement for the CIP was consistent with that used on TxDOT bridges. The surfaces of the precast beams were cleaned to remove dust and dirt particles before casting. The reinforcement cage was then placed on the beams and the concrete (Class "S") was cast as shown below.
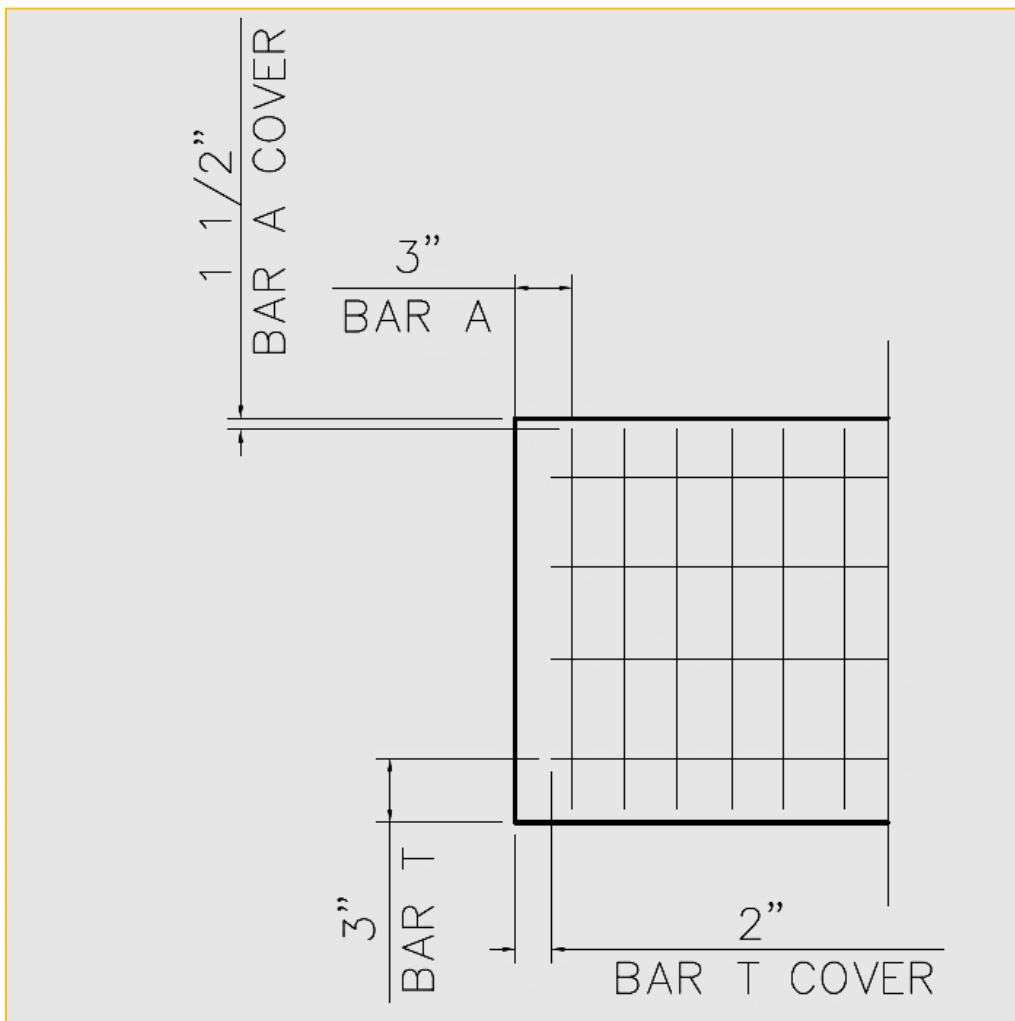
Figure 263. CIP slab reinforcement layout for box beam
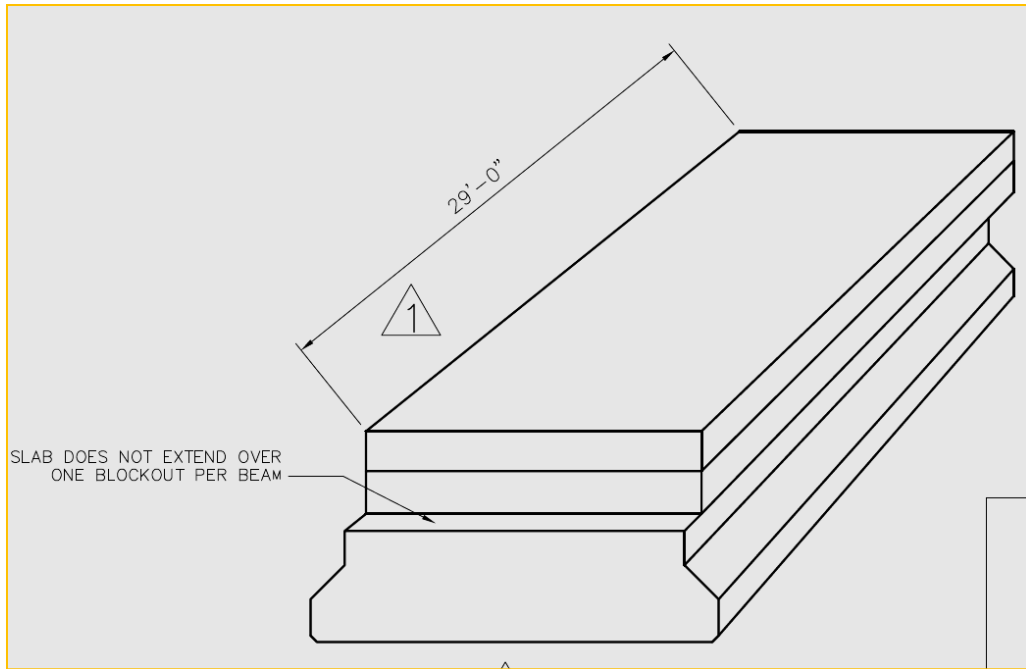
Figure 264. CIP slab does not extend to one blockout
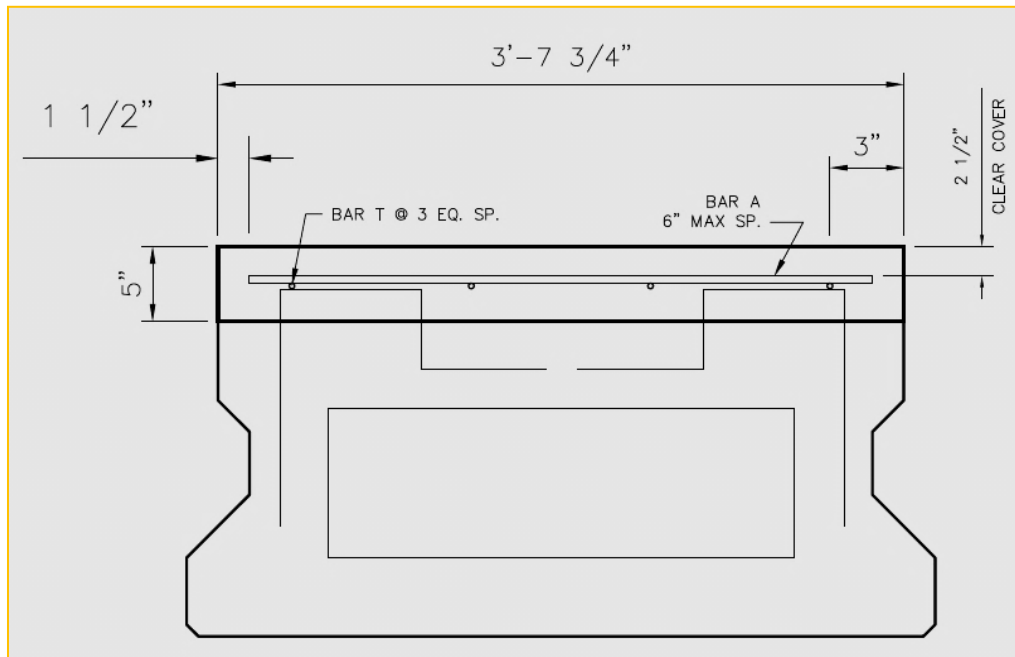
Figure 265. CIP slab detail for box beam
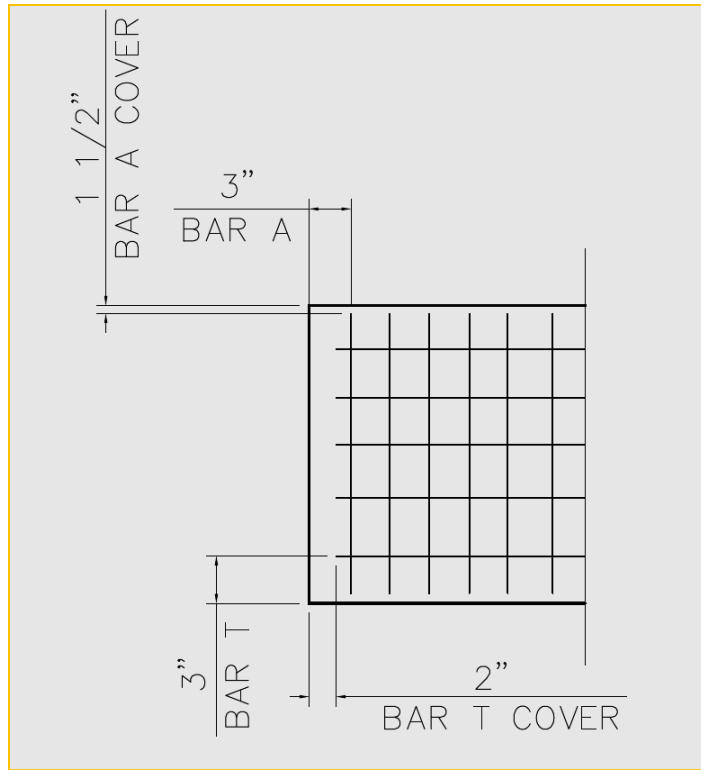
Figure 266. CIP slab reinforcement layout for slab beam
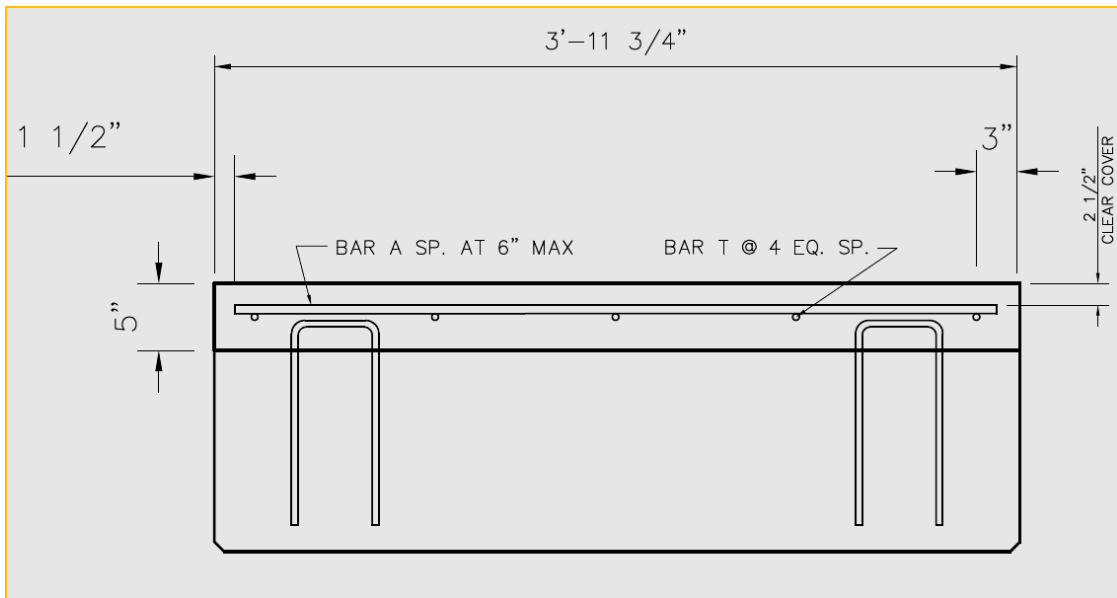
Figure 267. CIP slab detail for slab beam

285

Figure 268. Slab beam and CIP formwork

Figure 269. Box beam in CIP formwork

Figure 270. Box beam with CIP reinforcement

Figure 271. Slab beam with CIP reinforcement

Figure 272. Slab beam without shear reinforcement and CIP reinforcement
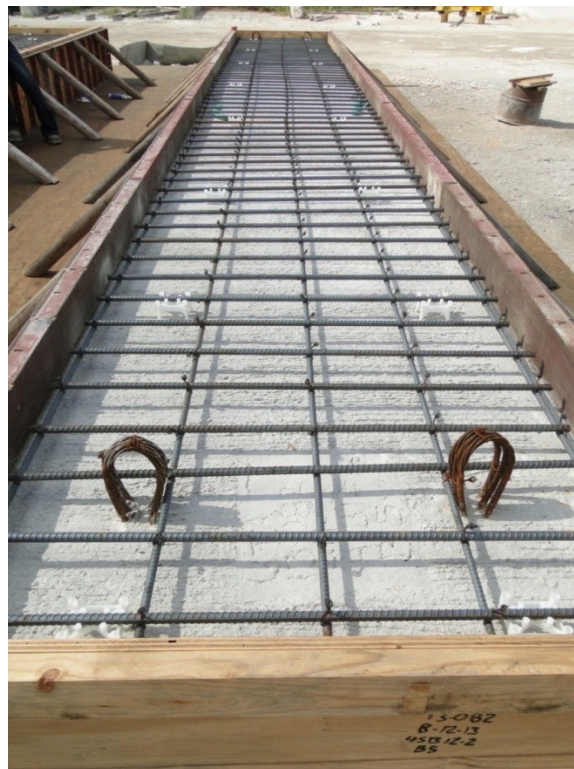
Figure 273. Box beam without shear reinforcement and CIP reinforcement

Figure 274. Wetting concrete surface prior to CIP casting

Figure 275. Vibrating and wood float finishing

Figure 276. CIP casting

Figure 277. Vibrating during CIP casting

Figure 278. Finishing of CIP part of specimens

Figure 279. Finished CIP surface

Figure 280. Finished specimens

The specimens were then covered with a plastic sheet and cured after which they were demolded and prepared for delivery to UTA. The concrete strength after 28 days was 11 ksi for the CIP slab.

Specimen Delivery

The beams were delivered to the UTA Civil Engineering Laboratory. A local crane company was hired to aid in unloading the beams from the delivery trucks and for placing the beams within the lab.

Figure 281. Beams arrive at UTA Civil Engineering Laboratory

(a)

(b)

(c)

(d)

Figure 282. Storing of the beams outside the lab

8.3.2 Task 7: Full-scale Tests on Composite Box and Slab Beams (Further Investigation)

8.3.2.1 Task 7: Specimen Design

Based on component testing from Task 2 through Task 5, it was discovered that a change in bar configuration with a 2 in embedment will have no effect on the shear strength of the beam. Task 6 proved that horizontal shear failure will not occur for TxDOT beams with a rake finish even without shear reinforcement. Therefore the proposed details for Task 7 are to ensure horizontal shear failure by reducing the interface area. It is expected that a reduction in shear reinforcement combined with wood float finish would significantly facilitate the fabrication of composite slab and box beams.

TxDOT is also pushing towards the use of self-consolidating concrete (SCC) on precast beams although it has not yet been widely accepted by fabricators. However, on our visit to Texas Prestressed Concrete plant, we observed that they do use SCC on their slab beams. It was observed that a wood float finish on SCC slab beams resulted in a much smoother interface (Figure 283) comparable to a CSP 4. There is currently no known research that investigates the horizontal shear resistance of beams constructed with SCC. Therefore, testing SCC beams would provide valuable information to determine the effect of a much smoother interface on the horizontal shear resistance. It should also be noted that although AASHTO recommends a cohesion factor of 0.28 ksi for a surface roughened to an amplitude of 0.25 in., it does not address the fact that a smoother interface may result from the use of SCC. Consequently, there is no cohesion and friction factor suggested in the case where SCC is used.

Figure 283. Surface finish on SCC slab beams comparable to CSP 4

Slab beam with reduced area (SCC and conventional concrete)

Two slab beams were designed; one of the beams was to be cast using Self-Consolidating Concrete (SCC) and conventional concrete was used on the other beam. Horizontal shear reinforcement was provided on both beams and the interface area was reduced to 12 in. to force a horizontal shear failure in order to better evaluate the contribution of the horizontal shear reinforcement. Flexural reinforcement was increased on both beams to increase the shear demand with the addition of 12 No. 8 longitudinal bars (Figure 284). Since PGSuper does not consider the additional mild steel flexural reinforcement in calculating the moment, hand calculations were performed to determine the moment capacity of the beams. A wood float finish was provided to the surface of both specimens.

Table 20 below summarizes the maximum moment, shear and horizontal shear results from the PGSuper design. The peak load shows the expected load needed to fail

the beam in flexure. This peak load has been calculated based on a point load application at midspan.

Table 20. Slab beam design

Beam Type	No. of Strands	No. of bars	Mu* (kip-ft)	ΦMn (kip-ft)	ΦVn (kip)	Vui (kip/ft)	Vni (kip/ft)	Peak Load (kips)	Peak load for horizontal shear
4SB12-reduced area	12	12	427.63	1163.43	337.59	50.50	72.40	160	674
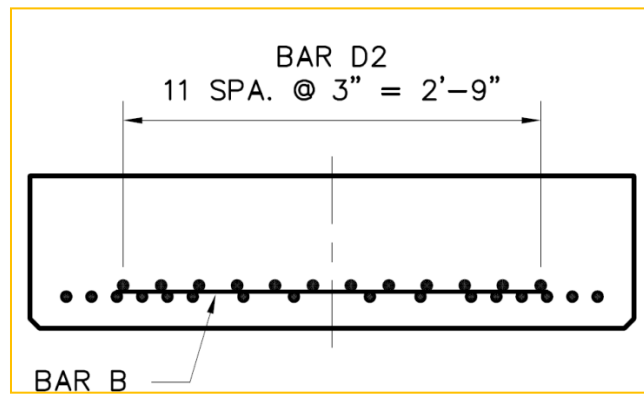
(a)
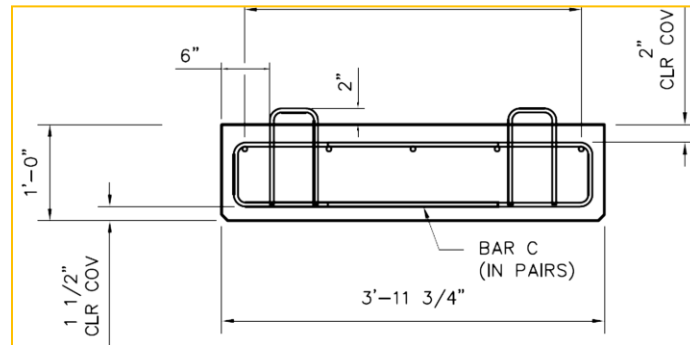
(b)

Figure 284. 4SB12 section with (a) Tension reinforcements and (b) Horizontal shear reinforcements

The size of interface area needed to ensure a horizontal shear failure was calculated based on both the elastic method (VQ/Ib_v) and the simplified elastic method (V/b_vd).

Reduced Area component tests

To ensure that the full-scale beams fail by horizontal shear, it is necessary to reduce the interface shear resistance by reducing the interface area. Three methods were attempted for reducing the interface area; using aluminum strips, using Styrofoam, or using a polyethylene foam tape at the interface to prevent contact between the precast beam and the CIP slab. The most suitable method will be the one providing the least resistance to sliding. Push-off specimens were therefore cast with the each different method to determine the best to use for the full-scale precast beams.

Figure 285. Push-off specimen with (a) foam tape, (b) aluminum strip and (c) Styrofoam to reduce interface area

The foam tape was found to provide less resistance to sliding compared to the steel plate and the Styrofoam. Foam tape was therefore chosen to reduce interface area on the full-scale specimens (Figure 286).

Foam tape
Peak load: 15 kips
C = 0.06 ksi

(a)

(b)

Figure 286. Foam tape specimen at failure

8.3.2.2 Task 7: Specimen Construction

After prestressing the strands, the longitudinal bars were placed in the formwork bed. The bars were supported on top of the strands by #4 bars placed transversely at intervals along the length of the slab beam without shear reinforcement (Figure 287). The stirrups (Bar C) were then placed with the stirrups containing strain gauges placed at 9 inch spacing from the center of the beams. The longitudinal bars with strain gauges were placed at the furthest bar from right beam edge, at the center and 13 in. from the left edge (Figure 287).
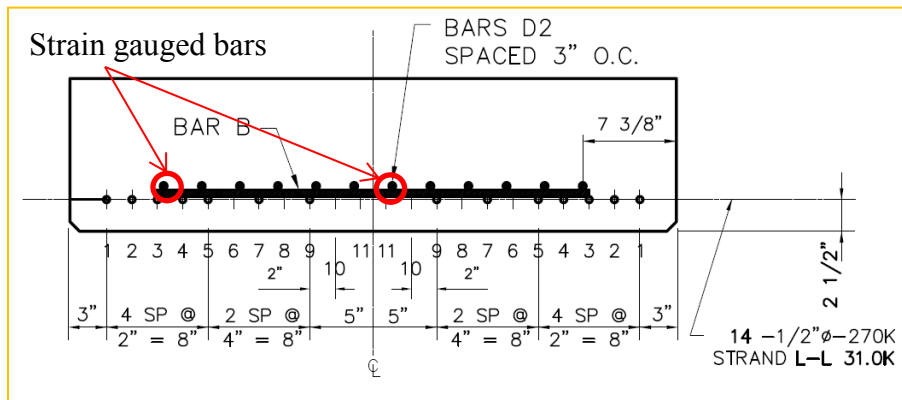
Figure 287. Slab beam section
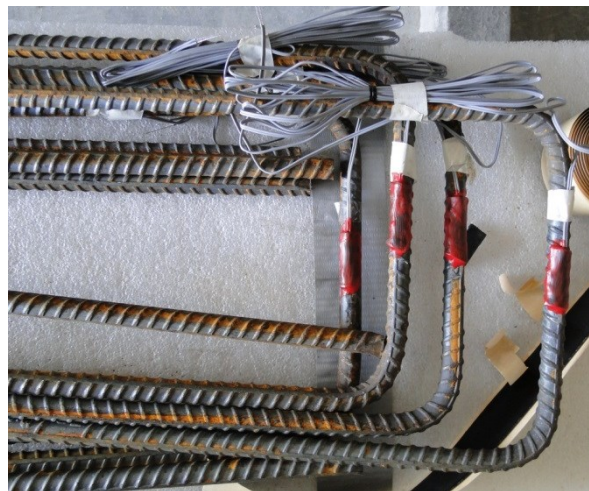
Figure 288. Strain gauges on stirrups

(a)

(b)

Figure 289. Placing of strain gauged stirrups

(a)

(b)

Figure 290. Placing of No. 8 longitudinal bars on slab beam

(a)

(b)

Figure 291. Finished slab beam reinforcement

Slab Beam Casting

The concrete mix used was chosen according to TxDOT specifications as mentioned earlier. Slab beam were cast in a single pour and a wood float finish provided at the surface. One of the slab beams was cast with SCC typically used in precast panels.

(a)

(b)

Figure 292. SCC slab beam casting

Figure 293. Wood float finish

A longitudinal line was then made on the wet concrete at 6 in. from the edge to mark the position of the horizontal shear reinforcement. The horizontal reinforcements were then pushed into the wet concrete to a height of 2 in. from the concrete surface (Figure 294).

Figure 294. Placing of horizontal shear reinforcement

Figure 295. Finished slab beam specimen

Figure 296. Surface finish on slab beam having conventional concrete

Figure 297. Surface finish on SCC slab beam

The reinforcement for the CIP was consistent with that used on actual bridges. Surfaces of the precast beam were cleaned to remove dust and dirt particles before casting. The reinforcement cage (Figure 302 and Figure 303) was then placed and the concrete (Class "S") was cast as shown below.
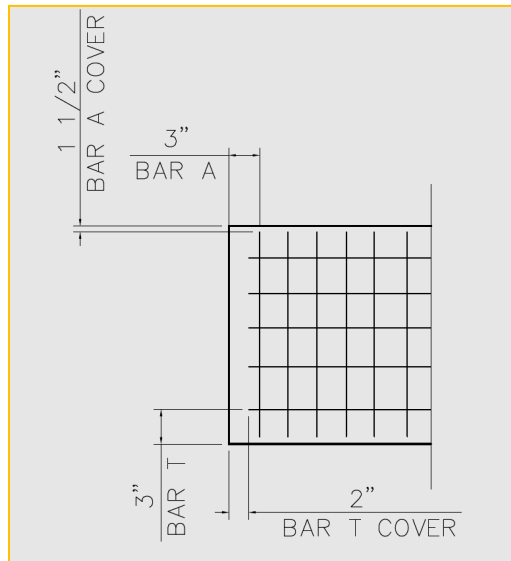
Figure 298. CIP slab reinforcement layout for slab beam
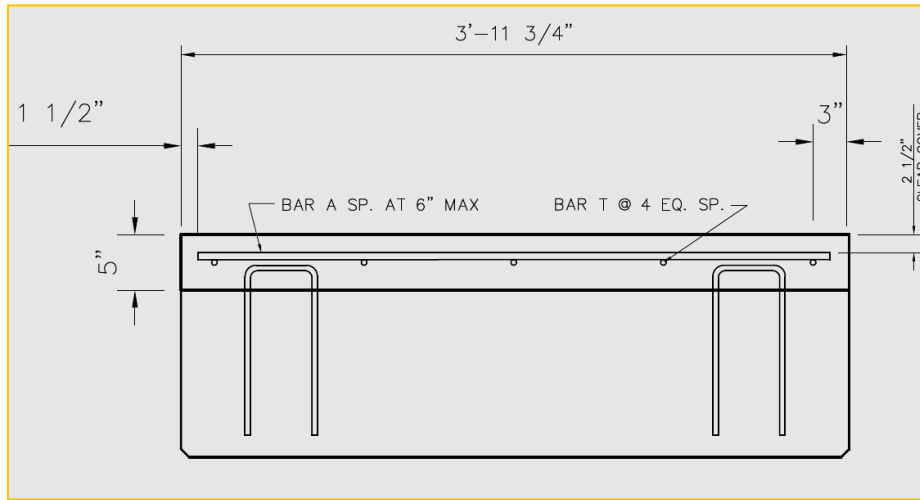
Figure 299. CIP slab detail for slab beam

Strain gauges were installed on the horizontal shear reinforcement prior casting of the CIP slab. The foam tape was then placed on the surface of the beam to reduce the interface area to 12 in. It was placed in two layers to guarantee that no tear will occur during casting of the CIP slab.

Figure 300. Strain gauges installation on horizontal shear reinforcements

(a)
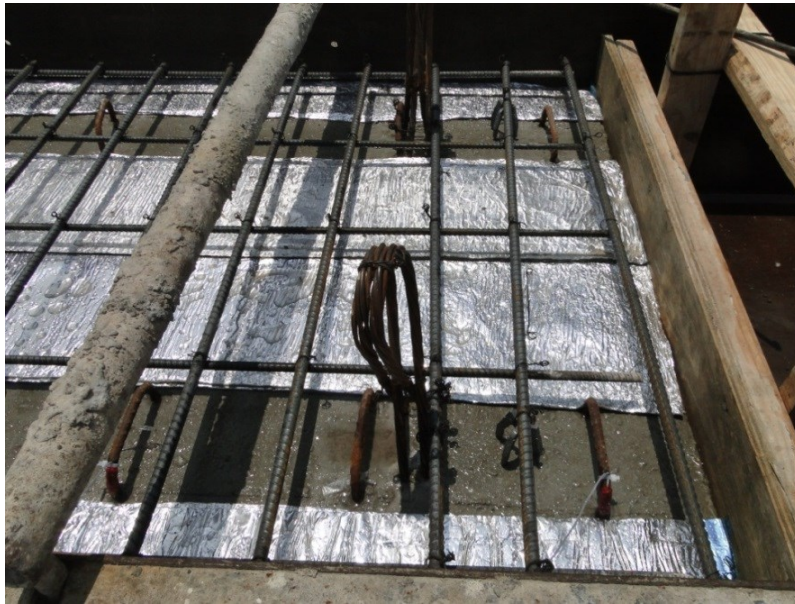
(b)

Figure 301. Foam tape on the slab beams

(a)

(b)

Figure 302. Casting of the CIP slab

Push-off specimens were also cast to determine the friction between the tape and the concrete. Six specimens were cast in which two had no tape at the interface while the rest had foam tape at the interface to reduce the interface area.

(a)

(b)
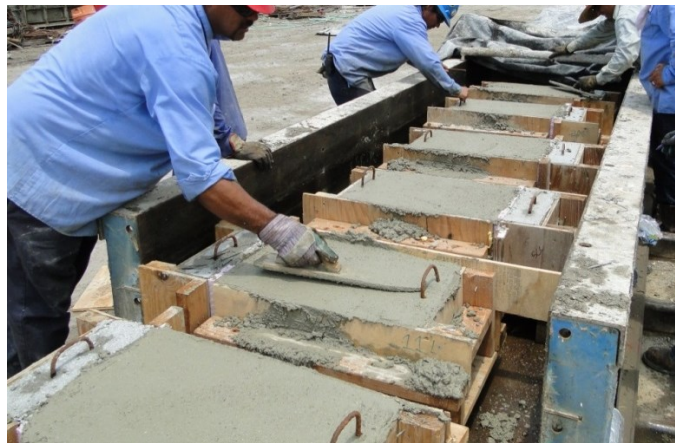
(c)

Figure 303. Casting of the push-off specimens

The specimens were then covered with a plastic sheet and cured for 28 days after which they were demolded and prepared for delivery to UTA.

Delivery of beams

The beams were delivered to the UTA Civil Engineering Laboratory. A local crane company was hired to aid in unloading the beams from the trucks.

Figure 304. Storing of the beams outside the lab

8.3.3 Full-Scale Test Setup

The proposed test setup for Task 6 and Task 7 was composed of an H-frame with a hydraulic cylinder attached to apply the load. Two W12x72 wide flange sections were used as the loading beam (one on top of the other) so as to apply the load uniformly along the width of the beam. A load cell was placed between the hydraulic cylinder and the loading beam to record the load being applied. The specimen was instrumented with two LVDT's placed on both the CIP and precast parts to measure the slip during testing. One LVDT was placed underneath the midpoint of the beam to measure the

displacement during loading whereas one LVDT each was placed at the supports to check for any displacements occurring at the supports.
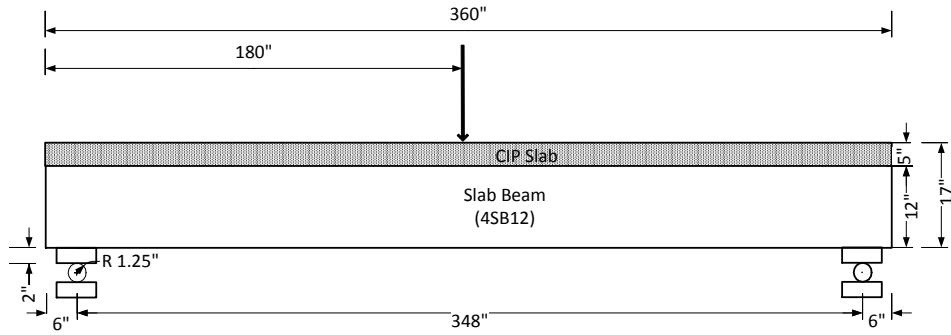
(a)
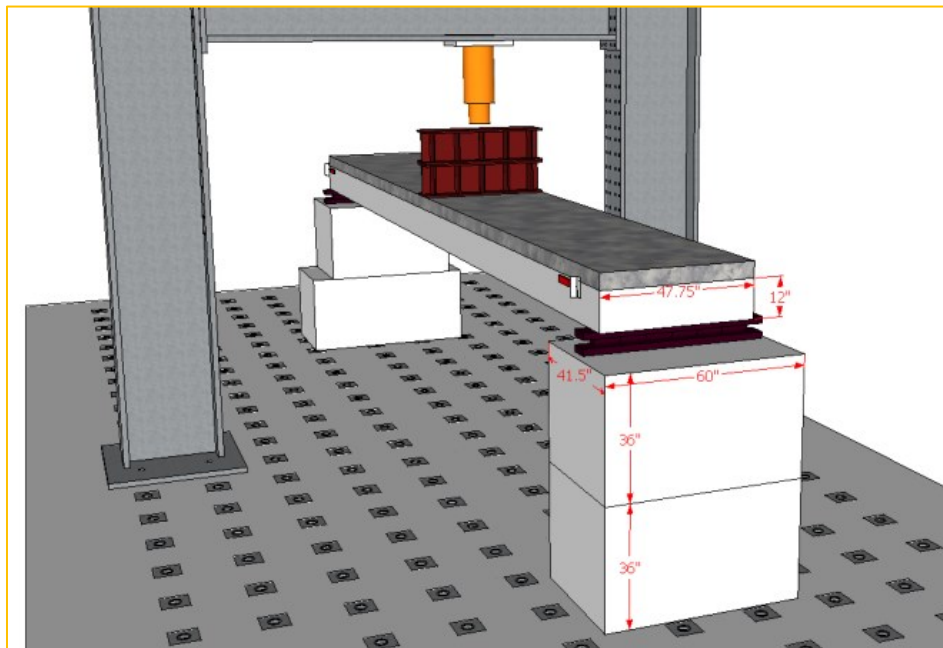
(b)

Figure 305. Schematic view of the slab beam test setup

Four LVDT's were placed to measure the slip at each end of the beam. Two LVDT's were placed at the center to measure the displacement of the beam. The load was then applied at the center of the beam at different intervals.

Figure 306. Test setup: LVDT's and loading beams

Figure 307. Test setup

Chapter 9

Part II: Test Results and Analysis

9.1 Component Test

9.1.1 Task 2 Test Results

Summary of the Task 2 results is given in Table 21 in terms of the peak load and cohesion factor. The results in Table 21 were obtained by dividing the peak load over the contact area to obtain the cohesion factor (*c*) as per the AASHTO (2014) nominal interface shear equation. Each specimen can be identified according to the specimen ID in the first column of Table 21 in which the three terms represent the location of casting (L=Laboratory, P=Precast Plant), the surface type (WF=Wood Float, RF= Rake Finish, CSP6…etc.), and the specimen test number (A=1, B=2, C=3). According to our survey, most of the precast box and slab beams across the country are finished with a wood float. Test results indicated that the average cohesion factor is approximately 0.14 ksi, significantly lower than the 0.28 ksi specified by AASHTO Section 5.8.4.3 for a surface roughened to an amplitude of 0.25 in.

Table 21. Task 2 Cohesion Factor Test Results

Specimen	Surface Type	Failure Mode	Failure Load (kip)	Shear Stress (ksi)
L-WF-A	Wood Float	Interface	38.5	
L-WF-B	Wood Float	Interface	23.7	0.14
L-WF-C	Wood Float	Interface	45.9	
L-C6-A	CSP 6	Interface	56.6	
L-C6-B	CSP 6	Interface	53.6	0.20
L-C6-C	CSP 6	Interface	42.0	
L-C7-A	CSP 7	Interface	49.6	
L-C7-B	CSP 7	Interface	70.6	0.23
L-C7-C	CSP 7	Interface	52.6	
L-C8-A	CSP 8	Interface	57.2	
L-C8-B	CSP 8	Interface	61.1	0.21
L-C8-C	CSP 8	Interface	41.9	
L-C9-A	CSP 9	Interface	47.7	
L-C9-B	CSP 9	Interface	57.5	0.21
L-C9-C	CSP 9	Interface	54.7	

** Each specimen can be identified according to the specimen id in the first column of Table 21 in which the three terms represent the location of casting (L=Laboratory, P=Precast Plant), the surface type (WF=Wood Float, RF= Rake Finish, CSP 6…etc.), and the specimen test number (A=1, B=2, C=3).

All three wood float finish specimens failed at the interface as seen in Figure 308. There was however some disparity in the shear stress recorded for the three wood float specimens. It was also noticed that some aggregates were dislodged (Figure 309) from the concrete when the precast part was observed after failure. The specimens with the dislodged aggregates showed a higher shear stress compared to the specimens with no visible aggregate dislodgement indicating that a stronger bond was created when there was adequate contact between the exposed aggregate of the precast segment and the concrete matrix of the CIP segment. The average shear stress was however 60% lower than that suggested by AASHTO (2014) (Figure 313).

(a)   (b)
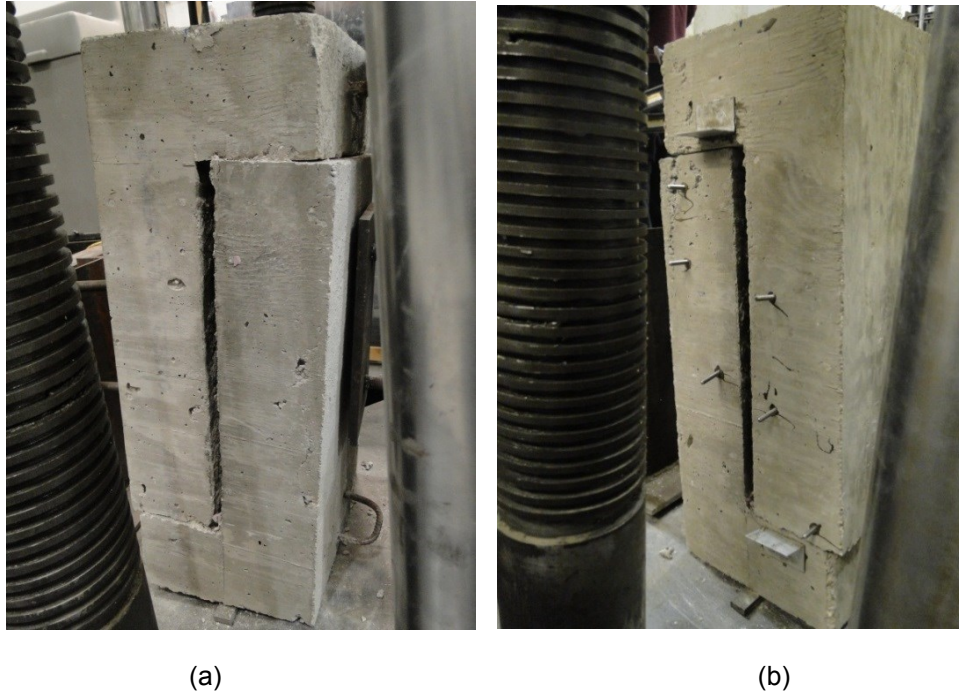
Figure 308. Wood Float Specimen #1 at failure (a) front view (b) back view

Figure 309. Precast failure plane showing dislodged aggregate

An increase in shear stress was observed in the CSP 6 specimens where an average cohesion factor of 0.20 ksi was recorded. The surface of the precast segment of

the CSP 6 specimen exhibited more aggregate exposure however very minor aggregate dislodgement was observed (Figure 310). The overall roughness was still relatively minor compared to that of the other CSPs.

Figure 310. CSP 6 Specimen precast surface profile

As the surface roughness increased from CSP 6 to CSP 7, an increase in the average shear stress of 0.03 ksi was also observed (Figure 313). The average cohesion factor of CSP 7 was 0.23 ksi in which the shear stresses ranged from 0.20 ksi to 0.28 ksi, but excluding the high value of 0.28 ksi, there seems to be little difference between the rest of the results for CSP 6 and CSP 7. The CSP 8 specimens averaged a cohesion factor 0.21 ksi. However, there was inconsistency in the results of all three specimens with a horizontal shear stress as low as 0.17 ksi being recorded. The failure of L-CSP8-B and L-CSP8-C specimens was by a small portion into the CIP part near the notch due to the strong bond at the interface. CSP 9 showed more consistency in the failure load of all three specimens with an average horizontal shear stress equal to that of CSP 8. A large amount of aggregate dislodgement and aggregate fracture was observed in both the CSP 8 and CSP 9 specimens (Figure 311). The general surfaces of these specimens exhibited

a rough surface with many protrusions and visible aggregate surfaces (Figure 312); however the cohesion values still remained well below the 0.28 ksi suggested by AASHTO (2014) (Figure 313). Overall, the cohesion factors for the different CSP profiles were all very similar averaging a shear stress of 0.21 ksi, suggesting that the cohesion factor cannot be further increased by increasing the level of surface roughness but the strength of the concrete matrix and its ability to bond the exposed aggregates.

Figure 311. CSP 8 specimen precast failure plane showing dislodged and fractured aggregates

Figure 312. CSP 9 specimen surface profile
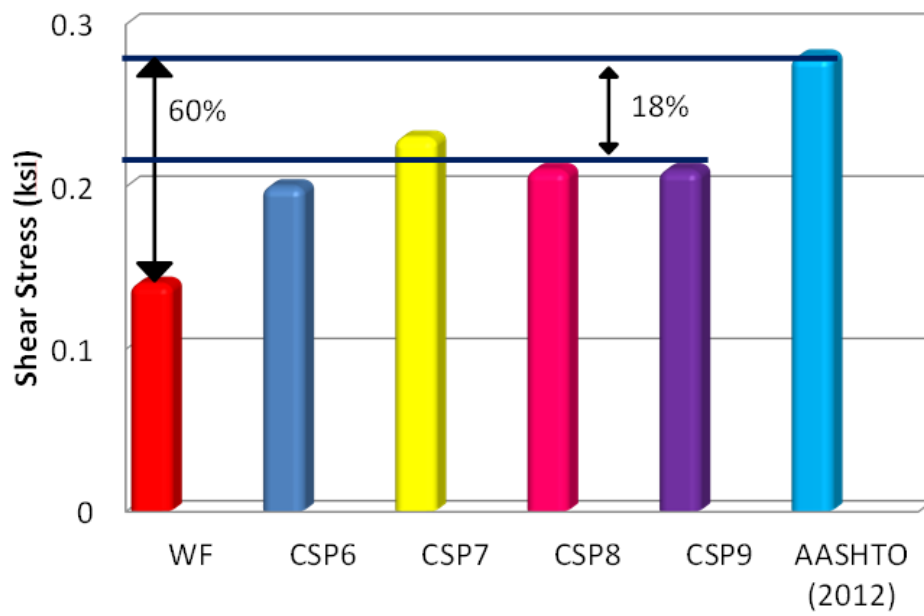
Figure 313. Cohesion factor comparison

This observation can be further supported by the tests conducted on the push-off specimens fabricated at the precast plant. A summary of the results for the tests conducted on the specimens fabricated at the precast plant with a wood float and rake finish can be seen in Table 22. The average cohesion factor for the wood float specimens was found to be 0.39 ksi; however some disparity was observed in the test results consistent with the disparity of the results for the previously tested wood float specimens. More consistent results were seen for the specimens prepared with a rake finish. The rake finish specimens had a much higher cohesion factor. The average cohesion factor for the rake finish specimens was observed to be 0.45 ksi. It is important to note that the specimens fabricated at the precast plant had a 28-day compressive strength twice as high (11 ksi) as the specimens constructed in the laboratory. The average cohesion factor for all the specimens constructed in the laboratory was found to be 0.21 ksi, and the average cohesion factor for the specimens constructed at the precast plant was 0.42 ksi. This suggests that there is a direct relation between the cohesion factor and the compressive strength of the concrete that is not explicitly accounted for in the AASHTO equation.

Table 22. Precast plant push-off specimens

Specimen	Surface Type	Failure Mode	Failure Load (kip)	Shear Stress (ksi)
P-WF-A	Wood Float	Interface	76	0.39
P-WF-B	Wood Float	Interface	121	
P-RF-A	Rake	Interface	112	0.45
P-RF-B	Rake	Interface	119	

9.1.2 Task 3 Results

A summary of the Task 3 results can be seen in Table 23 in terms of the cohesion factor from Task 2 and the calculated friction factor from Task 3. The results in

Table 23 were obtained by using the average cohesion factors (c) for each respective surface type from Task 2 together with the failure load from Task 3 and the applied 20 kip normal force (P_c), to calculate the friction factor (μ) as per the AASHTO (2014) nominal interface shear equation. As previously mentioned, it is important to observe the behavior of the wood float finish as it is the most common surface preparation method used in precast plants across the nation. The wood float specimens failed at an average load of 53 kips resulting in a friction factor of 0.85, lower than $\mu = 1.0$ specified in AASHTO Section 5.8.4.3 for a surface roughened to an amplitude of 0.25 in. The same issue experienced with the wood float specimens of Task 2 was observed once again where disparity was seen between the test results where two of the specimens had lower shear strength than the other. It was noticed that some aggregates were dislodged from the concrete in the precast after failure. Dark areas on the surface seem to indicate that there was lack of contact between the precast and CIP part of the specimen (Figure 315). Hence the whole interface area was not utilized leading to lower interface shear strength. The two specimens having a low shear stress were observed to have failure surfaces that were quite smooth after failure indicating there was not much aggregate interaction.

Figure 314. Typical failure mode
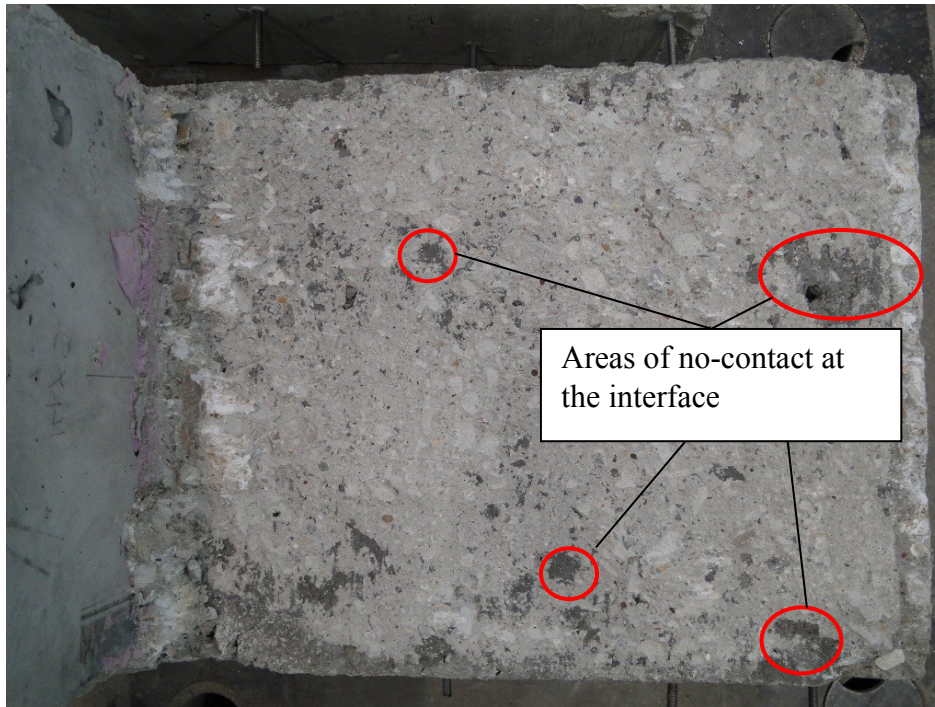
Figure 315. Interface after failure showing area of no-contact

The results for the CSP 6 specimens had much higher consistency in shear strengths for all three specimens. All the three specimens failed at the interface with an average peak load of 71.4 kips resulting in a friction factor of 1.0 equivalent to that suggested by AASHTO (2014). After failure the precast segment of the CSP 6 specimen was observed to have a relatively smooth surface with few protrusions from dislodged aggregates (Figure 316(a)). CSP 7 specimens showed significantly more interaction at the interface with aggregate fracture and pullout. Fracture of concrete from the CIP part was also observed in some specimens. The CSP 7 specimens failed at the interface at an average peak load of 85.6 kips which resulted in a friction factor of 1.4. Two of the CSP 8 specimens failed at exactly the interface while the third failed out of the interface suggesting that the bond on the interface was very strong. As the surface roughness increased so did the friction factor. The average peak load for the CSP 8 specimens was

88.9 kips which translates into a friction factor of 1.8. Considerable aggregate pullout and fracture was observed on the surface of the precast specimens of CSP 8 (Figure 316). A progressive increase in the friction factor was observed from CSP 6 to CSP 8 with CSP 8 and CSP 9 registering the same friction factor. Furthermore, the friction factor was seen to increase only to a certain extent in surface amplitude, also suggesting that the friction factor is limited by the strength of the concrete matrix. CSP 8 and CSP 9 recorded the highest friction factor of 1.8 which is 80% higher than the highest recommended by AASHTO for "normal-weight concrete placed monolithically" (Figure 317).

(a)

(b)

Figure 316. Task 3: horizontal push-off tested specimens (a) CSP 6 (b) CSP 8

The friction factor was calculated using the AASHTO equation and results from Task 2 and Task 3. Shear stress was calculated from Task 2 as shown in Table 23. Therefore using CSP 6 as an example,

323

Average cA_{cv} (Task 2): 50.7 kips

Shear strength from Task 3: 71.4 kips

$$V_{ni} = cA_{cv} + \mu\left(A_{vf}f_y + P_c\right)$$

71.43 kips = 50.74 kips +µ (0+20 kips)

µ = (71.4-50.7)/20 = 1.0

Table 23. Task 3 Push-off Test Results

Surface Type	Failure Mode	Failure Load (kip)	Shear Stress (ksi) (Task 2)	µ
Wood Float	Interface	38.1	0.15	
Wood Float	Interface	36.4	0.09	0.85
Wood Float	Interface	84.4	0.18	
CSP 6	Interface	75.8	0.22	
CSP 6	Interface	75.5	0.21	1.0
CSP 6	Interface	63	0.17	
CSP 7	Interface	81.1	0.20	
CSP 7	Interface	84.2	0.28	1.4
CSP 7	Interface	91.5	0.21	
CSP 8	Interface	84.5	0.23	
CSP 8	Not Interface	109*	0.24	1.8
CSP 8	Interface	93.2	0.17	
CSP 9	Not Interface	93.5*	0.19	
CSP 9	Interface	83.3	0.23	1.8
CSP 9	Interface	64**	0.22	

*Specimens did not fail at the interface, the ultimate loads were used here to conservatively estimate the horizontal shear strength.**Results not used as they were found to be unrealistically low as explained in results summary in CSP 9.
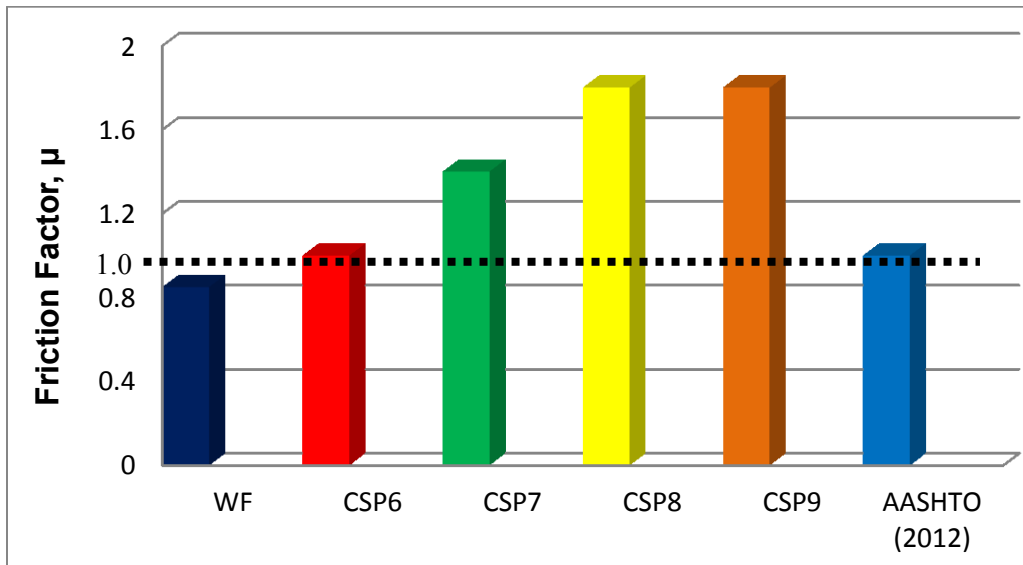
Figure 317. Friction coefficient comparison

9.2 Full-Scale Tests

9.2.1 Task 6 Results

9.2.1.1 4SB12#1 (slab beam)

The load was first applied at 5 to 10 kip interval until the first flexural crack was observed at 55 kips, near the mid-span of the beam. With an applied load to 82 kips, the cracks continued to propagate and eventually reached the interface between the CIP slab and the precast beam. At 90 kips, the flexural cracks propagated into the 5 in. CIP slab but not along the interface. The beam eventually failed in flexure at a peak load of 102 kips corresponding to a displacement of 7 in. Crushing of concrete occurred under the loading point (Figure 318) and the cracks significantly widened to more than 6 mm. No cracks at the interface were observed and no slips were recorded by the LVDTs. No significant strain was measured from the strain gauge data of the horizontal shear reinforcement, thus indicating that there was very minor contribution from the horizontal shear reinforcement.

9.2.1.2 4SB#2 (slab beam)

In the second slab beam which had no horizontal shear reinforcement, the first flexural crack was also observed at a load of 55 kips. The cracks had propagated into the CIP slab at a load of 180 kips. However, no cracks propagating along the interface were observed. The beam also failed by flexure at a load of 197 kips with crushing of the concrete at the loading point (Figure 318). The load then dropped to 177 kips after failure. With continued load application, an explosive failure occurred with a decrease in load of more than 100 kips and the formation of a horizontal crack 2 in. below the interface. The cracks widened to 5 mm and the concrete at the loading point was further crushed. The interface remained intact without any cracks forming across it. Although some hairline cracks propagated along the interface at failure on the south-face side, it did not extend further and was not observed on the north-face side of the beam.

9.2.1.3 4B20#1 (box beam)

The first flexural crack in the box beam specimen was observed at 110 kips. At a load of 170 kips, flexural cracks had progressed reaching the interface of the CIP slab and the precast beam. Cracks of 1.0 mm in width were recorded with some spalling being observed. At 189 kips, the cracks progressed into the CIP slab with crack widths as wide as 1.5 mm. It should be noted that the flexural cracks did not propagate along the interface but instead passed through the interface into the CIP slab. The beam failed in flexure due to concrete crushing in the compression zone within the CIP slab (Figure 318). No cracking was observed within the interface of the prestressed beam and the CIP slab.

9.2.1.4 4B20#2 (box beam)

Similar results were observed for the box beam without horizontal shear reinforcement. At 180 kips, cracks had progressed further up the beam with shear cracks

being observed. At a load of 350 kips, the cracks had progressed up to the interface of the CIP and precast sections. Initial crushing of the concrete under the loading point was observed at 400 kips. With increase in load, the concrete crushed and the cracking propagated into the interface leading to a sudden horizontal shear failure. However, the horizontal shear crack did not propagate the entire length of the beam. Therefore no slip was recorded by the LVDTs at the ends.

Figure 318. Flexural/ horizontal shear failure near midspan

Figure 319. Full-scale beam specimens at failure

Summary of all the test results is presented in Table 24.

Table 24. Task 6 Full-scale Beam Test Results

Specimen	Horizontal Shear Reinforcement	Design load (kips)	Failure Load (kips)	Failure Mode	Strain ε_{su} on horizontal shear reinforcement at failure (µε)
4SB12 #1	Yes	82	101	Flexure	100
4SB12 - modified	No reinforcement	160	195	Flexure	-
4B20 #1	Yes	160	193	Flexure	250
4B20 - modified	No reinforcement	318	407	Flexure / Horizontal Shear*	-

* Horizontal shear failure was a secondary failure after flexural failure had occurred.

9.2.2 Task 7 Results

9.2.2.1 4SB12#1 (conventional concrete slab beam)

The load was first applied at 5 to10 kips interval until the first flexural crack was observed at 55 kips, near the mid-span of the beam. With continued increase in applied load, the crack was observed to progress towards the top of the beam. Also more cracks began to form along the length of the beam and also at the bottom of the beam. The crack width also increased gradually. The crack continued to progress towards the interface with every increment in load up to a load of 120 kips. The crack did not continue propagating towards the interface with further increase in the load. However, an increase in the strain in the horizontal shear reinforcements was observed at 150 kips, and yielding of the horizontal shear reinforcements at the quarter span in the West-end of the beam was also observed. At a load of 160 kips, the strain on the horizontal shear reinforcement increased and yielding was observed on the horizontal shear reinforcement located at the beam ends. At 170 kips and a midspan displacement of 3.6 in., slip was recorded at the East-end of the beam with an increase in the crack width at that end of the beam. With the development of shear cracks at the beam ends, the strain on the horizontal shear reinforcement continued to increase. The width of the flexural cracks increased to 1 mm. At a displacement of 5.24 in. and a load of 180 kips (Figure 320), the slip at the East-end increased to 0.15 in. with an increase in the crack width at the interface. Fracture of the concrete was also observed on the East-end of the beam. The beam failed in flexure at a load of 181 kips and a displacement of 6.65 in. (Figure 321). Crushing of concrete occurred near the loading point and the flexural cracks significantly widened to more than 6 mm. A separation between the CIP slab and the precast beam was also observed with a slip of 0.15 in. being recorded (Figure 322). From

strain gauge information of the horizontal shear reinforcement, it was clear that almost all

the horizontal shear reinforcement had yielded at this point.

(a)
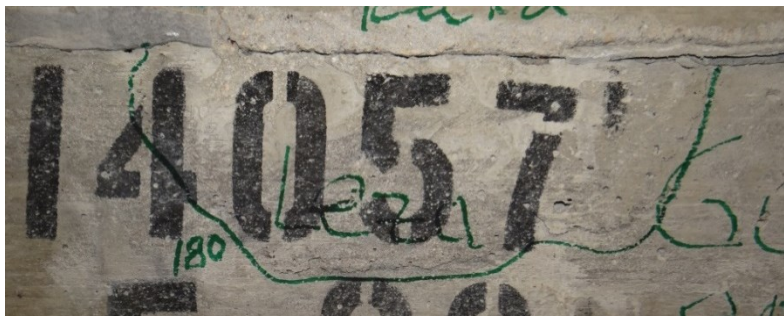
(b)

Figure 320. Crack at the interface widens at 180 kips

Figure 321. Beam at failure
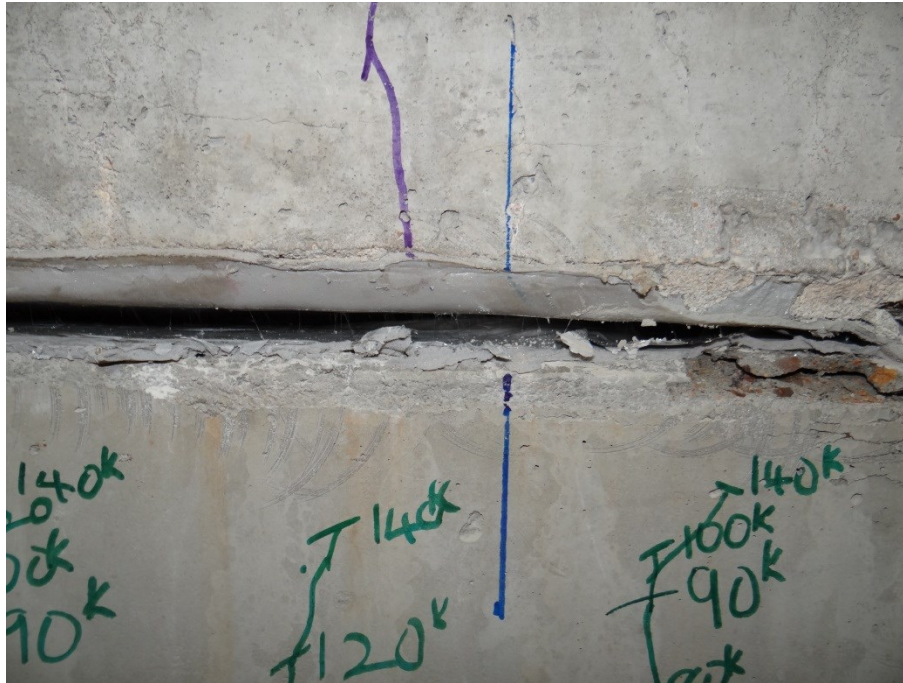
Figure 322. Separation of the interface at failure

9.2.2.2 4SB12#2 (SCC slab beam)

The beam was loaded at intervals of 10 kips with inspection after each interval to identify cracks. At a load of 50 kips, the first crack was observed on the beam. With increase in load to 80 kips, the cracks propagated upward and new flexural cracks formed along the beam. Cracks continued to progress upward as the load was increased with new cracks forming along the beam. At a load of 130 kips, the LVDTs started registering slip at the interface of 0.0024 in. Strains on the horizontal shear reinforcement began increasing gradually with yielding of the horizontal shear reinforcement at 6 ft. from the support. The flexural cracks continued to propagate towards the loading point with new flexural cracks forming along the length of the beam.

Slip gradually increased as the load was increased and at a load of 160 kips, a slip of 0.015 in. was recorded. Horizontal shear reinforcement near the support yielded at

this point including the longitudinal reinforcement. Cracks at the interface became noticeably larger at both ends of the beam (Figure 323).

(a) Crack on the East-end of beam

(b) Crack on the East-edge of beam

Figure 323. Visible interface cracks at beam ends

Cracks propagating from the interface towards the bottom of the beam started to appear at a load of 170 kips (Figure 324). The crack positions were approximately at the location of horizontal shear reinforcement.

(a) South-West side
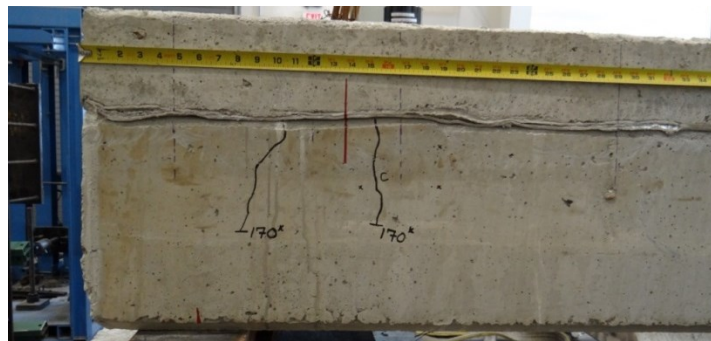
(b) North-East side

(c) South-East side

Figure 324. Vertical cracks close to beam ends

Cracks at the beam ends and the interface were also observed to widen with increase in load (Figure 325), as well as an increase in slip at a load of 180 kips as demonstrated by the red line in Figure 326.
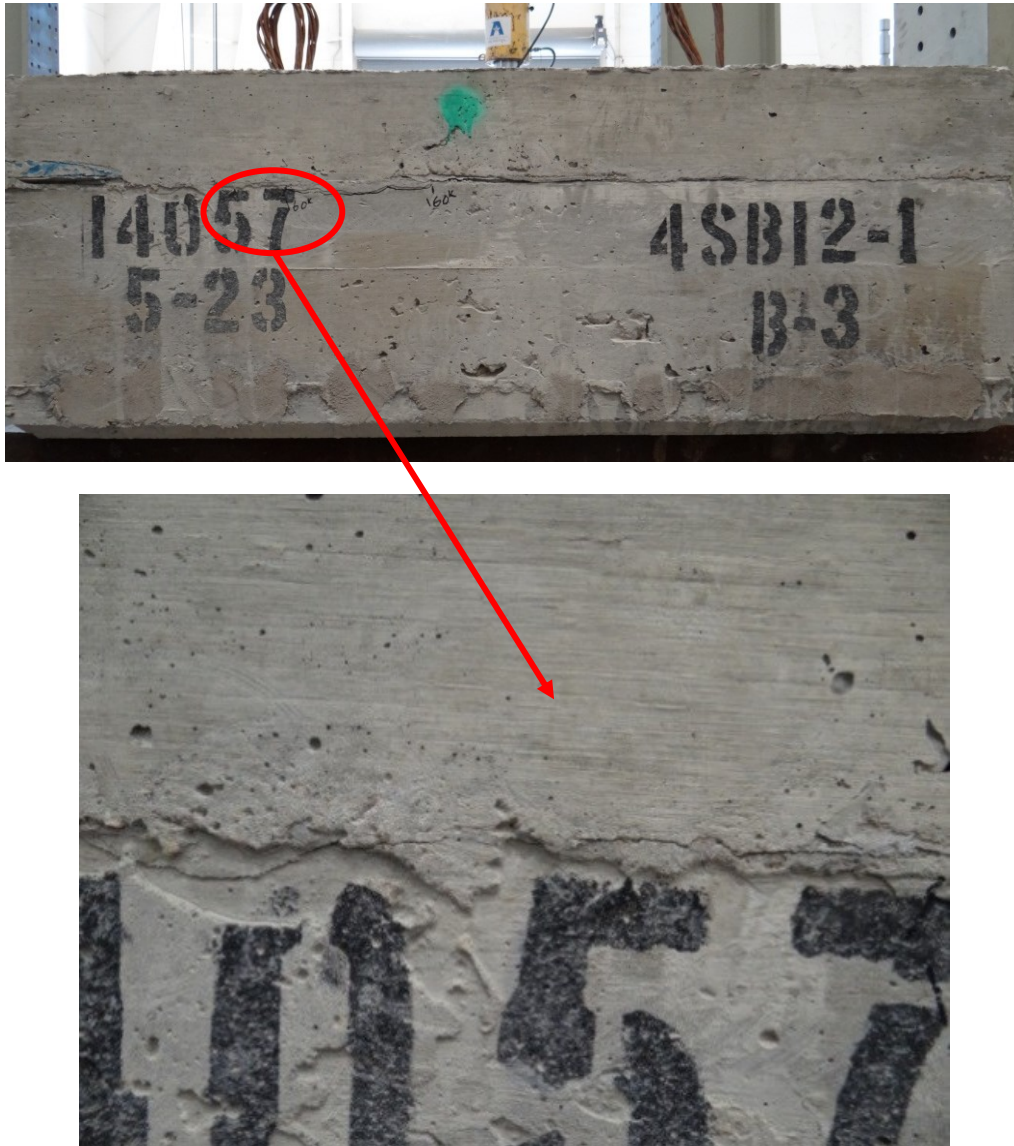
Figure 325. Interface cracks at beam ends

Figure 326. Interface slip at 180 kips

Cracks started to form at the CIP slab at a loading of 190 kips. These cracks did not originate from flexural cracks on the precast beam. Interface cracks were now wider and more visible on both ends of the beam as shown in Figure 327. More vertical cracks continued to appear on the beam with a slip of 0.10 in.
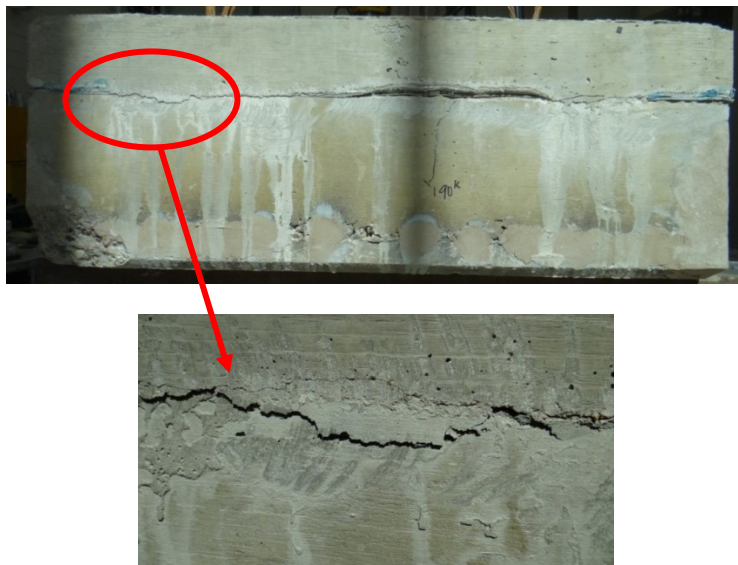
Figure 327. Cracking at the interface (photo taken at the beam end)

The beam failed by flexure at a load of 191.7 kips with crushing of the concrete under the loading point. A slip of 0.12 in. was recorded. Crushing of concrete was however observed on both the CIP slab and the precast beam (Figure 328). The wide crack opening at the interface (Figure 329) and the concrete crushing at both the slab and the beam indicated that the composite action is partly lost.
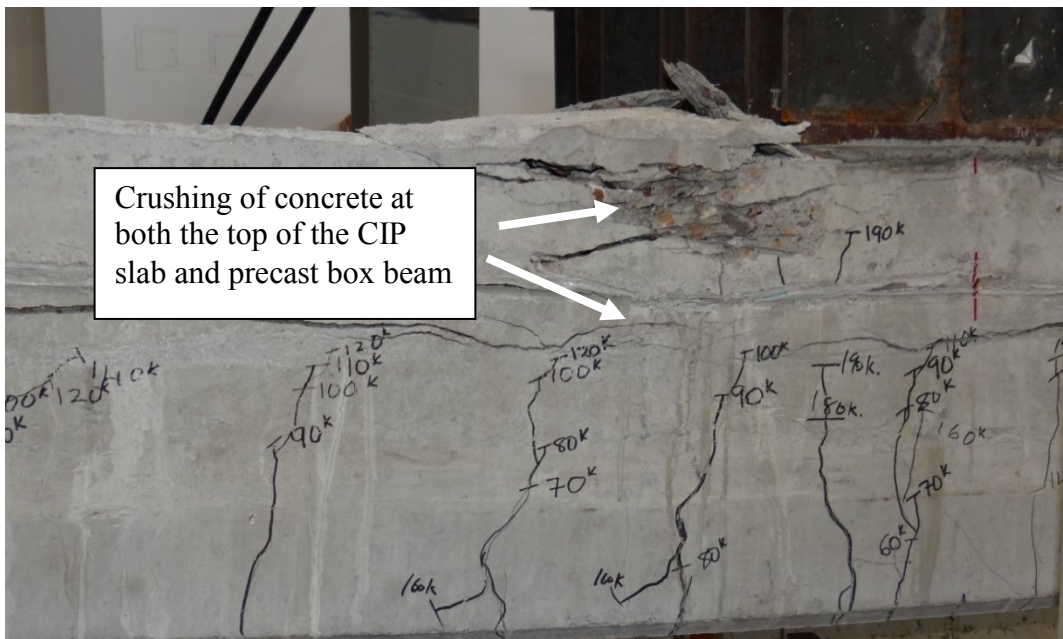
Figure 328. Crushing of concrete at failure

Figure 329. Separation between CIP slab and precast beam

Table 25. Task 7 Full-scale Beam Results

Specimen	Failure Load (kips)	Load at the onset of slip (kips)	Failure Mode	Strain ε_{su} on horizontal shear reinforcement at onset of slip ($\mu\varepsilon$)
4SB12 - conventional	181	156	Flexure*/Horizontal Shear	340
4SB12 -SCC	192	130	Flexure*/Horizontal Shear	560

Chapter 10

Part II: Summary, Conclusions, and Recommendations

10.1 Summary of Results

Behavior of component specimens

The results from Task 2 show that varying the CSPs has a limited effect on the shear stress values, and the wood float finish results in the lowest shear stress. This may indicate that there is no significant difference in using different CSPs on the shear stress between the precast and CIP sections of the bridge. However, all the surface finishes showed a shear stress that is less than that used in the AASHTO (2014) specifications as can be seen in Figure 313. The rougher surface is able to enhance the interface shear resistance but only to certain extent of roughness, after that limiting level of roughness the shear resistance is controlled by the strength of the concrete matrix. It was observed that failure occurs in the matrix around the aggregate; therefore the paste strength may be the dominating factor for interface strength. This was supported by the push-off tests conducted on the specimens fabricated at the precast plant in which doubling the concrete strength resulted in a cohesion factor twice as high.

In general there is an overall increase in the friction factor with increase in the surface roughness as demonstrated in Figure 317. Wood float gives the least friction coefficient. The CSP 6 specimens resulted in a friction factor of 1.0 equivalent to the value suggested by AASHTO (2014) which could be considered over-conservative as it does not include the effects of the aggregate-matrix interaction seen in the other CSPs. The friction factor progressively increases from CSP 6 to CSP 8, whereas CSP 9 has an equivalent friction coefficient to CSP 8. Friction component (μP_c) of the horizontal shear resistance can be increased by increasing the surface roughness; however beyond a certain extent of surface roughness (such as that of CSP 8) the increase would not be

significant. This is consistent with the results of Task 2, suggesting that a concrete strength parameter should be introduced to better define the cohesion and friction factors of the AASHTO nominal interface shear equation.

Task 6 results revealed that horizontal shear failure will not occur for TxDOT box and slab beams using the current design practice. Throughout the testing of box and slab beams with horizontal shear reinforcement, no significant strain was measured from the strain gauge data of the horizontal shear reinforcement because the beams always failed by flexure first. The horizontal shear strength contribution from concrete alone was sufficient to resist the shear stress at ultimate flexural failure.

In Task 7, interface areas of all beams were purposely reduced by foam tape to decrease the horizontal resistance and force the beams to fail along interface before flexural failure. The reduced areas in the slab beam were reduced by 75%. Slab beams tested in Task 7 revealed that the slab beam made with self-compacting concrete (SCC) experienced slip at a lower load (130 kips) as compared to the slab beam cast with conventional concrete (156 kips). The slip was noted to be equal on both ends of the beam for the SCC slab beam whereas the slip on the conventional concrete occurred on only the East half of the beam. However, after ultimate failure, the slip at a deflection of 6.8 in. was found to be approximately equal (Figure 330). Although the SCC slab beam experienced interface slip at a smaller load than the conventional concrete slab beam, it reached a slightly higher peak load compared to the conventional concrete. This shows that it still maintained some form of composite action. This is evident also from strain gauge information whereby the horizontal shear reinforcements yielded at a load of 190 kips compared to the conventional concrete whereby most horizontal shear reinforcement yielded at a load of 160 kips. Slip was observed to occur in both beams before the yielding of the horizontal shear reinforcement. It is noted from Figure 330 that in the SCC

beam the separation was much smaller than that in the beam with conventional concrete. As a result the interface reinforcement started to resist forces earlier; on the other hand, in the beam with conventional concrete, due to the presence of the rough surface, a large separation needs to occur first before slip. This in turn mobilized the interface reinforcement at later stage of the slip.
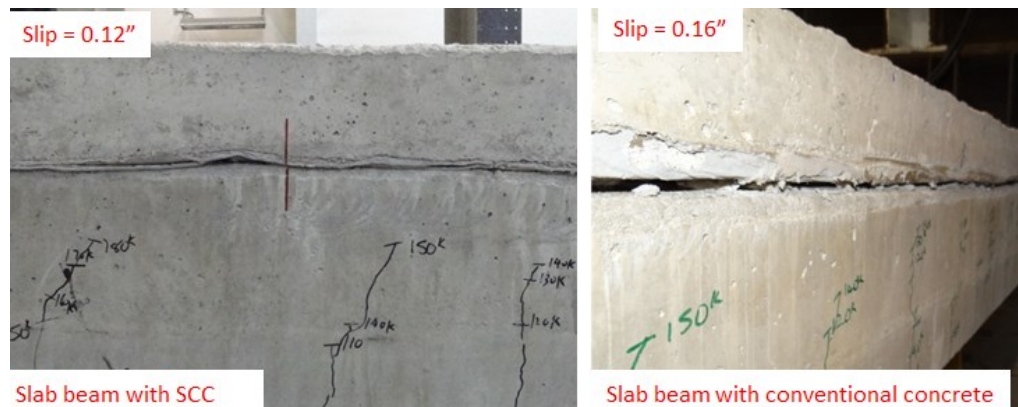
Figure 330. Slab beam slip at failure

It was also noted that due to a high compression force at the loading point, there was increased confinement and resistance to slip due to increased friction. This is also evident on the beams at failure as no slip was observed at or near the loading point. This may also be the case in actual bridges. Bridge design usually considers distributed loading from the CIP slab and live load. The compressive force from the live load (which is the one leading to failure, if that happens) on the bridge girder could provide increased friction at the interface.

The P_c (permanent net compressive force) force from the AASHTO equation could be modified to consider part of the live load which will lead to an increase in the friction force (μP_c) and consequently to an increase in the horizontal shear capacity.

10.2 Conclusions and Recommendations

1. Task 2 results indicate that a rougher surface is able to enhance the interface shear resistance (cohesion factor) but only to certain extent of roughness. It was observed that failure occurs in the matrix around the aggregate, therefore the paste strength may be the dominating factor for interface strength.

2. Friction component (μP_c) of the horizontal shear resistance can be increased by increasing the surface roughness; however beyond a certain extent of surface roughness (such as that of CSP 8) the increase would not be significant. This is consistent with the results of Task 2.

3. Concrete compressive strength appears to be an important factor that affects the horizontal shear resistance. This factor is not currently considered by AASHTO's equation. Further study in this regard is recommended.

4. Current TxDOT slab and box beams (with the 2 in. embedded length in the CIP deck) have sufficient horizontal shear strength up to flexural failure (even only with the surface roughness).

5. The use of SCC does reduce slightly the horizontal shear strength due to the reduction in cohesion and friction. However SCC has less separation at the interface thus maintaining a higher degree of composite action. Test result indicate that using SCC can provide sufficient horizontal shear strength for slab beams.

6. At ultimate horizontal shear capacity the horizontal shear force is mainly resisted by the cohesion/aggregate interlock and friction from the concrete, with minor contribution from the reinforcement. The interface shear reinforcement became engaged only after slip/separation occurred at the interface. (also indicated by Seible and Latham (1990), Hofbeck et al. (1969), and Kent et al. (2012))

7. Although the horizontal shear strength is predominantly controlled by the concrete behavior and not the interface shear reinforcement, the minimum amount of reinforcement currently specified by AASHTO (24 in. spacing) is useful in restraining separation of the interface after slip occurs (if that happens).

8. Current TxDOT practice for box and slab beams can be simplified (for example increasing the spacing of the horizontal shear reinforcement from 12 in. to 24 in. and providing a wood finish rather than rake finish) to aid in fabrication process.

9. Based on the findings from this study, in order to reflect the actual behavior of horizontal resistance, the interface shear resistance contribution from the reinforcement can be reduced, while the force (μP_c) can be increased by considering not only the permanent dead load but a partial live load.

Appendix A

Column Construction Manual

The construction procedure for the eight column specimens is discussed in this section. A total of six full-scale perimeter frame columns and two full-scale space frame columns were constructed. The first perimeter frame column (SP1) was partially constructed at the UTA CELB and cast at Hanson Pipe & Precast and will be discussed in the first section of the construction manual. The five remaining perimeter frame columns (SP2, SP3, SP4, and SP6) were all constructed in a similar fashion and cast completely at the UTA CELB. The only minor difference being in the use of Terminators for the bottom block construction of SP3 which will be shown in the second section of the column construction manual. The two space frame columns (SP5 and SP8) were also constructed and cast completely at UTA CELB. Column specimen SP5 was cast with reinforced concrete while the plastic hinge region of column SP8 was cast with UHP-FRC and will be explained in the third section of this construction manual. The fourth section of this manual provides detailed instructions on how the internal instrumentation was applied to all specimens.

First Perimeter Frame Column (SP1) Constructed at Hanson Pipe & Precast

This section covers the construction of the first perimeter frame column. The plan was to construct all of the reinforcing cages at The University of Texas at Arlington Civil Engineering Laboratory Building (UTA CELB) then transport the cages to Hanson Pipe & Precast for assembling and casting. For this reason all three of the main reinforcing cages were constructed simultaneously. It should be noted that the remainder of the column specimens were constructed entirely at the UTA CELB. For simplicity, the major steps of the construction process for the first column will be discussed in the following order:

- Construction of Bottom Block Cage
- Construction of Column Cage

- Construction of Top Block Cage

- Bottom Block Formwork and Casting

- Construction of Column Formwork

- Column Casting

- Top Block Casting

- Demolding of Formwork and Shipping of Column
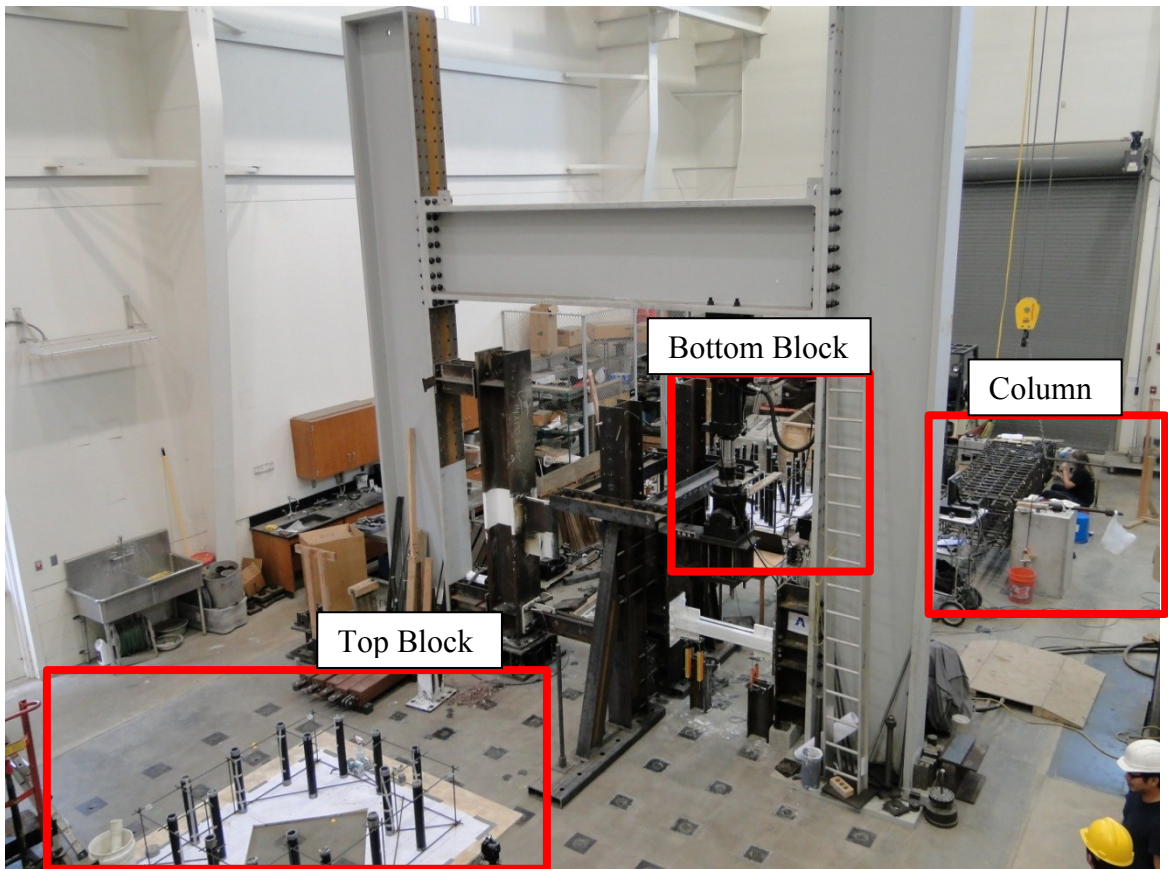
Figure 1. Simultaneous Construction of Reinforcing Cages at CELB
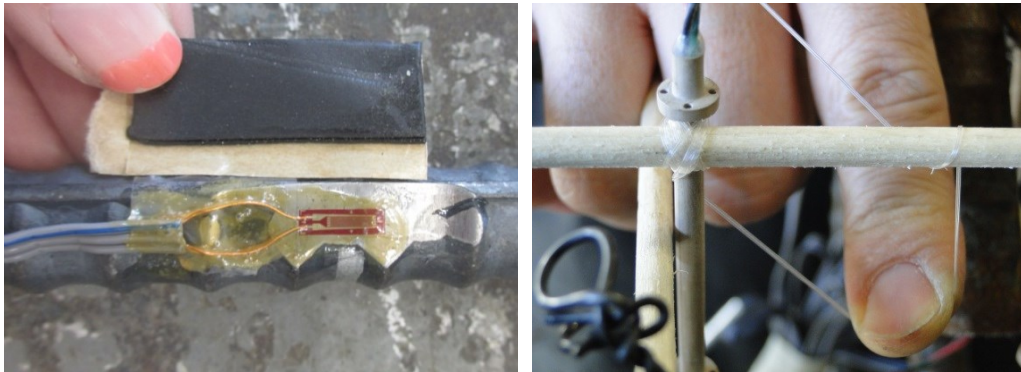
Figure 2. Instrumentation of reinforcing bars with steel and concrete strain gauges

The construction process begins with the instrumentation of the reinforcing bars. Once all the reinforcement has been completely instrumented the construction is ready to continue. The construction of the bottom block cage is independent of the steel strain gauge installation and may also be done simultaneously with the construction of the column cage and concrete gauge instillation.

Step 1: Construction of Bottom Block (Footing Block)

First lay 2 pieces of 4'x8' ply wood (of any thickness) on the floor. Make sure the floor is flat and clean before placing the ply wood. This grid will show the location of each of the pvc pipes that will be used as a reference during the construction of the bottom block cage as well as a reference through the remained of the column construction.
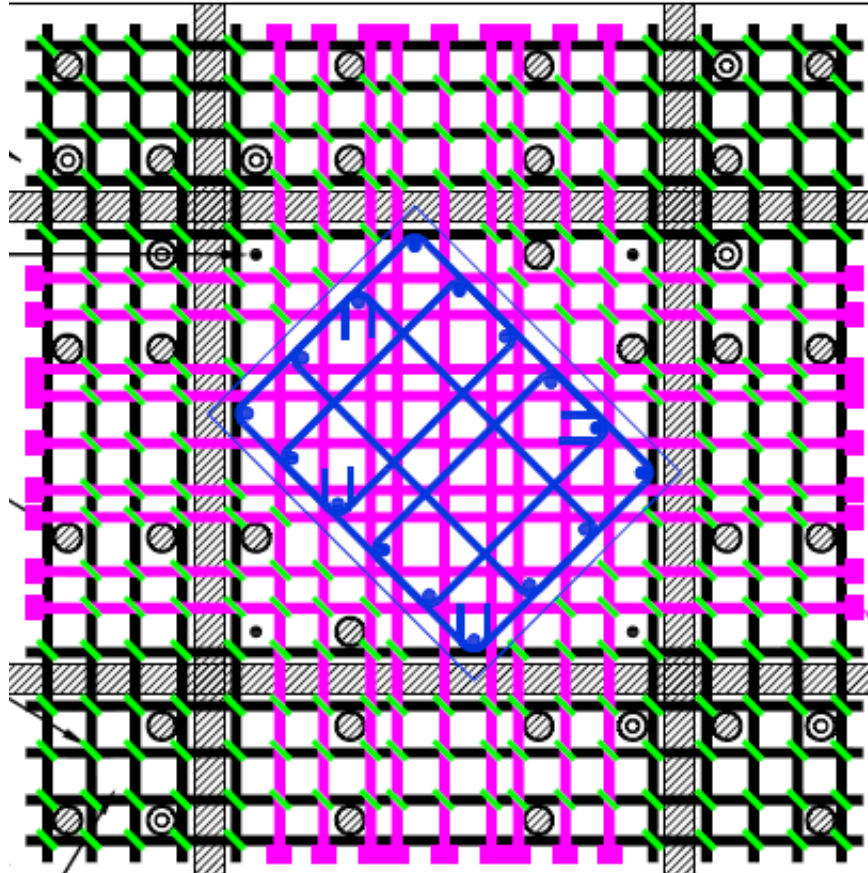
Figure 3. Bottom Block Cage Construction Drawings

Print the construction drawings shown in Figure 3 to scale and carefully place the drawings on the sheets of plywood. This may be done using small nails at the corners or duct tape along the edges to make sure that the sheet lies completely flat as shown in Figure 4 and Figure 5.
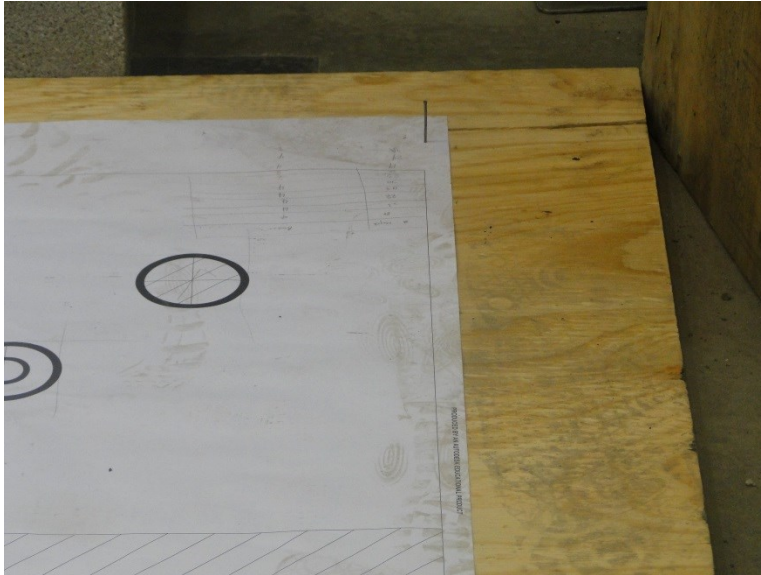
Figure 4. Nail on the corner of printed drawing.

Figrue 5. Printed out drawing placed on plywood with duct tape.

Now that the location of each of the pvc pipes is known wooden discs must be cut to be placed at the center of that exact location. The pvc pipes will then sit on top of the discs which will allow it to be held in place during construction and casting. It is very

important that the pvc pipes do not move and remain perfectly vertical so to prevent any instillation problems during the testing of the column. The discs are made of ply wood (of any thickness greater than 1/8") using hole drill bits of 2" and 2.5" similar to the one shown in Figure 6. Each hole drill bit corresponds to each size of pipe used in the bottom block. The hole drill bit is attached to the drill shown in Figure 7 and a piece of wood is placed underneath so as to not damage the drill during cutting. The wooden discs are then cut by turning on the drill and slowly lowering the knobl while holding the plywood in place as shown in Figure 7. Repeat this until all the discs have been cut. Figure 8 shows all of the cut discs.

Figure 6. Hole drill bit used for making discs

Figure 7. Cutting the wooden discs

Figure 8. Wooden Discs

After all of the wooden discs have been made they should be placed in the center of the circles shown on the drawings (Figure 9). All of the wooden discs are then drilled to the plywood using small 1 inch screws as shown in Figure 10 and Figure 11. This should be done very carefully as the location of the discs will be used as a reference during the rest of the construction.
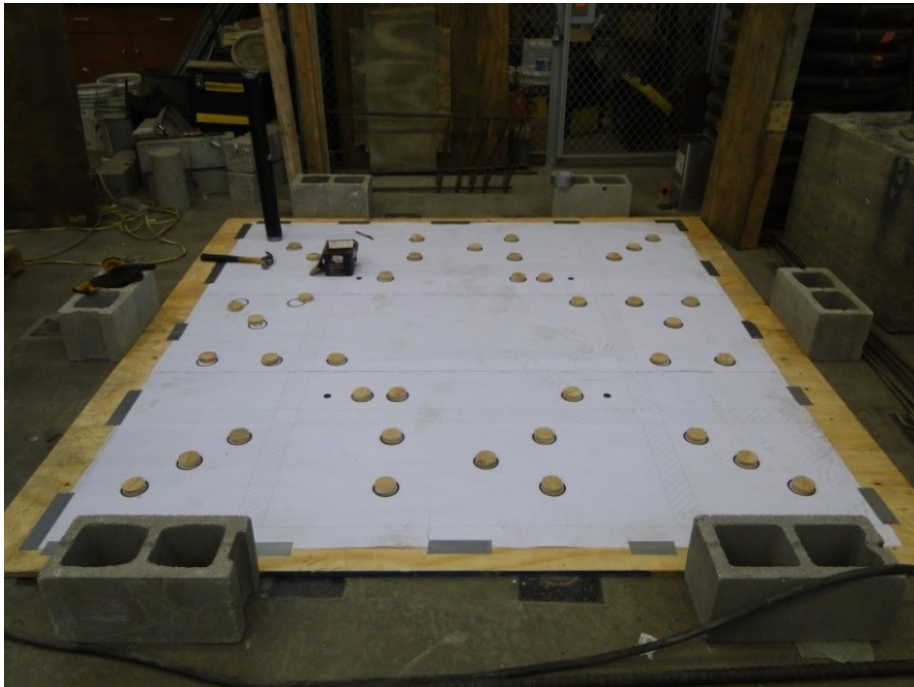
Figure 9. Placing discs on the plywood

Figure 10. Drilling the wooden discs to the plywood
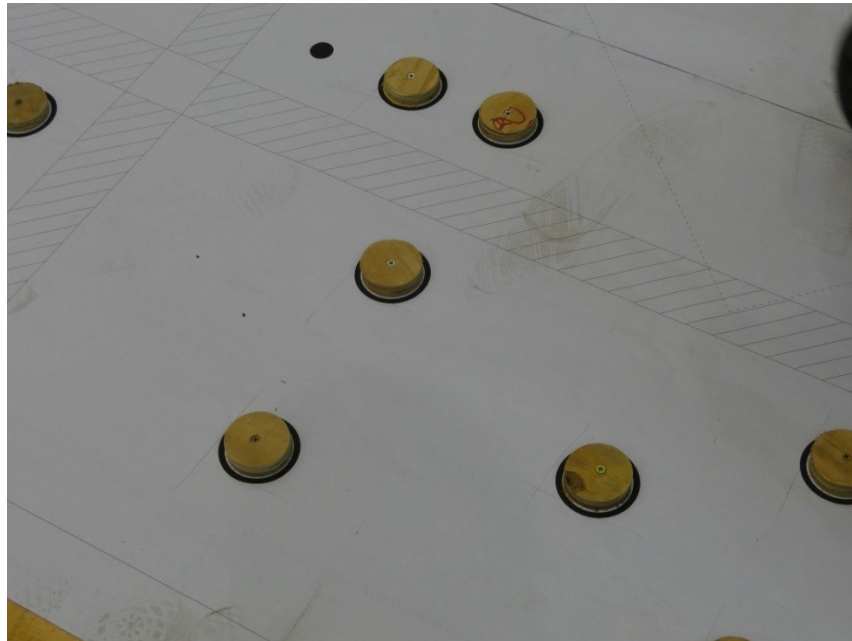
Figure 11. Wooden discs attached to plywood

The pvc pipes are cut according to the height of the bottom block drawings shown in Figure 12.Careful attention should be made to be as accurate as possible when

cutting the pvc pipes as the length of the pvc pipes will also be used as a guide during the construction of the bottom block cage. The pipes will be cut using a ban saw as shown in Figure 13. Two sets of 30" pipes will be cut. One of 2" diameter pipes that will be used for grouting during the instillation of the column on the test setup and another set of 2.5" pipes that will be used for post tensioning during transportation and to anchor the column to the test setup. Also 4 84" pipes of 2.5" diameter will be cut and placed in the column cage horizontally for the lifting and transportation purposes. Next, the pipes must be taped at one end to prevent concrete from seeping through the inside of the pipe. Also tape must be provided around the bottom edge that will sit on top of the disc for a better contact grip that will keep the pipe in place. The long horizontal pipes must be taped completely on both ends to prevent the concrete from entering. All of the 30" pvc pipes may now be placed on top of the discs as shown in Figure 16, while the 84" horizontal pipes are set aside to be used later on (Figure 15). During this step it is also necessary to cut the 4 1-1/8" post tensioning rods that will be inserted in the bottom block for the use of post tensioning during transportation. The rods should also be cut very carefully at the steel setting a very slow speed. The 4 rods should be cut at a length of 33" in which 3" will stick out above the footing enough for the coupler to be inserted. Also, the reinforcing bars (No. 3 and No. 4) are cut to provide a grid in which to secure the pvc pipes and place the top layer of reinforcement as shown in Figure 22 and Figure 23.

Elevation View - Main Footing Block
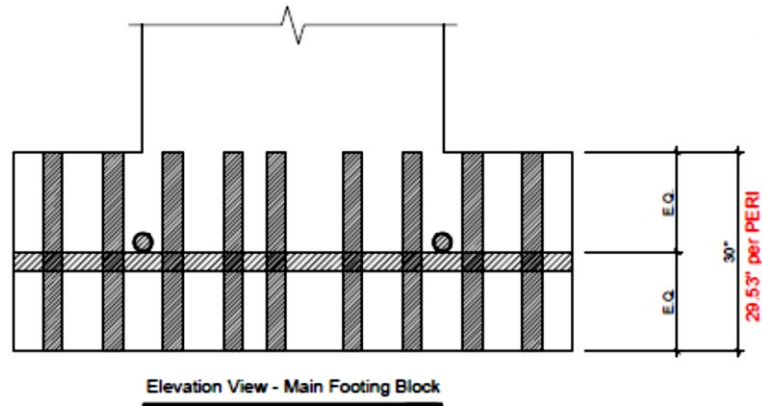
Figure 12. Drawings showing height of bottom block

Figure 13. Cutting reinforcing bars for bottom block grid

Figure 14. Cut reinforcing bars for bottom block grid

Figure 15. Long Horizontal pvc pipes used for lifting.

Figure 16. Placing of the pvc pipes on the wooden discs.

Now that the pvc pipes have been placed and the reinforcing bars have been cut, the next step is to construct the grid for the bottom block. First the 4 outside bars are laid out. Next lay out the rest of the reinforcement into a grid form in which there will be at least one corner where to tie the pvc pipe once it is raised as shown in Figure 17 and Figure 18. After the grid has been laid out, mark the locations of the reinforcing bars on the paper as well as the intersection in which where to weld as shown in Figure 19 and Figure 20. Figure 21 shows all of the reinforcing bars laid out, marked and ready to be welded. Next carefully weld the reinforcement grid as shown in Figure 22. Once the flat grid has been welded, add reinforcing bars vertically to raise it to the correct height. This may be done with 2 cinder blocks. Reinforcing bars may then be added in the bottom to stabilize the grid as shown in Figure 23.

Figure 17. The four outside bars of the grid

Figure 18. Bars intersecting next to the pvc pipe

Figure 19. Marking the location of the reinforcement grid on the paper printout.

Figure 20. Marking the location of the pipes on the paper and reinforcing bars.

Figure 21. All bars laid out, marked and ready to be welded.

Figure 22. Raising and welding the reinforcement grid.

Figure 23. Final bottom block reinforcing bar grid.

Finally we are ready to begin constructing the bottom block cage. The cage will be constructed based on the drawings shown in Figure 24. A 1.5" cover is required at the bottom of the block from the phase of the reinforcing bar to the outside phase of the bottom block. This will be accomplished by the use of rebar chairs as shown in Figure 28 and concrete blocks near the center to support the column cage as shown in Figure 29. First lay the bottom layer of reinforcing bars on the chairs and tie a number three bar at the ends to keep the bars standing straight as displayed in Figure 25. Next lay one U-bar on top of the bottom layer of reinforcement perpendicularly. Continue to place the second layer of reinforcement and tie them in a crisscross pattern to the bottom layer of U-bars, this may be done by hand or using a tie gun as shown in Figure 26 and Figure 27. Next tie the post tensioning rods to both the top and bottom reinforcement ensuring

that they will remain in place as shown in Figure 30 and Figure 31. Next add 3 bars on the top of the grid on each side. Finally, tie some shear reinforcement in the corners of the cage to the top and bottom as shown in Figure 32. The completed bottom block cage can be seen in Figure 33.
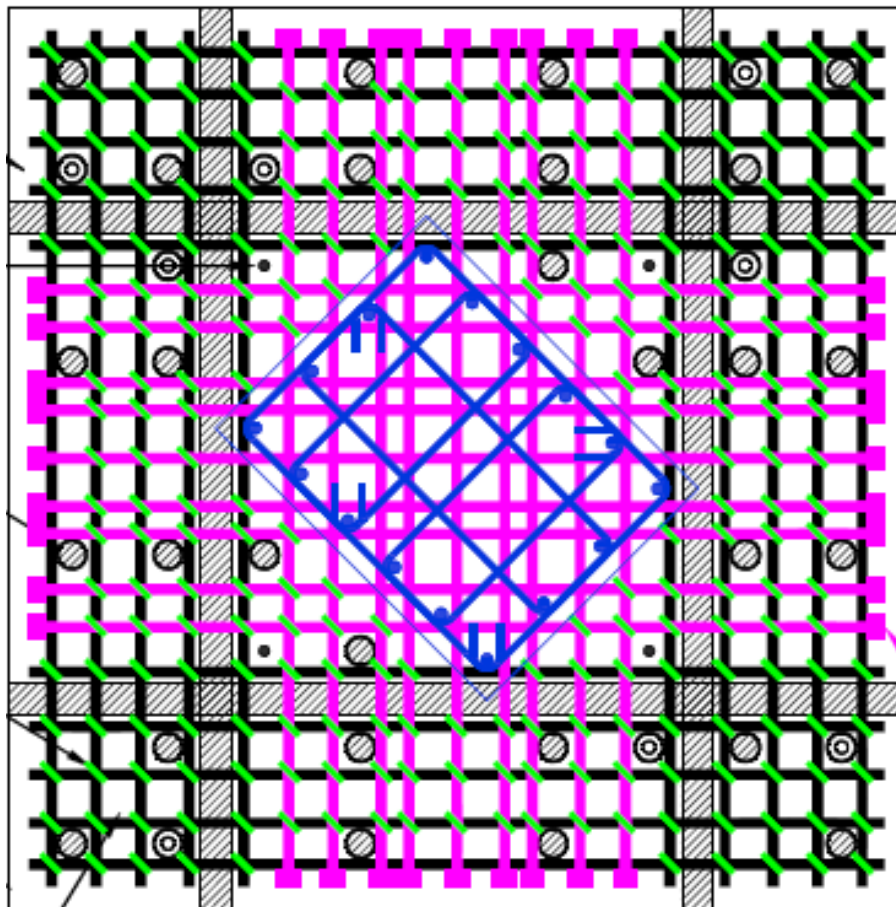
Figure 24. Bottom Block Cage Drawings

Figure 25. Bottom Block Construction

Figure 26. placement of second layer of bottom reinforcement

Figure 27. Bottom of Cage tied in a crisscross pattern

Figure 28. Chairs underneath bottom block for 1 ½ inch cover
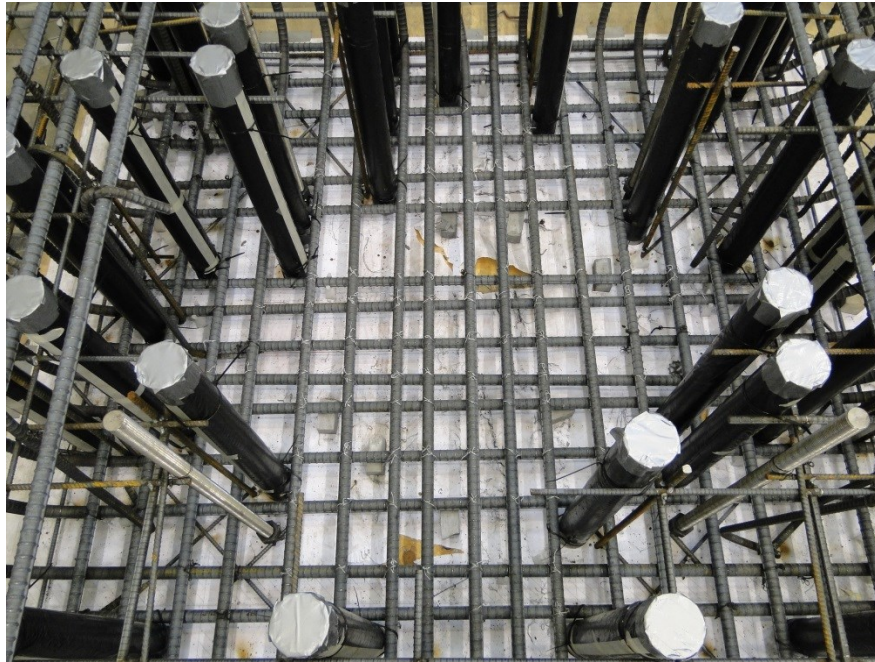
Figure 29. Bottom Block Cage with concrete blocks underneath
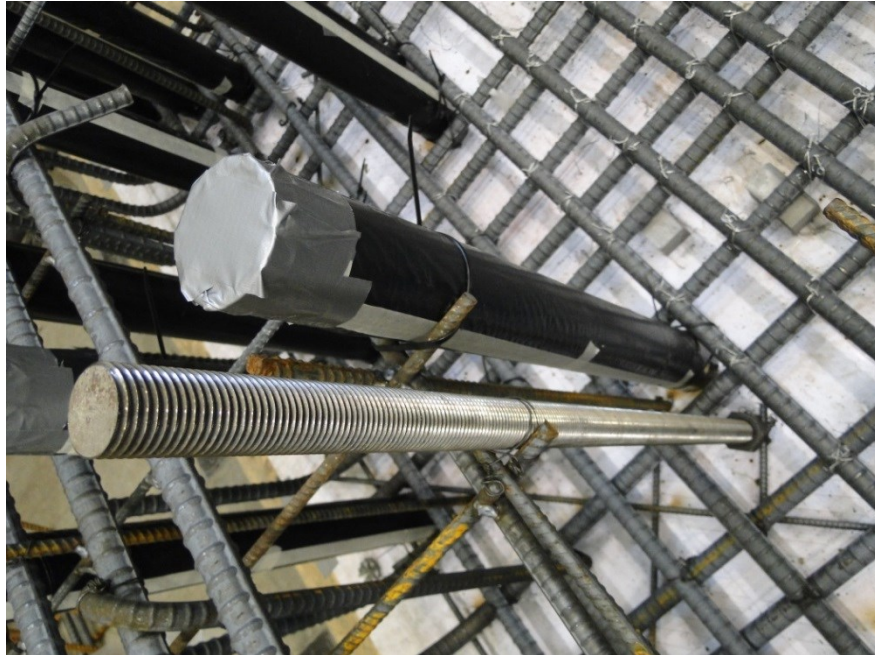
Figure 30. Tied Post Tensioning bar
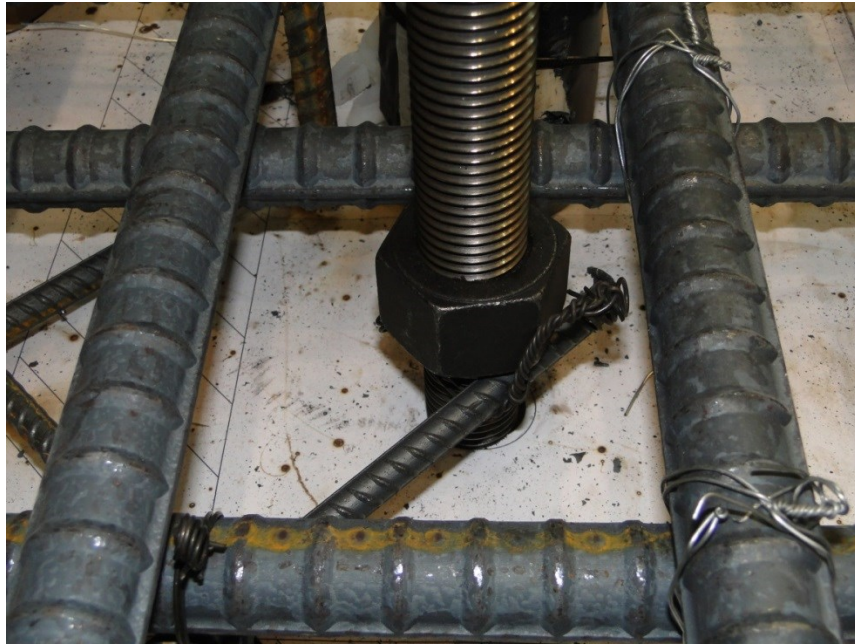
Figure 31. Tied post tensioning bar to the bottom of the bottom block cage.
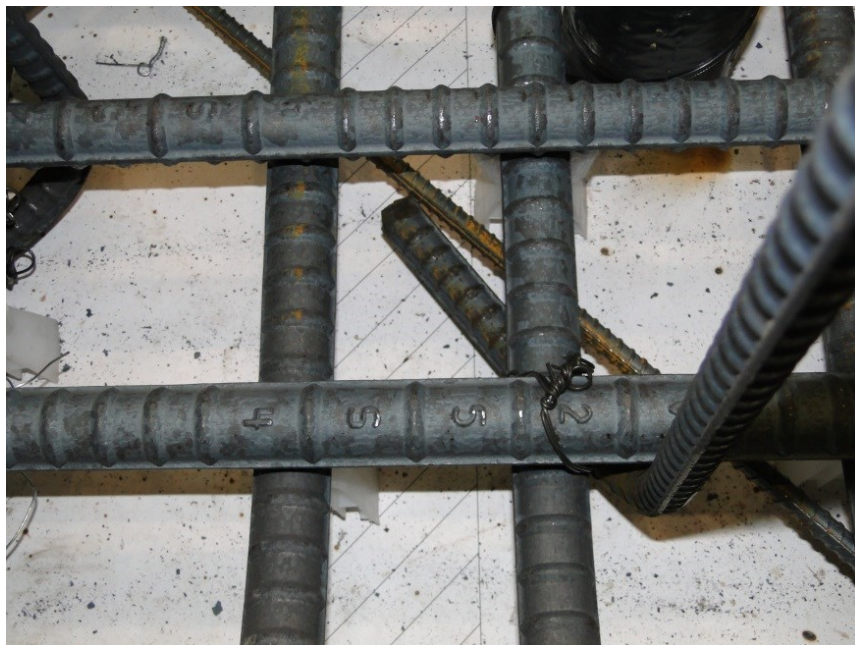
Figure 32. Tied Shear Reinforcement
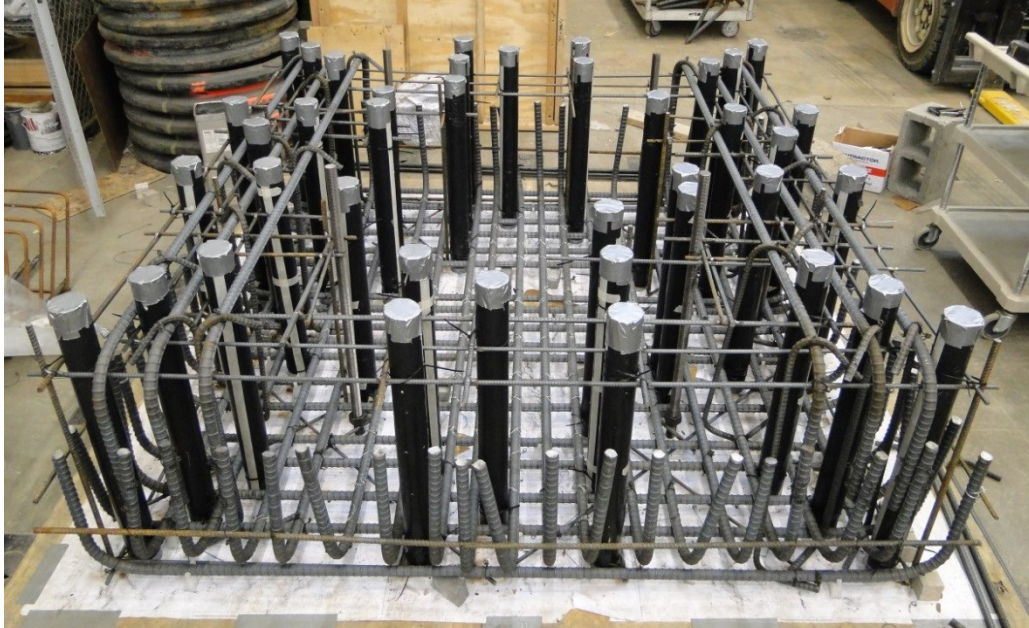
Figure 33. Completed Bottom Block Cage

Step 2: Construction of Column Cage

The construction of the column cage will be done according to the drawings in Figure 34. Next place two rods, strong enough to withstand the weight of the column reinforcing cage, on each side of the supports as shown in Figure 36.
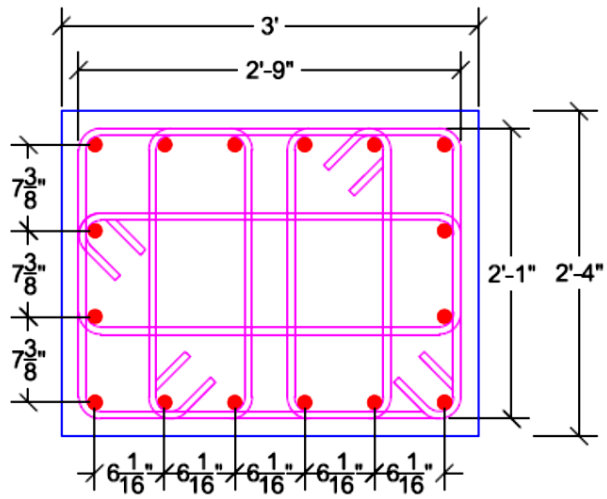
Section A-A
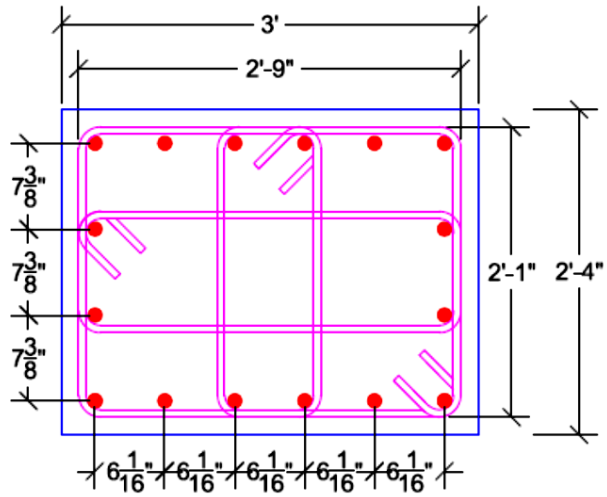
Section B-B

Figure 34. Perimeter Column Cage Construction Drawings

367
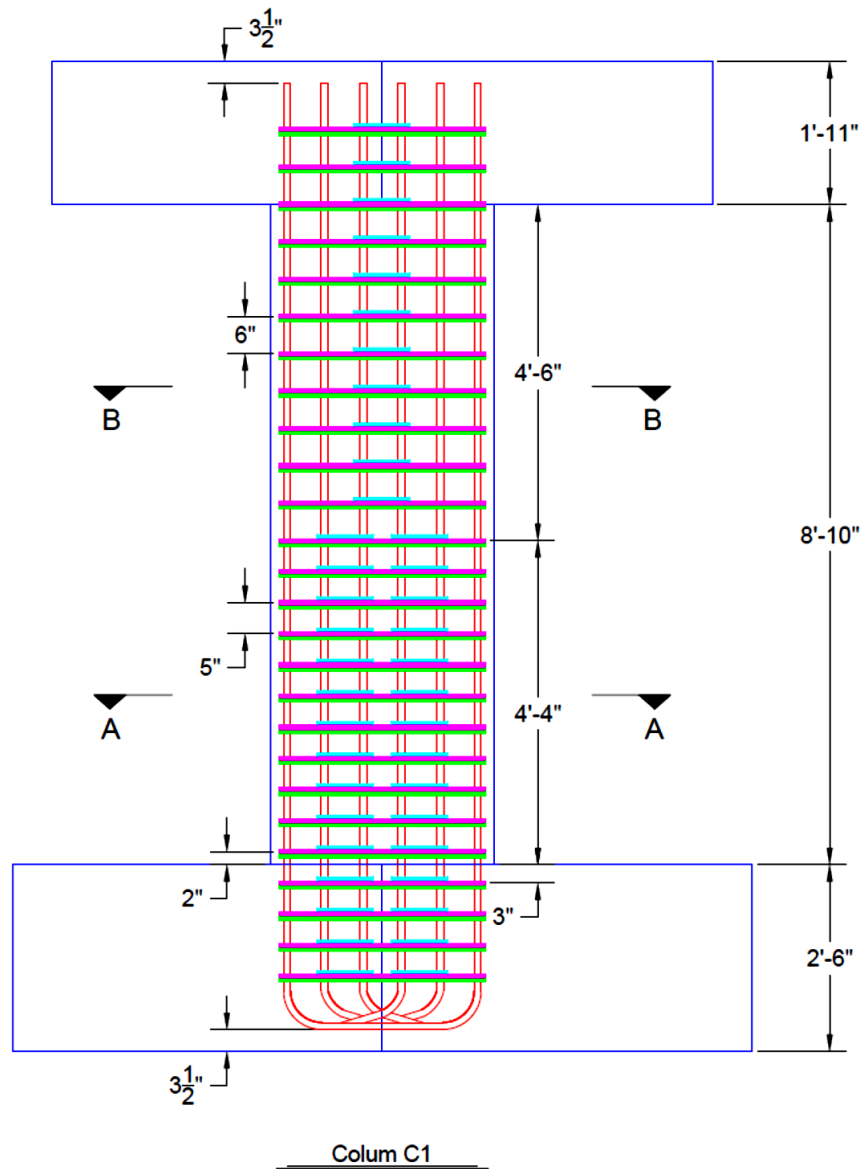
Figure 35. Column Construction Drawings

First place four supports of equal height distanced enough for the column cage to be placed between them. Place two small sheets of ply wood around the rod and hold them in place with a clamp. This is so that the heavy rod does not roll off the supports

during construction. Now place the top layer of longitudinal reinforcement as shown in Figure 36.

Figure 36. Placement of top layer of longitudinal bars

Note that special care should be taken with the bars that already have strain gauges on them to ensure that they are not damaged during the construction process. Once the top layer of longitudinal reinforcement has been placed the hoops may now be inserted in the correct order according to the construction drawings. This is done by lifting the longitudinal bars at the top end and sliding the hoops in the correct order as demonstrated in Figure 37 and Figure 38.

Figure 37. Placing of transverse reinforcement

Once again this is done with caution to ensure that the strain gauges on both the longitudinal reinforcement and the transverse reinforcement is not damaged during the construction.

Figure 38. Transverse reinforcement with strain gauges

Note that after the 15th hoop the configuration changes from to inner hoops to only one throughout the rest of the column.

Figure 39. Placement of upper hoop configuration

Place the bottom layer of longitudinal reinforcement inside the column cage. In Figure 40 the two configuration types of transverse reinforcement can be seen within the column.
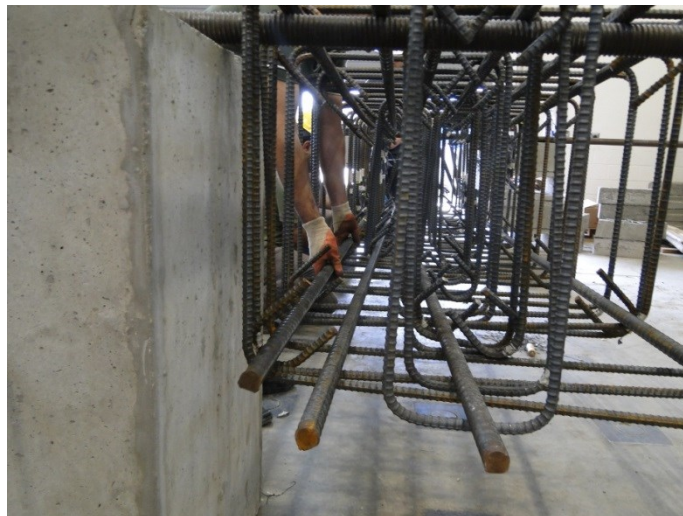
Figure 40. Two types of inner hoop configurations

Once all of the hoops have been placed it will be very heavy and will cause the cage to deflect. To prevent this, raise the cage with the crane to place two supports. Place two sawhorse supports on both sides of the column at around the midsection to prevent the deflection. The two supports must be leveled with the other four supports to ensure that the column remains perfectly horizontal.
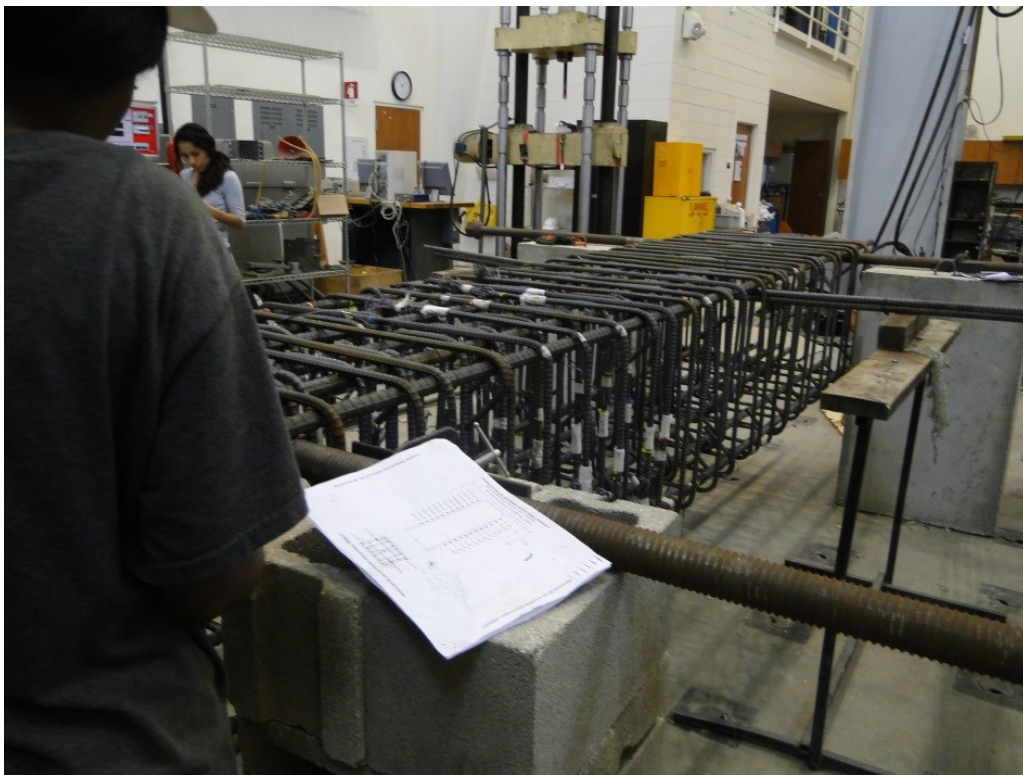
Figure 41. Sawhorse supports at midsection

Two wooden templates were made from AutoCAD drawing printouts according to the exact locations of the longitudinal reinforcement. The purpose of these templates to aid in obtaining the correct spacing throughout the column length.

Figure 42. Column templates

The templates will be placed at both ends so as to maintain the correct spacing. Place one half of a template at the end of the column cage by putting the longitudinal reinforcement through the spaces provided. Simultaneously, arrange the legs of the longitudinal reinforcement and tie them in place at the base of the column cage. The top and bottom layers of longitudinal reinforcement may be tied to one another to the four center bars while the corner bars are tied together.

Figure 43. Tied longitudinal bars at the base of the column

After the first half of the template has been placed, place the second half of the template accordingly.

Figure 44. Two halves of template at the top of the column cage

Tie the two halves of the template together and secure them to the longitudinal reinforcement using tie wire. Place the second template on the other end of the column cage.

Figure 45. Template placement near the base of the column cage

Next, place a flat piece of ply wood at the end of the column cage to measure the locations of the hoops relative to the base of the column cage. Make sure that the bottom of the legs of the longitudinal reinforcement is flush with the plywood. Mark the correct location of the hoops according to the drawings.

Figure 46. Marking of hoop location relative to the base.

Now the reinforcement may be tied at their correct location.
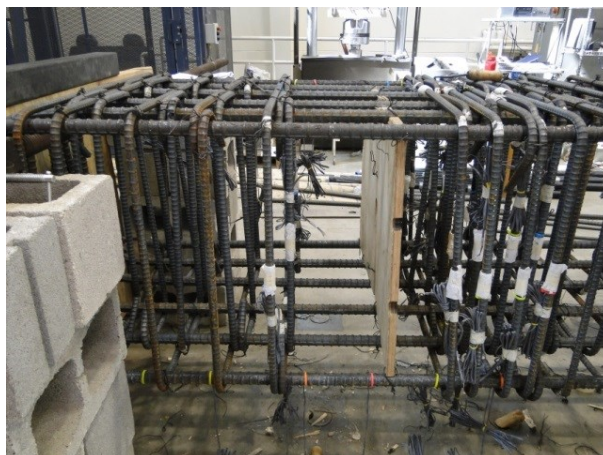
Figure 47. Placement of hoops at correct locations

The reinforcement will be tied at each location where reinforcement intersects with tie wire as shown in Figure 48.

Figure 48. Tying of transverse reinforcement

After all of the ties have been tied to the top and bottom layers of longitudinal reinforcement begin to place the longitudinal reinforcement located on the sides of the column cage. First the templates must be removed and placed on the side of the cage. Next begin to place the remaining longitudinal bars while carefully placing the remaining transverse hoops in their correct location and correct configuration. Continue to place all of the longitudinal reinforcement until all of the bars have been placed in the column cage.

Figure 49. Inserting the side longitudinal reinforcement

Tie the legs of all of the longitudinal reinforcement at the bottom of the cage towards the center of the column. This will be done in three layers as shown below. Tie all bar intersections until the column cage is complete.

Figure 50. Tied longitudinal reinforcement at the base of the column cage
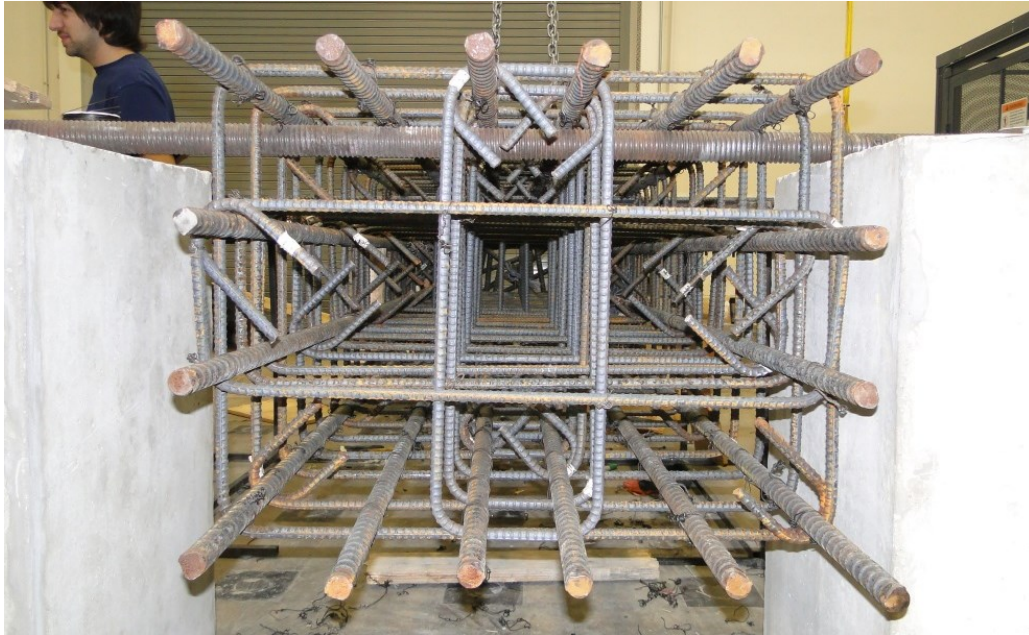
Figure 51. View of the "Top" of the completed tied column cage

Figure 52. Side view of the completed tied column cage

378

Step 3: Construction of Top Block Cage

The construction of the top block cage follows the same process as the construction of the bottom block cage. First lay two sheets of plywood side by side and print the construction drawings to scale and place on top of two plywood sheets.
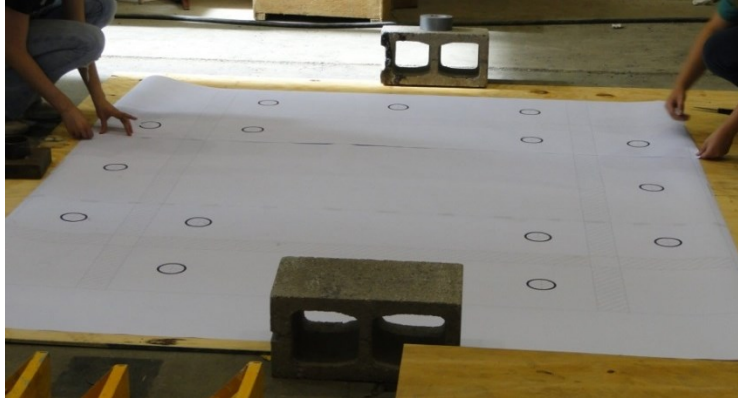
Figure 53. Attaching AutoCAD drawing to the plywood

Next, place the wooden discs on the corresponding circles and place the pvc pipes on the wooden discs. Also, lay the reinforcement grid for the top block cage in its correct location ready to be welded.

Figure 54. Top block reinforcement grid ready to be welded

After welding the reinforcement grid, raise it to the correct location just below the top layers of U-bar reinforcements. This may be done by placing the grid on top of a cinder block and a brick which would give the proper height as shown below.
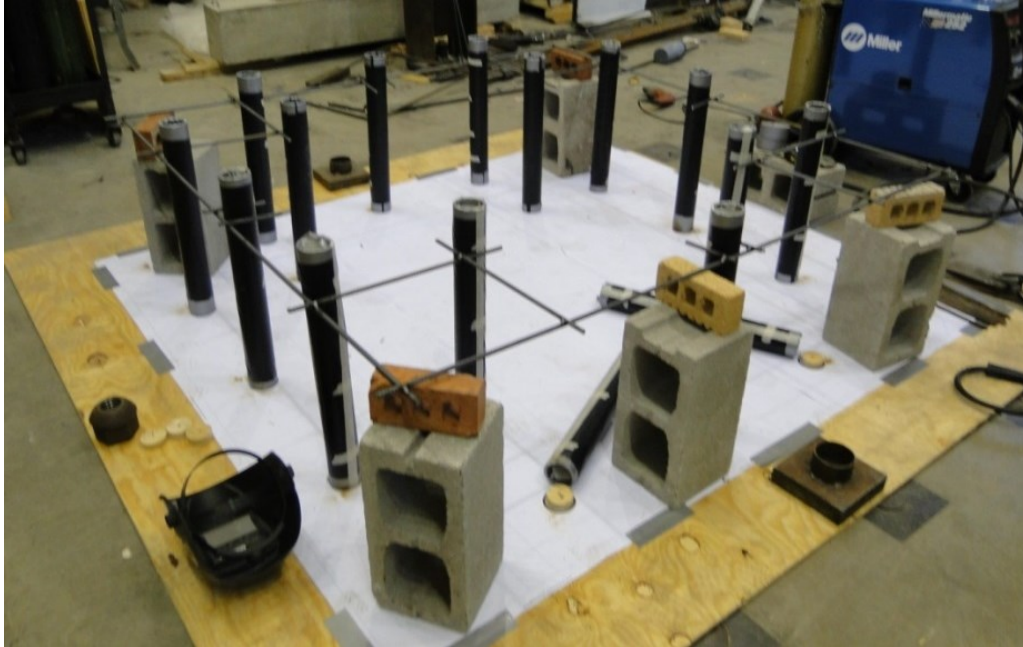
Figure 55. Raised reinforcing grid

After the grid has been raised, a vertical rebar may be welded to keep the grid upright. A lower layer of reinforcement is then added to stabilize the grid reinforcement as shown below. Next, remove the grid and pvc pipes leaving only the two sheets of plywood. Take one sheet of ply wood and using a saw cut the opening where the column should be placed. Do the same with the second sheet of ply wood and assemble the two pieces of plywood along with the reinforcement grid and pvc pipes as shown below.
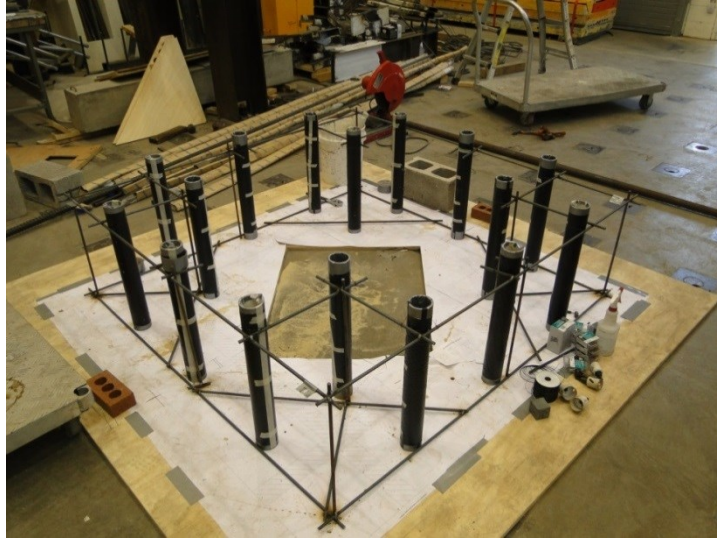
Figure 56. Finished reinforcing grid with plywood cutout

Place the bottom layer of reinforcement U-bars according to the drawings. Only place 3 on each of the four sides leaving an opening for the column cage to pass through the center.
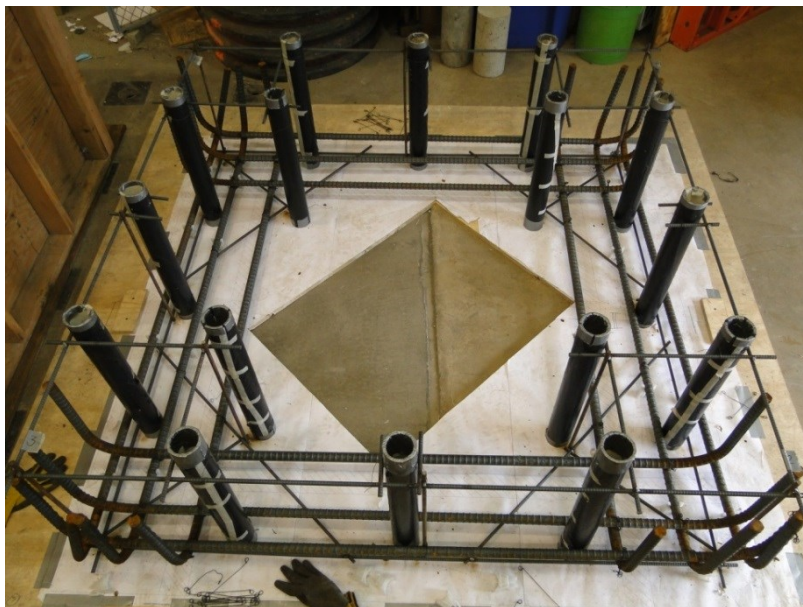
Figure 57. Placing bottom layer of reinforcement

The next step is to place the top layer or U-bar reinforcement. Place the first layer of reinforcement on top of the supports in one direction according to the drawings. Then place the second layer of top reinforcement perpendicular to the first layer of top reinforcement and tie them together.

Figure 58. Placing top layer of reinforcement

Double check that the concrete cover is 1.5 inches before tying the top and bottom layers of the reinforcement cage together.

Figure 59. Checking concrete cover

Tie together both of the top and bottom layers of the reinforcement cage as shown below. Also tie the horizontal pvc pipes that will later be used for lifting. Also make sure the cage is securely tied so that it may not fall apart during lifting and construction. At this time some of the shear reinforcement may also be tied to the cage.
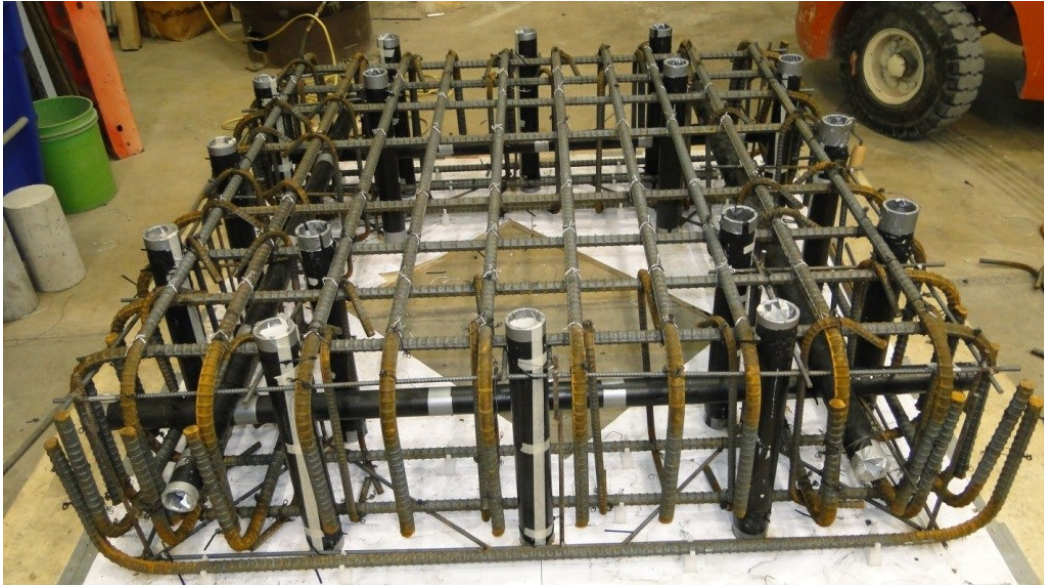
Figure 60. Tying top block cage

The shear reinforcement hooks on to the top and bottom layers of the reinforcement cage and are tied at both the top and bottom just as in the footing block. Make sure that the horizontal pvc pipes are securely tied to the reinforcing cage because they may move during casting.

Figure 61. Tying horizontal pvc pipe

Figure 62. Completed top block cage

Step 4: Bottom Block Formwork and Casting

The column formwork would be erected at Hanson Pipe & Precast. The formwork used for the construction of the column was ordered from PERI Formwork Systems, Inc. However, the exact dimension needed for the column were not available therefore the formwork would need to be adjusted based on the drawings below.
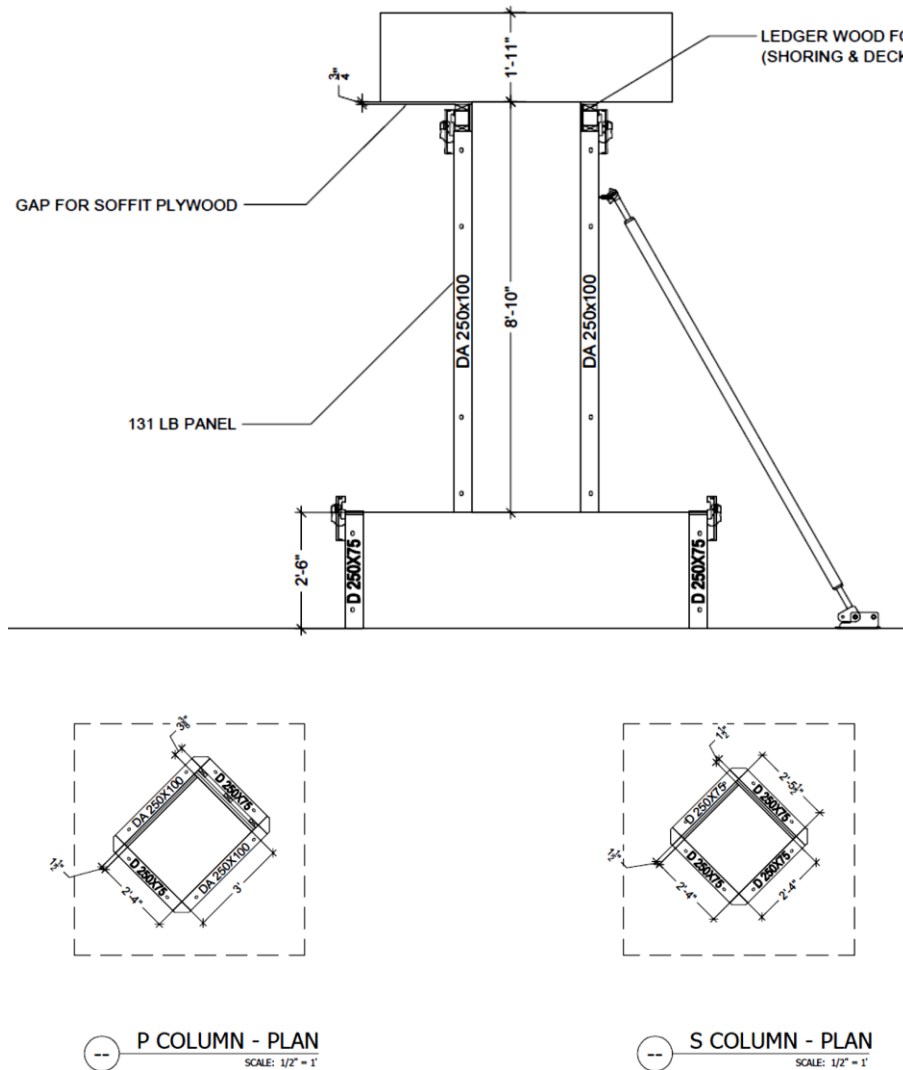
Figure 63. PERI Formwork Drawings

Plywood will be attached to the formwork to adjust it to the correct dimensions. Cut ¾ inch plywood to the dimensions of the two larger panels of the perimeter column (P Column). Drill the sheet of plywood to the formwork using 1 inch screws. Leave a 2 inch space near the top of the formwork to later place an extension. Cut the extension piece according to the drawings and place it flush against the plywood on top of the formwork panel. Drill the extension piece to the formwork panel until it is completely secure.

Figure 64. Drilling extension piece to modified column formwork

Place three wooden strips of $\frac{15}{16}$" equally spaced on the surface of the formwork. These pieces will be used to create the correct column dimensions. Place 2 more strips along the edge of the formwork to create a sealed form and prevent any concrete from seeping into the formwork. Put three more strips extending out through the formwork to be used as supports for the extension piece. Drill the plywood through the strips onto the formwork until it is securely in place.

Figure 65. Drilling plywood to the edge strips

Since the formwork will be used many times, the plywood needs to be securely attached to the formwork. Place a screw at about every 10 inches. Continue modifying the rest of the formwork panels. Note that for the larger panels a 1 $\frac{11}{16}$" gap is left at the edge so that the panels located in the perpendicular direction fit inside this gap producing the correct column dimensions. Complete the rest of the panels.

Figure 66. Completed column formwork modification

The rest of the column construction will take place at Hanson Pipe & Precast. Now that the reinforcement cages and formworks have been prepared they must be shipped to the construction site at Hanson. The column is first lifted by using 2 chains and collections of reinforcement bars. The cage is lifted at two points near the center assuring the column cage is balanced and lifted horizontally.

Figure 67. Shipping of column cage

At Hanson, the workers had already built the bottom block formwork and temporarily set up the frame.

Figure 68. Bottom block and frame setup

The bottom block cage arrived and was placed on supports away from the formwork. Once the bottom block cage has been placed, assemble the other two sides of the bottom block formwork. Return the frame to its correct location. Note that the frame has been secured to the floor. Using the crane place the column cage in the center of the footing cage.

Figure 69. Placement of the column cage

Two locations are measured and a 2x4 is used as a reference to orientate the column cage in the proper direction of 45 degrees.

Figure 70. Placing the column cage at 45°

Now that the column has been placed in its correct location, remove two sides of the bottom block formwork once again to place the top layers of reinforcing bars for the bottom block that will pass through the column cage. Pass the reinforcing bars through the column cage very carefully as to not damage the concrete gauges. Make sure to securely tie the reinforcing bars.

Figure 71. Placement of bottom block reinforcement through column cage

Level the column cage so that it is completely vertical. This is done by tying wire from the column cage to the 4 corner posts of the frame. Adjust the wires until the column cage is vertical.

Figure 72. Leveled column cage

Next, add the shear reinforcement. The shear reinforcement is placed in higher concentration around the perimeter of the column cage section. The shear reinforcement is hooked to the top of the bottom block cage and securely tied so that it does not rise during casting. Note the plastic bags in which the strain gauge wires are located have been removed prior to the placement of the shear reinforcement.

Figure 73. Placement of shear reinforcement

Add two No. 3 bars instrumented with strain gauges to the top surface of reinforcement through the column as shown in the drawings below.
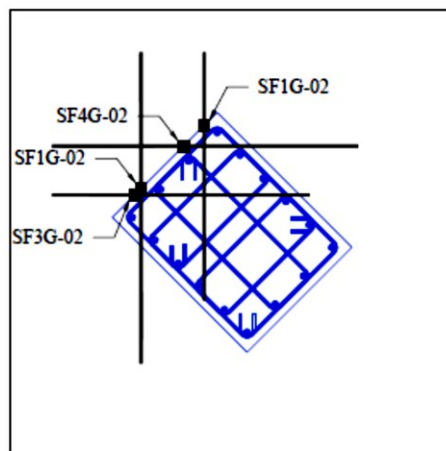
Figure 74. Placement of Footing Strain Gauges

Ensure that the specimen and formwork are completely leveled during the construction process. The column will be cast using the facilities at Hanson Pipe & Precast. The mixer that will be used is shown below.

Figure 75. Concrete Mixer

The mix design is input into the computer. The computer processes the information and instructs the mixer to begin mixing. The material is mixed.
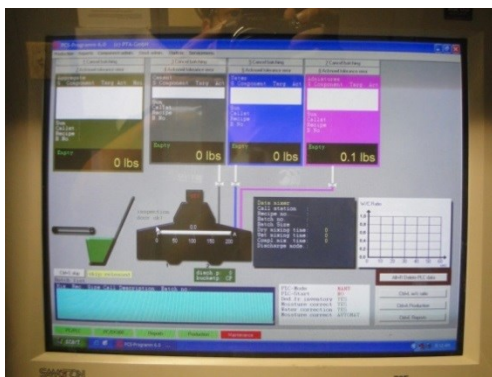
Figure 76. Inputting of mix design and mixing of material

Figure 77. Concrete mixing

The mix is then poured onto a truck that will deliver the concrete to the bottom block cage. The truck then begins to pour the concrete.

Figure 78. Pouring of concrete into the footing block

Figure 79. Bottom block casting

Once the bottom block has been filled about halfway it is vibrated. The vibration is done to eliminate any unwanted voids in the concrete and ensure a better uniform flow. The vibrating is done very carefully away from the center of the column cage so as to not damage any of the strain gauges.

Figure 80. Vibrating the bottom of the footing block

Special care should also be taken in vibrating at the locations where the strain gauge wires meet the top surface of the footing.

Figure 81. Bottom block casting

Continue to pour until the concrete has reached the top of the formwork. Carefully vibrate one more time and finish the surface.
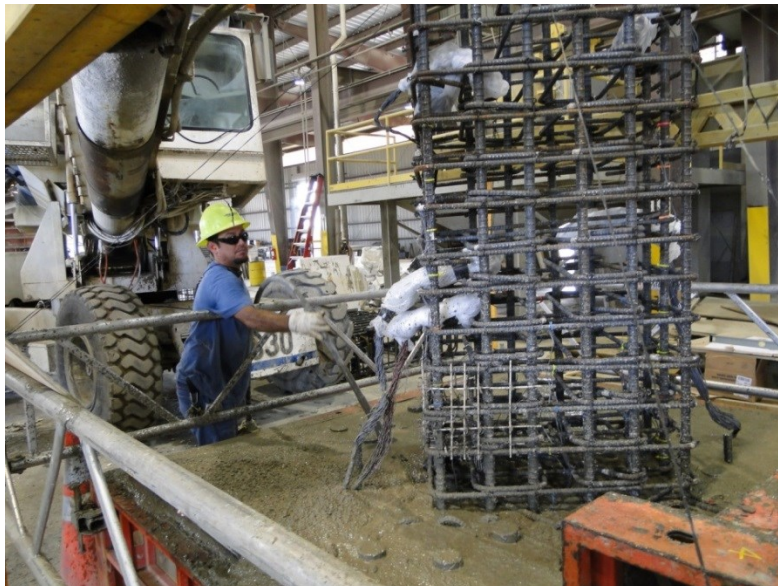
Figure 82. Vibrating near the top of the footing block

Figure 83. Cast bottom block

A wheel barrel of concrete is then taken to the material testing lab where the slump and temperature of the concrete is taken.24 cylinders are also made to evaluate the concrete strength at different time intervals.

Figure 84. 24 Concrete Cylinders

Back at the construction site, the surface of the footing block has been finished using a wood float.

Figure 85. Finished surface of bottom block

Figure 86. Completed bottom block casting

Step 5: Construction of Column Formwork

After 2 days the concrete should be sufficiently dry. Using the construction drawings draw the location of the column. This may be done in two ways. The first using the edges of the formwork as a reference to draw the center, or by using the location of the pvc pipes as a reference to draw the column.

Figure 87. Drawing reference lines

There should be a 1.5 inch concrete cover.

Figure 88. Checking column concrete cover

Place the first column formwork panel vertically flush on one face of the column cage.

Figure 89. Placing first column formwork panel

Using the crane place the second column formwork panel.

Figure 90. Lifting of formwork panel

Use the clamps to attach the two formwork panels so that they do not fall. Begin placing the LVDT rods on the side with the pre-drilled holes.

Figure 91. Inserting LVDT rods through the column formwork

Place 1.5 inch plastic chairs all along the perimeter of the column cage to ensure adequate concrete cover.

Figure 92. Placing concrete chairs

After the LVDT rods have been placed on one formwork panel, use the crane to place the second formwork panel.

Figure 93. Placing of second formwork panel

Note that the first transverse reinforcement hoop should be at 2 inches from the surface of the footing.

Figure 94. Checking of hoop spacing

Continue to place the LVDT rods on the second formwork panel. Special attention should be taken to not damage the concrete strain gauges during the instillation of the LVDT rods around this area.

Figure 95. Placing of LVDT rods on both formwork panels

The LVDT rods should be embedded about 10 inches from the outer surface of the column. This is to ensure that the rods are not lost during the crushing and spalling that may occur during the testing of the column.

Figure 96. 10" embedment of LVDT rods

Carefully collect the wires and place them through the hole that has been drilled in the column section at about mid height. Wrap the wires tightly in duct tape so that they may easily pass through the hole without being damaged.

Figure 97. Passing strain gauge wires through the column panel

Finish placing all LVDT rods and ensure that they are all secure and tied tightly to prevent them from moving during casting. After placing all of the LVDT rods, chip the upper laitance layer of concrete.

Figure 98. Chipping off top concrete layer

This is done by using a chisel all around the perimeter and interior of where the column will be located. The upper laitance layer is removed to ensure good bonding between the new and hardened concrete. Remove up to 3 inches of concrete from the perimeter of the column cage.

Figure 99. Removal of Laitance Layer

Once the column formwork has been placed raise the frame until the 2 supporting beams are well above the highest clamps on the formwork so that the rest of the support beams do not interfere with them. Continue to place the support beams equally spaced on both sides of the column cage.

Figure 100. Placement of supporting beams

Tie 2x4's together to two beams on either side of the column. This is done as an additional support to place the smaller size beams.

Figure 101. Column formwork construction

Place the smaller support beams near the column formwork. After all of the support beams have been placed, place sheets of plywood to create a deck above.

Figure 102. Attaching plywood to supporting beams

Figure 103. Raising frame flush with the top of the column formwork

Raise the frame on all sides until the deck is on the correct location with respect to the column formwork taking into consideration the thickness of the plywood sheets. Once the deck has been constructed attach the red lateral supports to the column formwork.

Figure 104. Attaching lateral supports

Drill the bottom of the lateral supports to the floor to secure stability.

Figure 105. Drilling supports to the floor

Note that all four of the columns of the frame have also been securely bolted to the floor. Place wooden pieces between the formwork and the embedded post tensioning rod so that the column formwork remains in place and does not move during casting.

Figure 106. Inserting wooden pieces to secure formwork

Place small pieces of wood underneath the formwork to prevent any leaking during casting.

Figure 107. Inserting small wooden pieces to prevent leaking

Place the yellow railing supports and beams all above the deck for safety purposes.

Figure 108. Placement of deck railing

Place 6 4x4's underneath the perimeter of the column formwork for precaution and to support the weight of the top block when pouring.

Figure 109. Additional wooden supports

Step 6: Column Casting

Prepare everything needed for casting the column section including the funnel and "elephant trunk".

Figure 110. Funnel and "elephant trunk"

Place the bucket underneath the mixer. Prepare the mix and pour the mix into the bucket.

Figure 111. Pouring concrete into bucket

Using the crane lift the bucket and attach the smaller funnel extension.

Figure 112. Attaching the funnel and "elephant trunk"

Next, add the "elephant trunk" extension. This will allow better control of the concrete pouring within the column section. Lift the bucket well above the column formwork. Guide the bucket of concrete towards the column formwork.

Figure 113. Lifting bucket over column

Lift the bucket straight over the column opening. Place the "elephant trunk" in the center of the column cage.

Figure 114. Placement of funnel

Pour the concrete carefully into the column formwork so as to not damage the concrete gauges and stop when the concrete is 1 foot below the top of the formwork.

Figure 115. Column Casting

Vibrate the column section taking special care not to damage the concrete
gauges.

Figure 116. Vibrating column section

Figure 117. Top view of column casting

Take a wheelbarrow of concrete to the material testing lab and do a slump test and measure the temperature of the concrete.

Figure 118. Material Testing

Prepare 24 cylinders that will later be tested to obtain the concrete strength at different time intervals and the testing day.

Figure 119. Concrete Cylinders

Step 7: Top Block Casting

Days after casting the column remove the formwork from the bottom block.

Figure 120. Removal of bottom block formwork

Assemble the formwork according to the dimensions of the top block as shown below.

Figure 121. Construction of top block formwork

Ensure that the top block will be 74 inches. Place the plywood on the top of the deck but do not attach it to the deck until it has been centered with respect to the bottom block.
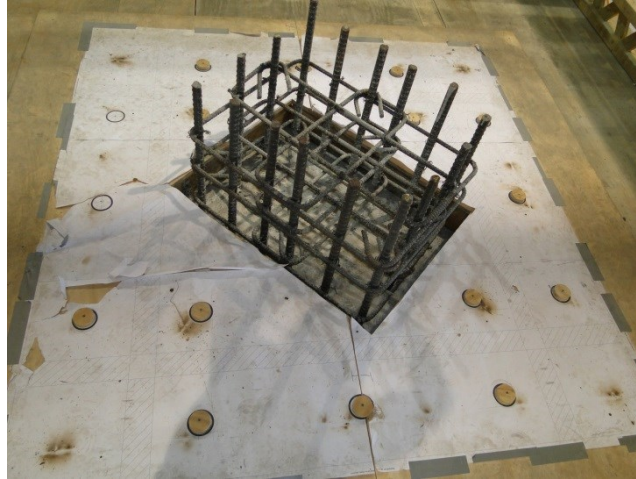
Figure 122. Placement of top block plywood

Drill small holes on the location where the post tensioning rods will pass through the top block. Place a laser straight down and see where it is located with respect to the post tensioning rod embedded on the bottom block. Do this until all four rods are aligned.

Figure 123. Aligning the top block with the bottom block

Prepare the surface of the top of the column once again removing the laitance layer with the chisel. This time adding a concrete adhesive to obtain a better bond between the two concretes. Dilute the concrete adhesive and pour it on the top surface of the column.

Figure 124. Addition of bonding adhesive

Using the crane place the top block cage on top of the deck centered around the column cage.

Figure 125. Placing of top block cage

Using the drawings place the remaining bottom layer of reinforcement (L-bars) through the column cage.

Figure 126. Placing bottom layer of top block reinforcement through column cage

Place the shear reinforcement mostly concentrated around the column cage. Next, using the crane place the formwork around the top block cage.

Figure 127. Top block cage and formwork ready for casting

The top block will be cast with .75 percent fibers to prevent any cracking during transportation since the concrete will still be in its early age strength. Pour the fibers into the concrete mixer.

Figure 128. Addition of steel fibers to mixer.

Place the bucket directly above the top block.

Figure 129. Lifting bucket above column

Pour the concrete on the top block until it has reached the top surface of the PVC pipes or 23 inches.

Figure 130. Top block casting.

Spread the concrete around until it is evenly settled. Vibrate the concrete and finish the surface.

Figure 131. Finishing top block surface

Take a wheelbarrow of concrete to the material testing lab to perform the necessary tests. Notice the high concentration of fibers in the mix. Perform a slump test and take the temperature of the concrete.

Figure 132. Material testing

Make 24 cylinders.

Figure 133. Top block cylinders

Step 8: Demolding of Formwork and Shipping of Column

Two days after casting remove the formwork from the top block as well as all of the protective railing.

Figure 134. Demolding of top block formwork

Remove all of the decking and lower the frame down. Also remove the two panels of formwork where there are no LVDT rods. Next, remove all of the LVDT rods from both of the column formwork panels.

Figure 135. Removing LVDT rods

After all of the LVDT rods have been removed, very slowly and carefully begin to remove the two remaining panels. Special care should be taken to not damage the wires that are now cast within the concrete column and also pass through the hole in the column formwork and can be very easily ripped out. After removing all of the formwork, wrap the wires coming out of the column to the column using plastic wrap. This is to protect the wires during shipping and transportation.

Figure 136. Wrapping wires to column section

Wrap the wires that are coming out of the footing block.

Figure 137. Wrapping footing block wires

Use the couplers to attach two rods together and then passing through the top block attach the two rods using another coupler to the portion of post tensioning rod embedded within the footing block.

Figure 138. Inserting post tensioning rods

Prepare all of the equipment for post tensioning (Plates, nuts, washers…etc.).

Figure 139. Post tensioning plates, nuts and washers

Figure 140. Post tensioning equipment

The post tensioning must be done from the top of the column.

Figure 141. Post tensioning of column

To post tension the rod, place the rod inside the jack. Pump to 3000 psi on each rod which has been calibrated to be a total force of approximately 20 kip. FEM analysis concluded that the best way to post tension the column without damage would be to post tension the rods from the top of the column cross alternating at 1000psi intervals.
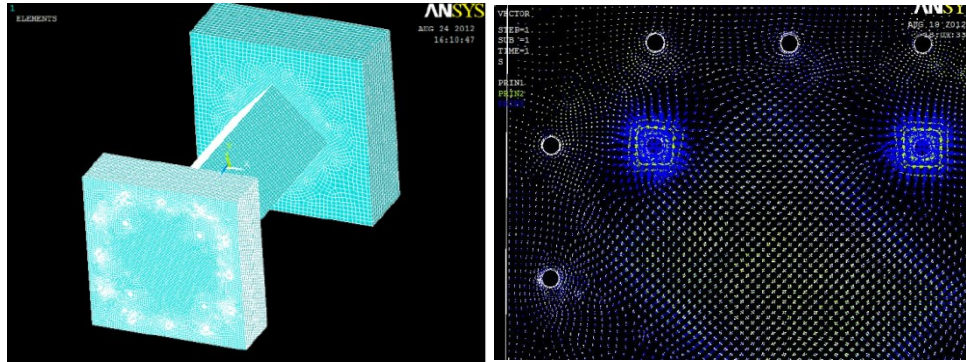
Figure 142. FEM analysis for post tensioning sequence

Once the column has been post tensioned chokers need to be placed inside the hooks to use the crane chains for lifting purposes.

Figure 143. Placing chokers for lifting

The column will be lifted using a 35 ton capacity crane located within the facilities at Hanson Pipe & Precast.

Figure 144. 35 ton capacity crane

A spreader beam will be used to better distribute the load.

Figure 145. Spreader beam

Slowly and carefully lift the column above the ground.

Figure 146. Lifting of column

Set the column on the forks of the forklift.

Figure 147. Setting column on forklift

Figure 148. Column on forklift

Attach the chains to the loops with two on each side on the phase opposite to the forklift. Place a piece of wood in between the chains and the concrete column. This is done so that the chains do not damage the concrete during lifting. Slowly begin to lift the column on one side using the crane. Place more wooden supports below the column to prevent it from crushing as it the column is laid down.

Figure 149. Starting to lower column

Continue to move the crane down while simultaneously moving it towards the door. Some crushing may still occur near the bottom of the footing.

Figure 150. Lowering column to the floor

Once the column is completely horizontal place supports at the bottom of the top block to keep it leveled.

Figure 151. Column laying horizontally

Bring the flat bed that will be used to transport the column around towards the gate.

Figure 152. Flatbed truck used for transportation

Using the spreader beam attach the chains to the lifting hooks.
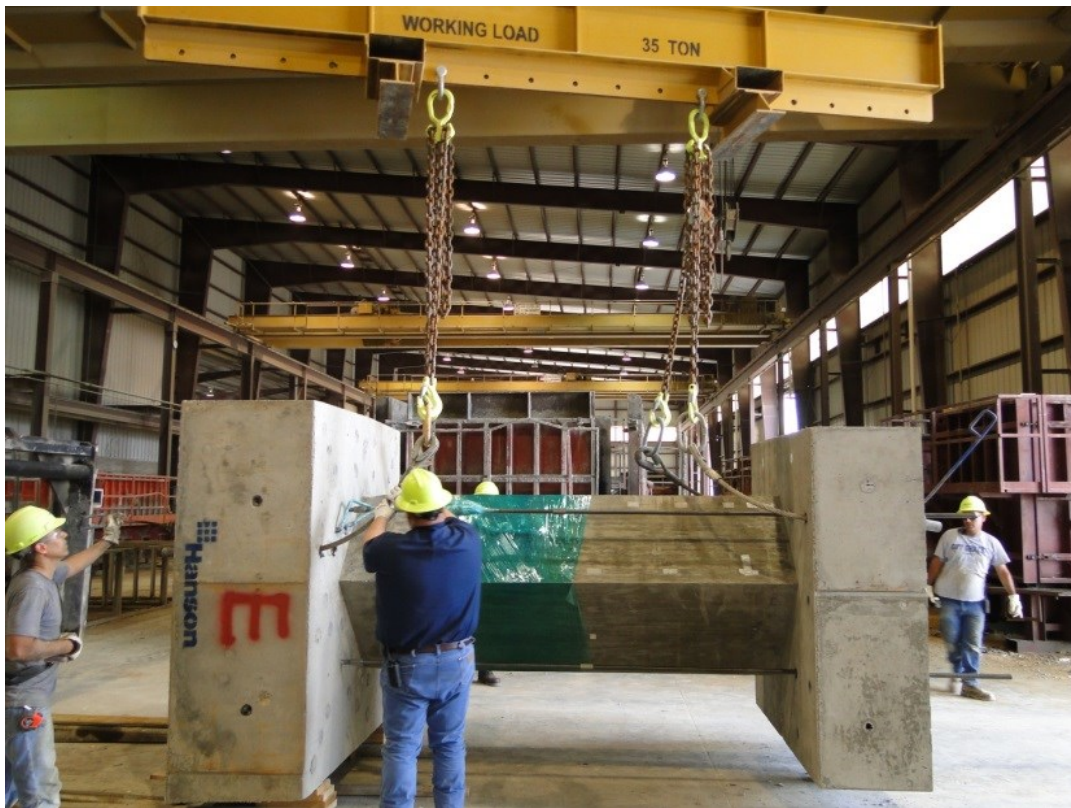
Figure 153. Placing hooks to lift column onto flatbed truck

Slowly lift the column horizontally and guide the column as close as possible to the gate.

Figure 154. Lifting column horizontally

Reverse the flatbed truck into the building to the ideal location to centralize the weight of

the column. Secure the column to the flatbed and begin transportation.

Figure 155. Setting column on flatbed truck

Space Frame Columns (SP5 and SP8) Constructed at UTA CELB

Following the casting of SP1, all of the remaining column specimens were constructed and cast completely at UTA CELB following the standard procedure established with SP1. This section will describe the construction of the space frame columns constructed at UTA CELB. The space frame column construction also followed the general procedure of the perimeter frame column. However the cross section of the space frame columns were smaller compared to that of the perimeter frame columns. The space frame column is a square column with cross-sectional dimensions of 28"x28" and is reinforced with twelve No. 8 bars distributed evenly around the perimeter of the cross section spaced at 7.5" on center. The transverse reinforcement consists of groups of 3 overlapping ties bent from No. 5 bars spaced at 5" to 6" throughout the length. The space frame reinforcement details can be seen in Figure 156 and Figure 157.
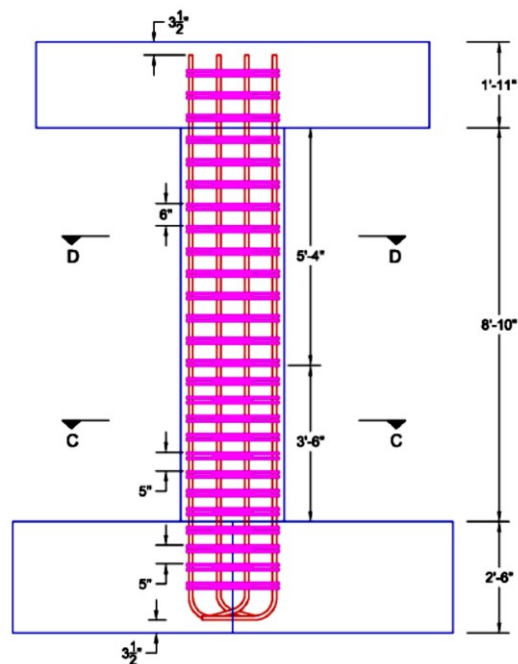
Figure 156. Space Frame Column Reinforcing Details
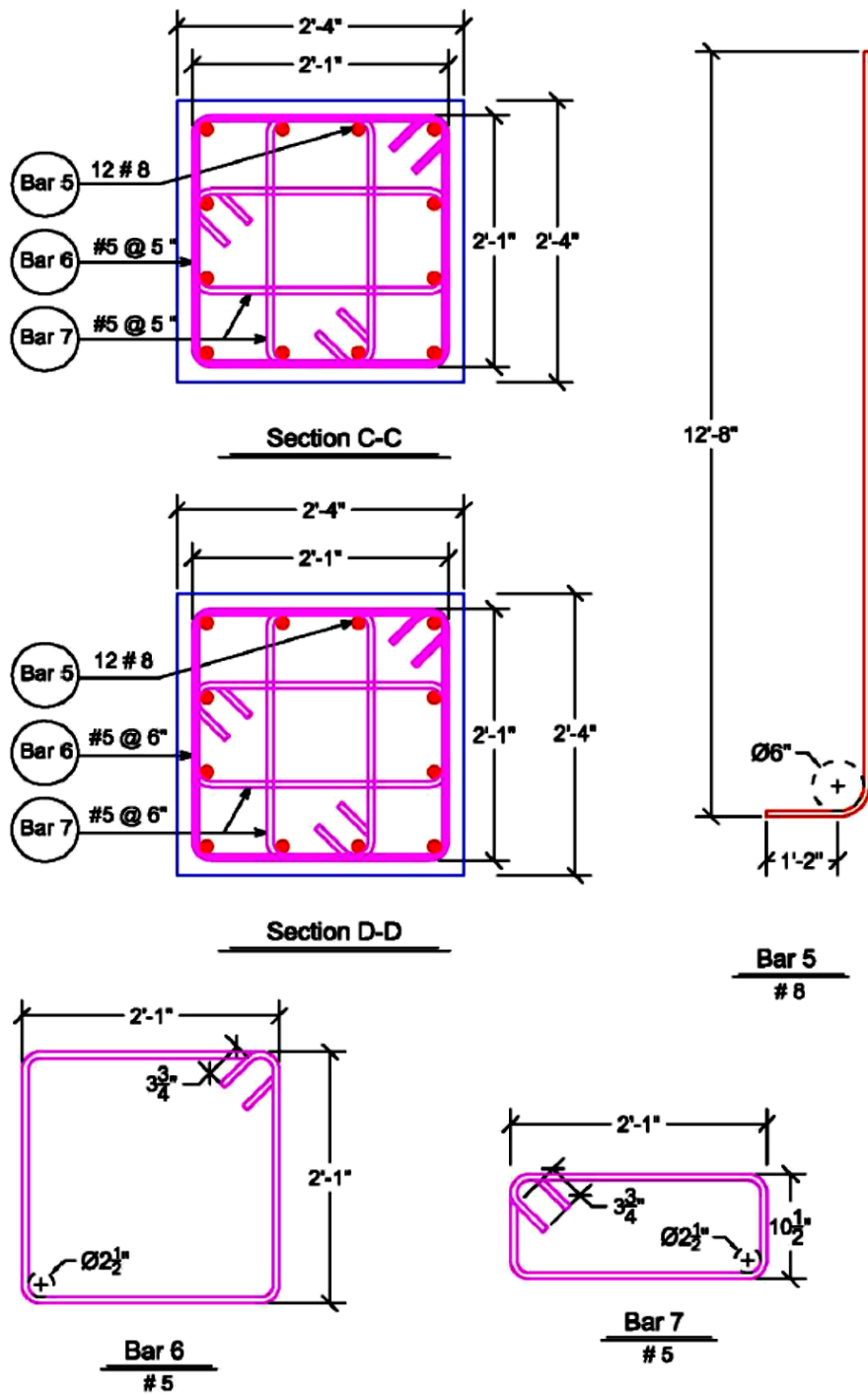
Figure 157. Space Frame Column Reinforcement Bar Details

438

Construction Sequence

All of the space frame column specimens were constructed at the UTA CELB. Each specimen was built in three major parts and cast vertically to simulate real world construction as accurately as possible. Before the construction began all steel strain gauges were placed on the reinforcing bars. The reinforcing cage for the footing block and column cage were constructed separately but simultaneously. Once the footing block cage was completed it was placed inside the formwork and the truss frame was erected as shown in Figure 158. After the column cage was completed and instrumented with concrete strain gauges as shown (Figure 159), it was placed inside the footing cage (Figure 160), centered and secured with straps to the truss frame to prevent it from moving during casting (Figure 161).

Figure 158. Footing Block Reinforcement and Formwork

Figure 159. Completed Column Reinforcement Cage

Figure 160. Placing of the Column Cage into the Footing Block
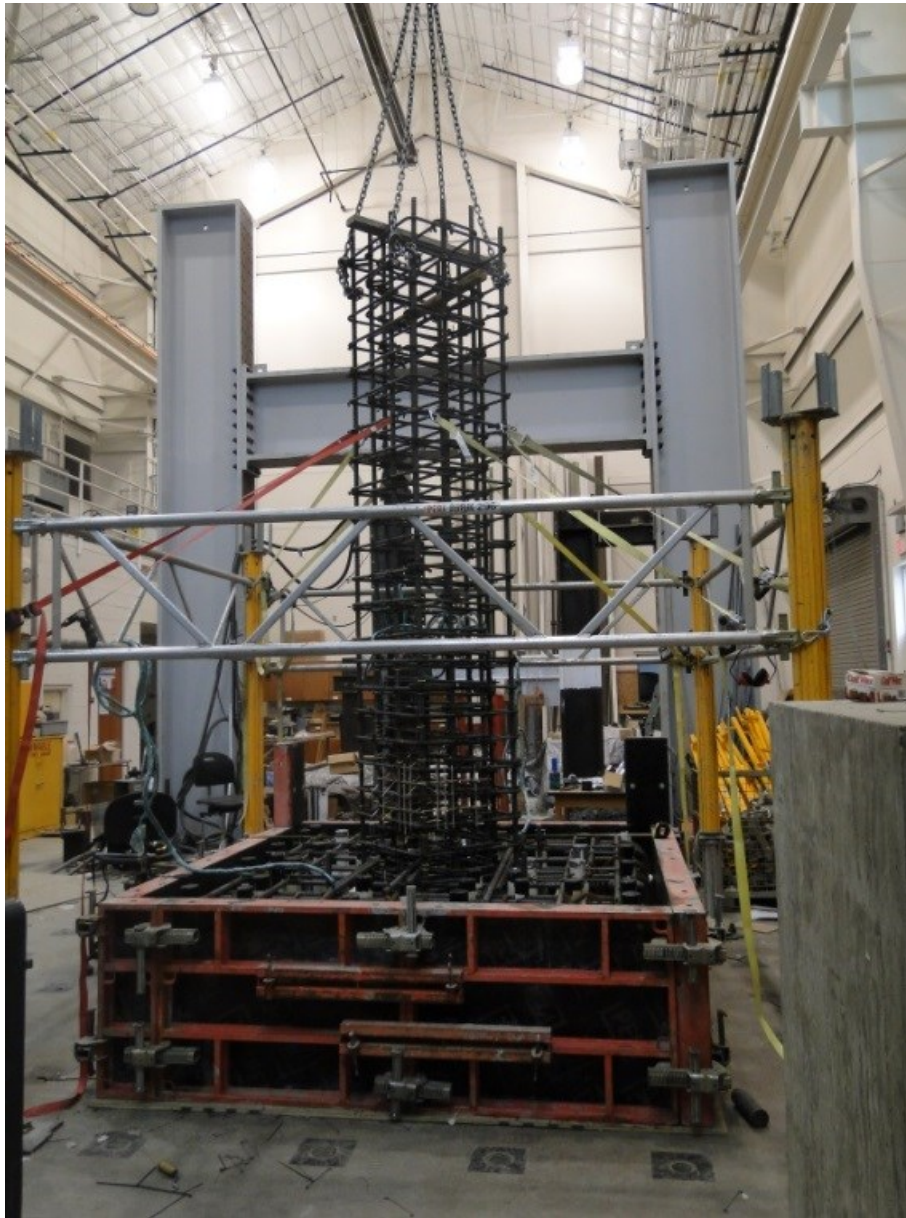
Figure161. Centered and Secured Column Cage

The bottom block was cast using 5 ksi concrete provided by a ready mix truck as shown in Figure 7.Twelve concrete cylinders were made to later be tested under uniaxial compression in order to determine the concrete strength progression.

Figure 162. Bottom Block Casting.

Figure 163. Finishing of bottom block surface

After the bottom block concrete had gained sufficient strength, the formwork for the column and platform was placed (Figure 164).

Figure 164. Column Formwork and Loading Block Platform

The top block reinforcing cage was constructed (Figure 165) and placed on the platform with the top block formwork.

Figure 165. Loading Block Cage and Formwork

Figure 166. Top block cage and formwork

The column section and the loading block were cast vertically to simulate real world construction. The specimen was cast using 5 ksi concrete provided by a ready mix truck. The concrete was poured into a large bucket which was then lifted with a crane to pour the concrete into the column section as shown in Figure 167.

Figure 167. Final Column and Loading Block Casting

Figure 168. Casting of loading block

After 2 days of curing the formwork is removed and the column is prepared for shipping. Four post tensioning rods were used to protect the specimen from cracking during lifting and transportation. The finished SP5 column specimen can be seen in Figure 170. The column was removed from the CELB by the use of heavy duty forklifts (Figure 171 and Figure 172) and placed on a flatbed truck to be transported to the University of Minnesota (Figure 173).

Figure 169. Finishing of top block surface and covering for curing

Figure 170. SP5 Space Frame Column Specimen.

Figure 171. Lifting of column with forklift

Figure 172. Removing Specimen from CELB.

Figure 173. Shipping of Column Specimen to Minnesota

UHP-FRC Space Frame Column Construction Procedure

Both column specimens SP5 and SP8 were built with the same construction sequence. However, there are 2 key differences between the two space frame columns. The differences featured in specimen SP8 include:

The first 40" above the footing is cast with Ultra High Performance Fiber Reinforced Concrete (UHP-FRC).

The first 40" of specimen SP8 was cast with UHP-FRC. Since no tests had been conducted with UHP-FRC on full scale structural elements, it presented an interesting construction challenge. In order to correctly mix the UHP-FRC in large quantities a special concrete mixer had to be designed. The mixer was designed and fabricated with the help of Bailey Tool & Manufacturing Company and can be seen in Figure 174.

Figure 174. Special UHP-FRC Mixer

Formwork was set up prior to casting to a height of 40" as shown in Figure 175. All of the dry materials for the casting were premeasured and placed inside of a large bucket (Figure 176). The dry material is then added to the mixture slowly followed by water and super plasticizer (Figure 177). The microfibers are added last as shown in Figure 178. In order to pour the 40" section the mixer must be elevated to a height well above the section to allow the UHP-FRC concrete to flow downwards into the column formwork. The mixer was raised with the crane and placed on an elevated platform as shown in Figure 179. An extension is placed to guide the UHP-FRC mix towards the column section. The UHP-FRC concrete is then poured into the formwork until it is

449

completely filled (Figure 180). The UHP-FRC mix is self-consolidating and requires no vibration.
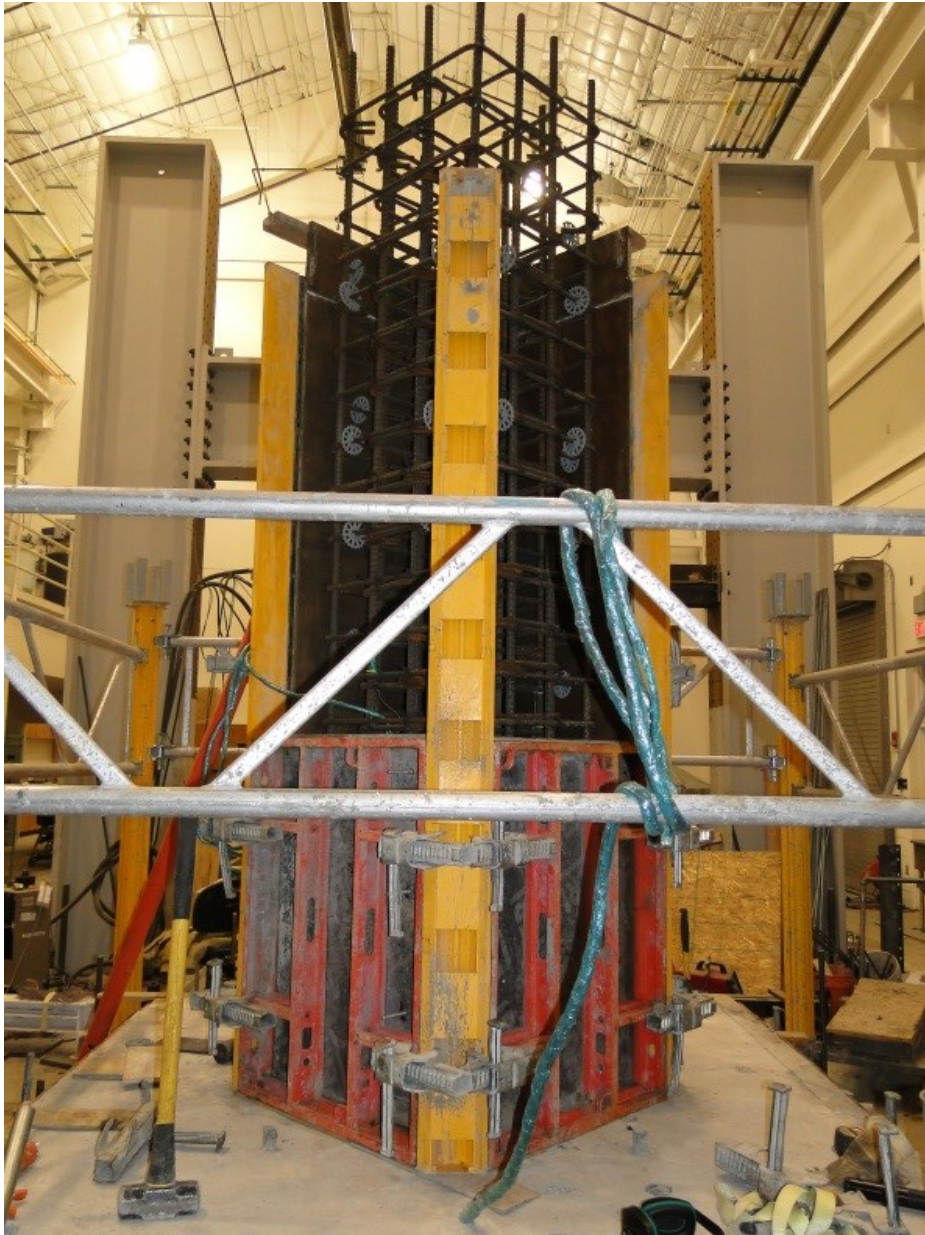
Figure 175. Formwork for 40" UHP-FRC Section of Column SP8

Figure 176. Premeasured Dry Materials

Figure 177. Pouring Dry Material

Figure 178. Addition of Micro-Fibers to Mixer

Figure 179. Elevated Mixer ready for pouring

Figure 180. Pouring of UHP-FRC 40" Section

Figure 181. UHP-FRC Section after Casting

After the casting of the UHP-FRC section the remainder of the column SP8 is cast identically to that of column SP5. The completed specimen SP8 can be seen in Figure 183.

Figure 182. 40" UHP-FRC Section After demolding

Figure 183. Space Frame Column Specimen SP8

<u>The bottom two layers of hoops below the footing have been removed</u>

As per ACI 318-14 specimen SP5 was constructed with the transverse reinforcement extending completely below the surface of the footing as shown in Figure 186 similar to what would be found in practice. To evaluate the necessity of transverse reinforcement below the surface of the footing, column specimen SP8 was constructed with the lower two layers of transverse reinforcement removed.
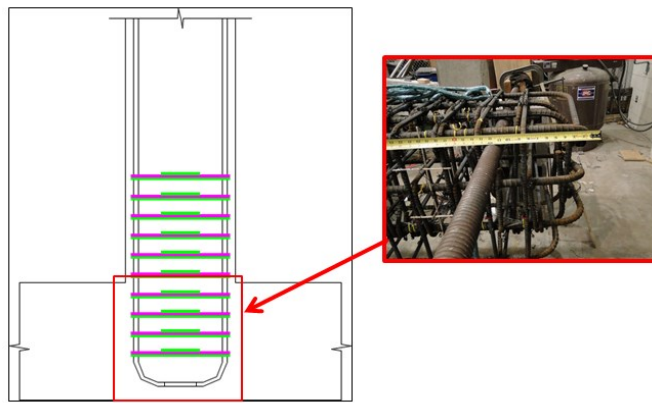
Figure 186. Transverse reinforcement extending below the footing of SP5
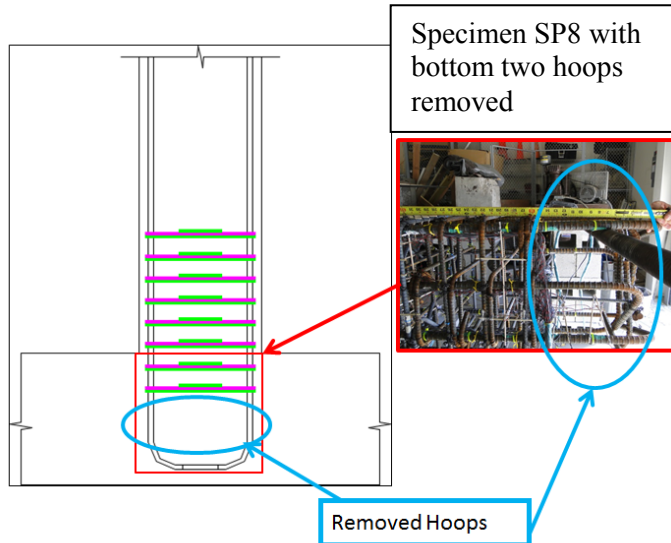
Figure 187. Column Specimen SP8 with the bottom two hoops removed.

Appendix B

Strain Gauge Installation Manual

Instrumentation of Reinforcing Bars

The determination of the strain development within both the longitudinal steel rebars, and the hoops and ties used in the specimens of this study are essential to analyzing the behavior of reinforced concrete columns. This information can be gathered by installing strain gauges, that measure changes in electrical resistance, directly to the surface of the steel rebars before constructing caging and pouring the concrete. In order to obtain accurate data from these devices, a special procedure was used that creates a smooth, flat surface to which the strain gauge is attached, and ensures protection of the device from damage due to the conditions of casting and pouring.

Strain Gauge Locations

In this experimental program, first the locations of the strain gauges are marked directly onto the steel rebars using the description described below.

Longitudinal Rebars

Strain gauges are to be placed onto the longitudinal L rebars as shown in the following diagram (S-01).

SL * G**

    Elevation of strain gauges
    referring to top face of the
    footing block ("Ground") - a
    negative sign denotes strain
    gauges below the surface

    Longitudinal rebar
    designation number

    Longitudinal rebar strain
    gauge

S-01

NOTE: The direction of NORTH is indicated
applying to each individual strain gauge drawing.
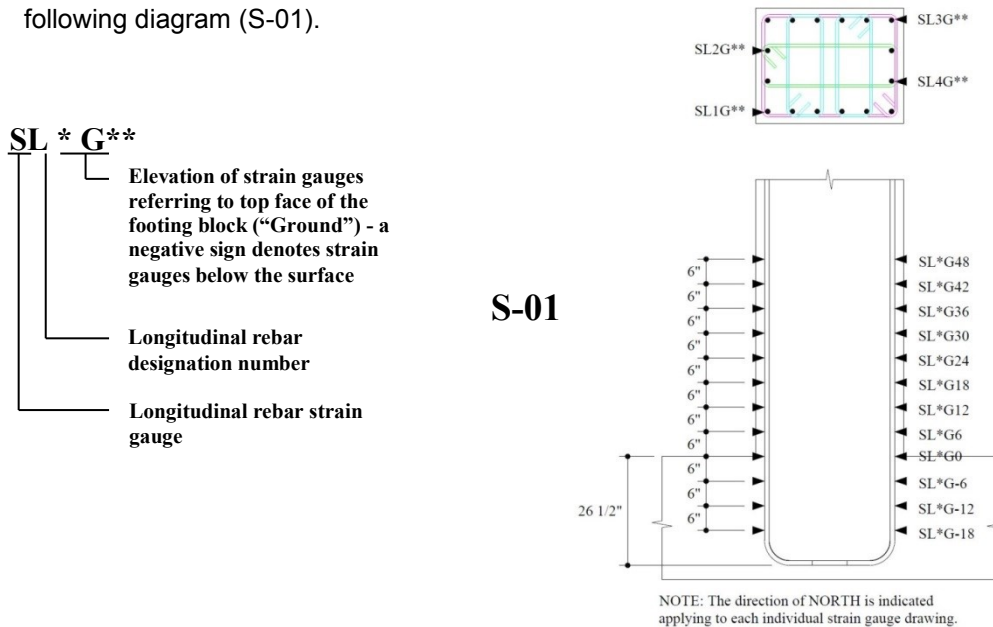
The locations shown in the above construction drawing should be marked accurately onto the L rebars (all from the same shipment batch) with a visible marker around the entire circumference of the rebars as shown in Figure.

Figure 1. Strain gauge location marking

This is done so that after attaching the strain gauges, and constructing the entire column and footing cages as one structure, the final locations of the strain gauges can be documented. Note that the locations are measured from the lowest point on the leg of the L rebar when the long leg rebar is perfectly level upward. That is, although the rebars are designed to be perfect 90˚ angles, they do not always come as such, and the locations of the strain gauges are measured from the point where the column and footing meet (the "footing" surface).

Figure and Figure depict on which side the strain gauges are to be attached. Ultimately, the strain gauges are to be attached to the strong axis of the rebars (on the ridge as shown in Figure) that does not eventually touch any of the hoops or ties when put together as one cage (note that some of the L rebars will be rotated at approximately 45˚). The strain gauges are mounted on the strong axis because buckling typically occurs along the weak axis of the rebar, which would lead to considerably different strains on the compression and tension faces. As a consequence, it was decided that the strain gauges should be mounted onto the strong axis face so that the measured strains would be the

458

average values. Figure through Figure show more details of the orientation of strain gauges on each longitudinal rebars.

Figure 2. Location of strain gauge on longitudinal rebars

Longitudinal **Bar 3**: place gauges on **bottom** strong axis

Longitudinal **Bar 2**: place gauges on **bottom** strong axis

Longitudinal **Bar 4**: place gauges on **top** strong axis

Longitudinal **Bar 1**: place gauges on **top** strong axis
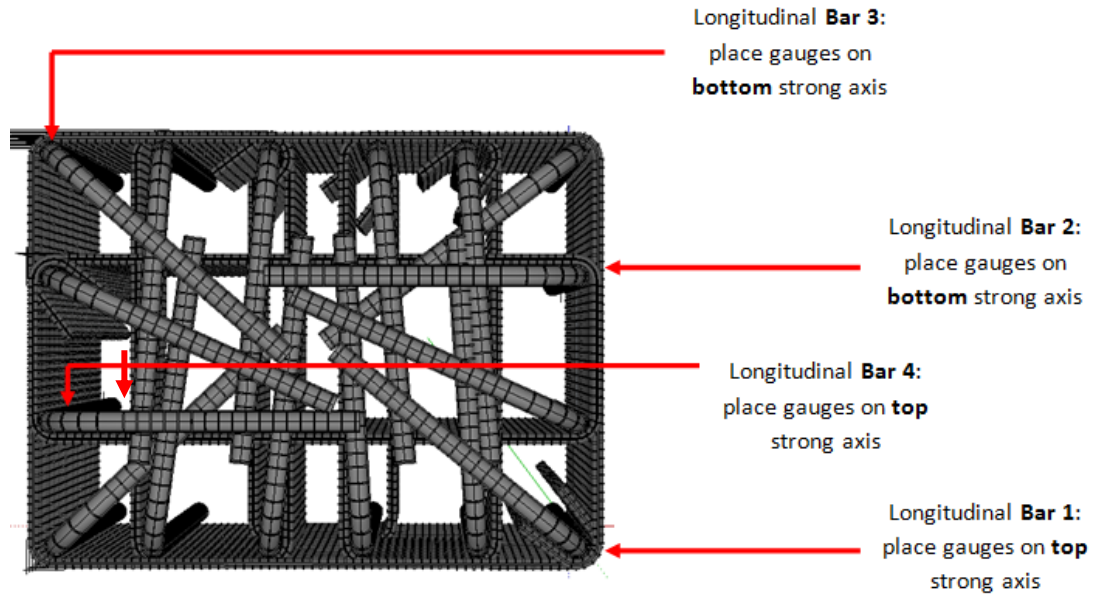
Figure 3. View from the bottom of the completed column caging

Figure 4. Photo of the bottom of the completed column caging

In order to do this, two L rebars can be placed with their short legs pointing in one direction, and the other two L rebars pointing in the opposite direction. Then, strain gauges would be placed on the strong axes (longitudinal ridge) on the tops of the L rebars.

Figure 5. Orientation of strain gauges on longitudinal Bar 1 (on top ridge)

Figure 6. Orientation of strain gauges on longitudinal Bar 2 (on bottom ridge)

Figure 7. Orientation of strain gauges on longitudinal Bar 3 (on bottom ridge)

Figure 8. Orientation of strain gauges on longitudinal Bar 4 (on top ridge)
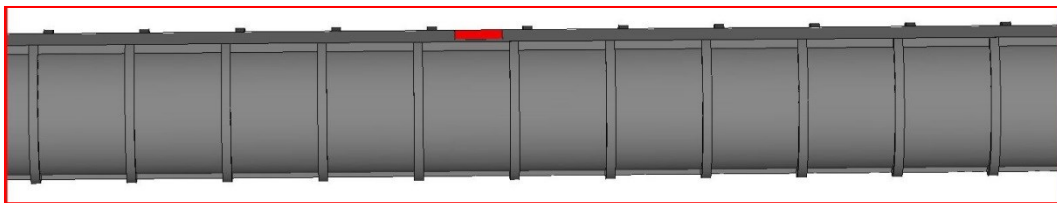
Figure 9. 3D rendering of strain gauge on Bar 1
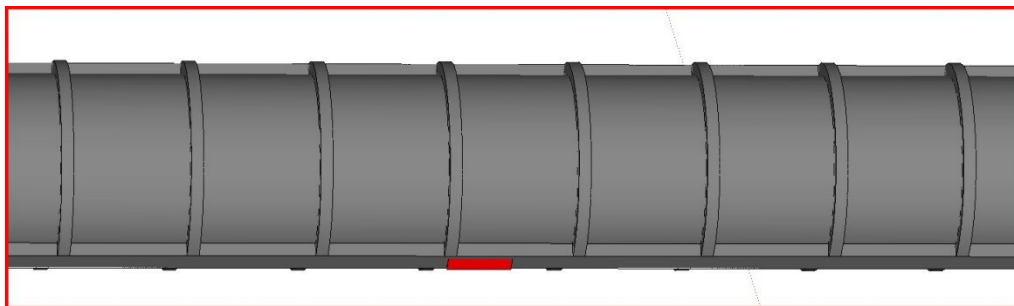
Figure 10. 3D rendering of strain gauge on Bar 2
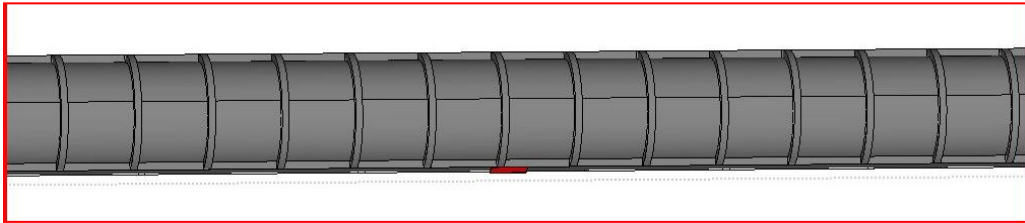
Figure 11. 3D rendering of strain gauge on Bar 3
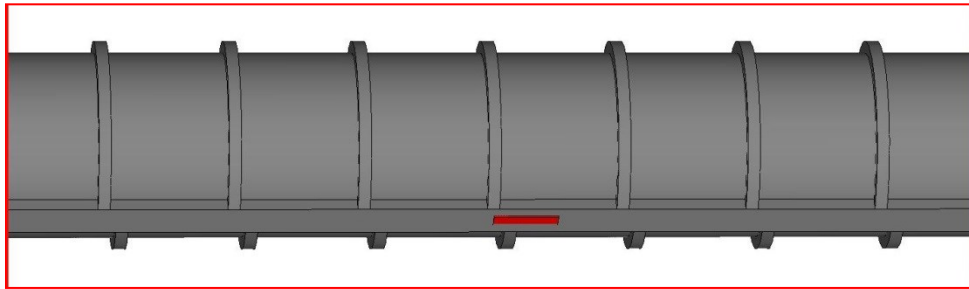
Figure 12. 3D rendering of strain gauge on Bar 4

Figure shows which rebars are placed in the same direction.
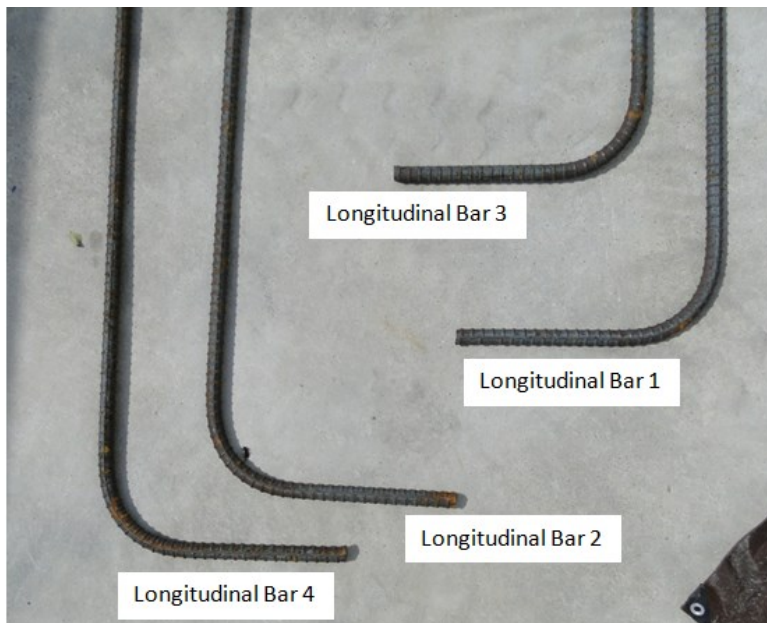
Figure 13. Orientation of L rebars for strain gauge installation

Hoops and Ties

Figure below shows both the layering and bar types to be used in the caging of these RC column specimens.
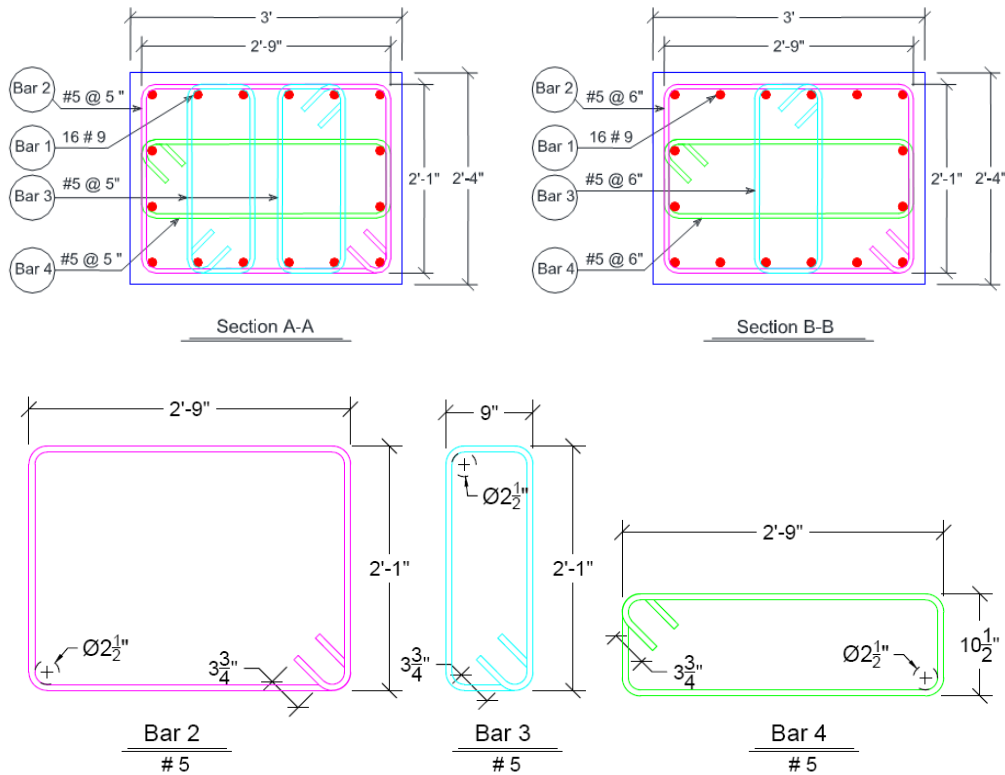
Figure 14. Hoop and tie layering (Bar 4 on bottom, Bar 2 in the middle, and Bar 3 on the top)

Note: Please see the construction drawings for the location of crossed-section A-A and B-B.

Before measuring the locations of the strain gauges, tie the hooks of the rebars into place tightly with steel wire so that the corresponding sides are perpendicular (as shown in Figure).

Figure 15. Hoop with hooks tied in place before measuring strain gauge locations

Also, it is important to note the locations of the hooks on these rebars in the critical region of the RC column (Figure and Figure).
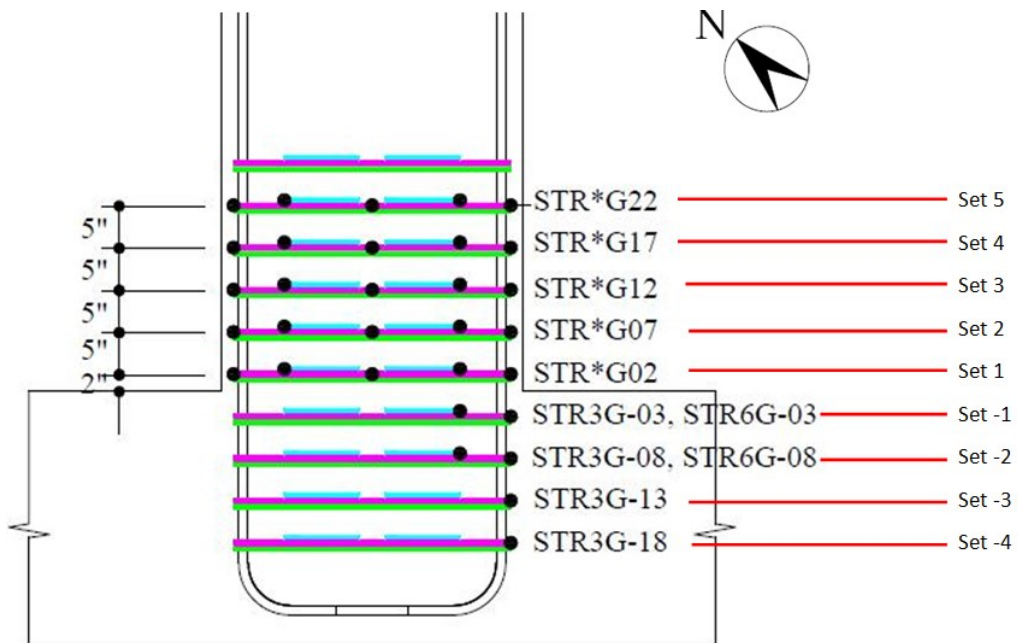
Figure 16. Critical region of column

Hook locations: hoop and tie sets as viewed from the top of the column
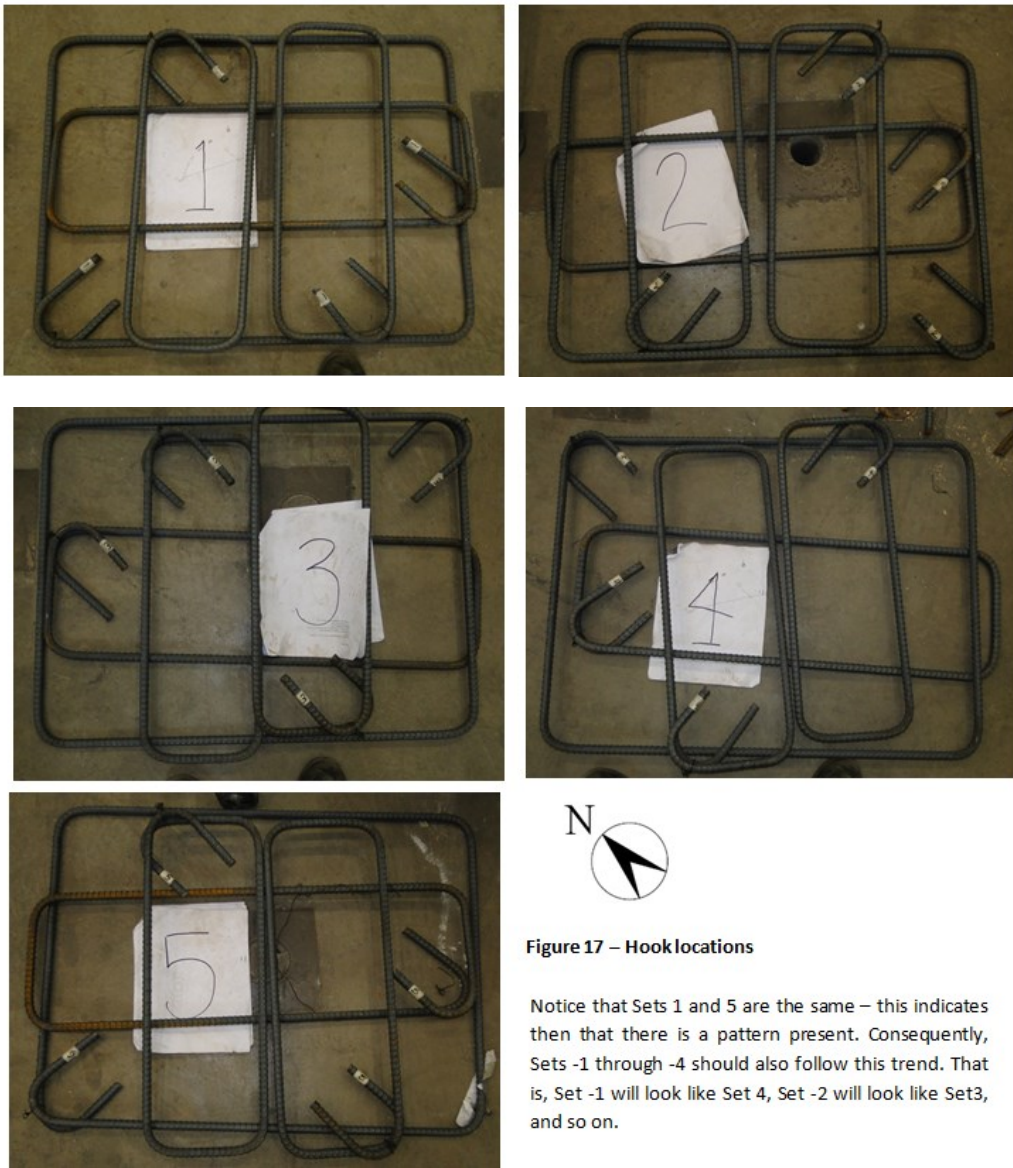
Figure 17 – Hook locations

Notice that Sets 1 and 5 are the same – this indicates then that there is a pattern present. Consequently, Sets -1 through -4 should also follow this trend. That is, Set -1 will look like Set 4, Set -2 will look like Set3, and so on.

Figure 17. Hook locations

With the hoop and tie locations clarified, the strain gauges then are to be placed at the center of each side as shown in the following drawing (S-02), on the top side of the sets (as seen in Figure).

STR1G**

STR4G**
STR5G**

STR3G**
STR6G**

STR2G**

STR * G**
- Elevation of strain gauges referring to top face of the footing block ("Ground") - a negative sign denotes strain gauges below the surface
- Strain gauge number on the crossed-section
- Hoop rebar strain gauge

STR*G22
STR*G17
STR*G12
STR*G07
STR*G02
STR3G-03, STR6G-03
STR3G-08, STR6G-08
STR3G-13
STR3G-18

5"
5"
5"
5"
2"

S-02
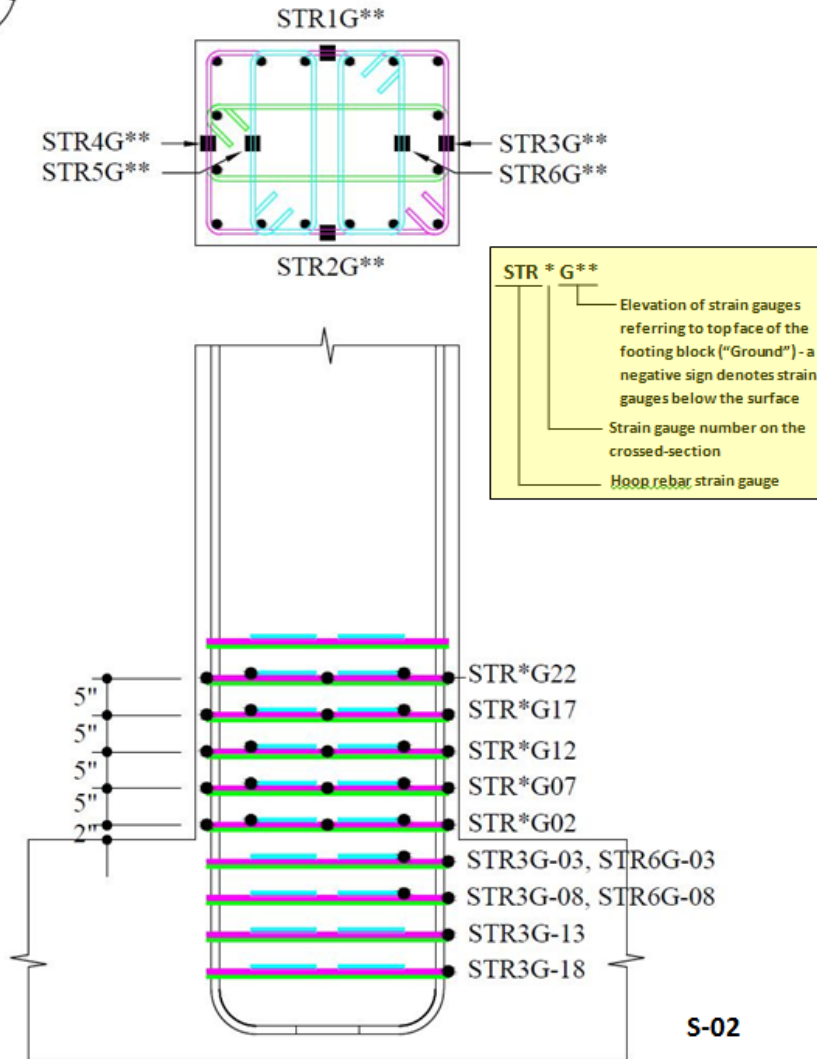
Note that the hoops and ties typically are not the exact size specified; therefore, the strain gauges should be put in the center of the actual length of the sides, and then the actual sizes documented for each batch of hoops and ties. To this same fact, one should use only hoops, ties, etc. from the same batch shipment, so that consistent sizing is maintained for each column specimen as best as possible.

S-02

Strain Gauge Orientations

Before moving on to the actual application of the strain gauges, there is one final detail to clarify: the strain gauge orientation. Strain gauge orientation refers to the direction in which the wires of the devices should face (see Figure).

Wires oriented downward

Figure 18. Strain gauge orientation

This detail is determined based on where the wires are planned to be pulled out of the formwork when casting the specimen. The goal is to have to gauges orientated so that the wire does not get folded back toward the actual electrical resistant gauge, risking it being damaged or even ripped off of the steel rebar. The below diagrams explain how to orient the gauges when placing on the longitudinal L rebars, hoops, and ties.
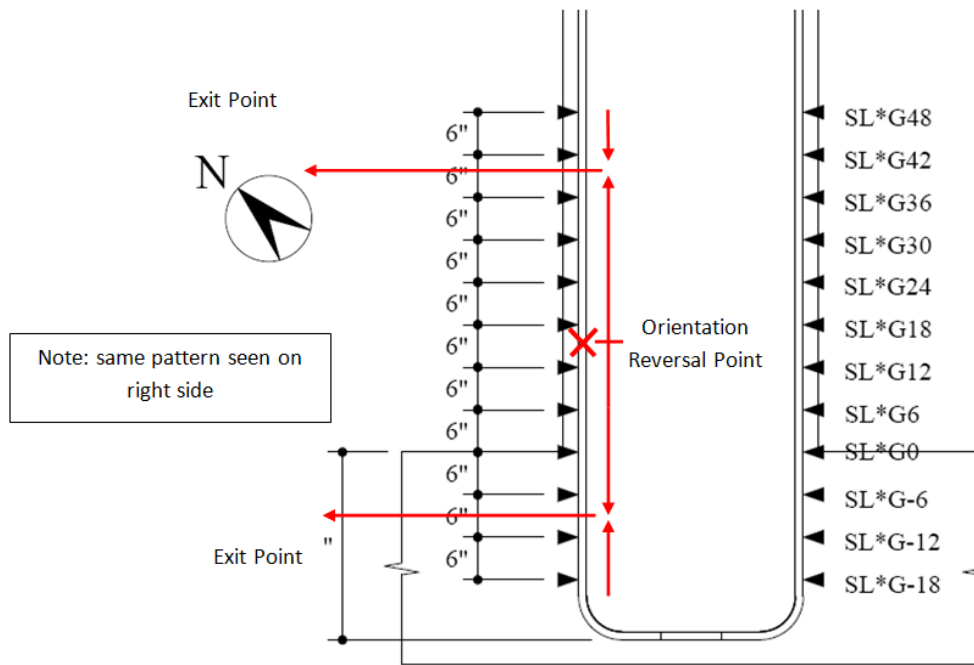
Figure 19. Orientation of wires along L rebars

View of Sets from top
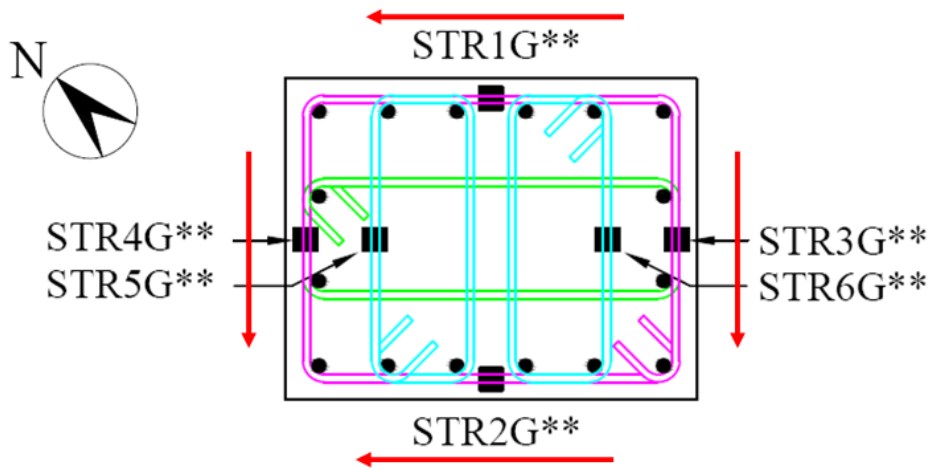
Figure 20. Orientation of wires on hoops and ties

Applying Strain Gauges to Rebars

Once marked properly, the grooved surfaces of the steel are ground and then sanded with 400 grit sandpaper until a flat, smooth surface is created for the strain gauge to be attached. Be careful to grind no more of the deformed bar than necessary for the strain gauge surface so as to not disrupt the bond between the concrete and rebar. Also, be cautious to create a level surface, rather than a scooped surface, to place the strain gauge. See Figure for this step.

Figure 21. Grinding and sanding of deformed rebars

Note: Here, a small sanding belt is used; however, to speed up the process, one can use a handheld grinder to grind down the ribs on the longitudinal (#9) rebars as shown in Figure , but it must be smoothed and leveled with the sanding belt after to ensure a flat surface is obtained.

Figure 22. Grinding of deformed rebars with handheld grinder

The smooth surface is then cleaned with an acid conditioner and neutralized with a base conditioner. The base should be applied with one smooth wipe with a separate paper towel than the acid, so as to not simply move around the acid. See Figure for this step.
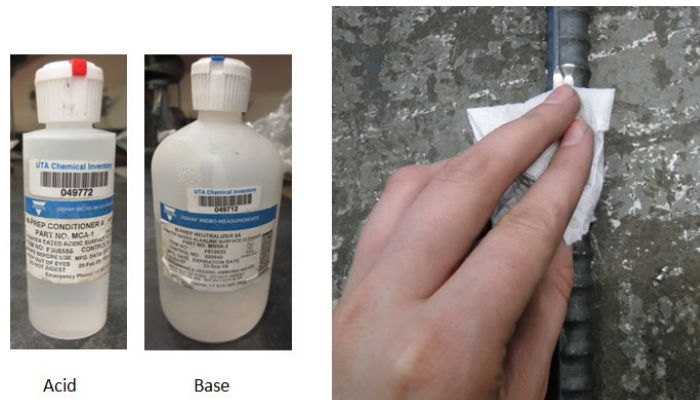
Figure 23. Cleaning of smooth surface

Before using any particular strain gauge, check that it has the proper resistance. With the signal wire (blue-striped wire) and one ground wire, the multimeter should read about 120 ohms (typically +2.5 ohms) – check with each ground wire. Then check that the two ground wires read close to 0 ohms (typically +2 ohms). See Figure for this step.
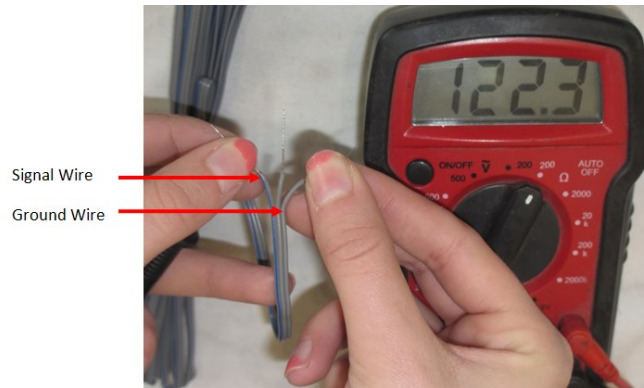
Figure 24. Multimeter test on strain gauges

Then, to line up the center crosshairs on the strain gauge itself to the accurate location on the rebar, apply a strip of scotch tape longitudinally to the top side of the strain gauge (the side that has wires soldered to the gauge), and place directly onto the rebar lining up the crosshairs on the device to the previously marked location (S-01 and S-02 on pages 1 and 7). See Figure for this step.

Figure 25. Lining up the gauge crosshairs to the proper location on the rebar

Note: Keep in mind the direction of the wires according to the wire bundling plan described above.

Slowly lift up the lower end of the tape toward the bottom of the gauge and place a piece of scotch tape horizontally under the exposed wires. This will allow for the steel to deform without the wires not consequently pulling the gauge and damaging it. Replace the longitudinal tape on top of the new horizontal tape. Be careful with the exposed wires and the location of the gauge itself during this step. See Figure for this step.

Edge of horizontal tape just below the bottom edge of the strain gauge, but not underneath the gauge
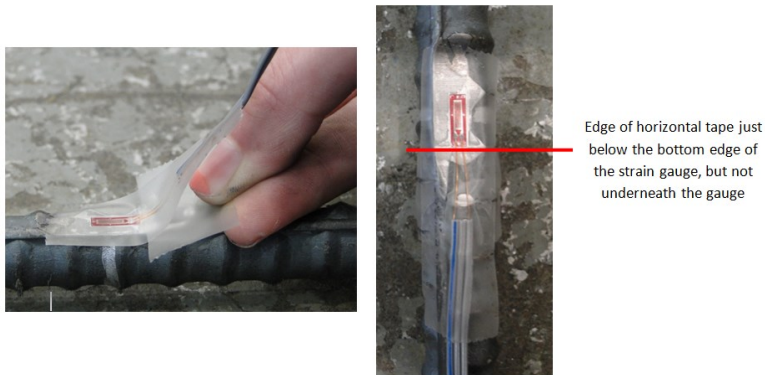
Figure 26. Horizontal tape

Now, lift the top end of the longitudinal tape, pulling the gauge off of the rebar and allowing space to place a strip of glue (Cyanoacrylate adhesive) under the location of the strain gauge. Replace the tape and gauge over the strip of glue, and firmly press the gauge down for about two minutes while it dries. See Figure for this step.

Figure 37. Glue application

Once dry, carefully remove the top, longitudinal scotch tape. The strain gauge should now be glued in place on the rebar. Allow to dry for about 15 more minutes.

The next step is to prepare the specimen for a series of layers that will protect the gauge from damage during construction and casting of the column specimen. At this point, carefully separate the exposed wires into a loop shape. This will not only keep the wires from touching and disrupting the electrical transmission, but it will give allowance for the steel to elongate during loading. Also, carefully trim the horizontal scotch tape around the wire loop with an exacto-blade. This is done to again prevent disruption of the bond between the concrete and rebar by using as little tape as possible on the steel surface. See Figure for this step.
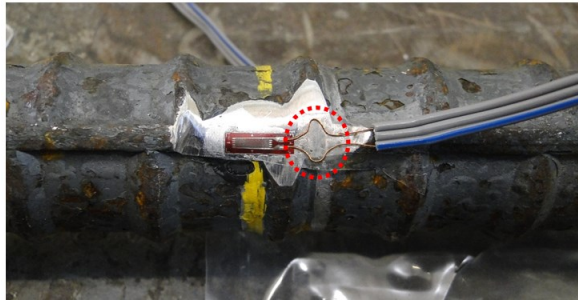
Figure 38. Creating wire loop

Now, apply a layer of polyurethane coating ("Coat A") from the bottom of the gauge to the top of the gauge, i.e. not on the exposed wires, and allow to dry for about 15 minutes. See Figure for this step.

Figure 39. Coat A application

Once Coat A has dried, apply a layer of nitrile rubber coating ("Coat B") all the way from the top of the gauge down just beyond the start of the coated wires, and allow to dry for about 2 hours. See Figure for this step.

Figure 40. Coat B application

Note: Here, a zip-tie is used strictly to hold the exposed wires in place while drying. It will be removed after drying. Other methods to do this are permitted, such as securing with masking tape.

Once Coat B has dried, cut a piece of moisture sealing electrical tape to an appropriate size that will cover the entire gauge, from just above the top of the device down a few centimeters from the start of the coated wires (approximately just beyond Coat B in Figure 21), and place over device. The tape should not be too large to minimize the disruption of bond between the rebar and concrete. See Figure for this step.
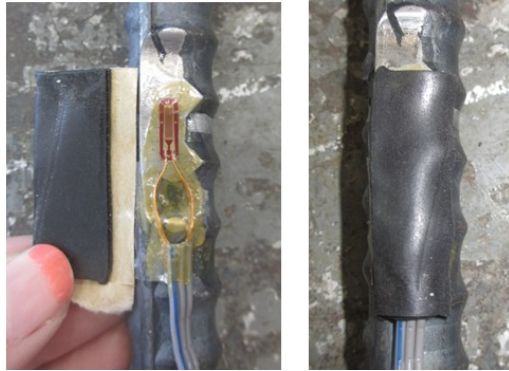
Figure 41. Moisture sealing electrical tape application

Seal the edges of the electrical tape using liquid electrical tape. Be sure the liquid tape creates a barrier that does not allow the moisture sealing tape to lift off of the rebar surface, breaking the seal of the liquid tape. The liquid tape only takes about 5 to 10 minutes to dry. See Figure for this step.

).

Figure 42. Liquid electrical tape application

Once the liquid electrical tape is dry, zip-tie on top of the bottom edge of the moisture sealing electrical tape. Be careful not to zip-tie over the exposed wire portion of the device below, for this would cause a weak point in the wire that will likely break under any additional stress. The goal is to zip-tie on top of the coated wires. The purpose of the zip-tie is to help protect the strain gauge from being pulled during the construction process. See Figure for this step.

Figure 43 Zip-tie

At this point, one can label the gauge according to the drawings above (S-01 and S-02). This is done by printing out labels (about 10 point font size), trimming them down to size, sticking them face up to the adhesive side of the tape, and wrapping it tightly around the coated wires at the end of the gauge wire. See Figure for this step.

Figure 44. Strain gauge label

Then, secure the bundle of wire to the rebar with masking tape for safekeeping as shown in Figure .

Figure 45. Secure wire bundle

Finally, once the column cage is completed, check all of the strain gauges for the proper resistance (as in Step 3) to be sure it has not been damaged during the construction process. If the strain gauge has not been damaged, add a second label (as in Step 14) a bit farther down the wire. The second label is there not only to demonstrate that the gauge has been checked a second time, but also so that there is a back-up label if one is lost in any transport or testing throughout the project.

Concrete Gauge Instillation

Concrete gauges are used to measure the strain in the concrete during testing of the RC column. This information is very useful in measuring the confinement provided by the eight column specimens. Based on this information, observations may be made with respect to column size, concrete strength, and hoop spacing to optimize the design of the reinforcement.

Location of Concrete Gauges

The location of the concrete gauges was determined initially by the location of the plastic hinge. After each test, observations were made in which the locations of the concrete gauges were altered to obtain more meaningful results. The concrete gauge locations for the first column are shown in Figure 46, Figure 47 and Figure 48. Note that the direction of the gauge in Figure 46 corresponds to the longitudinal direction; while Figure 47 and Figure 48 correspond to the transverse direction with reference to the height and width of the cross section respectfully.

The notation used to label each concrete strain gauge describes the location of that particular concrete strain gauge in space. For example, on the cross sectional view shown on the top of Figure 46 the label CL1G**, the C represents that the gauge is a concrete strain gauge. The L signifies that the gauge is oriented in the longitudinal direction. The transverse direction along the height of the cross section is represented by H, and the transverse direction along the width of the cross section is represented by B. The 1 defines the gauge number. The G** refers to the elevation of the strain gauges from the top face of the footing block or "Ground". For example, in the drawing shown on the bottom of Figure 1, CL*G15, the G15 signifies that the gauge is located 15 inches from the surface of the footing block or "Ground".
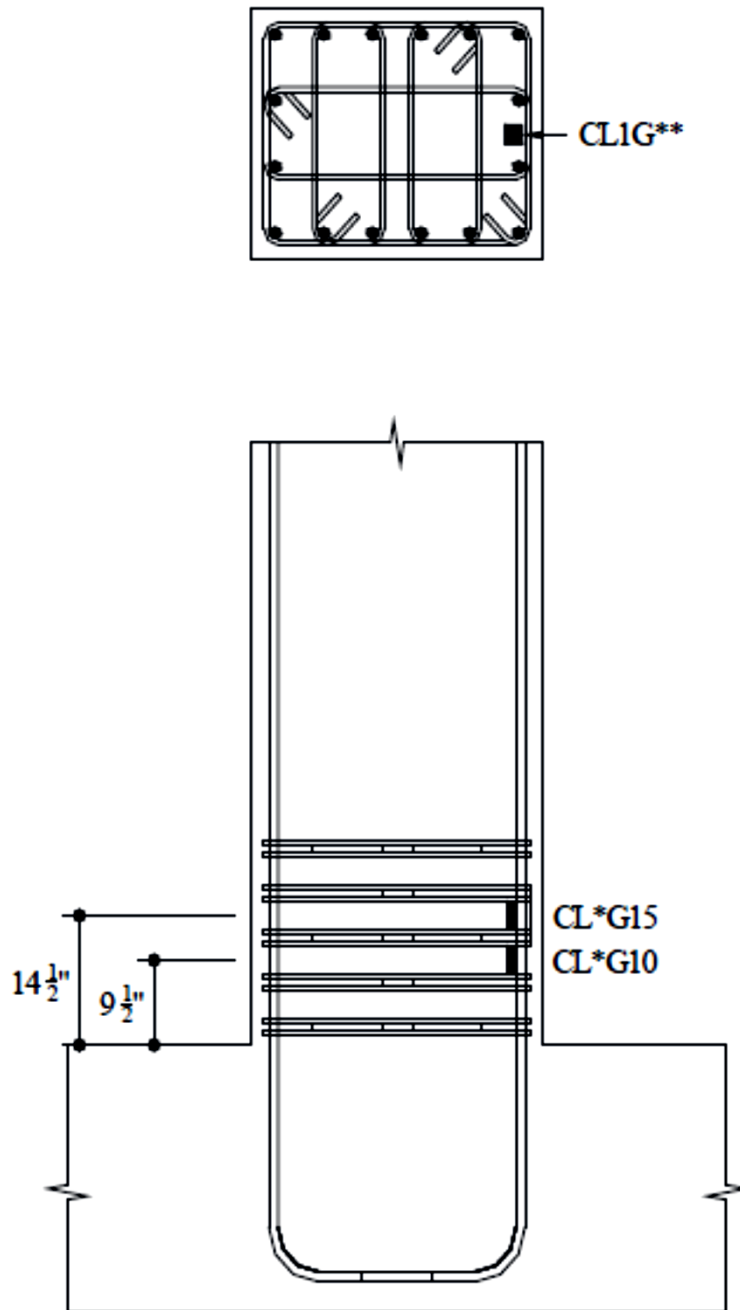
Figure 46. Concrete Internal Strain Gauge in the Longitudinal Direction

CTRH1G**
CTRH2G**
CTRH3G**
CTRH4G**

CTRH*G15
CTRH4G12
CTRH*G10
CTRH4G07

$14\frac{1}{2}$" $9\frac{1}{2}$"
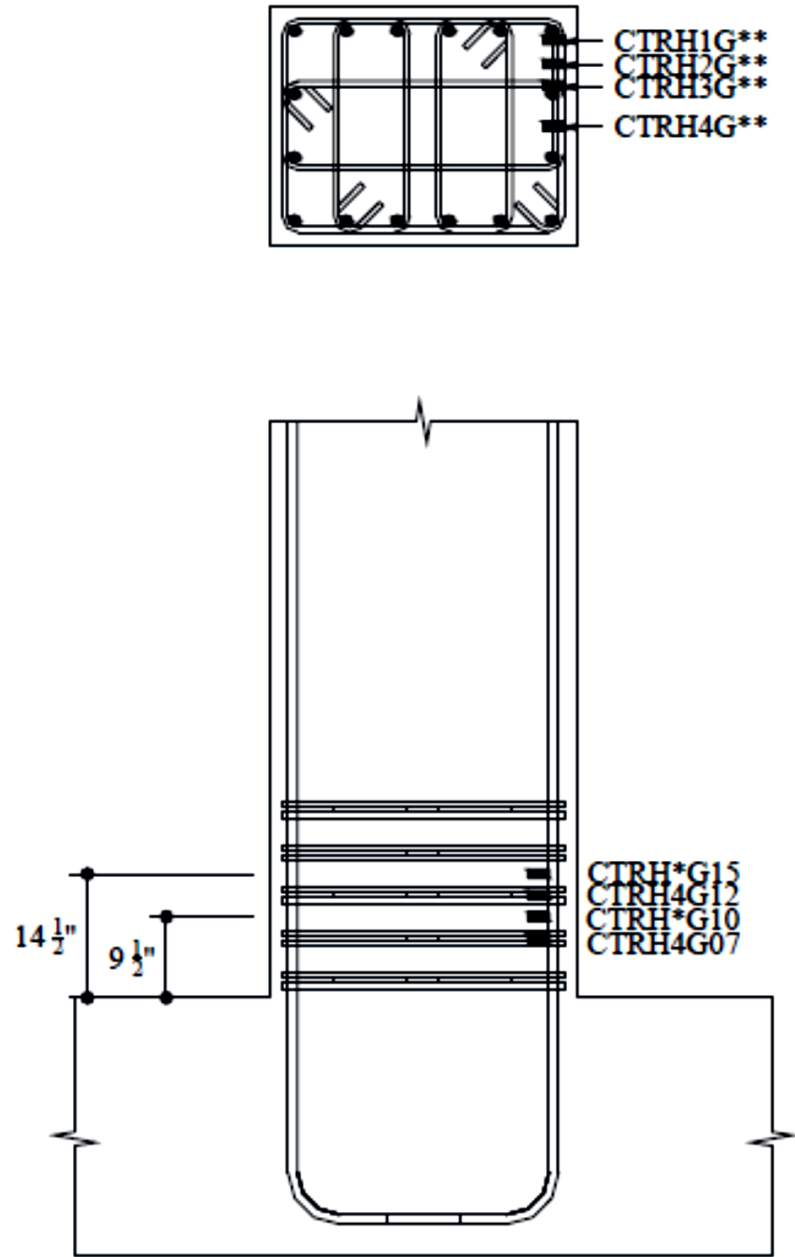
Figure 47. Concrete Internal Strain Gauge in the Transverse Direction (Along the Height of the Cross Section)
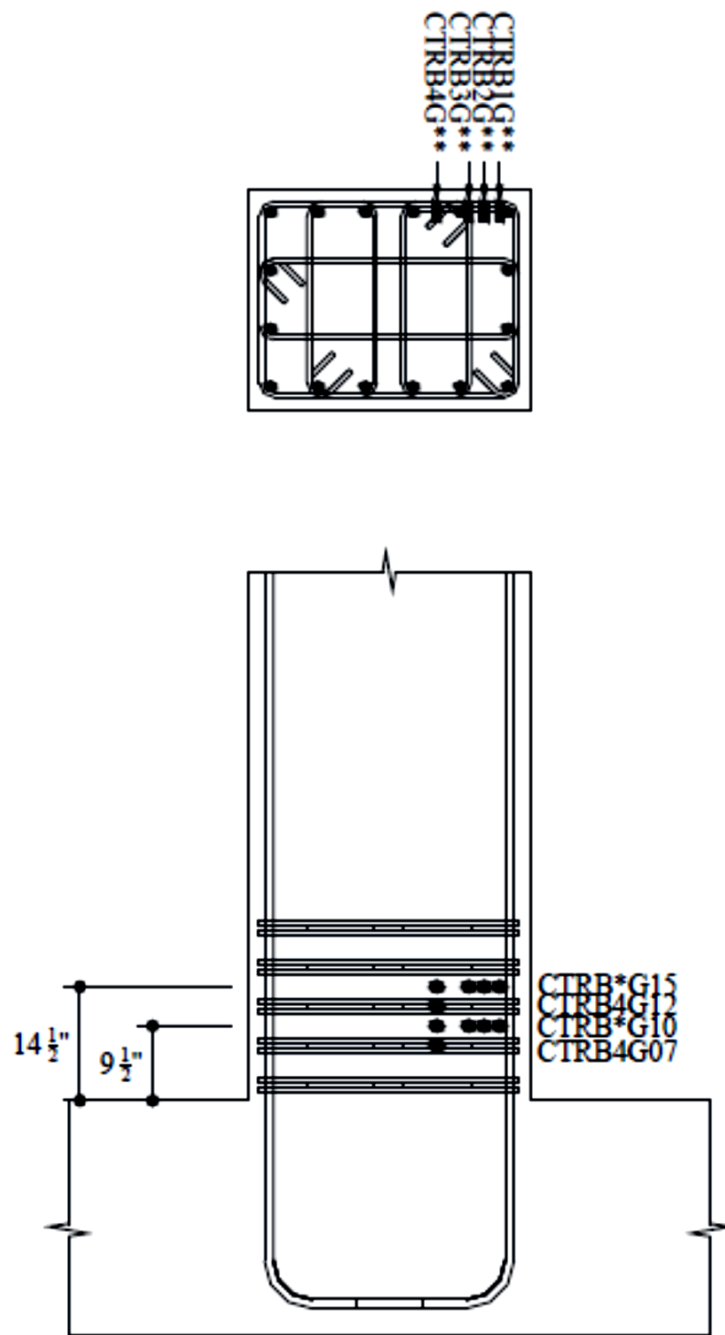
Figure 48. Concrete Internal Strain Gauge in the Transverse Direction (Along the Height of the Cross Section)

Materials

Concrete Strain Gauge

The concrete Strain Gauges used for this project were made by Japanese company TML (Tokyo Measuring Instruments Laboratory Co., Ltd.). Two types of concrete strain gauges were used from the Mold Strain Series, the PMFL-50 and the PMFL-60. According to TML, these gauges are designed for measuring interior strain in concrete or mortar under loading tests and their small construction enables instillation in a variety of areas. The concrete strain gauges are embedded within the concrete. A length of steel wire is tensioned within the concrete strain gauge. As the concrete deforms, the steel wire is pulled or loosened and strains are measured between the two flanges of the concrete gauge. The gauges are also covered by an engineered plastic with superior water proofing characteristics which protect the gauge during casting.

Instillation Materials

The materials necessary for the instillation of the concrete strain gauges are shown below in Figure 49.

Figure 49. Concrete Strain Gauge Instillation Materials.

Instillation Procedure

First, use the drawings to mark the location of the wooden sticks and concrete gauges on the reinforcement bars using a marker.

Figure 50. Marking of locations

Place the wooden stick along the yellow lines and tie it to the longitudinal bar using a concrete tie and tie tool carefully ensuring that the stick does not break.
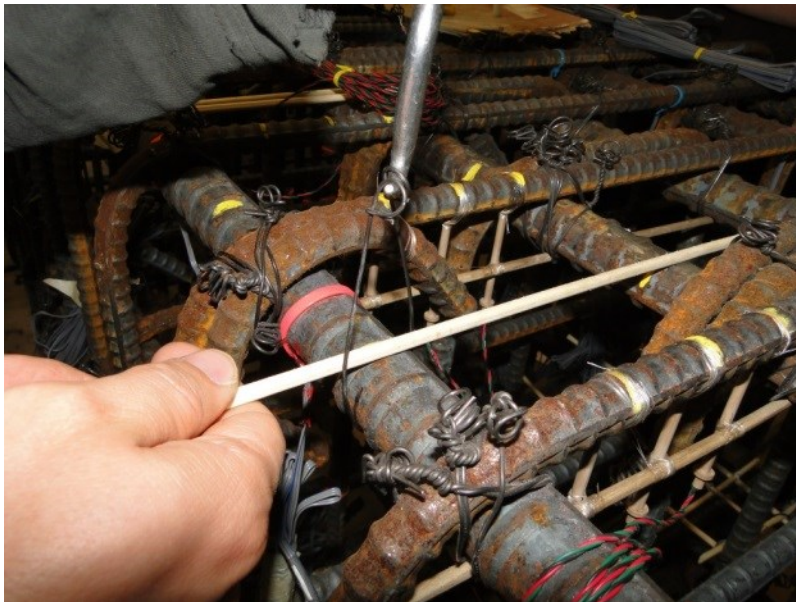
Figure 51. Tying of wooden sticks

Use scissors to trim off the excess wooden dowels.

Figure 52. Trimming of wooden dowels

Once an intersection of two wooden sticks has been created the concrete gauge
can be placed at the correct location and tied using the fishing line.
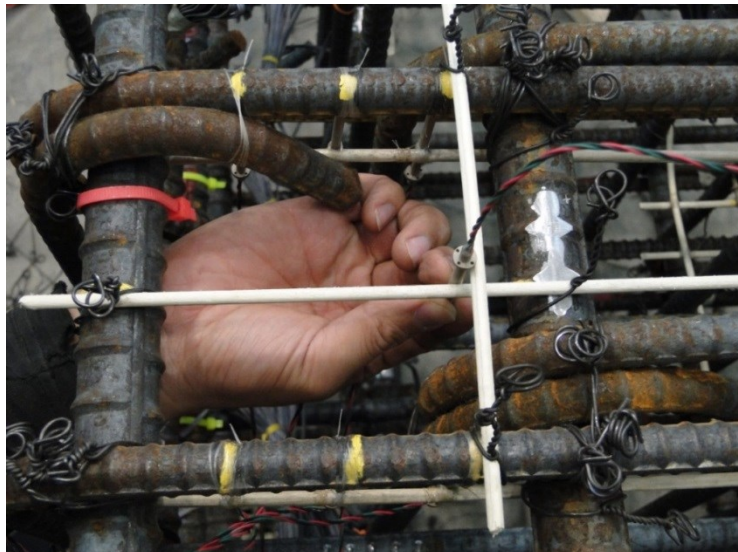
Figure 53. Placing of concrete gauges

The concrete strain gauges are located in between the column cage reinforcement. To obtain accurate data and prevent the device from being damaged during casting, two points along the concrete gauge are secured to ensure the stability of the device during the construction process.
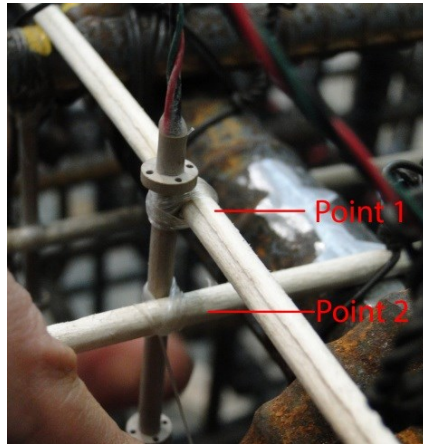
Figure 54. Tying of concrete gauges

A number of different knot tying techniques may be used but the preferred tying technique is the Overhand Knot.

Prepare the fishing line before tying concrete strain gauge in place

3.1.1 Cut fishing line to a length about 2 meters long

Figure 55. Measuring of string

3.1.2 Take the two ends of the fishing line and tie an Overhand Knot as shown in Figure 56.
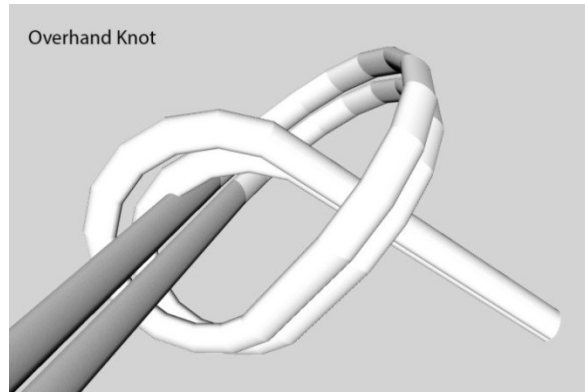
Figure 56. Overhand knot

To tie concrete gauge using fishing line in desired locations, there are two techniques can be used. One is for concrete gauges measuring the strain in concrete that are in contact with the steel rebar; another is for measuring the strain in concrete located in between the reinforcement, i.e. the concrete strain gauge is tied to wooden dowels.

Concrete strain gauge are tied to wooden dowel

Using the prepared fishing line shown in Step 3.1 to secure the concrete gauge to the wooden dowel. Wrap the concrete gauge and the wooden dowel by having the overhand-knot-end go through the loop of the fishing line. Then pull to tighten the concrete gauge to the wooden dowel.
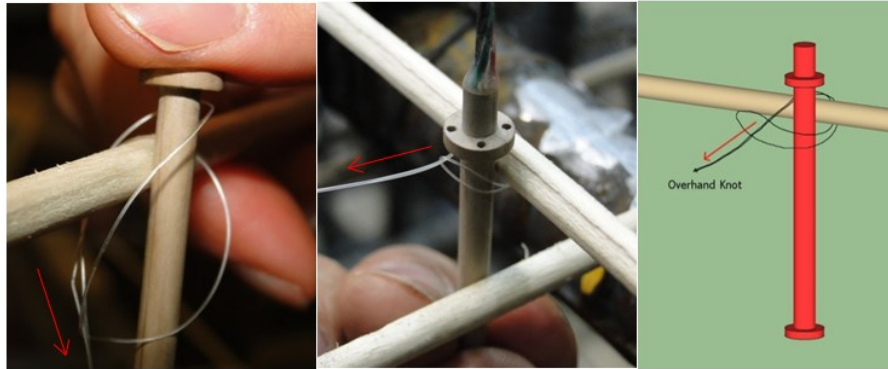
Figure 57. Using fishing line to secure concrete gauge onto wooden dowel

Hold the end of the fishing line, and fold it back tightly and wrap it around both the concrete gauge and the wooden dowel. To secure the concrete gauge in place, wrap the fishing line around concrete gauge and the wooden dowel a few cycles in the same direction, and then in the opposite direction in a crisscross pattern, repeat this step until the concrete gauge stays securely in place.
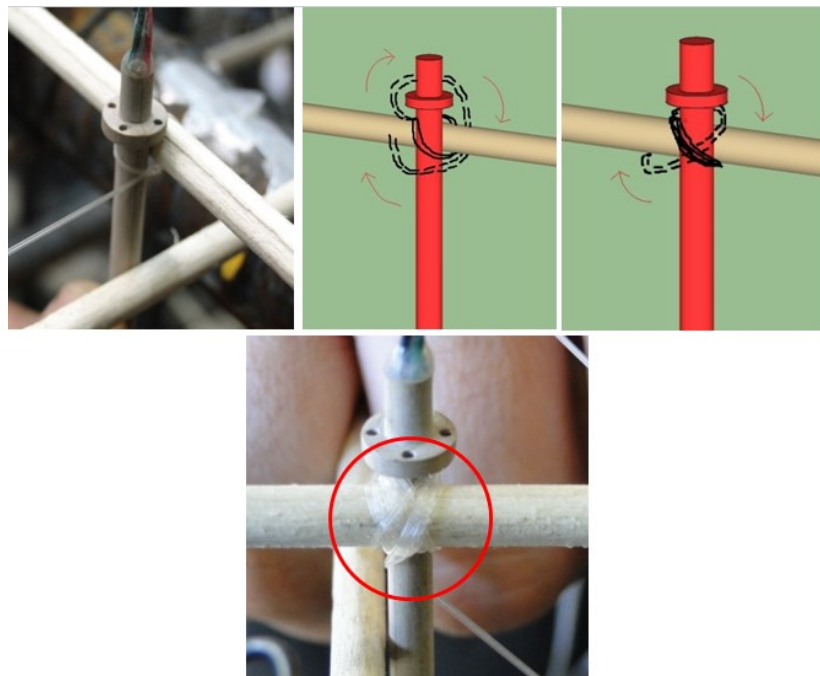
Figure 58. Tie concrete gauge onto wooden dowel

To secure the concrete gauge in the horizontal direction along the wooden dowel to which the concrete gauge is attached, the following steps are conducted. With one end tied to the concrete gauge and wooden dowel, hold the overhand-knot-end of the fishing line and wrap it once around the wooden dowel forming a loop with the other end, and then have the overhand-knot-end pass through the loop. Pull the split-end of the fishing line forming a loop wrapped on the wooden dowel. As one hand continuously pulls the overhand-knot-end of the fishing line tightly, the other hand pushes the loop toward the concrete gauge. Repeat this step a few times.
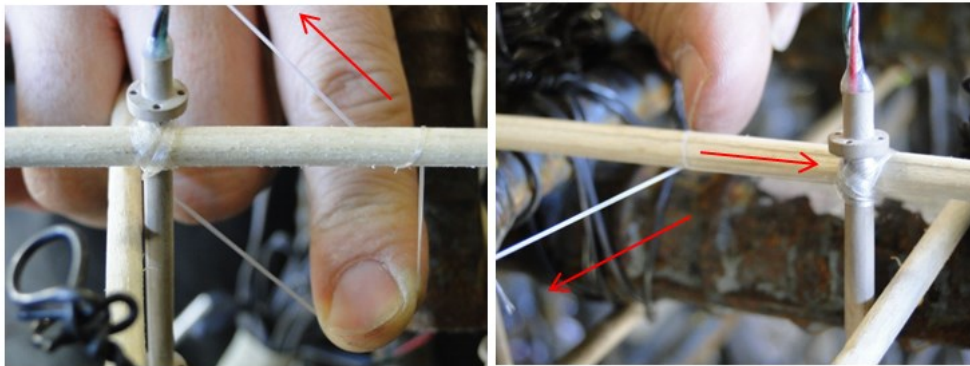
Figure 59. Securing the concrete gauge onto the wooden dowel in the horizontal direction

With the end of the fishing line pulled tightly, apply CN-Y adhesive to the fishing line tied to the wooden dowel. Then cut the excess part.

Figure 60. Apply super glue to fishing line and trim off the excess part

Concrete strain gauge with one end tied directly to the steel rebar

To measure the strain in concrete that is in contact with steel rebar, the concrete strain gauge is tied directly to the steel rebar.

Figure 61. Placing of concrete guage

4.5 Using the prepared fishing line shown in Step 3.1 to first, tie it on the concrete gauge as shown in figure 62.
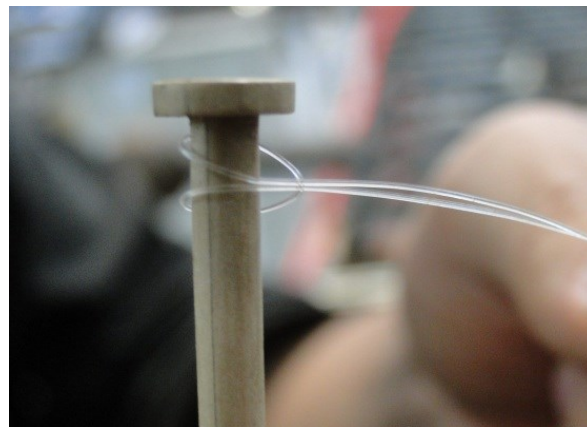
Figure 62. Tying of concrete gauge

4.6 Place the concrete strain gauge in contact with steel rebar.

Figure 63. Tying concrete gauge to rebar

4.7 To secure the concrete strain gauge in place, using fishing line make a loop, then put the overhand-knot-end around the steel bar and through the loop. Repeat this process for a few times until the concrete strain gauge stays securely in place. As shown in figure 64.

Figure 64. Securing gauge to bar

4.8 Apply CN-Y adhesive and trim off the excess part of the fishing line.

Figure 65. Applying glue

Continue to place the gauges according to the drawings until all of the concrete strain gauges have been installed.
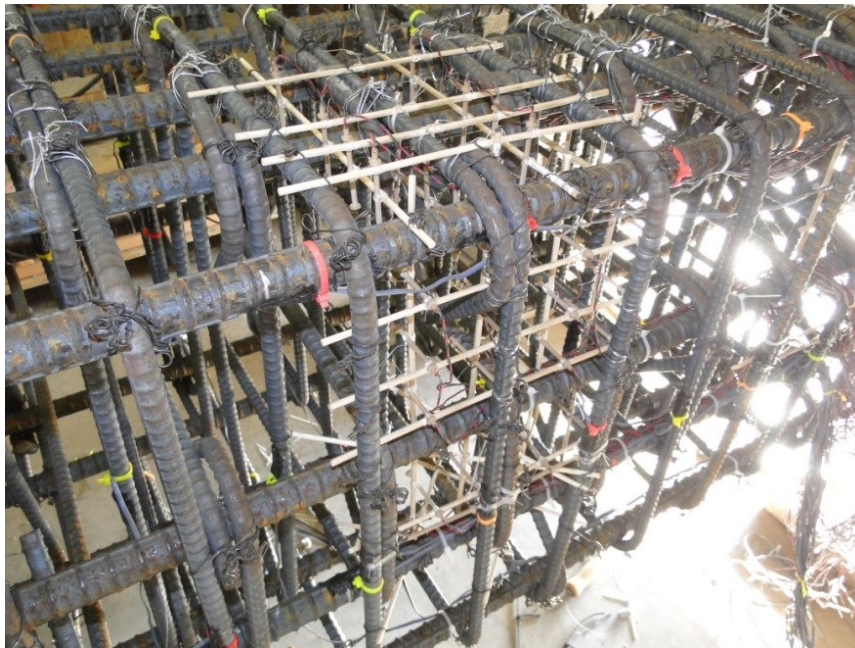
Figure 66. Completed concrete gauge instillation

Once all of the gauges have been installed the next step is to carefully wrap the wires using a plastic wrap. First all of the wires are carefully taken towards the 4 key locations of the column where the wrapping will occur.

Figure 67. Wrapping of wires

Two bunches of wires will come out at the bottom of the column cage below the footing and two bunches of wires will come out of the column section on opposite sides around mid-height as shown below.

Figure 69. Completed gauge instillation

Wrapping the wires is more easily done with two people. The first person should tightly and carefully pull on the wires so that the bunch is held tight and straight. The second person then wraps the wires continuously overlapping the wrap to prevent and openings or tears.

Appendix C

Review of 50 State DOTs

An investigation was conducted on other DOT practices as pertains to the construction of box and slab beams. Our main concern was on the details of the horizontal shear reinforcement (and the surface roughness implemented. Some of states do not have either box beams or slab beams and although others do use them; they do not have the plans on their website. The table below summarizes the findings on all the states.

There are generally five surface finishes that can be applied on concrete.

1. **As-placed roughness**: No attempt is made to smooth or roughened the surface after concrete is poured and vibrated.

2. **Float finish**: After concrete is poured and vibrated, a rough wooden float is run through the surface to smoothen it.

3. **¼" rake finish**: A rake is run across the interface transverse to the beam length leaving a very rough textured finish.

4. **Rough broom finish**: A stiff broom is run across the surface of the beam in the transverse direction.

5. Sheepsfoot voids: This represents a mechanical surface finish consisting of 1 in. diameter, ½ in. deep impressions made at a spacing of 3½ in.

Only three kinds of finishes are currently being used; that is the broom, rake and float finish as will be seen below. It has also been noticed that there are three different shapes of horizontal shear reinforcement used. The following summary is based on the forms of horizontal shear resistance.

Alaska DOT

Does not typically use slab beams with CIP decks therefore they do not have any standard plans for this type of structure. When they have designed this type of bridge in

the past, they extended the vertical shear reinforcing into the deck and verified that the requirements of AASHTO LRFD article 5.8.4 are met. They however specify a roughened interface.

Colorado DOT

The Colorado department of transportation use both the slab and box beams in their bridges. Although not much information is given in their design drawings, it is clear that the embedded length of the horizontal shear reinforcement in slab beams is 2.5 inches.
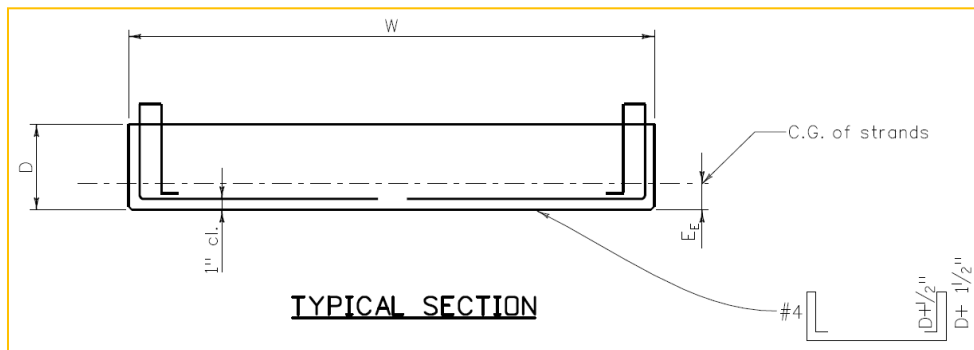
Figure 1. Typical slab beam section
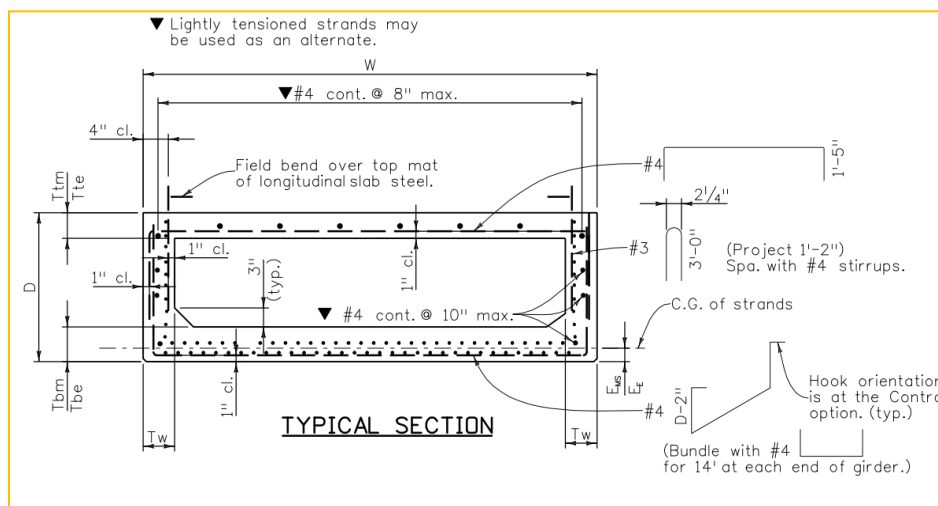
Figure 2. Typical box beam section

Delaware DOT

They do not provide any standard drawings on their website. They however have both slab and box beams and they use the M-shaped bar (Type 1) as the horizontal shear reinforcement. A broom finish is specified for the top of the slab and box beams.

Indiana DOT

Uses box beams on their bridges. Plans could not clearly show if there is horizontal reinforcement. The plan below is from a bridge replacement project on Pruce road. The embedded length of the horizontal reinforcement is seen to be $2\frac{1}{8}$ in. The horizontal reinforcement seems not to cover the entire length of the beam. The plans specify that the top of the beams should be scored transversely at approximately 3in. centers with a pointed tool.
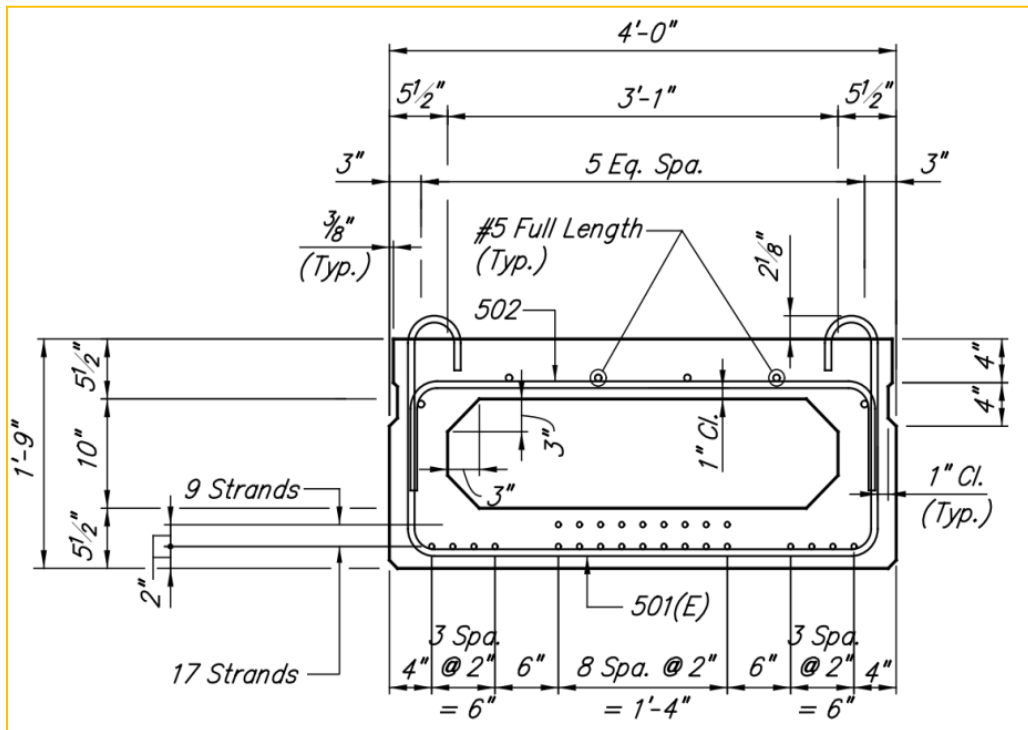
Figure 3. Typical box beam section
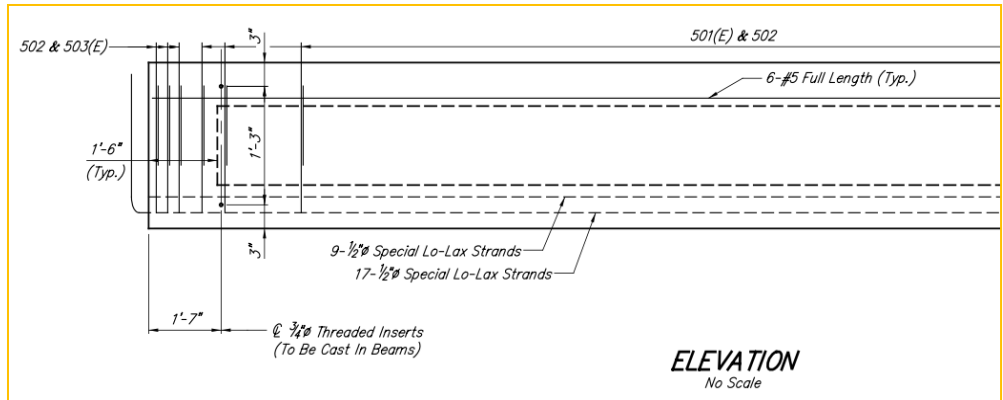
Figure 4. Elevation

Idaho DOT

They do use slab beams on their bridges although no information is provided for the horizontal shear reinforcement. On further inquiry I was informed that the girder stirrups are designed to project into the concrete decks and the top surface of the girders have a float finish.
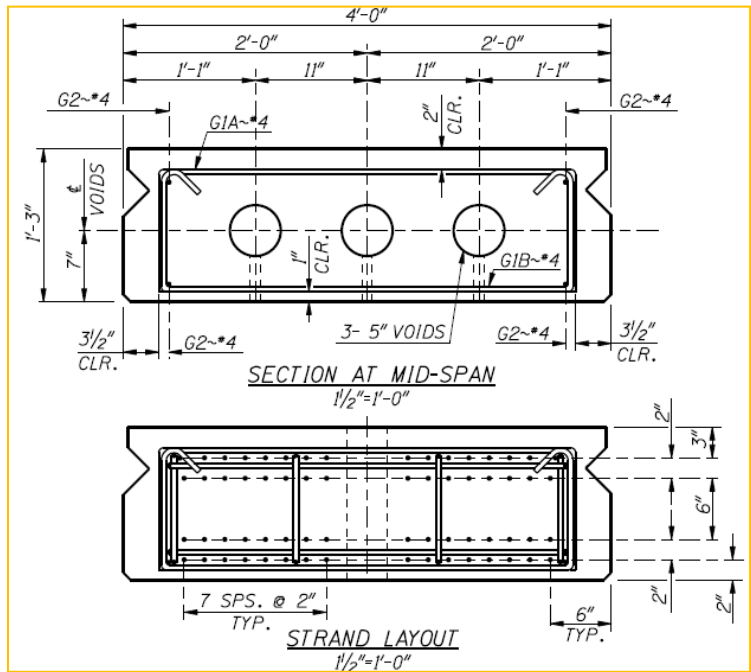
Figure 5. Typical slab beam section

New Jersey DOT

The specifications specify that the surface will be finished according to the designers specifications thus not giving a specific surface roughness to be used. Both the slab and box beam have type 1 horizontal shear reinforcement as shown below.
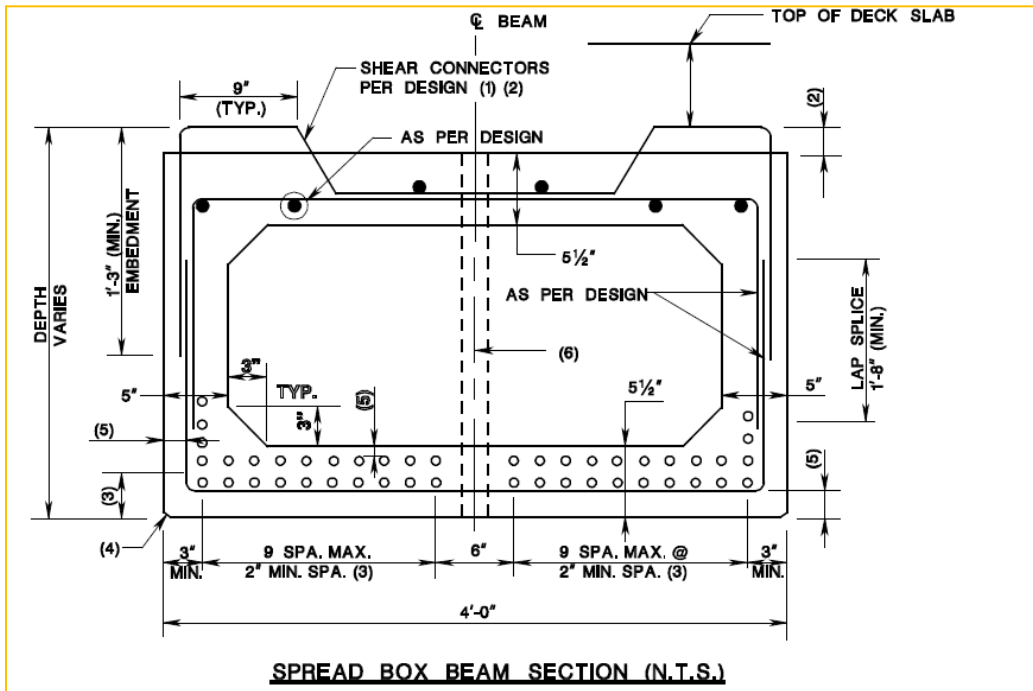
Figure 6. Typical box beam section

Kentucky DOT

Kentucky utilizes box beams in their bridges. The diagram below shows a typical box beam. The height of the horizontal shear reinforcement is seen to be about 2.5 in. whereas the width is unclear. A floated surface finish is specified.
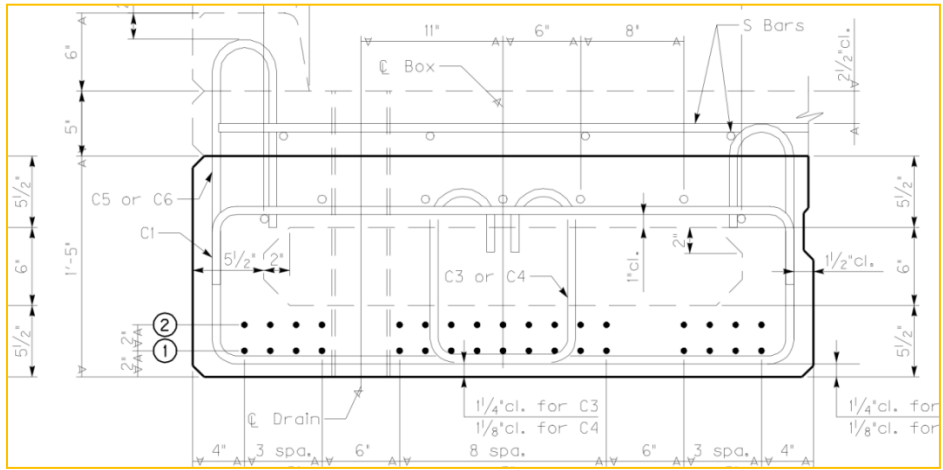
Figure 7. Typical box beam section
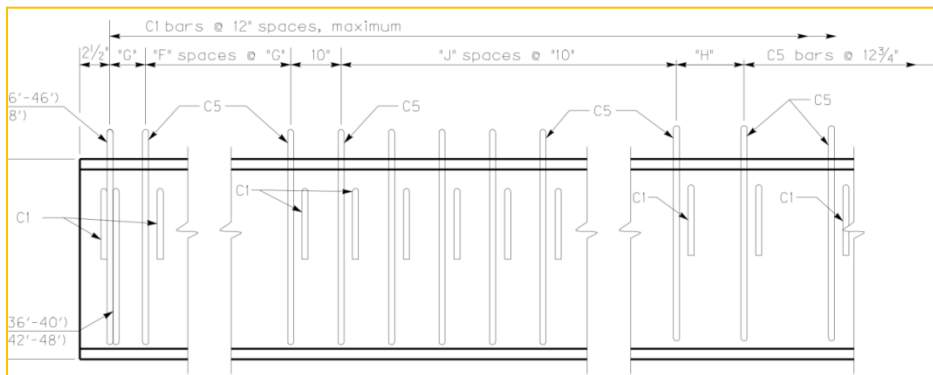
Figure 8. Elevation

Maine DOT

Details of Maine department of transportation box and slab beams are shown below. The embedded length of the horizontal shear reinforcement is shown to be 3 inches. Similar horizontal shear reinforcement is specified for the box beams.
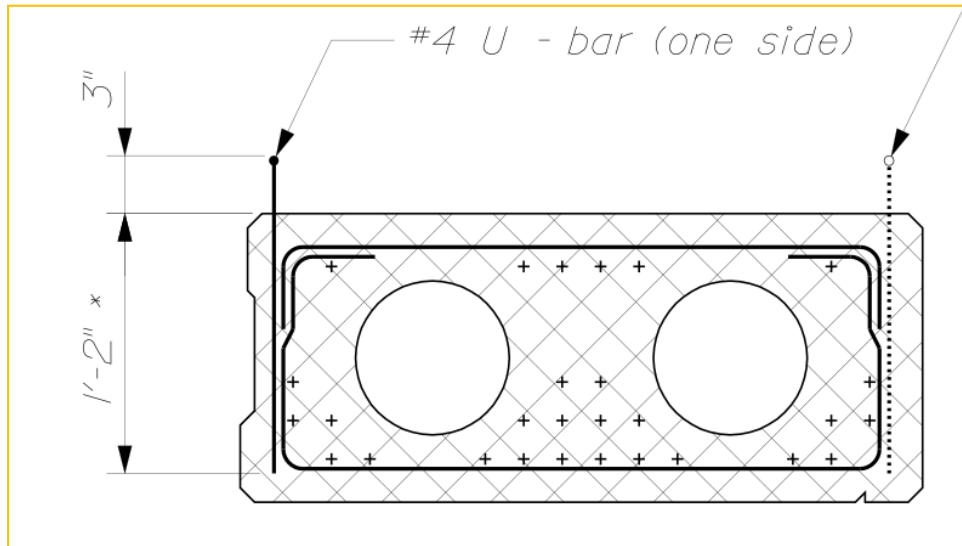
Figure 9. Typical slab beam section (Note that the direction of the horizontal shear reinforcement is perpendicular to the cross-section)
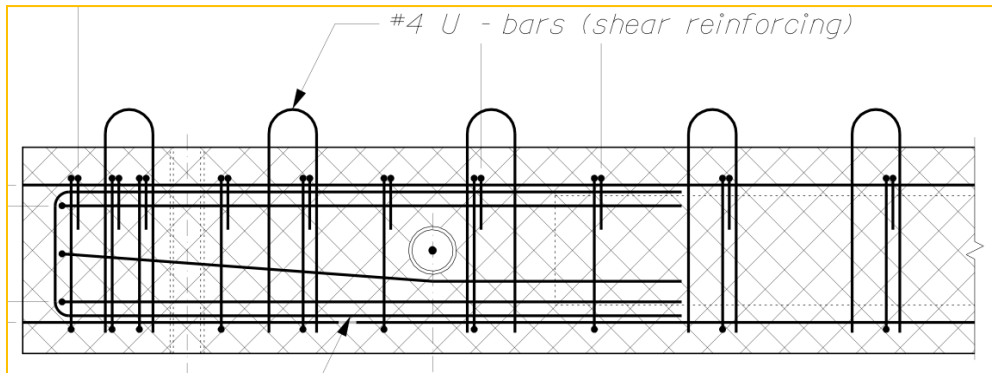
Figure 10. Elevation
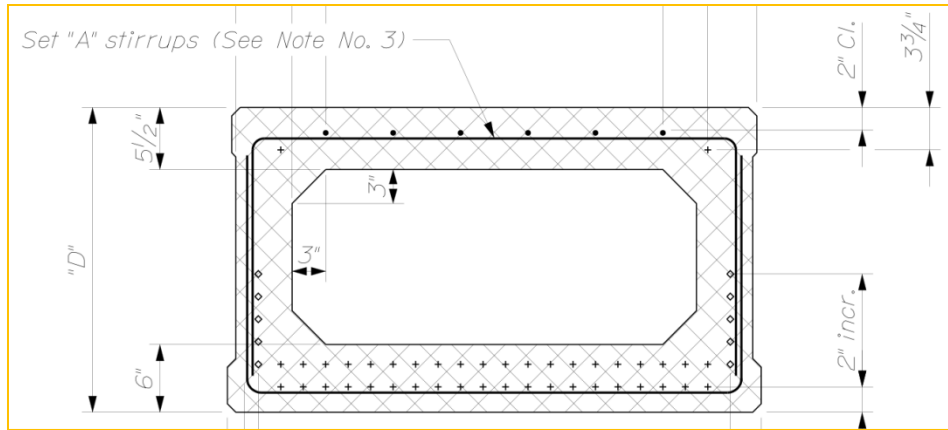
Figure 11. Typical Box beam section

Massachusetts DOT

Massachusetts utilizes both box and deck beams on their bridges. The deck beam is essentially similar to a slab beam as can be seen in the diagram below. The embedded length of the horizontal shear reinforcement is seen to be 2 in. whereas the width is not specified. A rake finish is specified (1/4 amplitude) across the width.
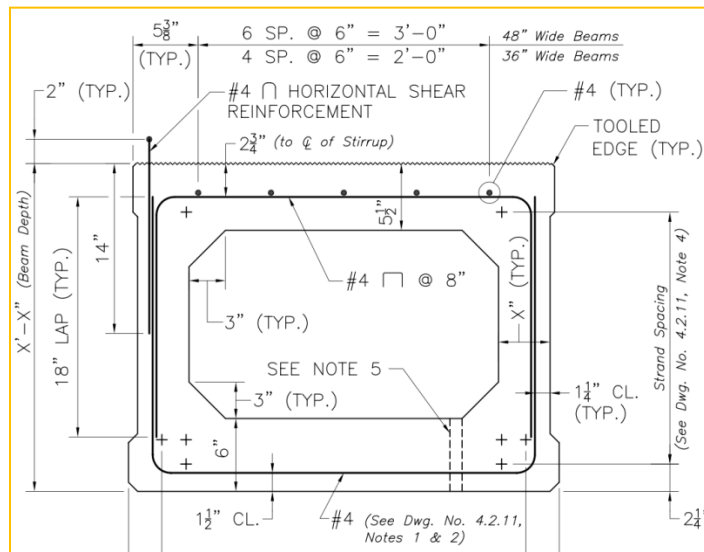
Figure 12. Typical box section (Note that the direction of the horizontal shear reinforcement is perpendicular to the cross-section)

503
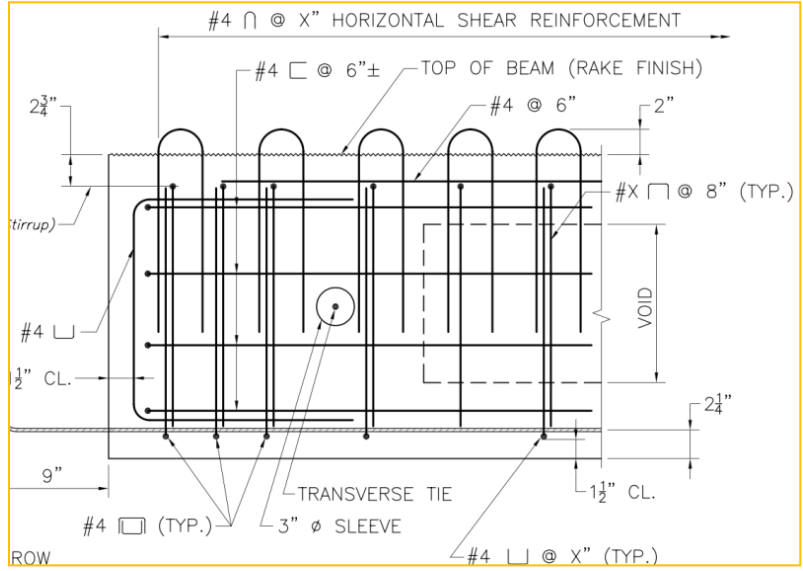
Figure 13. Elevation
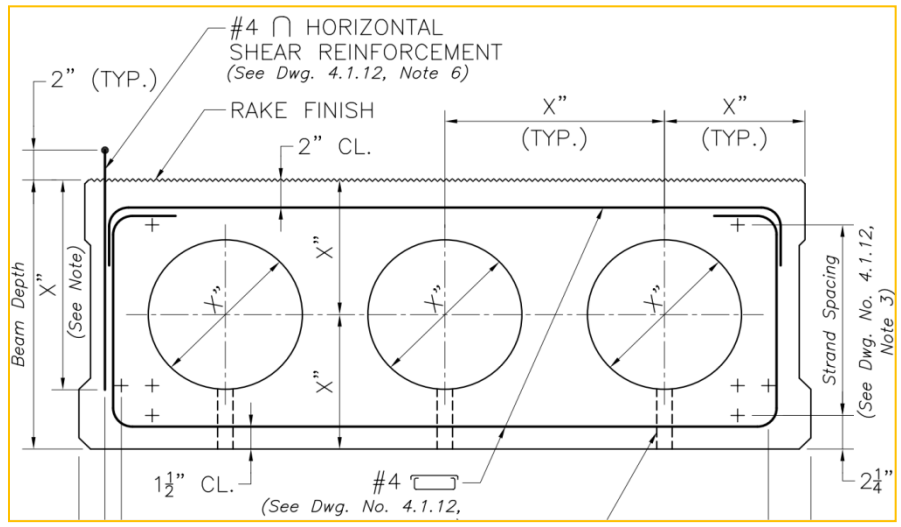
Figure 14. Typical slab (deck) beam section (Note that the direction of the horizontal

shear reinforcement is perpendicular to the cross-section)

504
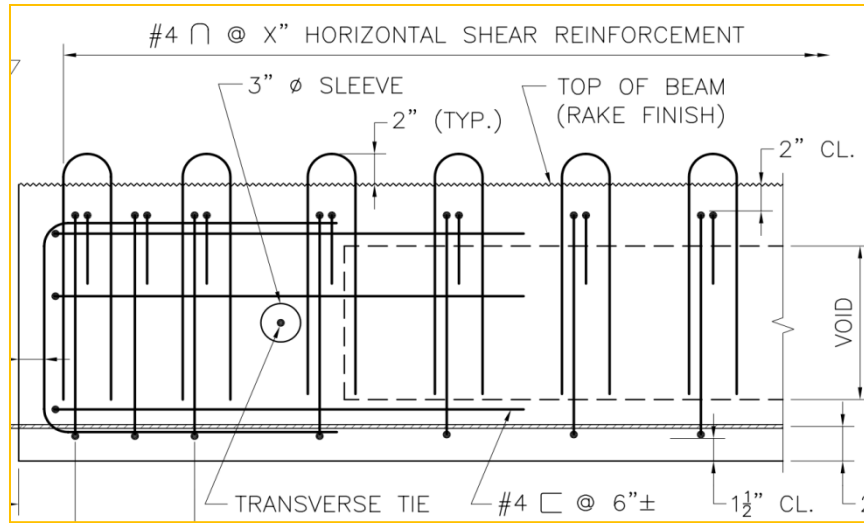
Figure 15. Slab (deck) beam elevation

Minnesota DT

Minnesota utilizes rectangular beams as shown below. The embedded length is seen to be 6 inches. The plans specify that the tops of beam should be rough floated and broomed transversely for bond.
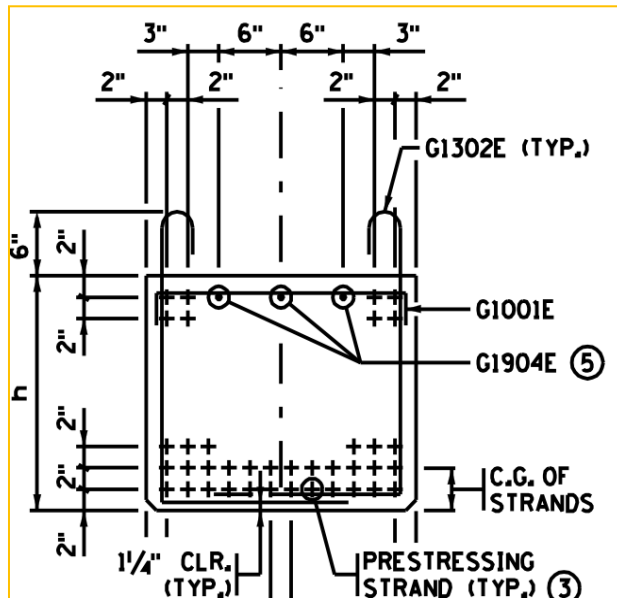
Figure 16. Typical rectangular beam section
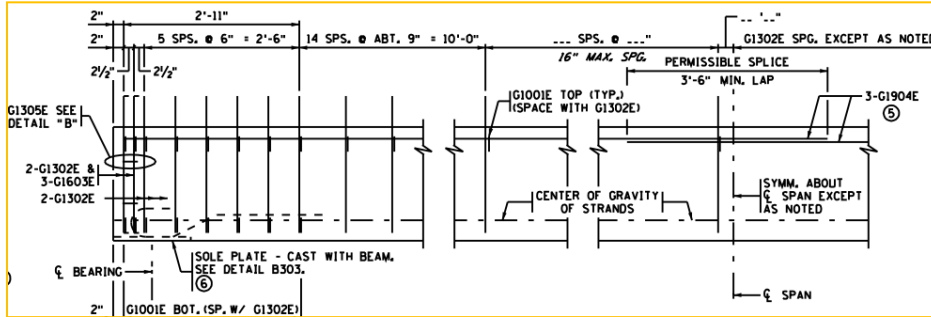
Figure17. Elevation

Missouri DOT

Missouri does not have standard drawings for prestressed box and slab bridges. They however use prestressed box beams and voided slab beams (no solid slabs) and rely on experience and their inventory of bridges they have designed in the past. The diagrams below show some of the details that have been used by consultants and the department. Top surface of all beams shall receive a scored finish (depth of scoring ¼") perpendicular to prestressing strands.
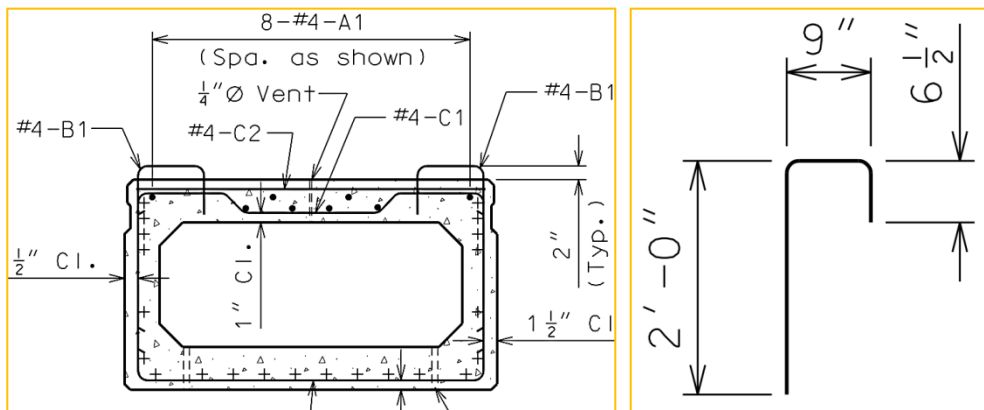
Figure 18. Typical box beam section

506
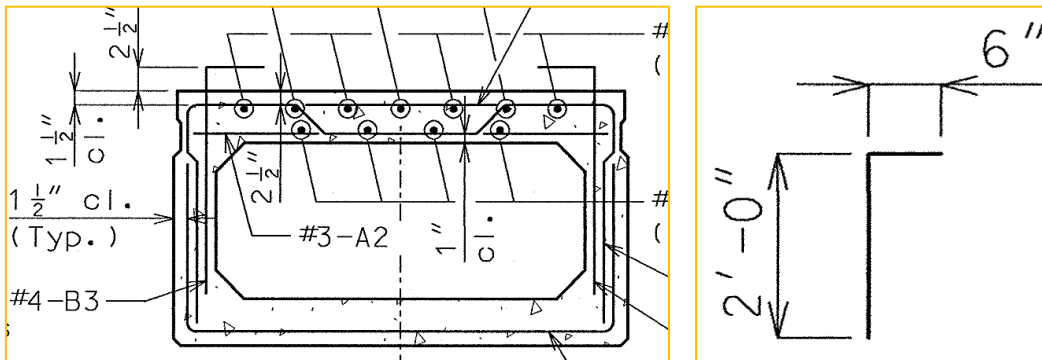
Figure 19. Typical box beam section
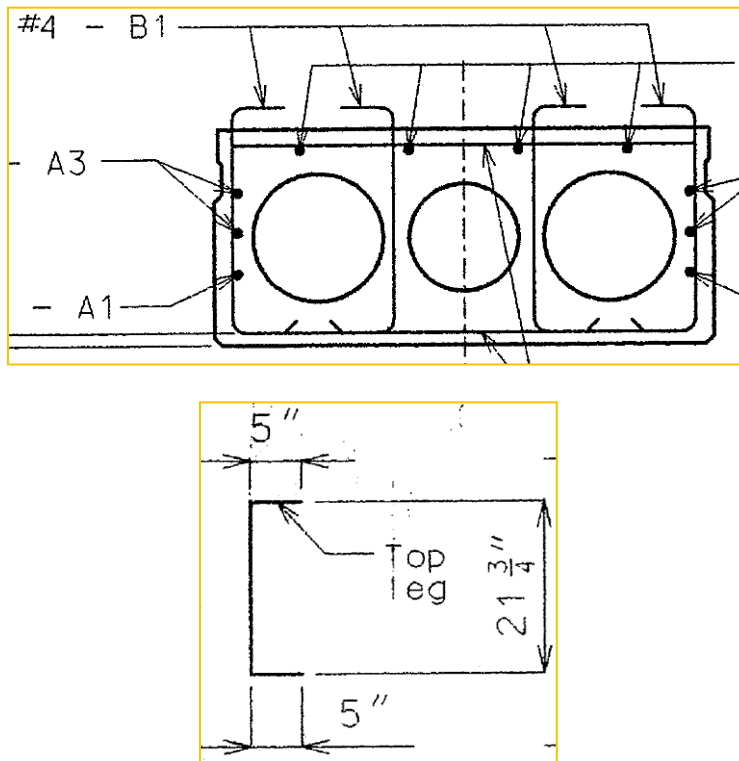
Figure 20. Typical slab beam section

Pennsylvania DOT

Uses box beams in their bridges. The embedded length of the horizontal shear reinforcement is seen to be 3 inches whereas the width is 4 inches.
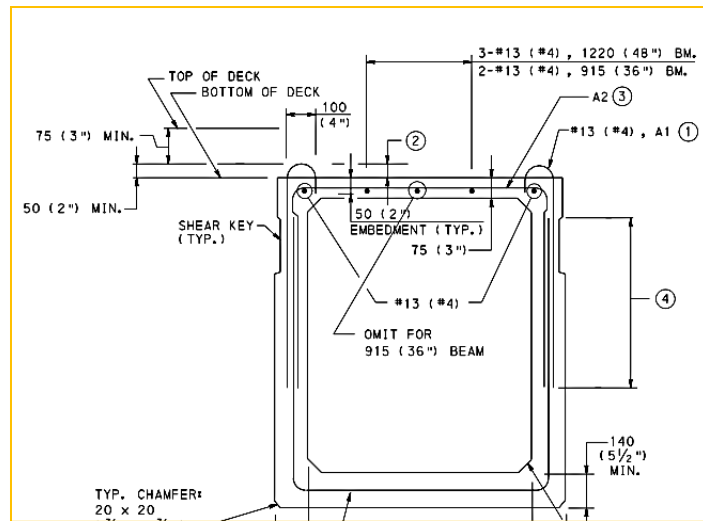
Figure 21. Typical box beam section

Rhode Island DOT

Has both slab and box beams. The embedded length is seen to be 2 inches for the horizontal shear reinforcement whereas no details are given on the width of the reinforcement. A raked surface finish is specified for butted box beam girders having a minimum of 5 inch composite deck overlay.
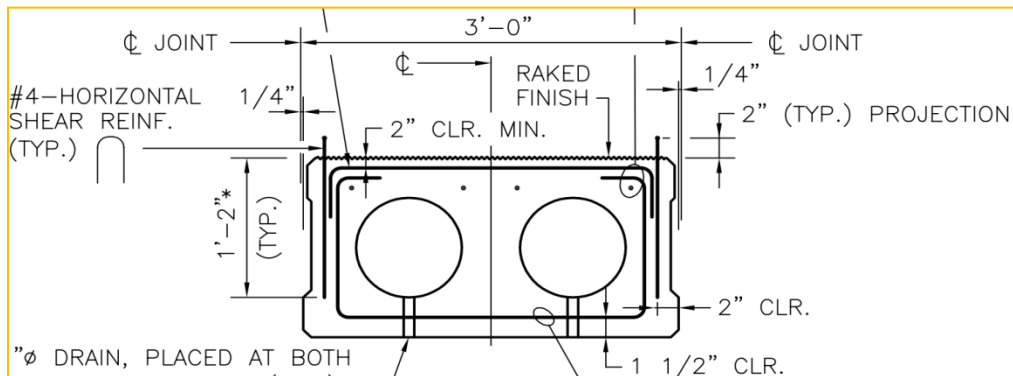
Figure 22. Typical slab section (Note that the direction of the horizontal shear reinforcement is perpendicular to the cross-section)
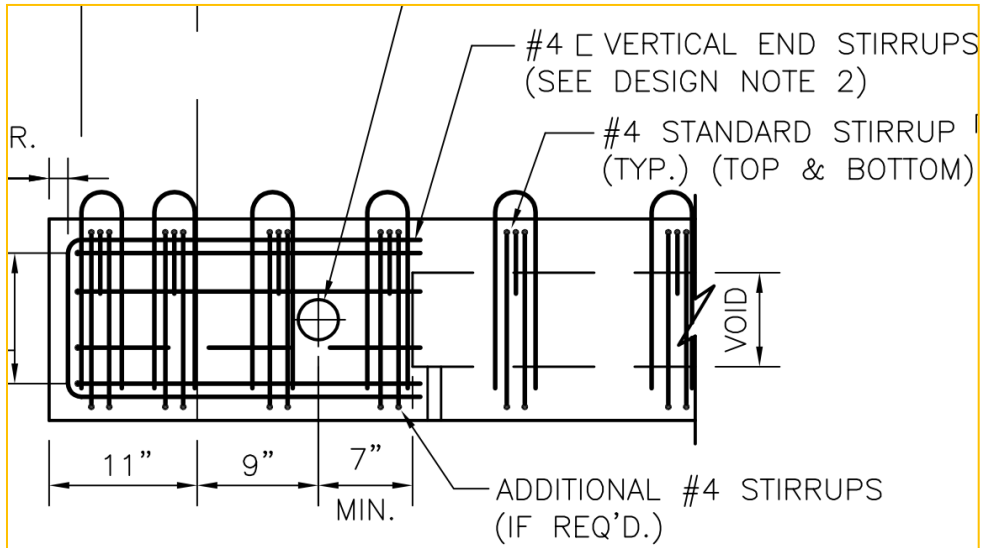
Figure 23. Elevation
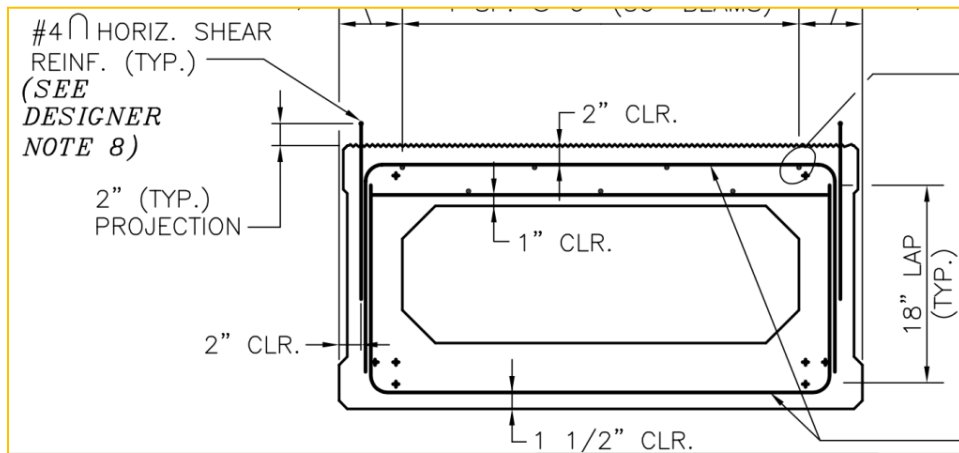
Figure 24. Typical box beam section (Note that the direction of the horizontal shear reinforcement is perpendicular to the cross-section)
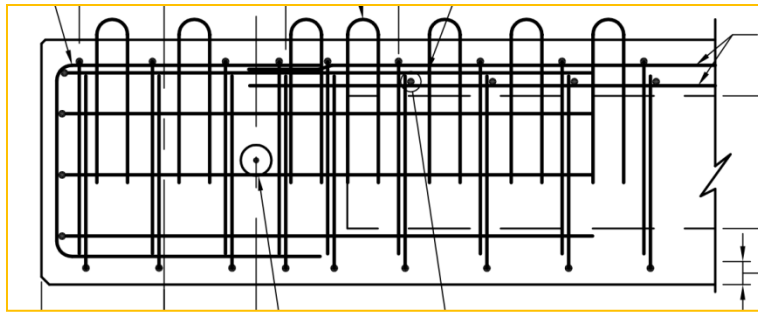
Figure 25. Elevation

New York DOT

Utilizes both the box and slab beam on their bridges. The embedded length of the horizontal shear reinforcement is shown to be 2 inches. No information is provided on the width of the horizontal shear reinforcement. A transverse rough surface finish with an amplitude of 1/4in. is specified.
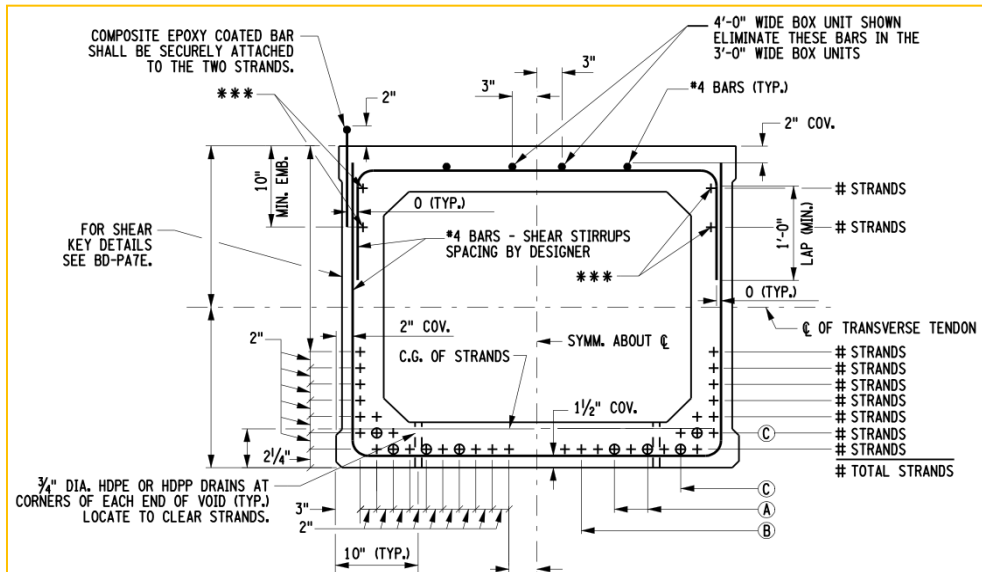
Figure 26. Typical box beam section (Note that the direction of the horizontal shear reinforcement is perpendicular to the cross-section)

510
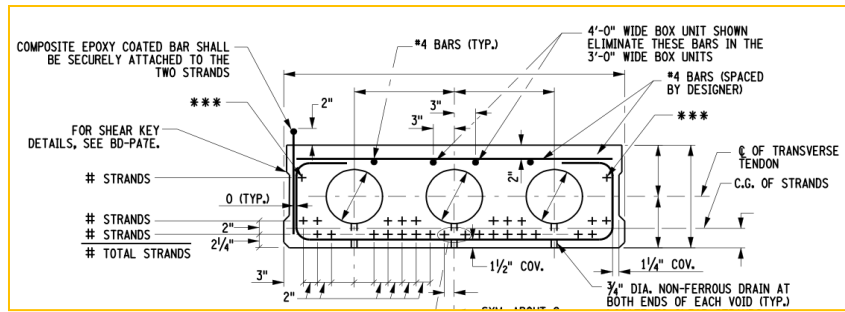
Figure 27. Typical slab section (Note that the direction of the horizontal shear

reinforcement is perpendicular to the cross-section)

Connecticut DOT

Details on both the box beam and slab beam are shown below. A water proof membrane is used on top of the precast beams with a minimal of 3.5 in. bituminous overlay. However, 20 years later, they began to experience some pre-mature failures of those structure types due to the failure of the waterproof membrane. They have more recently started using cast in-place slab but have not yet have standard details available yet. The plans specify a float finish on the top of the beams.
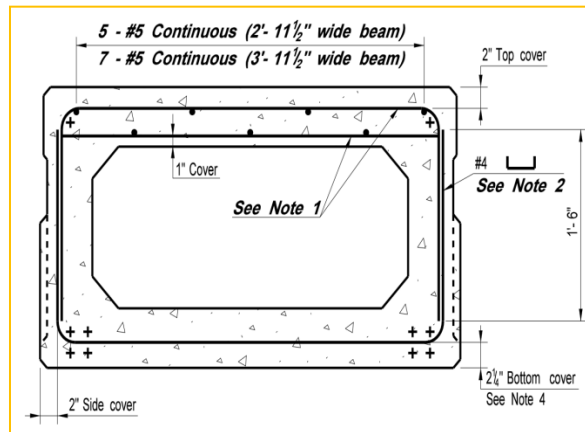
Figure 28. Typical midspan box beam section (the layout of horizontal shear

reinforcement is not clear)
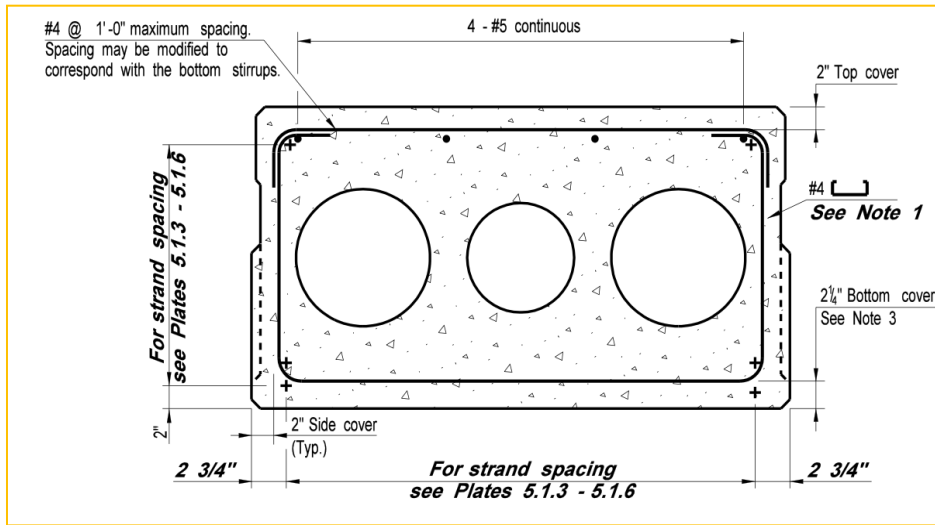
Figure 29. Typical midspan slab beam section (the layout of horizontal shear

reinforcement is not clear)

Alabama DOT

The Alabama DOT has voided slab beams but no box beams. The details are as shown below whereby the width of the horizontal reinforcement is seen to be 4 inches whereas the embedded length is 2.5 inches.
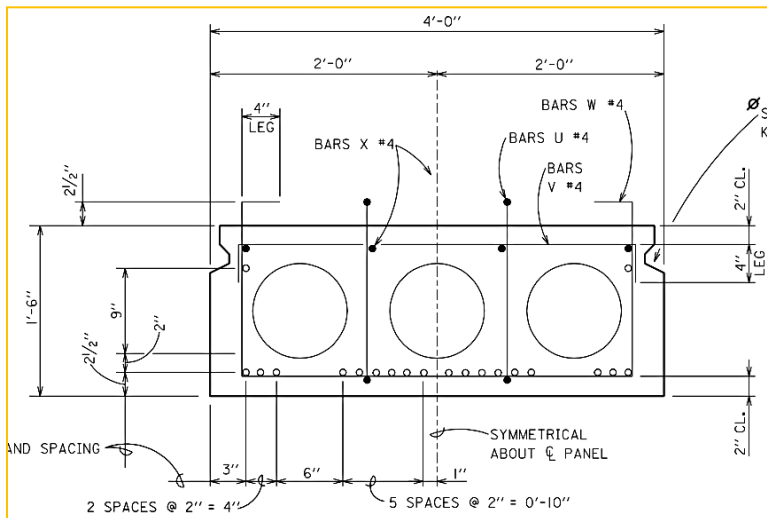
Figure 30. Typical slab beam section

Washington DOT

Has only the slab beam whose details are shown below. The width of the horizontal reinforcement is 9 inches while the embedded length is 2.5 in. The top surface of the beam is float finished.
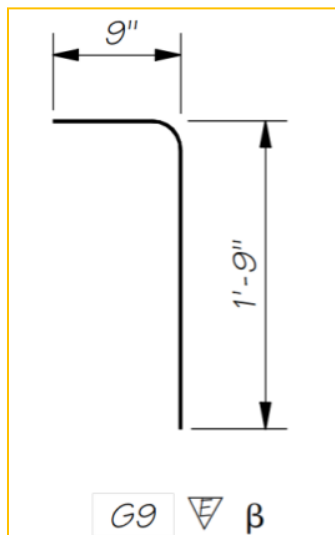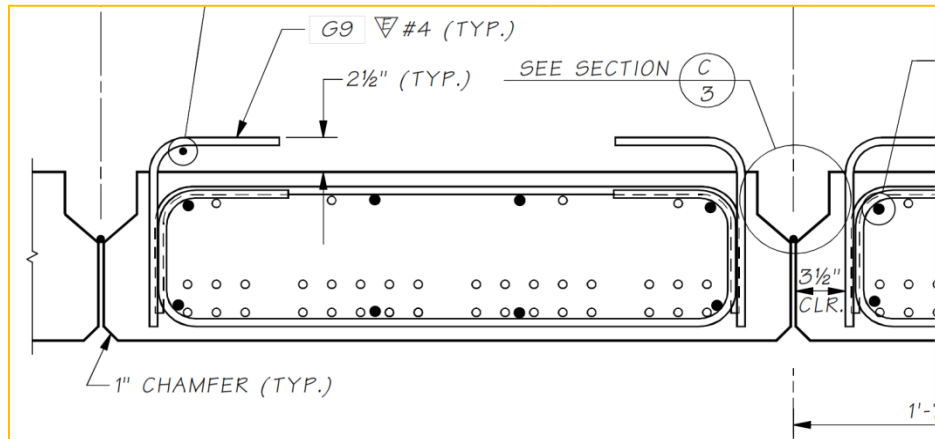
Figure 31. Typical Slab section
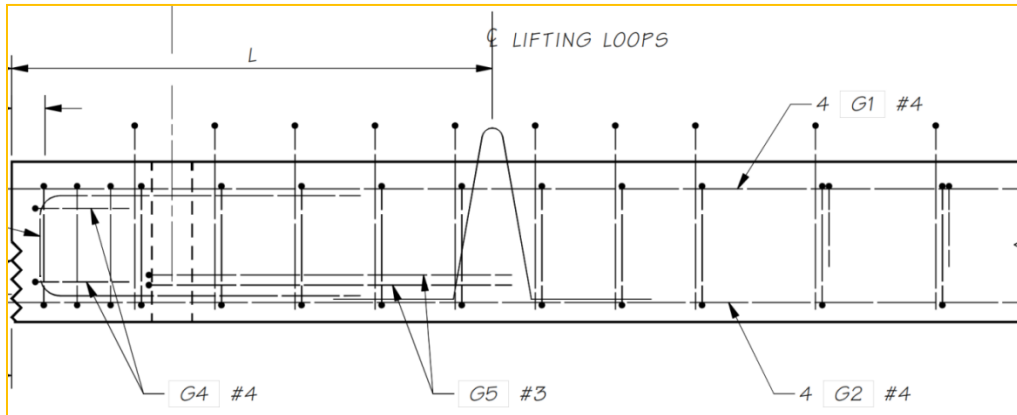
Figure 32. Elevation

Michigan DOT

Uses only slab beams whose section is shown below. The height of the horizontal shear reinforcement is shown to be 2.75 inches whereas the width of the reinforcement is 31 inches. The top of the beam is float finished.
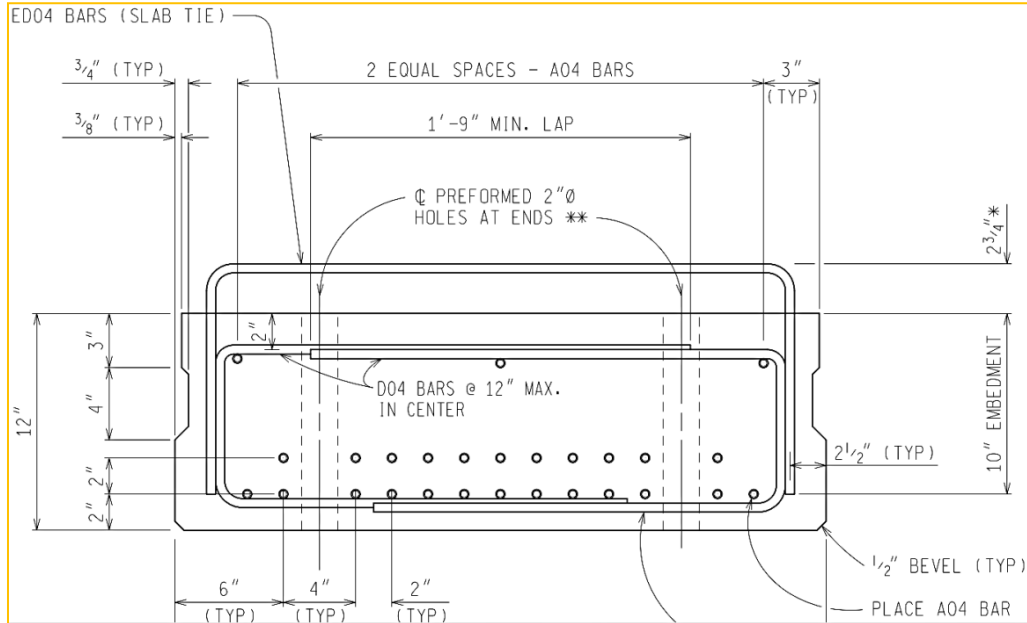
Figure 33. Typical box beam section

North Carolina

Typically use both slab and box beams but employ an asphalt wearing/riding surface or thin lightly reinforced concrete overlay. As such, the beams are designed to perform as non-composite structural elements and hence do not require horizontal shear reinforcement.

Ohio DOT

Has both the slab and box beams. The specifications recommend roughening the surface to an amplitude of ¼ inch.

Figure 34. Typical box beam section

North Dakota DOT

Utilizes box beams in their bridges. The diagram below shows a typical box beam section. The embedded length of the horizontal shear reinforcement is shown to be 3 inches whereas the width is 6 inches. A wood float finish is specified.
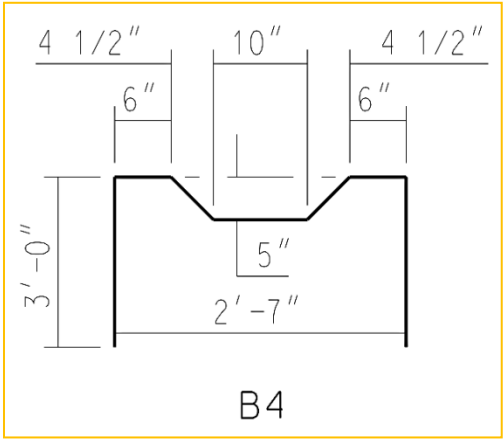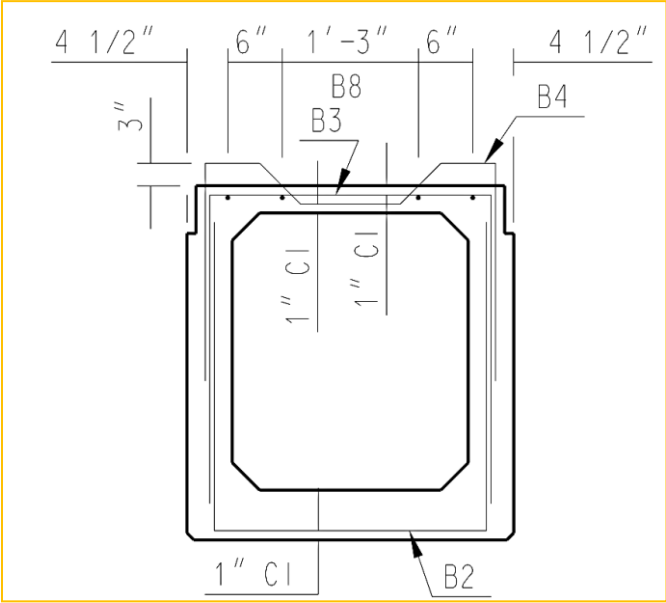
Figure 35. Typical box beam section

West Virginia DOT

Has box beams. The embedded length is seen to be 5 inches whereas the width is 7 inches. The plans specify that the top surface should be roughened to an amplitude of ¼ inches.
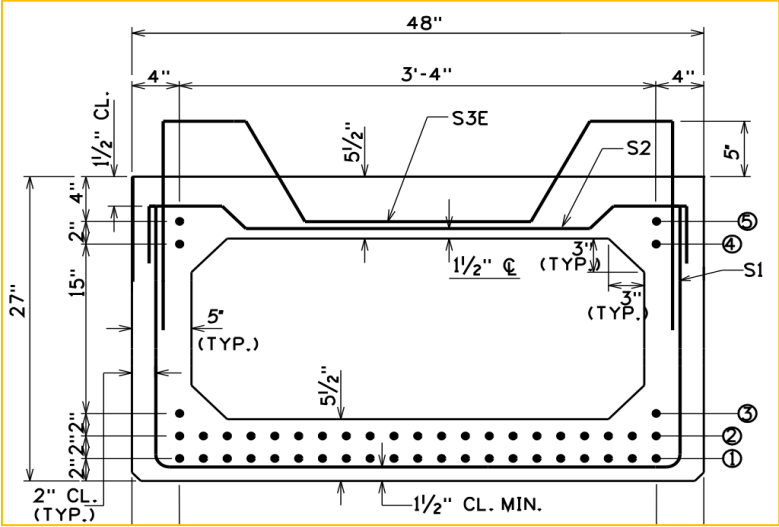
Figure 36. Typical box beam section
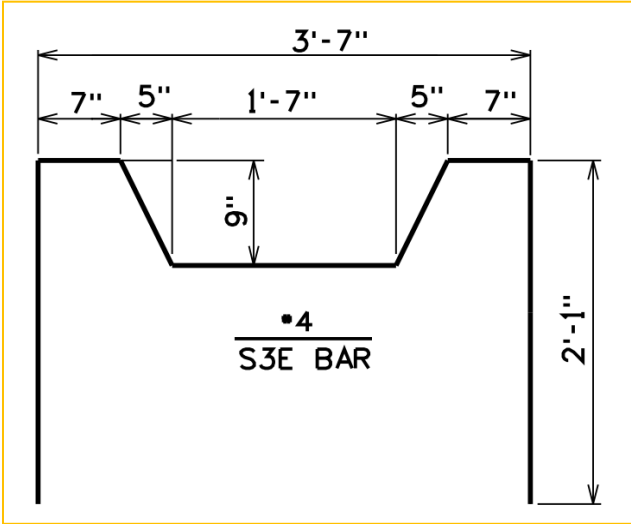
Figure 37. Elevation

From the study conducted it has been observed that there are essentially five types of horizontal shear reinforcement as shown below.
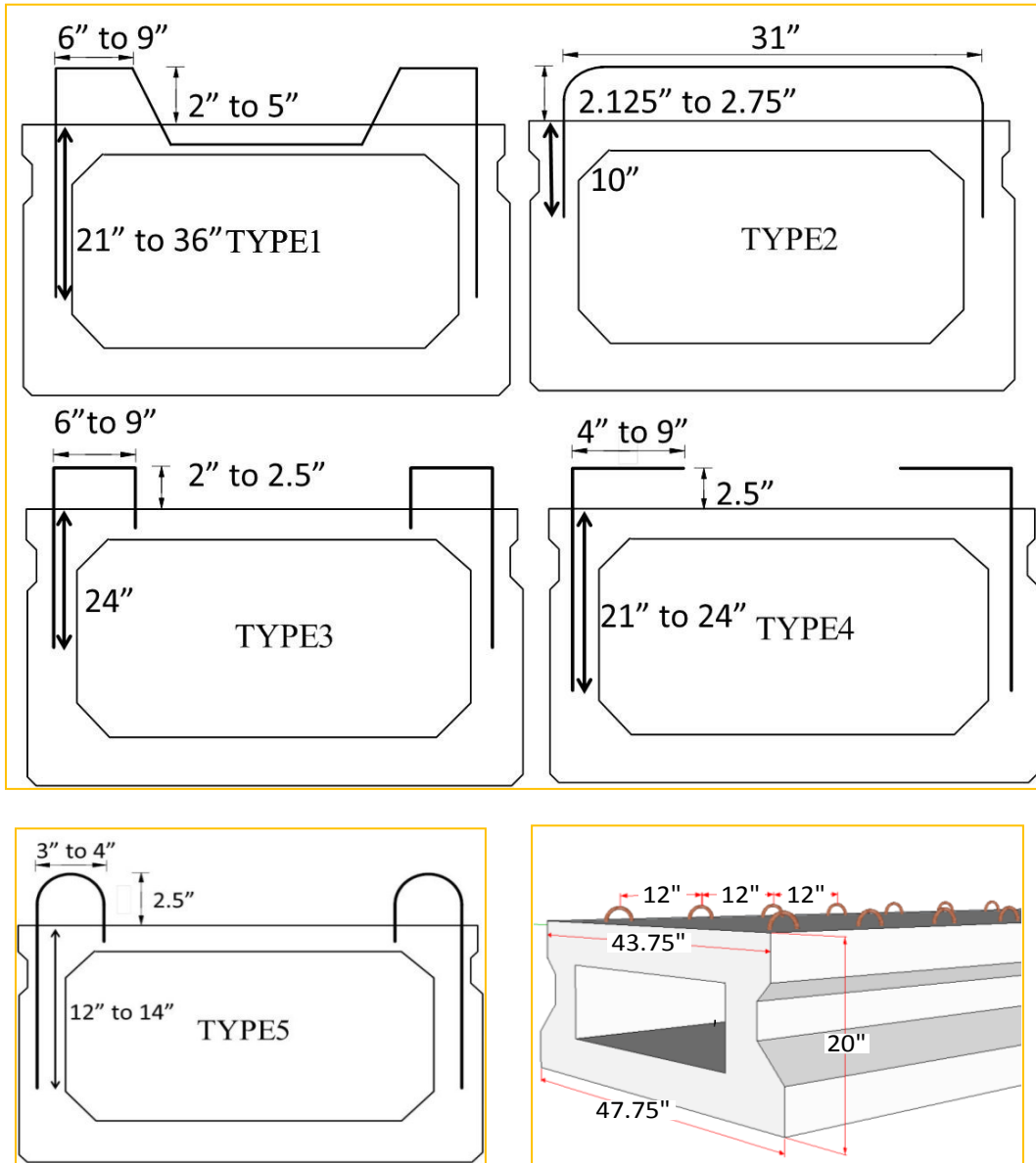
Figure 38. Five types of horizontal shear reinforcement

A wood float surface finish is also shown to be the most used type of finishing on the beams. The table below gives a summary of the findings.

Table 1. State DOT configuration for horizontal shear reinforcement

Type of horizontal shear reinforcement	State DOT
1	Ohio, North Dakota, West Virginia, Texas, Delaware, Illinois
2	Maryland, Michigan
3	Colorado, Missouri, Texas
4	Missouri, Alabama, Washington, Tennessee
5	Indiana, Kentucky, Minnesota, Pennsylvania, Texas*
6	Maine, Massachusetts, Rhode Island

* TxDOT standard prior to 2012.

It is clear from this study that the width of horizontal shear reinforcement used in other states is generally greater than that used in TxDOT practice. Also of interest is the effectiveness of using the reinforcement perpendicular to the cross-section. Therefore the testing matrix adopted in task 5 (Bar-pullout test) is justified as it will enable us to determine the effectiveness of different widths and curvatures of the reinforcement. The above report also shows that although wood float finish is the most popular finish being used, other kind of finishing (broom finish, rake finish) should also be considered for their effectiveness.

.

Appendix D

Task 2 Test Results

Wood Float Finish

The three wood float specimens failed at loads of 38.5 kips, 23.6 kips and 45.9 kips. The failure occurred at the interface and no flexural cracks were observed. It was noticed that some aggregates were dislodged from the concrete when the precast part was observed after failure. The places where this occurred on the precast part are represented by black markings.

Wood float 1

(a)   (b)
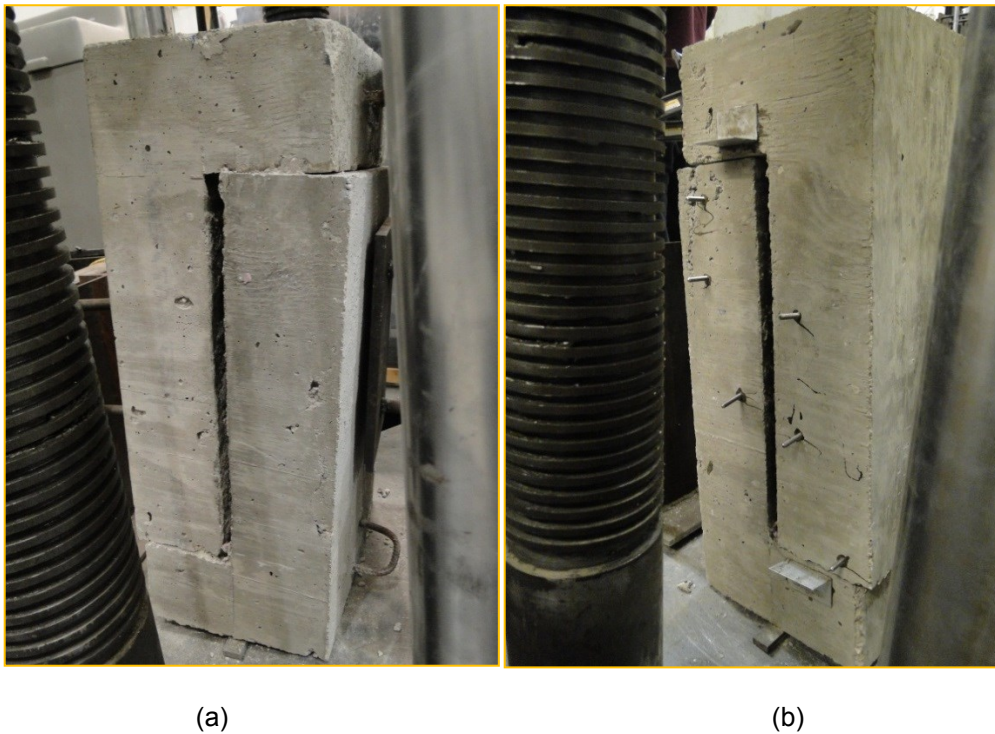
Figure 1. Wood Float Specimen #1 at failure (a) front view (b) back view.
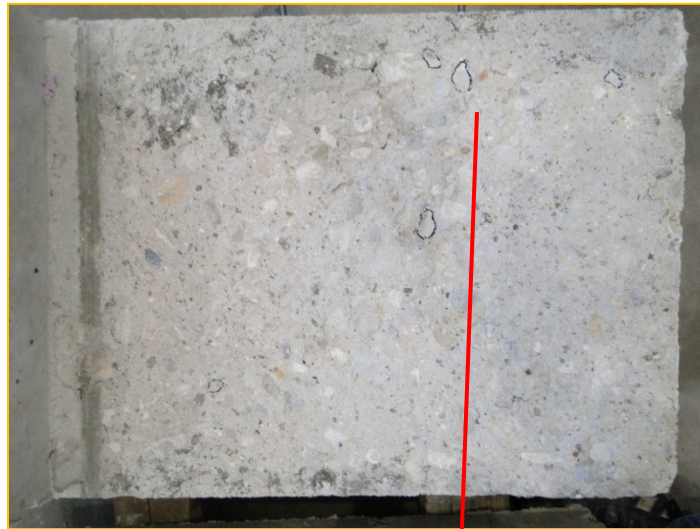
(a)

(b)

Figure 2. Wood float specimen # 1 precast (a) failure plane showing aggregate pullout and (b) surface profile.

(a)

(b)

Figure 3. Wood Float Specimen #1 Cast in-place (a) failure plane and (b) surface profile.

Wood float 2

(a)

(b)

Figure 4. Wood Float Specimen #2 at failure (a) front view (b) back view.

(a)

(b)

Figure 5.Wood Float Specimen #2 CIP (a) failure plane and (b) surface profile.
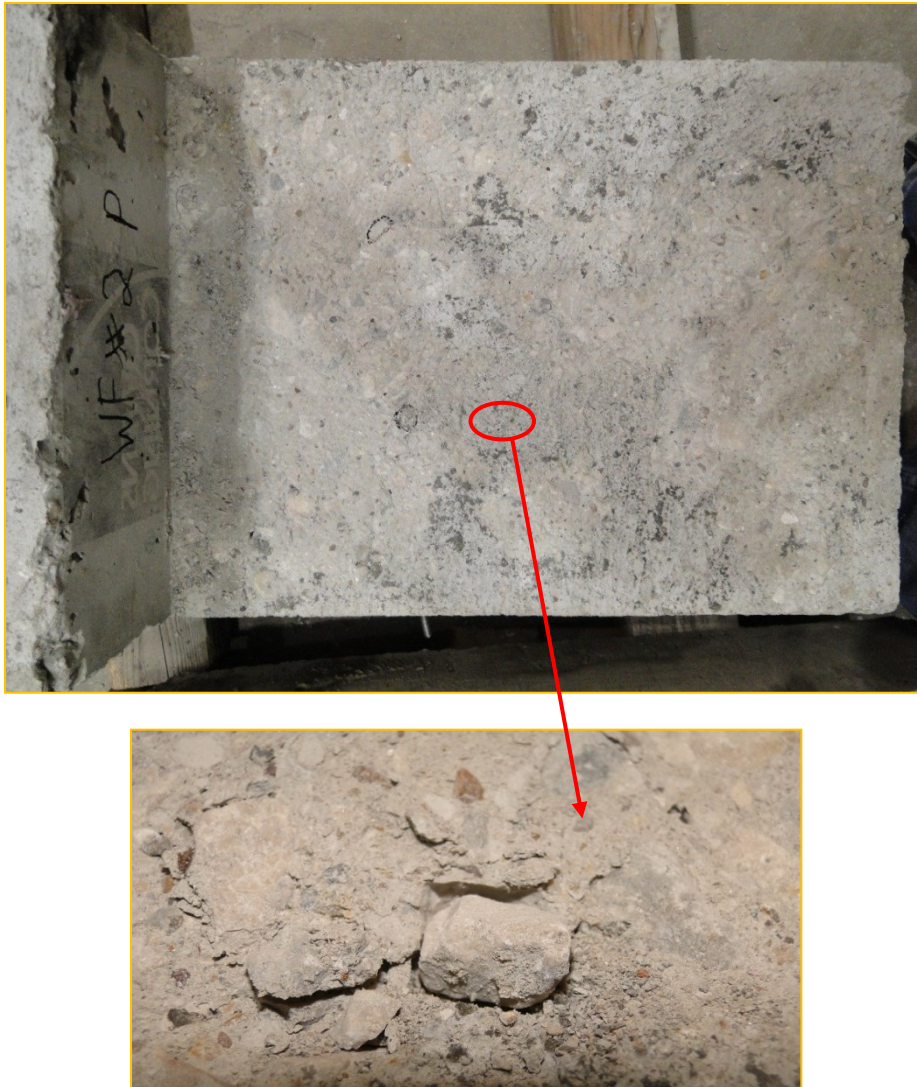
Figure 6. Wood Float Specimen #2 precast failure plane showing dislodged aggregate.

Wood float 3

(a)

(b)

Figure 7. Wood Float Specimen #3 at failure (a) front view (b) back view.

(a)

(b)

Figure 8. Wood Float Specimen #3 CIP (a) failure plane and (b) surface profile.

(a)

(b)

Figure 9. Wood Float Specimen #3 precast (a) failure plane showing dislodged

aggregates and (b) surface profile.

CSP 6

Figures 110 through 118 show the testing of both of the CSP 6 specimens. All three specimens failed at the interface with peak loads of 49.6 kips, 53.6 kips and 42.0 kips.

<table>
<tr><td>(a)</td><td>(b)</td></tr>
</table>
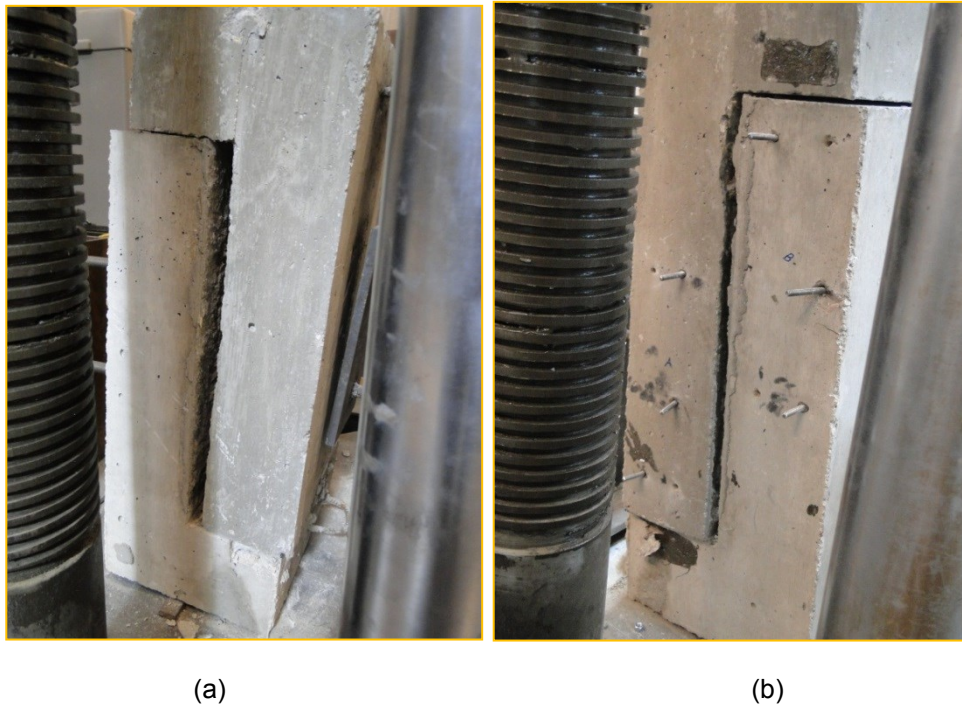
Figure 10. CSP 6 Specimen #1 failure (a) front view (b) back view.
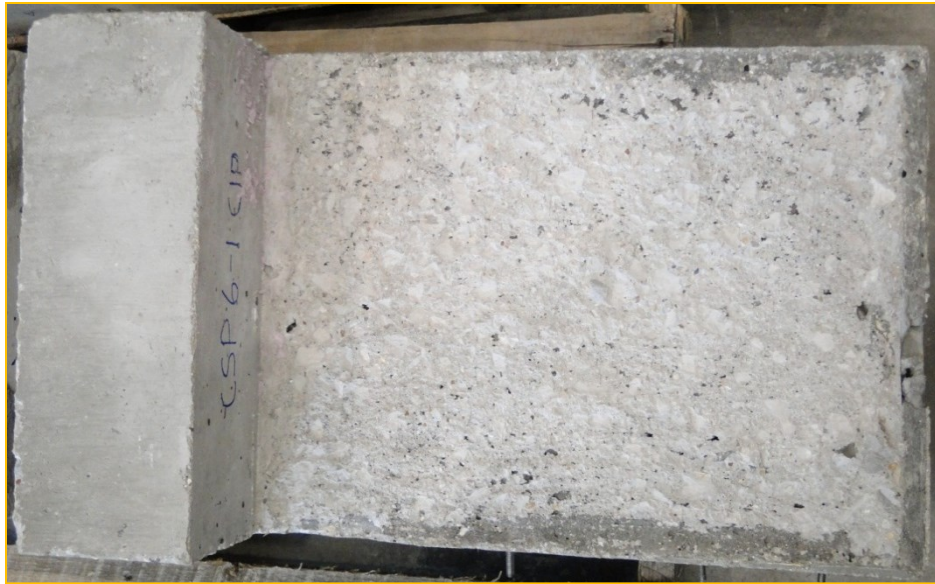
(a)
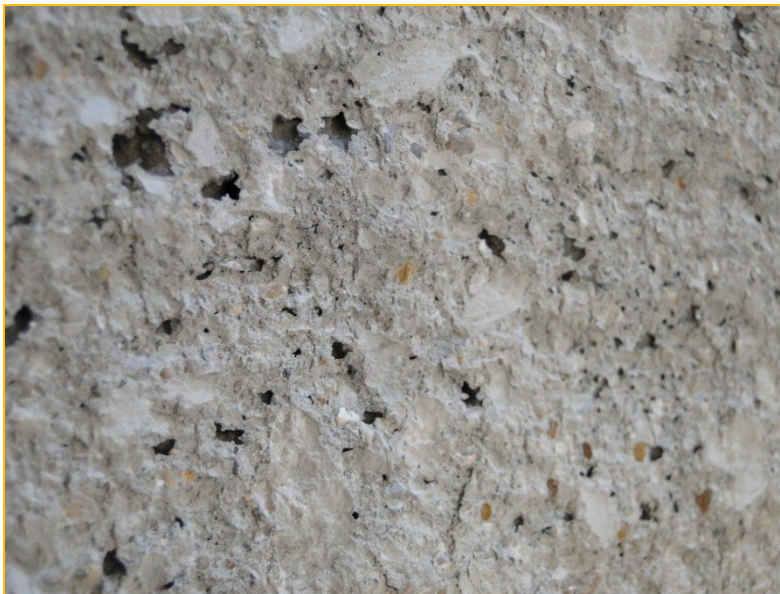
(b)

Figure 11. CSP 6 Specimen #1 CIP (a) failure plane and surface profile.

(a)

(b)
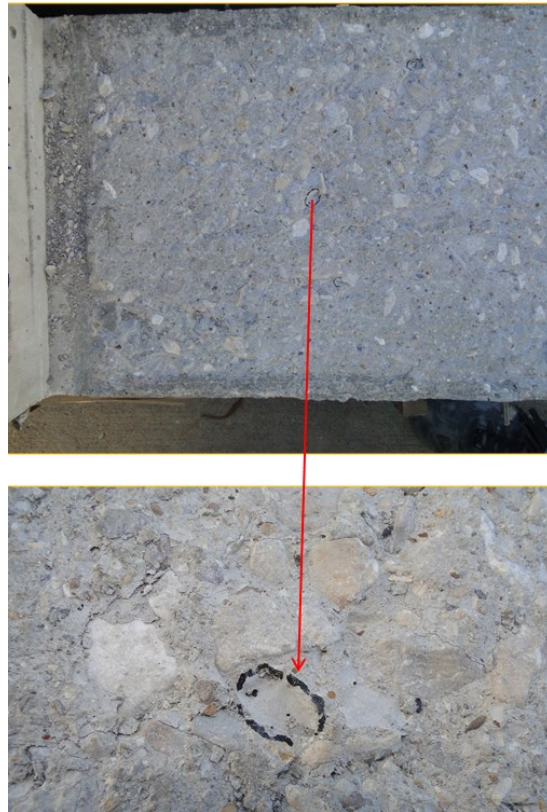
Figure 12. CSP 6 Specimen #1 precast (a) failure plane and (b) surface profile.

CSP 6_2
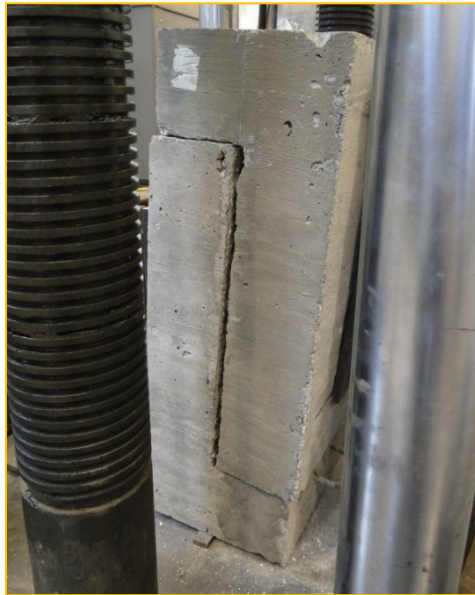
(a) Front view

(b) Back view

Figure 13. CSP 6 Specimen #2 failure

(a)
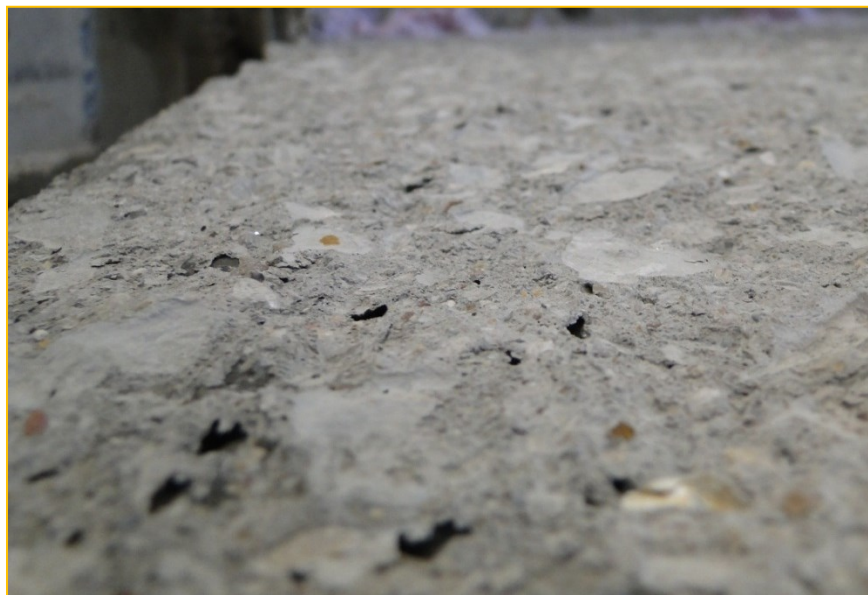
(b)

Figure 14. CSP 6 Specimen #2 CIP (a) failure plane and (b) surface profile.

(a)

(b)

Figure 15. CSP 6 Specimen #2 precast (a) failure plane and (b) surface profile.

CSP 6_3

(a) front view

(b) back view

Figure 16. CSP 6 Specimen #3 failure.

(a)

(b)

Figure 17. CSP 6 Specimen #3 CIP (a) failure plane and (b) surface profile.

(a)

(b)

Figure 18. CSP 6 Specimen #3 precast (a) failure plane and (b) surface profile.

CSP 7

Figures 119 through 127 below show the testing of the CSP 7 specimens. No flexural cracking was observed during testing and both specimens failed along the interface at peak loads of 49.6, 70.6, and 52.6 kips. There seems to be not much difference between the peak loads of CSP 6 and CSP 7 except for the second CSP 7 specimens that gave the highest peak.
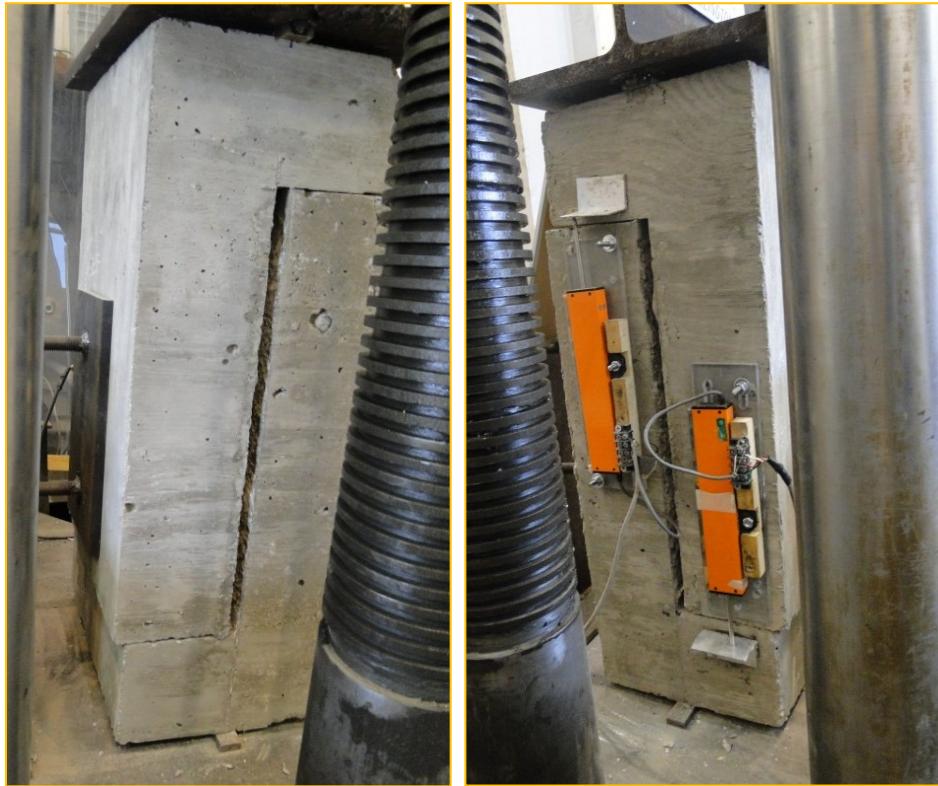
Figure 19. CSP 7 Specimen #1 failure (a) front view (b) back view.

(a)

(b)

Figure 20. CSP 7 Specimen #1 CIP failure plane

(a)

(b)

Figure 21. CSP 7 Specimen #1 precast (a) failure plane and (b) surface profile.

CSP7_2

(a) front view

(b) back view

Figure 22. CSP 7 Specimen #2 failure

(a)

(b)

Figure 23. CSP 7 Specimen #2 CIP (a) failure plane and (b) surface profile.

(a)

(b)

Figure 24. CSP 7 Specimen #2 precast (a) failure plane and (b) surface profile.

CSP7_3

(a) front view

(b) back view

Figure 25. CSP 7 Specimen #3 failure

(a)

(b)

Figure 26. CSP 7 Specimen #3 CIP (a) failure plane and (b) surface profile.

(a)

(b)

Figure 27. CSP 7 Specimen #3 precast (a) failure plane and surface profile.

CSP 8

Figures 128 through 138 below show the testing of the CSP 8 specimens. All three specimens failed mostly along the interface at peak loads of 61.1, 57.2 and 41.9 kips. The failure of the second and third specimen was by a small portion, into the CIP part near the notch. The was observed a lot of aggregate dislodgement and fracture as is shown in the diagrams.

CSP8_1

Figure 28. CSP 8 Specimen #1 failure (a) front view (b) back view.

(a)

(b)

Figure 29. CSP 8 Specimen #1 CIP (a) failure plane and (b) surface profile.

(a)

(b)

Figure 30. CSP 8 Specimen #1 precast (a) failure plane and (b) surface profile.

CSP8_2

Figure 31. CSP 8 Specimen #2 failure (a) front view (b) back view.

Figure 32: Failure into the CIP at the notch.

(a)

(b)
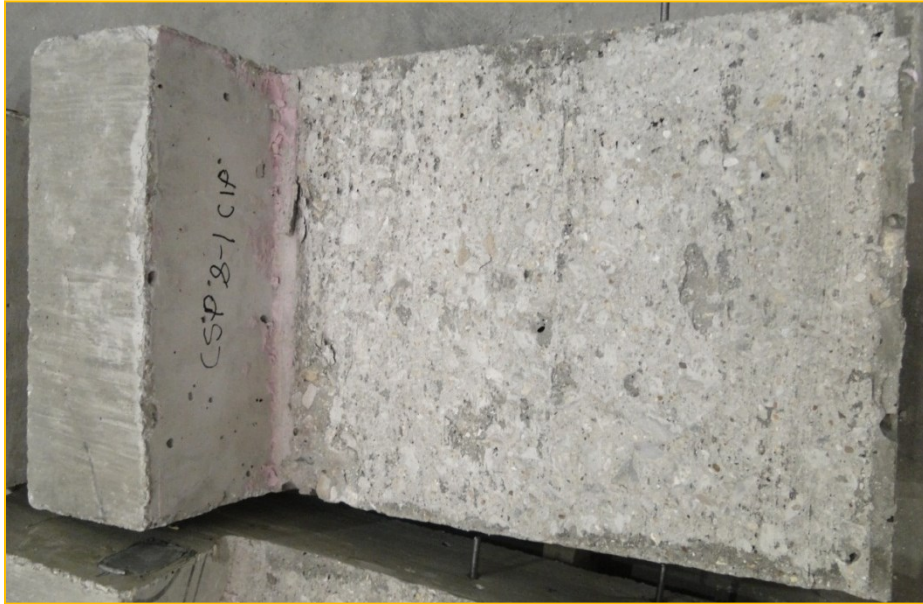
Figure 33. CSP 8 Specimen #2 CIP (a) failure plane and (b) surface profile.
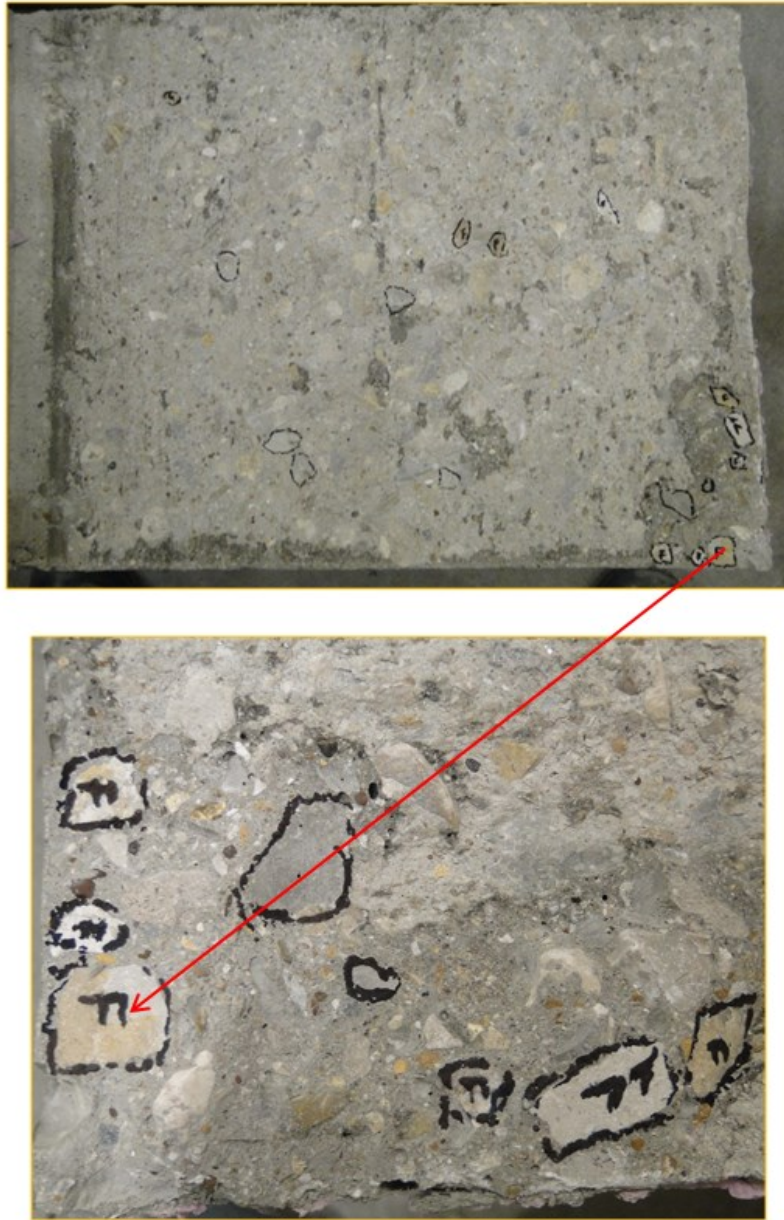
Figure 34. CSP 8 Specimen #2 precast failure plane showing dislodged and fractured aggregates.

CSP8_3

Figure 35. CSP 8 Specimen #3 failure (a) front view (b) back view.

Figure 36: Failure into the CIP at the top notch.

(a)

(b)

Figure 37. CSP 8 Specimen #3 CIP (a) failure plane and (b) surface profile.

(a)

(b)

Figure 38. CSP 8 Specimen #3 precast (a) failure plane and (b) surface profile.

CSP 9

Figures 39 through 47 below show the testing of the CSP 9 specimens. All three specimens failed along the interface with peak loads of 47.72, 54.66 and 57.46kips.

Figure 39. CSP 9 Specimen #1 failure

(a)

(b)

Figure 40. CSP 9 Specimen #1 CIP (a) failure plane and (b) surface profile.

(a)

(b)

Figure 41. CSP 9 Specimen #1 precast (a) failure plane and (b) surface profile.

CSP9_2

Figure 42. CSP 9 Specimen #2 failure (a) front view (b) back view.
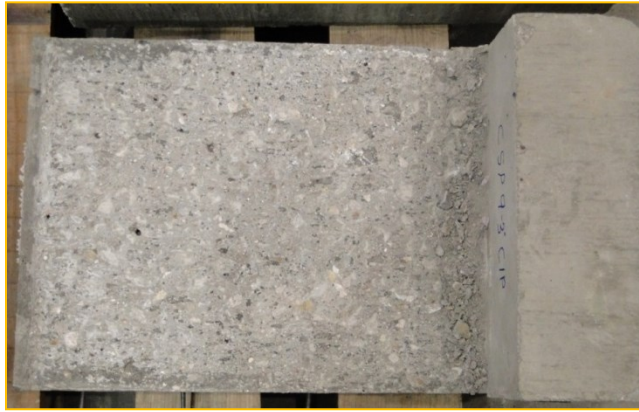
(a)

(b)

Figure 43. CSP 9 Specimen #2 CIP (a) failure plane and (b) surface profile.

(a)

(b)

Figure 44. CSP 9 Specimen #2 precast (a) failure plane with dislodged aggregate and (b) surface profile.

CSP9_3

Figure 45. CSP 9 Specimen #3 failure front view

(a)

(b)

Figure 46. CSP 9 Specimen #3 CIP (a) failure plane and (b) fractured aggregate.

(a)

(b)

Figure 47. CSP 9 Specimen #3 precast (a) failure plane and (b) surface profile.

Summary of Test Results

Table 1 and Figure 48 summarize the experimental results for the fifteen specimens.

Table 1. Push off test results.

Specimen	Surface Type	Failure Mode	Failure Load (kip)	Shear Stress (ksi)
1	Wood Float	Interface	38.5	0.15
2	Wood Float	Interface	23.7	0.09
3	Wood Float	Interface	45.9	0.18
4	CSP 6	Interface	56.6	0.22
5	CSP 6	Interface	53.6	0.21
6	CSP 6	Interface	42.0	0.17
7	CSP 7	Interface	49.6	0.20
8	CSP 7	Interface	70.6	0.28
9	CSP 7	Interface	52.6	0.21
10	CSP 8	Interface	57.2	0.23
11	CSP 8	Interface	61.1	0.24
12	CSP 8	Interface	41.9	0.17
13	CSP 9	Interface	47.7	0.19
14	CSP 9	Interface	57.5	0.23
15	CSP 9	Interface	54.7	0.22
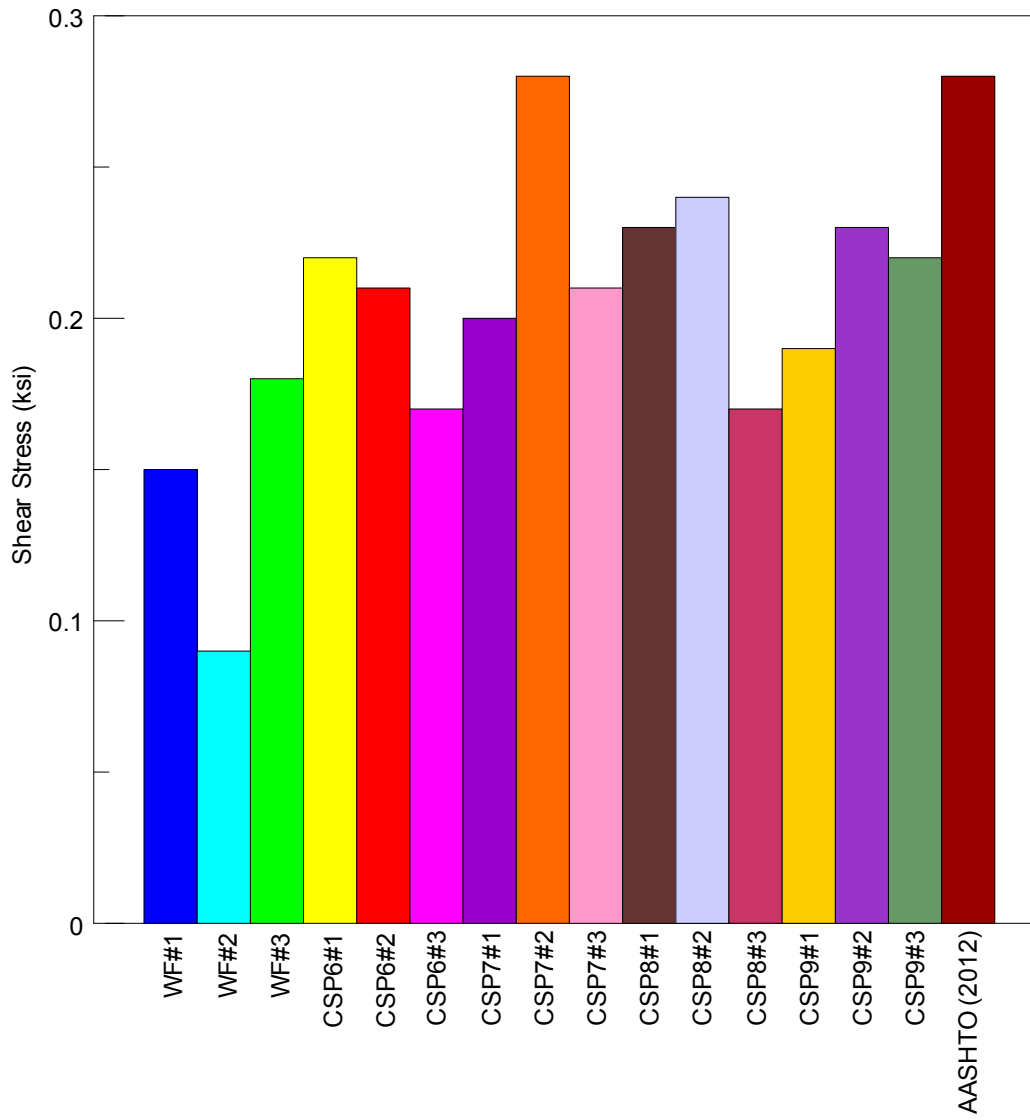
Figure 48. Shear stress comparison.

Appendix E

Task 3 Test Results

After 28 days of curing, Task 2 specimens were tested. Once completed, Task 3 specimens were prepared for testing. Two LVDT's were placed to measure the slip at each notch. The top surface of the specimen was grouted and the 2 inch thick plate was placed on the top followed by the load cell. The compression force was applied first by the 400-kip machine and kept constant at 20 kips after which the horizontal force was applied. The horizontal load was applied at a rate of approximately 100 lb/sec, up to failure.
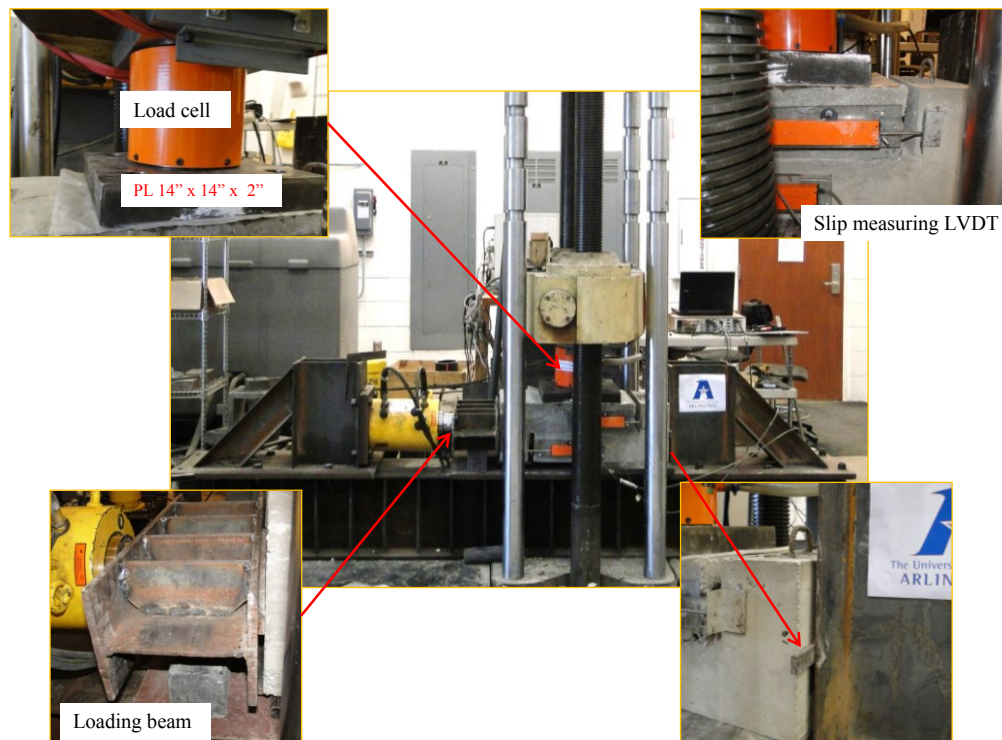
Figure 1. Test set-up.

Since there is expected to be some friction between the compression loading plate and the plastic sheet between the specimen and also between the 400 kip machine top plate and the load cell, a testing was conducted to find out how much friction these two would have contributed to the total shear recorded. The set-up below was used to

analyze this. The rollers were used so that there is no shear between the specimen and the plate on top of the roller and then a compression load of 20 kips was applied to the specimen. This compression load was kept constant while a horizontal load was progressively applied. The specimen moved almost immediately and the force applied for it to move was recorded. This is the force due to friction between the loading plate and specimen and between the load cell and top plate.

Friction between the top plate and load cell and the loading plate and specimen.
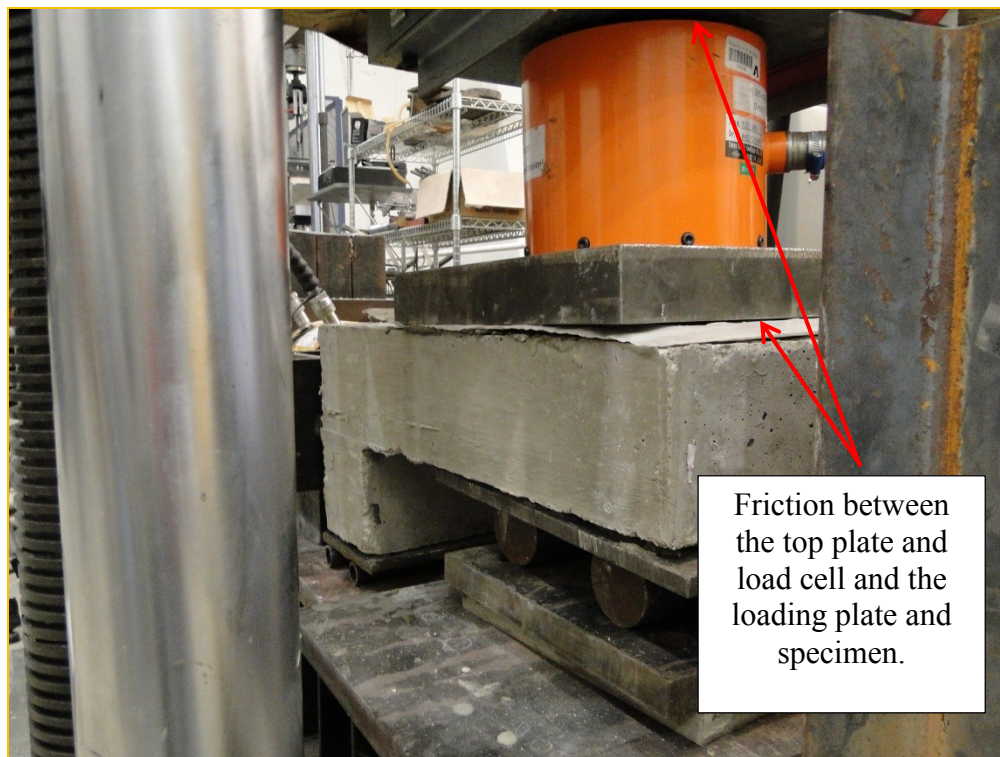
Figure 2. Shear between the loading plate set-up.

It was discovered that the contribution from these two factors was only 0.5 kips. Therefore it does not adversely affect the results shown above.

Wood Float Finish

The wood float specimens failed at an average load of 53 kips. The failure occurred at the interface and no flexural cracks were observed. Specimen #1 and

specimen #3 had much lower strength compared to specimen #2. This can be attributed to the hardening of concrete while the specimens were being cast thus resulting in less workability and compaction. For this reason the bond between the precast and cast in-place was poor leading to early failure. It was recommended that the three specimens be cast again with Task 4 to verify this. It was noticed that some aggregates were dislodged from the concrete when the precast part was observed after failure.

Wood float 1
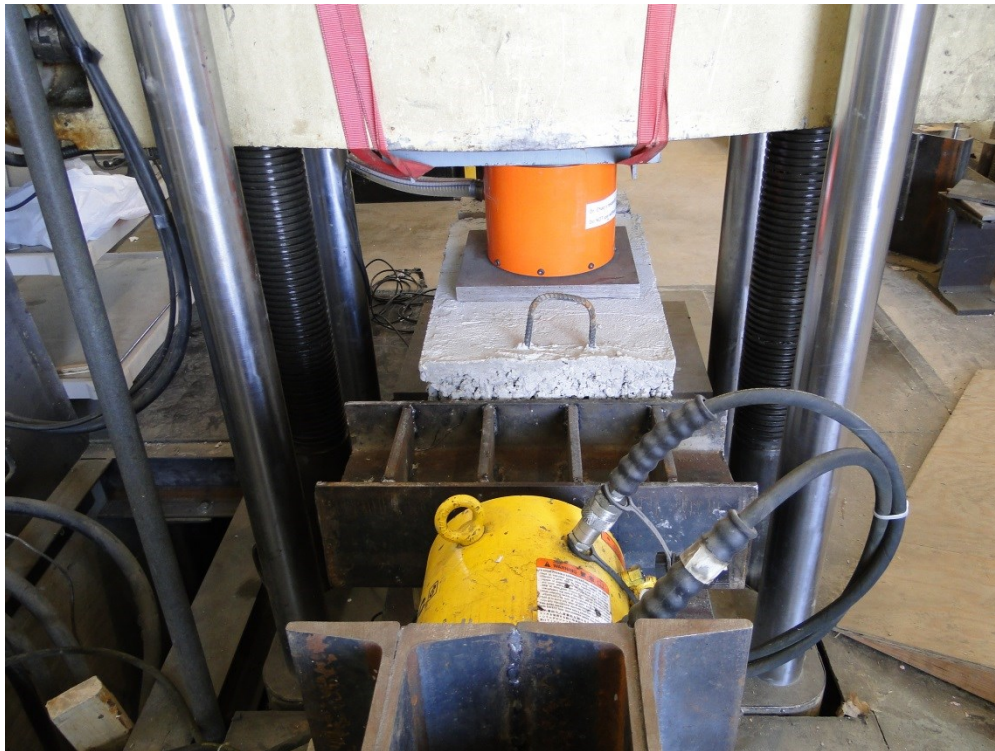
Figure 3. Wood Float Specimen #1 at failure (a) front view

Figure 4. Wood float specimen # 1 precast failure plane showing aggregate pullout.

Figure 5. Wood Float Specimen #1 Cast in-place failure plane.

Dark areas on the surface (circled) show areas where it is believed there was lack of contact between the precast and cast in-place part of the specimen. Hence the whole interface area was not utilized hence lower interface shear strength.

Wood float 2

Showed the highest strength among the wood float specimens of 84.4 kips. This is evident also from inspection of specimen after failure which shows more aggregate pullout and also fracturing of the concrete near the notch indicating higher bond strength.

(a)

(b)

Figure 6. Wood Float Specimen #2 at failure (a) front view (b) back view.

(a)

(b)

Figure 7.Wood Float Specimen #2 CIP failure plane.

(a)

(b)

(c) Fracturing of concrete near notch.

Figure 8. Wood Float Specimen #2 precast failure plane showing dislodged aggregate.

Wood float 3

Showed the lowest strength of 36.4 kips which is caused by lack of complete contact between the cast in-place and precast part as is evident in the pictures. The failure surfaces were also observed to be quite smooth after failure indicate there was not much aggregate interaction.

(a)

(b)

Figure 9. Wood Float Specimen #3 at failure (a) front view (b) back view.

(a) Fairly smooth surface at failure.

(b) Surface profile.

Figure 10. Wood Float Specimen #3 CIP failure plane.

(a)

(b)

Figure 11. Wood Float Specimen #3 precast failure plane showing areas of no contact. Circled areas indicate areas where it is believed to have no contact between the cast in-place and precast part.

CSP 6

The Figures below show the testing of the CSP 6 specimens. All the three specimens failed at the interface with an average peak load of 71.43 kips. The failure load for the first two specimens was equal whereas for the third it was fairly close. Specimens #1 and #2 showed a very rough interface after failure which consisted of aggregate pullout and fracture whereas for the third, the surface was fairly smooth which can explain the slight drop in the peak load.

(a)

(b)

Figure 12. CSP 6 Specimen #1 failure (a) front view (b) back view.

(a)

(b)

Figure 13. CSP 6 Specimen #1 CIP failure plane.

(a)

(b)Rough surface profile

Figure 14. CSP 6 Specimen #1 precast failure plane.

CSP 6_2

(a)

(b)

Figure 15. CSP 6 Specimen #2 failure (a) front view (b) back view.

(a)

(b)

Figure 16. CSP 6 Specimen #2 CIP failure plane.

(a)

(b) Aggregate fracture

(c) Fracture near notch.

Figure 17. CSP 6 Specimen #2 precast failure plane.

CSP 6_3

(a)

(b)

Figure 18. CSP 6 Specimen #3 failure (a) front view (b) back view.

(a)

(b) Concrete fracture near interface

(c) Fairly smooth surface

Figure 19. CSP 6 Specimen #3 CIP failure plane.

(a)

(b)

Figure 20. CSP 6 Specimen #3 precast failure plane.

CSP 7

The Figures below show the testing of the CSP 7 specimens. No flexural cracking was observed during testing and both specimens failed along the interface at an average peak load of 85.6 kips. There was also some fracture of concrete near the interface. CSP 7 specimens showed significantly more interaction at the interface with aggregate fracture pullout and also specimen #1 showed failure that dislodge some part of the concrete from the precast part. Specimen #3 showed the highest strength and it can be observed from the interface after failure that there is more obvious aggregate fracture, pullout and concrete dislodged from the precast part.

(a)

(b)

Figure 21. CSP 7 Specimen #1 failure (a) front view (b) back view.

(a)

(b) dislodged from the precast part.

Figure 22. CSP 7 Specimen #1 CIP failure plane.

(a)

(b)

Figure 23. CSP 7 Specimen #1 precast failure plane.

CSP7_2

(a)

(b)

Figure 24. CSP 7 Specimen #2 failure (a) front view (b) back view.

(a)

(b)

Figure 25. CSP 7 Specimen #2 CIP failure plane.

(a)

(b)

Figure 26. CSP 7 Specimen #2 precast failure plane.

CSP7_3

(a)

(b)

Figure 27. CSP 7 Specimen #3 failure (a) front view (b) back view.

(a)

(b) Extremely rough surface showing both fracture and pullout

(c)

Figure 28. CSP 7 Specimen #3 CIP failure plane.

(a) Dislodged concrete and aggregates.

(b)

(c)

Figure 29. CSP 7 Specimen #3 precast failure plane.

CSP 8

The Figures below show the testing of the CSP 8 specimens. Two of the specimens failed at exactly the interface while Specimen #3 failed out of the interface suggesting that the bond on the interface was very strong. The average peak load was 88.85 kips. Specimen #2 showed the highest peak load which is evident from the surface after failure whereby there is a piece of concrete dislodged from the precast part and also considerable aggregate pullout and fracture.

CSP8_1

(a)

(b)

Figure 30. CSP 8 Specimen #1 failure (a) front view (b) back view.

(a)

(b)

Figure 31. CSP 8 Specimen #1 CIP failure plane.

(a)

(b)

Figure 32. CSP 8 Specimen #1 precast failure plane.

CSP8_2

(a)

(b)

Figure 33. CSP 8 Specimen #2 failure (a) front view (b) back view.

(a)

(b) Dislodged concrete.

Figure 34. CSP 8 Specimen #2 CIP failure plane.

(a)

(b)

Figure 35. CSP 8 Specimen #2 precast failure plane showing dislodged and fractured

aggregates.

CSP8_3

(a)

(b)

Figure 36. CSP 8 #3 failure.

CSP 9

The Figures below show the testing of the CSP 9 specimens. Two specimens failed along the interface while the third failed at the legs. The average peak load was 80.22 kips. Specimen #1 showed a much smaller peak load compared to #2 and #3. It is believed that this specimen was one of the latest to be cast thus the concrete was less workable and hence poor bonding. Since the results were much lower than expected, they were not used in the calculation on the friction coefficient. Specimen 3 did not fail at the interface but started progressing into the precast part as can be seen in Figure 64 this is believed to indicate that the bond at the interface was so strong that failure followed the path of least resistance.

(a)

(b)

Figure 37. CSP 9 Specimen #1

(a)

(b)

(c)

Figure 38. CSP 9 Specimen #1 CIP failure plane.

(a)

(b)

Figure 39. CSP 9 Specimen #1 precast (a) failure plane and (b) surface profile.

(a)

(b)

Figure 40. CSP 9 Specimen #2 failure (a) front view (b) back view.

(a)

(b)

(c)

Figure 41. CSP 9 Specimen #2 CIP failure plane.

(a)

(b)

Figure 42. CSP 9 Specimen #2 precast failure plane.

CSP9_3

(a) Failure progressing into precast part.

(b)

Figure 43. CSP 9 Specimen #3 failure

Summary of Test Results

Table 2 and Figure 44 summarize the experimental results for the fifteen specimens. The friction factor was calculated using the AASHTO equation and results from Task 2 and Task 3. Shear stress was calculated from Task 2 as shown in Table 2 . Therefore using CSP 6 as an example,

<div align="center">

Average cA_{cv} (Task 2): 50.74 kips

Shear strength from Task 3: 71.43 kips

$$V_{ni} = cA_{cv} + \mu\left(A_{vf}f_y + P_c\right)$$

71.43 kips = 50.74 kips +μ (0+20 kips)

μ = (71.43-50.74)/20 = 1.0

</div>

Table 1. Push off test results (Task 2).

Specimen	Surface Type	Failure Mode	Failure Load (kip)	Shear Stress (ksi)
1	Wood Float	Interface	38.47	0.15
2	Wood Float	Interface	23.74	0.09
3	Wood Float	Interface	45.90	0.18
4	CSP 6	Interface	56.61	0.22
5	CSP 6	Interface	53.56	0.21
6	CSP 6	Interface	42.00	0.17
7	CSP 7	Interface	49.55	0.20
8	CSP 7	Interface	70.61	0.28
9	CSP 7	Interface	52.59	0.21
10	CSP 8	Interface	57.22	0.23
11	CSP 8	Interface	61.11	0.24
12	CSP 8	Interface	41.88	0.17
13	CSP 9	Interface	47.72	0.19
14	CSP 9	Interface	57.46	0.23
15	CSP 9	Interface	54.66	0.22

Table 2. Push off test results (Task 3).

Specimen	Surface Type	Failure Mode	Failure Load (kip)	Shear Stress (ksi) (Task 2)	μ
1	Wood Float	Interface	38.1	0.15	
2	Wood Float	Interface	36.4	0.09	0.85
3	Wood Float	Interface	84.4	0.18	
4	CSP 6	Interface	75.8	0.22	
5	CSP 6	Interface	75.5	0.21	1.0
6	CSP 6	Interface	63	0.17	
7	CSP 7	Interface	81.1	0.20	
8	CSP 7	Interface	84.2	0.28	1.4
9	CSP 7	Interface	91.5	0.21	
10	CSP 8	Interface	84.5	0.23	
11	CSP 8	Not Interface	109*	0.24	1.8
12	CSP 8	Interface	93.2	0.17	
13	CSP 9	Not Interface	93.5*	0.19	
14	CSP 9	Interface	83.3	0.23	1.8
15	CSP 9	Interface	64**	0.22	

*Specimens did not fail at the interface, the ultimate loads were used here to conservatively estimate the horizontal shear strength.

**Results not used as they were found to be unrealistically low as explained in results summary in CSP 9.
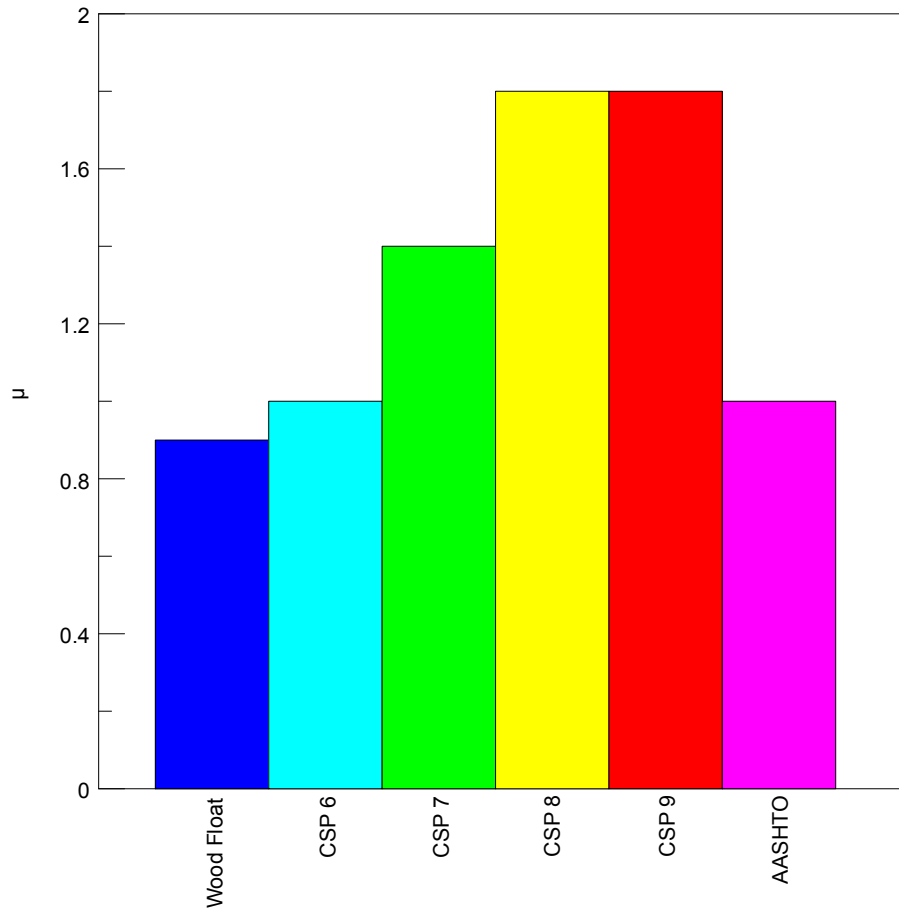
Figure 44. Friction coefficient comparison.

References

AASHTO, "LRFD Bridge Design Specifications," American Association of State Highway and Transportation Officials (AASHTO), Washington, D.C., 2014.

ACI 374.1-05: Acceptance Criteria for Moment Frames Based on Structural Testing and Commentary. American Concrete Institute, Farmington Hills, Michigan, 2005.

ACI 441R-96: High Strength Concrete Columns: State of the Art. American Concrete Institute, Farmington Hills, Michigan, 1996.

ACI 318, Building Code Requirements for Structural Concrete (ACI 318-14) and Commentary (ACI 318-14), American Concrete Institute, Farmington Hills, Michigan, 2014.

ACI ITG-4.3R, "Report on Structural Design and Detailing for High-Strength Concrete in Moderate to High Seismic Applications," ACI Innovation Task Group 4, American Concrete Institute, Farmington Hills, Michigan, 2007.

ACI-363R. High-Strength Concrete. ACI 363 Committee Report, American Concrete Institute, 2010.

Aghdasi, P., "Development Of Ultra-High Performance Fiber-Reinforced Concrete (UHP-FRC) For Large-Scale Casting," Master's Thesis, The University of Texas at Arlington, Arlington, Texas, 2013.

Aghdasi, P., Palacios, G., Heid, A.E., and Chao, S.-H., 'Mechanical properties of a highly flowable ultra-high-performance fiber-reinforced concrete mixture considering large-size effects,' High Performance Fiber Reinforced Cement Composites (HPFRCC 7), International Workshop, Stuttgart, Germany, June 1-3, 2015.

Ali, M. A., and White, R. N., "Enhanced Contact Model for Shear Friction of Normal and High-Strength Concrete," ACI Structural Journal, 96(3): 348-360, 1999.

Anderson, A.R., "Composite Designs in Precast and Cast in place Concrete," Progressive Architecture, 41(9): 172-179, 1960.

Aoude, H., Cook, W.D., and Mitchell, D. "Behavior of Columns Constructed with Fibers and Self-Consolidating Concrete." ACI Structural Journal, 2009.

ASTM C 39 (2001), Standard Test Method for Compressive Strength of Cylindrical Concrete Specimens, Annual Book of ASTM Standards, ASTM International, Vol. 04. 02, West Conshohocken, PA, 2003.

Aviram, A., Stojadinovic, B., Parra-Montesinos, G.J., and Mackie, K.R. 'Structural response and cost characterization of bridge construction using seismic performance enhancement strategies.' PEER Report No. 2010/01, (Pacific Earthquake Engineering Research Center, University of California, Berkeley CA., 2010).

Badoux, J. C., and Hulsbos, C. L., "Horizontal Shear Connection in Composite Concrete Beams under Repeated Loads," ACI Journal, 64(12): 811-819, 1967.

Bae, S. and Bayrak, O. (2008). "Seismic Performance of Full-Scale Reinforced Concrete Columns," *ACI Structural Journal*, V. 105, No. 2, March-April, pp. 123-132.

Bae, S., "Seismic Performance of Full-Scale Reinforced Concrete Columns," PhD Dissertation, The University of Texas at Austin, Austin, Texas, 2005.

Bass, R. A., Carrasquillo, R. L., and Jirsa, J. O., "Shear Transfer across New and Existing Concrete Interfaces," ACI Structural Journal, 86(4): 383-393, 1989.

Birkeland, H. W., Class Notes for Course, "Precast and Prestressed Concrete," University of British Columbia, 1968.

Birkeland, P., and Birkeland, H., "Connections in Precast Concrete Construction," ACI Journal, 63(3): 345-368, 1966.

Caldarone, Michael A. *High-strength Concrete: A Practical Guide*. London: Taylor & Francis, 2009.

Chao, S.-H. "Bond Characterization of Reinforcing Bars and Prestressing Strands in High Performance Fiber Reinforced Cementitious Composites under Monotonic and Cyclic Loading," Ph.D. Dissertation, University of Michigan, Ann Arbor, MI, 2005.

Choi, Y.-J., and Chao, S.-H., "Seismic Performance of Full-Scale High-Performance Fiber-Reinforced Concrete (HPFRC) Special Moment Frame Slab-Beam-Column Subassemblage Using Joint as the Major Energy Dissipation Source," High Performance Fiber Reinforced Cement Composites (HPFRCC 7), International Workshop, Stuttgart, Germany, June 1-3, 2015.

Chung, H. W. and Chung, T. Y., "Prestressed Concrete Composite Beams Under Repeated Loading," ACI Journal, 1976.

Collins, M. P.; Mitchell, D.; and MacGregor, J. G., "Structural Design Considerations for High-Strength Concrete," *Concrete International*, V. 15, No. 5, May 1993, pp. 27-34.

Cusson, D., and Paultre, P., "High-Strength Concrete Columns Confined by Rectangular Ties," Journal of Structural Engineering, 120(3): March, 1994.

del Viso, J.R., Cannona, J.R., Ruiz, G. "Shape and Size Effects on the Compressive Strength of High-Strength Concrete," Cem Concr Res, 2008;38(3):386–95.

Digital image. Concrete Columns-Structural Design Overview. ASDIP structural software, 17 Jan. 2015. Web. 24 Mar. 2015. <http://www.asdipsoft.com/concrete-columns-structural-design-overview/>.

Evans, R. H., and Chung, H. W., "Horizontal Shear Failure of Prestressed Composite T-Beams with Cast in-Situ Lightweight Concrete Deck," Concrete, pp. 124 – 126, 1969.

Foster, Stephen J. "On Behavior of High-Strength Concrete Columns: Cover Spalling, Steel Fiber and Ductility." ACI Structural Journal, 2001.

Frenay, J. W., "Shear Transfer Across a Single Crack in Reinforced Concrete Under Sustained Loading," Part 1, Experiments, Stevin Report, 5-85-5, 1985.

French CW, Schultz AE, Hajjar JF, Shield CK, Ernie DW, Dexter RJ, Du DHC, Olson SA, Daugherty DJ, Wan CP. Multi-Axial Subassemblage Testing (MAST) System: Description And Capabilities. Paper No. 2146, Proceedings of the 13[th]World Conference on Earthquake Engineering, Vancouver, BC, Canada, August 1-6, 2004.

Gohnert, M., "Horizontal Shear Transfer Across a Roughened Surface," Cement & Concrete Composites, V. 25, No. 3, pp 379 – 385, 2003.

Graybeal, B., "Compressive Behavior of Ultra-High-Performance Fiber-Reinforced Concrete," ACI Materials Journal, V. 104, No. 2, March-April 2007, pp. 146-152.

Hanson, N. W., "Precast-Prestressed Concrete Bridges: (2) Horizontal Shear Connections," PCA Journal, 2(2): 38-58, 1960.
High Performance, Flow Ability, and Fiber Reinforcement of a Concrete Matrix," BAC2010—2nd Iberian Congress on Self Compacting Concrete, University of Minho-Guimaraes, Portugal, July 1-2, 2010.

Hofbeck, J. A., Ibrahim, I. O., and Mattock, A. H., "Shear Transfer in Reinforced Concrete," ACI Journal, 66(13): 119-128, 1969.

Hsu, T. T. C., "Horizontal Shear Tests of PSI Prestressed Composite Beams," Report to Prestressed Systems Inc., 1976.

Hsu, T. T. C., Mau, S. T., and Chen, B., "Theory of Shear Transfer Strength of Reinforced Concrete." ACI Journal, 84(2), 149-160, 1987.

Hwang, S. J., Yu, H. W., and Lee, H. J., "Theory of Interface Shear Capacity of Reinforced Concrete," Journal of Structural Engineering, 126(6): 700-707, 2000.

ICRI Technical Guideline No. 03732 "Specifying Concrete Surface Preparation for Sealers, Coatings, and Polymer Overlays," 2012.

John, H. Thomsen IV, and W. Wallace John. "Lateral Load Behavior of Reinforced Concrete Columns Constructed Using High-Strength Materials." ACI Structural Journal, 1994.

Kaar, P.H., Kriz, L.B., and Hognestad, E., "Precast-prestressed concrete bridges, Pilot Tests of Continuous Girders." J. PCA Research and Development Laboratories, 2(2), 21-37, 1960.

Kahn, L. F., and Mitchell, A. D., "Shear Friction Tests with High-Strength Concrete," ACI Structural Journal, 99(1): 98-103, 2002.

Kamel M. R., "Innovative Precast Concrete Bridge Systems," Dissertation, University of Nebraska, Lincoln, Nebraska, 1996.

Kent, A. H., Gabriel, Z., Bahram, S., "Toward an Improved Understanding of Shear-Friction Behavior," ACI Journal, 109(6): 835-844, 2012.

Kono, S., and Tanaka, H., "Interface Shear Transfer for High Strength Concrete and High Strength Shear Friction Reinforcement," ASCE Journal, 2003.

Kovach, J. D., and Naito, C., "Horizontal Shear Capacity of Composite Concrete Beams without Interface Ties," ATLSS report 08-05, ATLSS Center, Lehigh University, Bethlehem, Pa, 2008.

Kriz, L. B., and Raths, C. H., "Connections in Precast Concrete Structures-Strength of Corbels," PCI Journal 10(1): 16–6, 1965.

Légeron, F. and Paultre, P. (2000) "Behavior of High-Strength Concrete Columns under Cyclic Flexure and Constant Axial Load," ACI Structural Journal, V. 97, No. 4, July-Aug., pp. 591-601.

Loov, R. E., and Patnaik, A. K., "Horizontal Shear Strength of Composite Concrete Beams with a Rough Interface," PCI Journal, 39(1): 48-69, 1994.

Loov, R.E., "Design of Precast Connections," Paper presented at a seminar organized by Compa International Ltd., Singapore, 1978.

Mander, J. B., J. N. Priestley, and R. Park. "Observed Stress-Strain Behavior of Confined Concrete ." ASCE - Journal of Structural Engineer, August 1988.

Mander, John B., J. N. Priestley, and R. Park. "Theoretical Stress-Strain Model For Confined Concrete." ASCE - Journal of Structural Engineering, August 1988.

Marques, J. L. G., and Jirsa, J. O., "A Study of Hooked Bar Anchorages in Beam-Column Joints," ACI Journal, 72(5): 198-209, 1975.

Mast R. F., "Auxiliary Reinforcement in concrete Connections, "Journal of the Structural Division, ASCE, 94(6)6: 1485-1504, 1968.

Mattock, A. H., "Anchorage of Stirrups in a Thin Cast in-Place Topping," PCI Journal, 32(6): 70-85, 1987.

Mattock, A. H., "Cyclic Shear Transfer and Type of Interface," ASCE Structural Journal, 107(10): 1945-1964, 1981.

Mattock, A. H., "Shear Friction and High-Strength Concrete," ACI Structural Journal, 98(1): 50-59, 2001.

Mattock, A. H., "Shear Transfer in Concrete Having Reinforcement at an Angle to the Shear Plane," ACI, Special Publication, 42: 17-42, 1974.

Mattock, A. H., and Hawkins, N. M., "Research on Shear Transfer in Reinforced Concrete," PCI Journal, 17(2): 55-75, 1972.

Mattock, A. H., Discussion of the paper, "Modified Shear-Friction Theory for Bracket Design," by B. R. Hermansen and J. Cowan, ACI Journal, 71(8): 421-423, 1974.

Mattock, A. H., Hofbeck, J. A., and Ibrahim, I. O., "Shear Transfer in Reinforced Concrete," ACI Journal, American Concrete Institute, 66(2): 119-128, 1969.

Mattock, A. H., Li, W. K., and Wang, T. C., "Shear Transfer in Lightweight Reinforced Concrete," PCI Journal, 21(1): 20-39, 1976.

Mattock, A.H., Johal, L., and Chow, H.C., "Shear Transfer in Reinforced Concrete with Moment or Tension Acting Across the Shear Plane," PCI Journal, 20(4): 76-93, 1975.

Menkulasi, F. and Roberts-Wollmann, C. L., "Horizontal Shear Connections for Full-Width, Full-Depth Precast Concrete Bridge Deck Panels on Prestressed I-Girders," Virginia Tech, Blacksburg, 2003.

Menkulasi, F., "Horizontal Shear Connectors for Precast Prestressed Bridge Deck Panels," Virginia Tech, Blacksburg, 2002.

Mindess, Sidney, James Francis Young, and David Darwin. Concrete. 2nd Edition. Englewood Cliffs, NJ: Prentice-Hall, 2003.

Mitchell, A. D., and Kahn, L. F., "Shear Friction Behavior of High-Strength Concrete", Georgia Department of Transportation Project No. 2005, , School of Civil and Environmental Engineering, Georgia Institute of Technology, Atlanta, Georgia, 2001.

Mwafy, A., Hussain, N., and El-Sawy, K. 'Seismic performance and cost-effectiveness of high-rise buildings with increasing concrete strength', Struct. Design Tall Spec. Build. 24 (2015) 257–279

Naaman, A. E., "Prestress Concrete Analysis and Design: Fundamentals," Third Edition, Techno Press 3000, Ann Arbor MI, 2012, 1176 pages.

Naaman, A.E., and Wille, K., "Some Correlation between High Packing Density, Ultra-

NCHRP Report 584, "Full-Depth Precast Concrete Bridge Deck Panel System."
Transportation Research Board, Washington, D.C, 2008.

Nojavan A, Schultz AE, Chao S-H, Haselton C, Simasathien S, Palacios G, and Liu X.
"Preliminary results of NEESR full-scale RC columns subjected to collapse-
consistent loading protocols for enhanced collapse simulation," Proceedings of
the 10th National Conference in Earthquake Engineering, Earthquake
Engineering Research Institute, Anchorage, AK, 2014.

Park R., and Paulay T., "Reinforced Concrete Structures," John Wiley and Sons, 1975.

Patnaik, A. K., "Behavior of Composite Concrete Beams with Smooth Interface." Journal
of Structural Engineering 127(4): 359-366, 2001.

Paulay T., Park R., and Phillips M. H., "Horizontal Construction Joints in Cast in Place
Reinforced Concrete," Shear in Reinforced Concrete, ACI Special Publications
42, Vol. 2: 599-616, Detroit, 1974.

PCI Design Handbook, Precast and Prestressed Concrete, Seventh Edition,
Precast/Prestressed Institute, Chicago, IL, 1992.

PGSuper Bridge Design Software, version 2.8.2, 2014.

Portland Cement Association. "High-Strength Concrete." Concrete Technology Today,
1994.

Pruijssers, A. F., and Liqui Lung, G., "Shear Transfer Across a Crack in Concrete
Subjected to Repeated Loading—Experimental Results," Part 1, Stevin Report 5-
85-12, 178 pp, 1985.

Pruijssers, A. F., and Lung, G., "Shear Transfer Across a Crack in Concrete Subjected to
Repeated Loading—Experimental Results," Part 1, Stevin Report, 1985.

Razvi, Salim, and Murat Saatcioglu. "Confinement Model for High Strength Concrete." ASCE - Journal of Structural Engineering, March 1999: 281-289.

Razvi, Salim, and Murat Saatcioglu. "Strength and Deformability of Confined High-Strength Concrete Columns." ACI Structural Journal, June 1994.

Razvi, Salim, R., and Murat Saatcioglu. "Strength and Deformability of Confined High-Strength Concrete Columns." ACI Structural Journal, December 1994: 678-687.

Rehm, G., "Criteria for Evaluation of Reinforcement Bars with High Quality Composite, Reinforced Concrete, Reports from Research and Practice", Commemorative frilly, Wilhelm Ernst & Sohn, Berlin, pp. 79-96, 1969.

Revesz, S., "Behavior of Composite T-Beams with Prestressed and Un-prestressed Reinforcement," ACI Journal, V. 24, No. 6, (Proceedings V.49), pp. 585 – 592, 1953.

Richart, F.E., Brandtzaeg, A., and Brown, R. L., "A study of failure of concrete under combined compressive stresses." Bulletin 185, Univ. of Illinois Engineering Experimental Station, Champaign, Ill, 1928.

Rossi, P, (2000), "Ultra-high Performance Fibre Reinforced Concrete (UHPFRC): An Overview," in Proceedings of Fifth RILEM Symposium in Fibre-Reinforced Concretes (FRC) - BEFIB' 2000, pp. 87 – 100.

Saemann, J. C., and Washa, G. W., "Horizontal Shear Connections between Precast Beams and CIP Slabs," ACI Journal, 61(11): 1383-1409, 1964.

Scholz D. P., "Performance Criteria Recommendations for Mortars used in Full-depth Precast Concrete Bridge Deck Panels Systems," Master's Thesis, Virginia Polytechnic Institute and State University, Blacksburg, Virginia, 2004.

Seible, F., and Latham, C. T., "Horizontal Load Transfer in Structural Concrete Bridge Deck Overlays," Journal of Structural Engineering, ASCE, V. 116, No. 10, pp. 2691 – 2710, 1990.

Shaikh, A. F., "Proposed Revisions to Shear-Friction Provisions." PCI Journal, 23(2), 12 - 21, 1978.

Shim C., Lee P., Chang S., "Design of Shear Connection in Composite Steel and Concrete Bridges with Precast Decks," Journal of Constructional Steel Research, 57: 203-219, 2001.

Shim C., Lee P., Yoon T., "Static Behavior of Large Stud Shear Connectors," Journal of Engineering Structures, 26: 1853-1860, 2004.

Shim, C. S., Kim, J. H., Chang, S. P., and Chung, C. H., "The Behavior of Shear Connections in a Composite Beam with a Full-Depth Precast Slab," Proceedings of the Institute of Civil Engineers, Structures and Buildings, Vol. 140:101-110, 2000.

Sugano, S. (1996) "Seismic Behavior of Reinforced Concrete Columns which used Ultra-High-Strength Concrete," Eleventh World Conference on Earthquake Engineering, Acapulco, Mexico, Paper No. 1383.

Sungjin, Bae, and Oguzhan Bayrak. "Early Cover Spalling in High-Strength Concrete Columns." Journal of Structural Engineering, ASCE, March 2003.

Tan, K. H., Guan, L. W., Lu, X., and Lim, T. Y., "Horizontal Shear Strength of Indirectly Loaded Composite Concrete Beams," ACI Structural Journal, 96(4): 533 – 539, 1999.

Tassios, T. P., and Vintzeleou, E. N., "Concrete to Concrete Friction," Journal of Structural Engineering, 113 (4): 832-849, 1987.

Texas Department of Transportation, Standard Specifications for Construction and Maintenance of Highways, Streets, and Bridges, June 1, 2004.

Trejo, D. and Kim, Y.H., "Development of Precast Bridge Deck Overhang System," Research Report 0-6100-3, FHWA/TX-10/0-6100-R3, 2011.

Walraven, J. C., and Reinhardt, H. W., "Theory and Experiments on the Mechanical Behavior of Cracks in Plain and Reinforced Concrete Subjected to Shear Loading," Heron, V. 26, No. 1, 1981.

Walraven, J., Frenay, J., and Pruijssers, A., "Influence of Concrete Strength and Load History on the Shear Friction Capacity of Concrete Members," PCI Journal, 32(1): 66-84, 1987.

Waweru, R., "The Strength of Horizontal Shear Reinforcement with Limited Development," PhD Dissertation, The University of Texas at Arlington, Arlington, Texas, 2015.

Wille, K.; Naaman, A.E.; and Parra-Montesinos, G.J., "Ultra-High Performance Concrete with Compressive Strength Exceeding 150 MPa (22 ksi): A Simpler Way," *ACI Materials Journal*, V. 108, No. 1, Jan.-Feb. 2011a, pp. 46-54.

Biographical Information

Guillermo Palacios was born on March 22, 1990. After graduating early from Grand Prairie High School in 2007 he then enrolled at The University of Texas at Arlington. During his senior year he met Dr. Andreas Stavridis who first introduced him to earthquake engineering research. He then became the founding president of the UTA Earthquake Engineering Research Institute Student Chapter and briefly worked with Dr. Stavridis on analyzing the results of shake-table tests of a full-scale, three-story reinforced masonry shear-wall structure. In 2012, Guillermo graduated Cum Laude with a Bachelor's of Science in Civil Engineering with an emphasis in Structural Engineering.

Shortly after graduation, Guillermo began his graduate studies working with Dr. Shih-Ho Chao. While working with Dr. Chao, his interest in research grew and he quickly became involved in a number of concrete projects including "Full-Scale RC and HPFRC Frame Subassemblages Subjected to Collapse-Consistent Loading Protocols for Enhanced Collapse Simulation and Internal Damage Characterization" and "Strength of Horizontal Shear Reinforcement with Limited Development" and temporarily worked on "The Effect of Fiber Corrosion on Shear Capacity of Steel Fiber Reinforced Concrete Beams".

Guillermo is a member of the American Concrete Institute (ACI) and the American Society of Civil Engineers (ASCE). During his final year of graduate studies, he began an internship at Jaster-Quintanilla located in Dallas, Texas. After receiving his M.S. in Structural Engineering and Applied Mechanics, Guillermo plans to work as a Structural Engineer and gain valuable design experience working toward his P.E. license. The possibility will always exist that his passion for research may lead him to return to school and pursue his PhD.